

**NASA Technical Memorandum 100541**

**AVSCOM  
Technical Memorandum 88-B-004**

**INFLOW MEASUREMENT MADE WITH A LASER VELOCIMETER ON A  
HELICOPTER MODEL IN FORWARD FLIGHT**

**Volume I      RECTANGULAR PLANFORM BLADES AT AN ADVANCE  
                  RATIO OF 0.15**

**Joe W. Elliott and Susan L. Althoff  
Aerostructures Directorate  
USAARTA-AVSCOM  
Langley Research Center  
Hampton, Virginia**

**Richard H. Sailey  
PRC Kentron Inc.  
Aerospace Technologies Division  
Hampton, Virginia**

**April 1988**

**(NASA-TM-100541) INFLOW MEASUREMENTS MADE  
WITH A LASER VELOCIMETER ON A HELICOPTER  
MODEL IN FORWARD FLIGHT. VOLUME 1:  
RECTANGULAR PLANFORM BLADES AT AN ADVANCE  
RATIO OF 0.15 (Army Aviation Systems**

**N88-24607**

**Unclassified  
G3/02 0149014**



**National Aeronautics and  
Space Administration**

**Langley Research Center  
Hampton, Virginia 23665-5225**

## SUMMARY

An experimental investigation was conducted in the 14- by 22-Foot Subsonic Tunnel at NASA Langley Research Center to measure the inflow into a scale model helicopter rotor in forward flight ( $\mu_{\infty} = 0.15$ ). The measurements were made with a two component Laser Velocimeter (LV) one chord above the plane formed by the path of the rotor tips (tip path plane). A conditional sampling technique was employed to determine the azimuthal position of the rotor at the time that each velocity measurement was made so that the azimuthal fluctuations in velocity could be determined. Measurements were made at a total of 147 separate locations in order to clearly define the inflow character. This data is presented herein without analysis. In order to increase the availability of the resulting data, both the mean and azimuthally dependent values are included as part of this report on two 5.25 inch floppy disks in Microsoft Corporation MS-DOS format.

## INTRODUCTION

One of the many problems confronting the helicopter aerodynamic community is the lack of a comprehensive database which includes the measurements of the velocities into and through the rotor systems. These measurements are necessary for a more complete understanding of the fluid dynamics associated with the rotor and its thrust/lift producing process, and to provide data for the validation of the rapidly emerging computer codes intended to predict the behavior of this process. One explanation for the lack of available data is the absence, until recent years, of a suitable device for making such measurements. Making measurements in and around a system of rotating blades requires a nonintrusive measurement capability that presents a minimum risk to the systems involved and provides an accurate means of making such measurements. The Laser Velocimeter (LV), which uses high energy light beams to measure velocities, is ideally suited to this task.

The Laser Velocimeter has been successfully used to measure specific areas and localized phenomena within the rotor disk (refs. 1 through 3). In addition, the hotwire anemometer and pressure probes, both having directional measuring limitations, have been employed in similar programs (refs. 4 and 5). This is, however, the first time that a comprehensive program has been undertaken to map the flow into the complete rotor disk. An investigation has been conducted to measure the flow into a representative rotor system as a function of azimuth using a two-component (streamwise and vertical direction) LV system.

## NOTATION

$A_0$	constant term in Fourier series of blade feathering (collective) at $r/R = 0.75$ , deg
$A_1$	coefficient of cosine term in Fourier series of blade feathering, deg
$B_1$	coefficient of sin term in Fourier series of blade feathering, deg
$b$	number of blades
$C_D$	rotor drag coefficient, $D/\rho A (V_{tip})^2$ , nondimensional

$C_Q$	rotor torque coefficient, $Q/\rho A R (v_{tip})^2$ , nondimensional
$C_T$	rotor thrust coefficient, $T/\rho A (v_{tip})^2$ , nondimensional
$c$	rotor blade chord, inches
$D$	rotor Drag, positive to the rear
$Q$	rotor Torque, ft-lb
$q$	dynamic pressure, lb/ft <sup>2</sup>
$r$	local radius of the rotor system, ft
$R$	rotor radius, ft
$T$	thrust produced by the rotor, lbf
$U$	free-stream component of velocity, positive downstream, ft/sec
$U_\infty$	free-stream velocity, positive downstream, ft/sec
$u_i$	induced component of velocity parallel to the tip path plane (positive flow down stream), ft/sec
$v$	vertical component of velocity, positive up, ft/sec
$v_i$	induced component of velocity normal to the tip path plane (positive flow up), ft/sec
$v_{tip}$	rotor blade tip velocity, ft/sec
Greek	
$\alpha$	angle between rotor disk and free-stream velocity (positive nose up), deg
$\lambda$	inflow ratio normal to Tip Path Plane (positive up), $(U \sin \alpha + v_i)/v_{tip}$
$\lambda_i$	induced inflow ratio normal to Tip Path Plane, (positive up), $v_i/v_{tip}$
$\mu_\infty$	rotor advance ratio, $U_\infty \cos \alpha/v_{tip}$
$\mu$	inflow ratio parallel to Tip Path Plane (positive down stream), $(U \cos \alpha + u_i)/v_{tip}$
$\mu_i$	induced inflow ratio parallel to Tip Path Plane (positive down stream) $u_i/v_{tip}$
$r$	rotor rotational speed, radians/sec
$\psi$	rotor azimuth measured from downstream position positive counterclockwise as viewed from above, deg
$\rho$	air density, slugs/ft <sup>3</sup>

$\theta$  blade pitch angle at a specific azimuth,  $\theta = A_0 - A_1 \cos \psi - B_1 \sin \psi$ , deg  
xx mean values

#### EXPERIMENTAL APPARATUS

The experimental apparatus used in this investigation included the NASA Langley Research Center 14- by 22-Foot Subsonic Tunnel, the 2-Meter Rotor Test System (2MRTS), and a two-component laser velocimeter system.

The 14- by 22-Foot Subsonic Tunnel is an atmospheric, closed-circuit wind tunnel of conventional design with enhancements for the testing of powered and high-lift configurations (ref. 6). The tunnel is shown in figure 1 and schematically in figure 2. When the test section is configured open, with the walls and ceiling lifted out of the flow leaving only a solid floor and a flow collector at the rear, it can be driven to about 170 knots. This investigation was conducted with the tunnel in this configuration to allow complete optical access to the rotor flowfield produced by the 2MRTS that was mounted on a strut in the forward part of the test section as is shown in figure 3.

The 2MRTS is a general purpose rotorcraft model testing system. The system consists of a 29-horsepower electric drive motor and 90 degree speed-reducing transmission, a blade pitch control system, and two six-component strain gage balances used for measuring forces and moments on the rotor system and fuselage shell. The four-bladed rotor hub is fully articulated with viscous dampers for lead-lag motion and coincident flap and lag hinges. A more detailed description of the 2MRTS including the ROBIN fuselage can be found in reference 7. The characteristics of rotor blades used in this investigation can be found in table 1. No attempt was made to dynamically scale the rotor blades, rather they were made as stiff as possible to minimize deflection while being tested.

The LV system used in this investigation was designed to measure the instantaneous components of velocity in the longitudinal (free stream) and vertical directions. The LV system is described in reference 8. The system is comprised of four subsystems: optics, traverse, data acquisition, and seeding. The optics subsystem, which is shown in figure 4, operates in backscatter mode and at high power (4 watts in all lines) in order to accommodate the long focal lengths needed to scan the wide test section. The transmitting and receiving optics packages are augmented by a zoom lens system consisting of a 3-in. clear aperture negative lens and a 12-in. clear aperture positive lens. Bragg cells in each of the optical paths provide a directional measurement capability. The velocity measurements are made at a point in space where the four beams cross, called the sample volume. The length of the sample volume (transverse to the flow direction) increases as the sample volume is moved away from the optics assembly. The sample volume is, over the 10- to 20 ft focal length of the system, less than 1 cm long with a near constant diameter of 0.2 mm.

The traverse subsystem provides five degrees of freedom in positioning the sample volume and is controlled by the same computer that is used for data acquisition. Translation of the sample volume in the horizontal and vertical direction is accomplished by displacing the entire optics platform. Translation along the lateral axes is accomplished by displacing the negative lens located in the zoom lens assembly, thus refocusing the sample volume along the axis of optical transmission. The other two degrees of freedom, pan and tilt, are implemented by rotating the final mirror about its vertical and horizontal axis in order to change the direction of optical transmission. The total inclusive range of the traversing system is 7 ft vertically,

6 ft streamwise, 16.5 ft laterally, and 10° in both pan and tilt. Measurements can be made outside of this envelope by repositioning the optics platform, which is mounted on wheels to facilitate such relocations. For this study the traversing system was positioned to the right of the test section when looking upstream as shown in figure 5.

The data acquisition subsystem is shown schematically in figure 6 and interfaces with the optical signal processing equipment to receive two channels of raw LV data and up to five channels of auxiliary data. In this investigation four of the auxiliary channels were used for the acquisition of data relative to blade position. Two of the channels (one each for the U and V components) measured the azimuthal position of the rotor shaft and the other two the lead/lag and flapping motion. The system converts the raw LV data to engineering units and determines the statistical characteristics of the acquired data so that the test results can be evaluated during the acquisition process. The raw data which is acquired from the buffer interface device, the data which has been converted to engineering units, and up to 64 parameters which are acquired from the tunnel static data acquisition system are written to magnetic tape for later analysis. The final function performed by the data system is to interface with and control the five degree-of-freedom scan system.

The seeding subsystem, shown schematically in figure 7, is a solid particle, liquid dispensing system (ref. 9). Polystyrene latex microspheres are suspended in a mixture containing, by volume, 50 percent water and 50 percent ethyl alcohol. The advantage of the polystyrene particles is their low density, high reflectivity, and precise particle size. The size of the particles used in this investigation was 1.7 microns in diameter with a standard deviation of 0.0239 microns. This mixture is pumped to an array of 32 nozzles where compressed air is used to atomize the mixture. These nozzles are mounted on a frame 8 ft wide by 6 ft high which is suspended on cables in the settling chamber of the tunnel. The low vapor pressure of water/alcohol mixture allows it to evaporate as it travels the 85 ft from the settling chamber to the test section. This process provides isolated single particles in the flow field whose velocities are measured as they pass through the sample volume, from which the local fluid velocity is inferred.

#### ERROR ANALYSIS

The overall LV system error is obtained by summing the error of all of the components that contribute to an error in the velocity measurement. The error sources are summarized in the table below, and are defined in ref. 10. They result in a bias error of -0.81 percent to 1.82 percent and a random error of 1.12 percent. Taking the square root of the sum of the squares of these gives a total system error of 1.38 percent to 2.14 percent (1.76 percent  $\pm$  0.38 percent).

Error source	Bias percent	Random percent
Cross beam angle measurement	0.81	None
Diverging fringes	A	A
Time jitter	N/A	N/A
Clock synchronization	0.51	$\pm 0.51$
Quantization	A	$\pm 0.99$
Velocity bias	B	B
Brag bias	B	B
Velocity gradient	B	B
Particle lag	$\pm 0.50$	B
Total error	-0.81 to 1.82	1.12
A NOT MEASURED		
B NEGLIGIBLE		

#### TEST PROCEDURES

Measurements were made at azimuthal increments of 30° from  $\psi = 0^\circ$ , excluding 120 and 270°, at 3.0 in. (approximately one chord) above the plane formed by the tips of the blades. Measurements were made from radial location of  $r/R = 0.2$  to  $r/R = 1.1$ , with the majority of the measurement locations concentrated toward the outboard portion of the disk. Figure 8 shows the measurement locations superimposed on the rotor disk. During the test the rotor tip path plane was maintained at -3° relative to the free stream by zeroing the blade flapping relative to the shaft and setting the shaft angle to -3°. The operating rotor speed for the test was held at 2113 rpm, the nominal tunnel speed was 94 ft/sec ( $\mu_\infty = 0.15$ ), and the nominal rotor thrust coefficient was 0.0064. Table 2 lists the target flight conditions, and selected parameters acquired during the test. The acquisition process consisted of placing the sample volume at the location to be measured and acquiring data for a period of one minute or until 4096 velocity measurements were made in either the U or the V components. During this time conditional sampling techniques were employed to determine the location of the four blades and to permanently associate each measured velocity with the location of the blade when the measurement was made. At the conclusion of that process the measurement location was changed and the acquisition process was repeated.

#### DATA REDUCTION

Independent velocity measurements in the free stream and vertical direction were made at each measurement location. At the same instant in time that a velocity

measurement was made, the location of the blades was recorded for that velocity component. The maximum time required to acquire this data was one minute (2100 rotor revolutions for this test) and the minimum approximately 20 sec. These data were collected over many spaced azimuth segments that are representative of blade position and include the corrections for blade lead/lag motion. The velocity value assigned to each azimuthal interval is the arithmetic mean of all of the measurements that were taken in the respective  $2.81^\circ$  wide azimuth range. The results of this sorting process provide the azimuth dependent velocity data. The "mean" velocity value refers to the arithmetic mean, calculated from all of the measurements made at a single measurement location.

#### EXPERIMENTAL RESULTS

Table 3 lists the measurement locations, the mean and standard deviation of the 2 components of induced inflow velocity, and the number of measurements made on the U and V components. In figure 9 the mean induced component of velocity (longitudinal)  $\mu_i$  with a band of  $\pm$  one standard deviation is plotted vs. radius for each radial scan. Figure 10 presents in the same format the mean induced component of velocity (normal)  $\lambda_i$ . The  $\pm$  one standard deviation is not indicative of the error but rather of the unsteady nature of the flow. The error of 1.76 percent  $\pm$  -0.38 percent is approximately equal to the size of the symbols in figures 9 and 10. The same data, without the one standard deviation, is presented in a contour plot format in figures 11 and 12 in order to more clearly show the mean induced flow over the whole disk (viewed from above). The format of each of figures 13 through 158 is the induced velocity vs. azimuth at the top of the figure, the number of measurements that went into determining the mean for each bin in the center, and an order ratio analysis of the time dependent data at the bottom of the figure. The figure numbers for the azimuthal and radial locations are indicated below.

Azimuth r/R	0	30	60	90	120	150	180	210	240	270	300	330
0.20	13	--	41	56	--	71	86	--	115	--	130	145
0.40	14	--	42	57	--	72	87	101	116	--	131	146
0.50	15	28	43	58	--	73	88	102	117	--	132	147
0.60	16	29	44	59	--	74	89	103	118	--	133	148
0.70	17	30	45	60	--	75	90	104	119	--	134	--
0.74	18	31	46	61	--	76	91	105	120	--	135	149
0.78	19	32	47	62	--	77	92	106	121	--	136	150
0.82	20	33	48	63	--	78	93	107	122	--	137	151
0.86	21	34	49	64	--	79	94	108	123	--	138	152
0.90	22	35	50	65	--	80	95	109	124	--	139	153
0.94	23	36	51	66	--	81	96	110	125	--	140	154
0.98	24	37	52	67	--	82	97	111	126	--	141	155
1.02	25	38	53	68	--	83	98	112	127	--	142	156
1.04	26	39	54	69	--	84	99	113	128	--	143	157
1.10	27	40	55	70	--	85	100	114	129	--	144	158

The results shown in table 3, the mean and standard deviation of the induced inflow velocities, and the results shown in figures 13 through 158, the azimuth dependent induced inflow velocities, are included on a 5.25 in. floppy disk in Microsoft Corporation MS-DOS format (see pocket inside rear cover). The details of the data format, and file structure is located in the file "README.DOC". The disk is double sided with a density of 360 kbytes.

#### CONCLUDING REMARKS

The Laser Velocimeter provides an effective system for making measurements in the dynamic environment associated with rotorcraft. It has in fact been used on numerous occasions to measure the localized phenomena encountered in such flows. This investigation demonstrates the use of a mature system in mapping the flow into a representative rotor in forward flight. These measurements provide not only the mean values but azimuth dependent values as well, and they provide a detailed look at the nature of this flow.

REFERENCES

1. Landgrebe, A. J.; and Johnson, B. V.: Measurement of Model Helicopter Rotor Flow Velocities With a Laser Doppler Velocimeter. American Helicopter Society, Journal, Vol. 19, July 1974, pp. 39-43.
2. Biggers, J. C.; and Orloff, K. L.: Laser Velocimeter Measurements of the Helicopter Rotor-Induced Flowfield. American Helicopter Society, Annual National V/STOL Forum, 30th, Washington, D.C., May 7-9, 1974.
3. Owen, F. K.; and Taubert, M. E.: Measurement and Prediction of Model-Rotor Flow-fields. AIAA, 18th Fluid Dynamics, Plasmadynamics and Laser Conference, Cincinnati, Ohio, July 16-18, 1985.
4. Tangler, J. L.; Wohlfeld, R. M.; and Miley, S. J.: Analysis of Wakes Generated by Hovering Model Propellers and Rotors Using Schlieren Photography and Hot-Wire Anemometry. Bell Helicopter Company, Fort Worth, Texas, NASA CR-2305, September 1973.
5. Junker, B.: Investigations of Blade-Vortices in the Rotor Downwash. Twelfth European Rotorcraft Forum, Garmish-Partenkirchen, Federal Republic of Germany, September 22-25, 1986.
6. Applin, Z. T.: Flow Improvements in the Circuit of the Langley 4- by 7-Meter Tunnel. NASA TM-85662, December 1983.
7. Phelps, A. E. III; and Berry, J. D.: Description of the U.S. Army 2-Meter Rotor Test System. NASA TM-87762, AVSCOM TM-86-B-4, January 1987.
8. Sellers, W. L.; and Elliott, J. W.: Applications of a Laser Velocimeter in the Langley 4-by 7-Meter Tunnel. Proceedings of the Workshop on Flow Visualization and Laser Velocimetry for Wind Tunnels. NASA CP-2243, March 1982, pp. 283-293.
9. Elliott, J. E.; and Nichols, C. E.: Seeding Systems for use With a Laser Velocimeter in Large Scale Wind Tunnels. Proceedings of the Workshop on Wind Tunnel Seeding Systems for Laser Velocimeters, NASA CP-2393, March 1985, pp. 93-103.
10. Young, W. H.; Meyers, J. F.; and Hepner, T. E.: Laser Velocimeter Systems Analysis to a Flow Survey Above a Stalled Wing. NASA TN D-8408, August 1977.
11. Dring, R. P.: Sizing Criteria for Laser Anemometry Particles. Journal of Fluid Engineering, Vol. 104, March 1982, pp. 15-17.

TABLE 1.- 2MRTS ROTOR AND BLADE CHARACTERSTICS

Hub Type .....	Fully Articulated
Number of blades .....	4
Airfoil section .....	NACA 0012
Hinge offset, in, r/R .....	2.00, .06
Root cutout, in, r/R .....	8.25, .24
Pitch-flap coupling angle, deg .....	0.0
Twist linear, deg .....	-8.0
Radius, R, in .....	33.88
Airfoil chord, C, in .....	2.6
Rotor solidity, $bc/\pi R$ .....	0.0977
Blade Stiffness	
Flapwise lb-in <sup>2</sup> .....	11500
Torsional lb-in <sup>2</sup> .....	25500
Blade Weight, grams .....	259.3
Lead/lag damping in-lb/deg/sec .....	182.4

TABLE 2.- NOMINAL ROTOR CONTROLS AND PERFORMANCE PARAMETERS

$C_D$ .....	0.0002
$\alpha$ , deg .....	-3.00
$A_0$ , deg .....	9.37
$A_1$ , deg .....	-1.11
$B_1$ , deg .....	3.23
Coning, deg .....	1.50
$\mu_\infty$ .....	0.149
$C_T$ .....	0.0063
$C_Q$ .....	0.00036
$V_\infty$ , knots .....	55.4
$V_{tip}$ , ft/sec .....	624.3
$M_{tip}$ , nondimensional .....	0.5533
Lag angle, (mean), deg .....	0.95

TABLE 3.- INFLOW VELOCITY SUMMARY

$\mu_1$				$\lambda_1$			
$\psi$	r/R	Mean	Standard deviation	# measurements	Mean	Standard deviation	# measurements
0	.20	.0193	.0186	555	-.0125	.0059	889
0	.40	.0181	.0169	467	-.0258	.0072	1015
0	.50	.0169	.0169	377	-.0313	.0081	861
0	.60	.0148	.0170	268	-.0369	.0090	709
0	.70	.0135	.0160	186	-.0425	.0098	589
0	.74	.0106	.0168	175	-.0449	.0096	482
0	.78	.0126	.0176	109	-.0479	.0101	424
0	.82	.0051	.0167	89	-.0502	.0094	286
0	.86	.0006	.0188	1490	-.0493	.0091	3535
0	.90	-.0004	.0188	1571	-.0499	.0086	3558
0	.94	-.0020	.0183	1449	-.0503	.0076	3360
0	.98	-.0040	.0171	999	-.0493	.0063	2252
0	1.02	-.0064	.0182	787	-.0478	.0051	1645
0	1.04	-.0070	.0175	689	-.0472	.0046	1561
0	1.10	-.0113	.0177	740	-.0442	.0046	1370
30	.50	.0167	.0159	2185	-.0348	.0095	3336
30	.60	.0143	.0154	2199	-.0411	.0100	3295
30	.70	.0086	.0161	2191	-.0462	.0096	3672
30	.74	.0084	.0162	2244	-.0473	.0097	3655
30	.78	.0065	.0156	2301	-.0477	.0105	3320
30	.82	.0040	.0174	2183	-.0480	.0105	3444
30	.86	.0011	.0157	2128	-.0480	.0106	3260
30	.90	-.0002	.0159	2108	-.0482	.0106	3069
30	.94	-.0017	.0159	2140	-.0484	.0094	3539
30	.98	-.0030	.0151	2075	-.0475	.0087	3531
30	1.02	-.0062	.0158	2114	-.0461	.0082	3574
30	1.04	-.0069	.0155	2064	-.0452	.0078	3548
30	1.10	-.0081	.0157	1883	-.0430	.0072	3522
60	.20	.0168	.0189	2375	-.0079	.0091	2059
60	.40	.0153	.0154	2129	-.0297	.0077	2870
60	.50	.0107	.0146	2161	-.0346	.0085	3050
60	.60	.0101	.0162	1509	-.0352	.0109	1866
60	.70	.0086	.0163	1771	-.0357	.0109	2321
60	.74	.0089	.0161	908	-.0354	.0114	1245
60	.78	.0072	.0151	1715	-.0382	.0056	1717
60	.82	.0055	.0140	1772	-.0376	.0056	1910
60	.86	.0034	.0163	1207	-.0381	.0073	1361
60	.90	.0033	.0164	879	-.0366	.0076	1059
60	.94	-.0023	.0169	585	-.0338	.0079	731
60	.98	-.0032	.0128	565	-.0210	.0094	855
60	1.02	-.0055	.0139	159	-.0111	.0043	211
60	1.04	-.0066	.0142	254	.0017	.0040	220
60	1.10	-.0042	.0132	290	.0262	.0023	179

TABLE 3.- Continued

$\psi$	$r/R$		$\mu_1$			$\lambda_1$	
		Mean	Standard deviation	# measurements	Mean	Standard deviation	# measurements
90	.20	.0016	.0280	462	-.0065	.0032	564
90	.40	.0117	.0206	543	-.0234	.0050	980
90	.50	.0111	.0176	476	-.0255	.0061	906
90	.60	.0121	.0188	779	-.0232	.0067	1429
90	.70	.0128	.0168	702	-.0241	.0072	1248
90	.74	.0117	.0170	827	-.0224	.0071	1402
90	.78	.0098	.0151	923	-.0195	.0073	1855
90	.82	.0079	.0161	790	-.0161	.0082	1321
90	.86	.0082	.0160	580	-.0112	.0090	962
90	.90	.0060	.0151	377	-.0008	.0075	606
90	.94	.0046	.0160	336	.0111	.0047	551
90	.98	.0044	.0133	321	.0195	.0037	572
90	1.02	.0001	.0113	244	.0214	.0030	520
90	1.04	-.0042	.0148	256	.0224	.0017	362
90	1.10	-.0043	.0127	227	.0182	.0018	431
150	.20	-.0016	.0167	1277	-.0030	.0033	1445
150	.40	.0069	.0183	1220	-.0138	.0055	1925
150	.50	.0096	.0181	1983	-.0122	.0066	2920
150	.60	.0107	.0181	1823	-.0090	.0060	2917
150	.70	.0110	.0172	1525	-.0041	.0080	3008
150	.74	.0116	.0170	1291	-.0020	.0079	3007
150	.78	.0131	.0149	1899	.0030	.0072	1453
150	.82	.0136	.0149	2449	.0063	.0069	1580
150	.86	.0118	.0126	1458	.0086	.0074	875
150	.90	.0082	.0135	3167	.0103	.0069	2339
150	.94	.0071	.0132	3232	.0111	.0059	1645
150	.98	.0025	.0143	956	.0114	.0036	879
150	1.02	-.0007	.0143	2787	.0110	.0029	1953
150	1.04	-.0002	.0151	2715	.0101	.0026	2088
150	1.10	-.0025	.0147	2687	.0087	.0023	2060
180	.20	.0639	.0140	1496	-.0090	.0056	798
180	.40	.0092	.0123	1430	-.0142	.0078	1278
180	.50	.0124	.0147	1738	-.0119	.0072	1442
180	.60	.0163	.0142	1731	-.0100	.0116	1574
180	.70	.0170	.0140	1991	-.0057	.0133	1560
180	.74	.0170	.0138	2294	-.0018	.0123	1580
180	.78	.0162	.0134	2362	.0012	.0123	1654
180	.82	.0155	.0130	2845	.0035	.0115	1619
180	.86	.0118	.0150	3089	.0047	.0122	1760
180	.90	.0102	.0154	3065	.0074	.0124	1581
180	.94	.0067	.0147	3158	.0103	.0113	1537
180	.98	.0031	.0142	3243	.0135	.0074	1473
180	1.02	.0005	.0135	3156	.0133	.0064	1464
180	1.04	-.0012	.0144	3243	.0127	.0064	1393
180	1.10	-.0043	.0143	3218	.0105	.0059	1671

TABLE 3.- Continued

$\mu_1$				$\lambda_1$			
$\psi$	r/R	Mean	Standard deviation	# measurements	Mean	Standard deviation	# measurements
210	.40	.0083	.0154	3101	-.0151	.0076	1951
210	.50	.0117	.0161	3114	-.0152	.0095	1768
210	.60	.0132	.0168	3013	-.0141	.0115	1524
210	.70	.0170	.0167	3028	-.0111	.0127	1342
210	.74	.0183	.0164	3054	-.0072	.0116	1193
210	.78	.0169	.0164	3027	-.0012	.0132	1003
210	.82	.0163	.0178	2945	-.0009	.0119	1026
210	.86	.0141	.0178	2795	.0036	.0152	1046
210	.90	.0131	.0165	1154	.0080	.0120	306
210	.94	.0079	.0159	1693	.0146	.0069	378
210	.98	.0065	.0171	2149	.0136	.0070	538
210	1.02	.0017	.0151	2876	.0131	.0062	739
210	1.04	.0013	.0155	3086	.0126	.0062	727
210	1.10	-.0026	.0154	3099	.0116	.0067	804
240	.20	.0057	.0141	2950	-.0089	.0055	1297
240	.40	.0080	.0149	3002	-.0168	.0066	1665
240	.50	.0107	.0150	2923	-.0184	.0071	1577
240	.60	.0140	.0170	1554	-.0191	.0086	708
240	.70	.0154	.0174	1486	-.0158	.0102	648
240	.74	.0151	.0185	1580	-.0169	.0119	602
240	.78	.0170	.0192	2041	-.0133	.0117	717
240	.82	.0163	.0190	2102	-.0092	.0111	742
240	.86	.0179	.0189	2547	-.0048	.0130	817
240	.90	.0178	.0192	2711	.0005	.0158	798
240	.94	.0149	.0194	3045	.0056	.0159	798
240	.98	.0110	.0204	2293	.0135	.0095	475
240	1.02	.0068	.0169	2079	.0161	.0081	433
240	1.04	.0056	.0176	2065	.0158	.0091	404
240	1.10	.0032	.0171	1601	.0134	.0076	381
300	.20	.0109	.0160	1725	-.0064	.0047	2953
300	.40	.0090	.0162	1721	-.0141	.0059	3601
300	.50	.0105	.0170	989	-.0192	.0069	2160
300	.60	.0116	.0165	421	-.0245	.0074	874
300	.70	.0107	.0180	187	-.0294	.0087	374
300	.74	.0099	.0180	158	-.0312	.0088	308
300	.78	.0076	.0177	1549	-.0331	.0087	3481
300	.82	.0086	.0175	1022	-.0350	.0089	2500
300	.86	.0077	.0170	724	-.0366	.0085	1787
300	.90	.0061	.0168	327	-.0384	.0079	949
300	.94	.0029	.0192	178	-.0375	.0070	497
300	.98	.0021	.0171	291	-.0377	.0068	692
300	1.02	.0002	.0201	84	-.0259	.0067	152
300	1.04	.0003	.0165	123	-.0296	.0065	280
300	1.10	-.0002	.0210	211	-.0073	.0081	263

TABLE 3.- Concluded

$\psi$	r/R	$\mu_1$			$\lambda_1$		
		Mean	Standard deviation	# measurements	Mean	Standard deviation	# measurements
330	.20	.0157	.0150	535	-.0078	.0048	1252
330	.40	.0164	.0156	429	-.0133	.0074	1162
330	.50	.0174	.0145	456	-.0191	.0080	1630
330	.60	.0164	.0153	520	-.0248	.0089	2170
330	.74	.1644	.0161	359	-.0385	.0096	1531
330	.78	.0144	.0152	235	-.0355	.0108	1564
330	.82	.0124	.0154	191	-.0383	.0106	1449
330	.86	.0139	.0154	171	-.0409	.0109	1348
330	.90	.0061	.0144	177	-.0430	.0102	1282
330	.94	.0042	.0155	129	-.0447	.0097	1036
330	.98	.0002	.0183	203	-.0451	.0084	887
330	1.02	-.0013	.0156	189	-.0446	.0070	750
330	1.04	-.0062	.0175	182	-.0424	.0057	616
330	1.10	-.0052	.0161	108	-.0394	.0051	430

ORIGINAL PAGE IS  
OF POOR QUALITY.



Figure 1.- Aerial view of 14- by 22-foot tunnel.

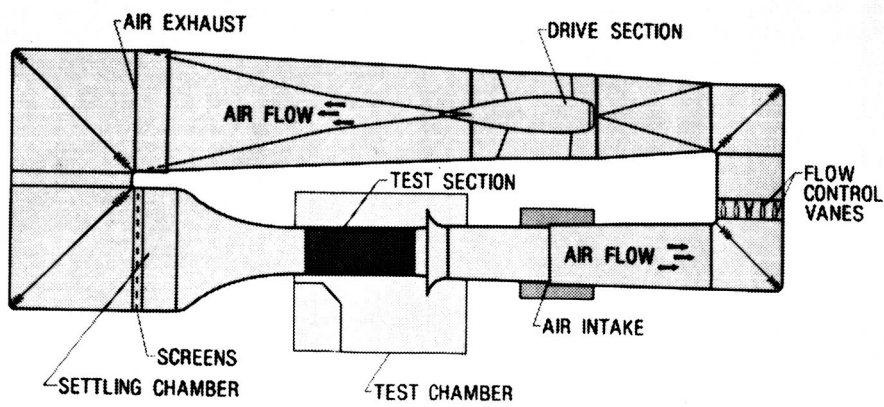
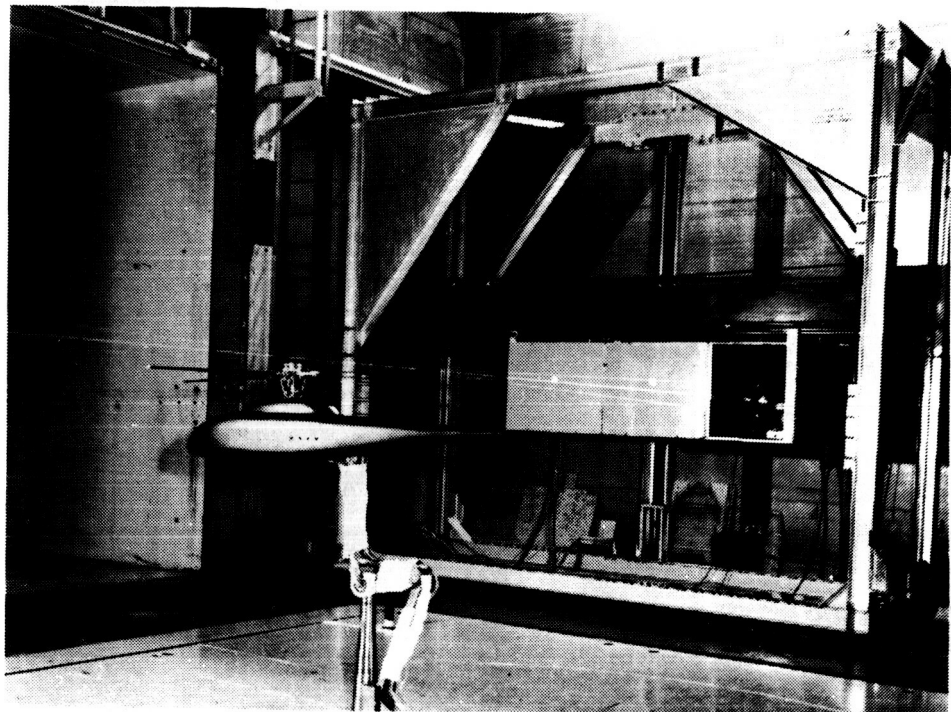


Figure 2.- Schematic view of 14- by 22-foot  
subsonic wind tunnel.

**ORIGINAL PAGE IS  
OF POOR QUALITY**



**Figure 3.- 2MRTS mounted in forward bay  
of the test section.**

ORIGINAL PAGE IS  
OF POOR QUALITY

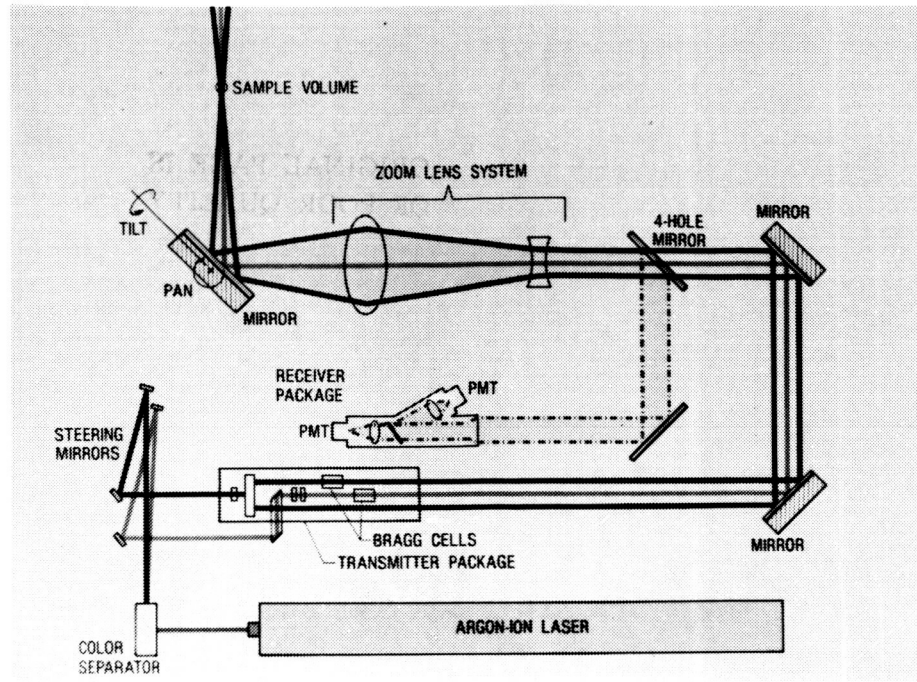


Figure 4.- Schematic diagram of Laser Velocimeter  
Optics Sub-system.

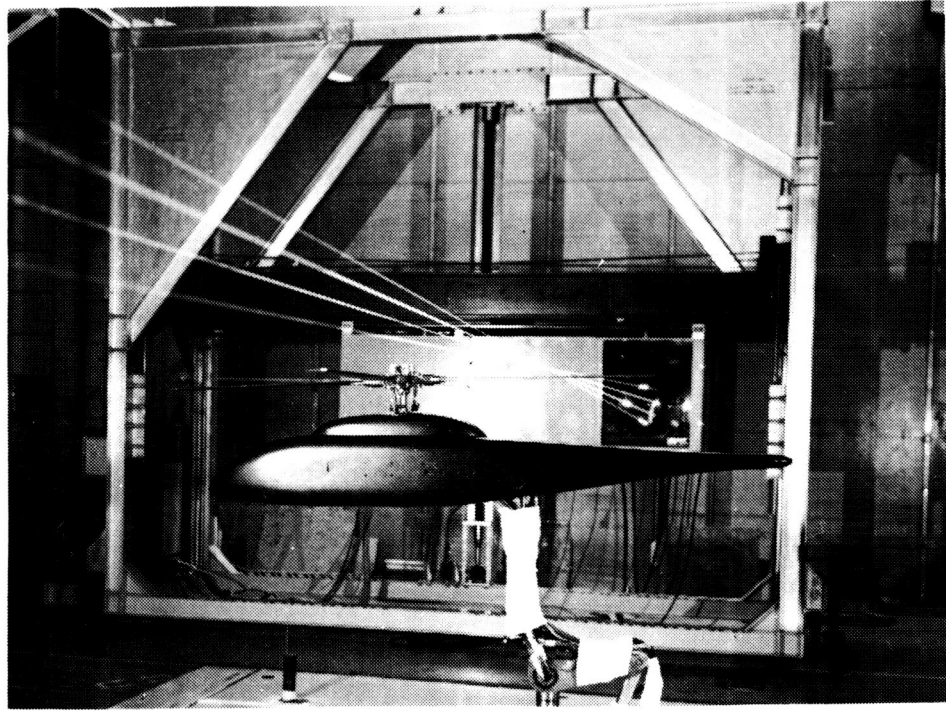


Figure 5.- Laser Velocimeter positioned in  
test chamber.

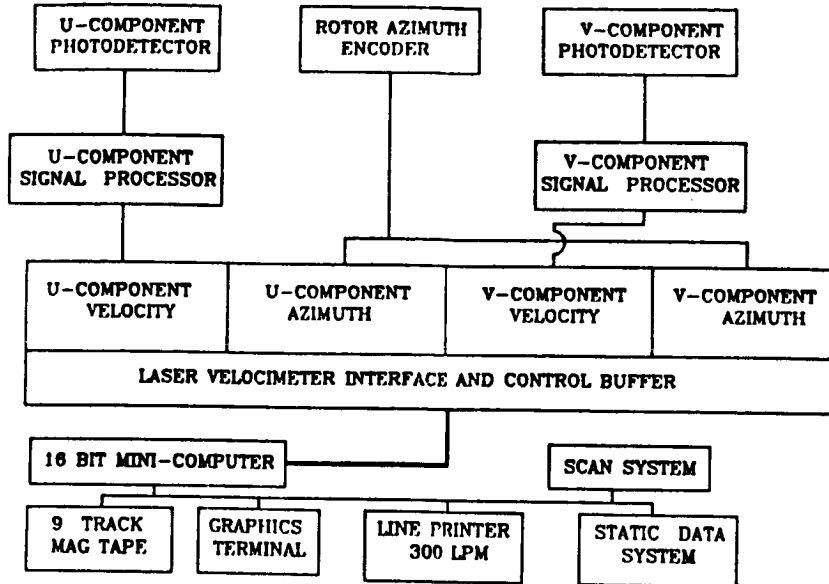


Figure 6.- Schematic view of data aquisition and control subsystem.

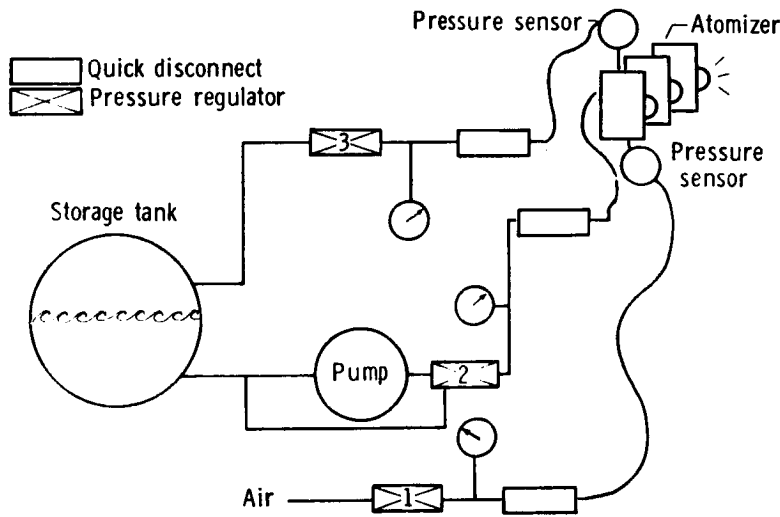
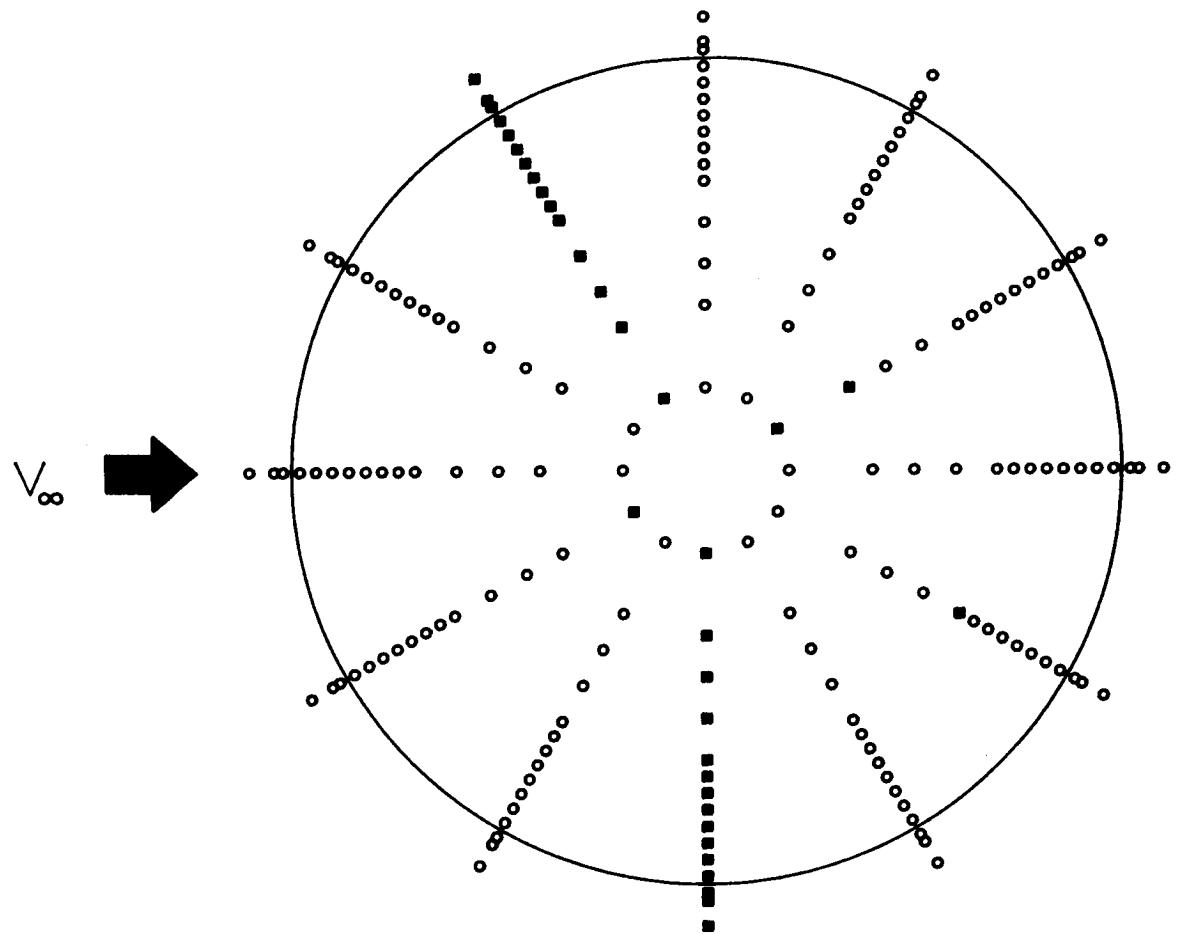


Figure 7.- Schematic of Seeding system.



**MEASUREMENTS**

- U and V
- None

Figure 8.— Locations of velocity measurements,  
3.0 inches above rotor tip path plane.

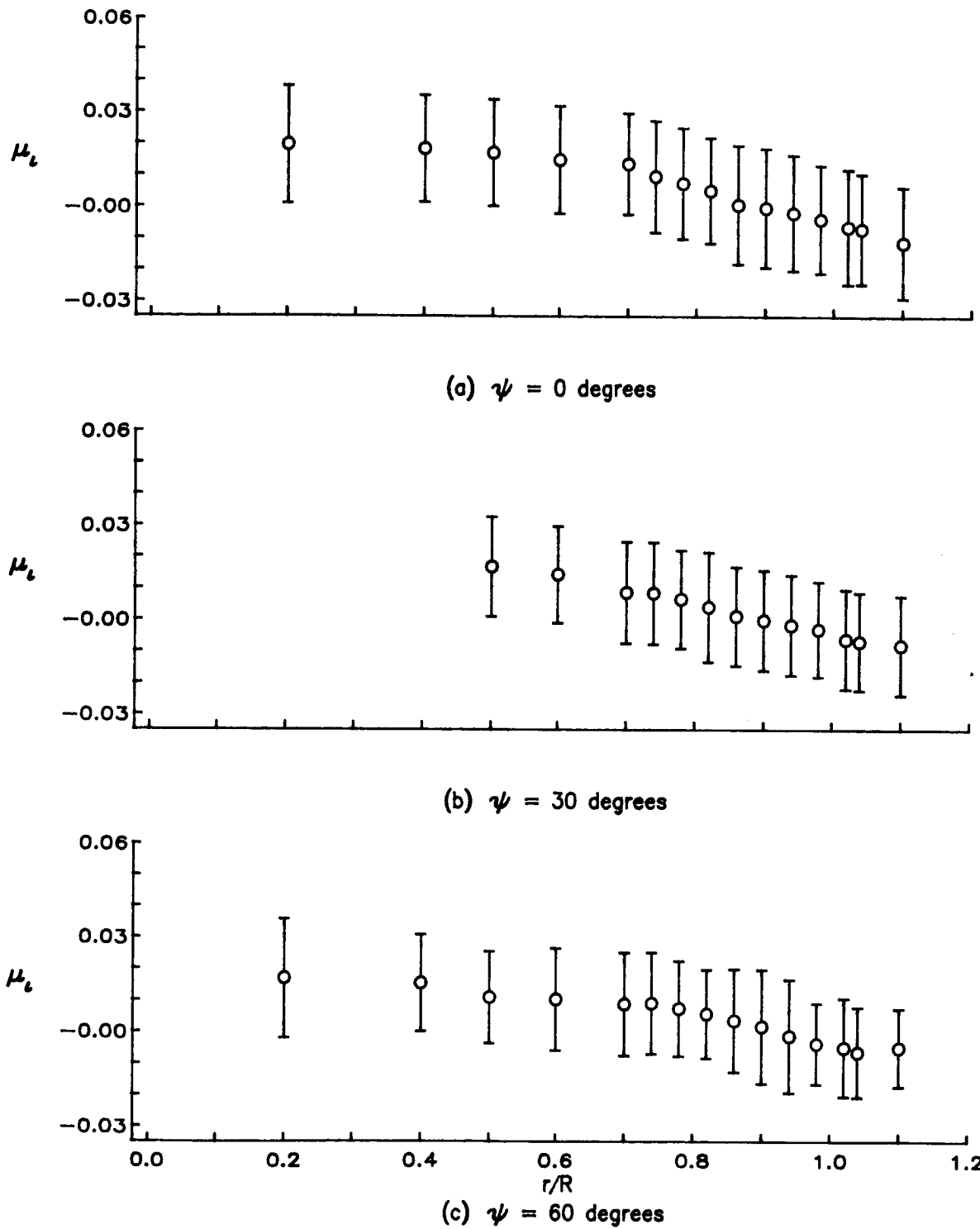
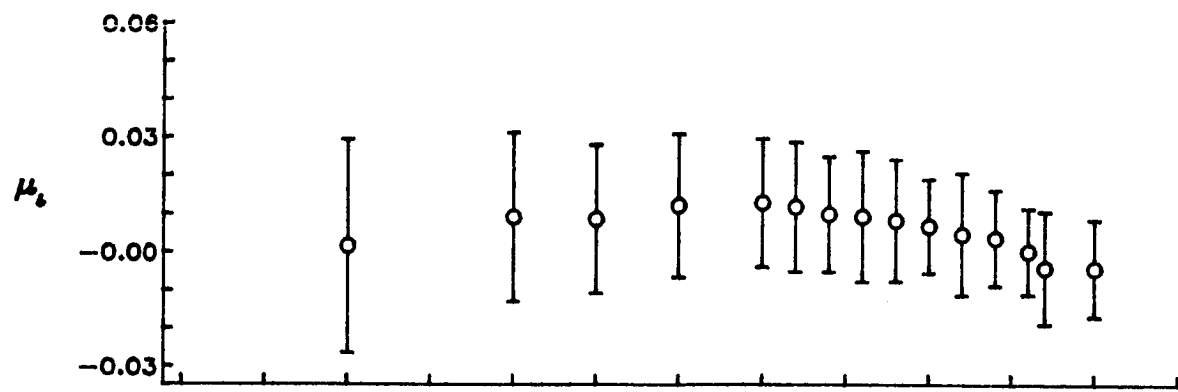
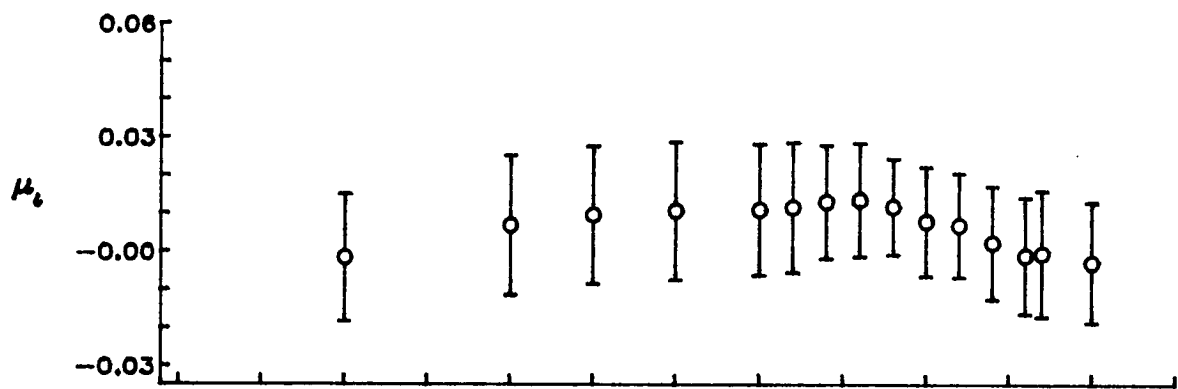


Figure 9.— Radial distribution of mean induced inflow ratio ( $\mu_i$ ).



(d)  $\psi = 90$  degrees



(e)  $\psi = 150$  degrees

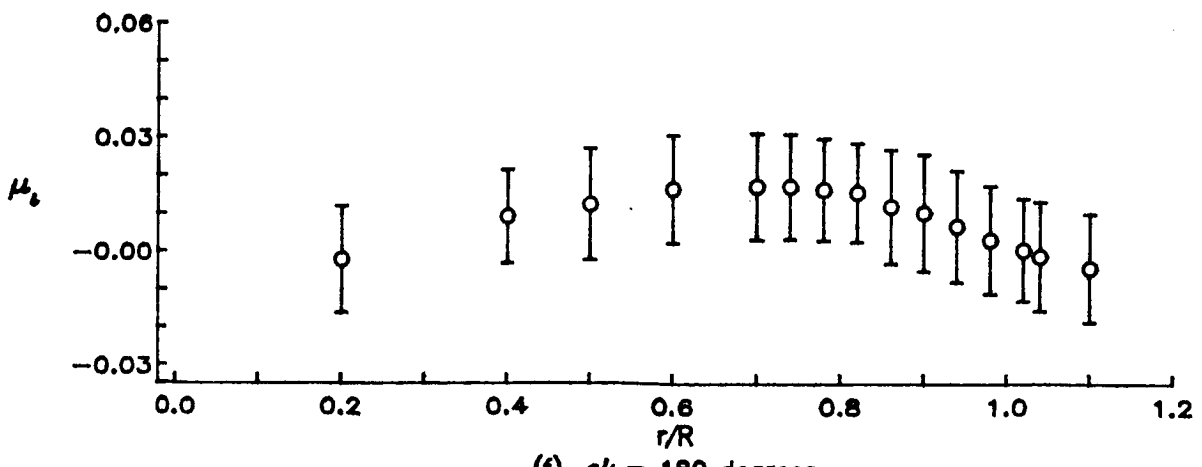


Figure 9.— Continued.

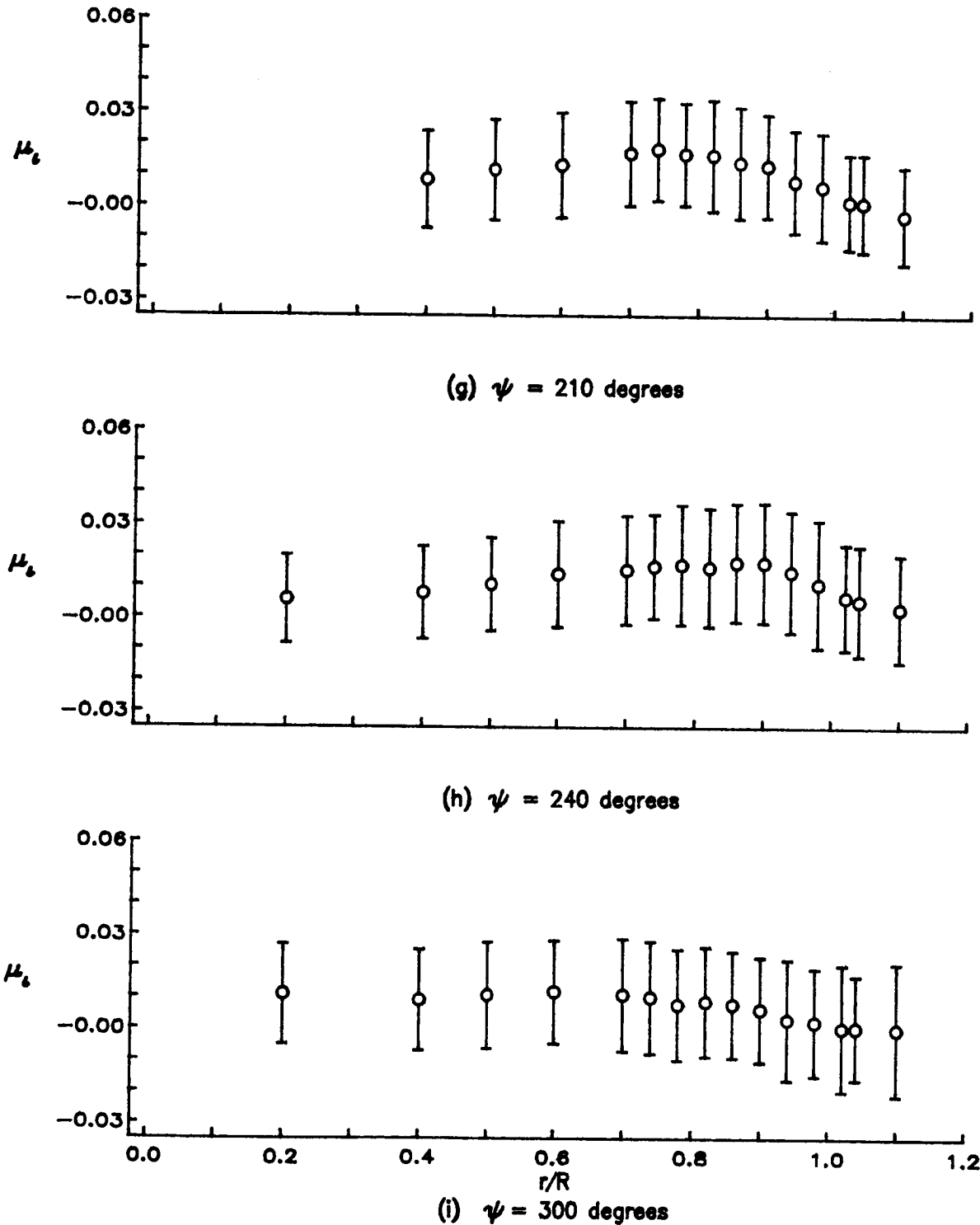


Figure 9.— Continued.

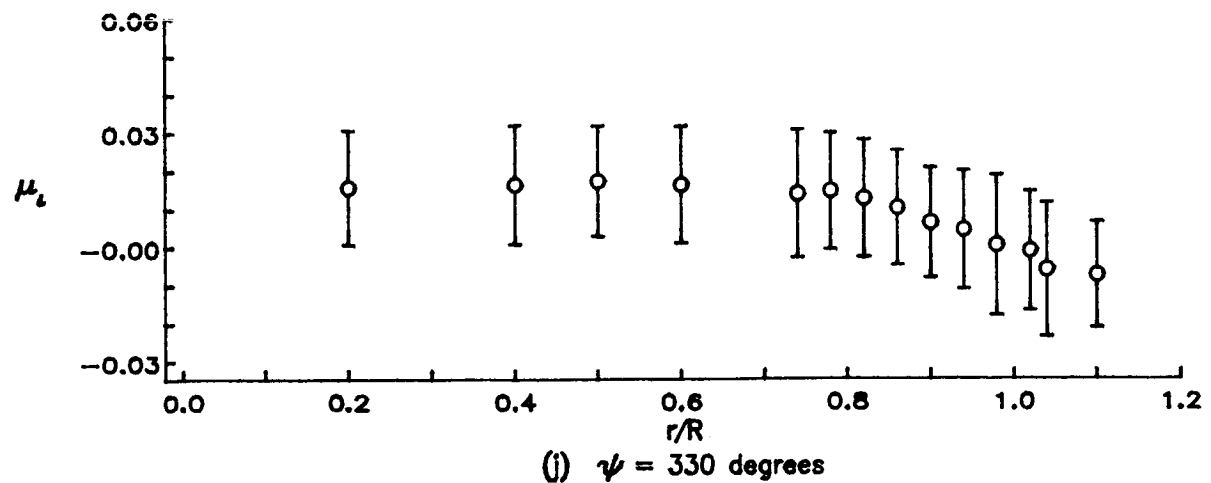


Figure 9.— Concluded.

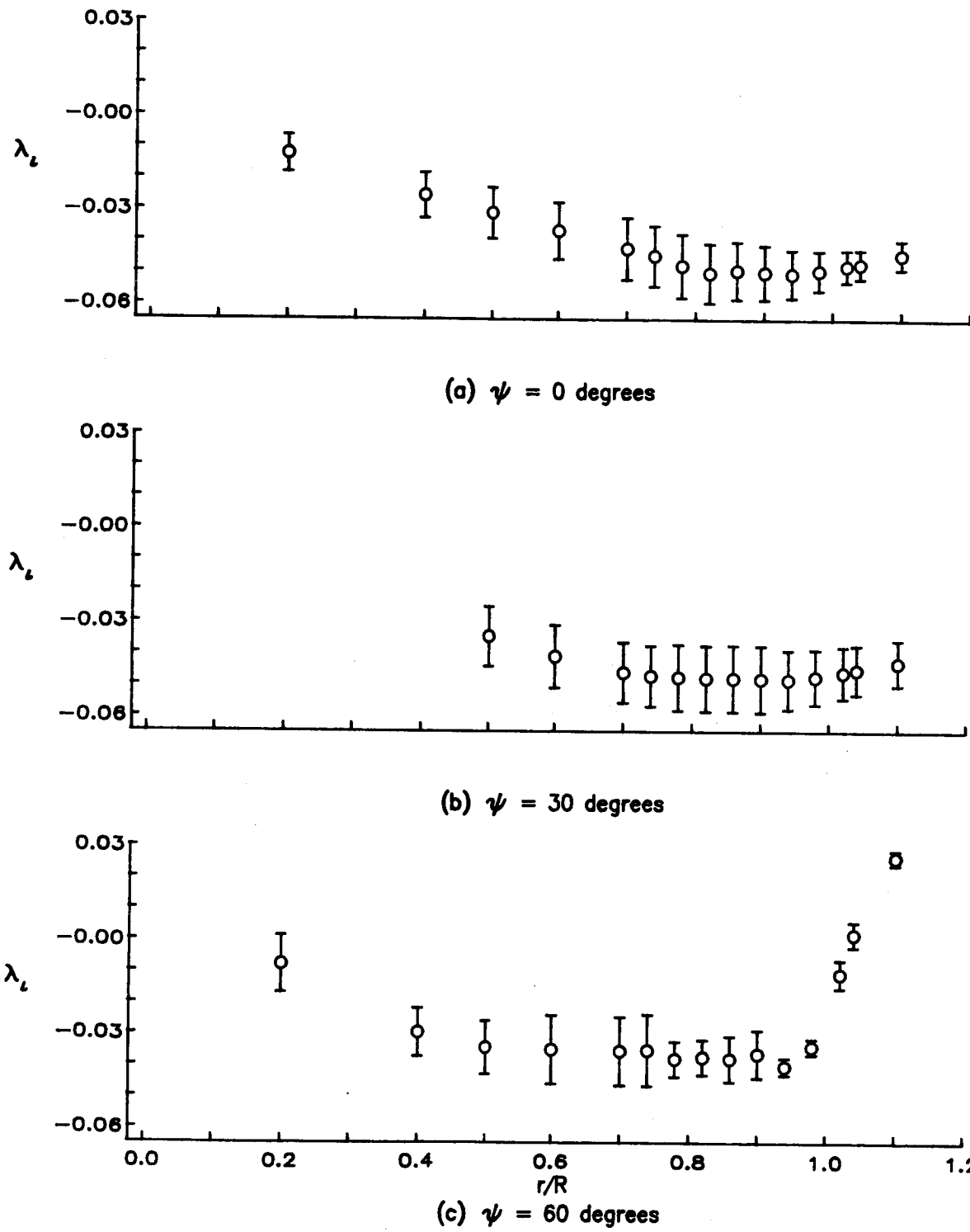
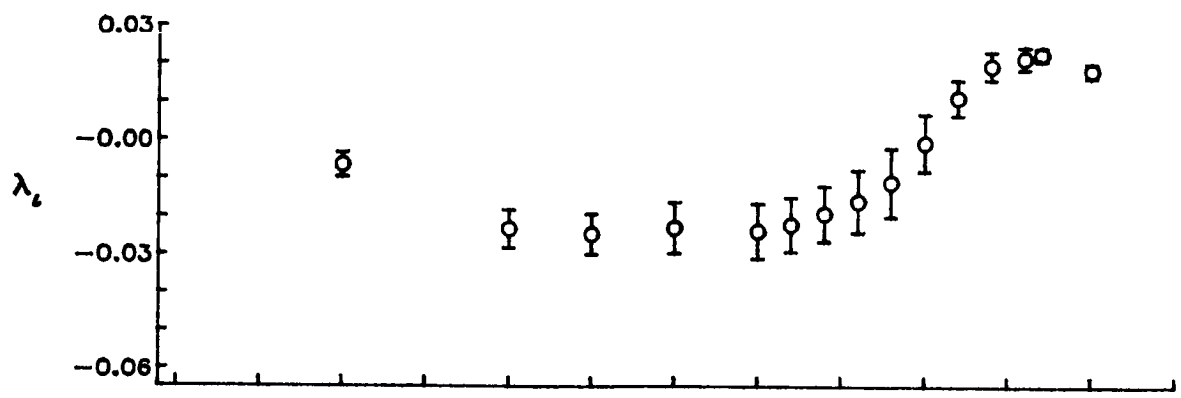
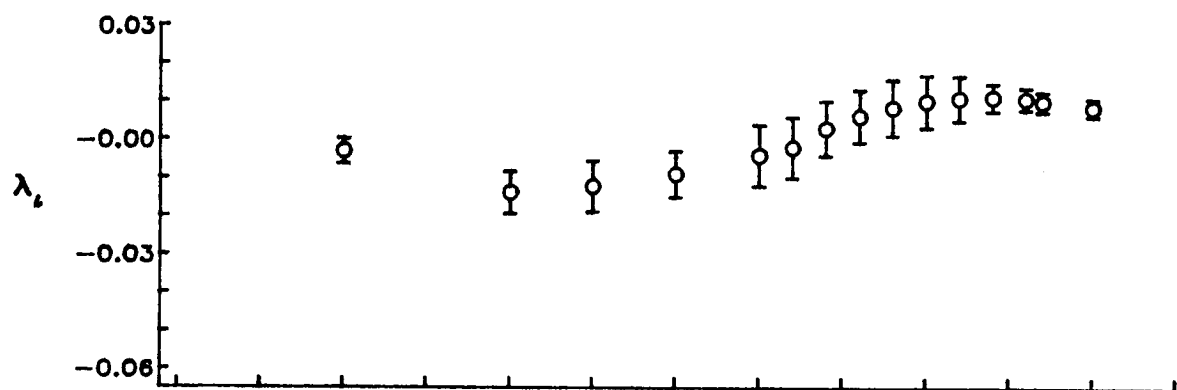


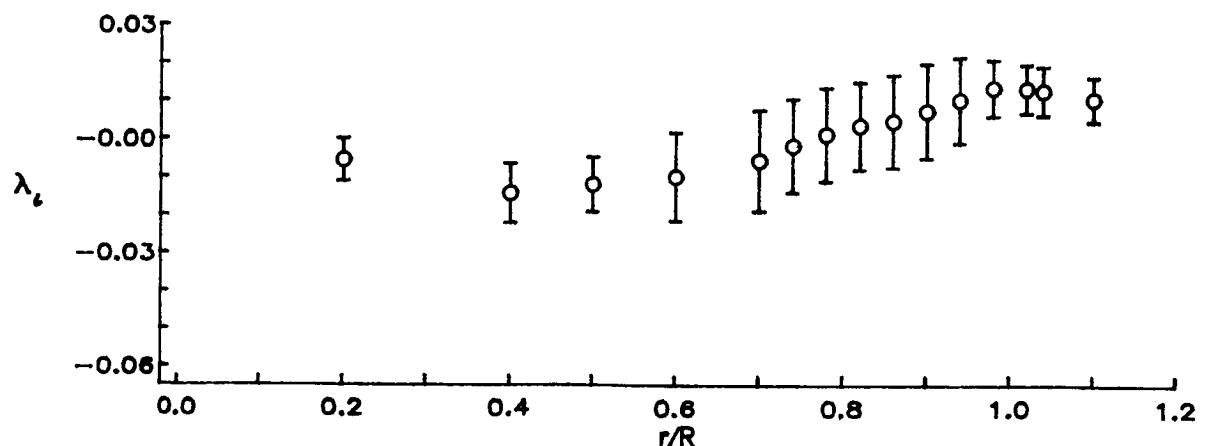
Figure 10.— Radial distribution of mean induced inflow ratio ( $\lambda_i$ ).



(d)  $\psi = 90$  degrees



(e)  $\psi = 150$  degrees



(f)  $\psi = 180$  degrees

Figure 10.-- Continued.

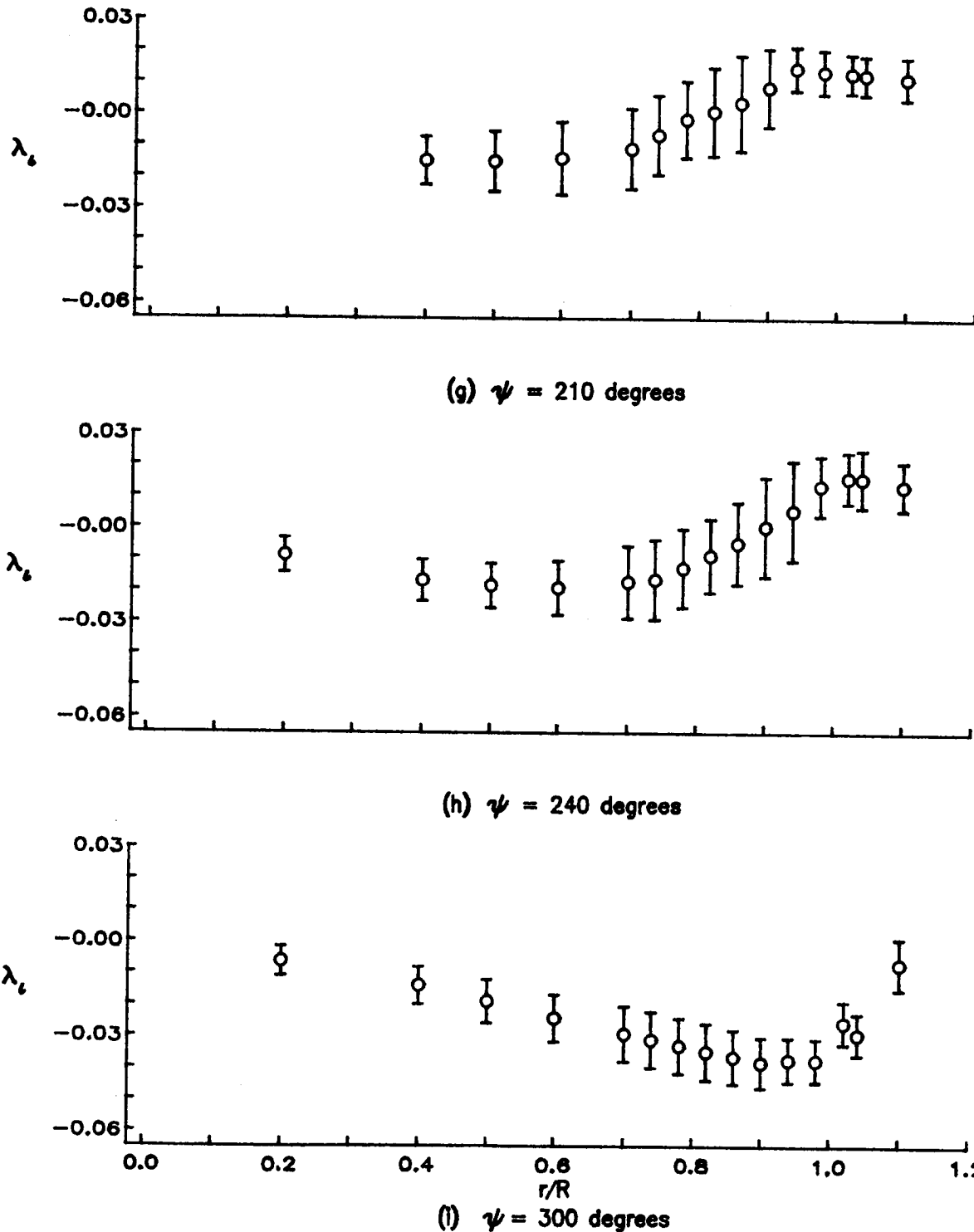
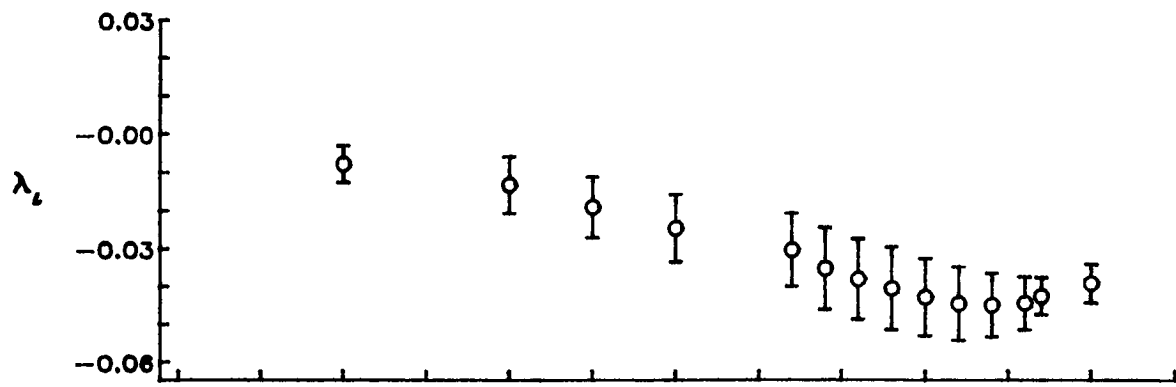
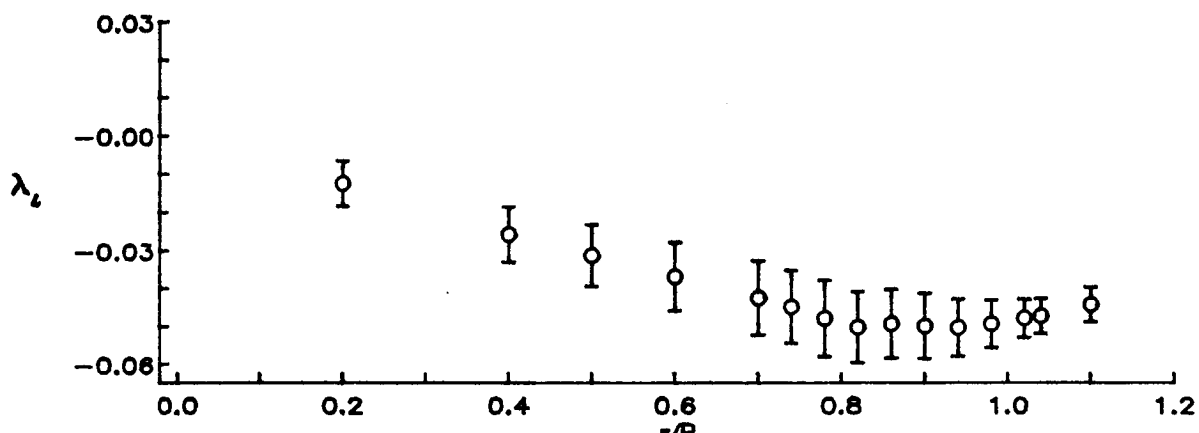


Figure 10.— Continued.



(j)  $\psi = 330$  degrees



(k)  $\psi = 360$  degrees

Figure 10.- Concluded.

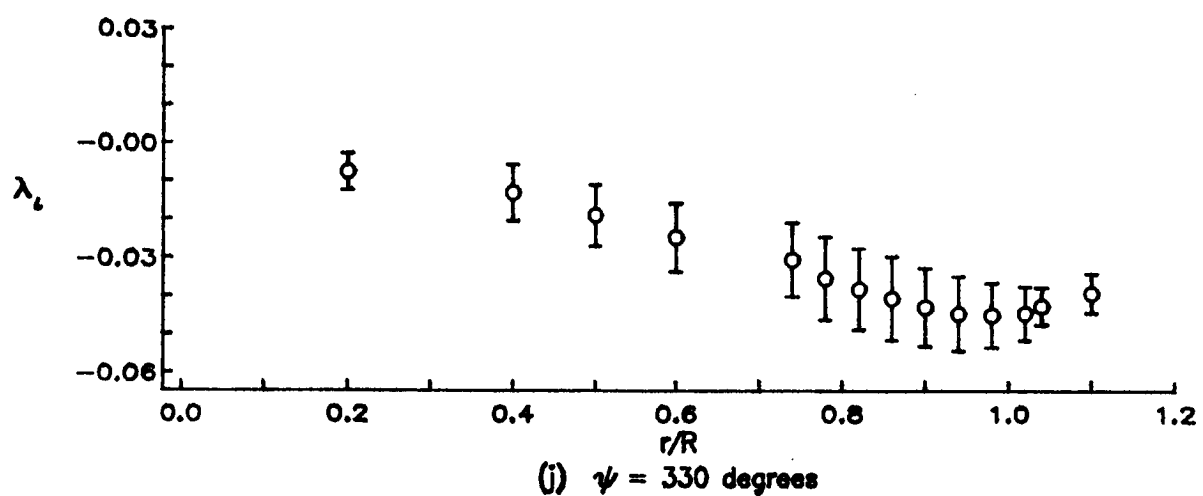


Figure 10.- Concluded.

ORIGINAL PAGE  
COLOR PHOTOGRAPH

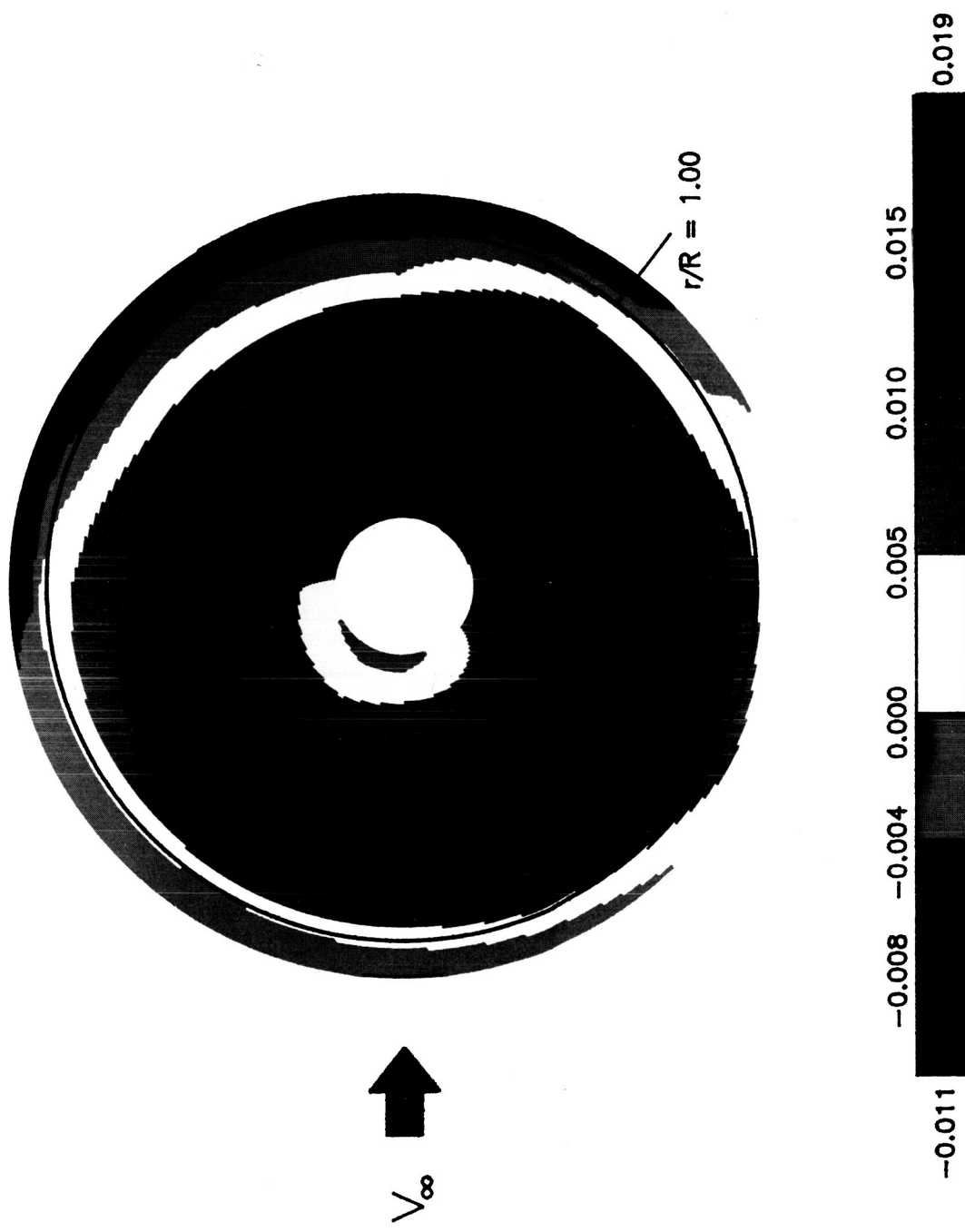


Figure 11.— Contour plot of mean induced inflow ratio ( $\mu_L$ ).

ORIGINAL PAGE  
COLOR PHOTOGRAPH

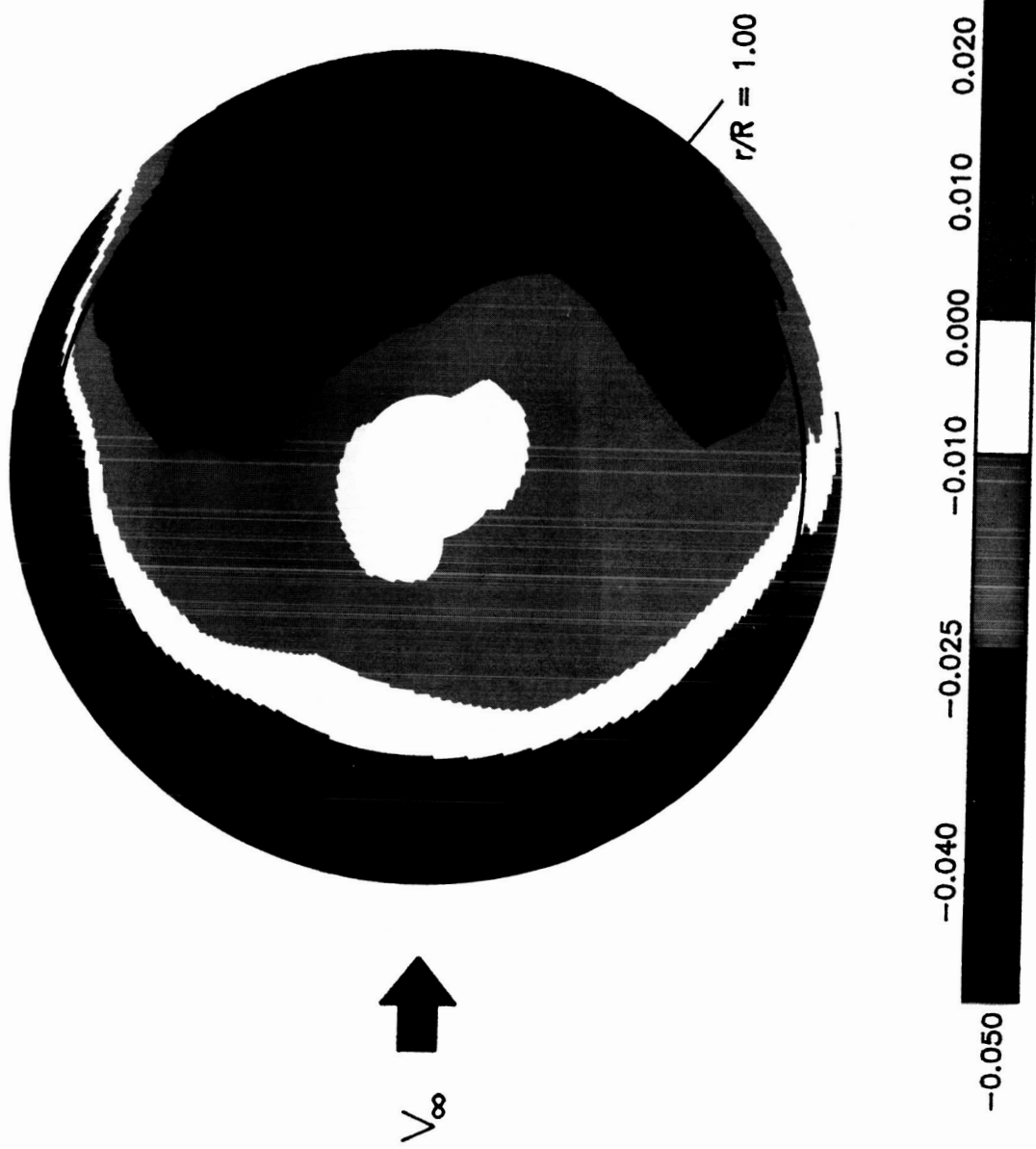


Figure 12.— Contour plot of mean induced inflow ratio ( $\lambda_L$ ).

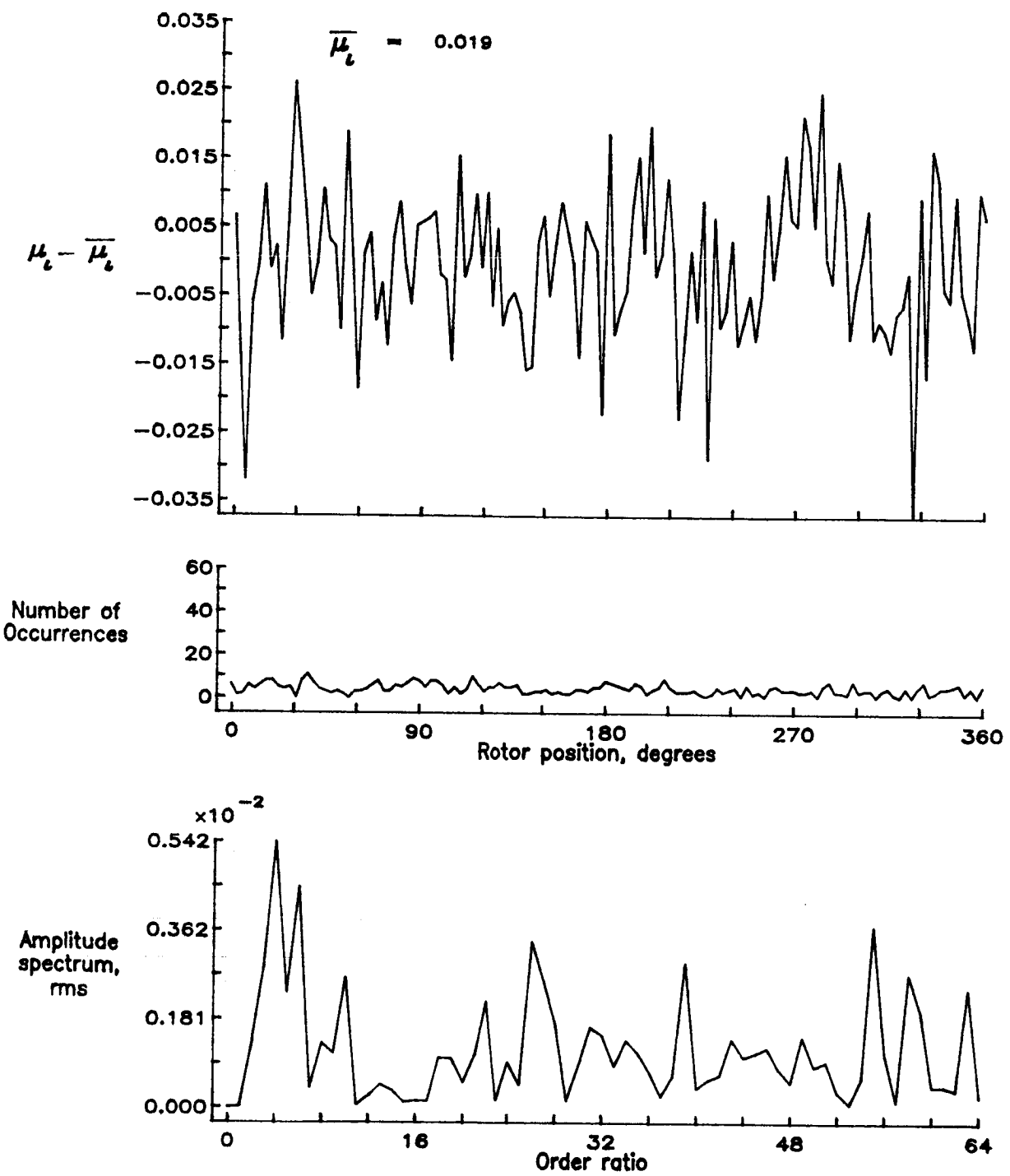


Figure 13.— Induced inflow velocity measured at 0 degrees and  $r/R$  of 0.20.

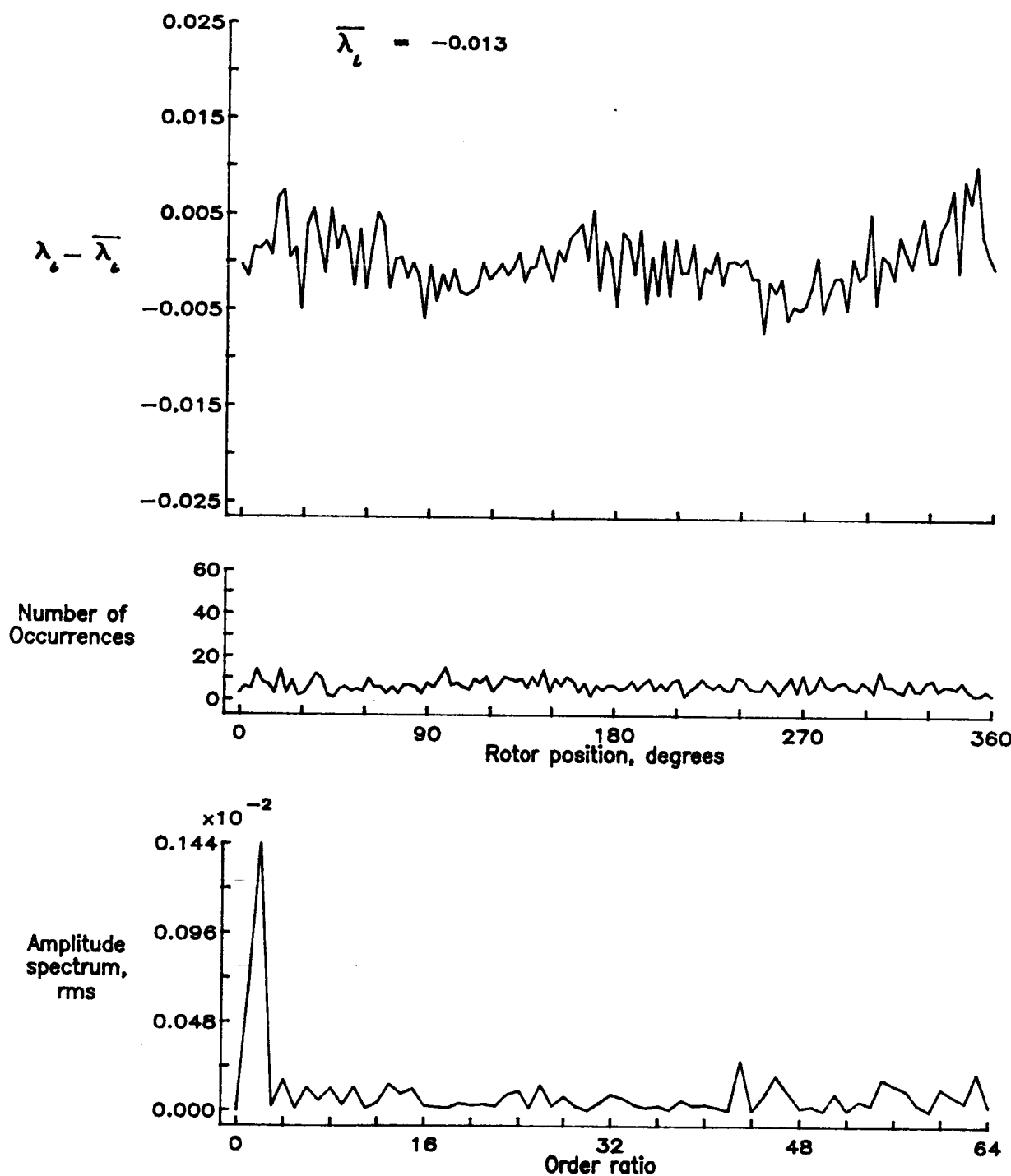


Figure 13.— Concluded.

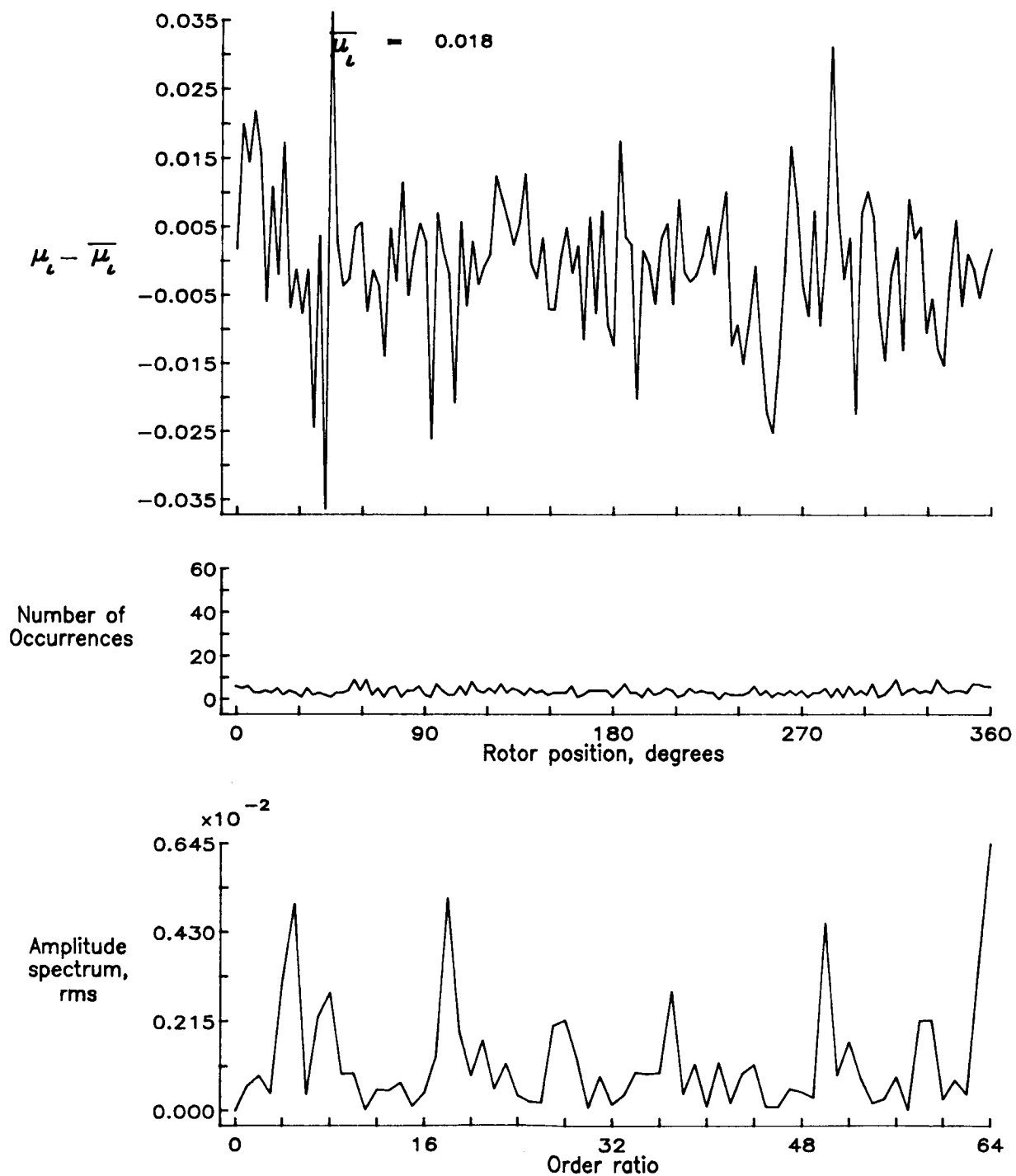


Figure 14.— Induced inflow velocity measured at 0 degrees and  $r/R$  of 0.40.

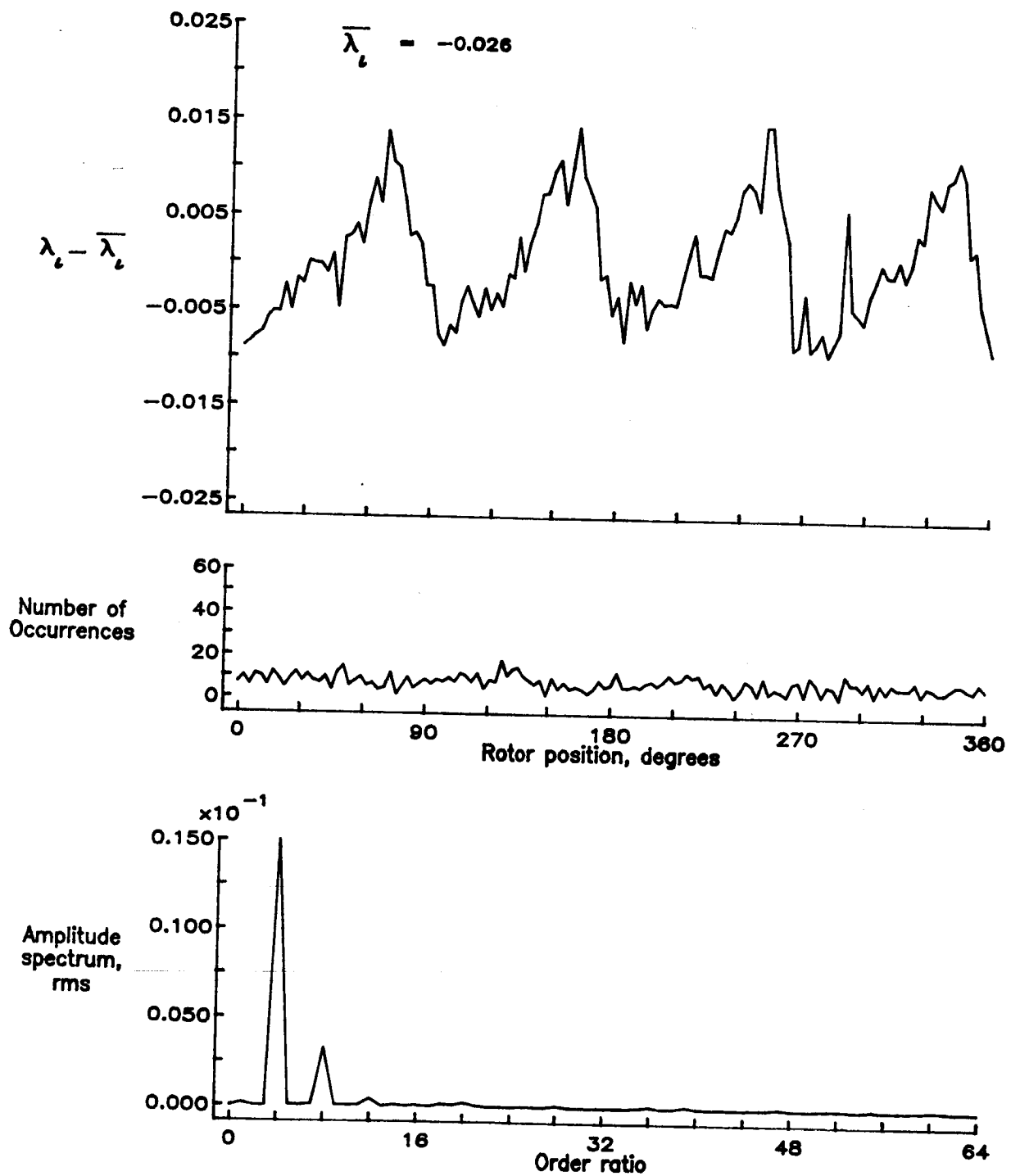


Figure 14.— Concluded.

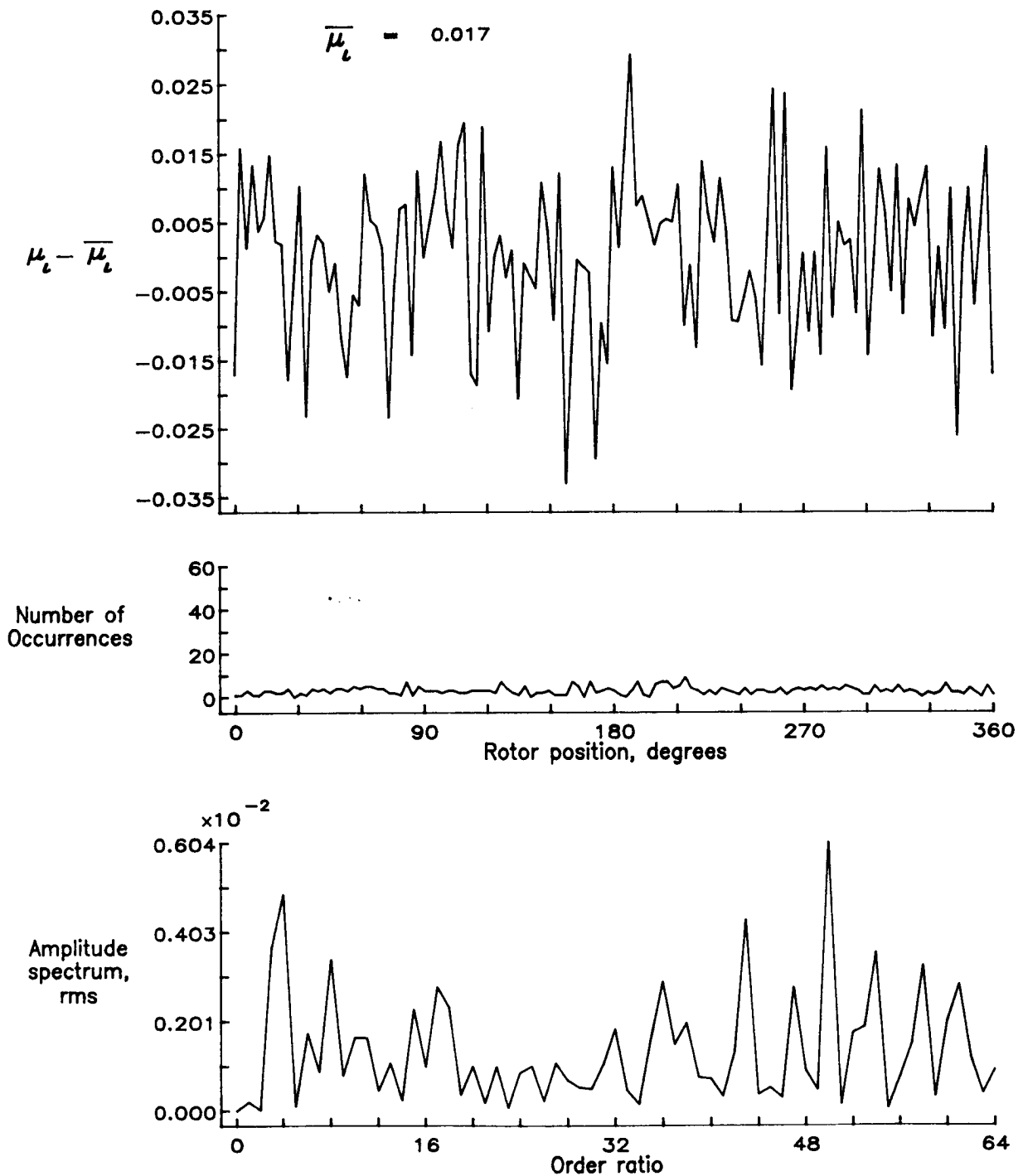


Figure 15.— Induced inflow velocity measured at 0 degrees and  $r/R$  of 0.50.

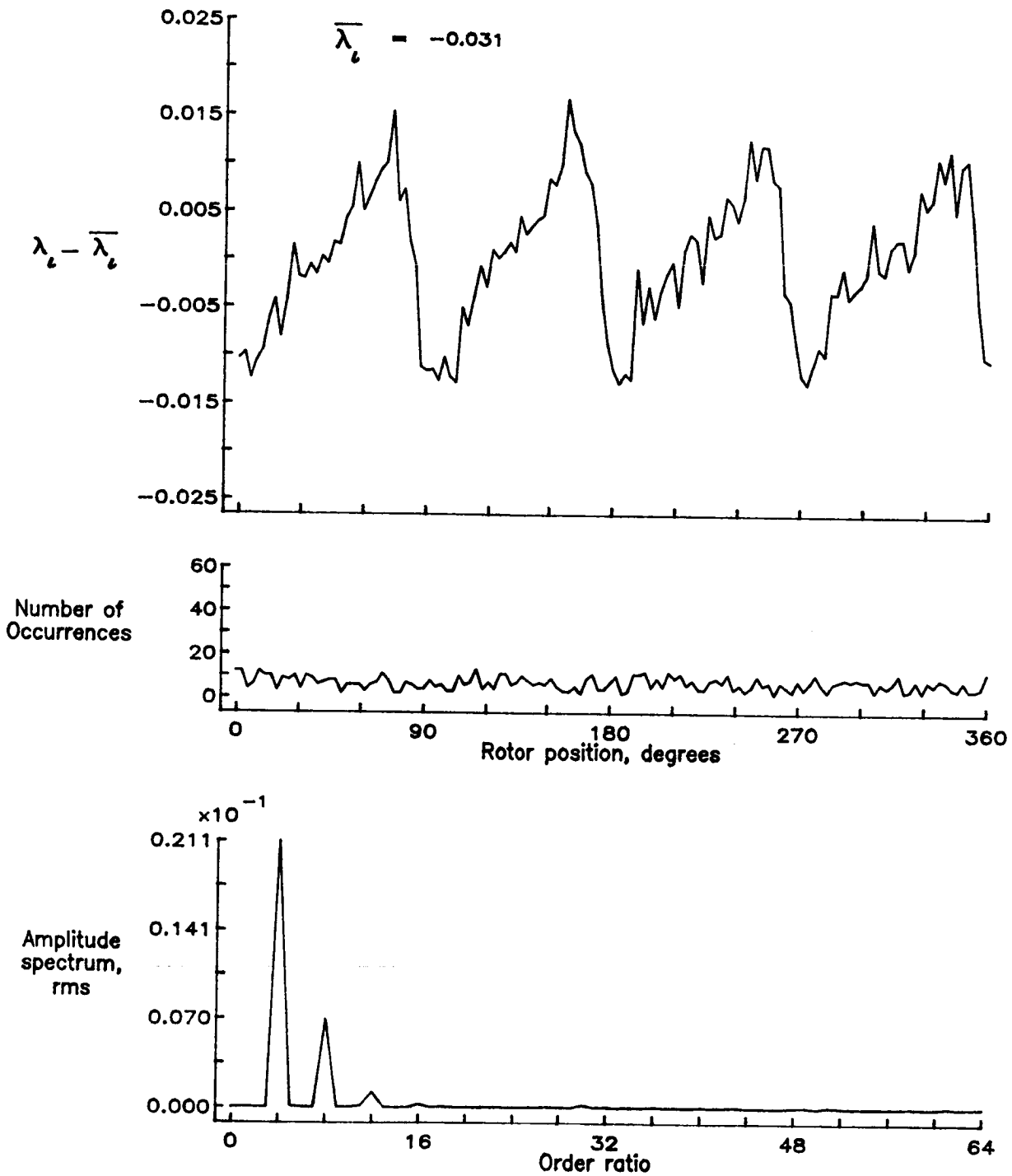


Figure 15.— Concluded.

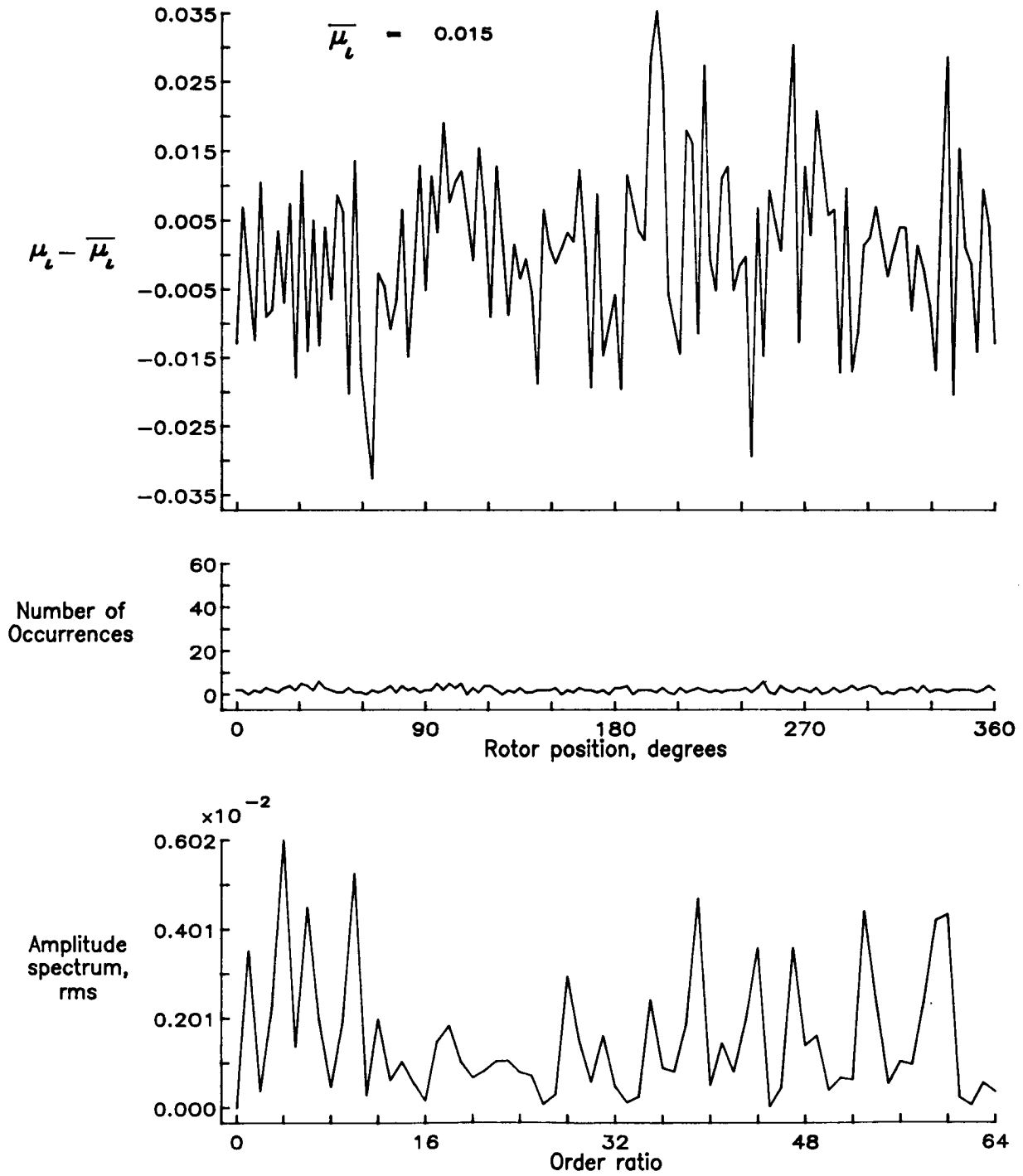


Figure 16.— Induced inflow velocity measured at 0 degrees and  $r/R$  of 0.60.

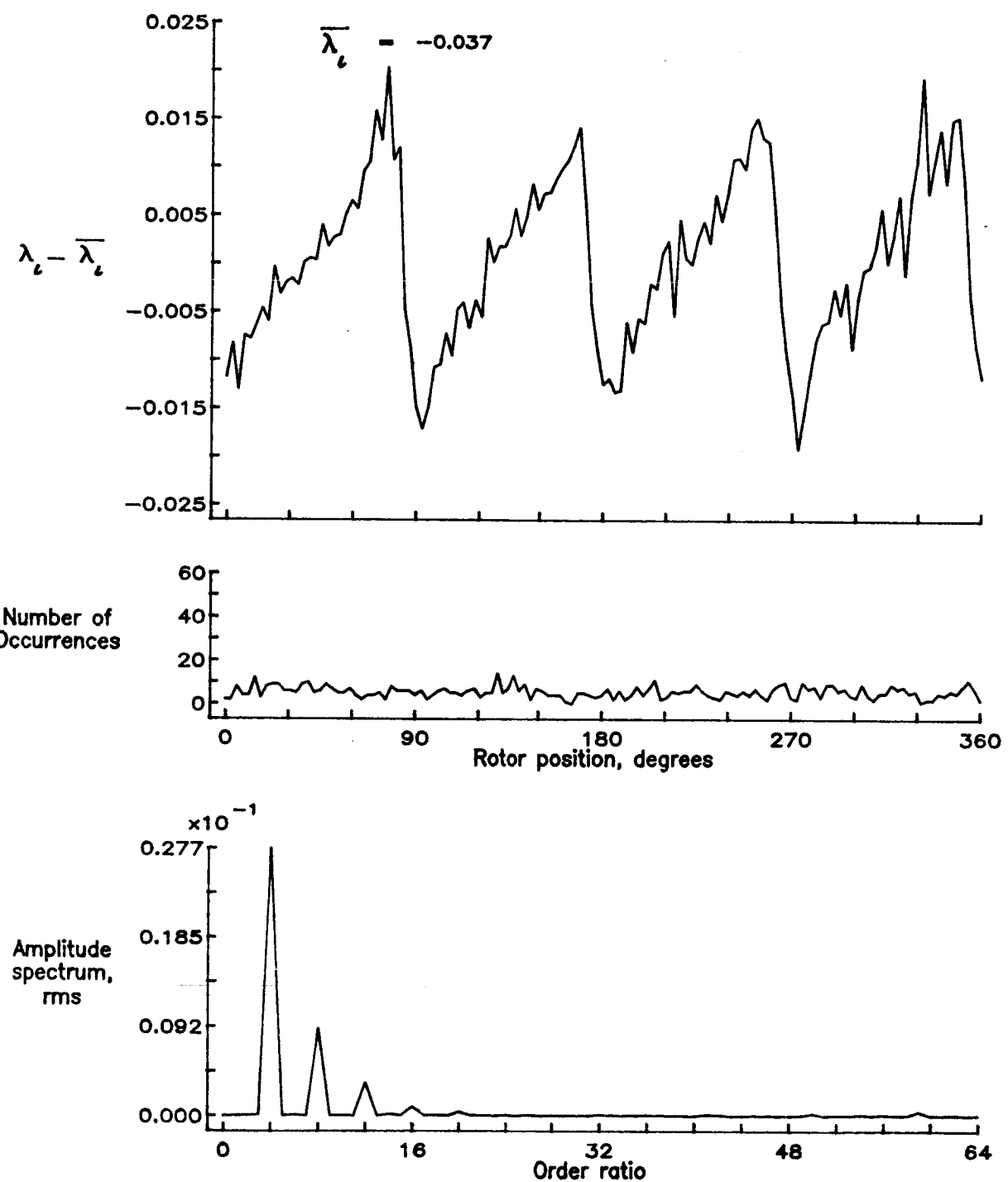


Figure 16.— Concluded.

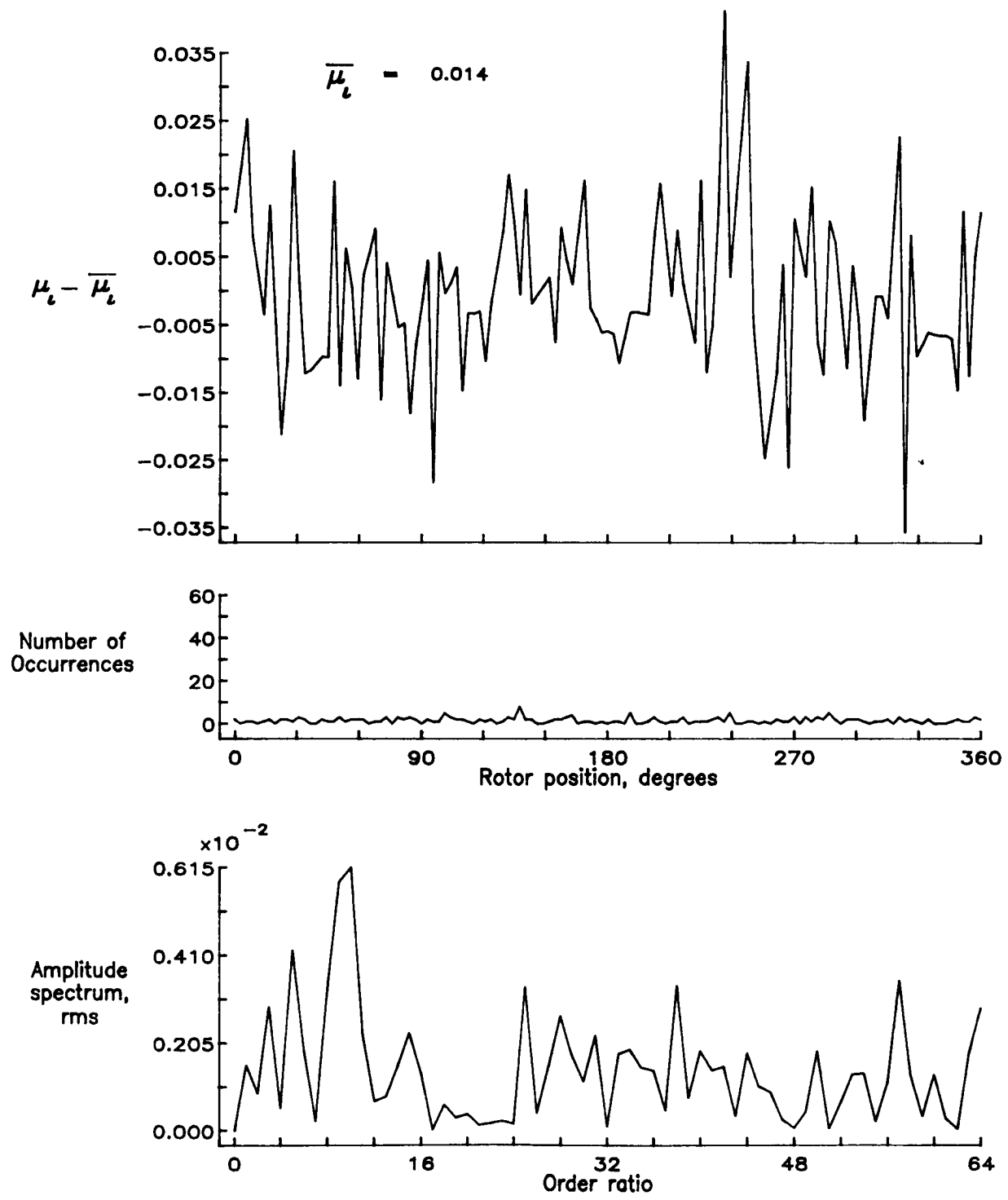


Figure 17.— Induced inflow velocity measured at 0 degrees and  $r/R$  of 0.70.

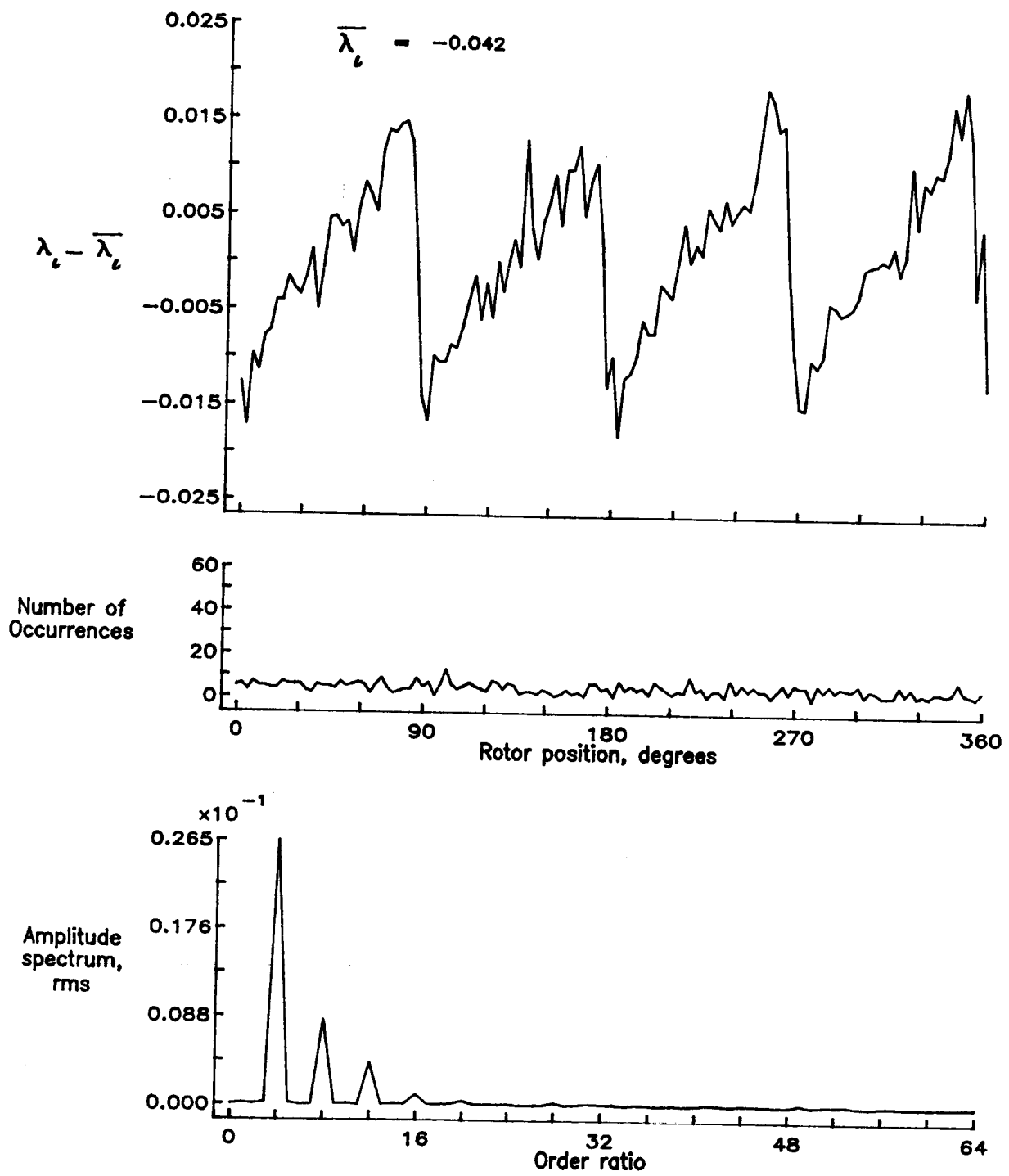


Figure 17.— Concluded.

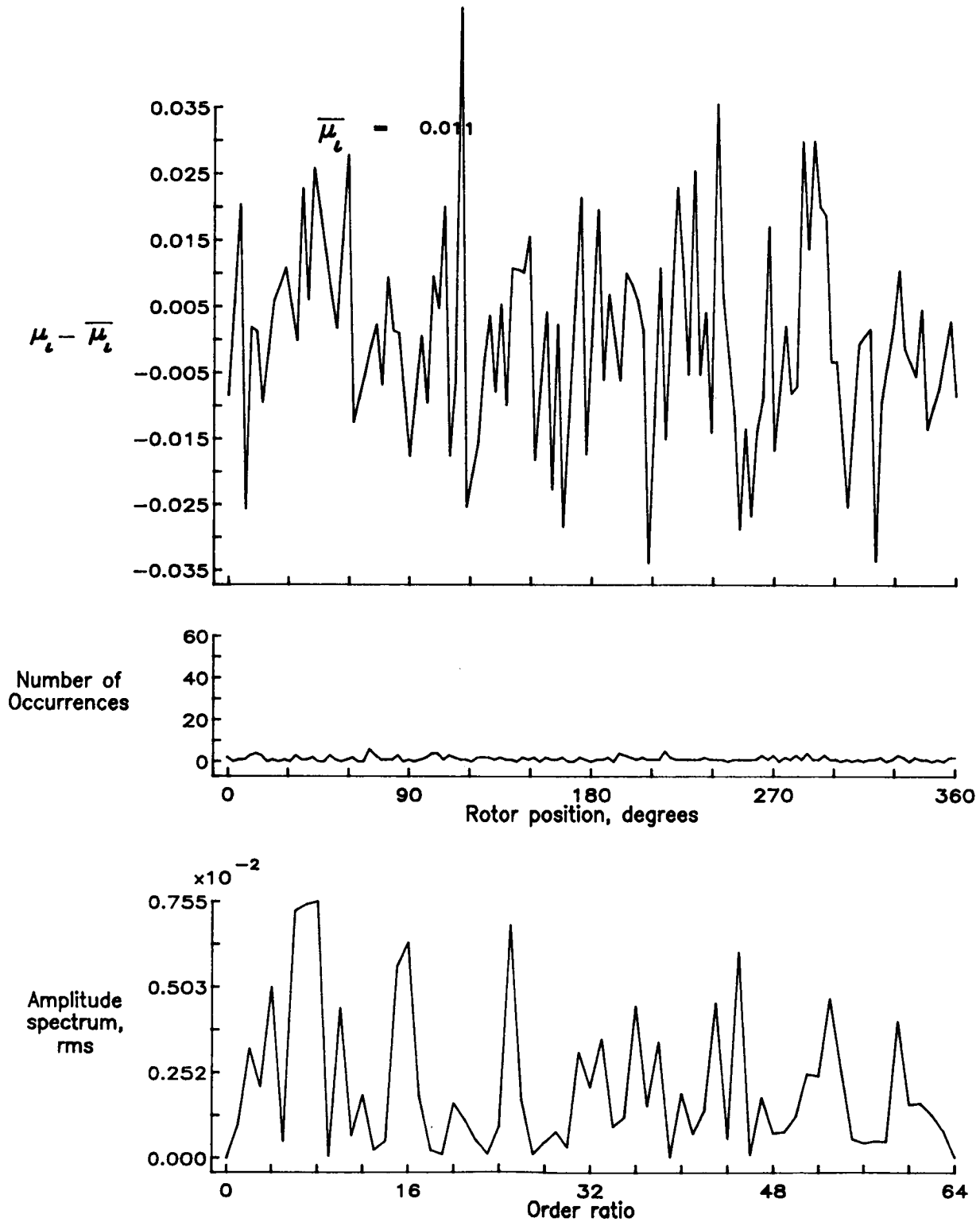


Figure 18.— Induced inflow velocity measured at 0 degrees and  $r/R$  of 0.74.

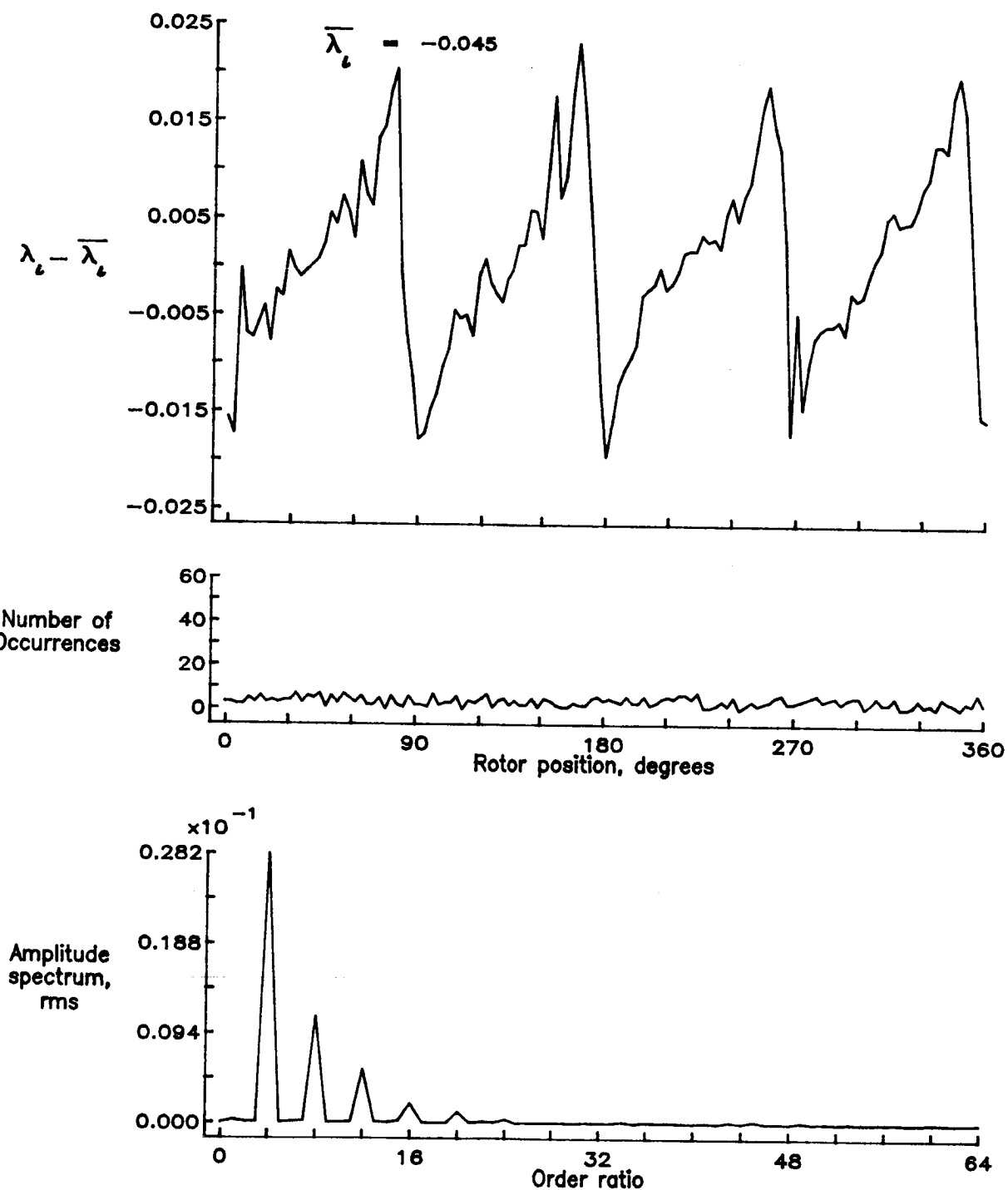


Figure 18.— Concluded.

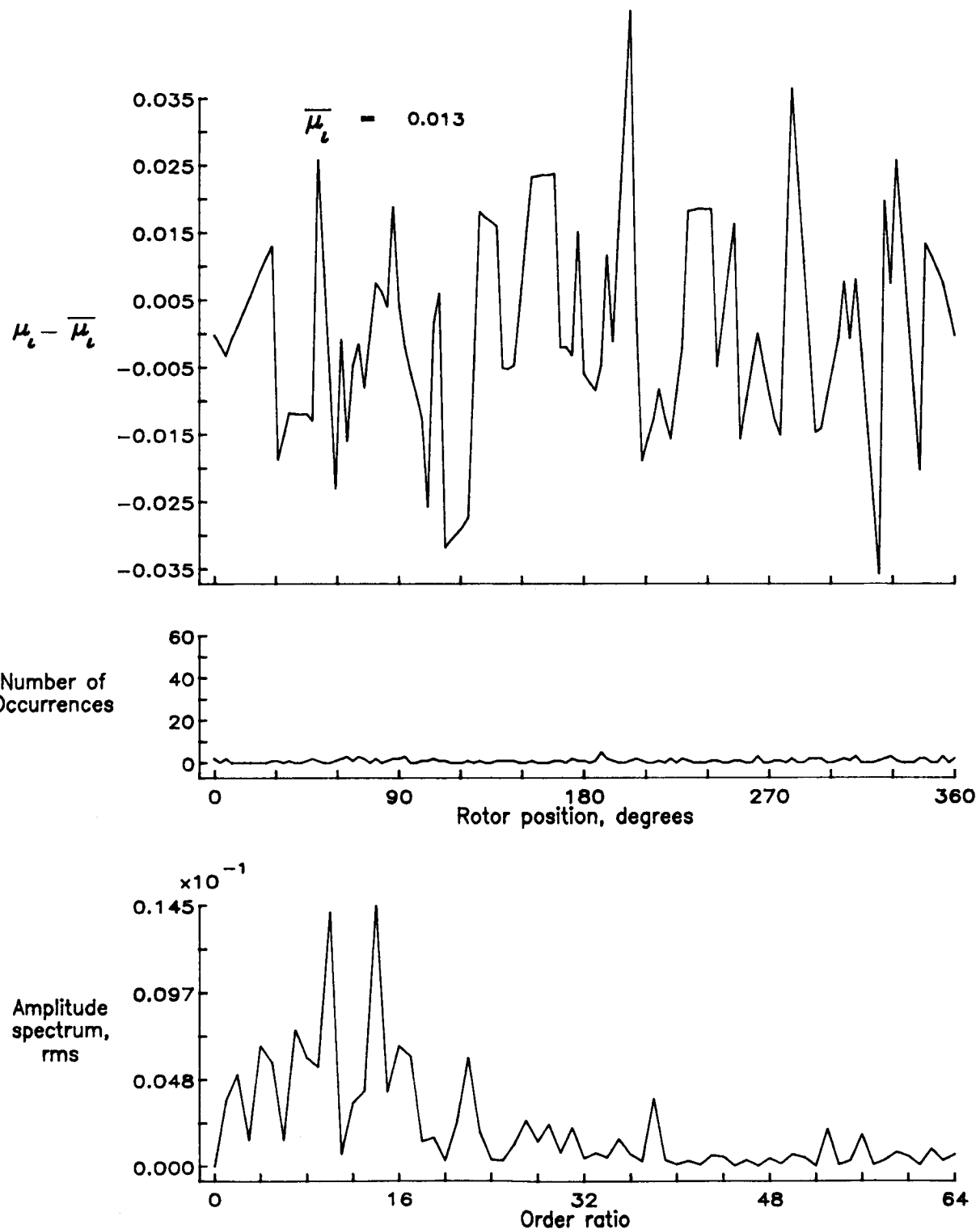


Figure 19.— Induced inflow velocity measured at 0 degrees and  $r/R$  of 0.78.

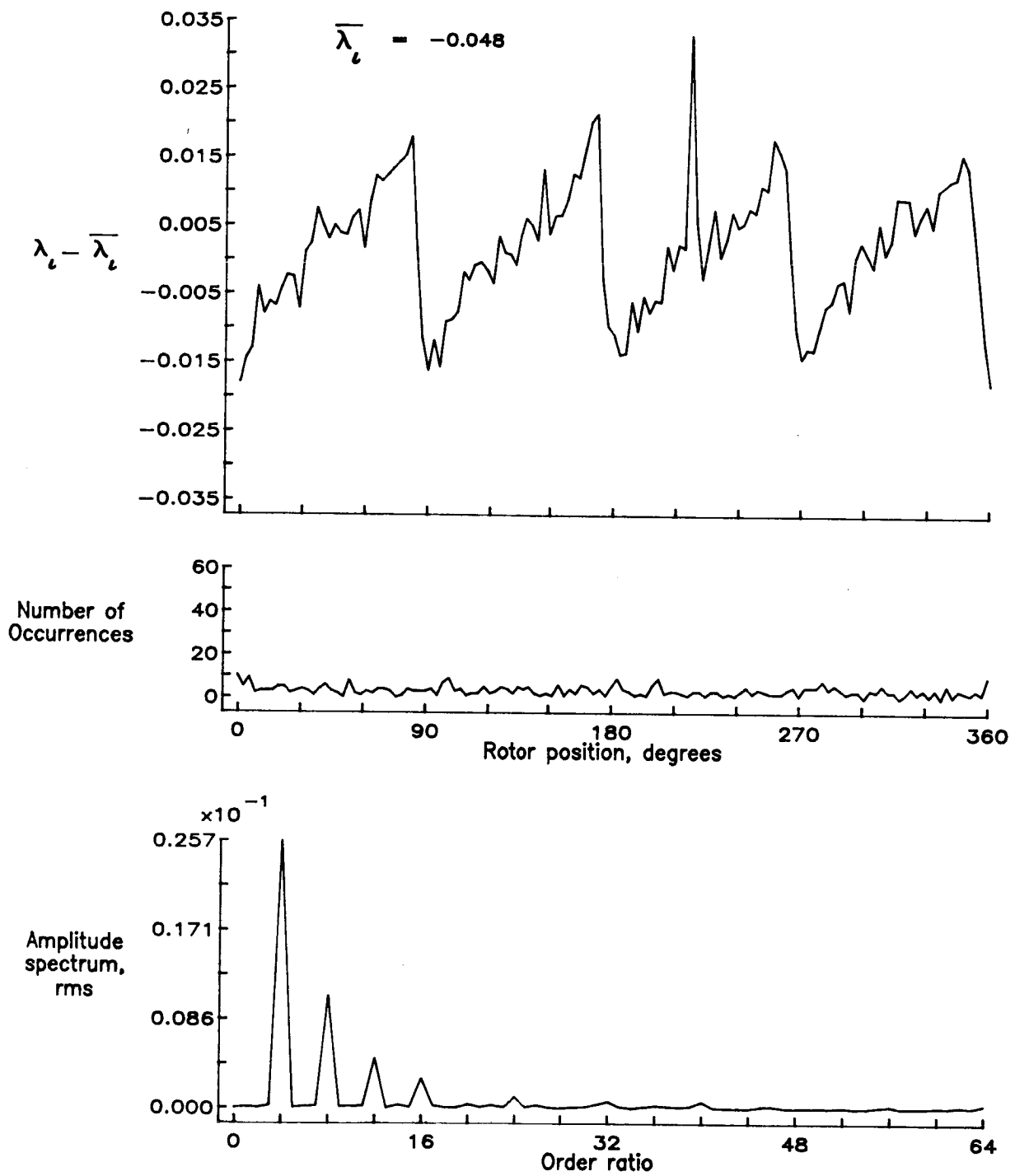


Figure 19.— Concluded.

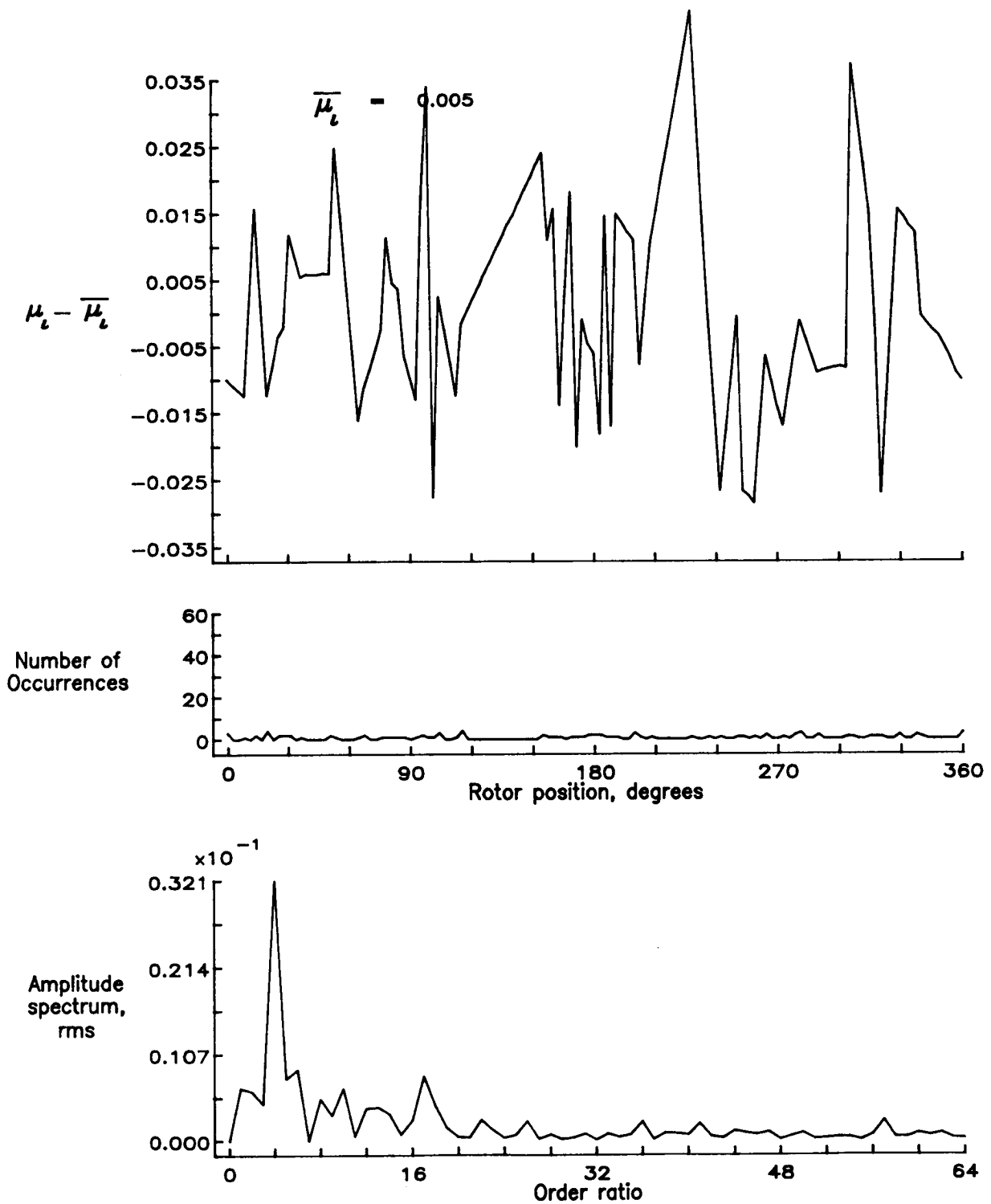


Figure 20.— Induced inflow velocity measured at 0 degrees and  $r/R$  of 0.82.

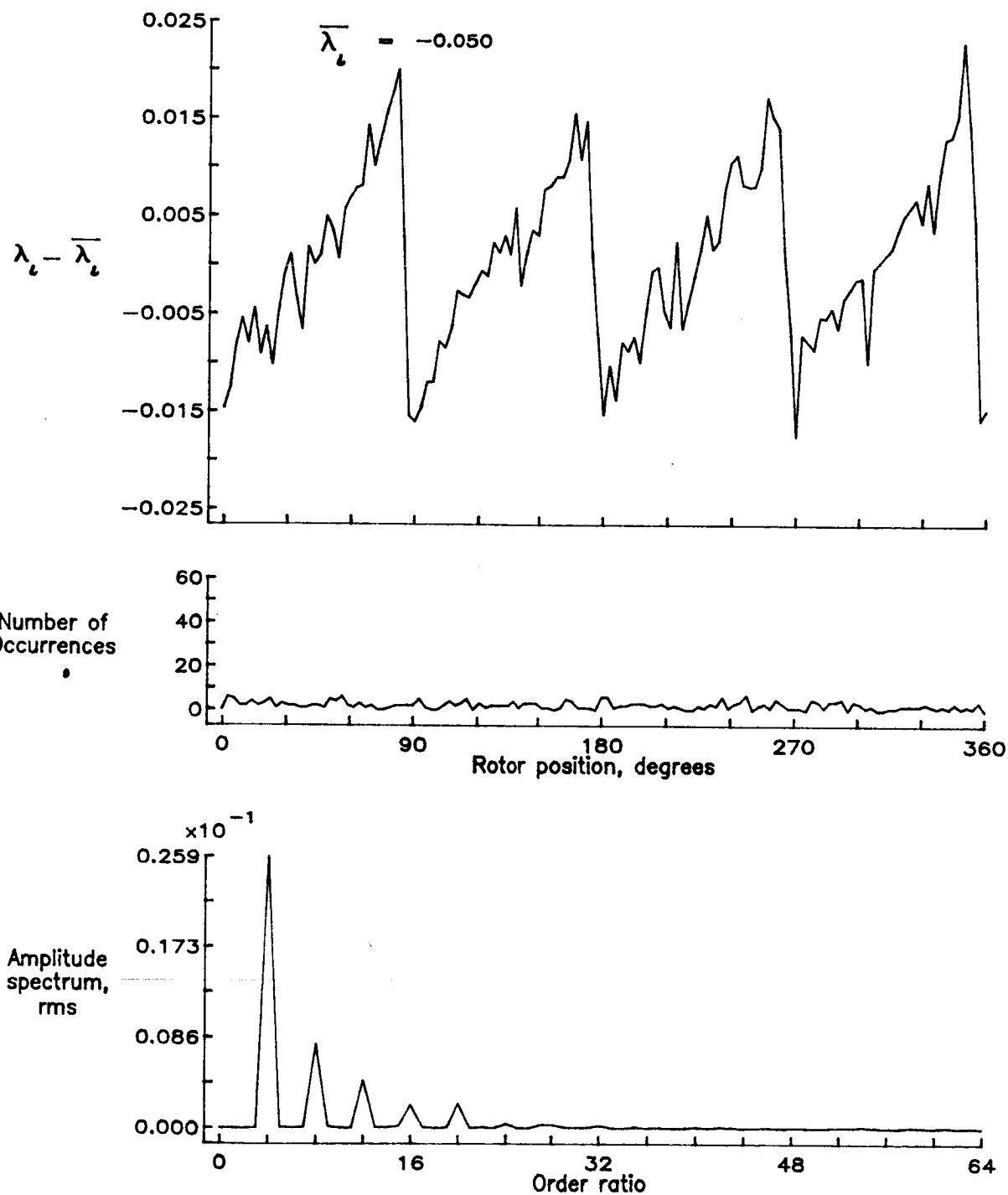


Figure 20.— Concluded.

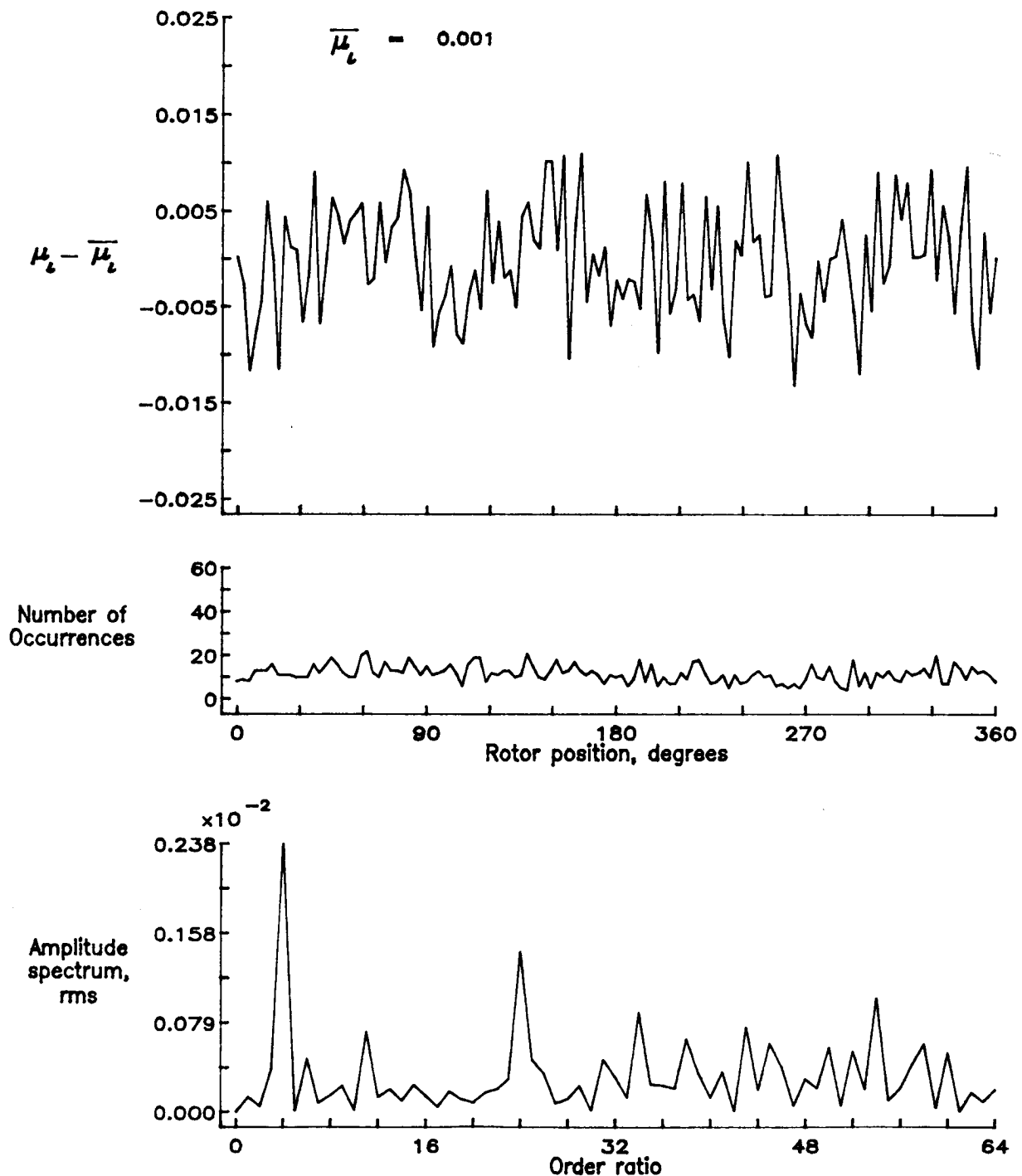


Figure 21.— Induced inflow velocity measured at 0 degrees and  $r/R$  of 0.86.

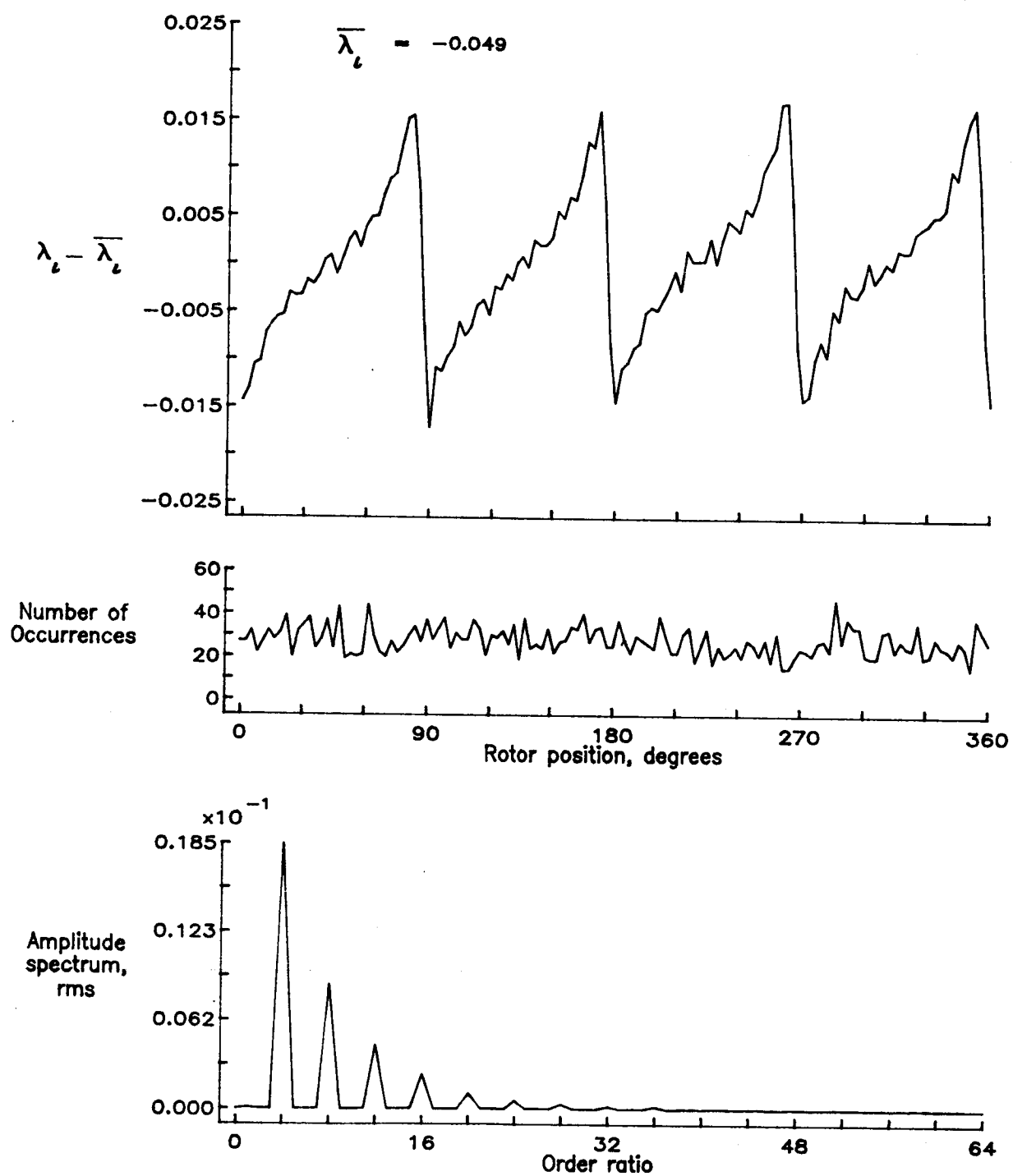


Figure 21.— Concluded.

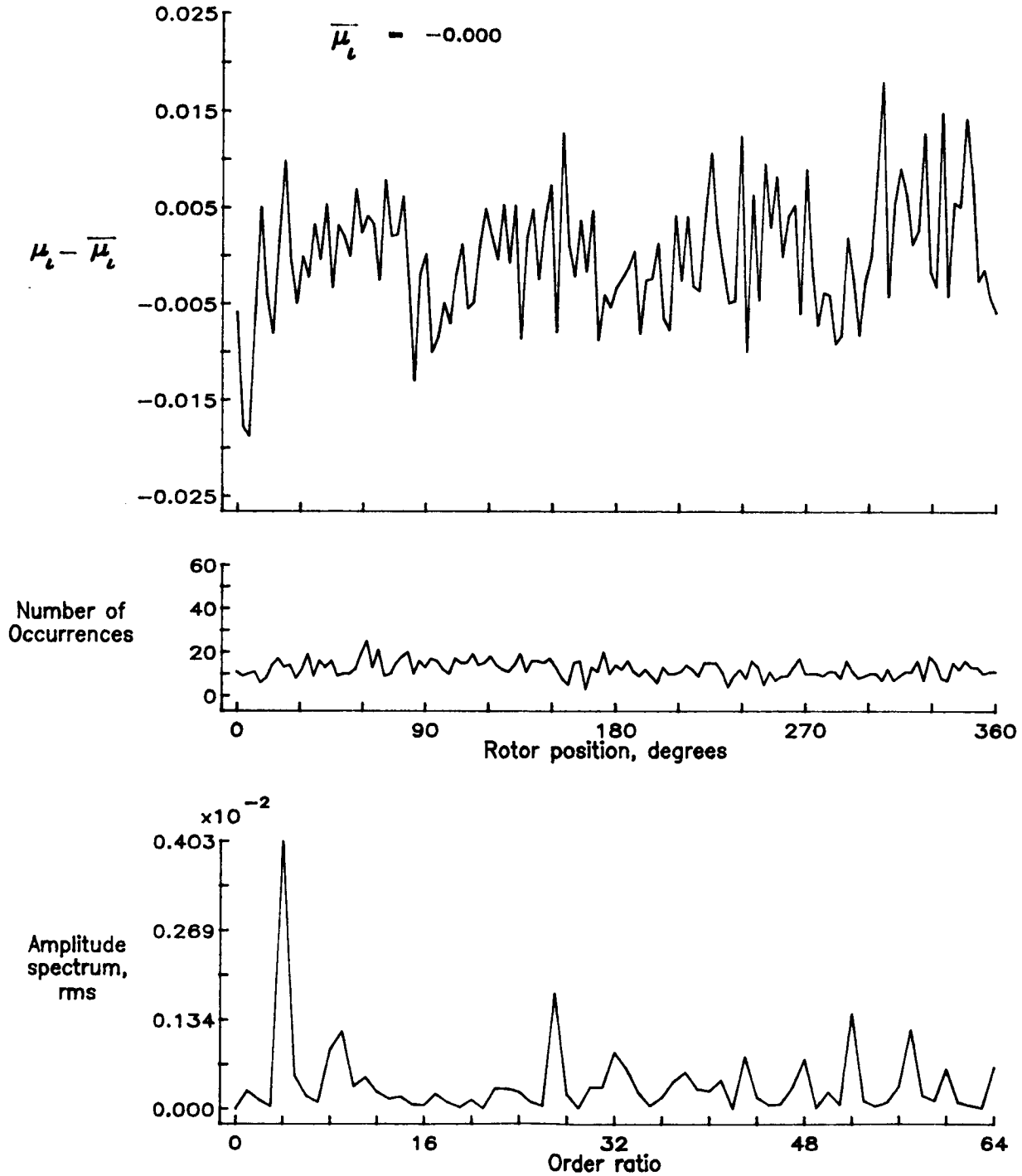


Figure 22.— Induced inflow velocity measured at 0 degrees and  $r/R$  of 0.90.

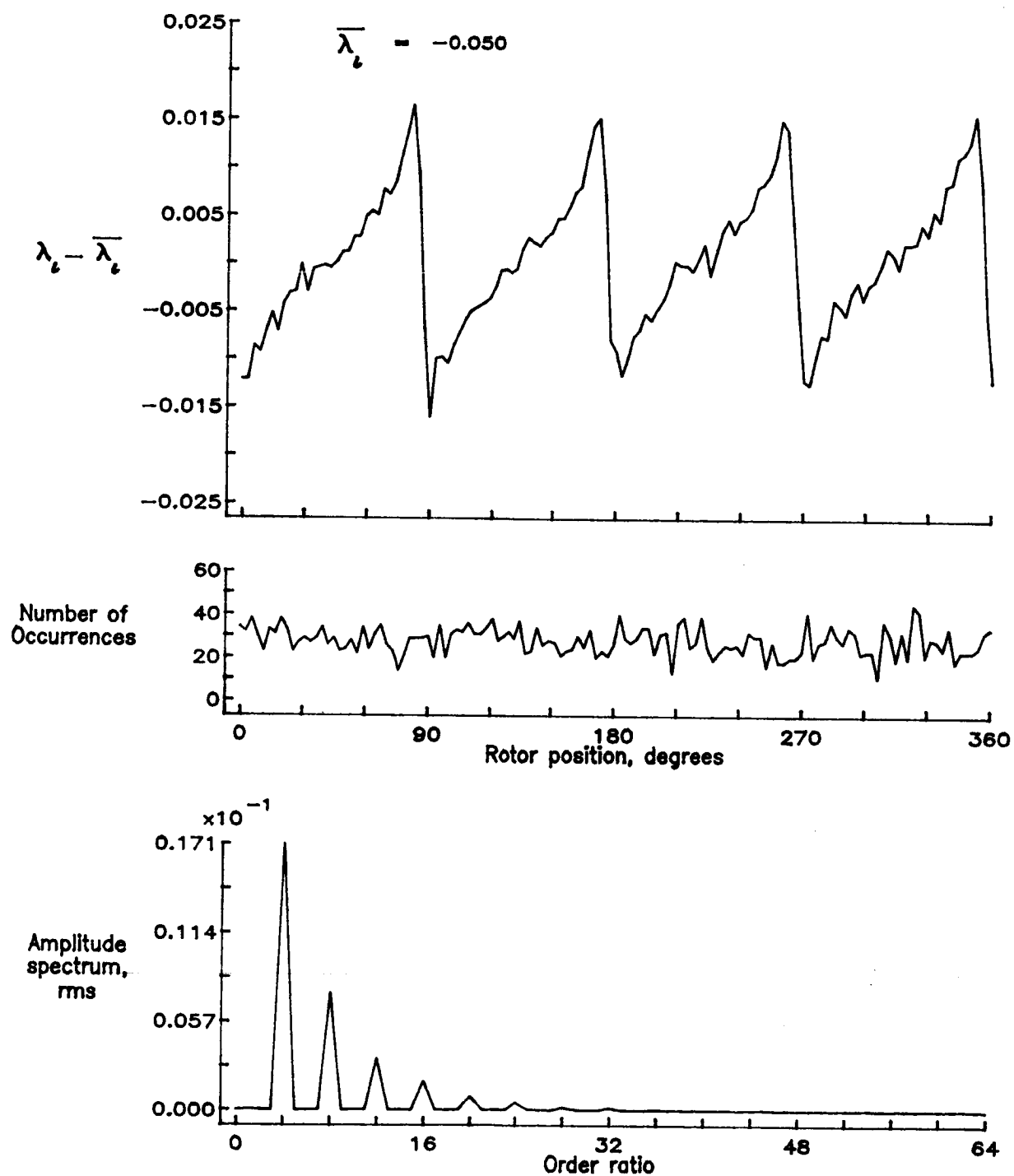


Figure 22.— Concluded.

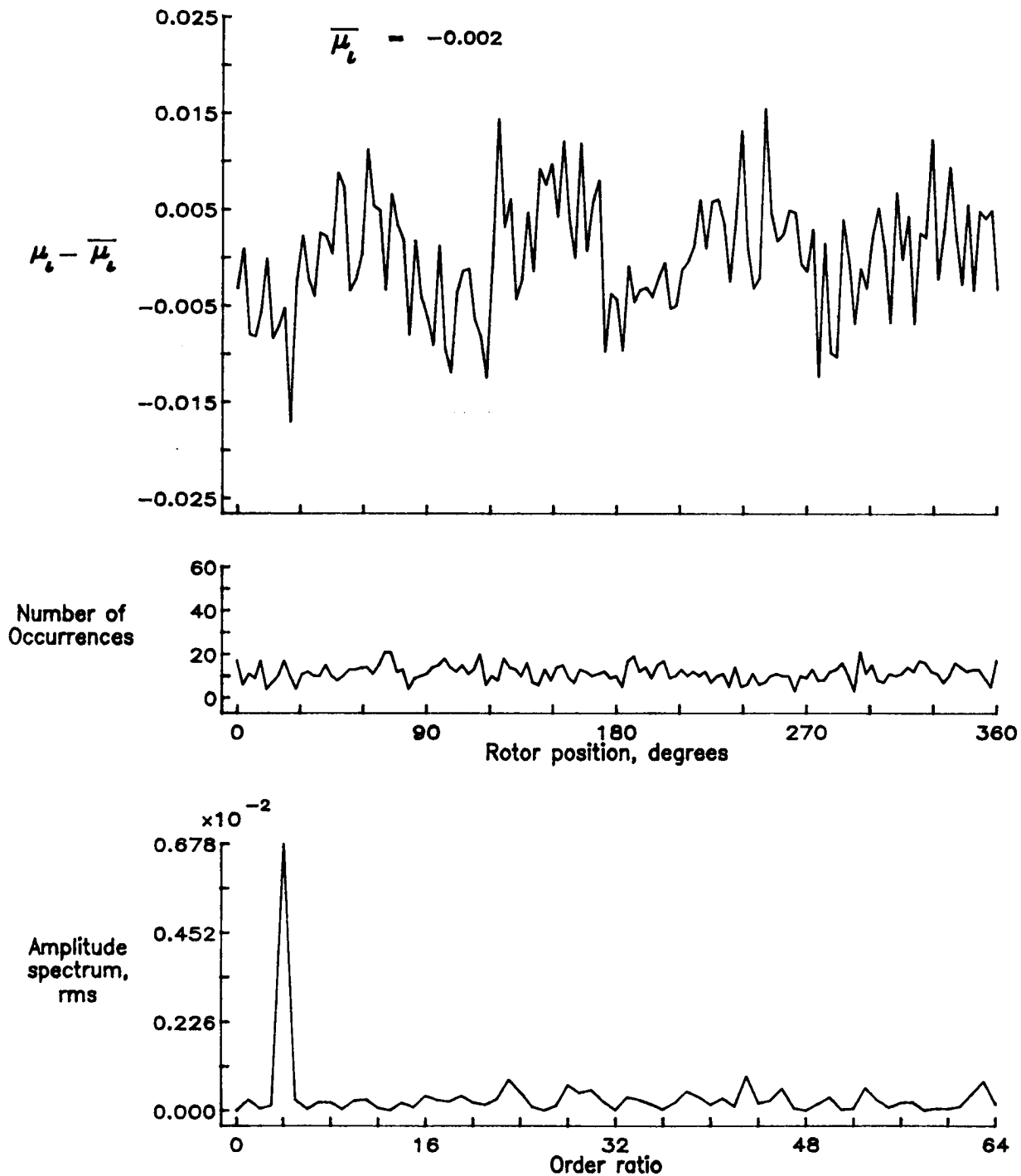


Figure 23.— Induced inflow velocity measured at 0 degrees and  $r/R$  of 0.94.

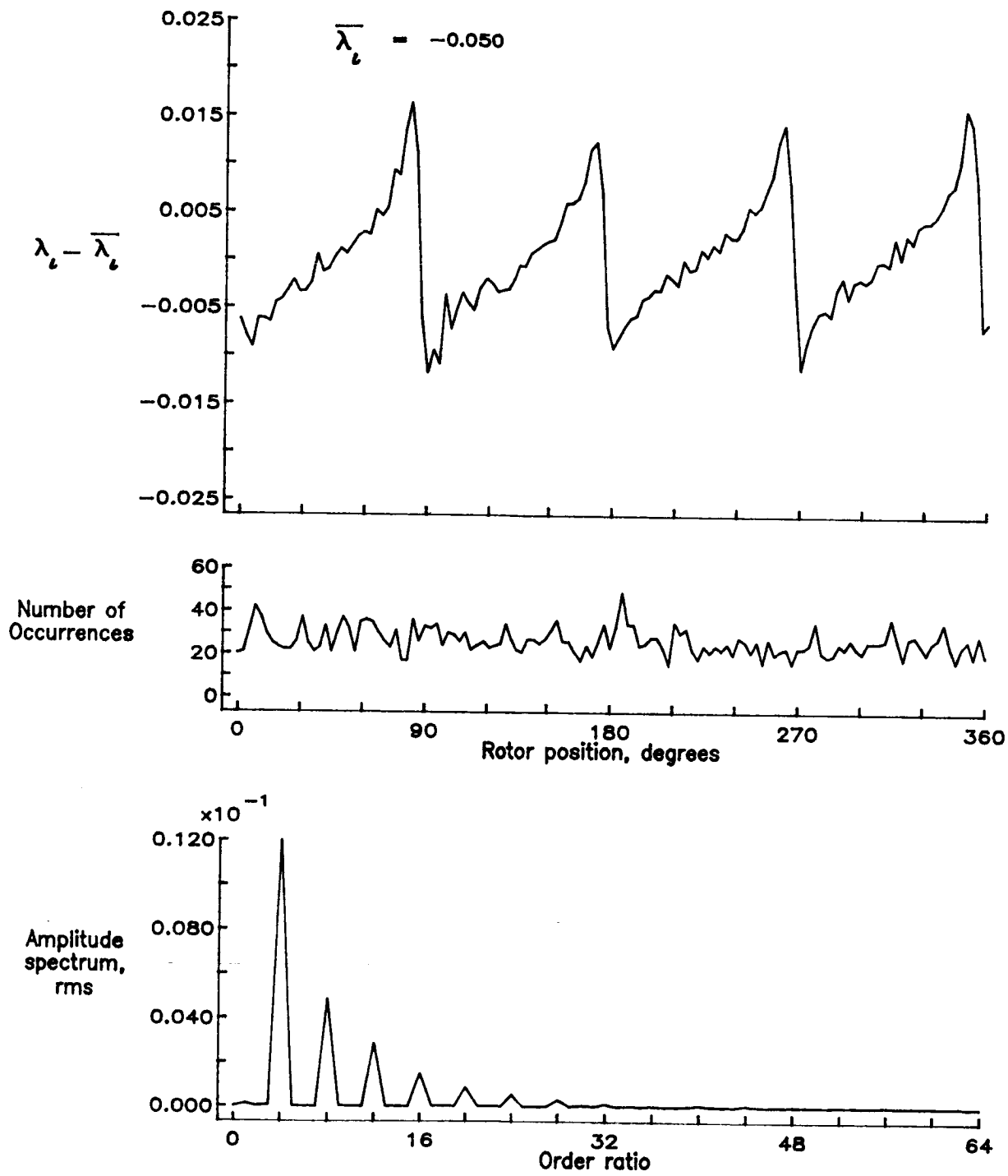


Figure 23.— Concluded.

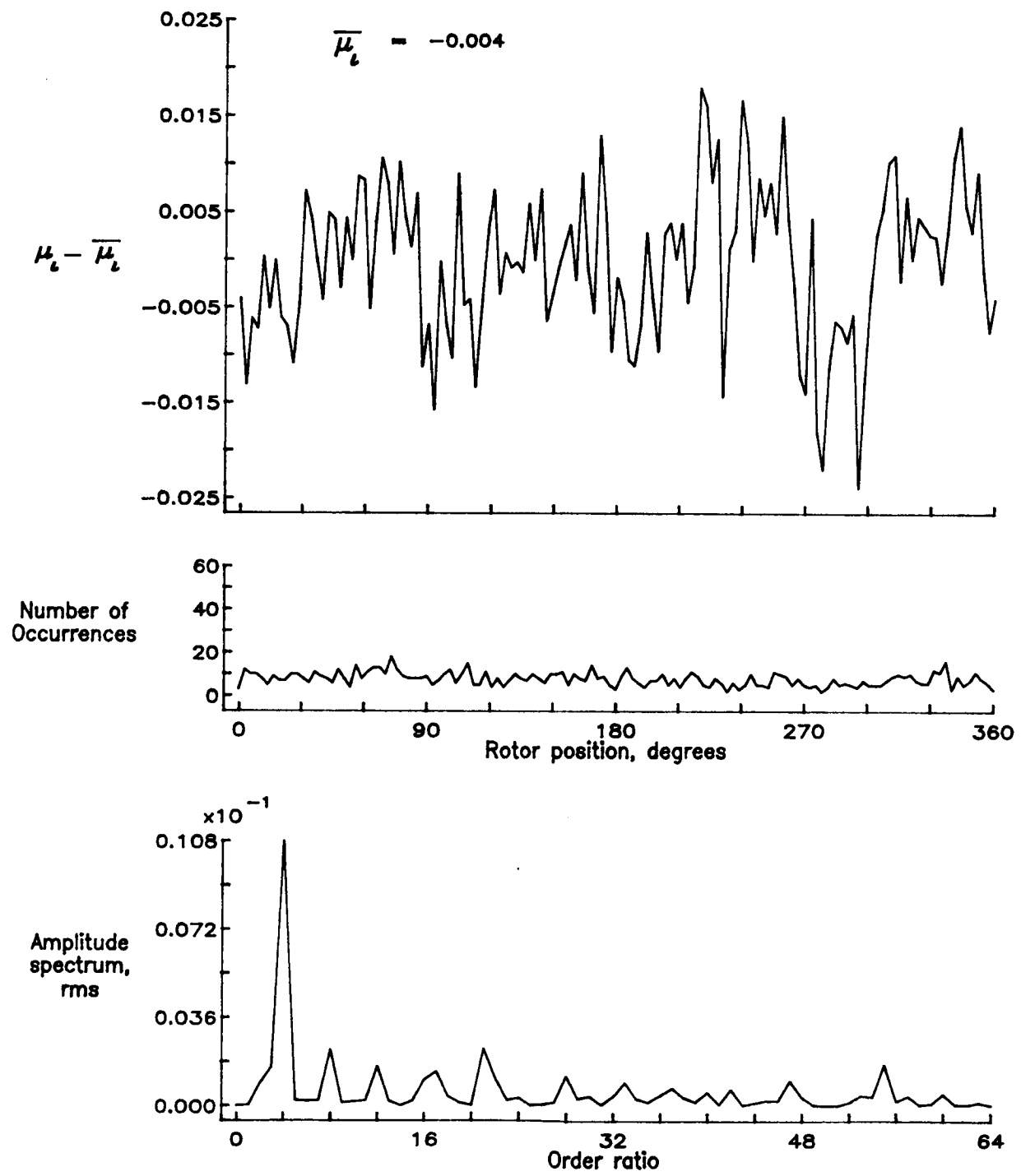


Figure 24.— Induced inflow velocity measured at 0 degrees and  $r/R$  of 0.98.

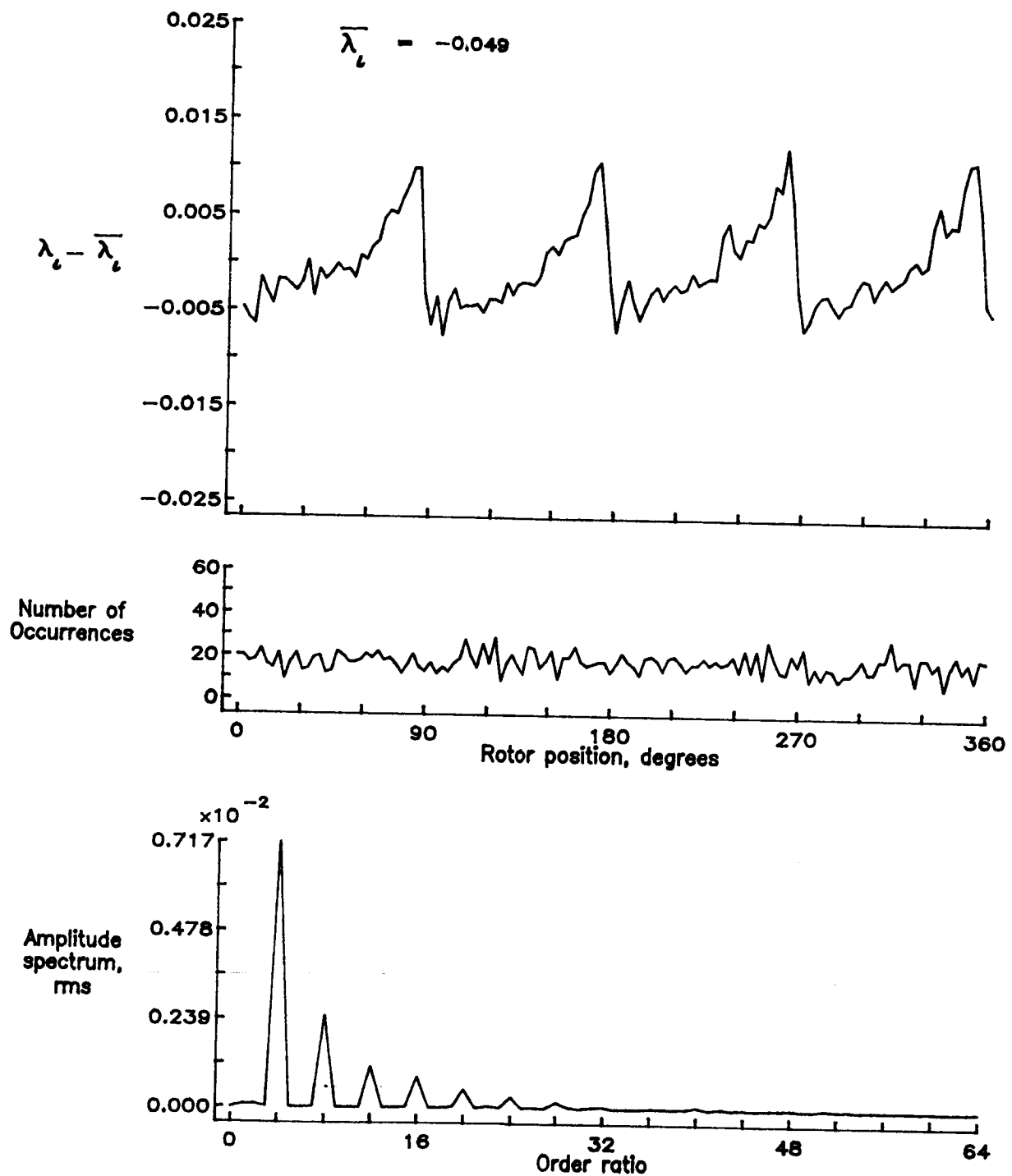


Figure 24.— Concluded.

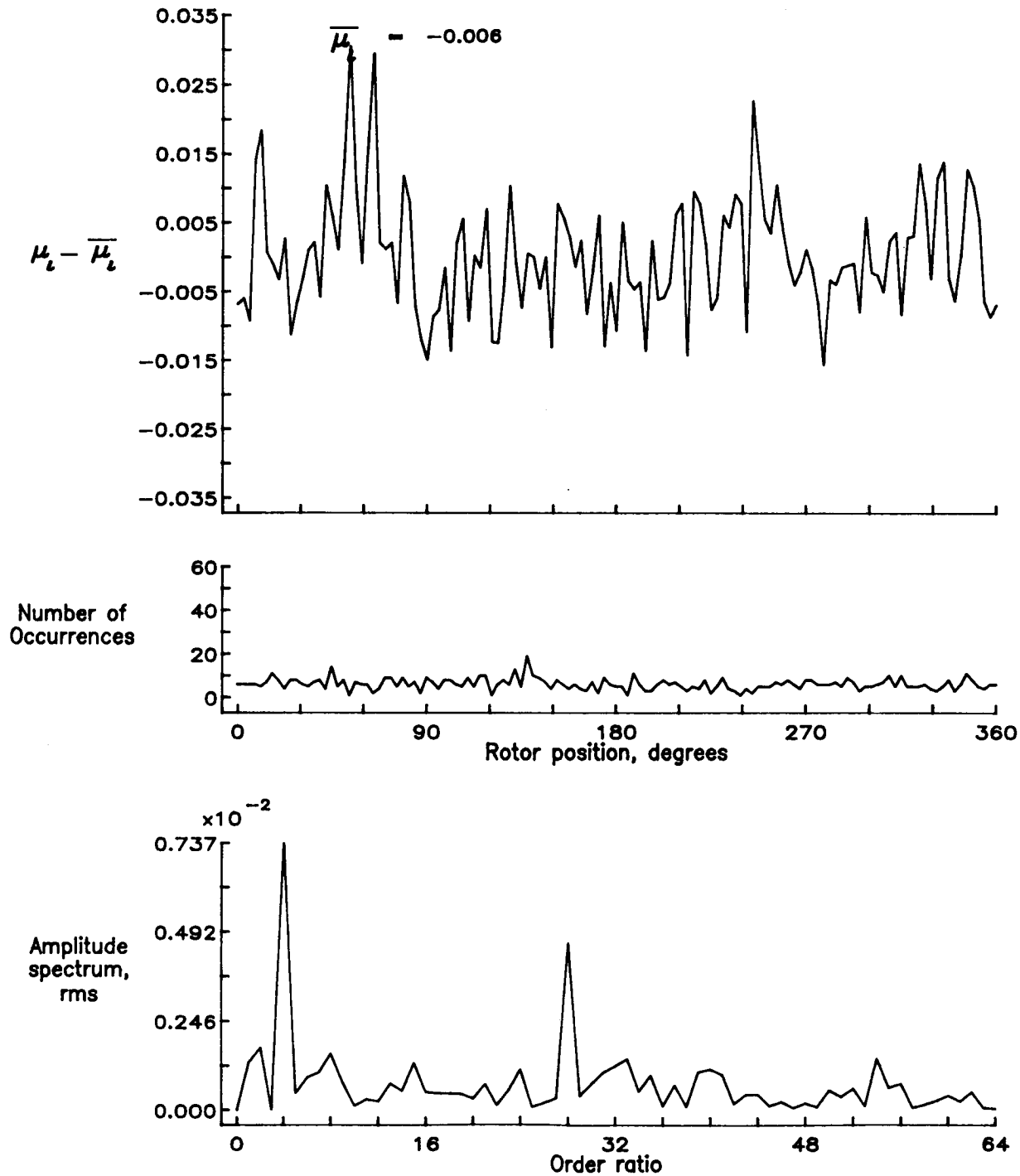


Figure 25.— Induced inflow velocity measured at 0 degrees and r/R of 1.02.

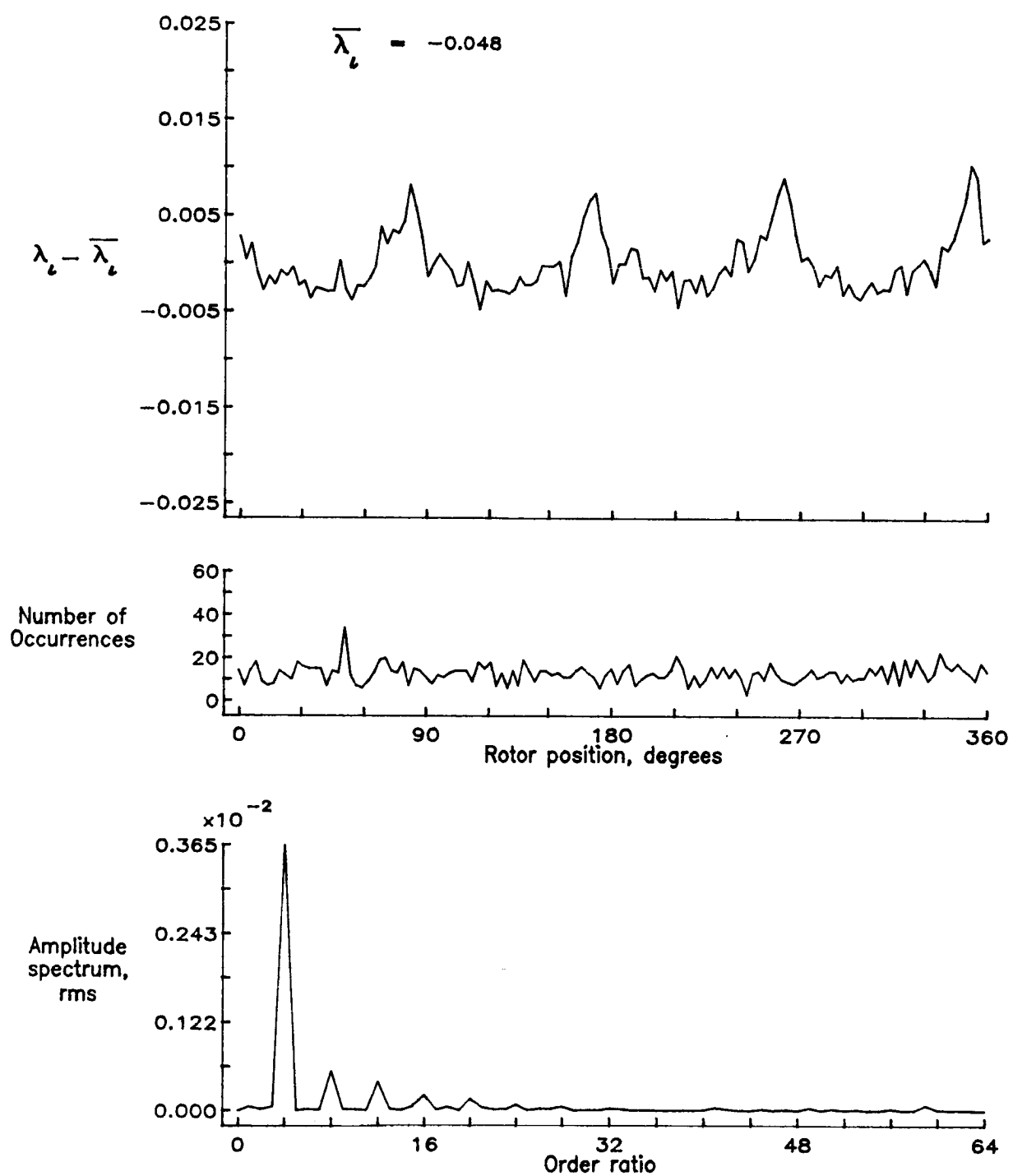


Figure 25.— Concluded.

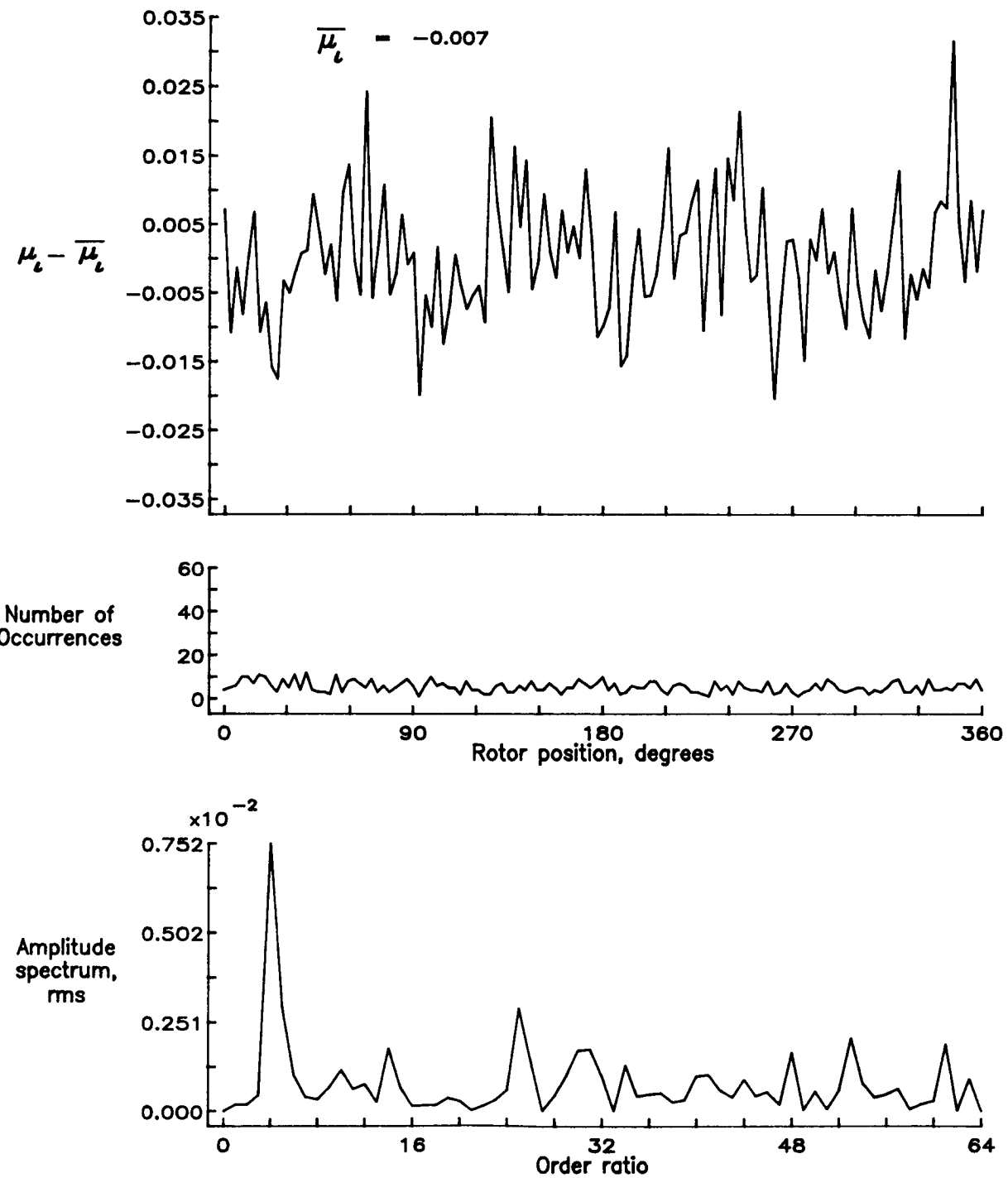


Figure 26.— Induced inflow velocity measured at 0 degrees and  $r/R$  of 1.04.

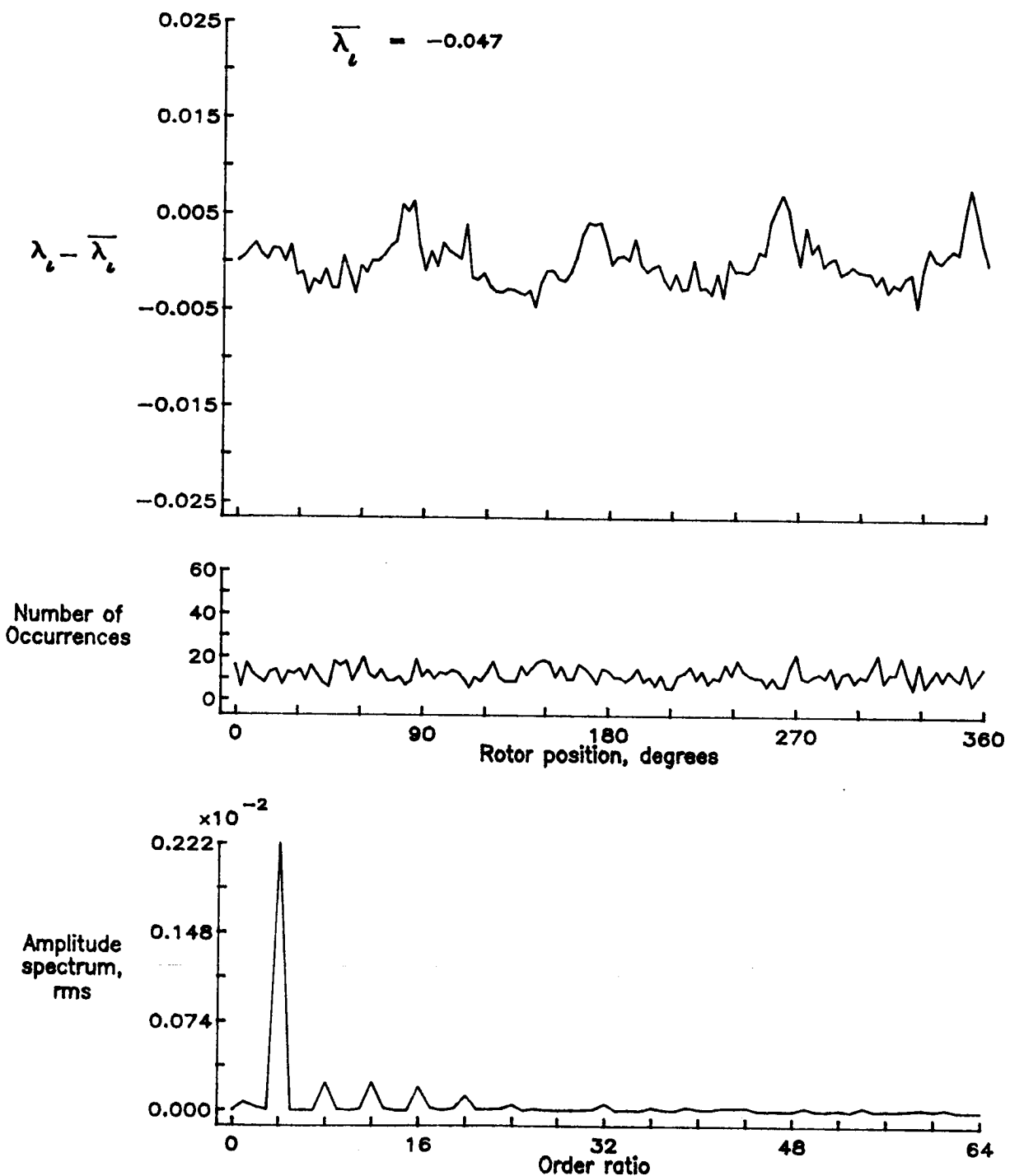


Figure 26.— Concluded.

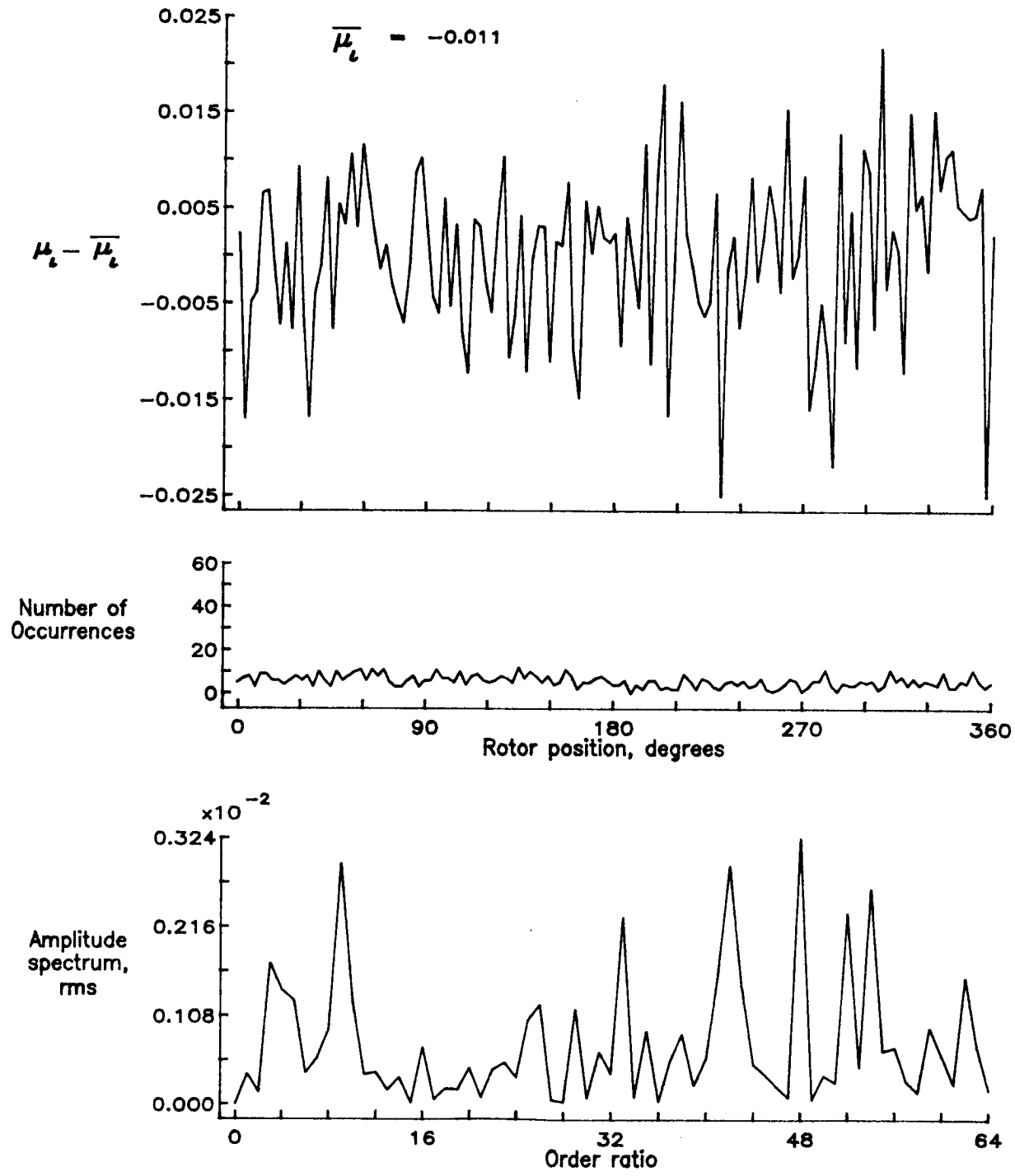


Figure 27.— Induced inflow velocity measured at 0 degrees and  $r/R$  of 1.10.

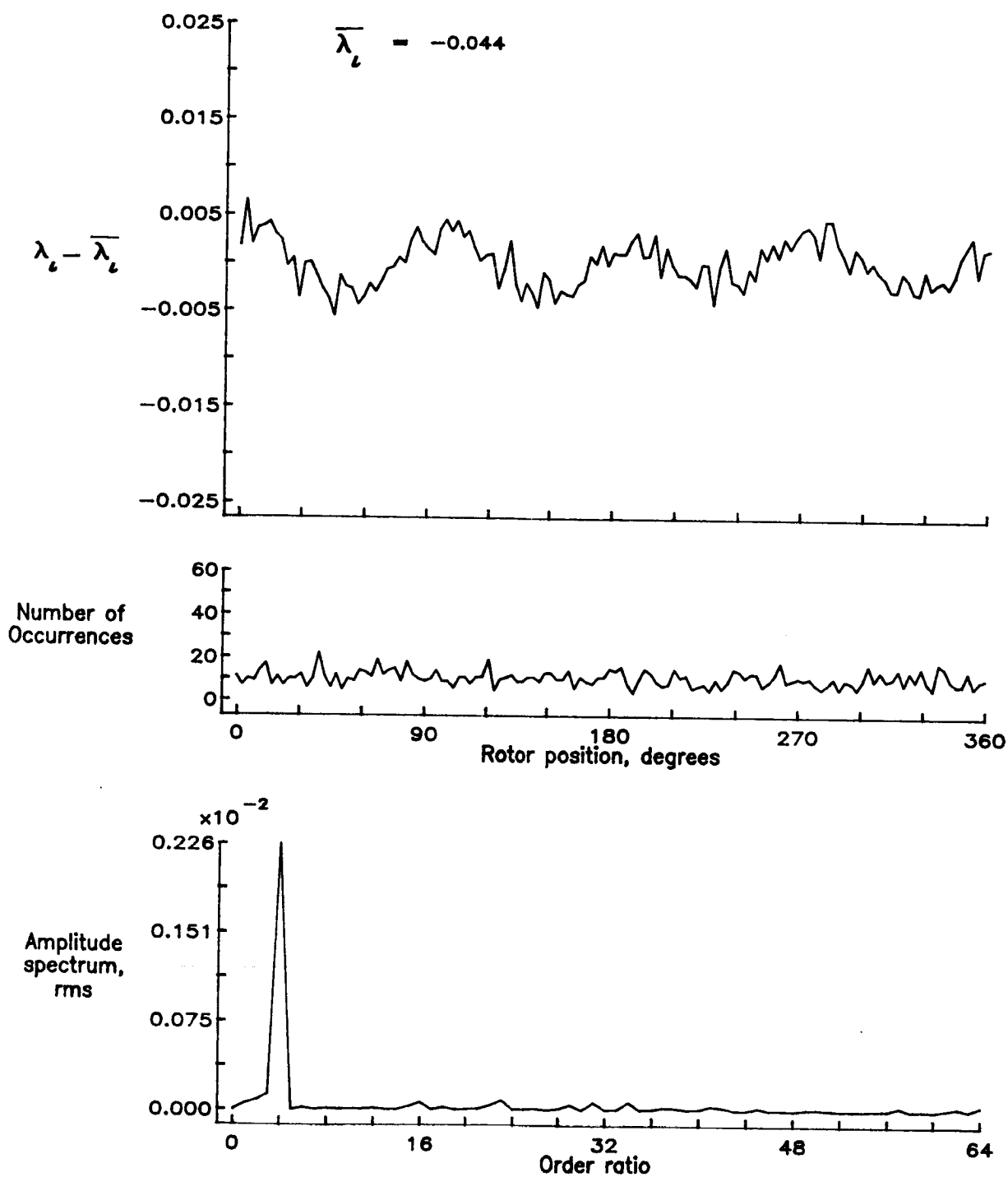


Figure 27.— Concluded.

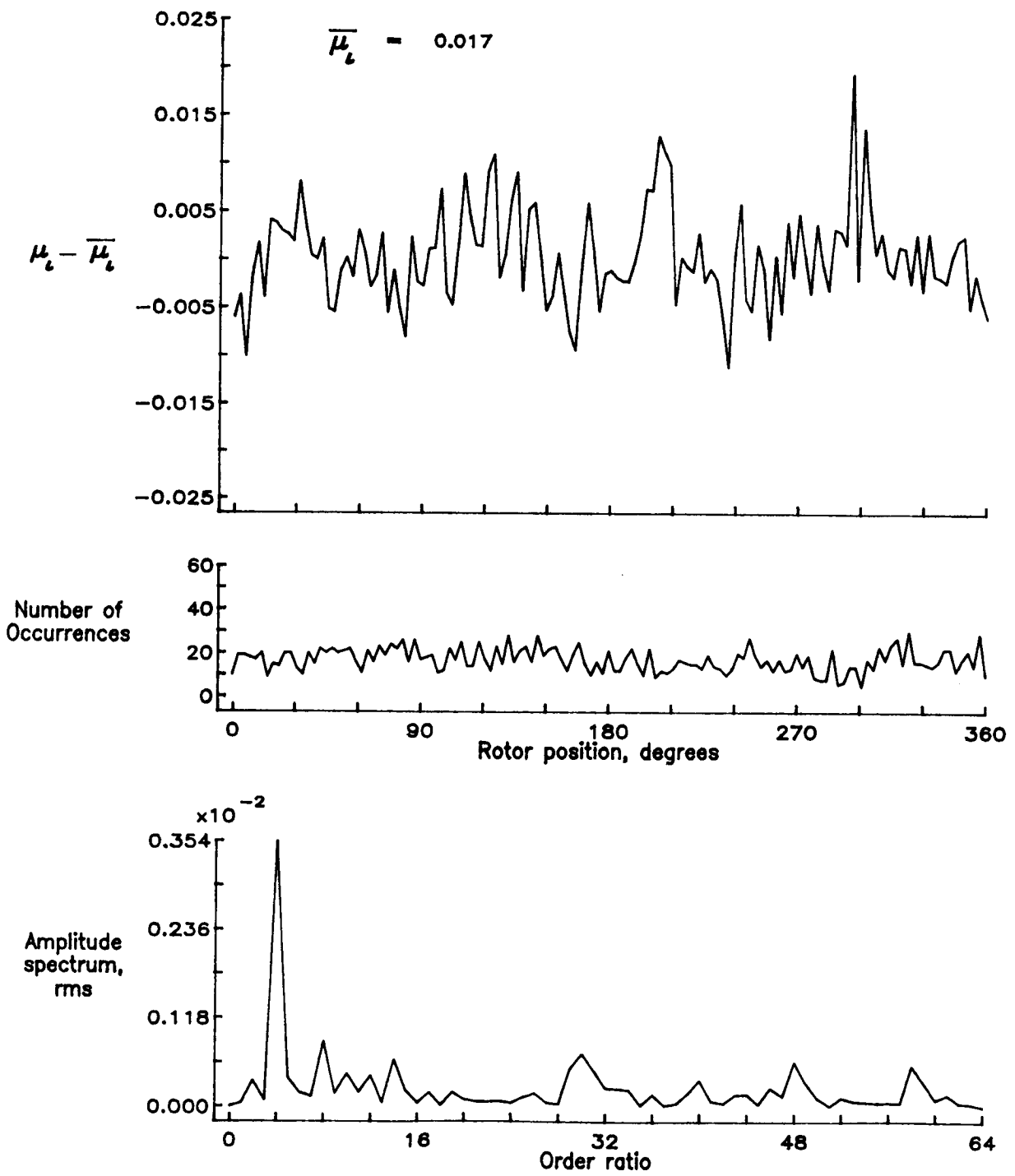


Figure 28.— Induced inflow velocity measured at 30 degrees and r/R of 0.50.

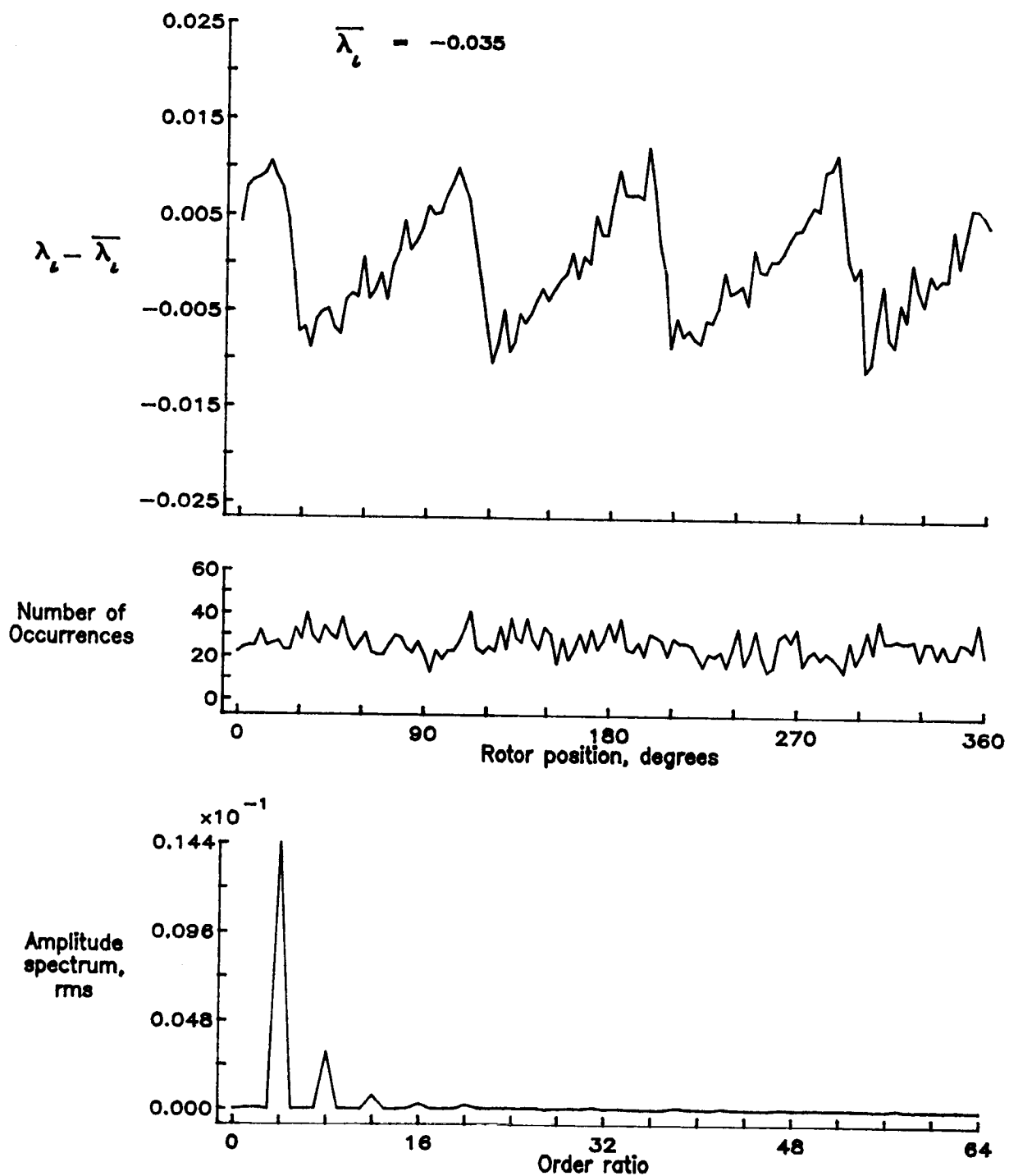


Figure 28.— Concluded.

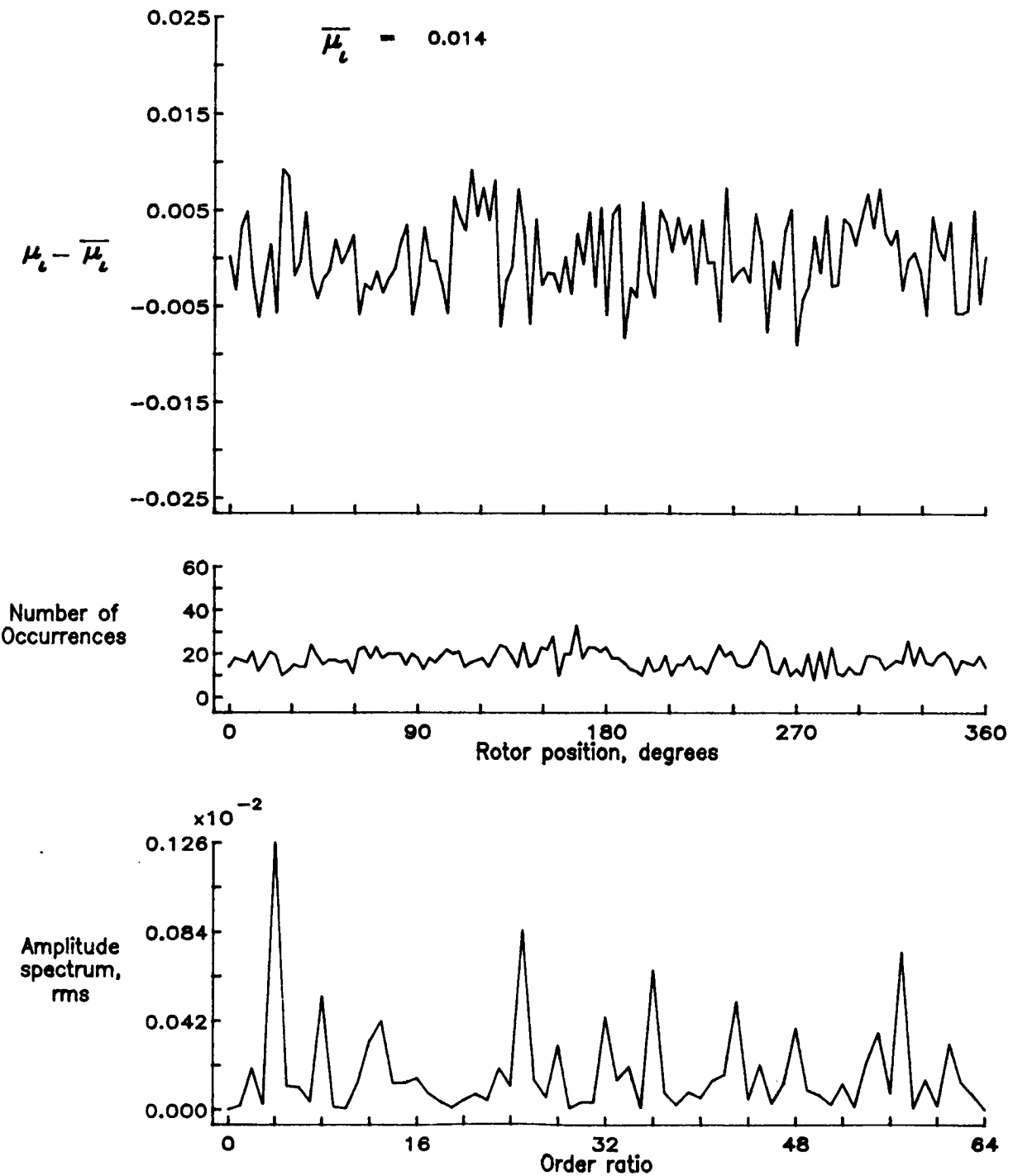


Figure 29.— Induced inflow velocity measured at 30 degrees and  $r/R$  of 0.60.

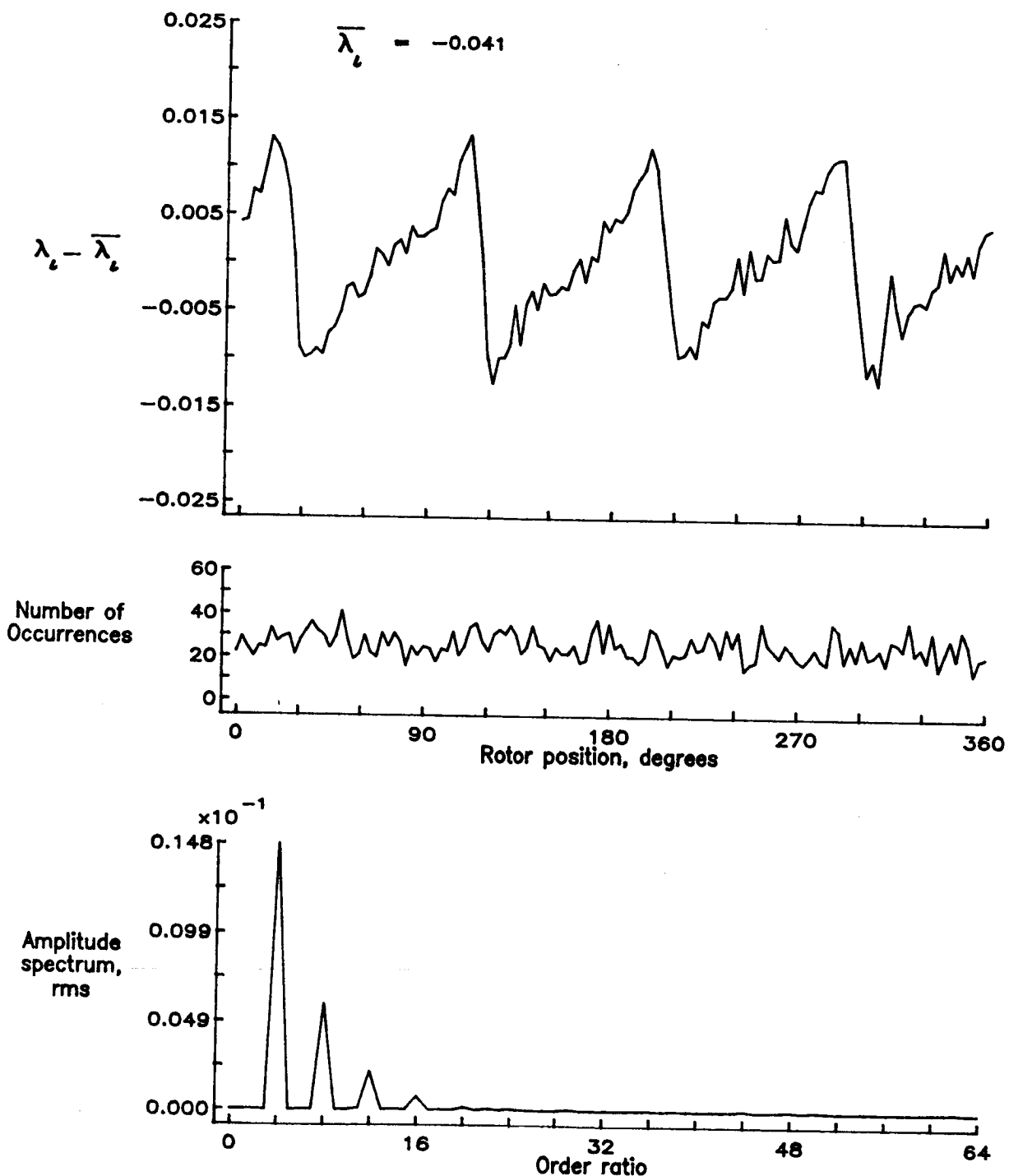


Figure 29.— Concluded.

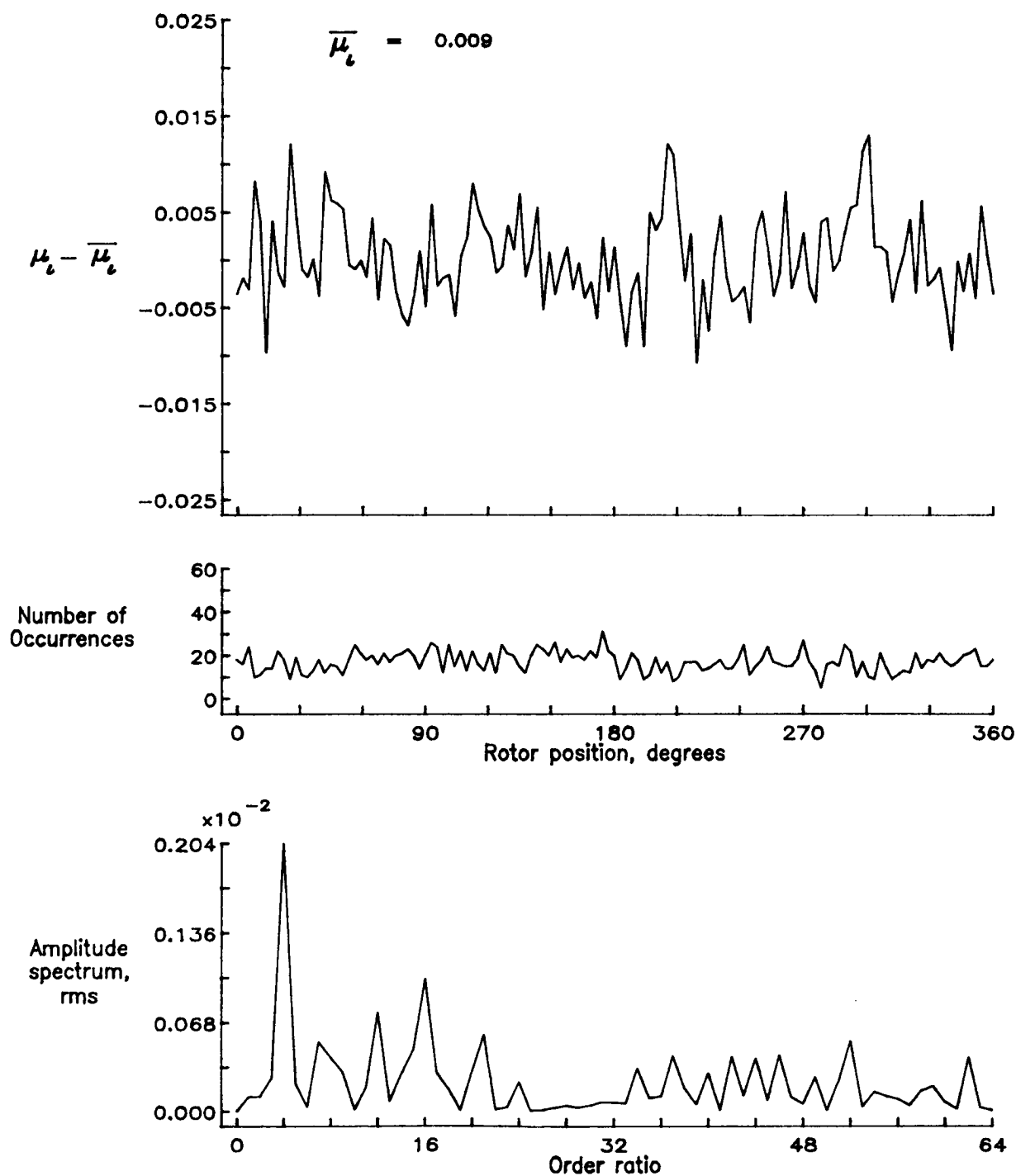


Figure 30.— Induced inflow velocity measured at 30 degrees and r/R of 0.70.

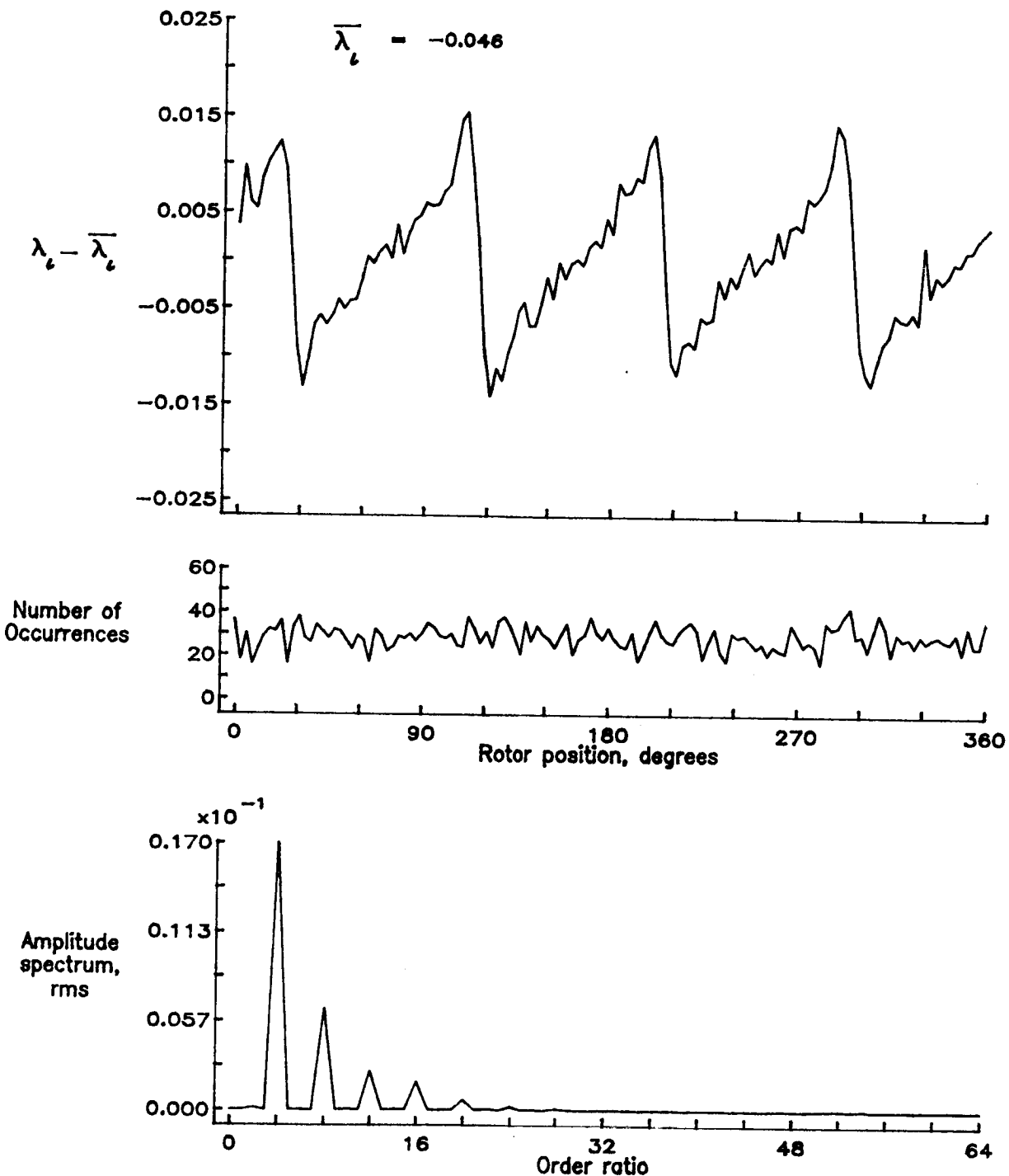


Figure 30.— Concluded.

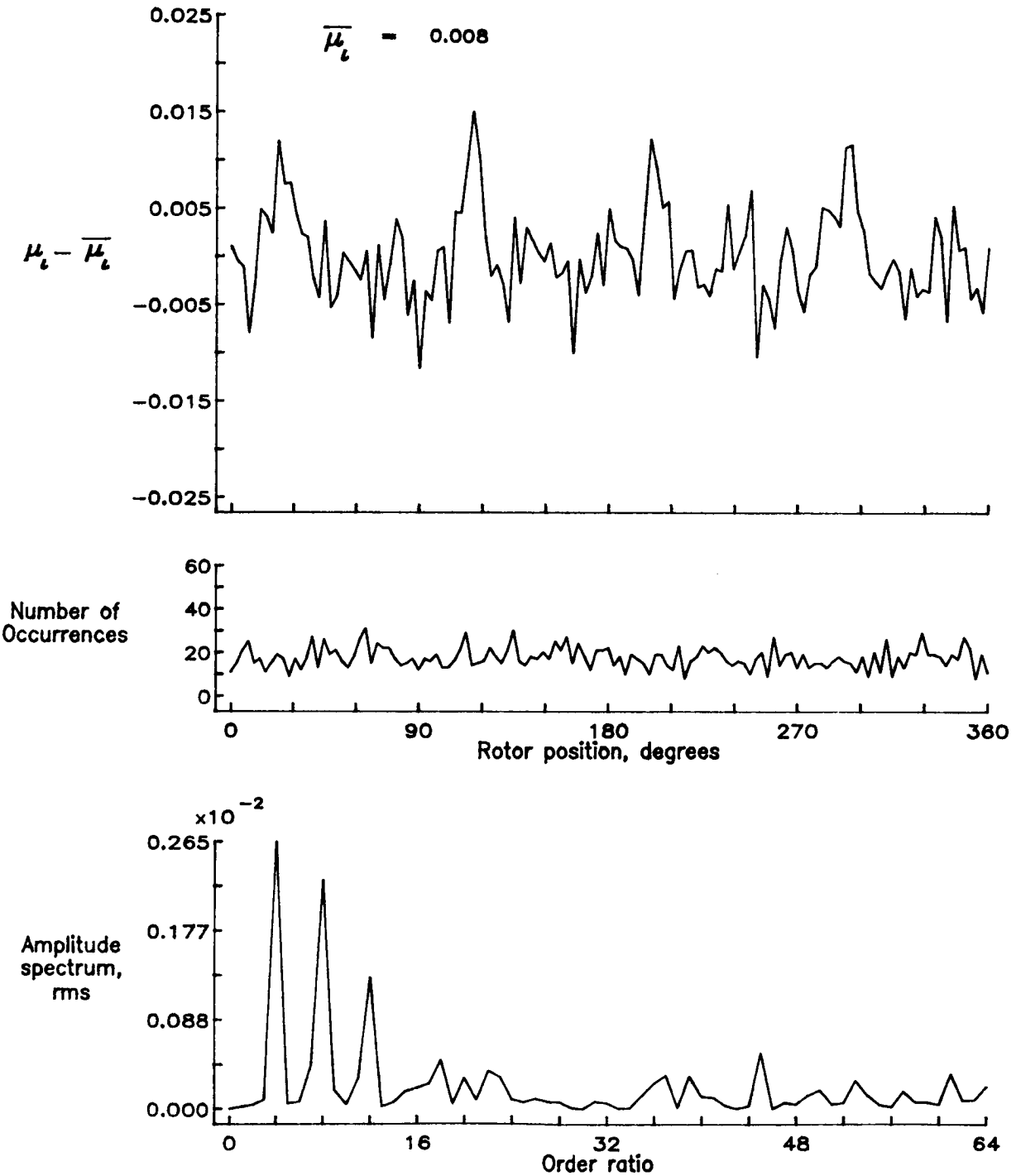


Figure 31.— Induced inflow velocity measured at 30 degrees and  $r/R$  of 0.74.

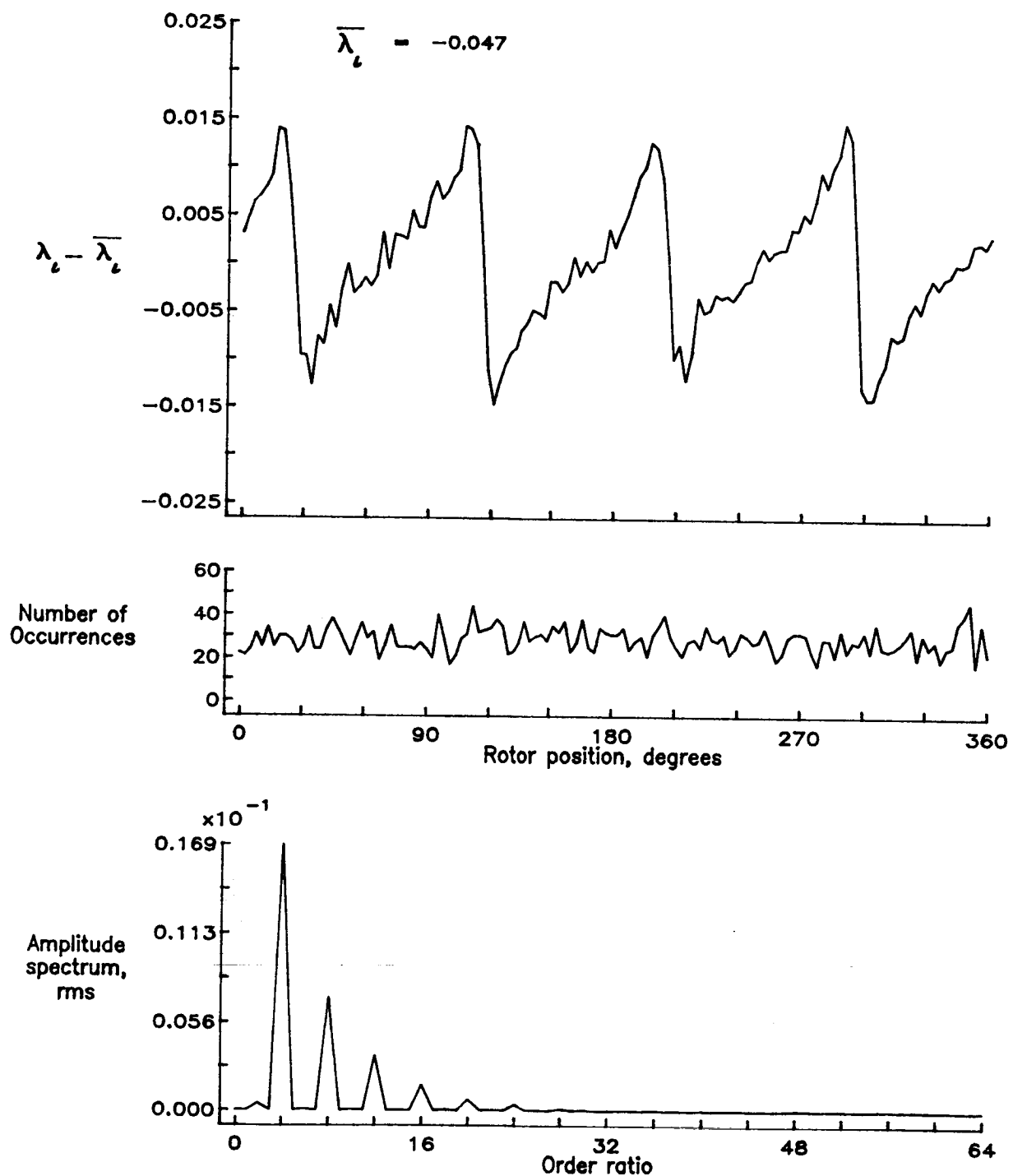


Figure 31.— Concluded.

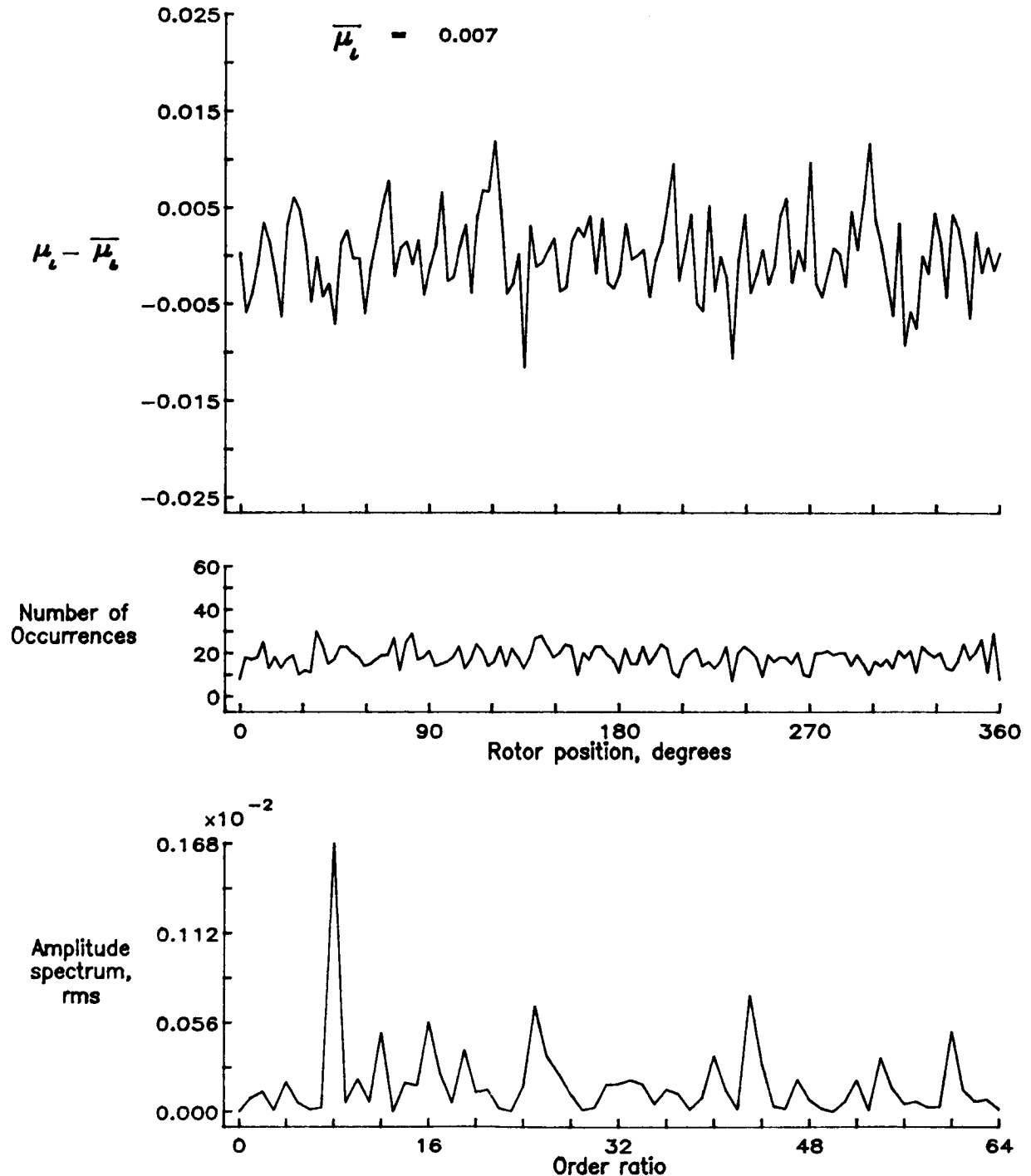


Figure 32.— Induced inflow velocity measured at 30 degrees and  $r/R$  of 0.78.

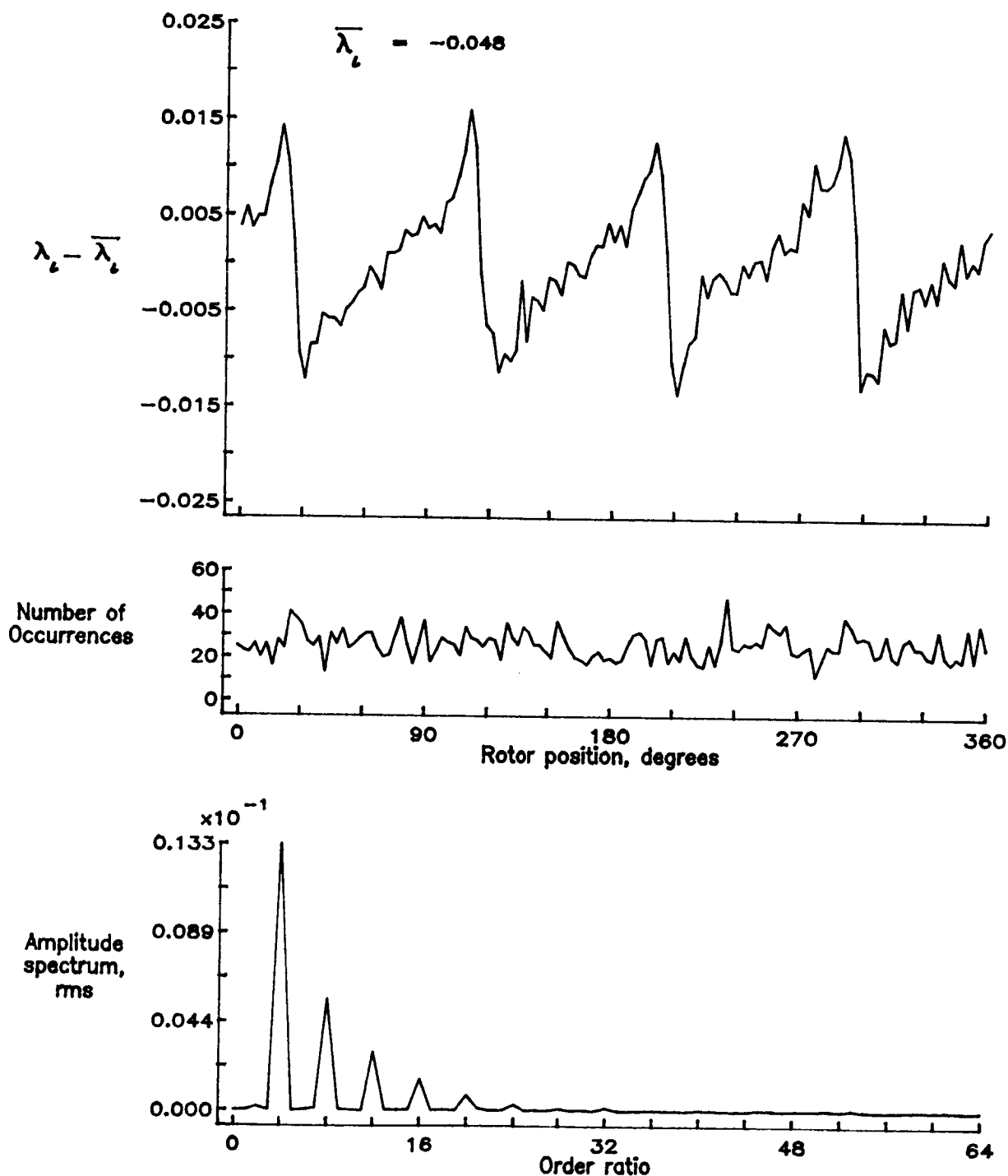


Figure 32.— Concluded.

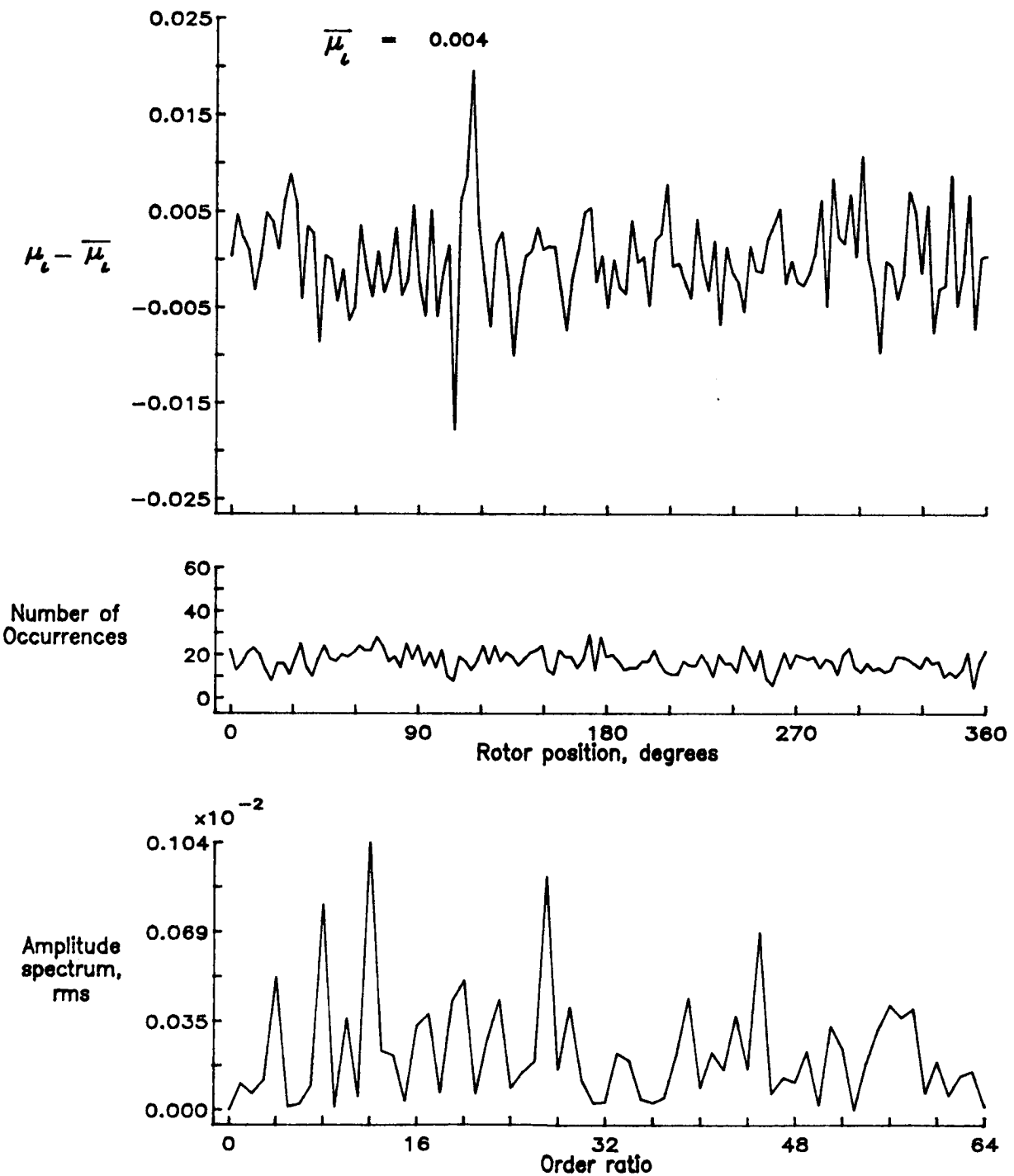


Figure 33.— Induced inflow velocity measured at 30 degrees and r/R of 0.82.

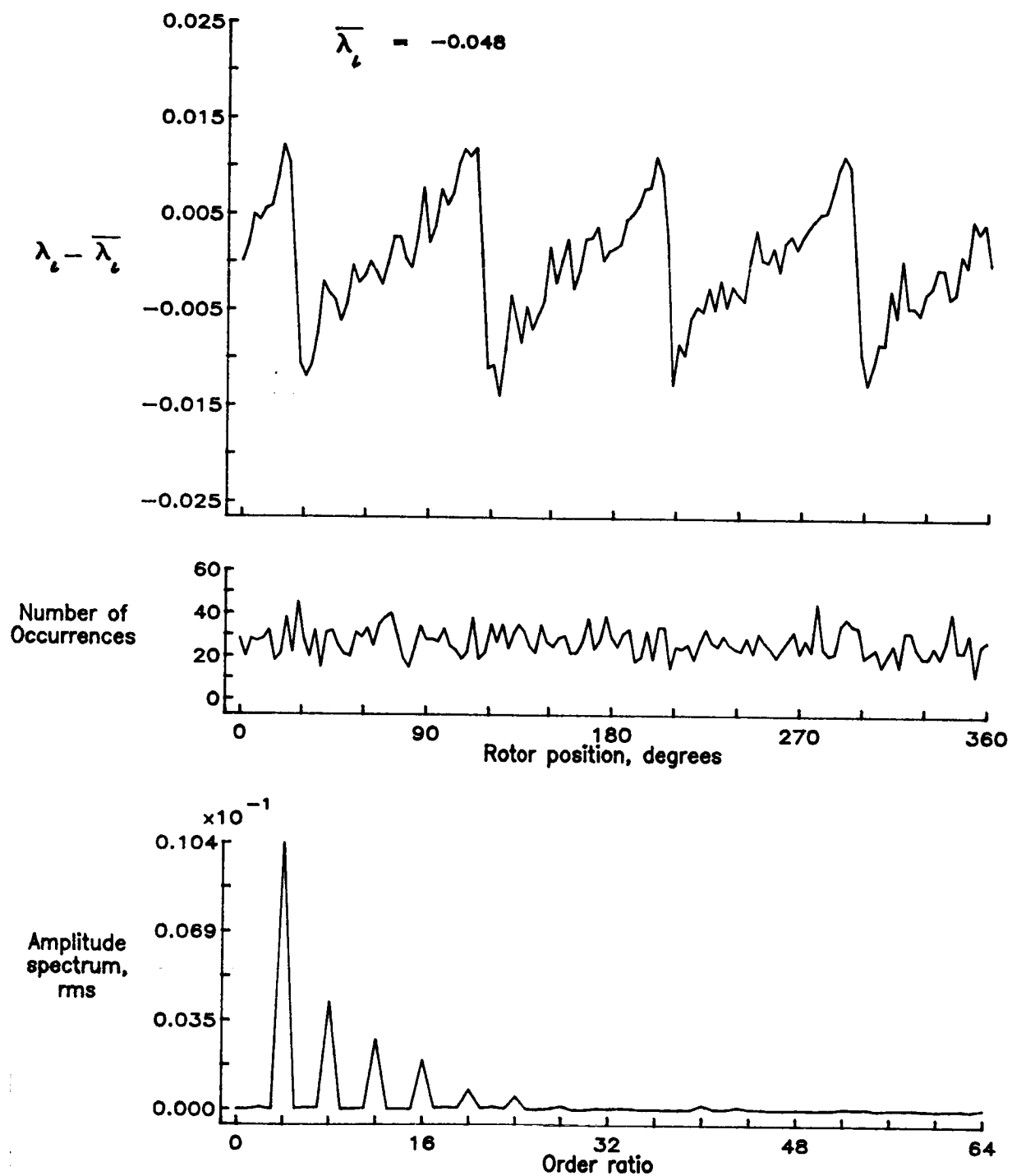


Figure 33.— Concluded.

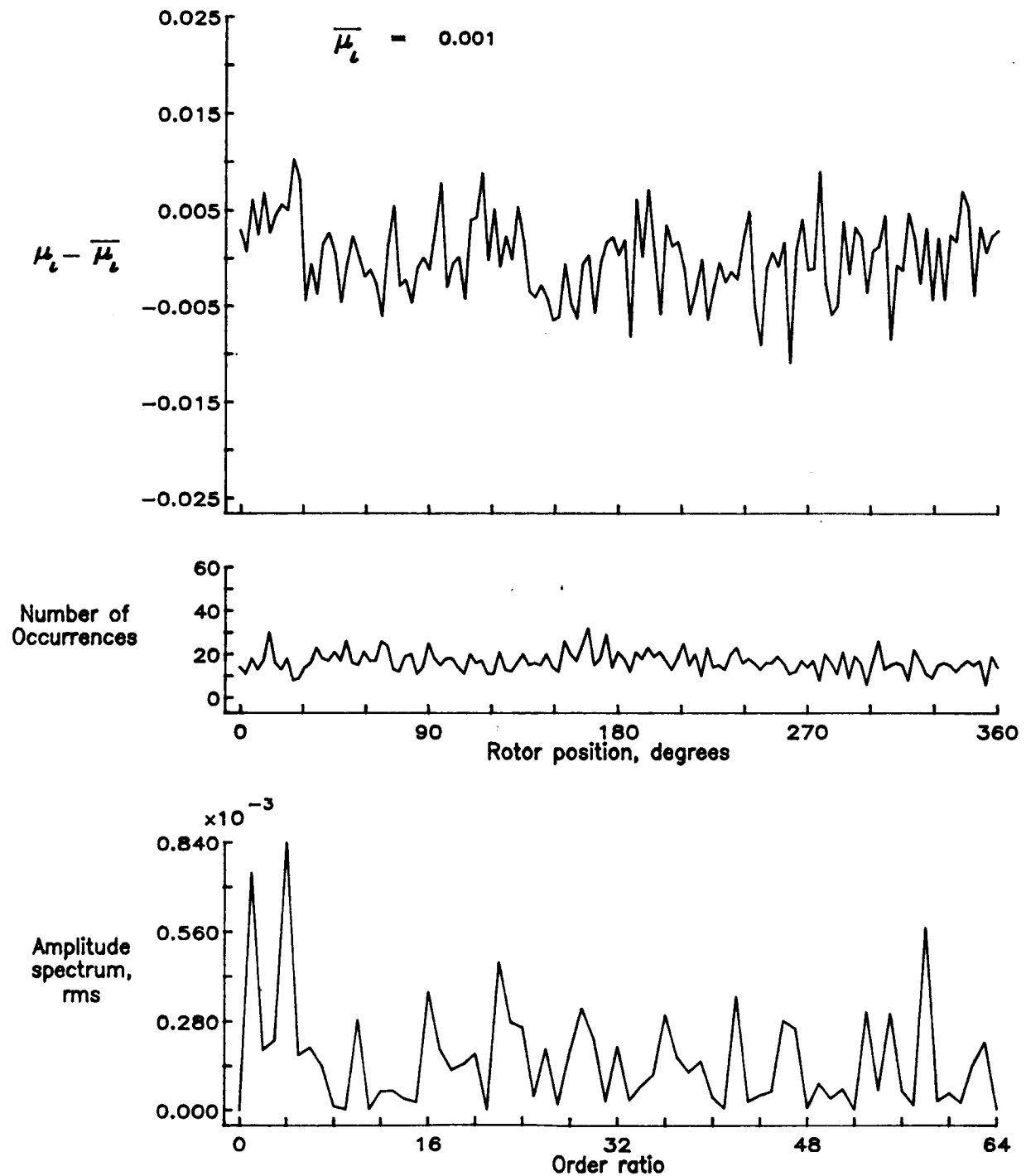


Figure 34.— Induced inflow velocity measured at 30 degrees and r/R of 0.86.

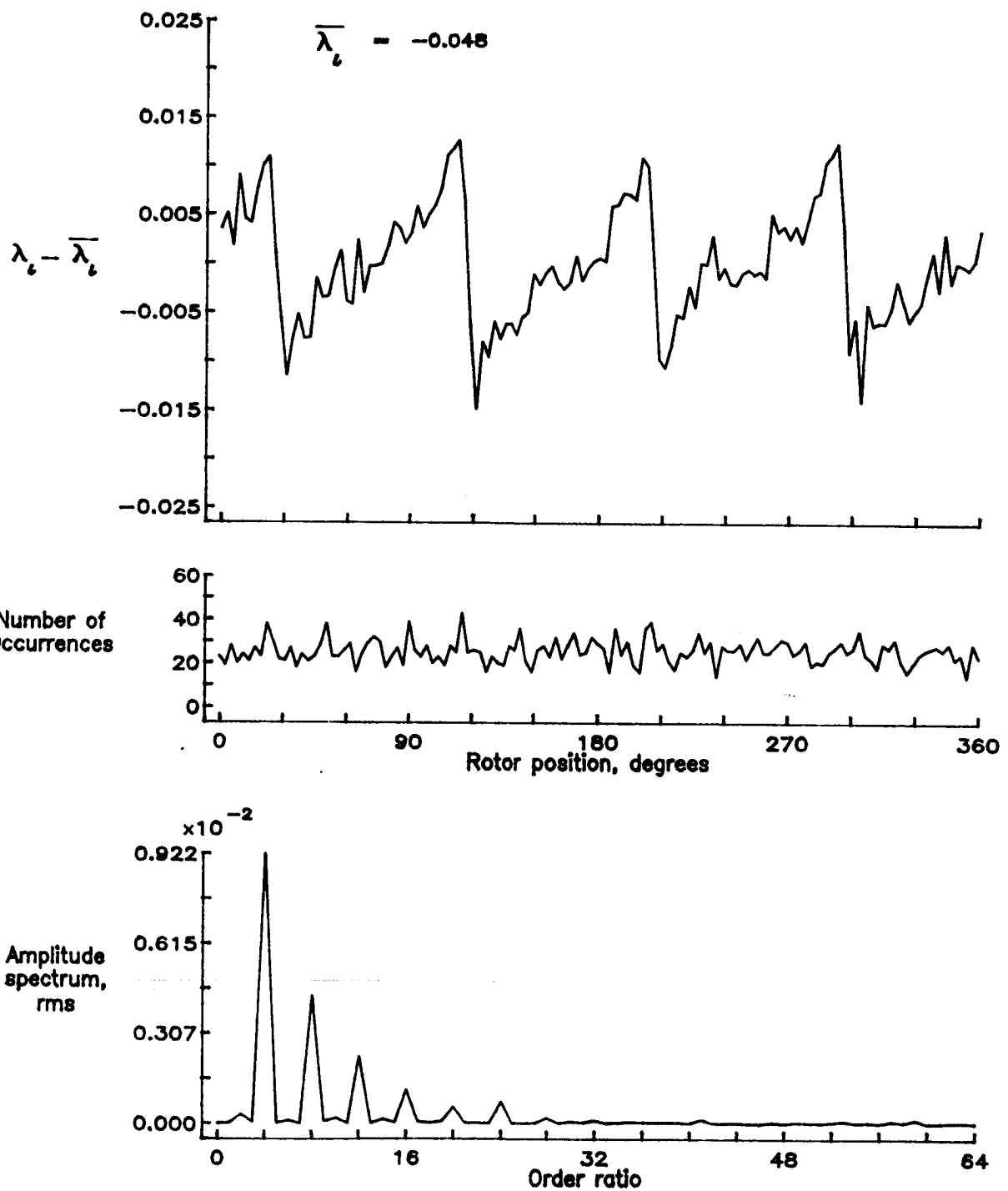


Figure 34.— Concluded.

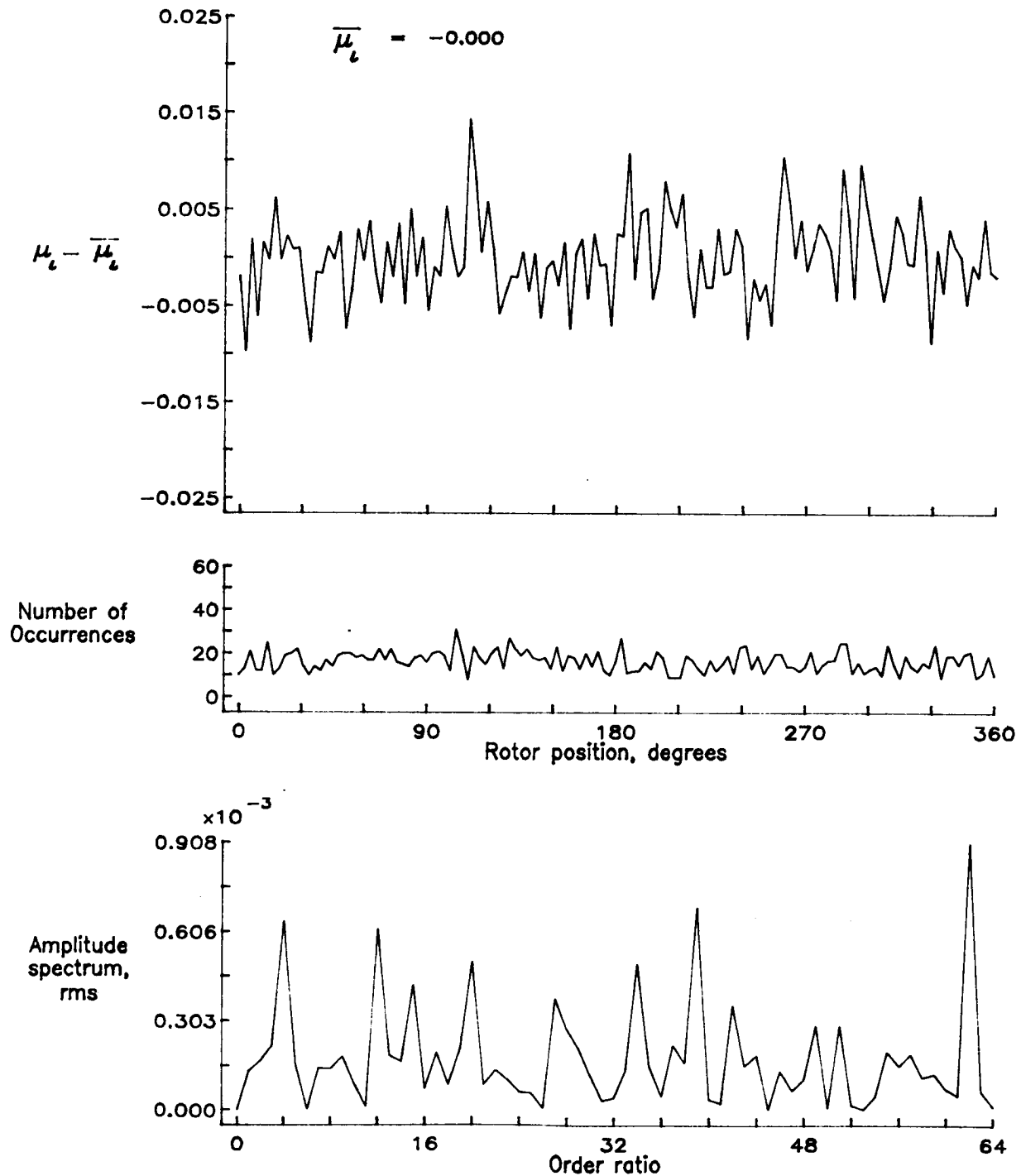


Figure 35.— Induced inflow velocity measured at 30 degrees and  $r/R$  of 0.90.

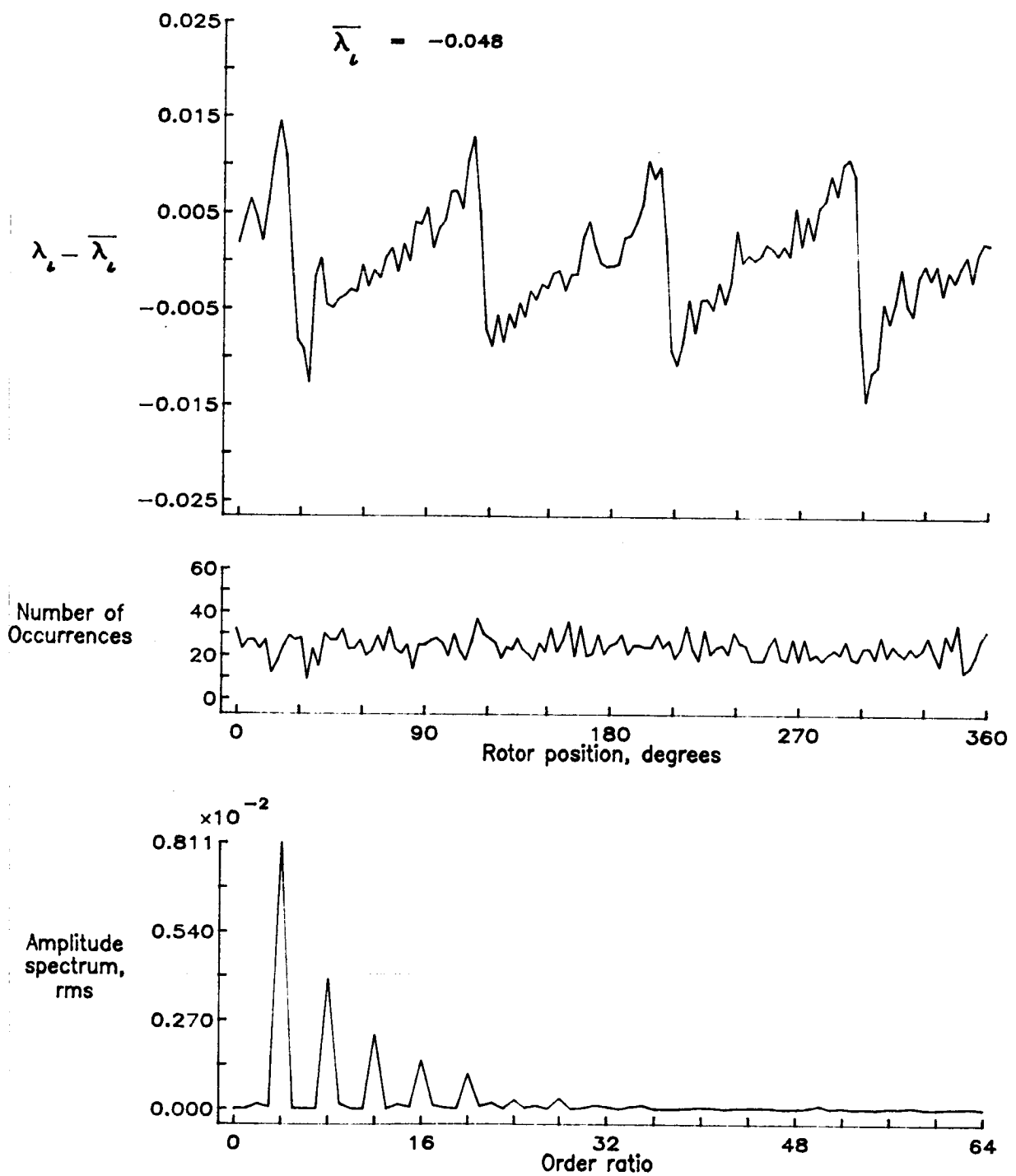


Figure 35.— Concluded.

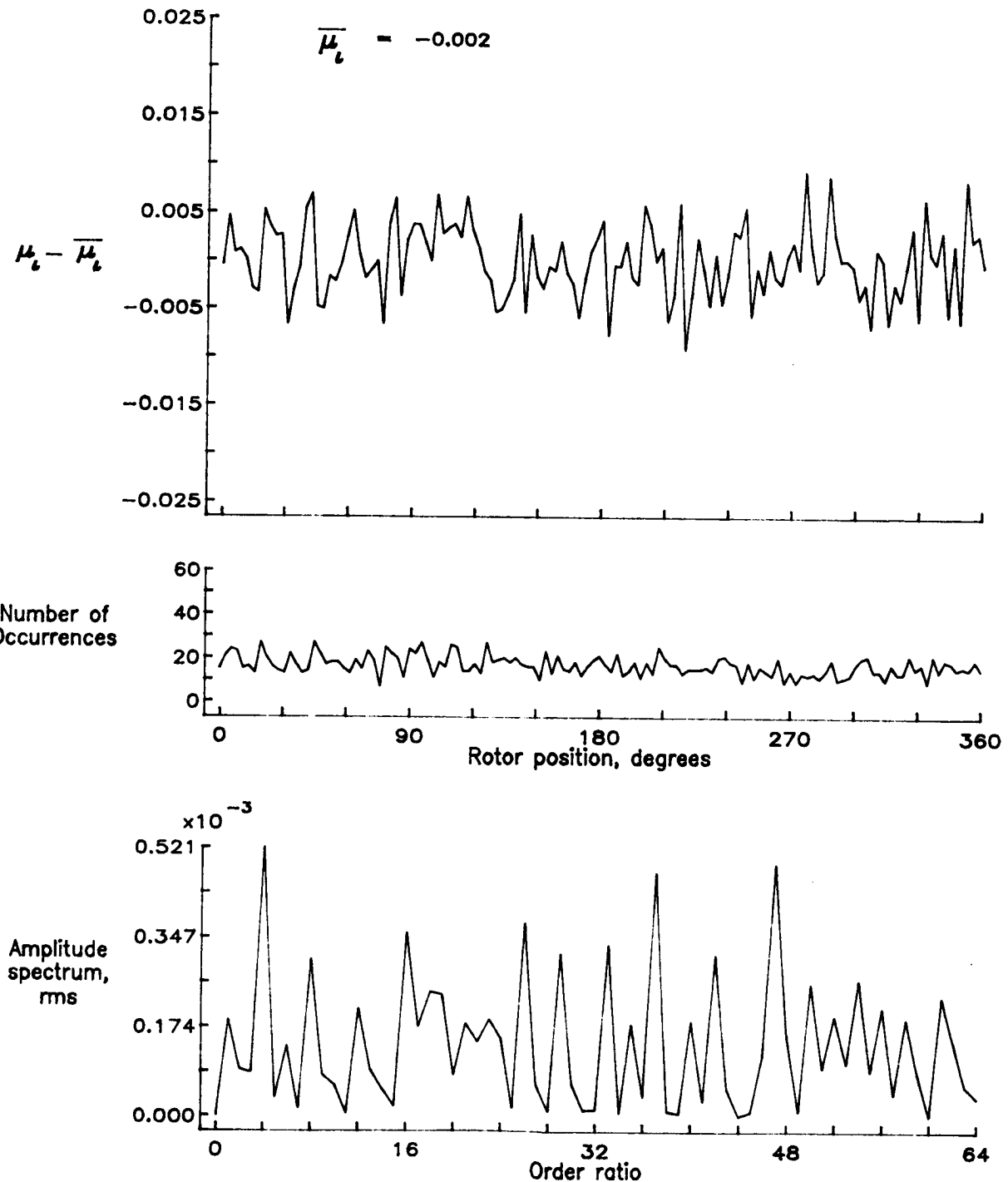


Figure 36.— Induced inflow velocity measured at 30 degrees and  $r/R$  of 0.94.

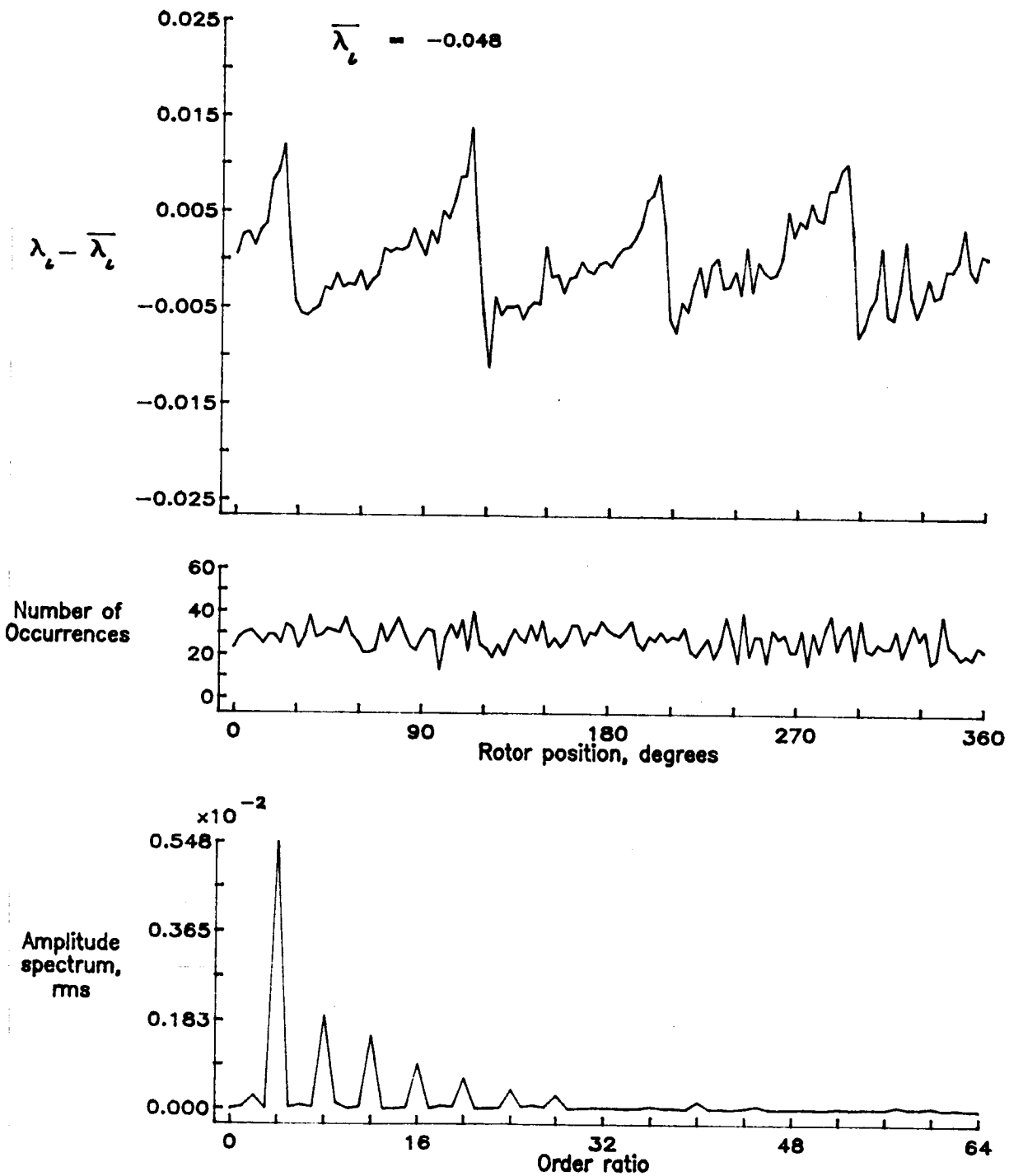


Figure 36.— Concluded.

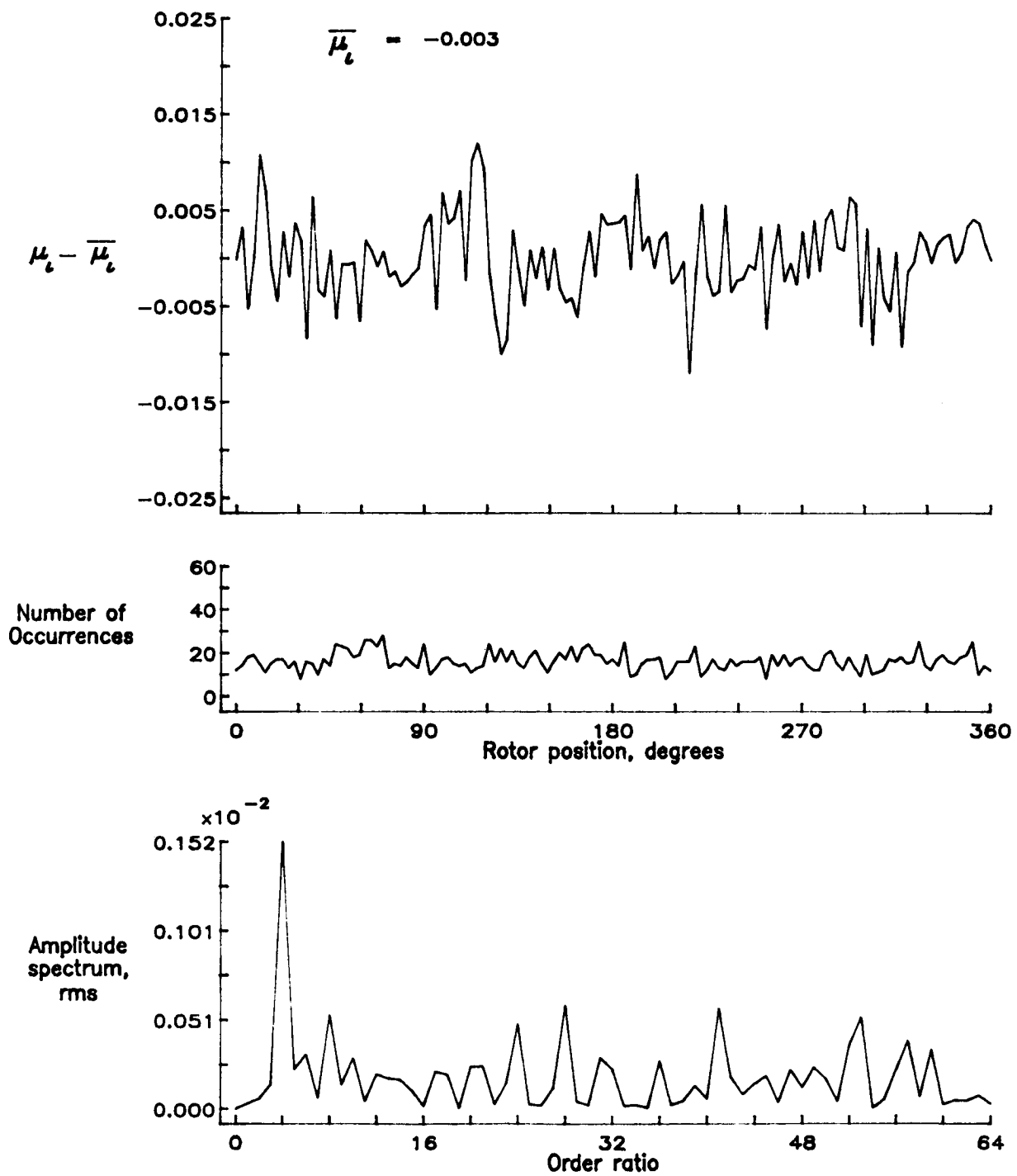


Figure 37.— Induced inflow velocity measured at 30 degrees and r/R of 0.98.

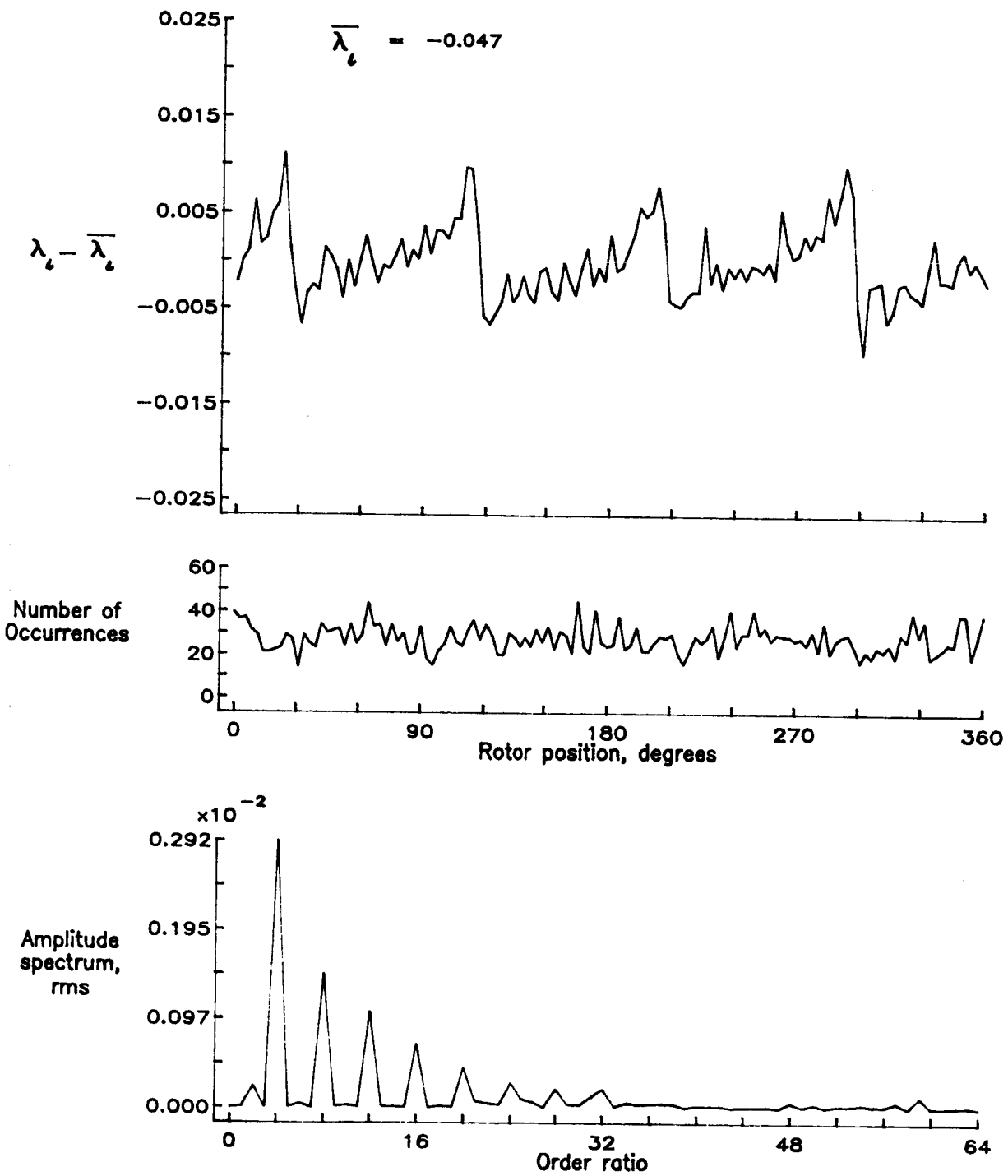


Figure 37.— Concluded.

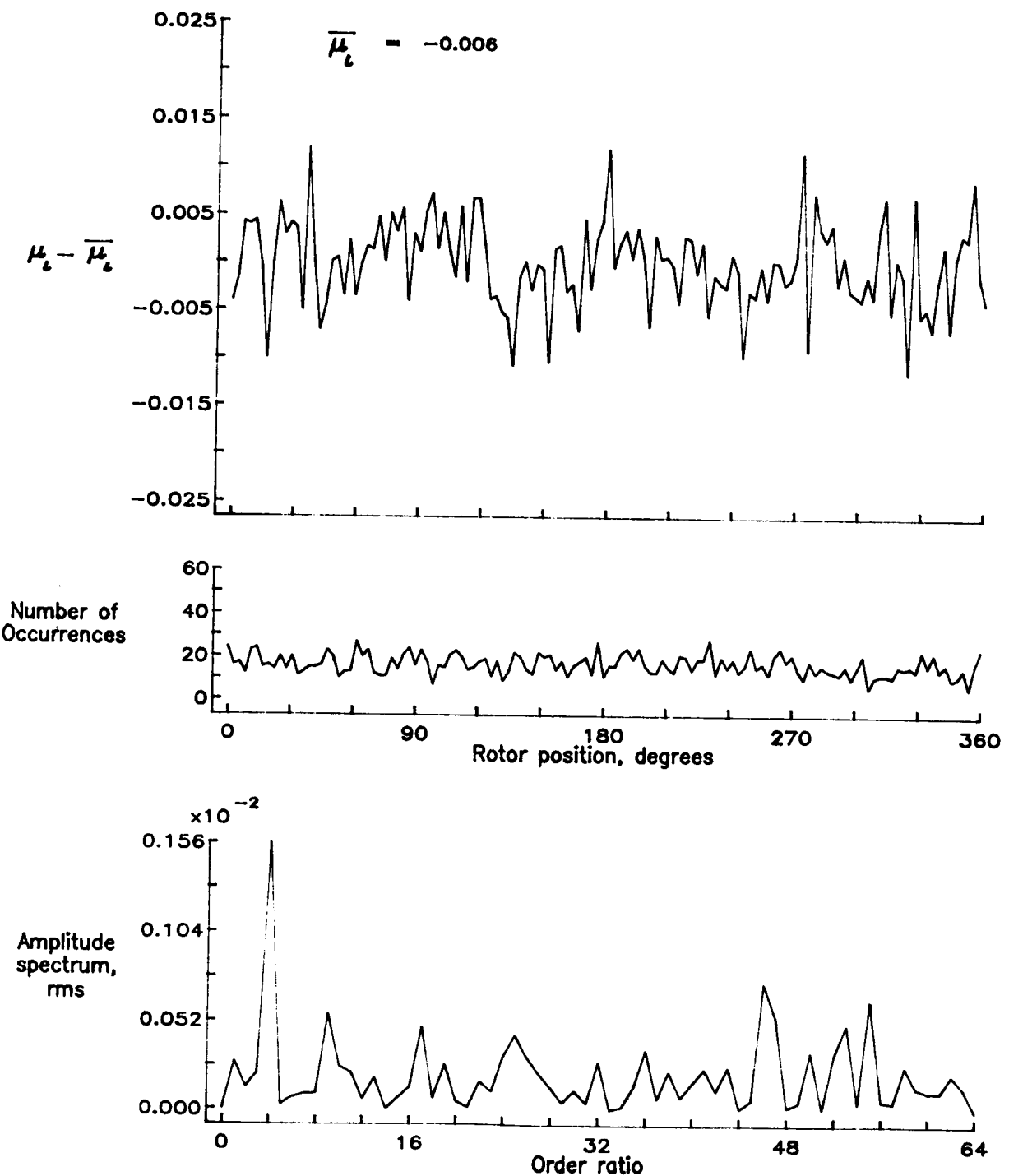


Figure 38.— Induced inflow velocity measured at 30 degrees and  $r/R$  of 1.02.

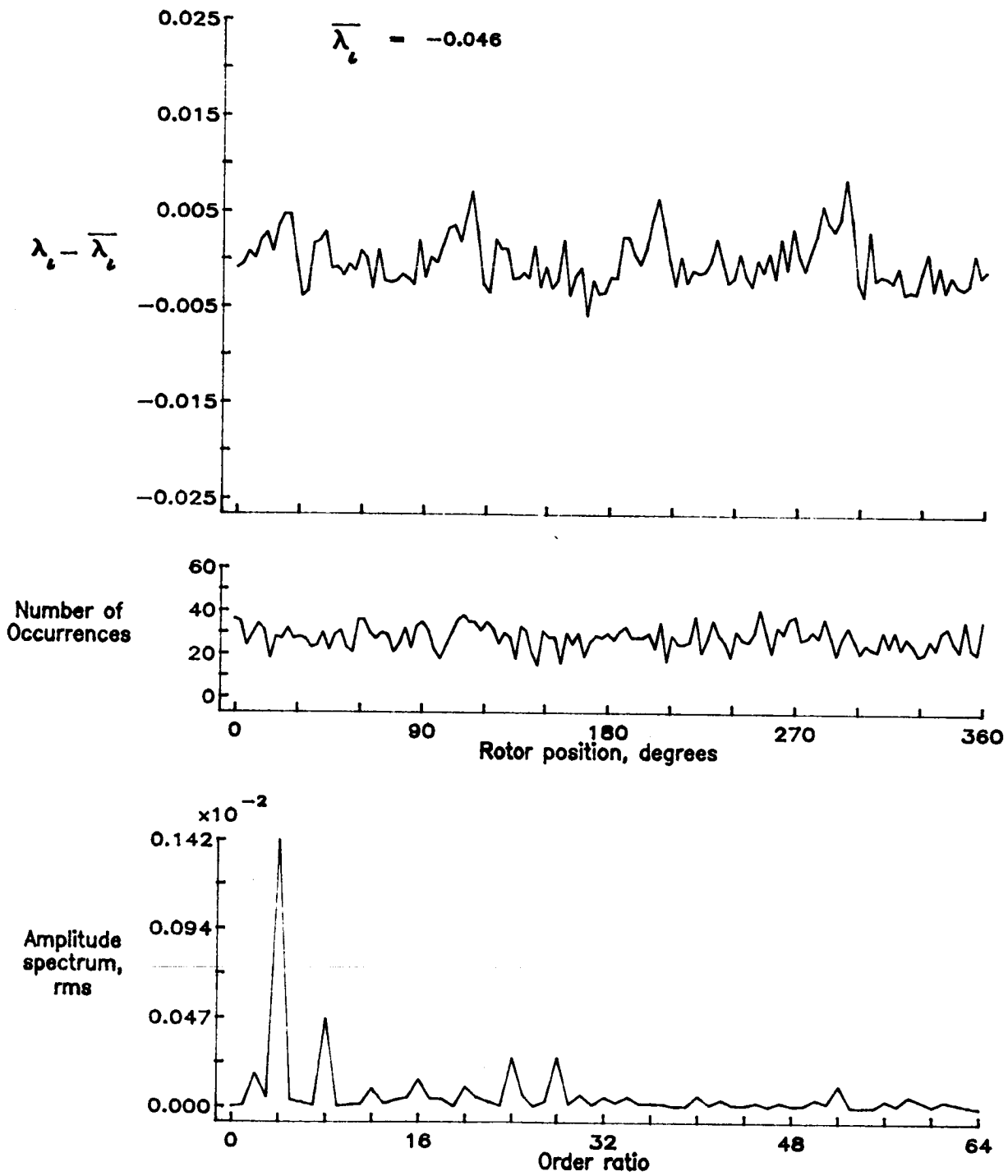


Figure 38.— Concluded.

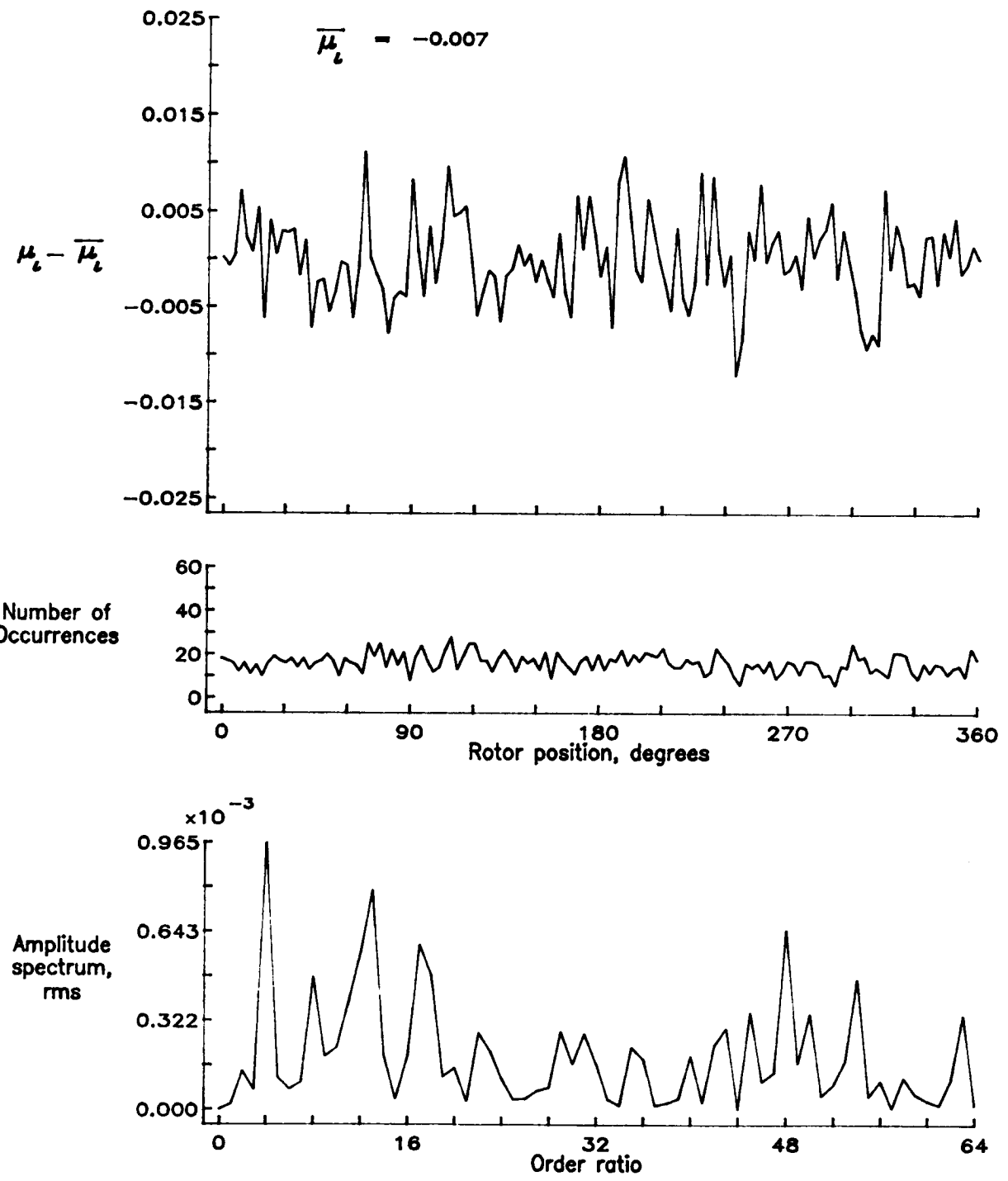


Figure 39.— Induced inflow velocity measured at 30 degrees and  $r/R$  of 1.04.

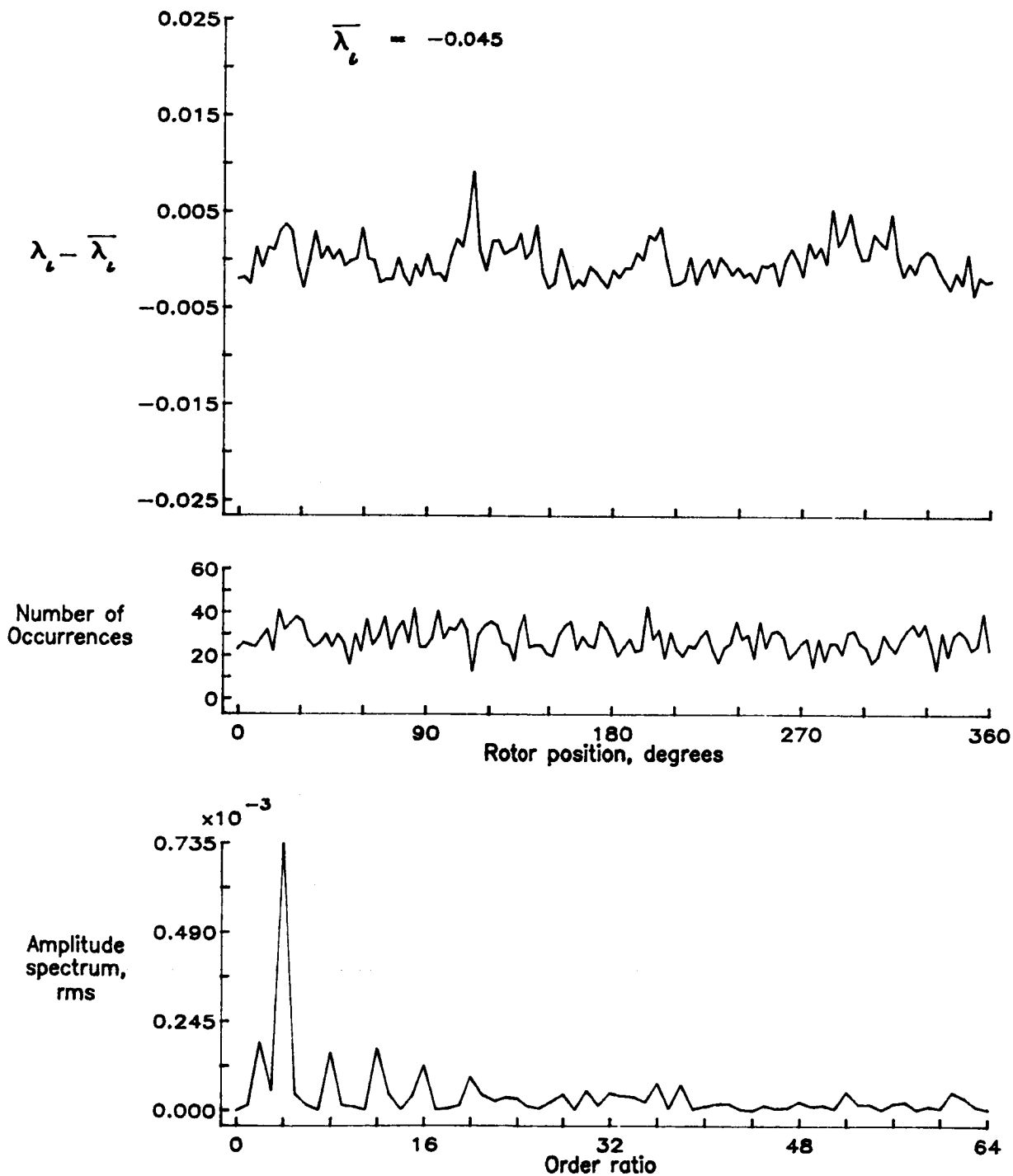


Figure 39.— Concluded.

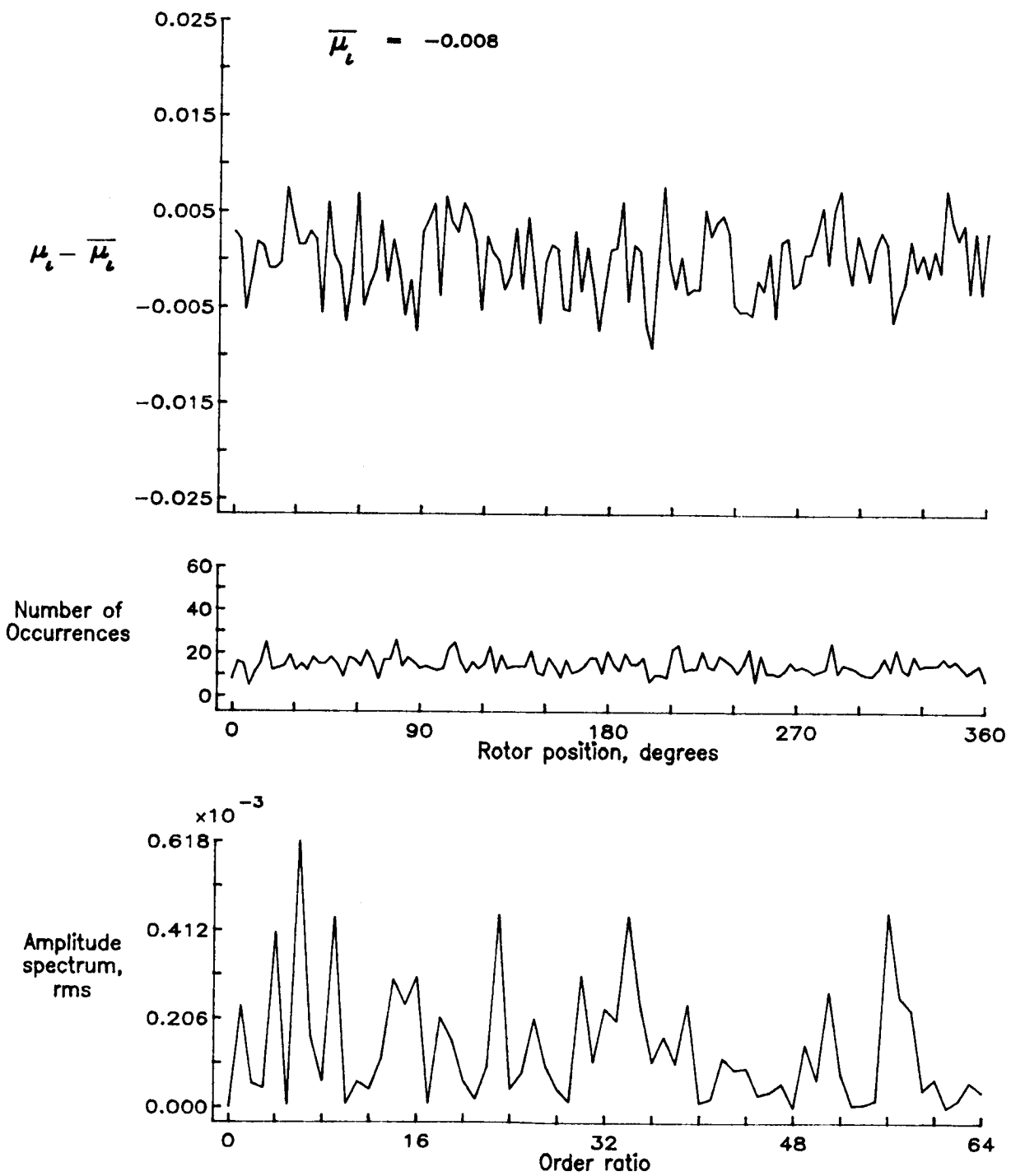


Figure 40.— Induced inflow velocity measured at 30 degrees and r/R of 1.10.

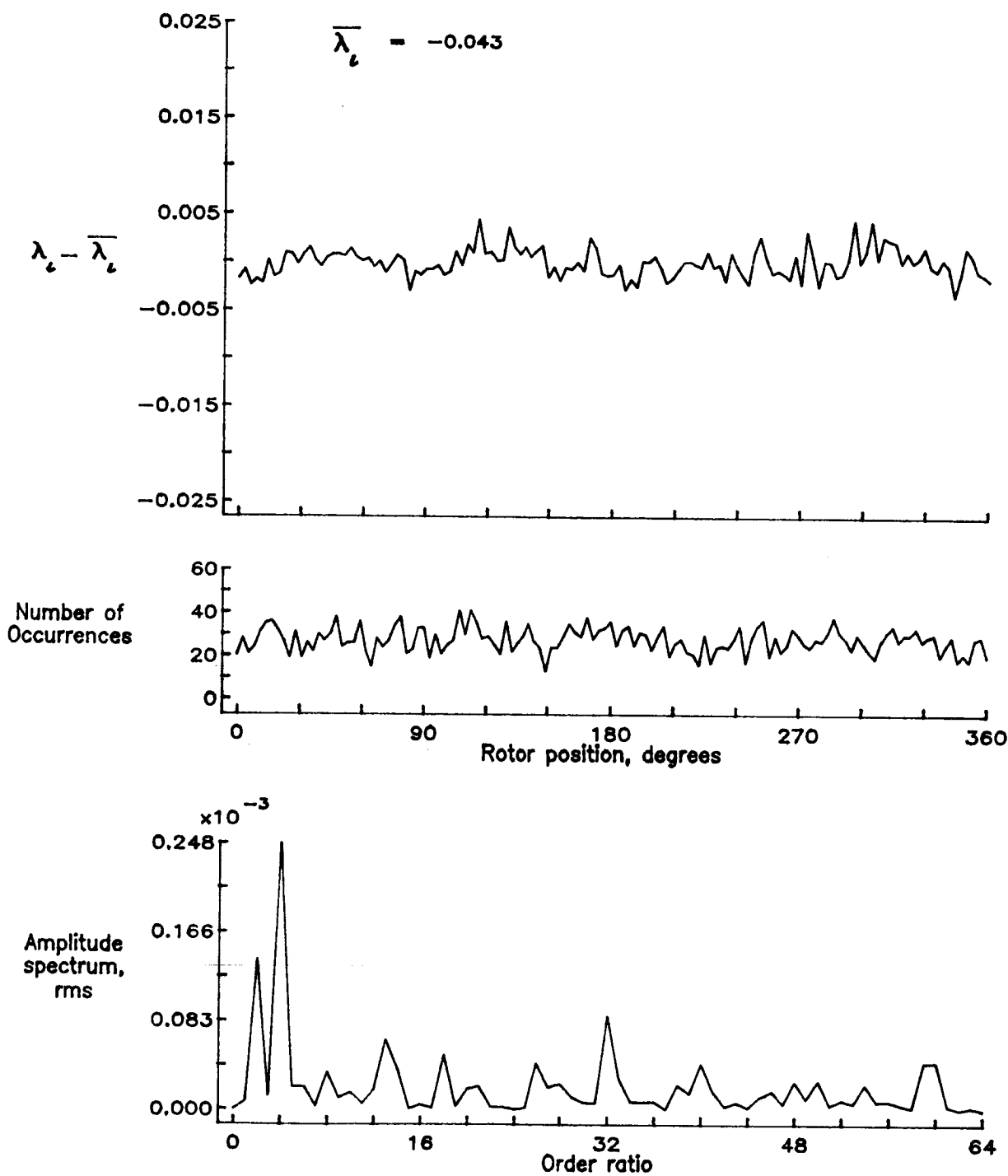


Figure 40.— Concluded.

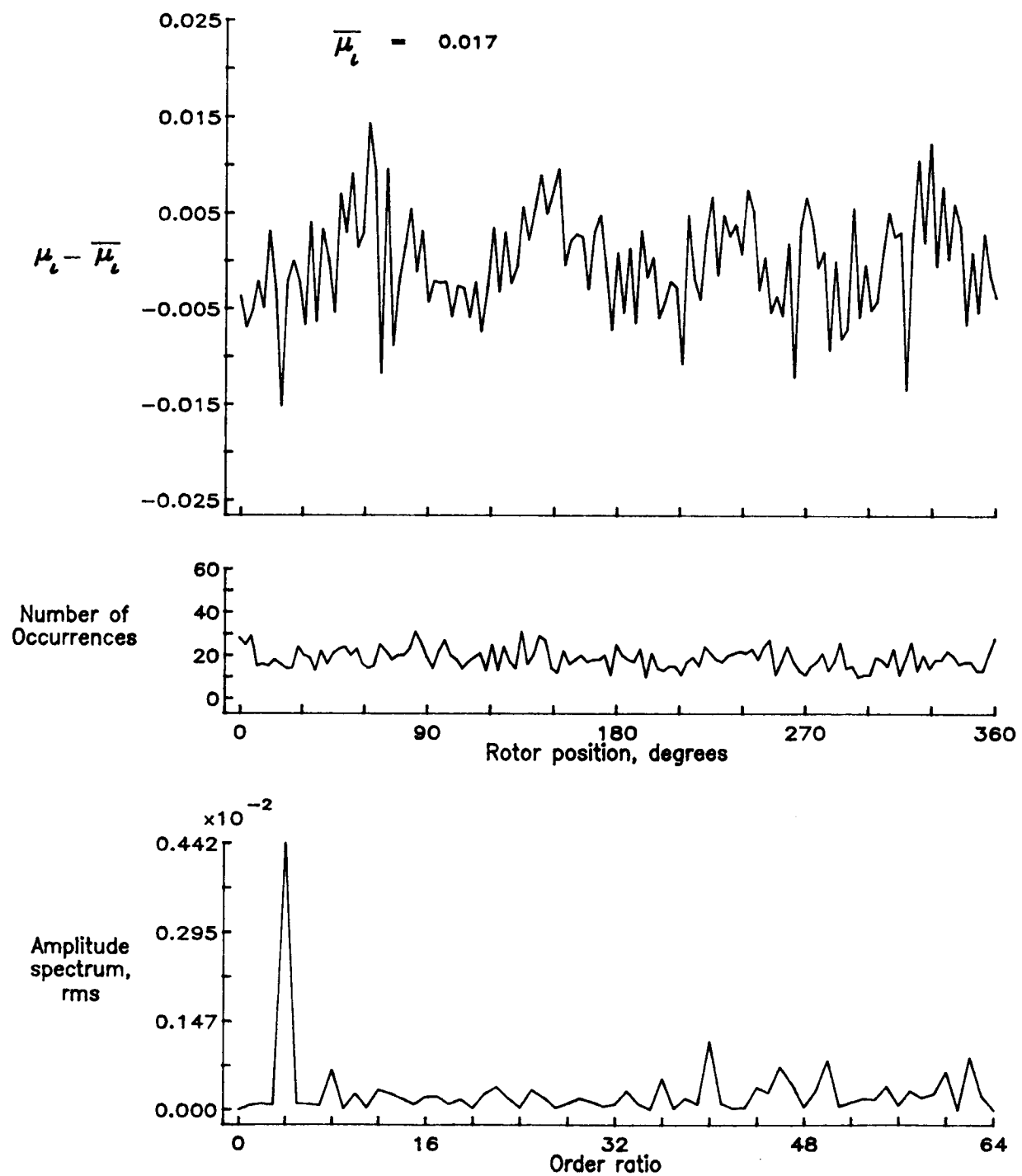


Figure 41.— Induced inflow velocity measured at 60 degrees and  $r/R$  of 0.20.

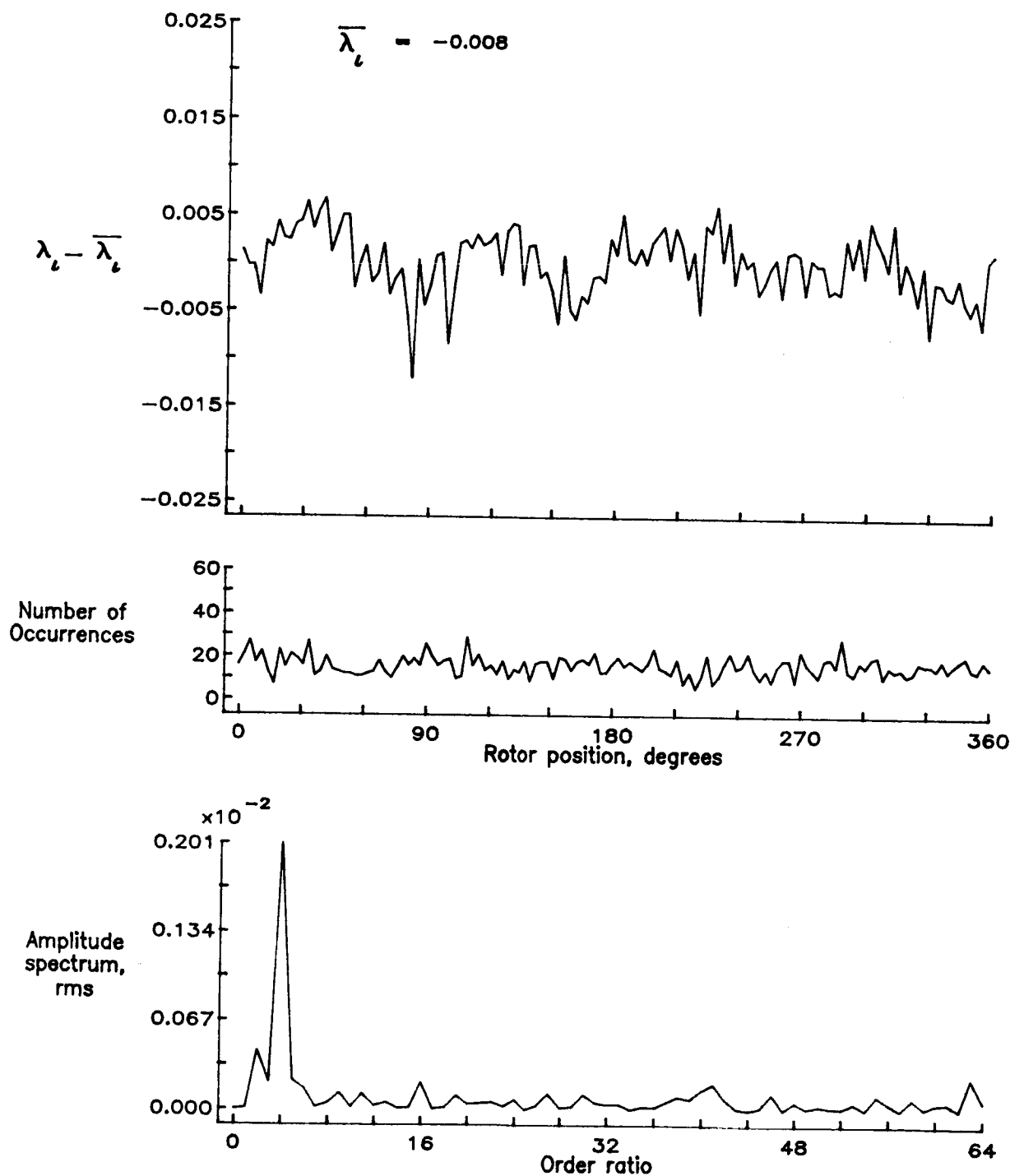


Figure 41.— Concluded.

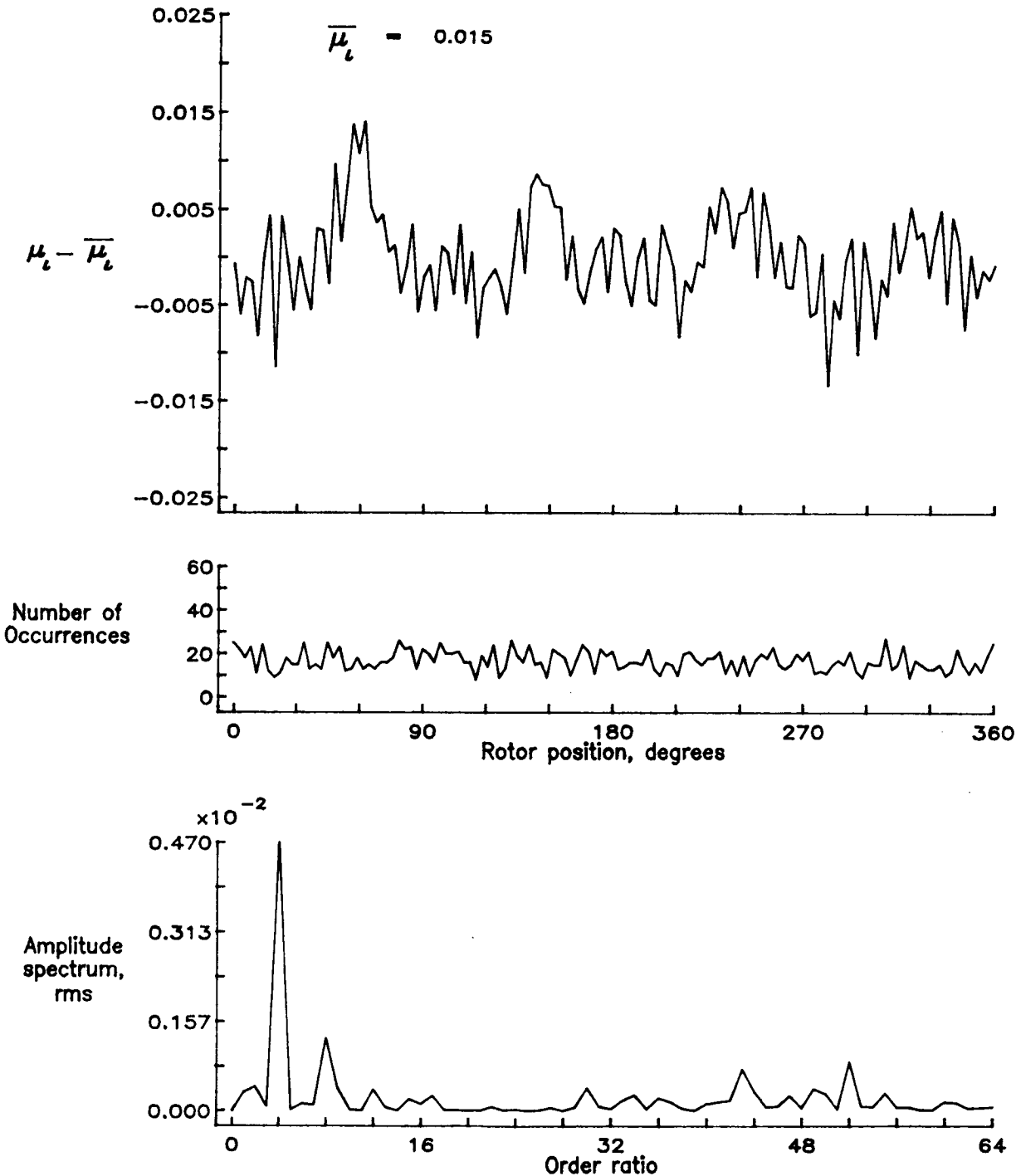


Figure 42.— Induced inflow velocity measured at 60 degrees and  $r/R$  of 0.40.

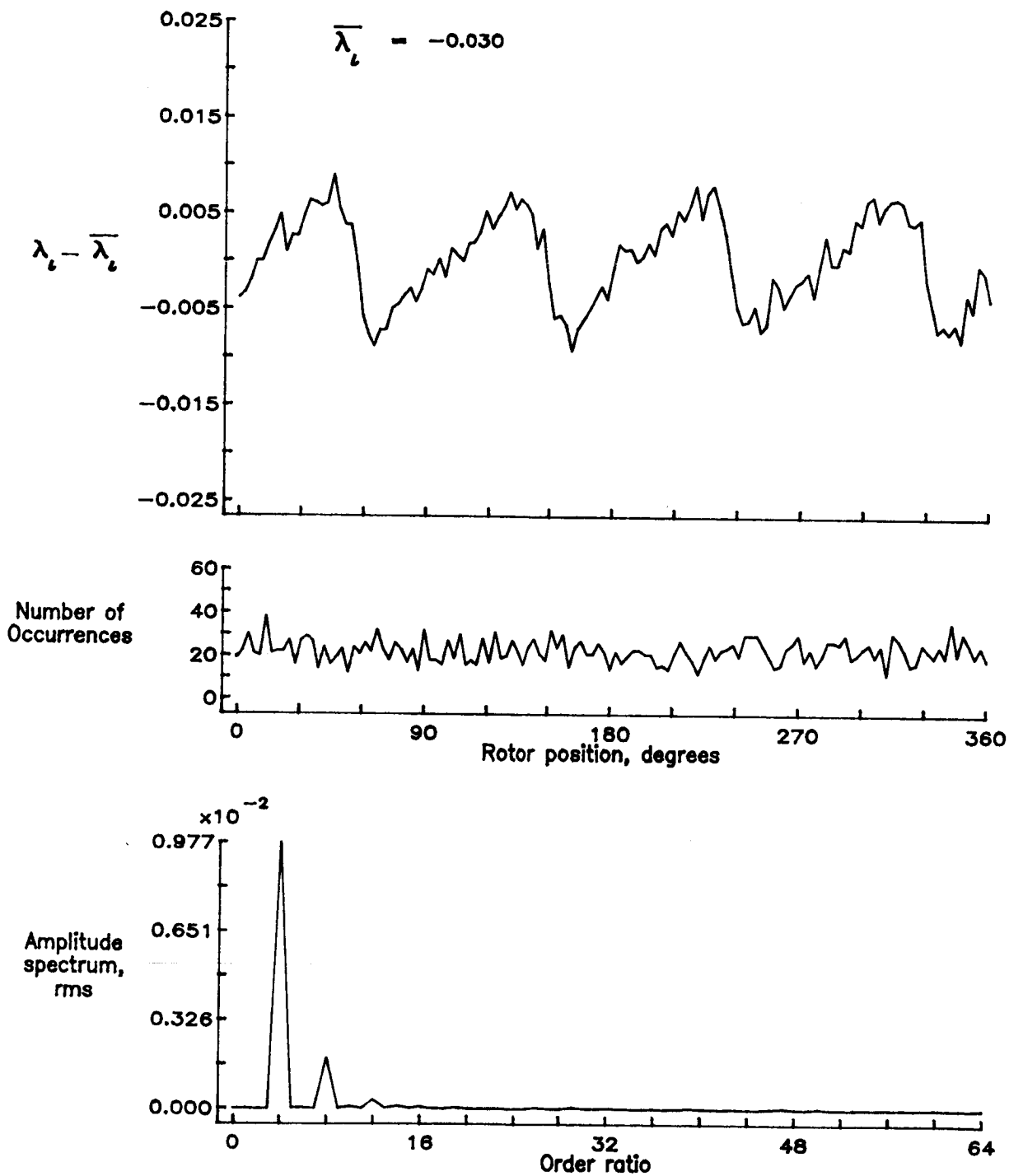


Figure 42.— Concluded.

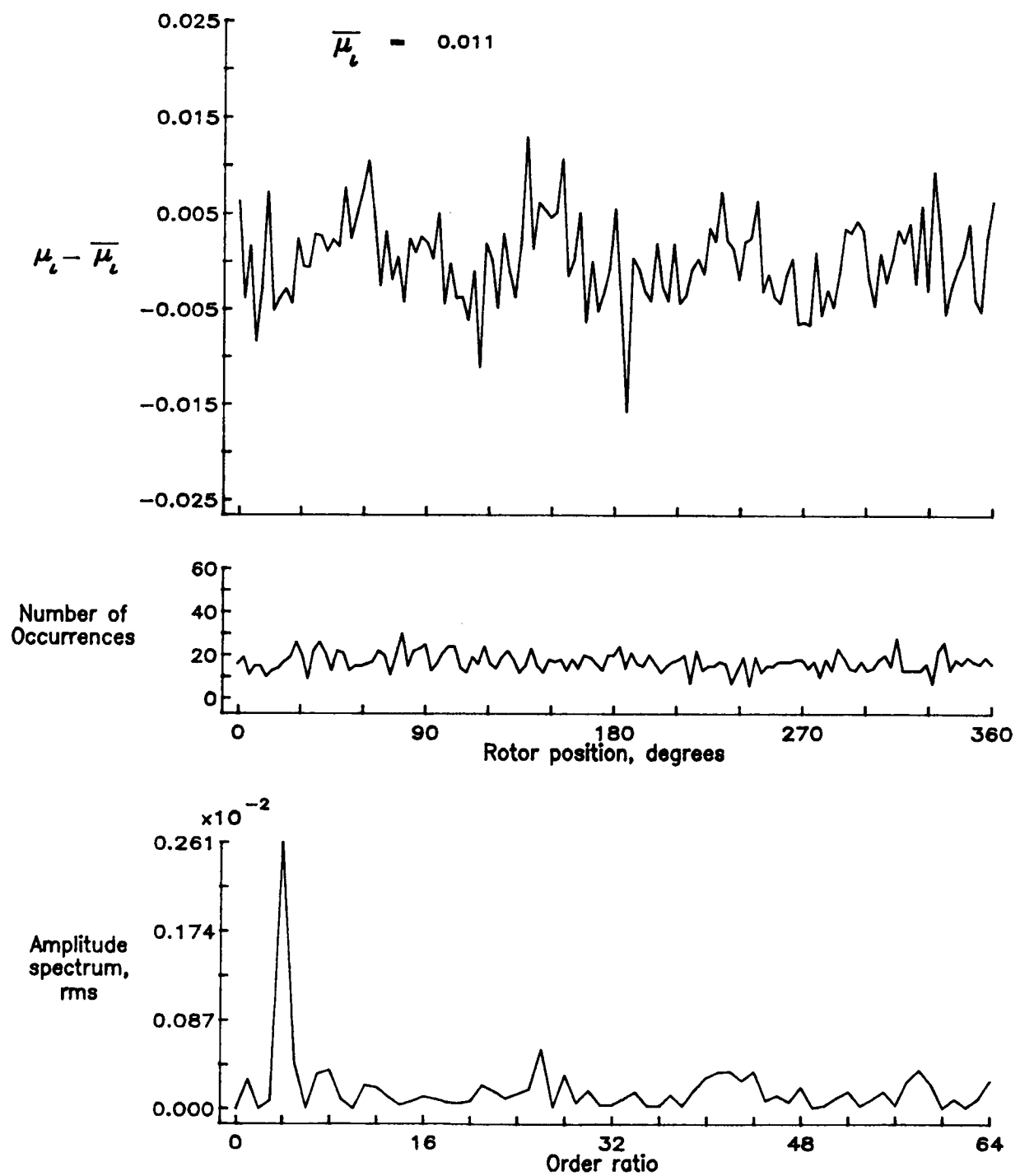


Figure 43.— Induced inflow velocity measured at 60 degrees and r/R of 0.50.

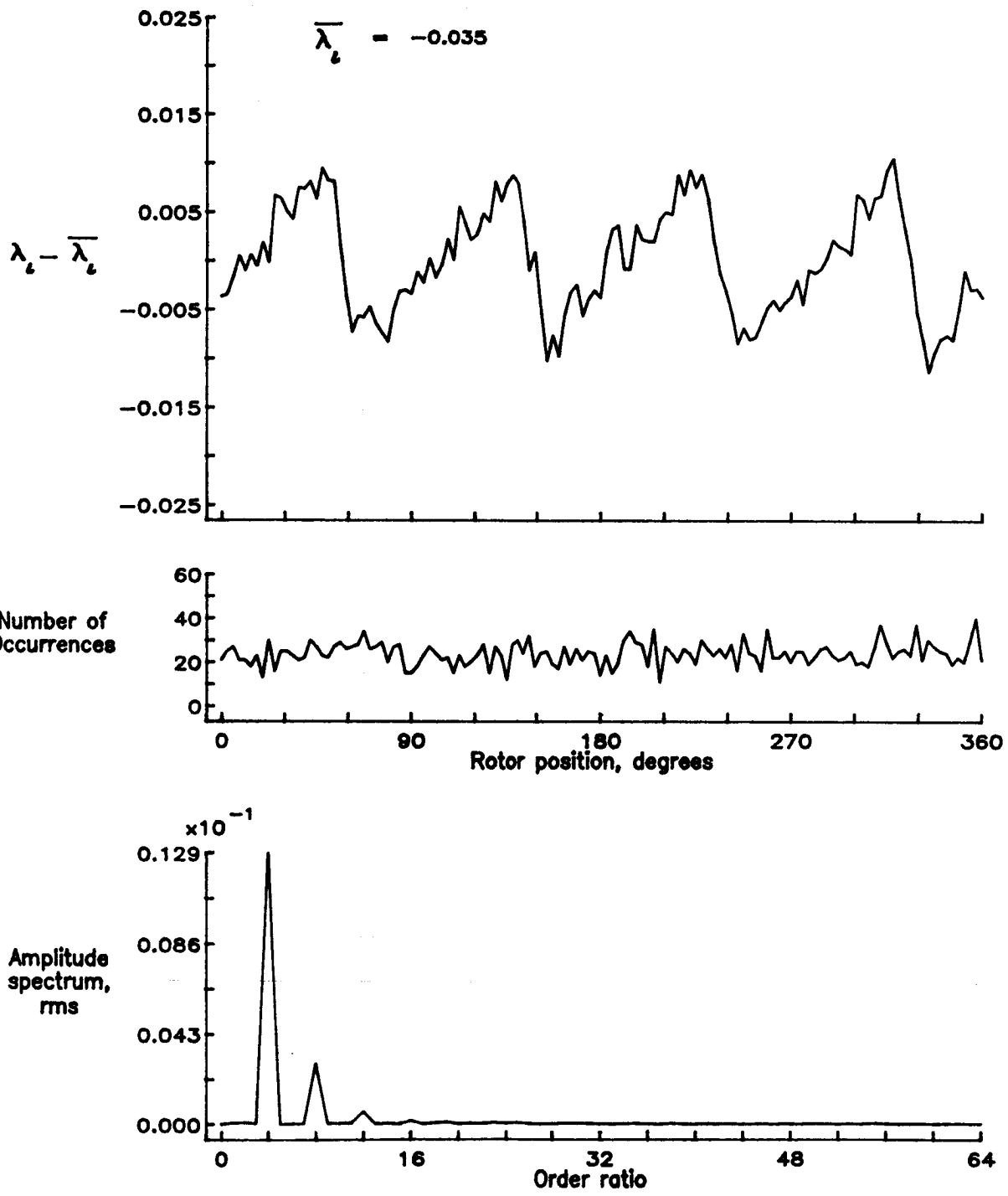


Figure 43.— Concluded.

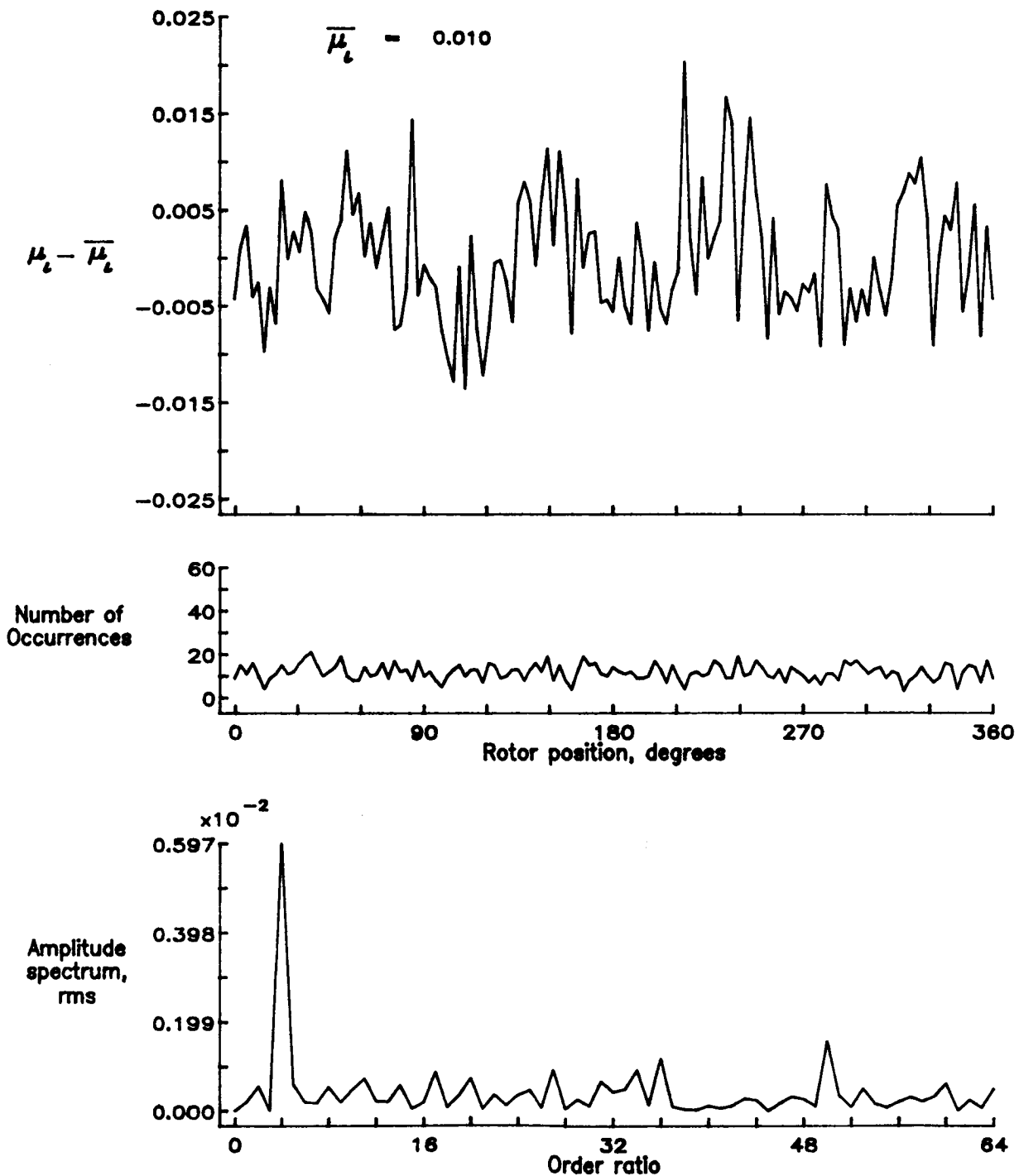


Figure 44.— Induced inflow velocity measured at 60 degrees and  $r/R$  of 0.60.

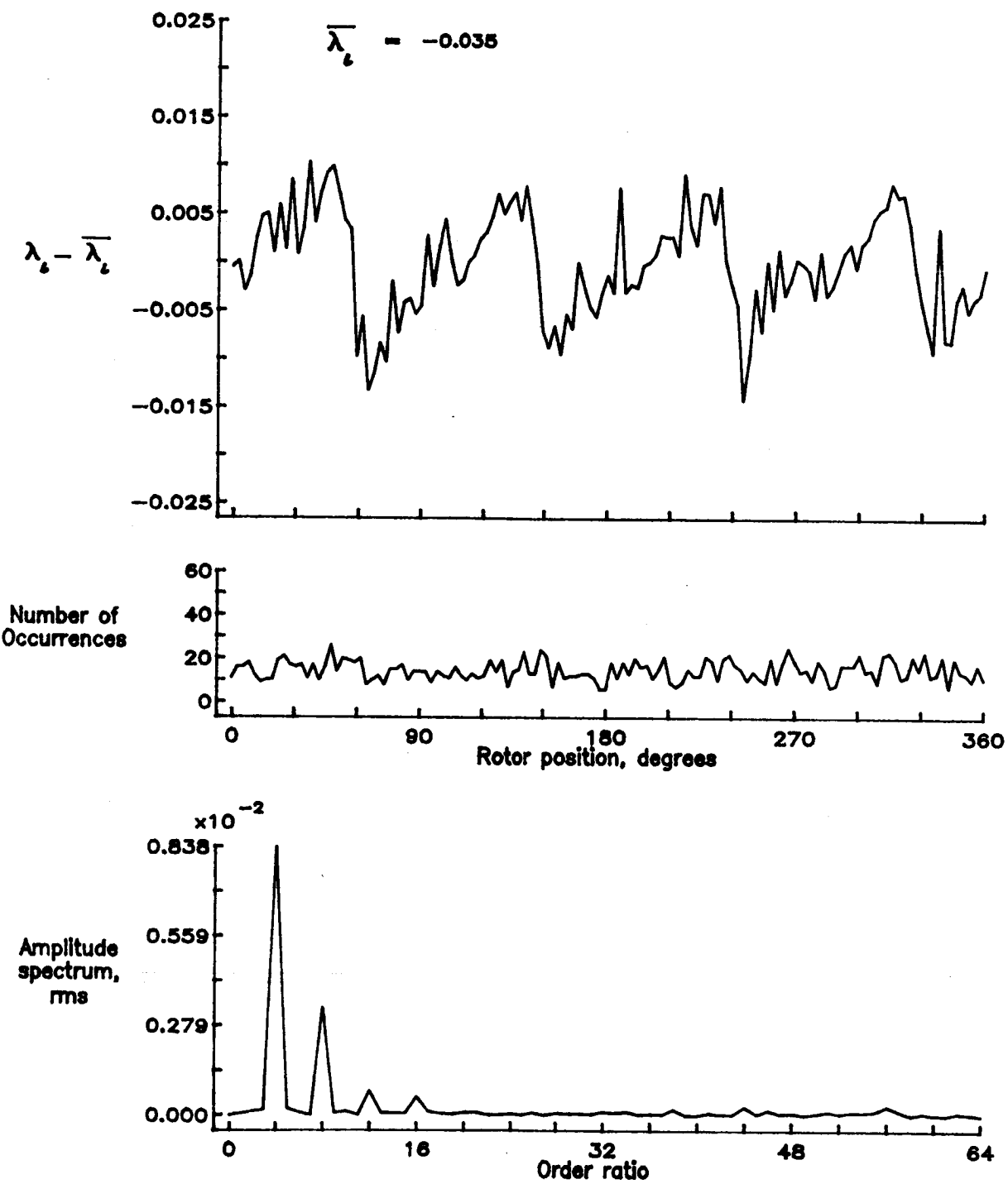


Figure 44.— Concluded.

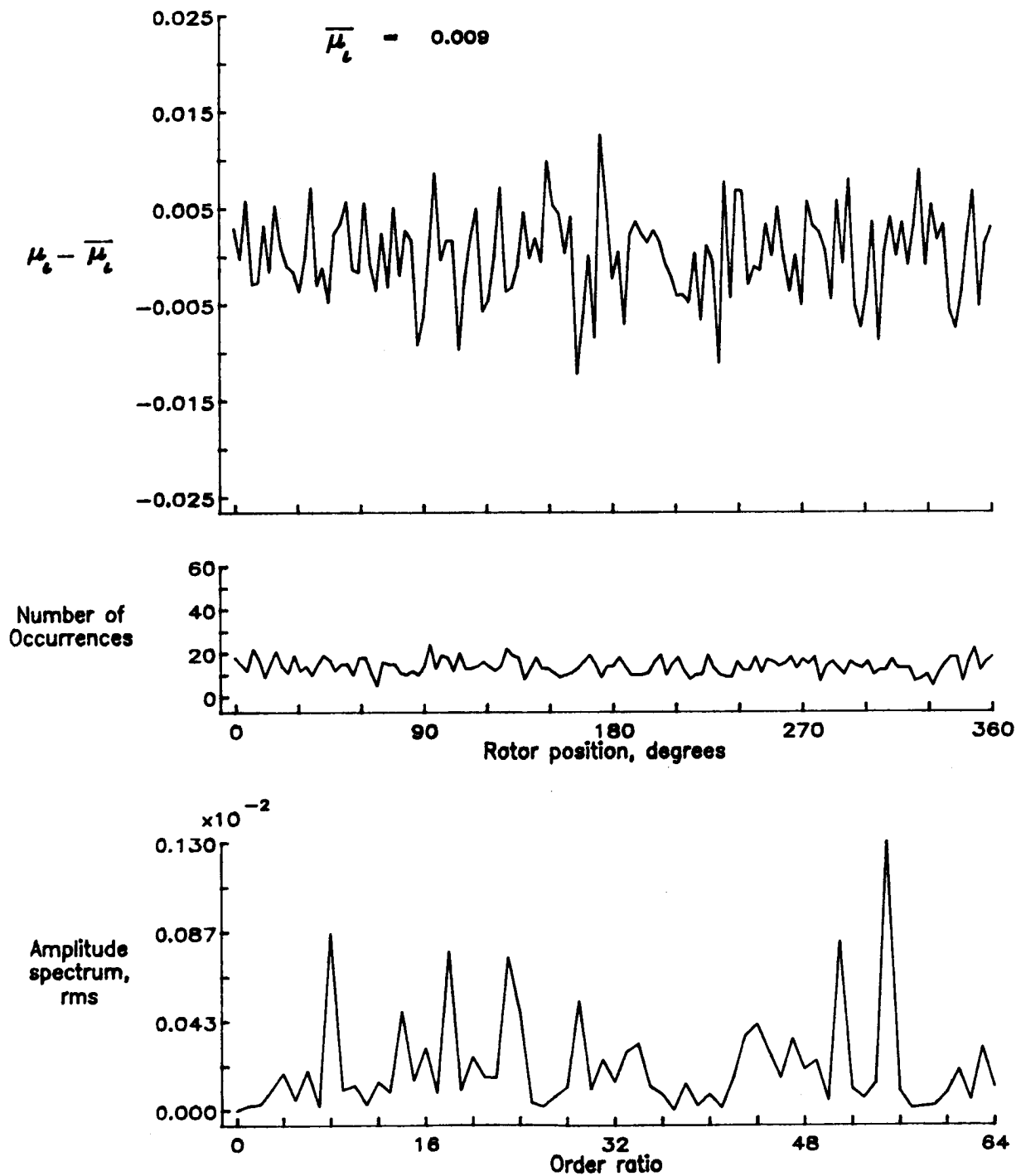


Figure 45.— Induced inflow velocity measured at 60 degrees and r/R of 0.70.

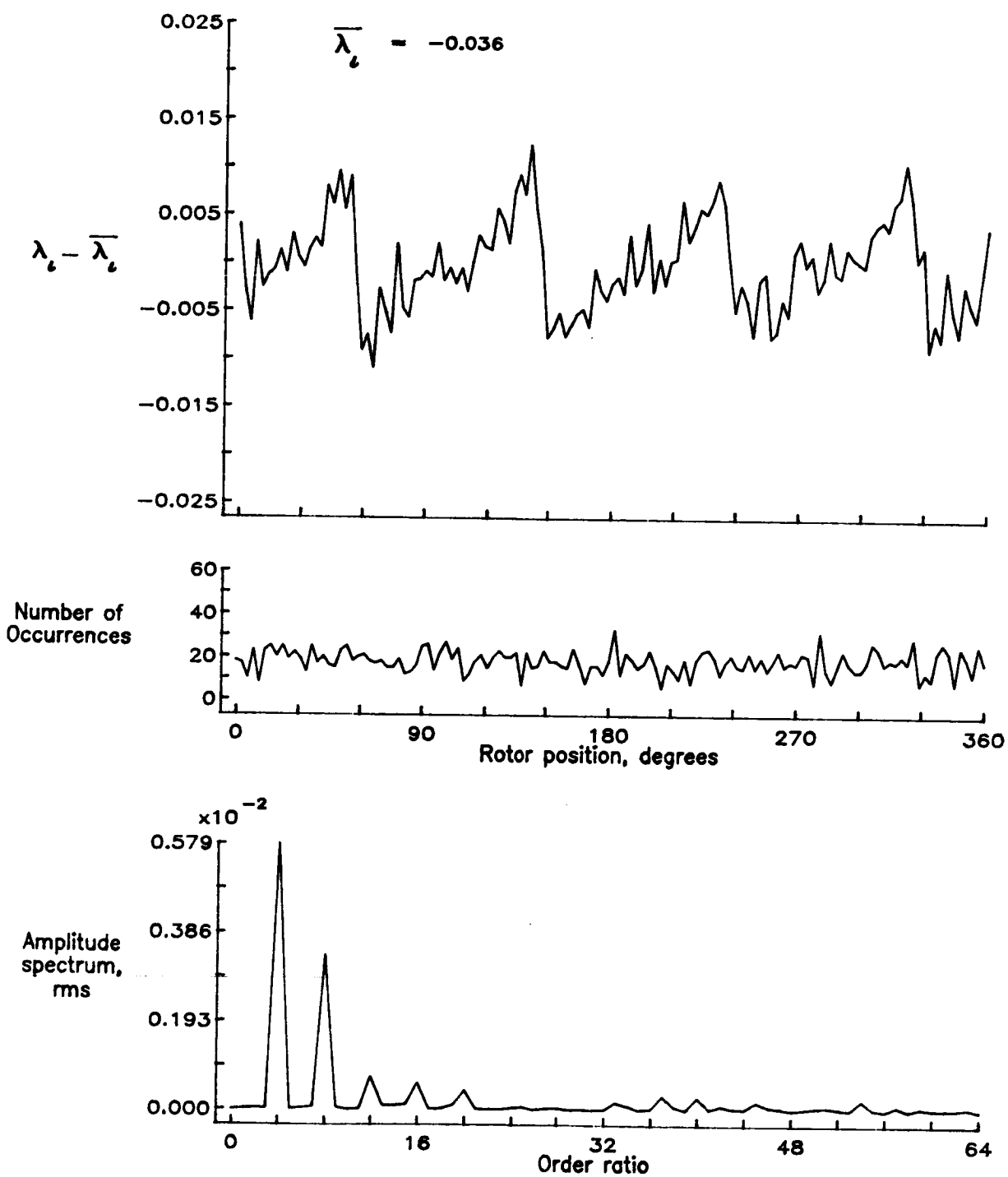


Figure 45.— Concluded.

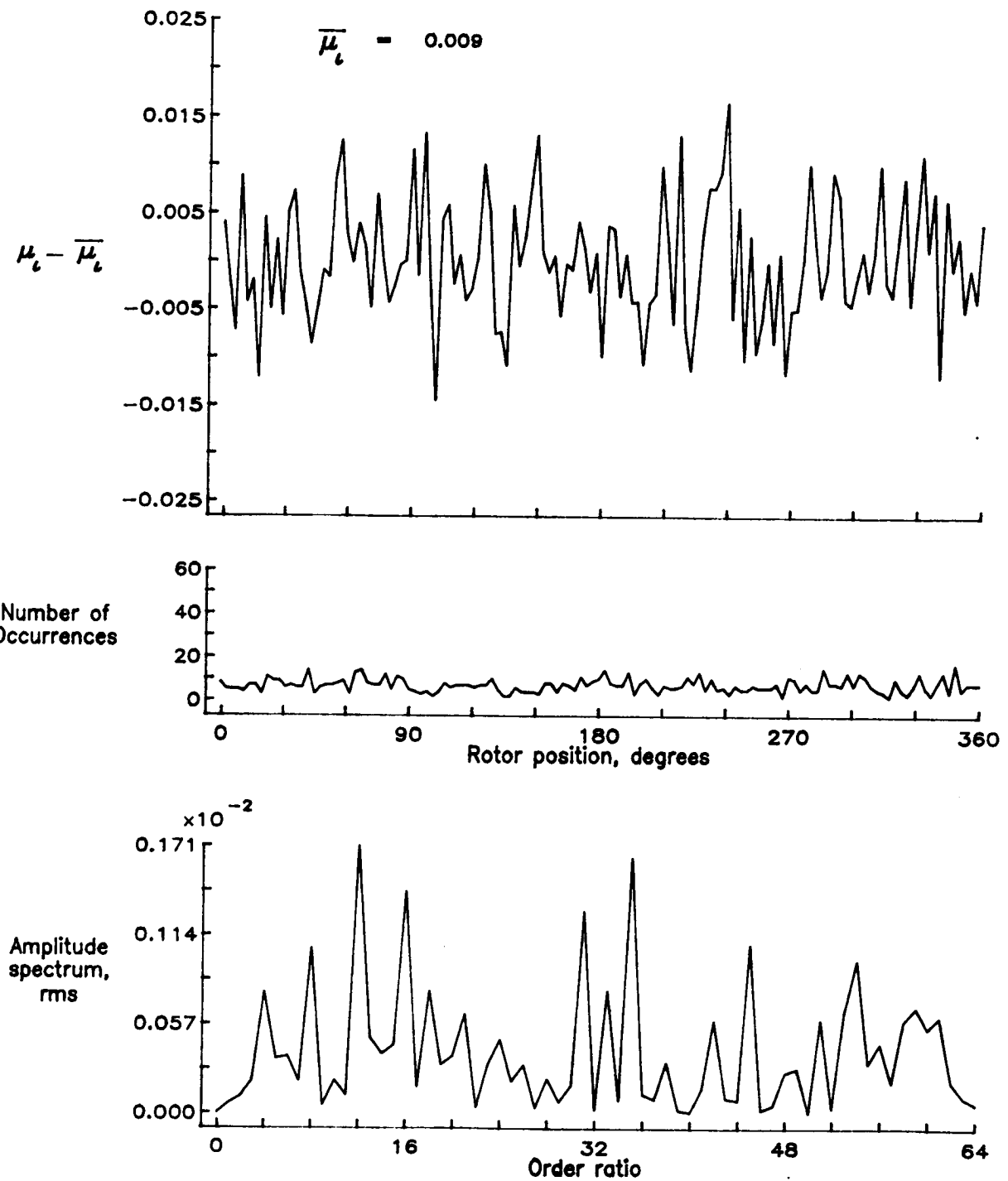


Figure 46.— Induced inflow velocity measured at 60 degrees and r/R of 0.74.

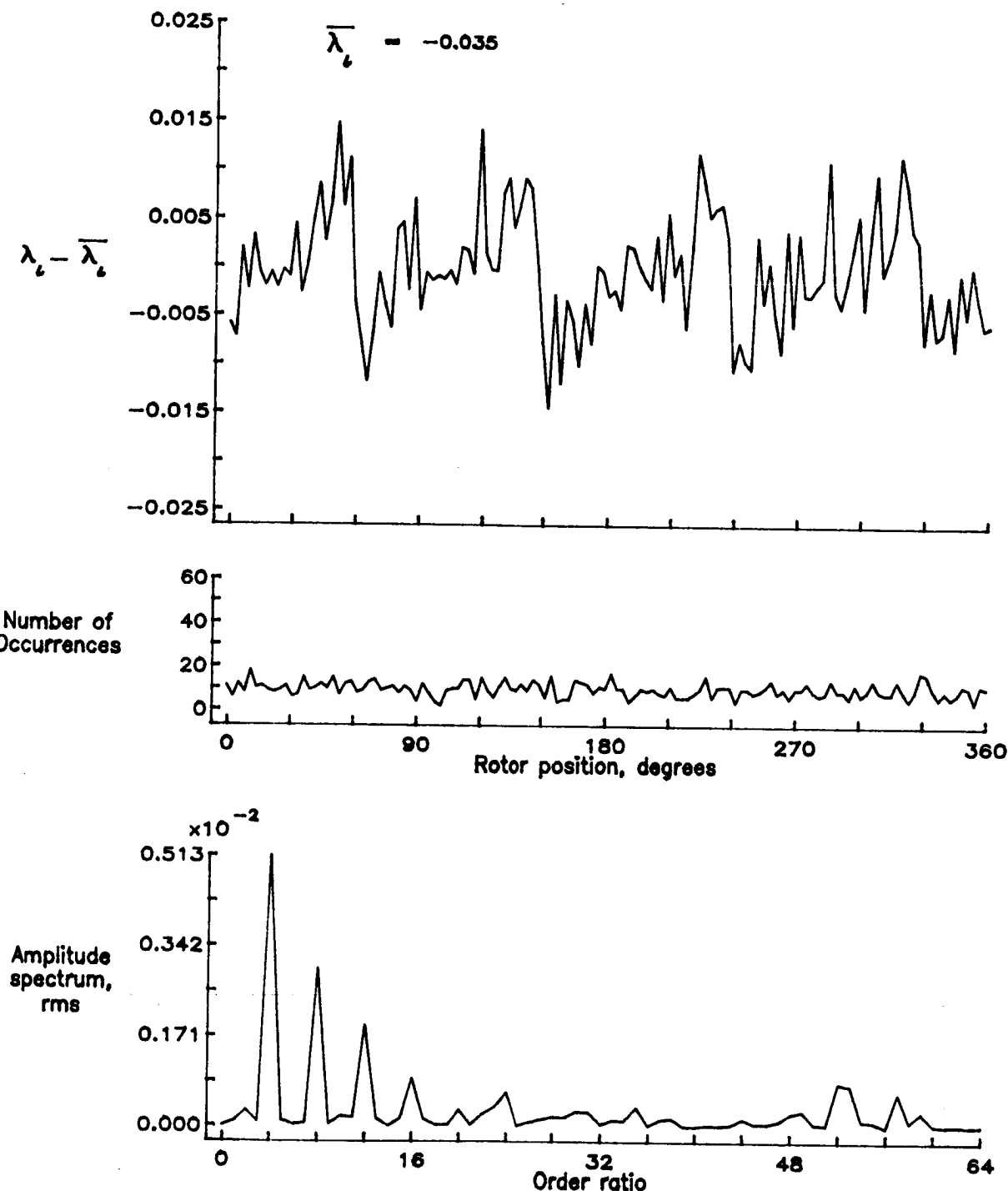


Figure 46.— Concluded.

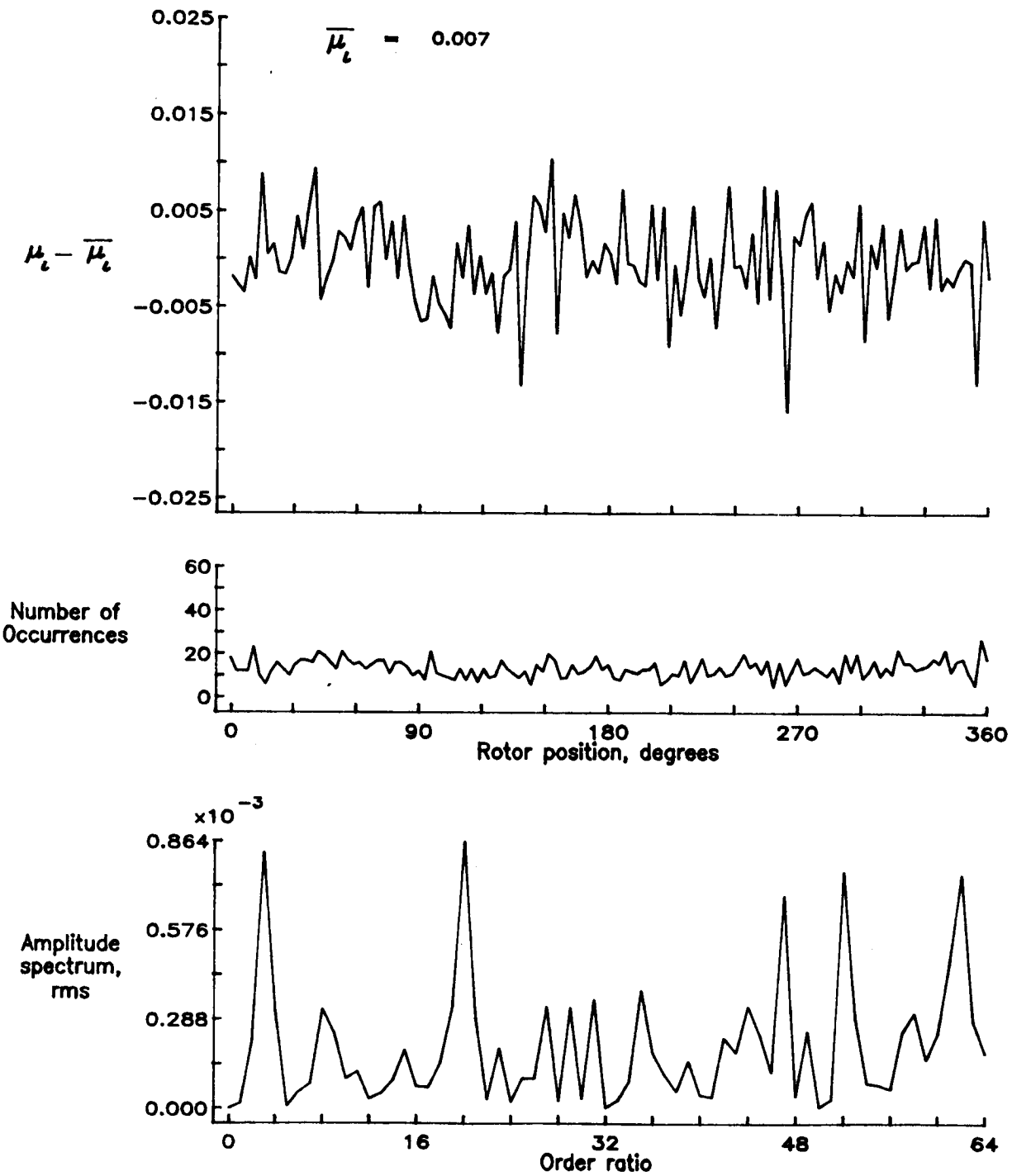


Figure 47.— Induced inflow velocity measured at 60 degrees and r/R of 0.78.

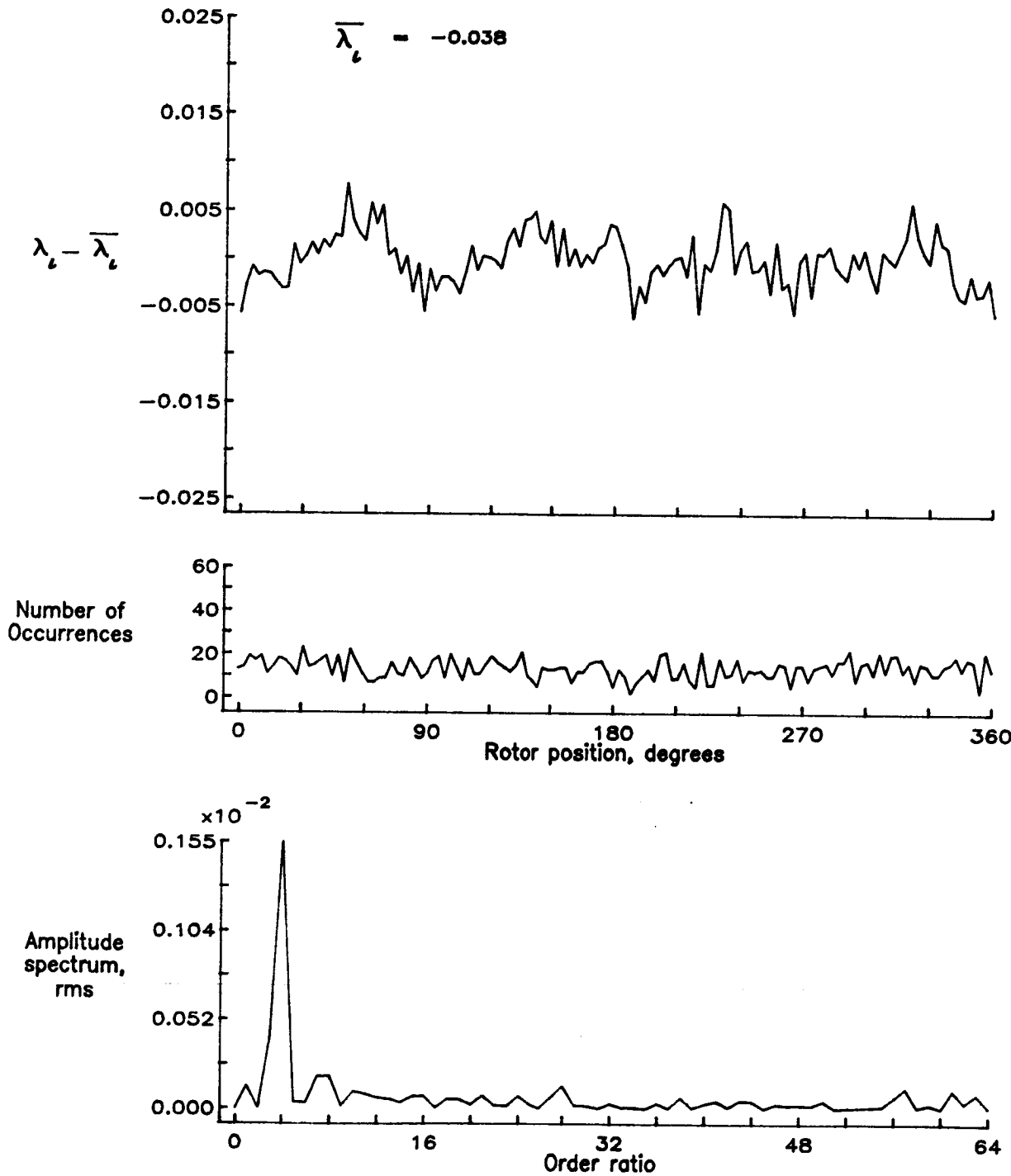


Figure 47.— Concluded.

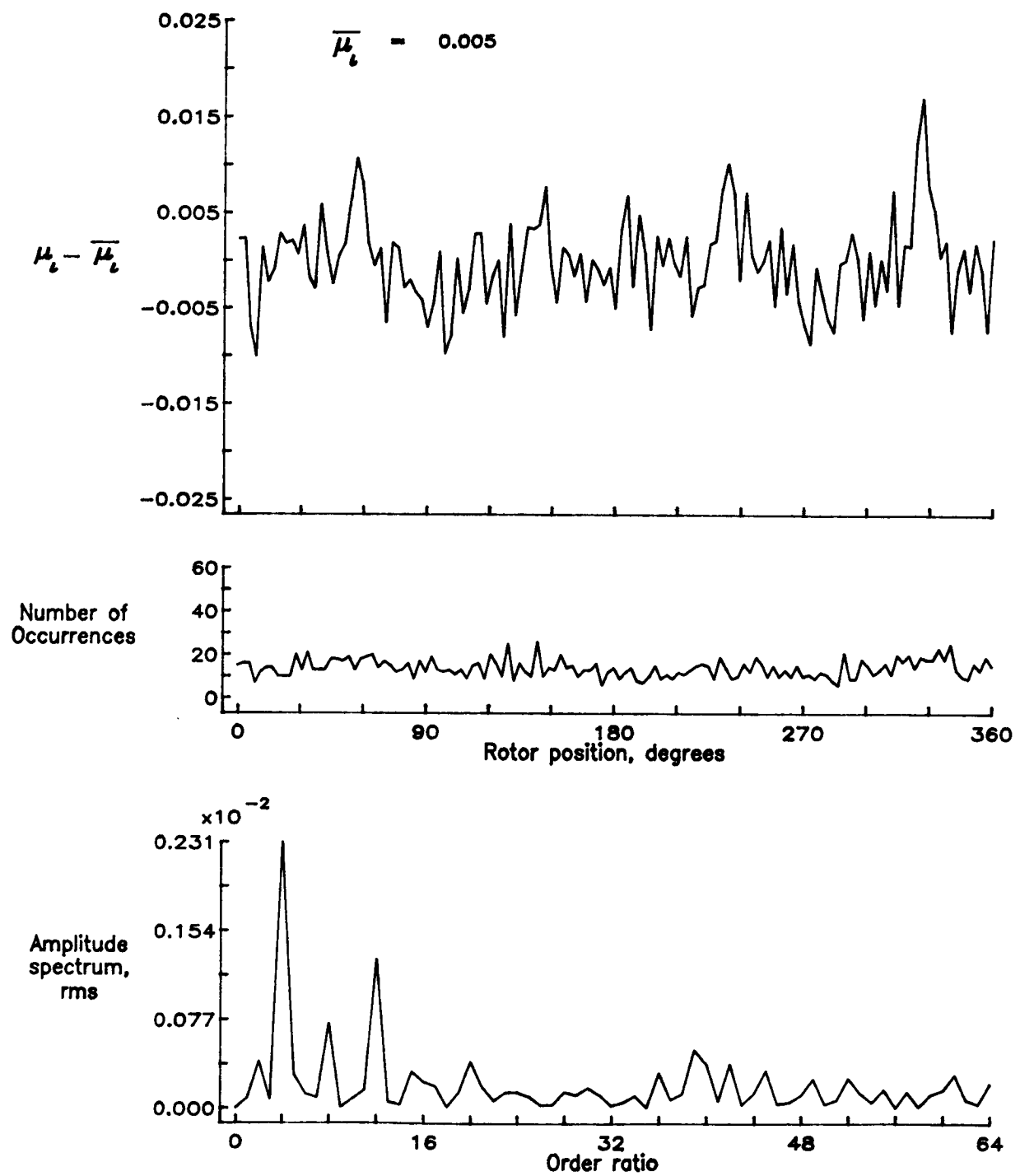


Figure 48.— Induced inflow velocity measured at 60 degrees and r/R of 0.82.

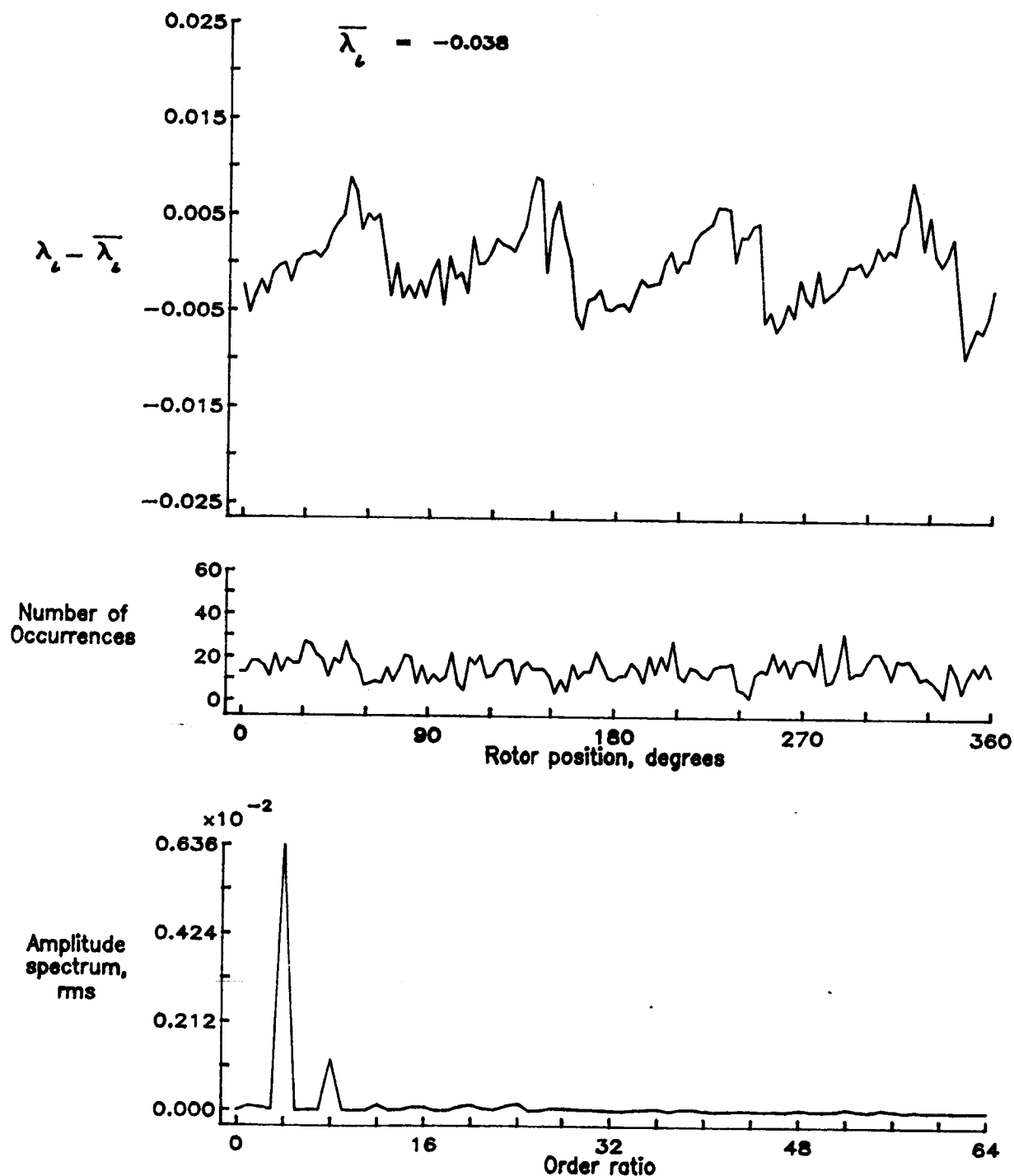


Figure 48.— Concluded.

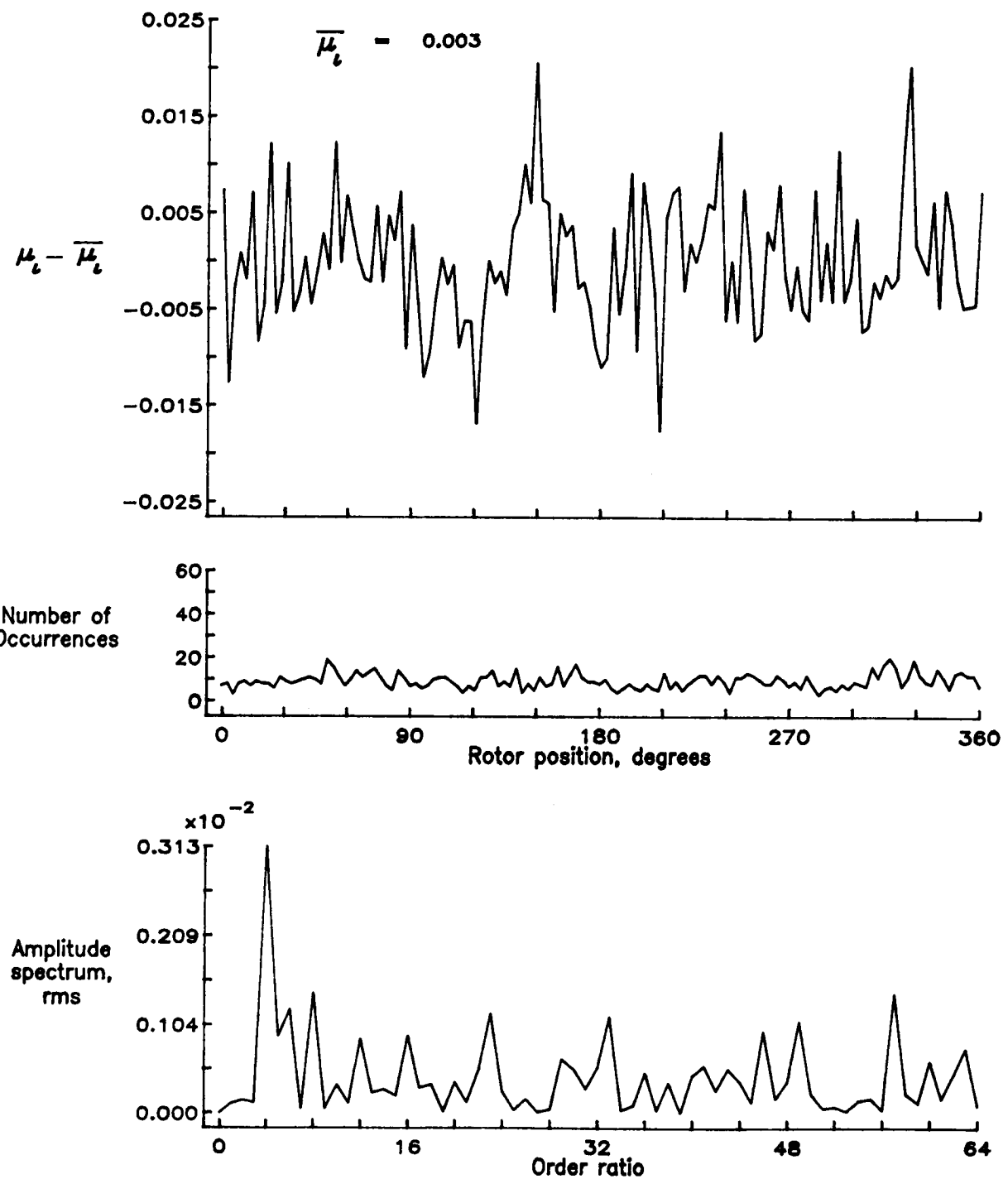


Figure 49.— Induced inflow velocity measured at 60 degrees and r/R of 0.86.

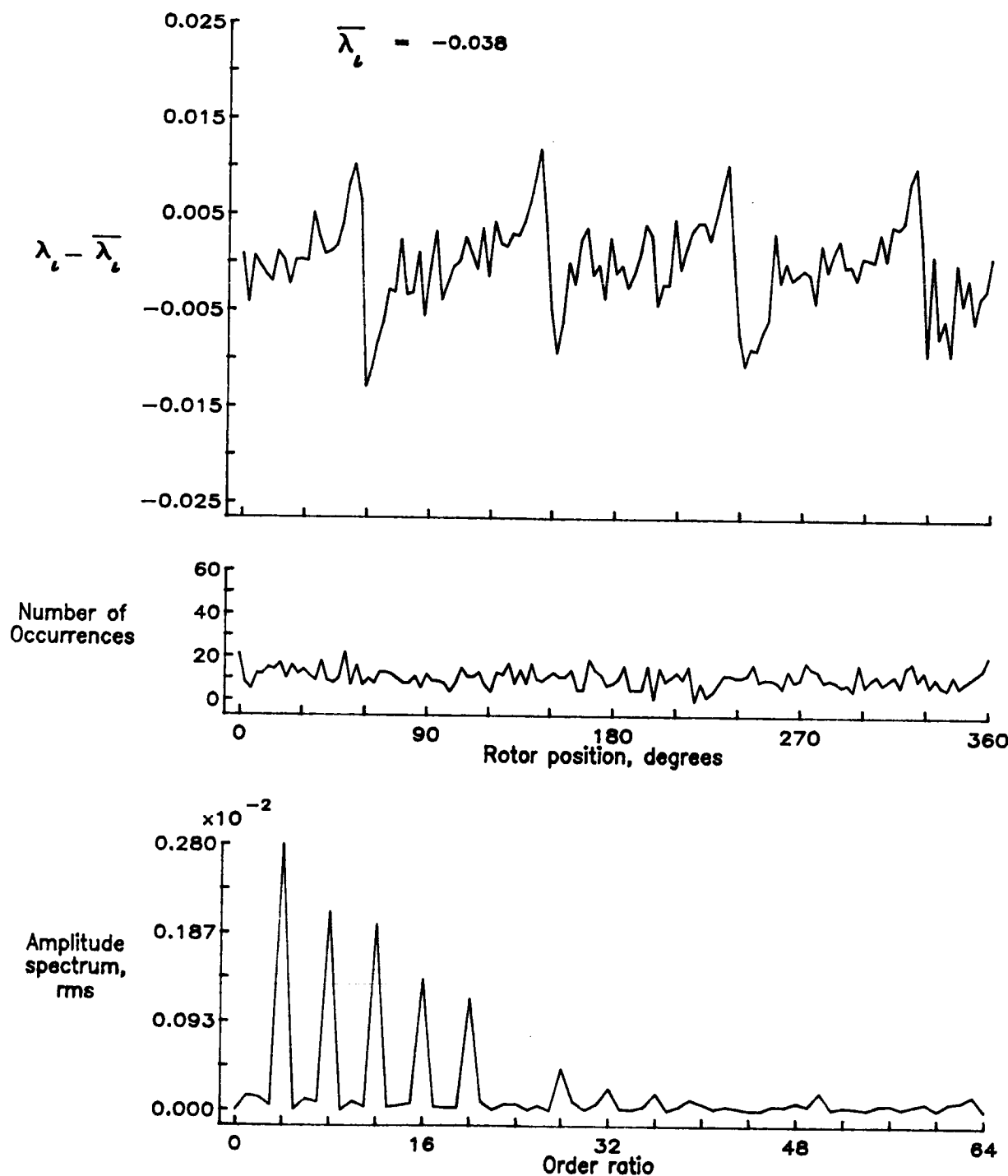


Figure 49.— Concluded.

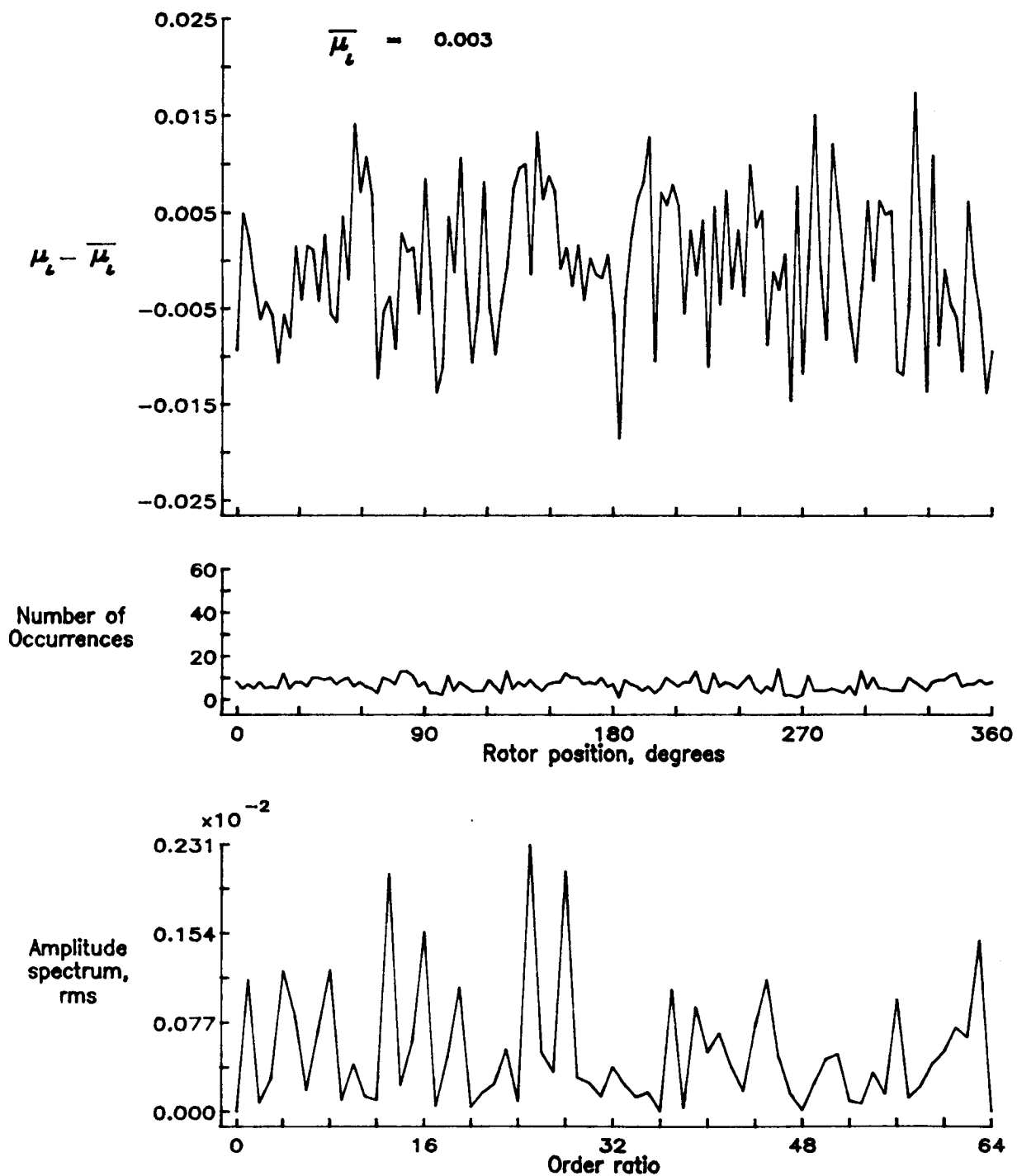


Figure 50.— Induced inflow velocity measured at 60 degrees and r/R of 0.90.

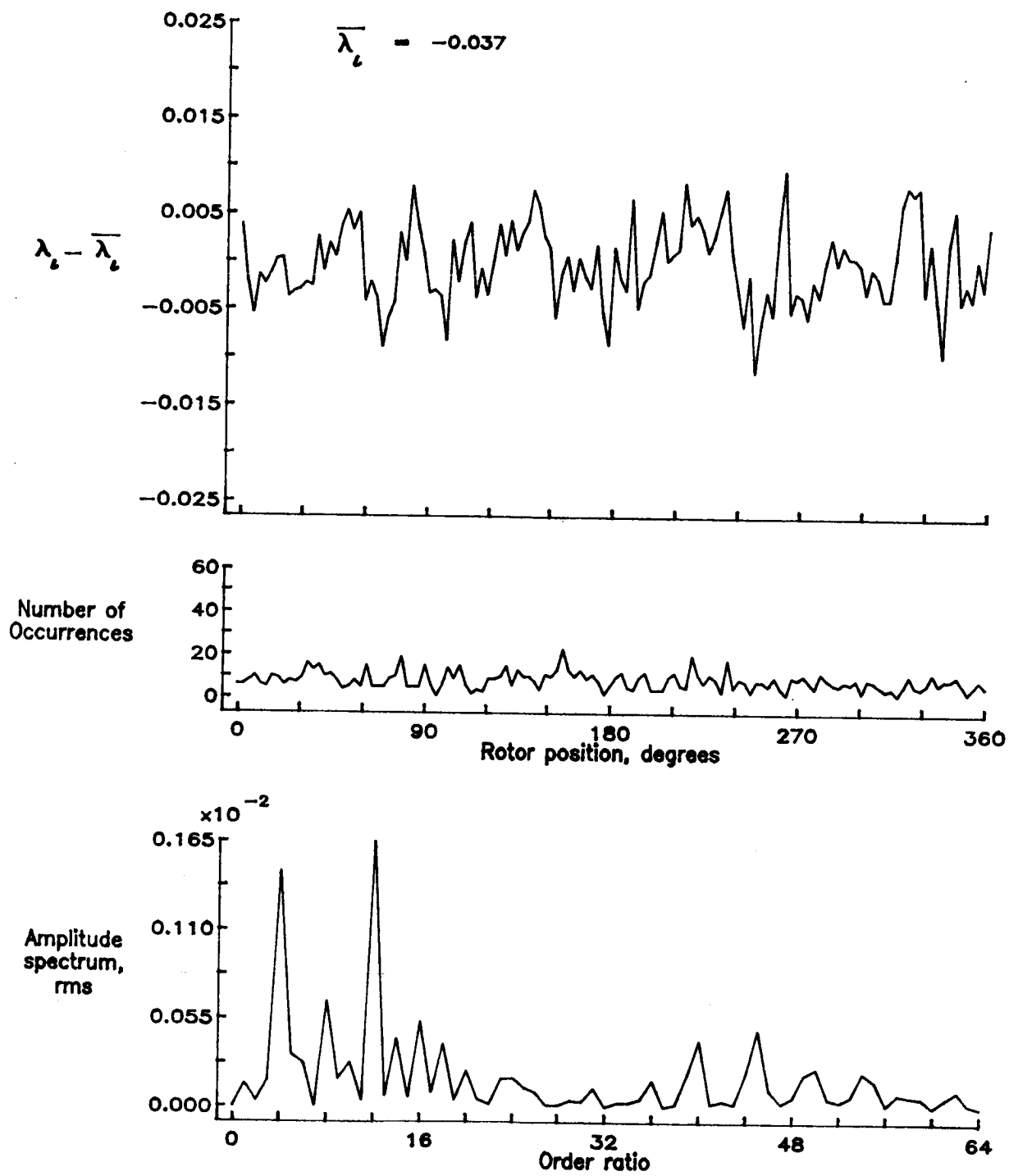


Figure 50.— Concluded.

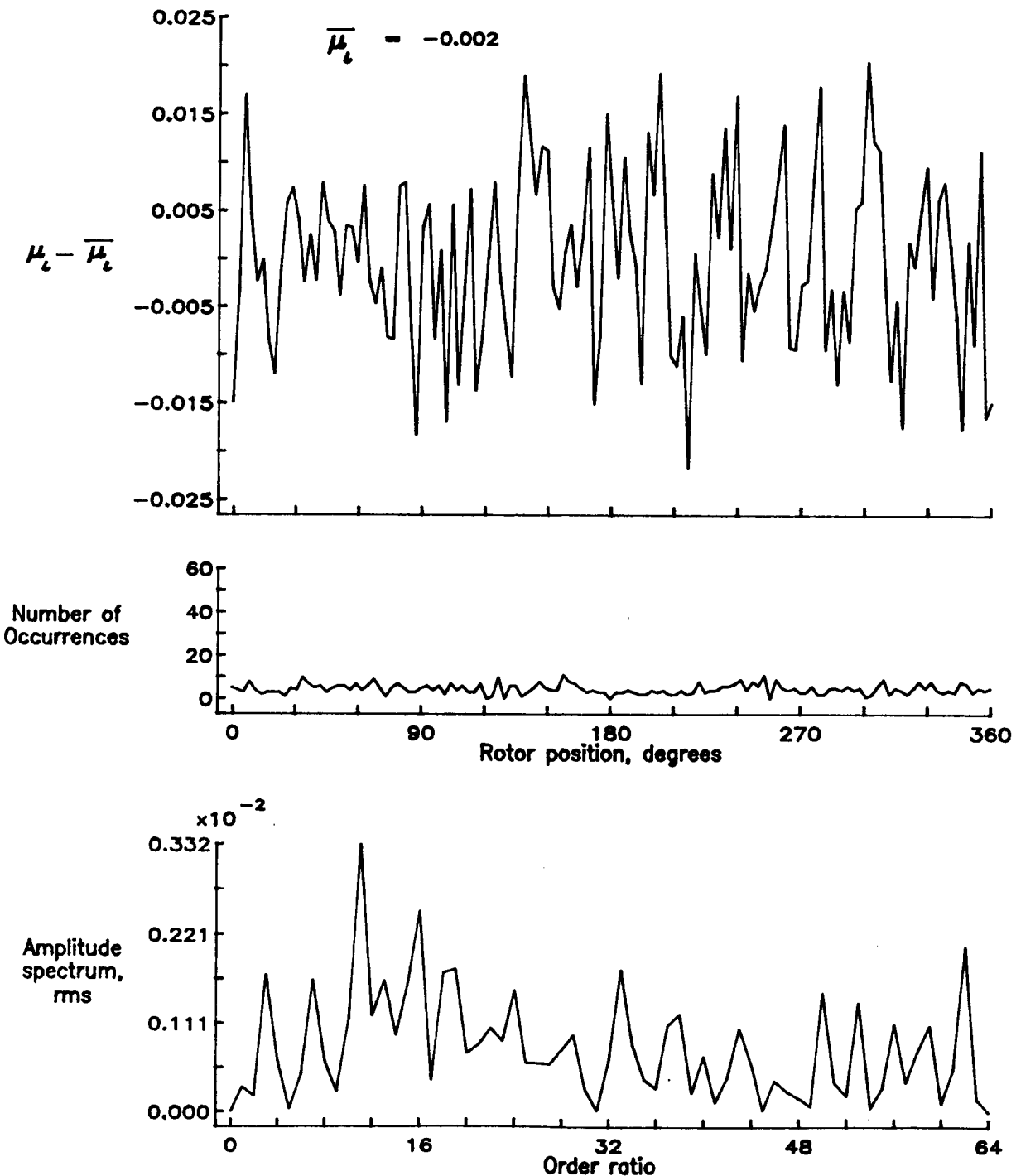


Figure 51.— Induced inflow velocity measured at 60 degrees and r/R of 0.94.

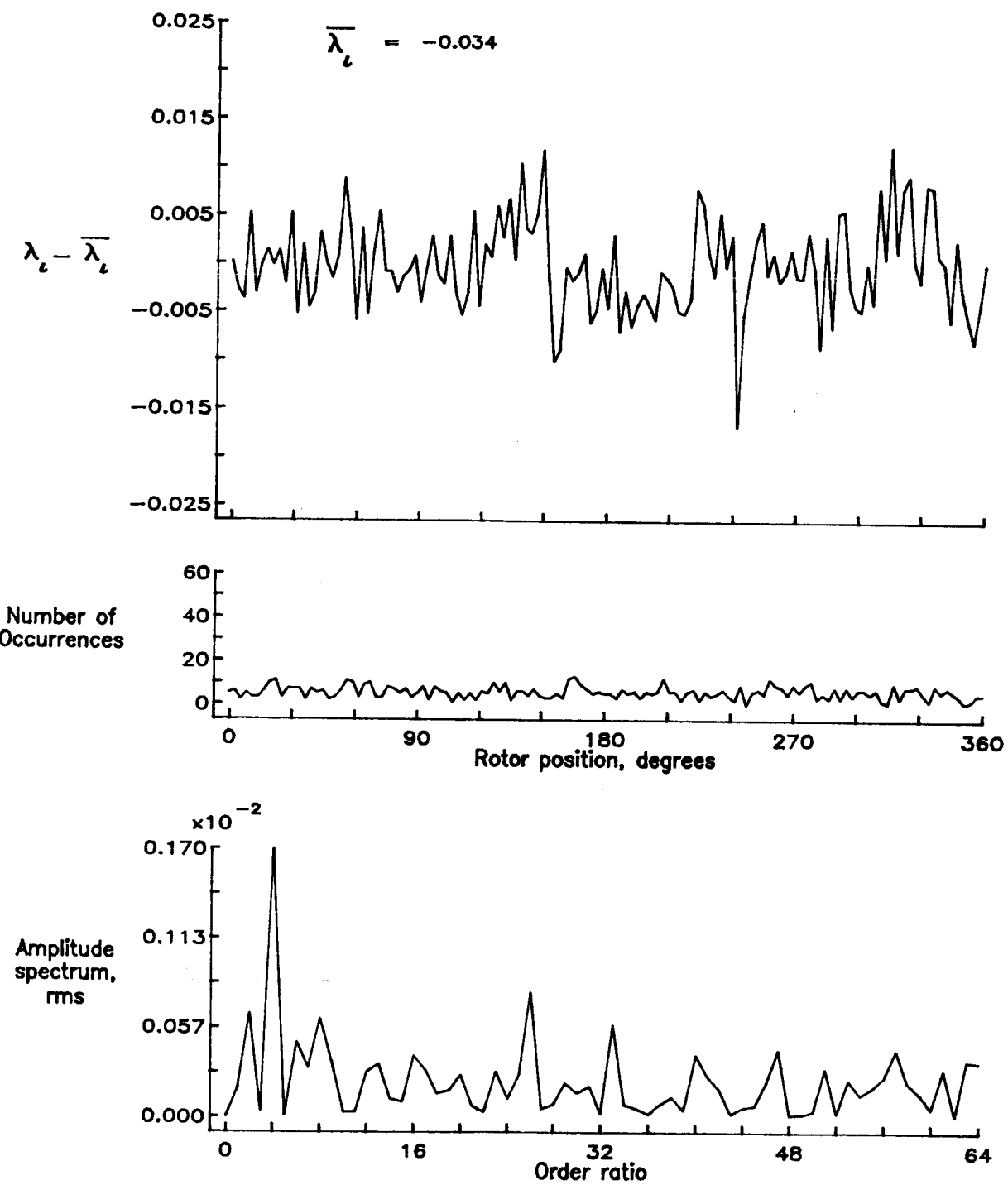


Figure 51.— Concluded.

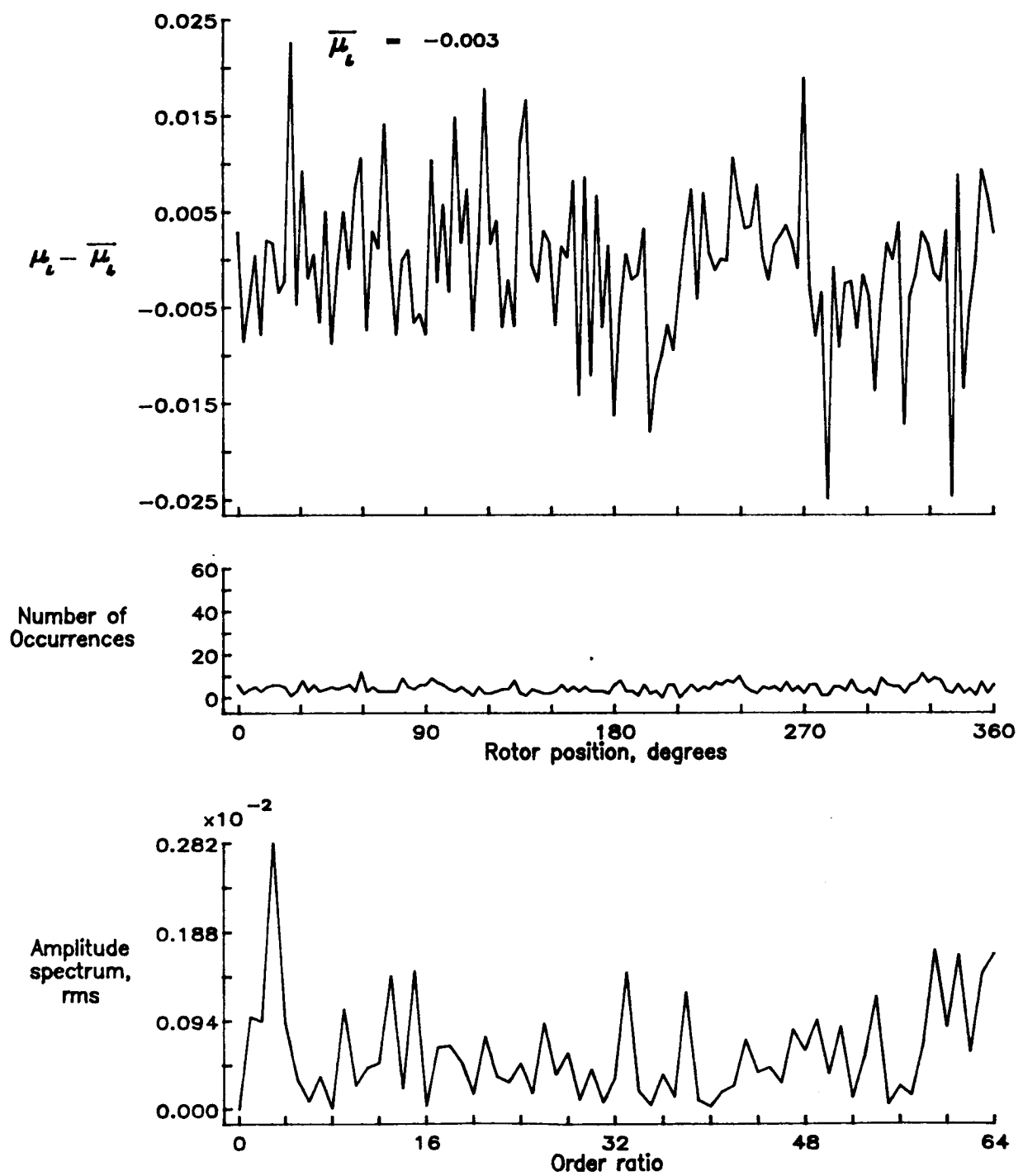


Figure 52.— Induced inflow velocity measured at 60 degrees and r/R of 0.98.

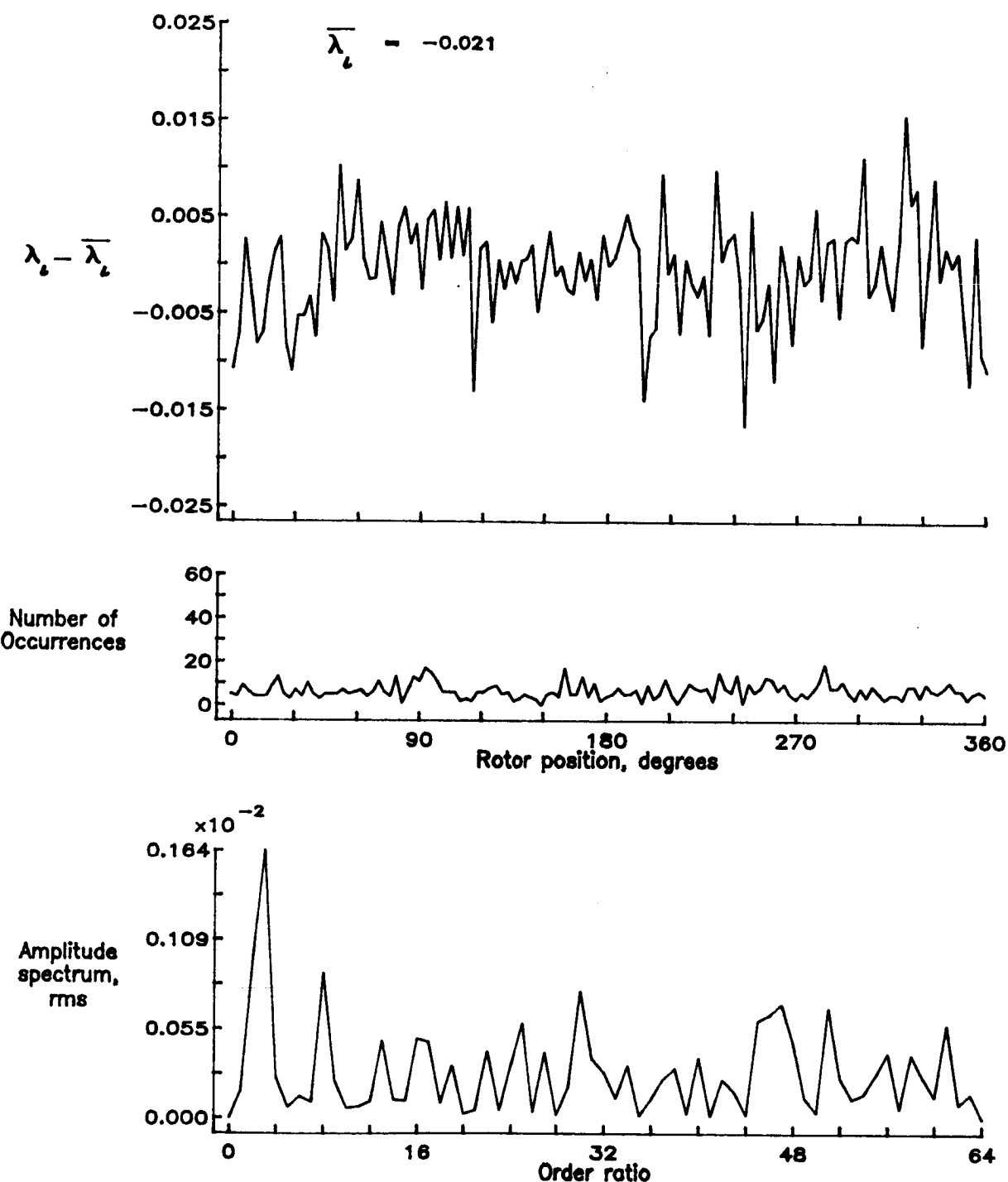


Figure 52.— Concluded.

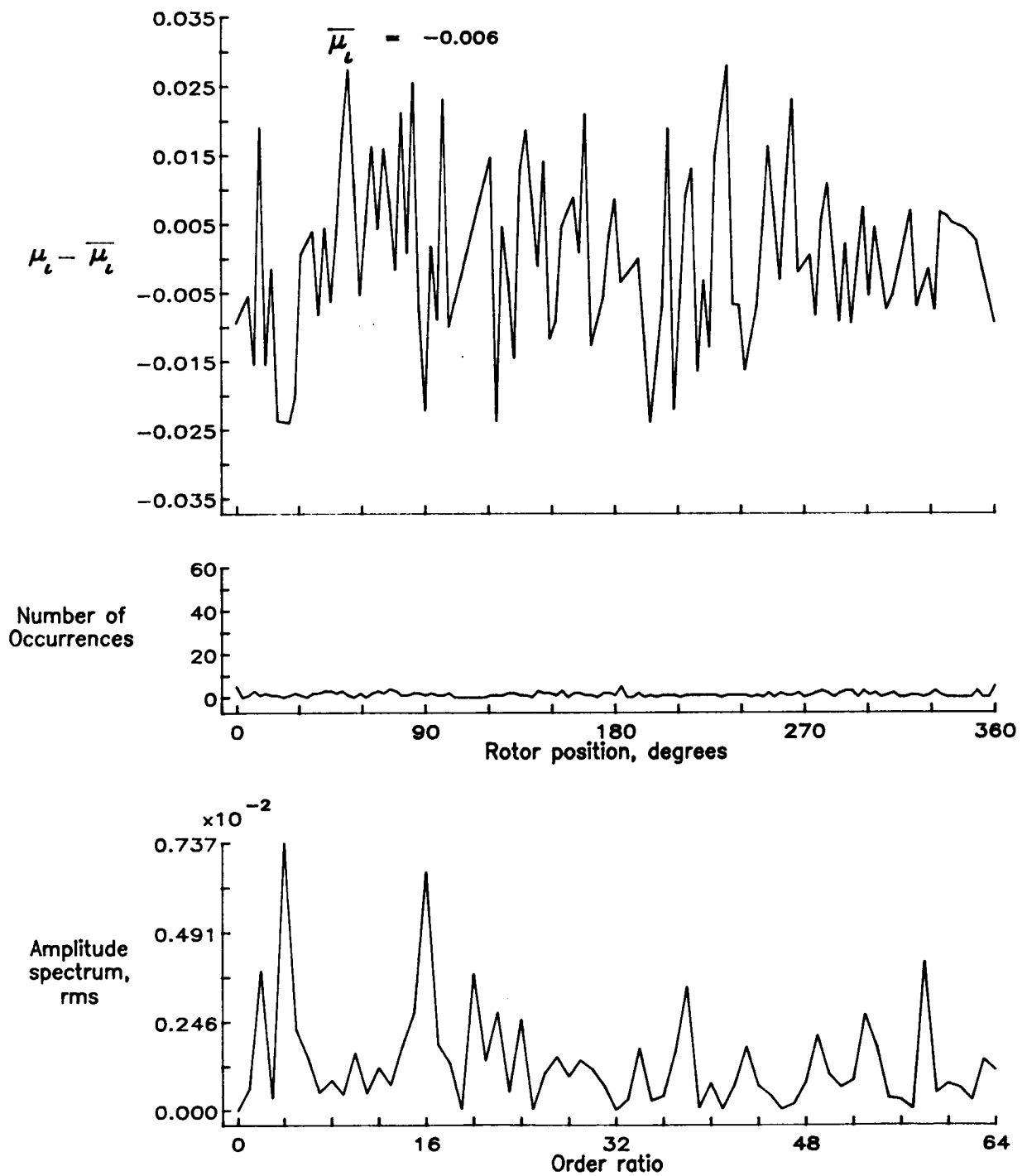


Figure 53.— Induced inflow velocity measured at 60 degrees and r/R of 1.02.

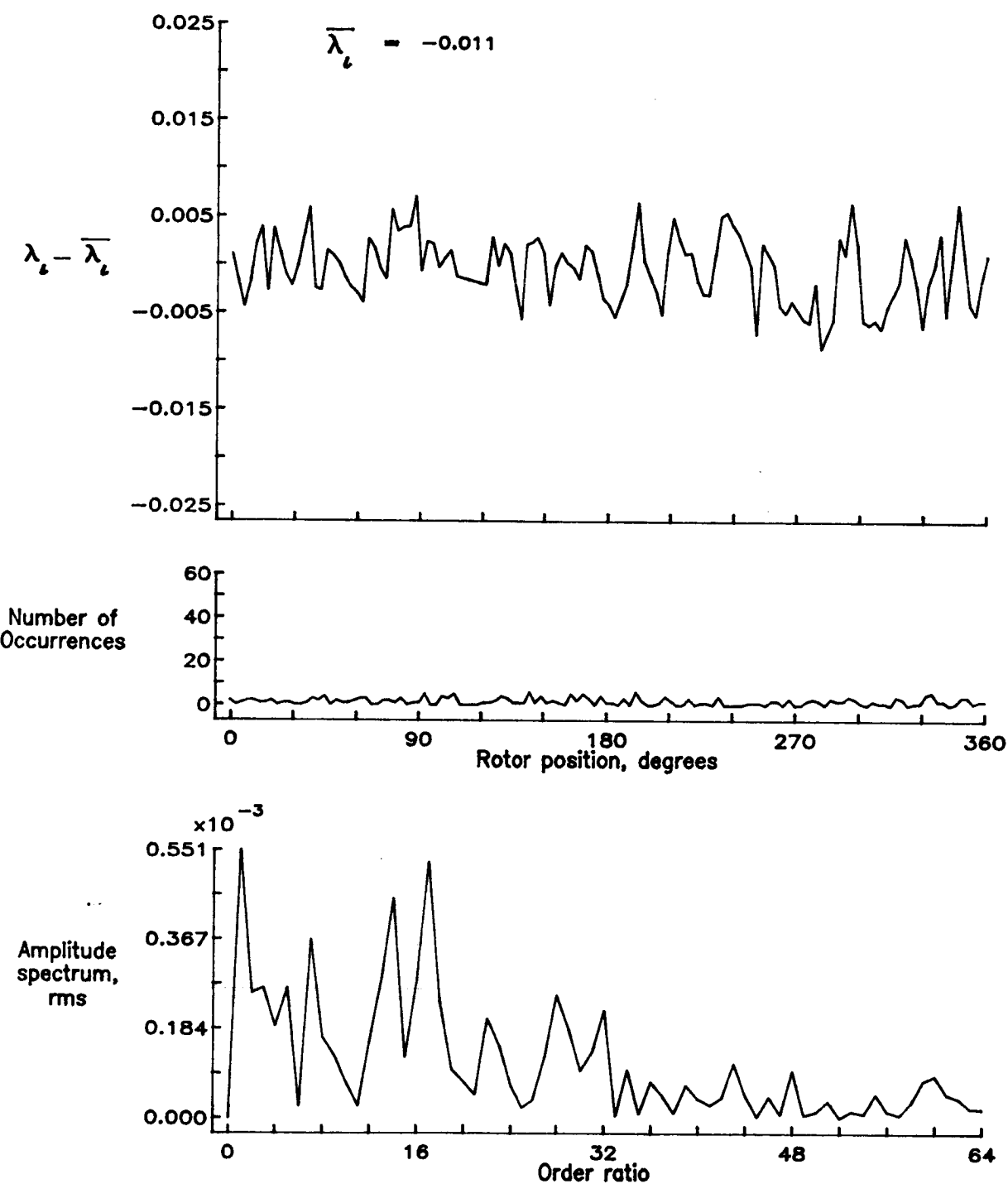


Figure 53.— Concluded.

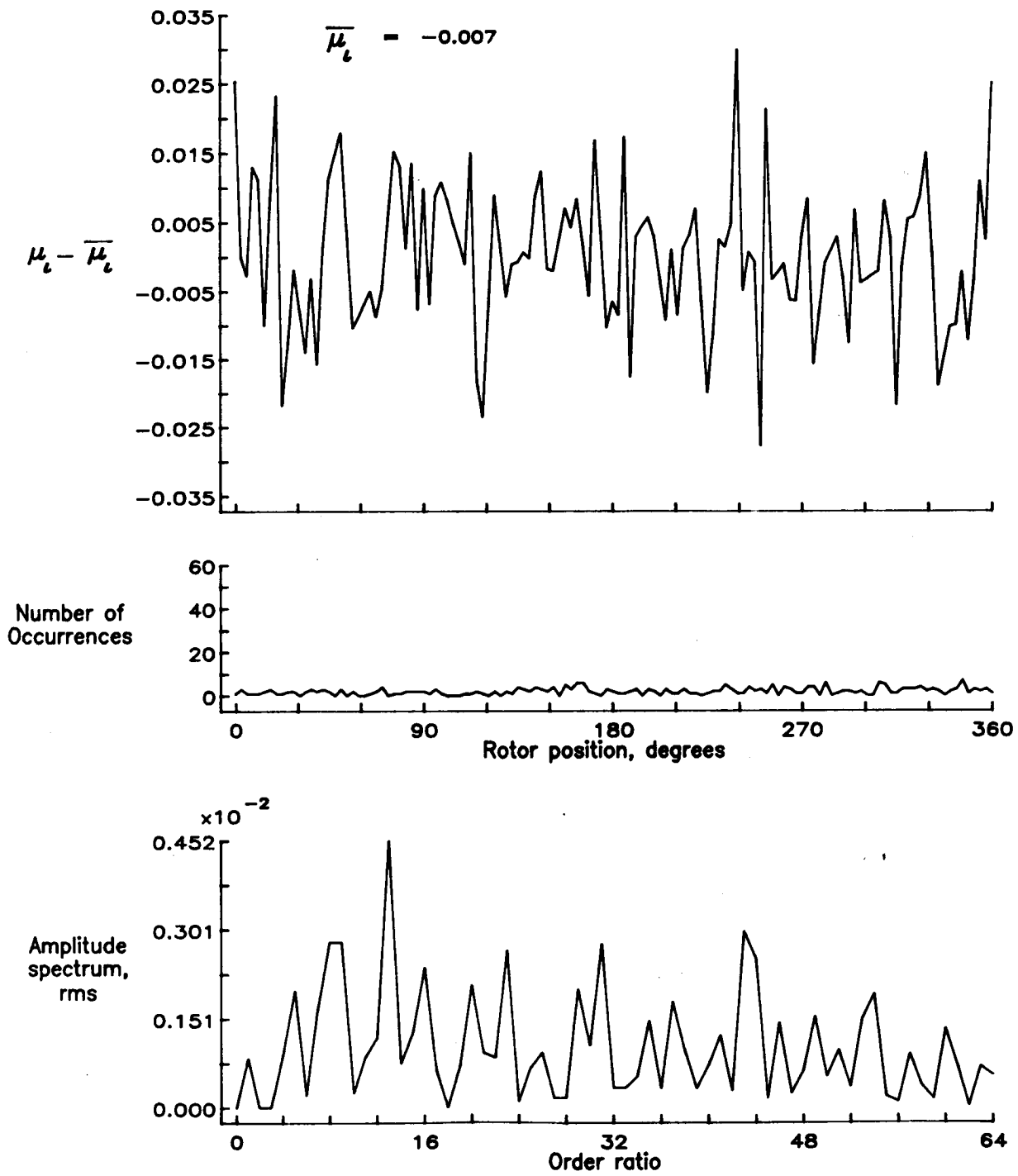


Figure 54.— Induced inflow velocity measured at 60 degrees and r/R of 1.04.

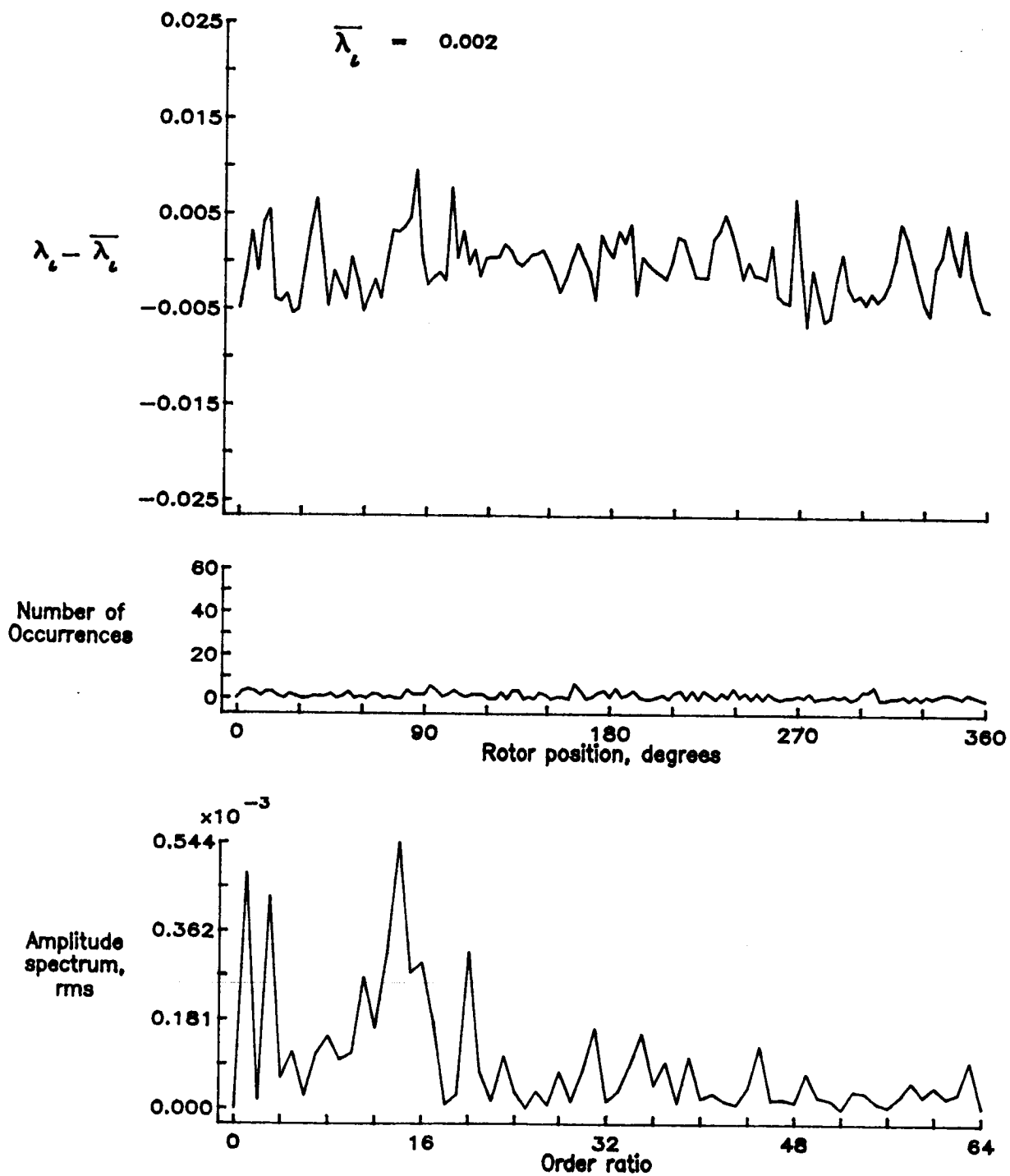


Figure 54.— Concluded.

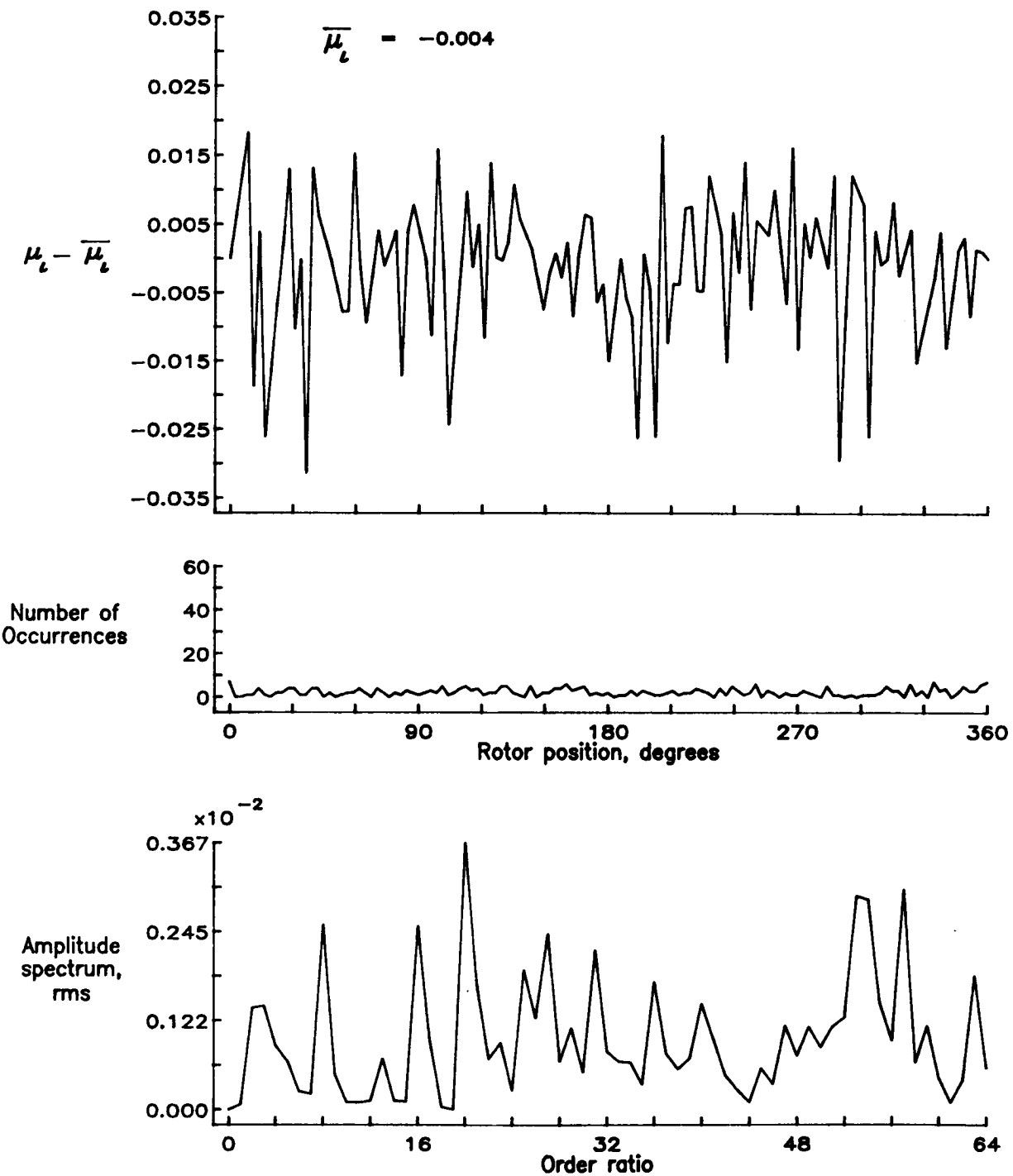


Figure 55.— Induced inflow velocity measured at 60 degrees and r/R of 1.10.

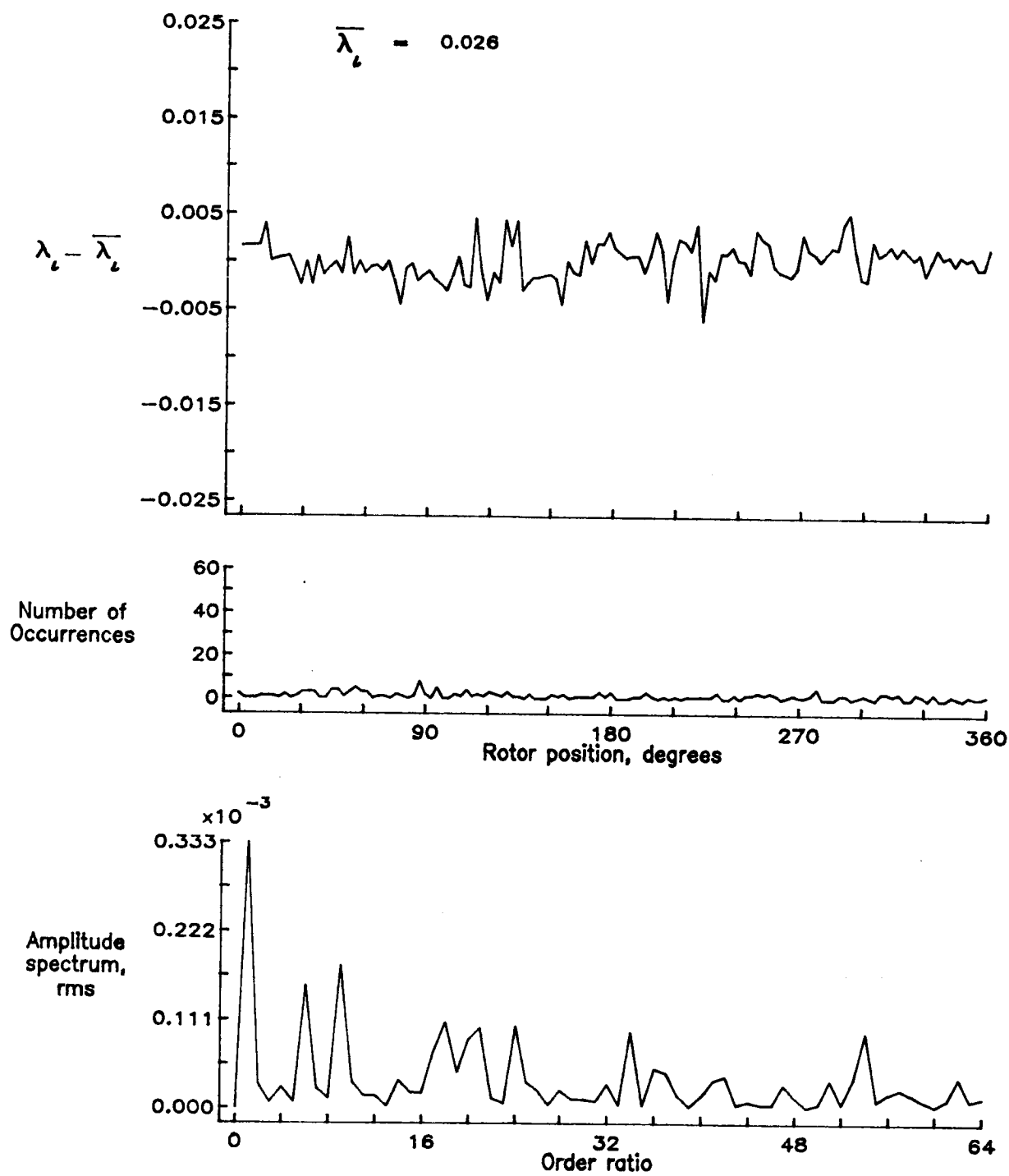


Figure 55.— Concluded.

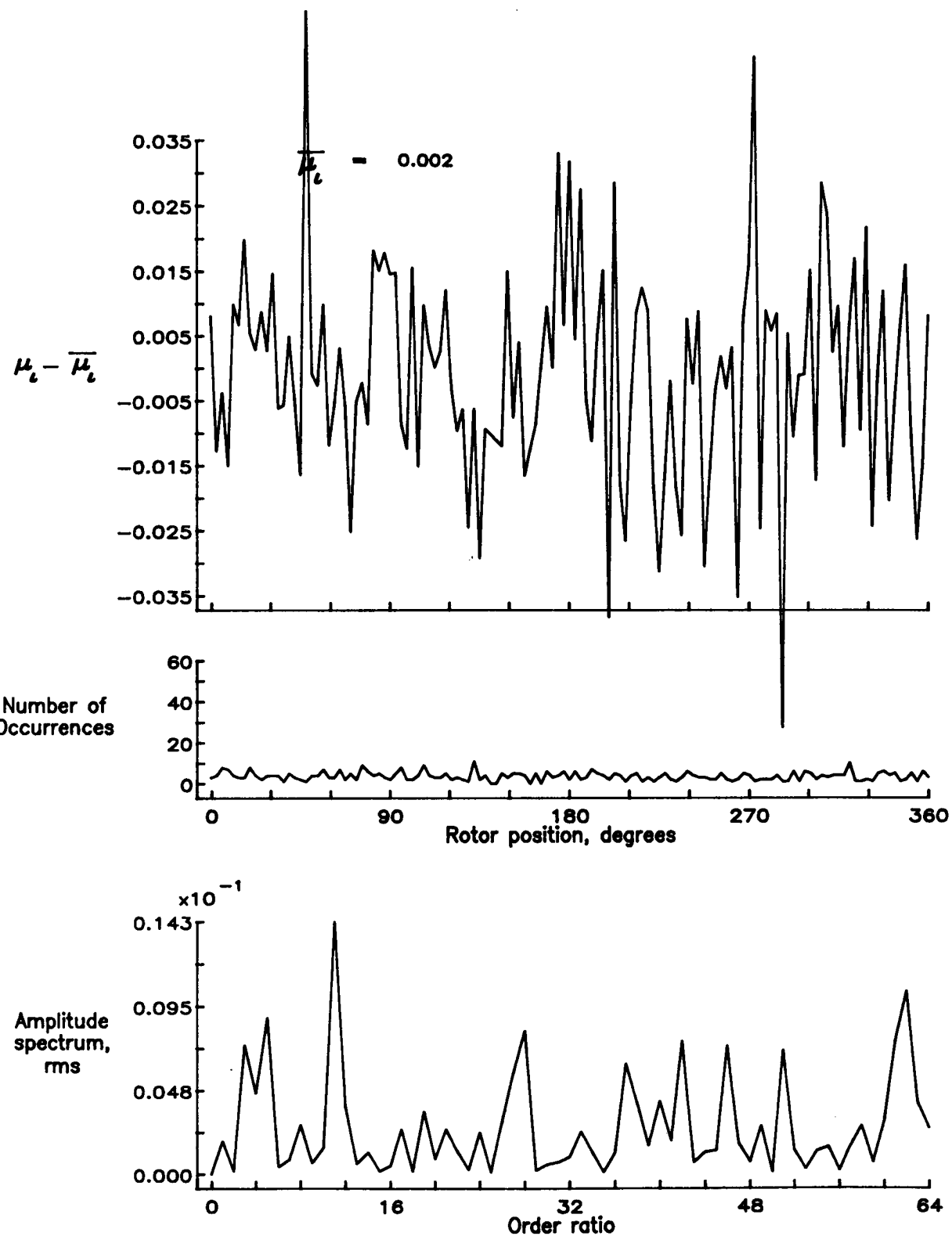


Figure 56.— Induced inflow velocity measured at 90 degrees and  $r/R$  of 0.20.

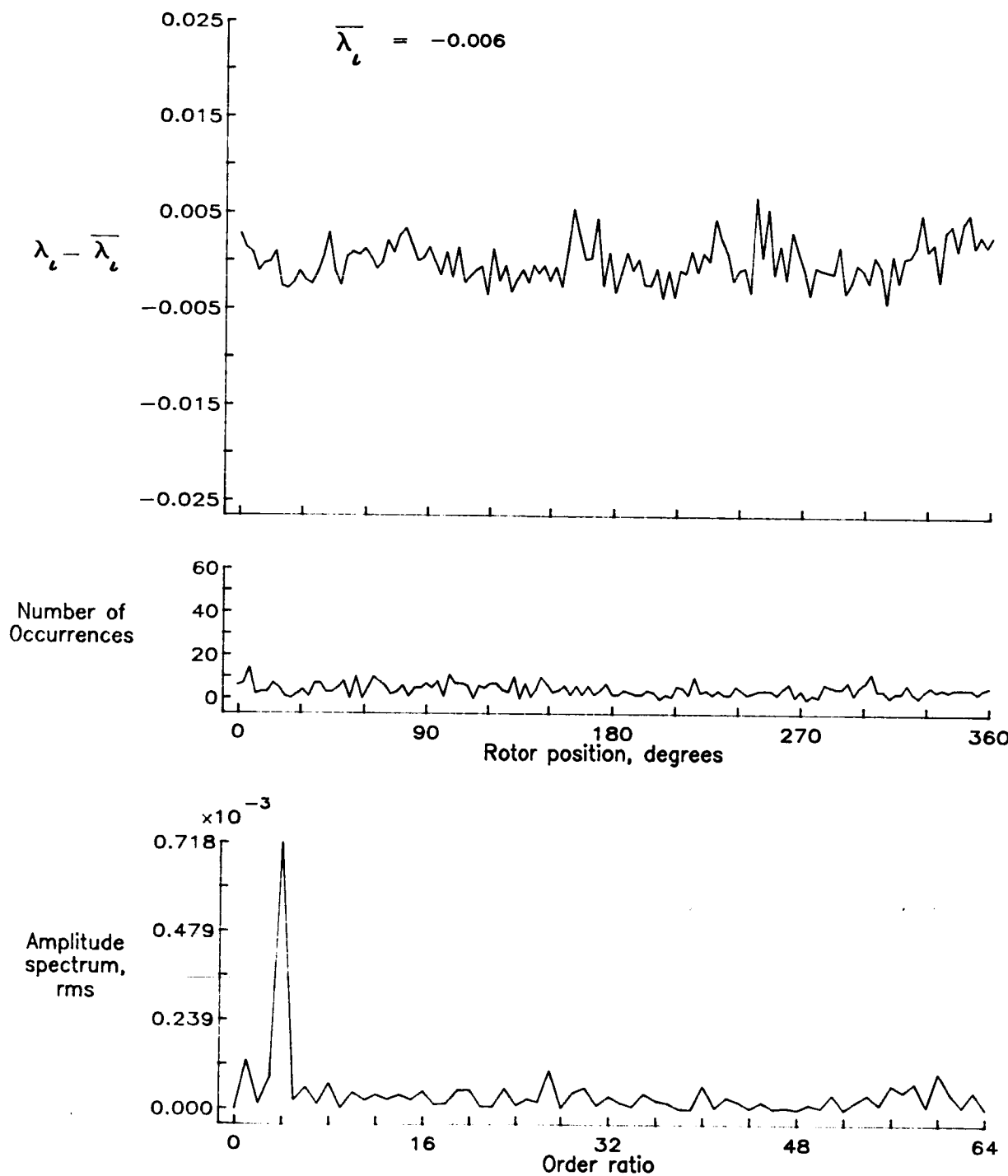


Figure 56.— Concluded.

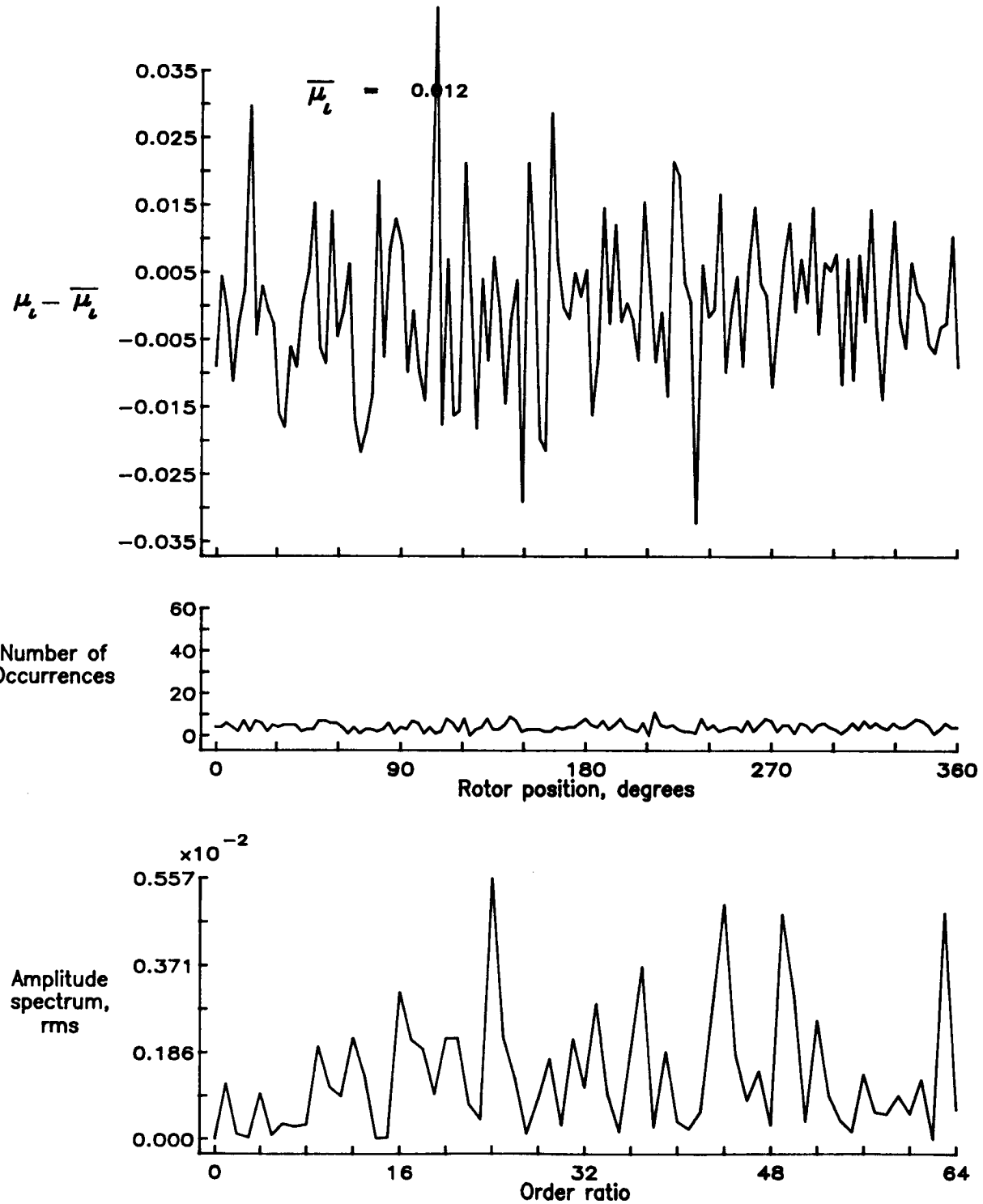


Figure 57.— Induced inflow velocity measured at 90 degrees and r/R of 0.40.

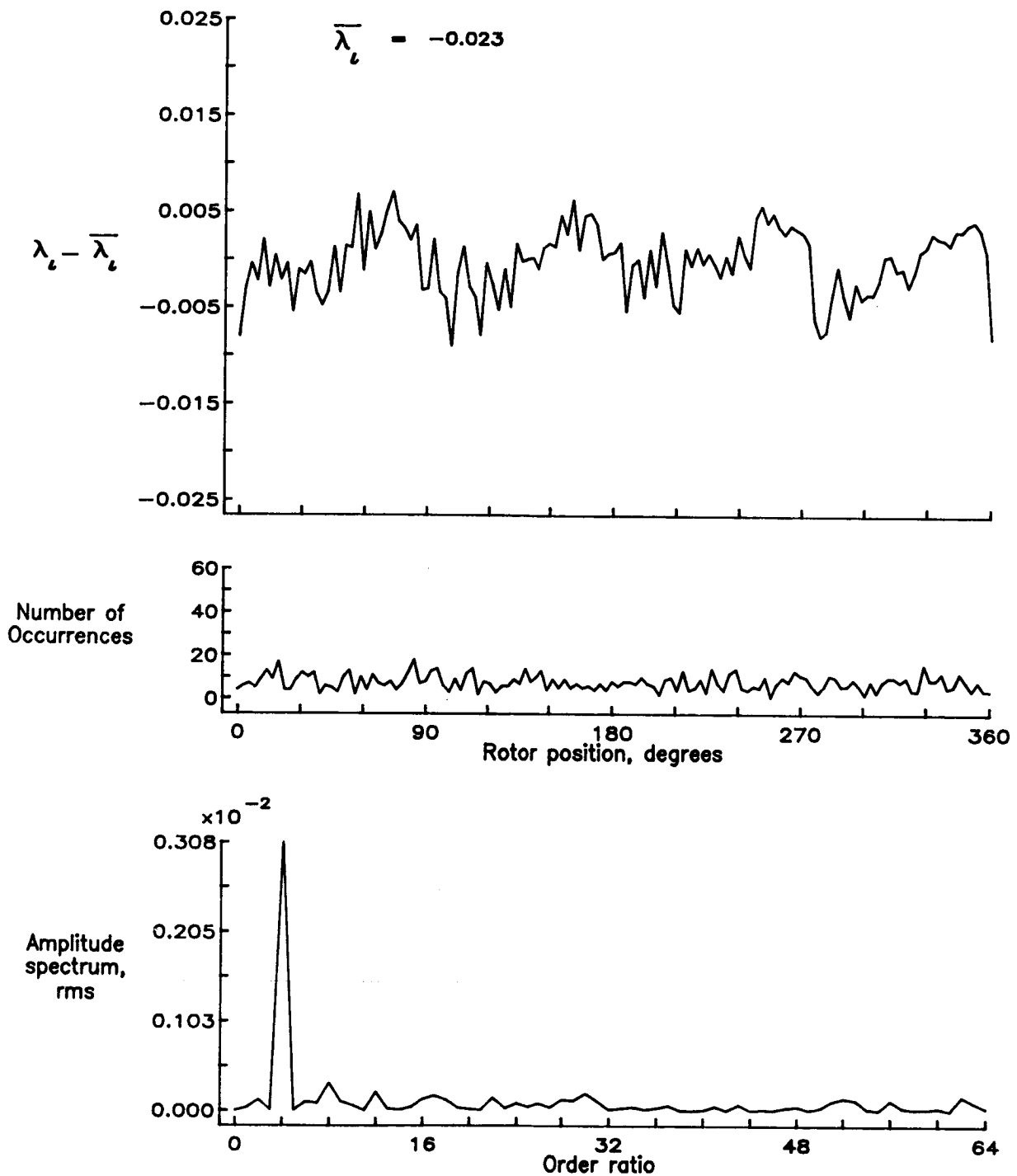


Figure 57.— Concluded.

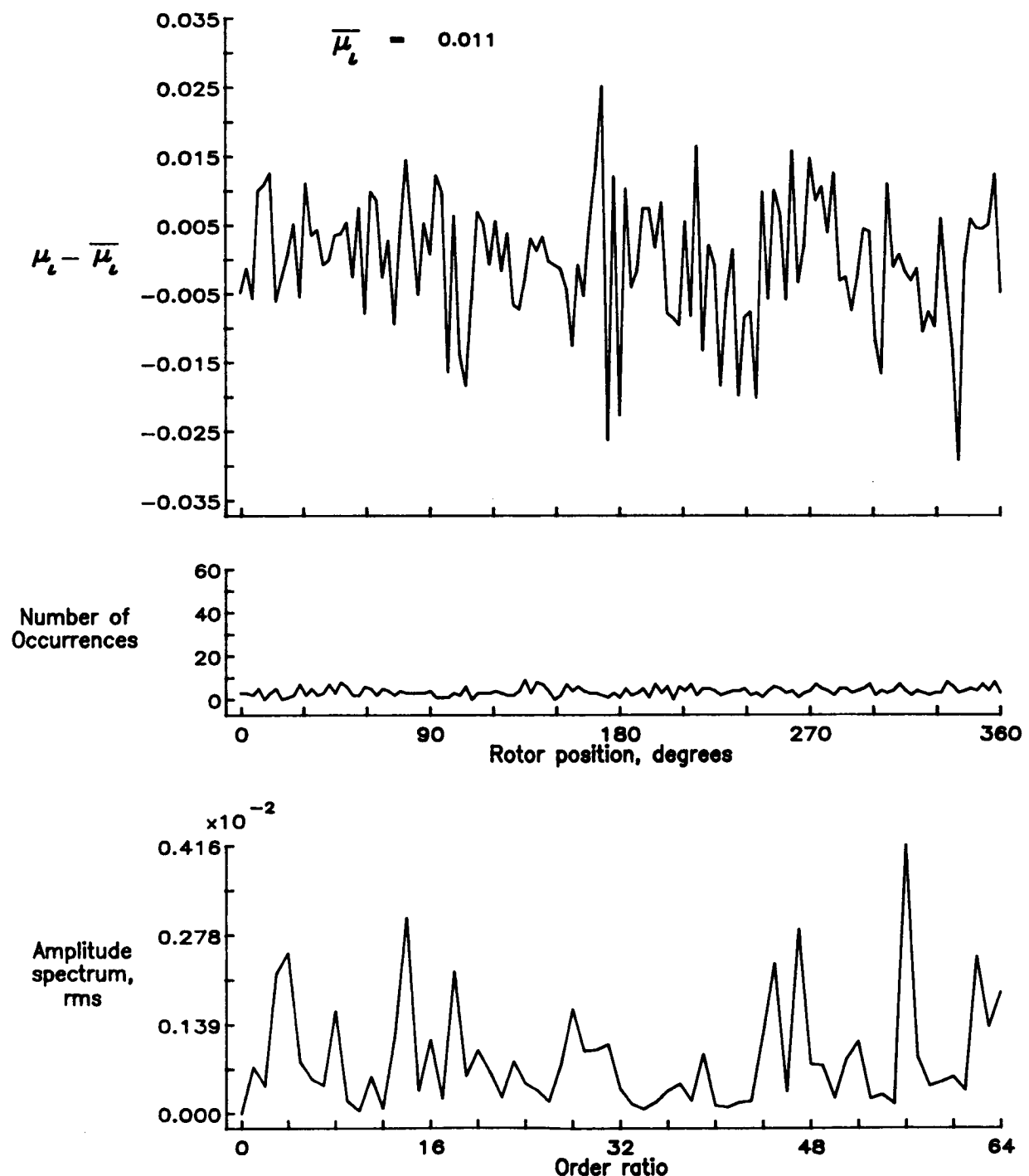


Figure 58.— Induced inflow velocity measured at 90 degrees and r/R of 0.50.

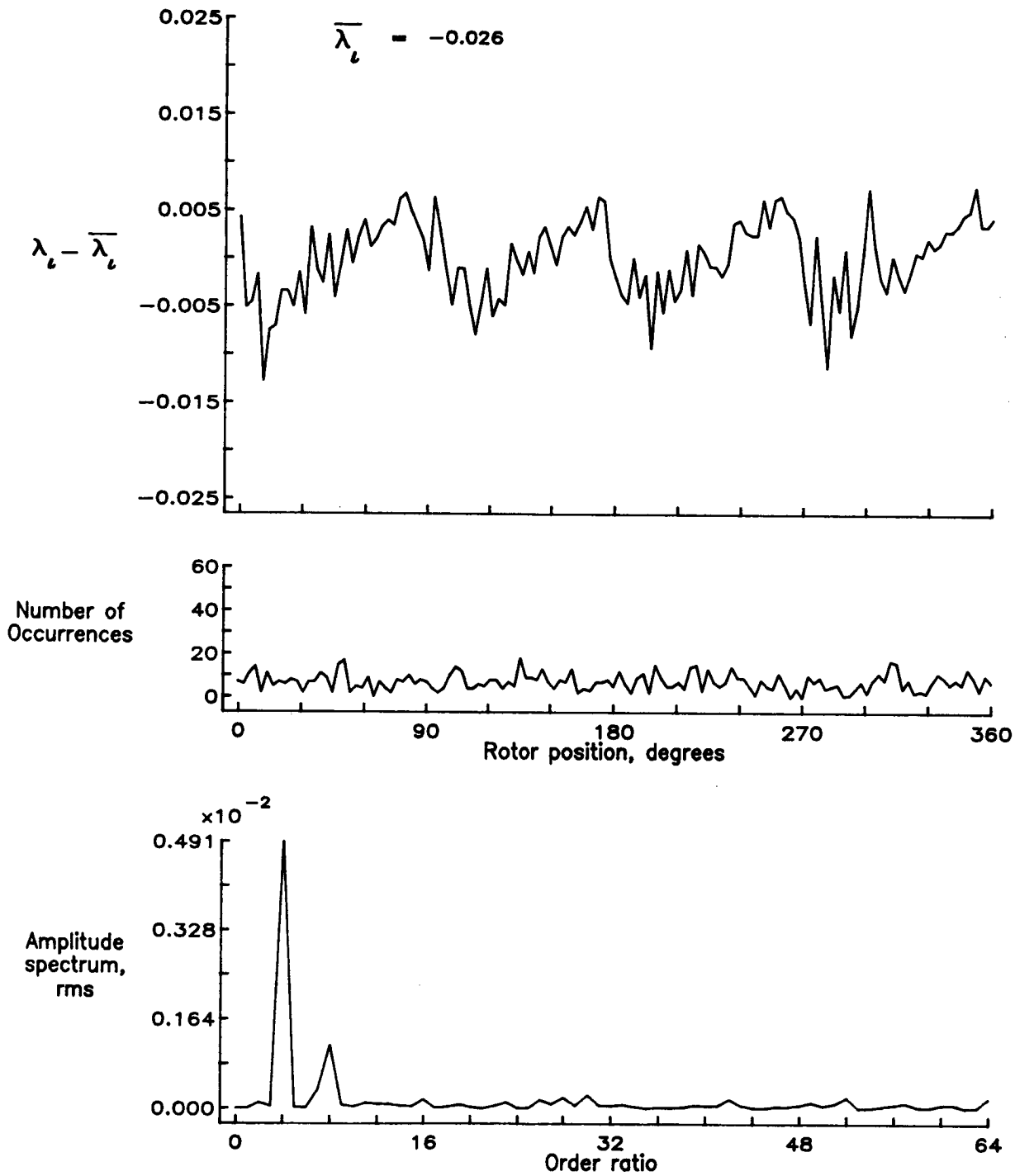


Figure 58.— Concluded.

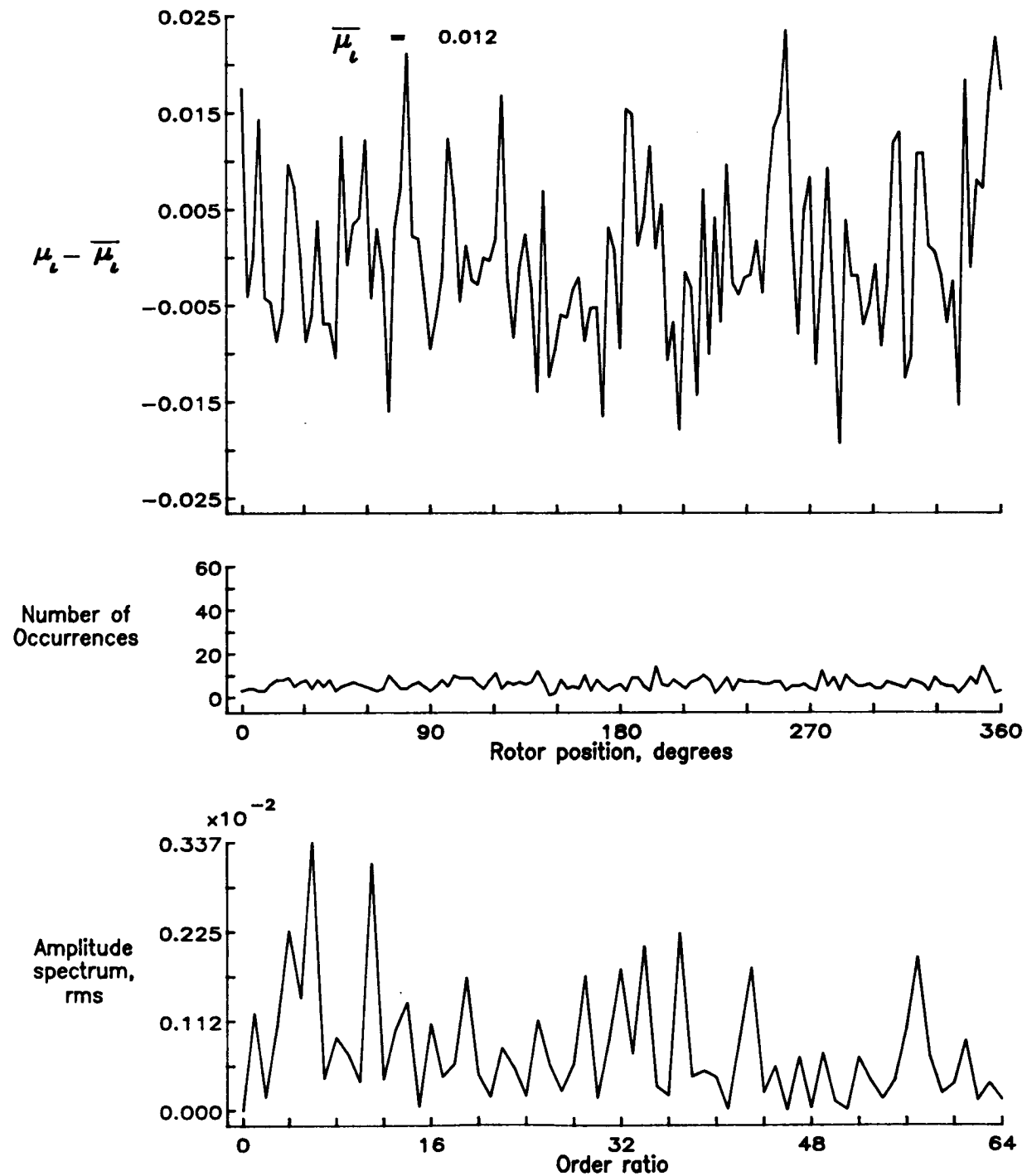


Figure 59.— Induced inflow velocity measured at 90 degrees and  $r/R$  of 0.60.

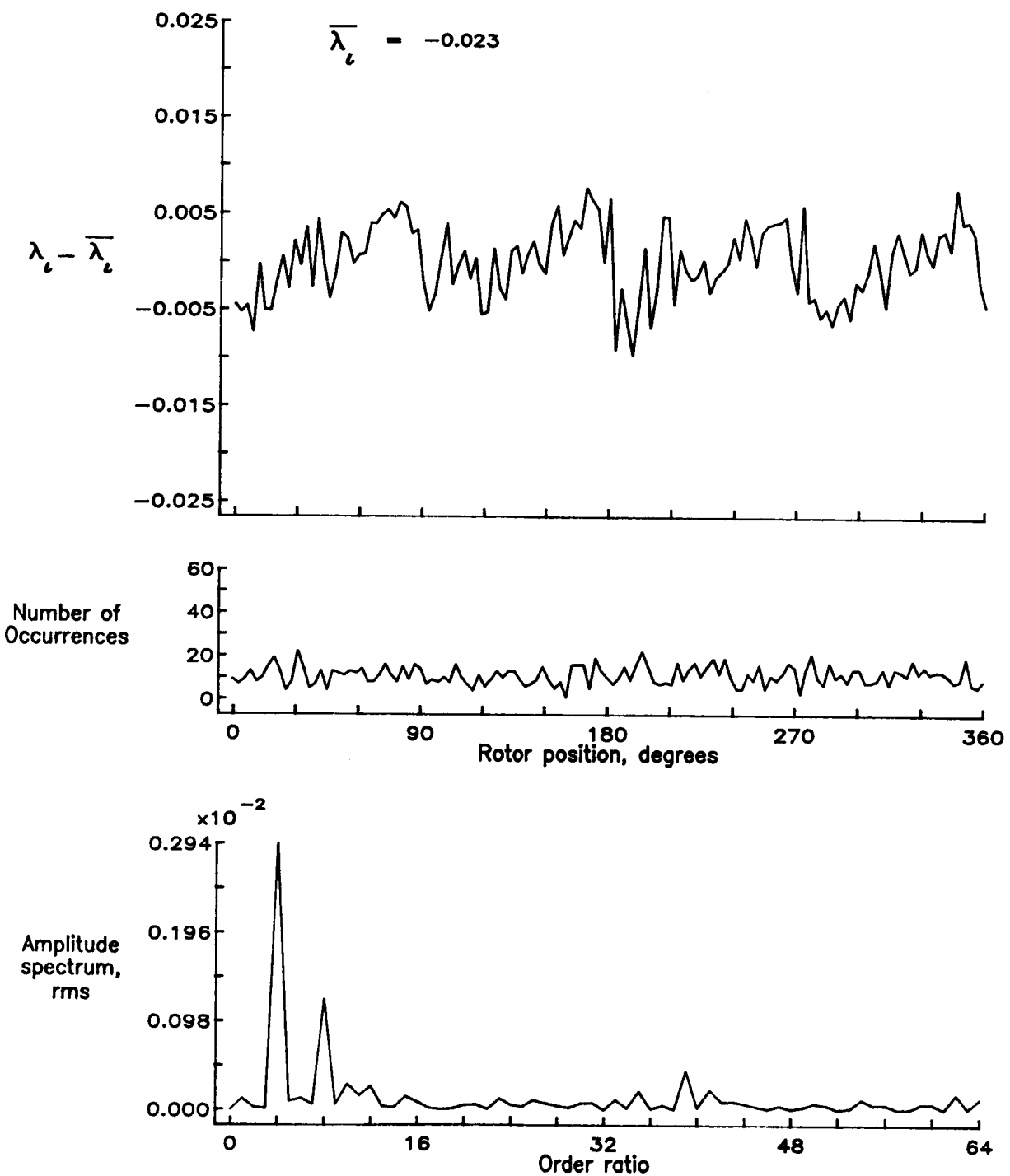


Figure 59.— Concluded.

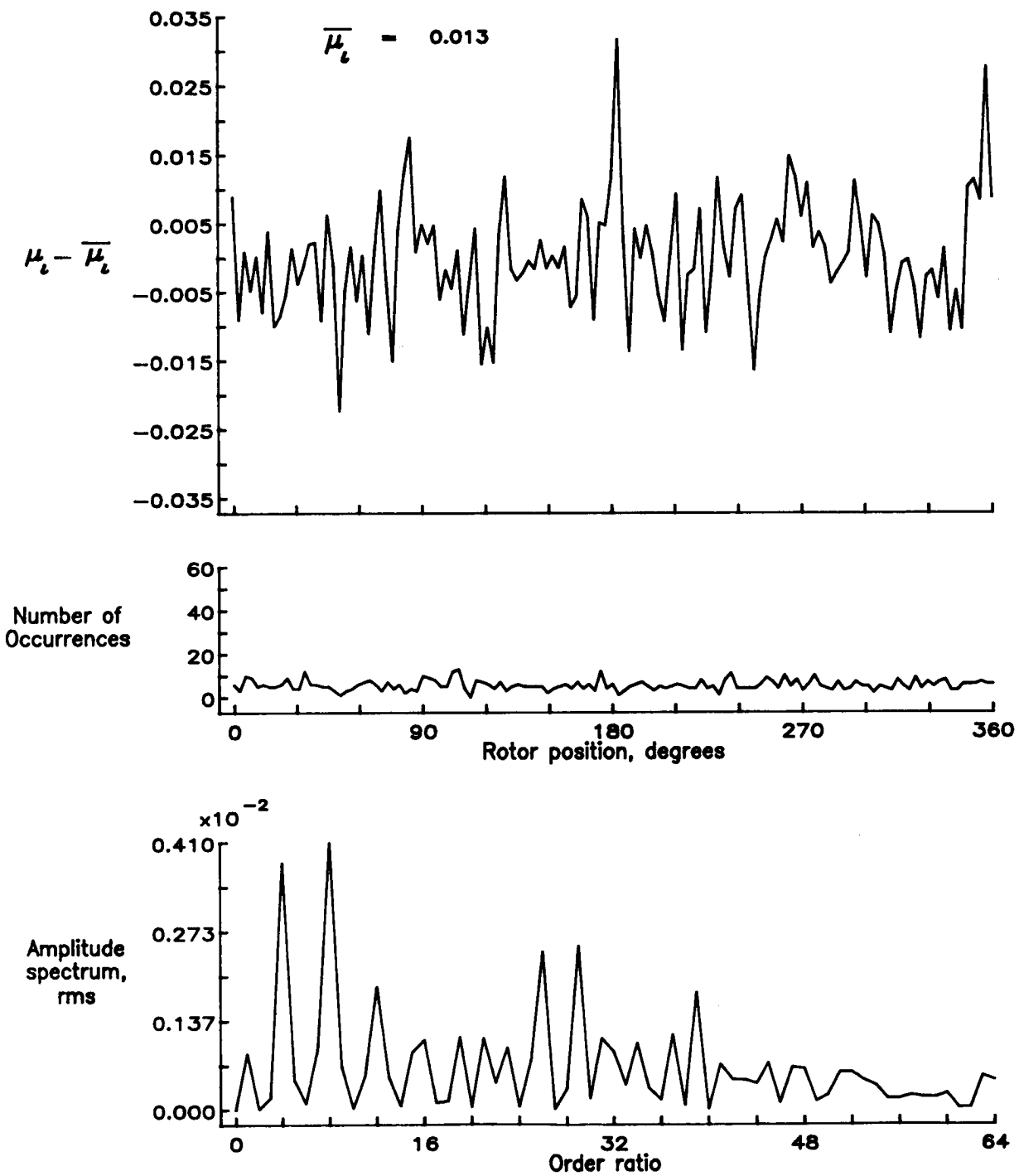


Figure 60.— Induced inflow velocity measured at 90 degrees and r/R of 0.70.

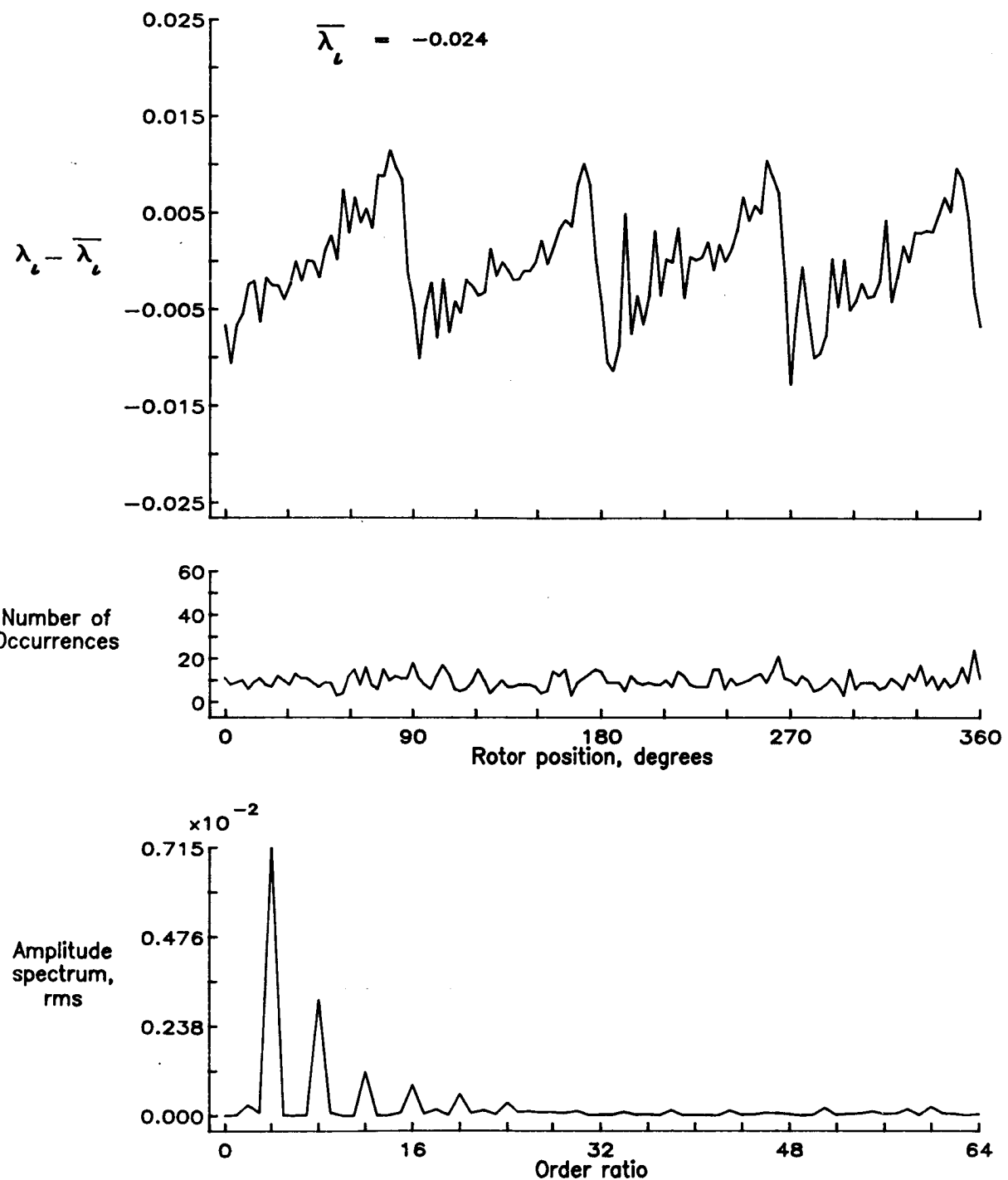


Figure 60.— Concluded.

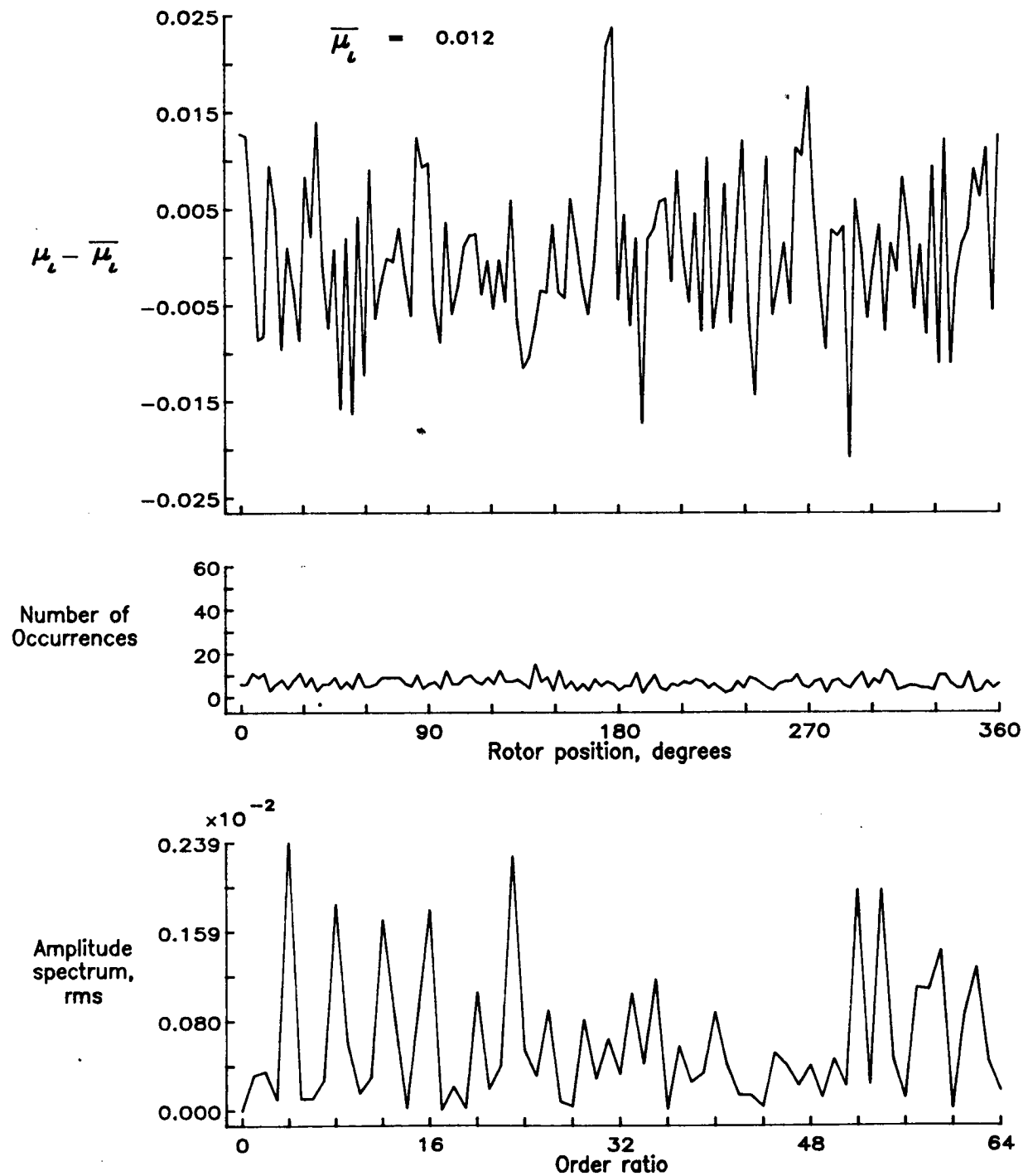


Figure 61.— Induced inflow velocity measured at 90 degrees and  $r/R$  of 0.74.

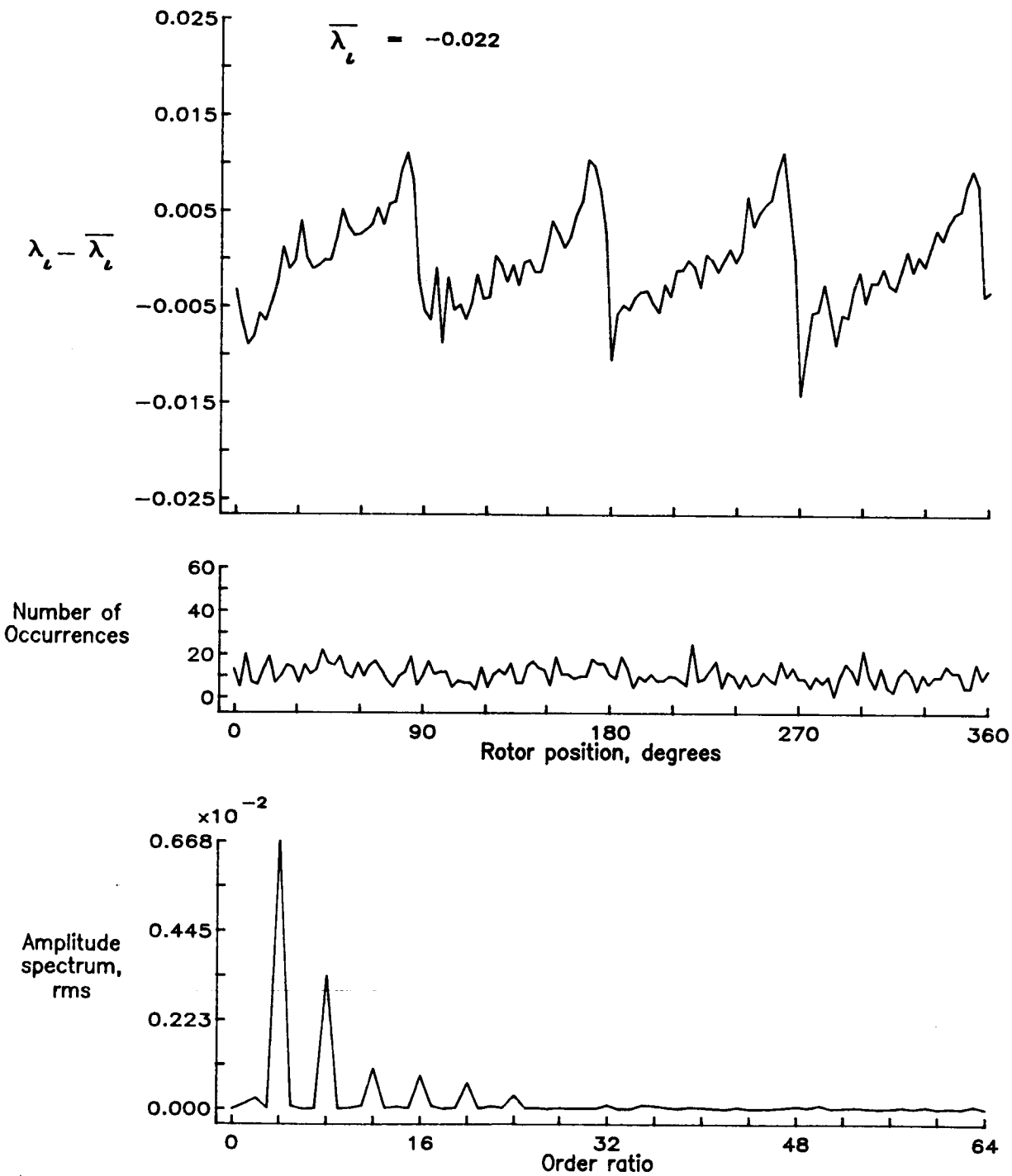


Figure 61.— Concluded.

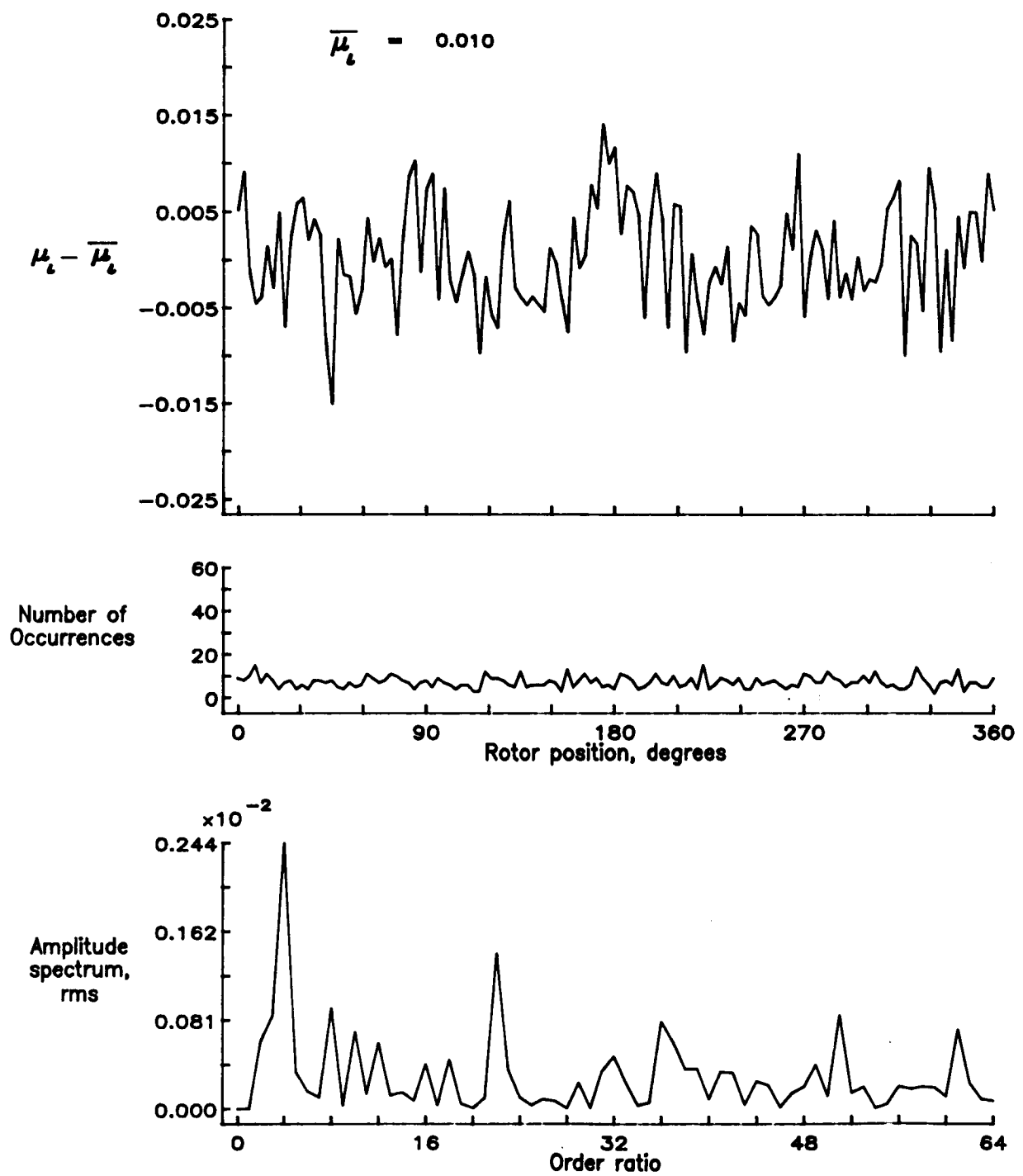


Figure 62.— Induced inflow velocity measured at 90 degrees and r/R of 0.78.

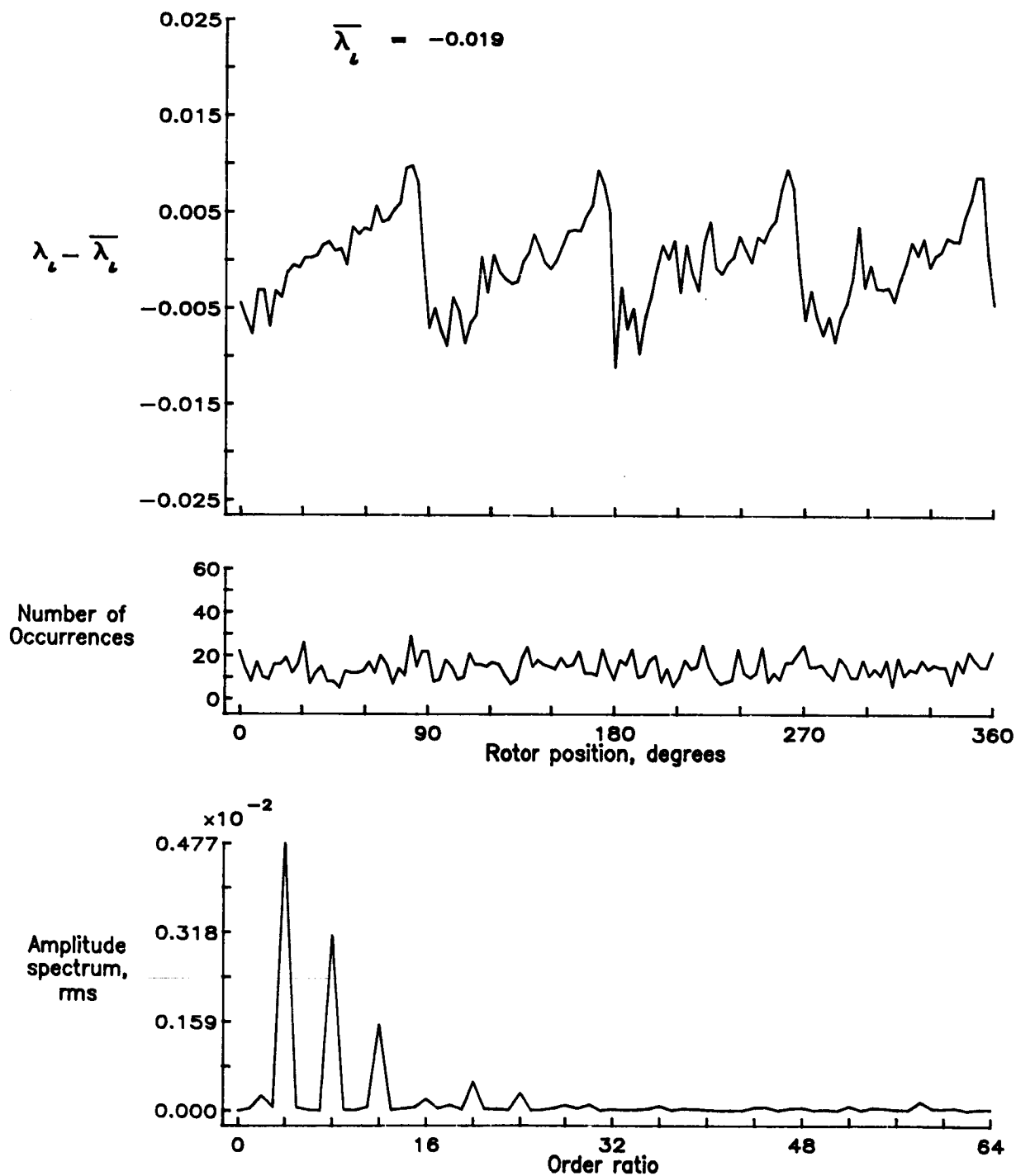


Figure 62.— Concluded.

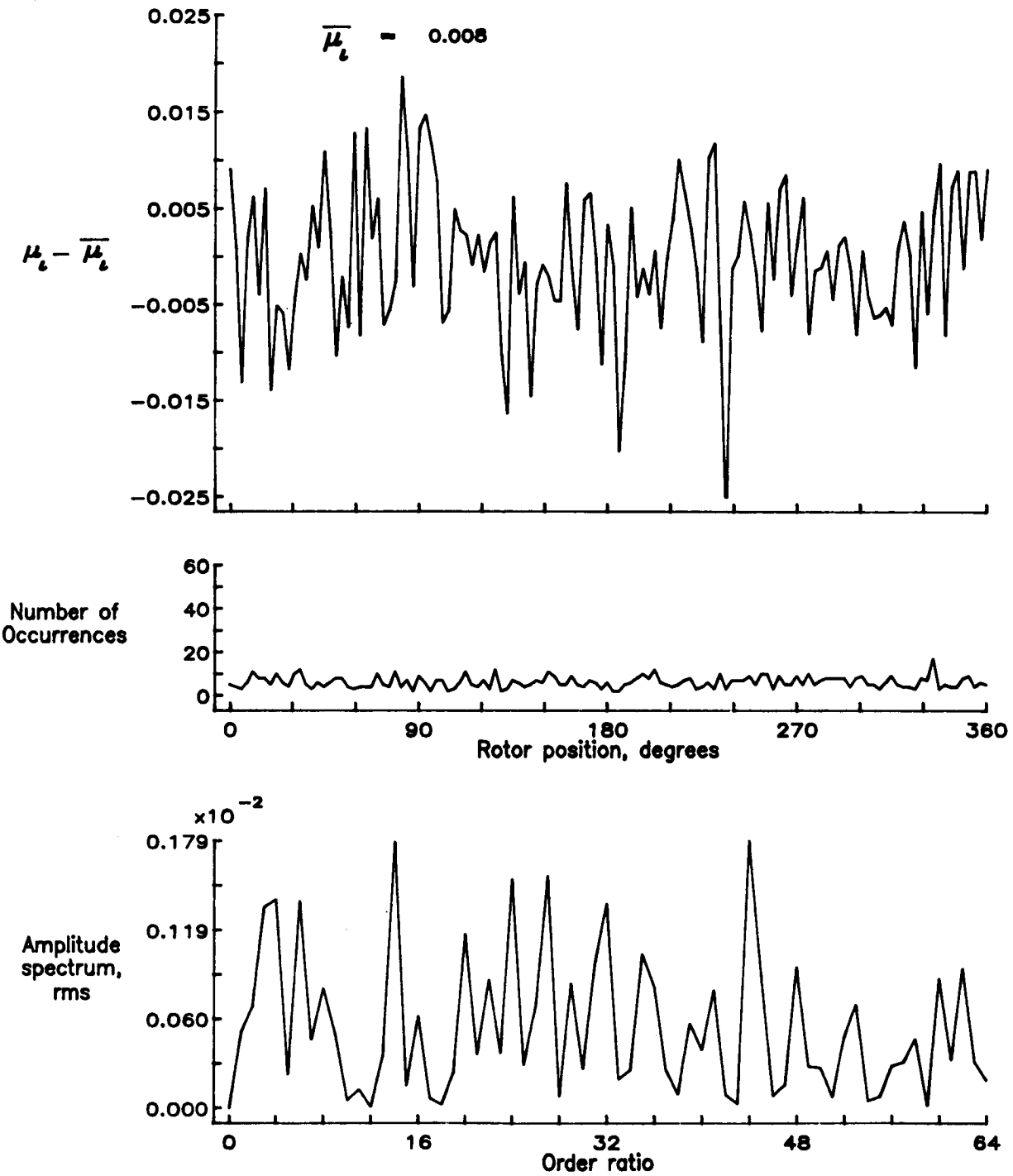


Figure 63.— Induced inflow velocity measured at 90 degrees and r/R of 0.82.

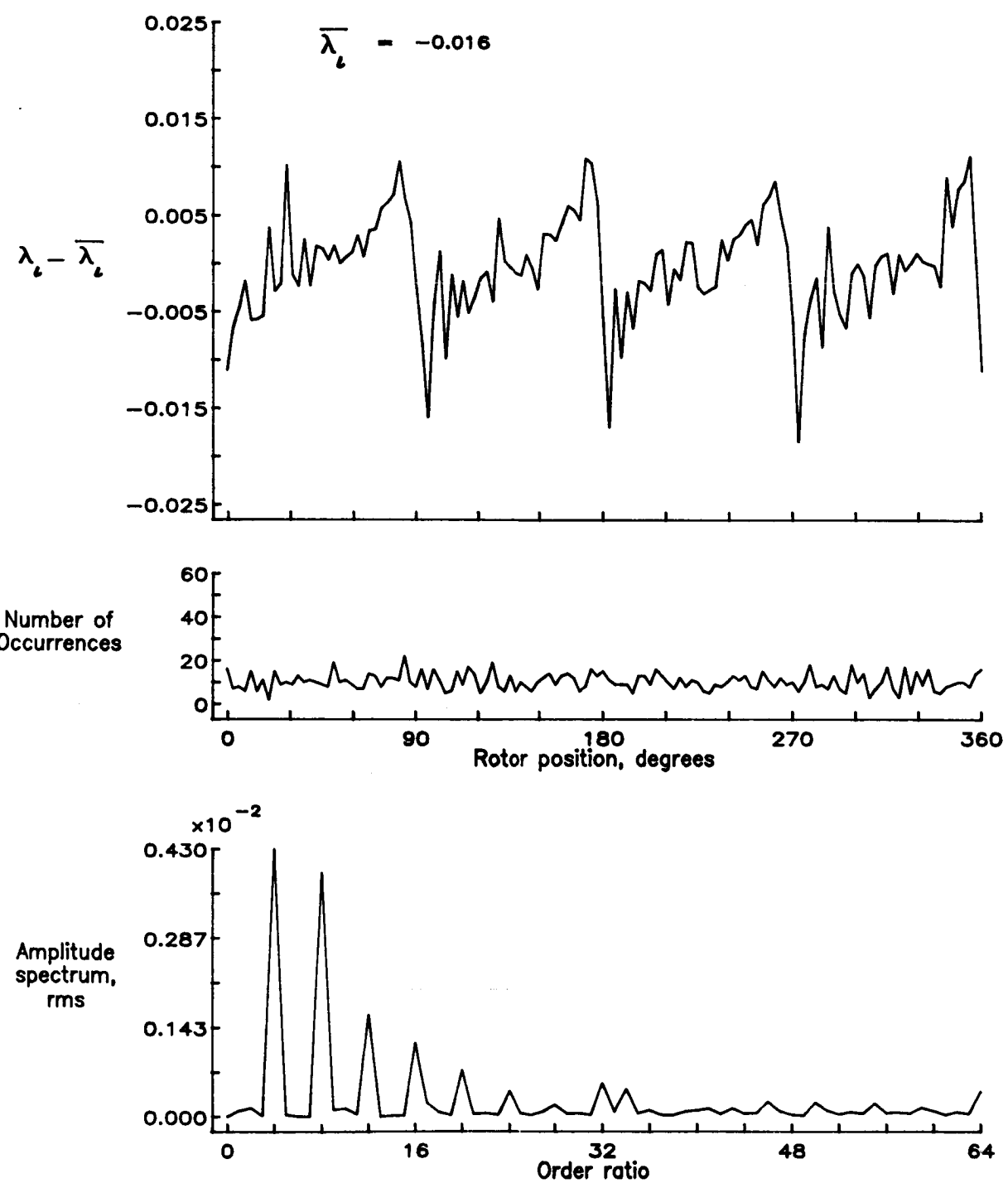


Figure 63.— Concluded.

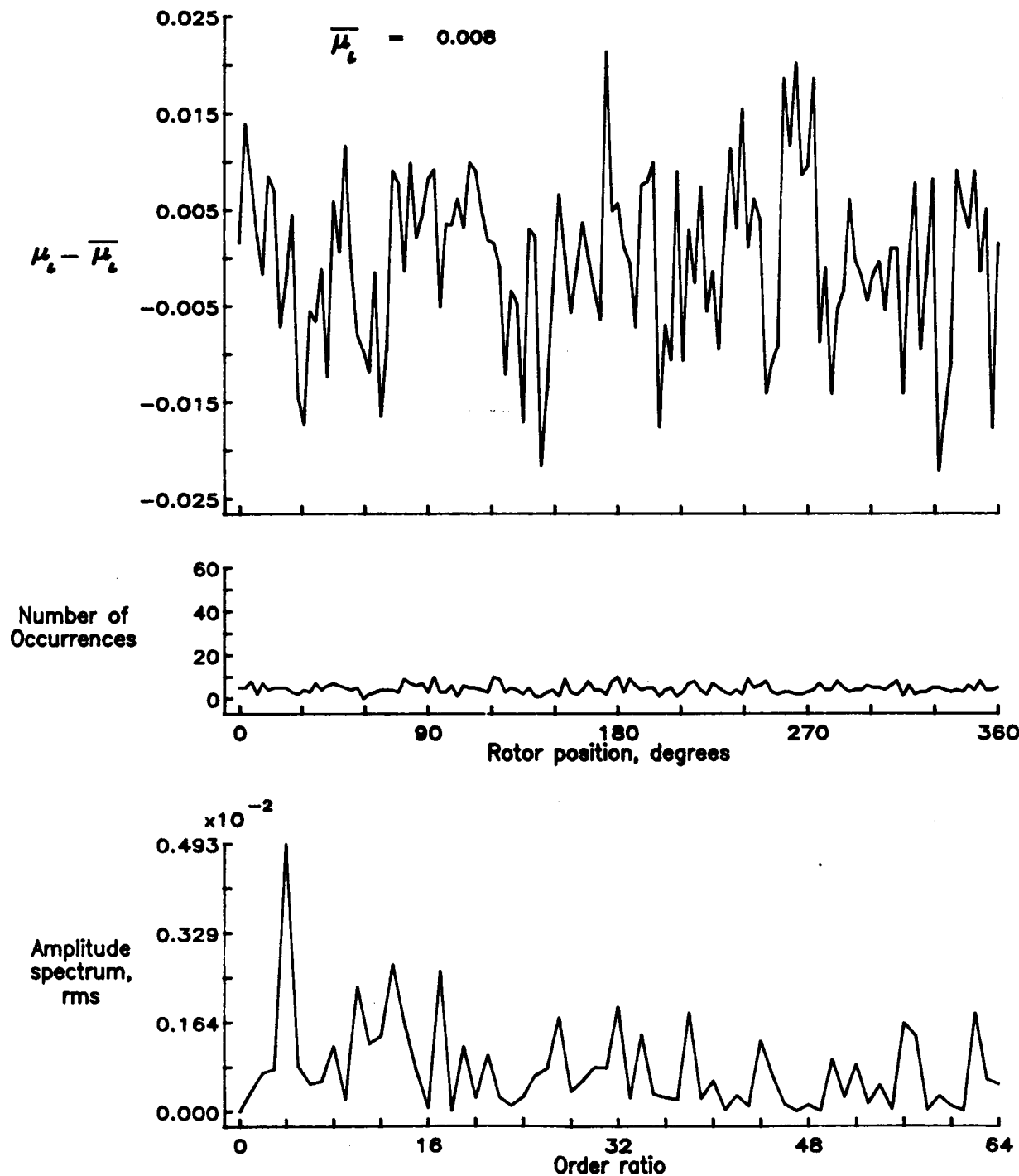


Figure 64.— Induced inflow velocity measured at 90 degrees and  $r/R$  of 0.86.

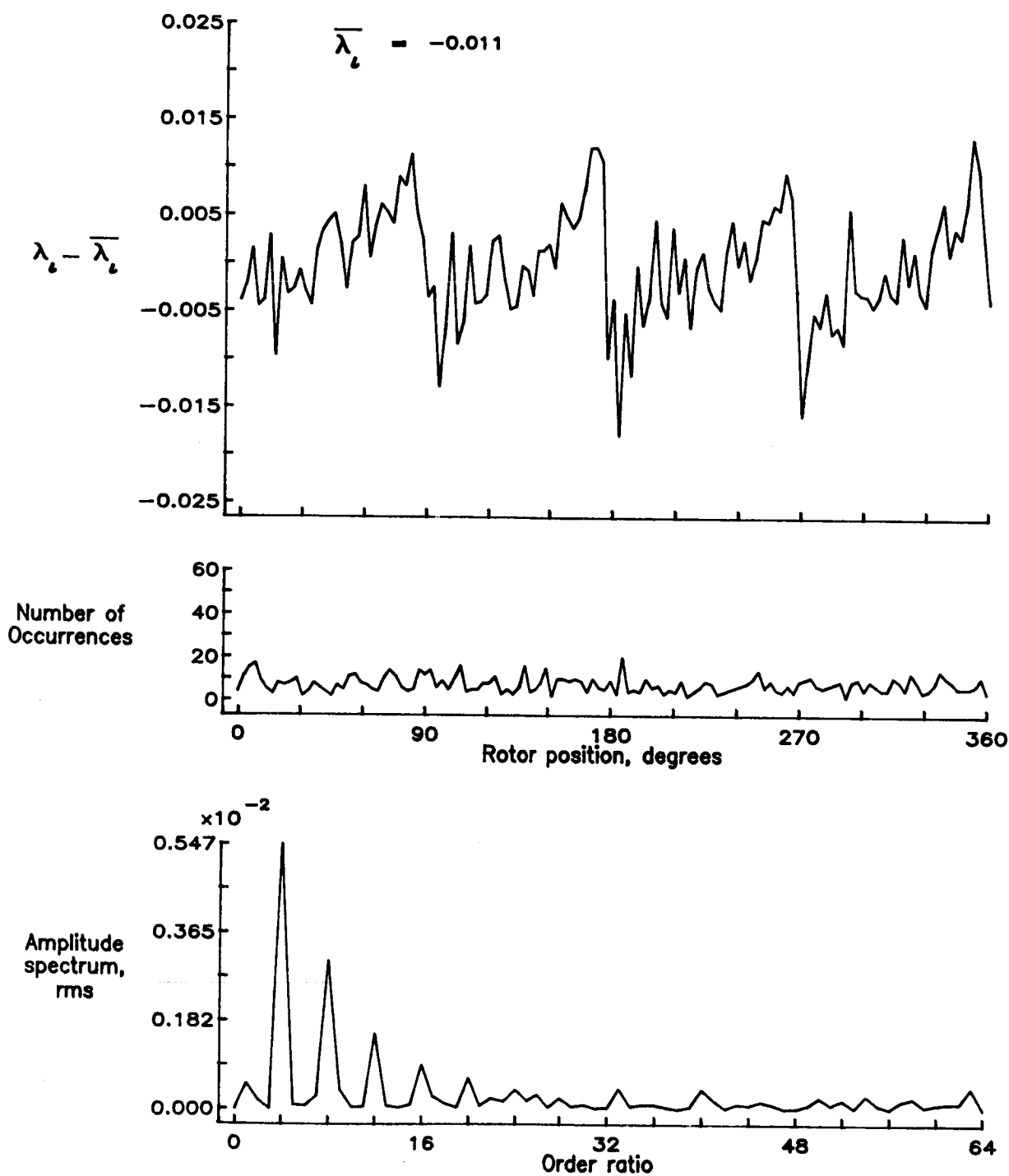


Figure 64.— Concluded.

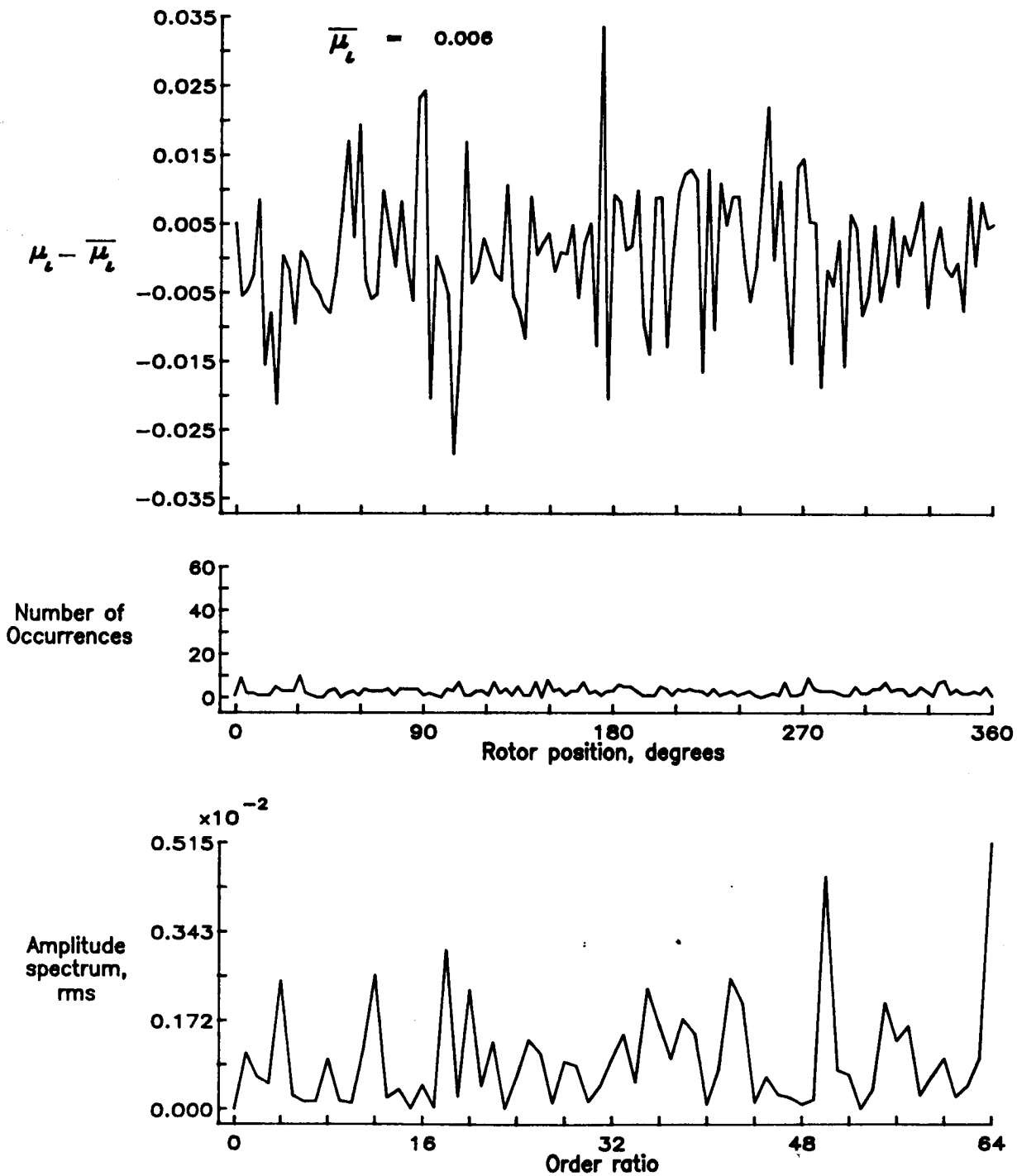


Figure 65.— Induced inflow velocity measured at 90 degrees and  $r/R$  of 0.90.

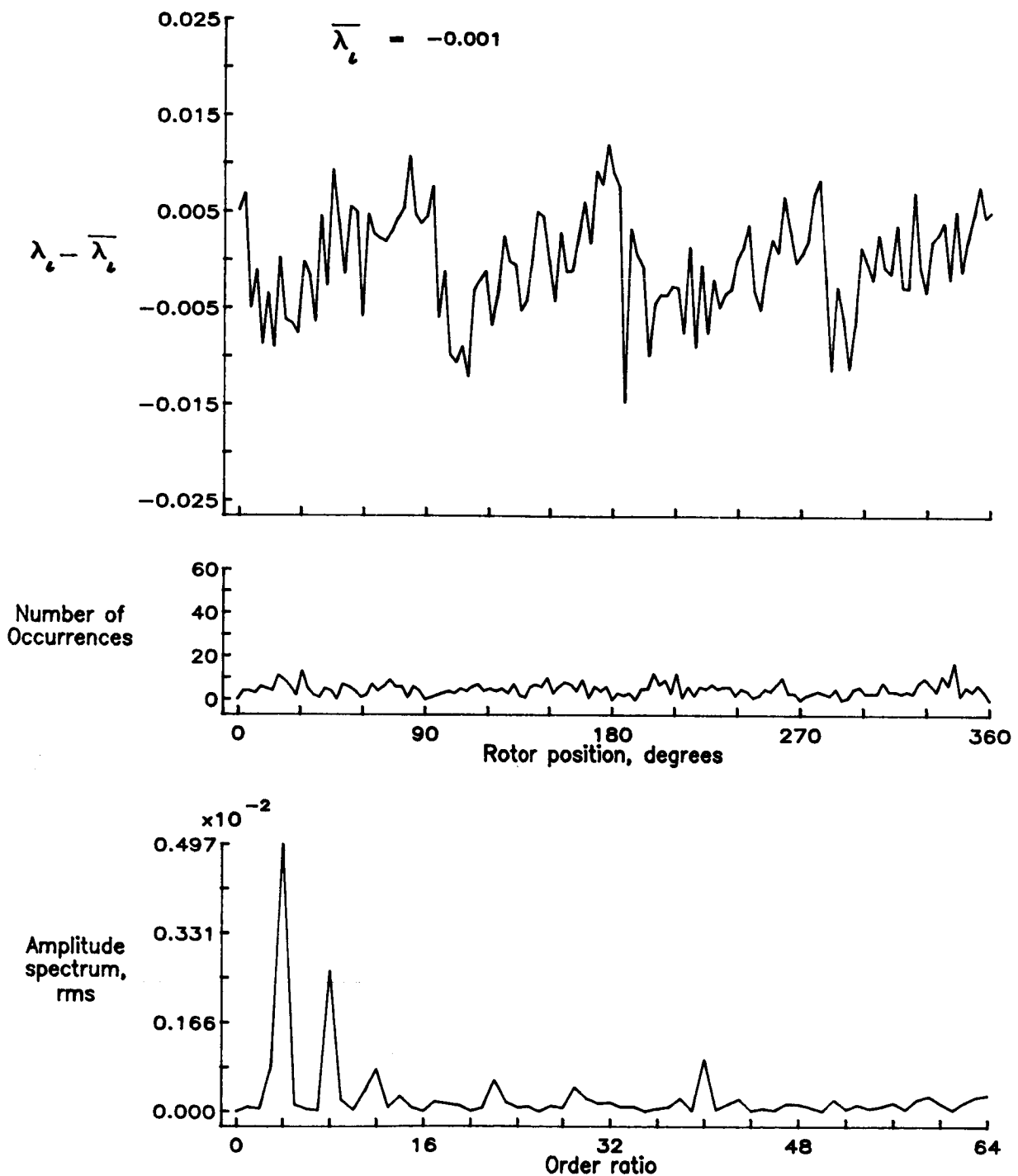


Figure 65.— Concluded.

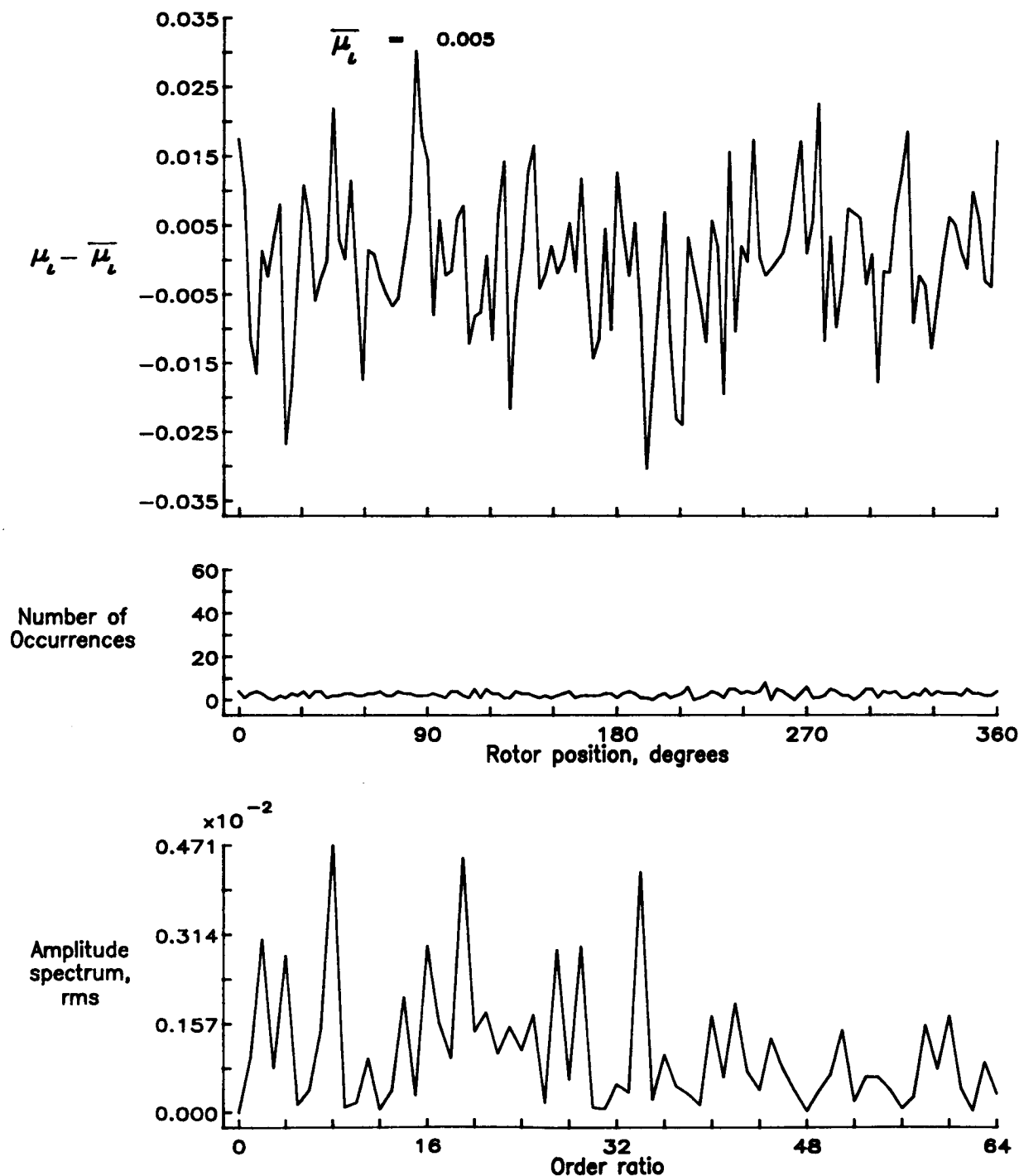


Figure 66.— Induced inflow velocity measured at 90 degrees and  $r/R$  of 0.94.

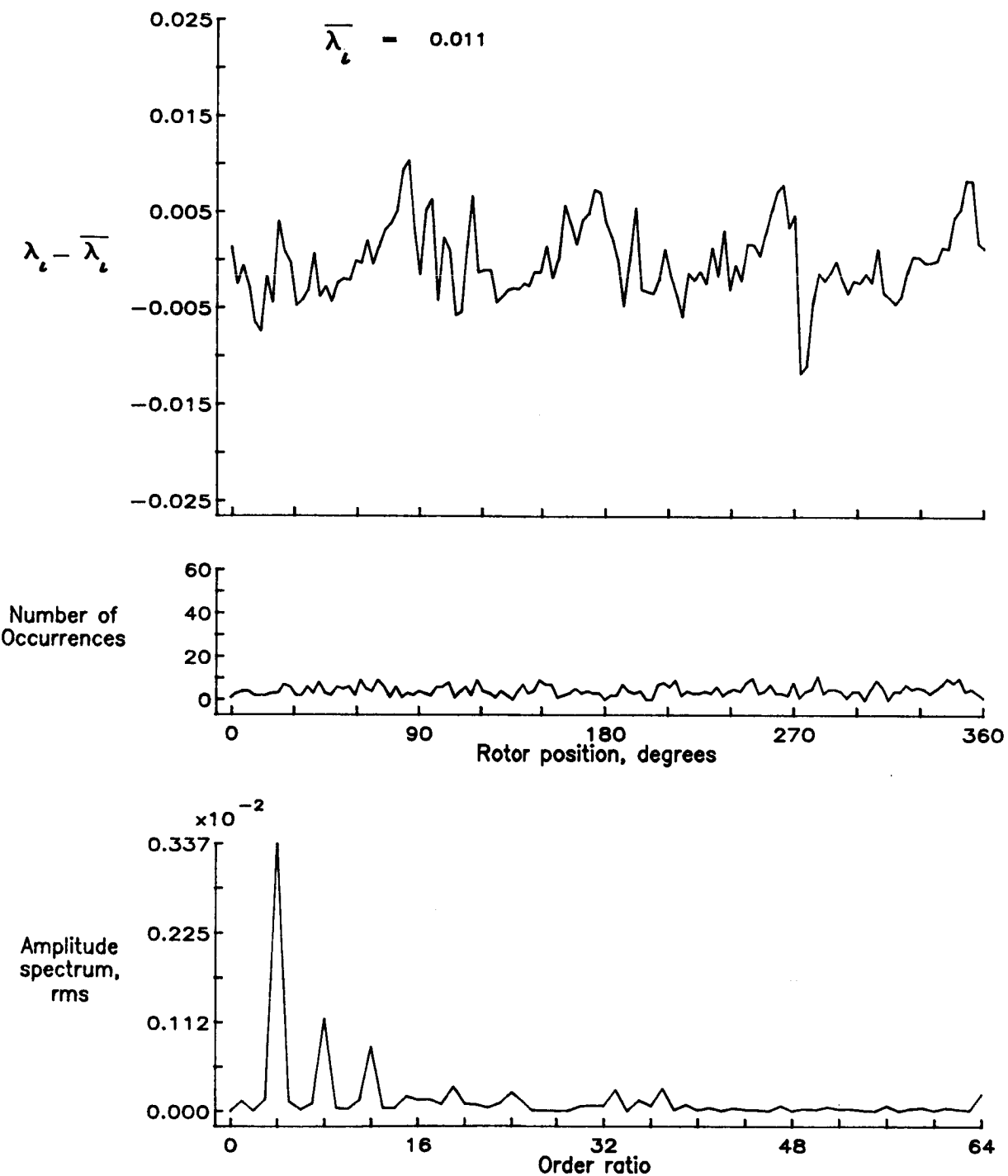


Figure 66.— Concluded.

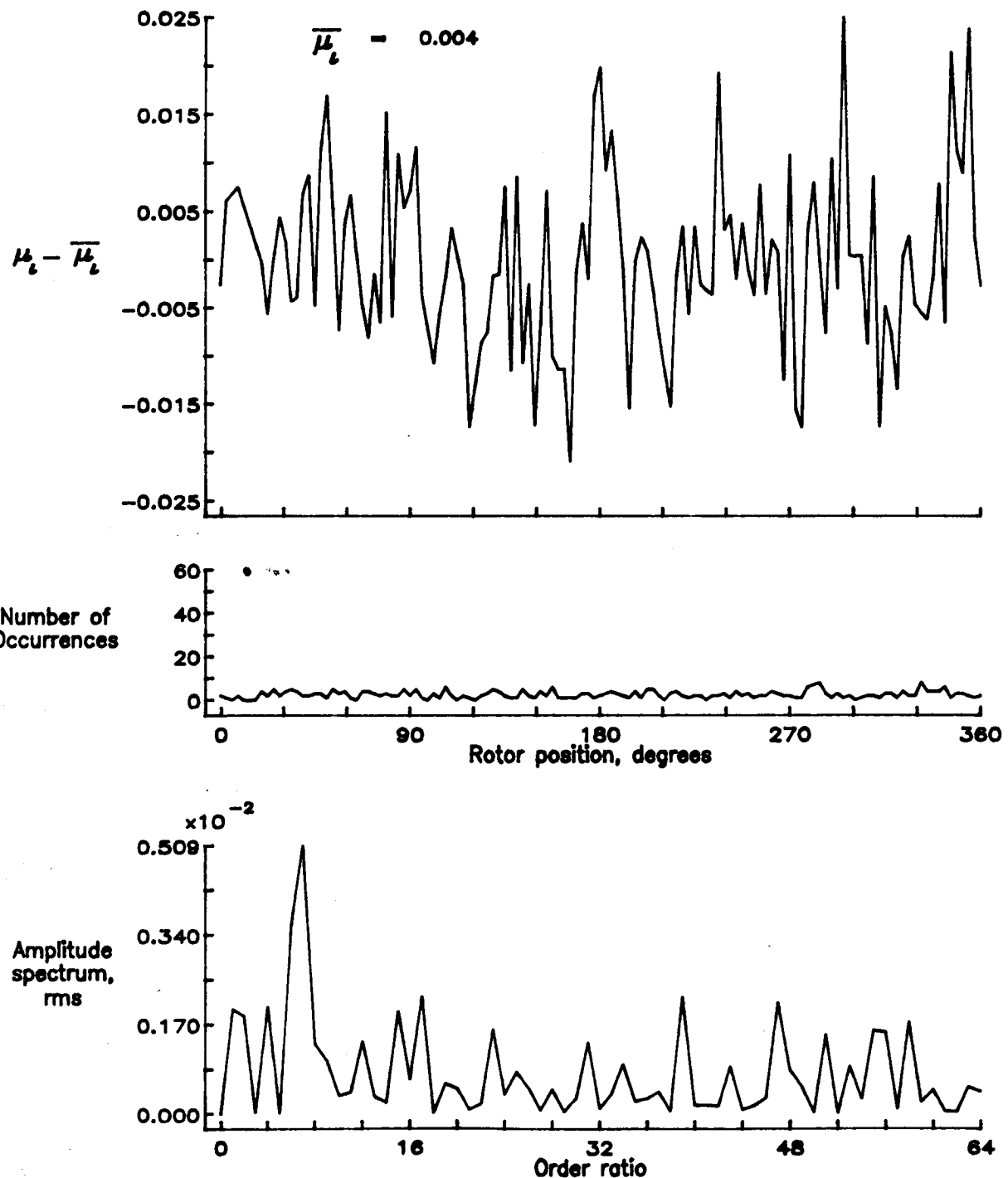


Figure 67.— Induced inflow velocity measured at 90 degrees and r/R of 0.98.

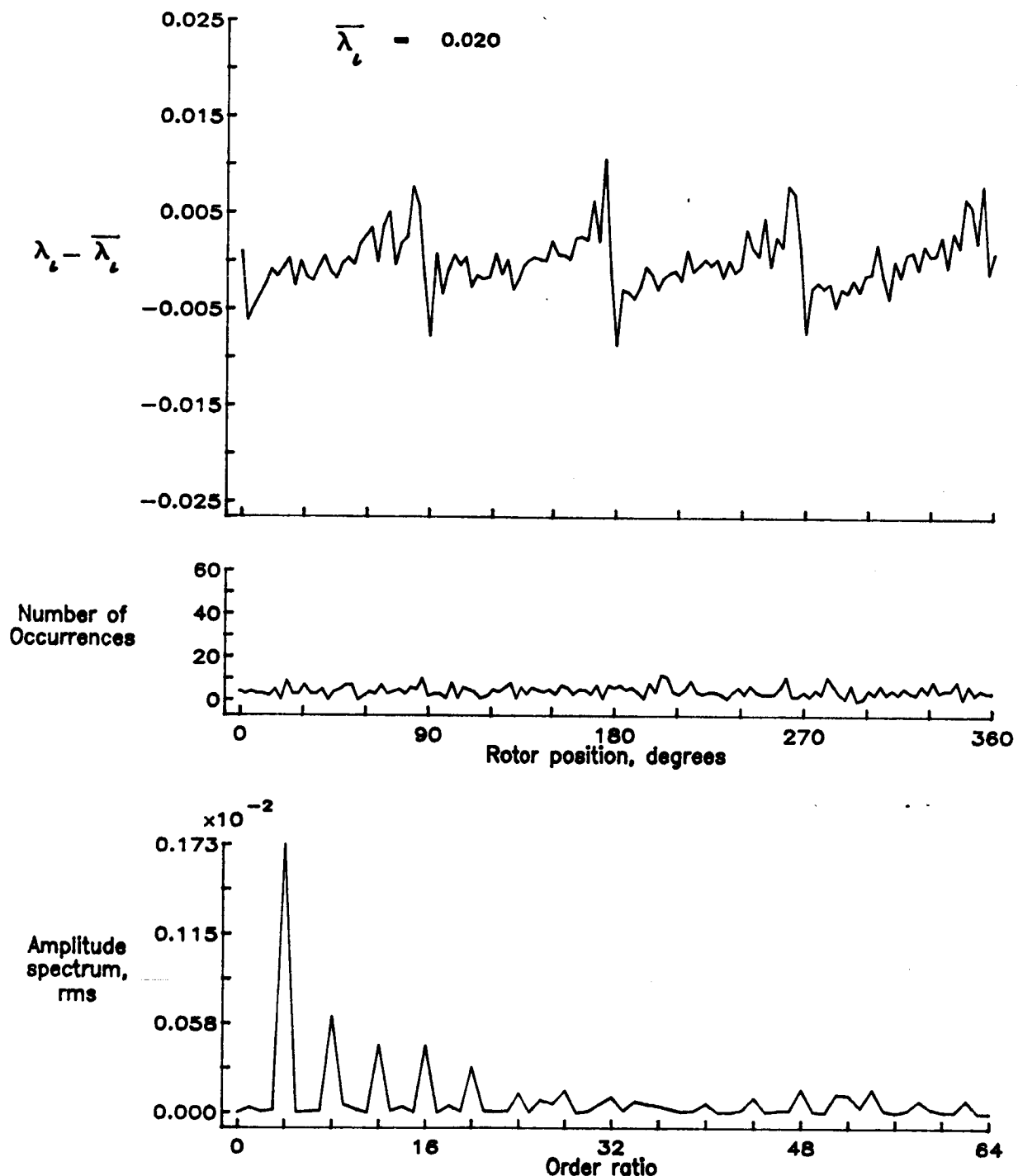


Figure 67.— Concluded.

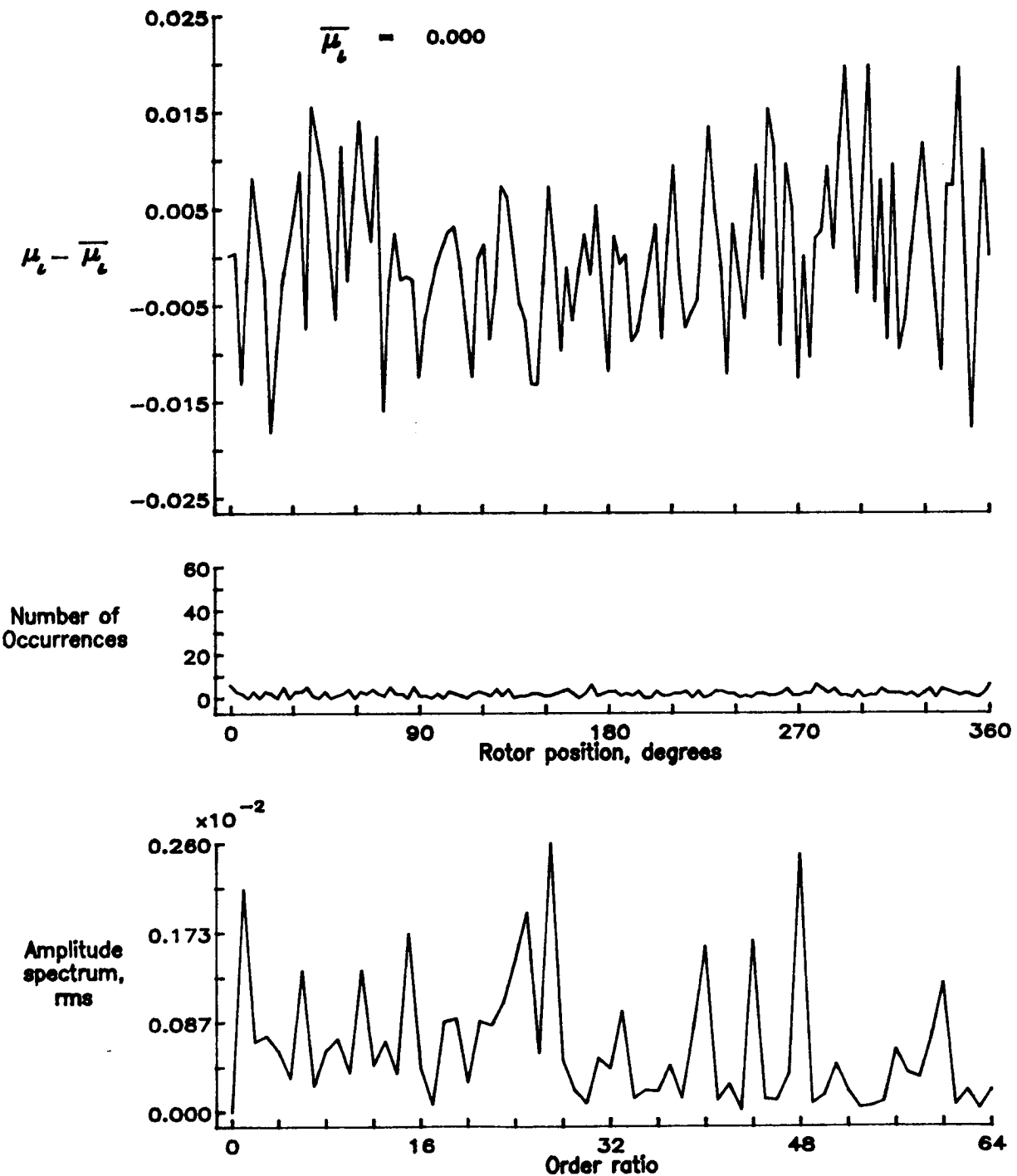


Figure 68.— Induced inflow velocity measured at 90 degrees and r/R of 1.02.

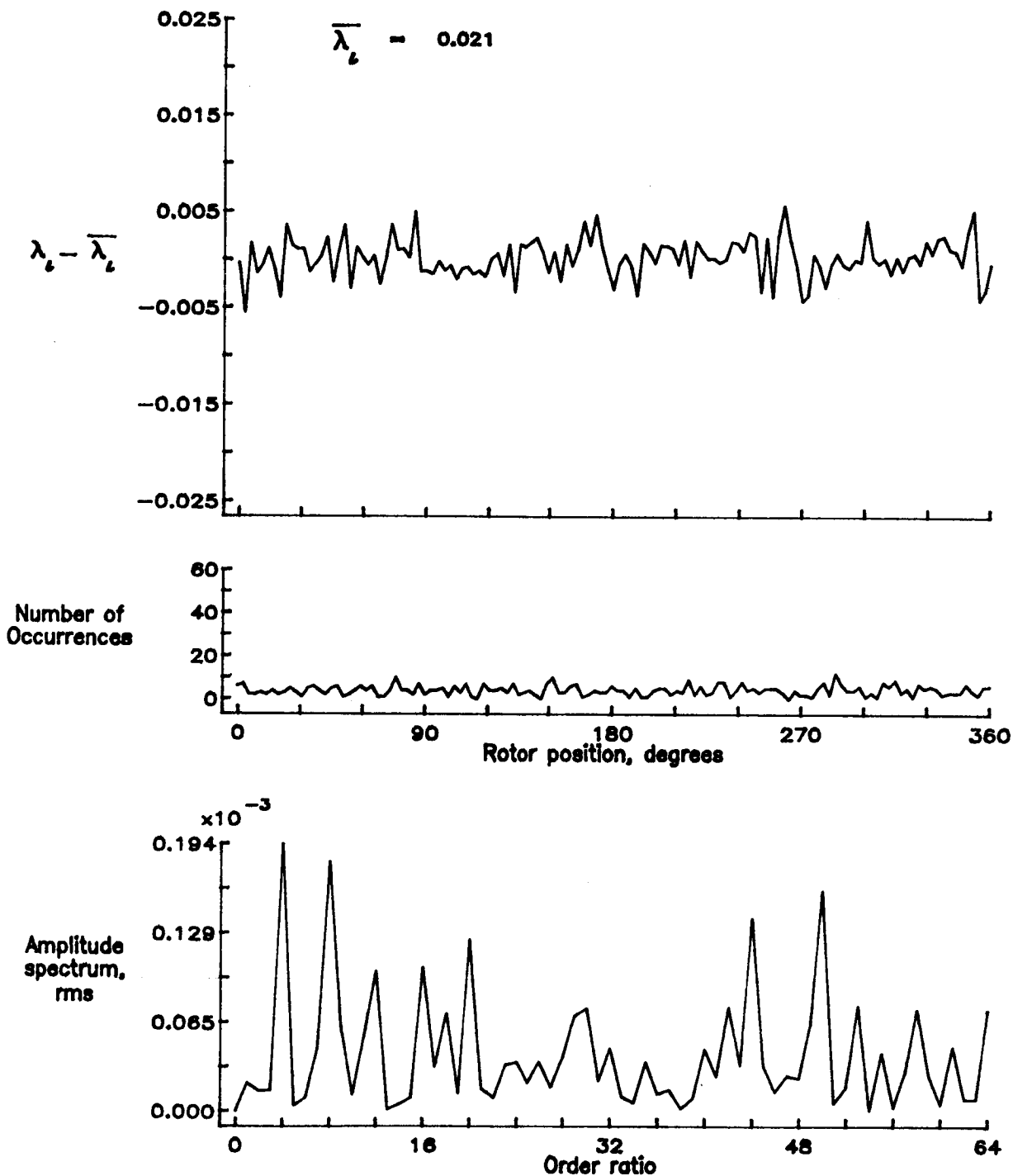


Figure 68.— Concluded.

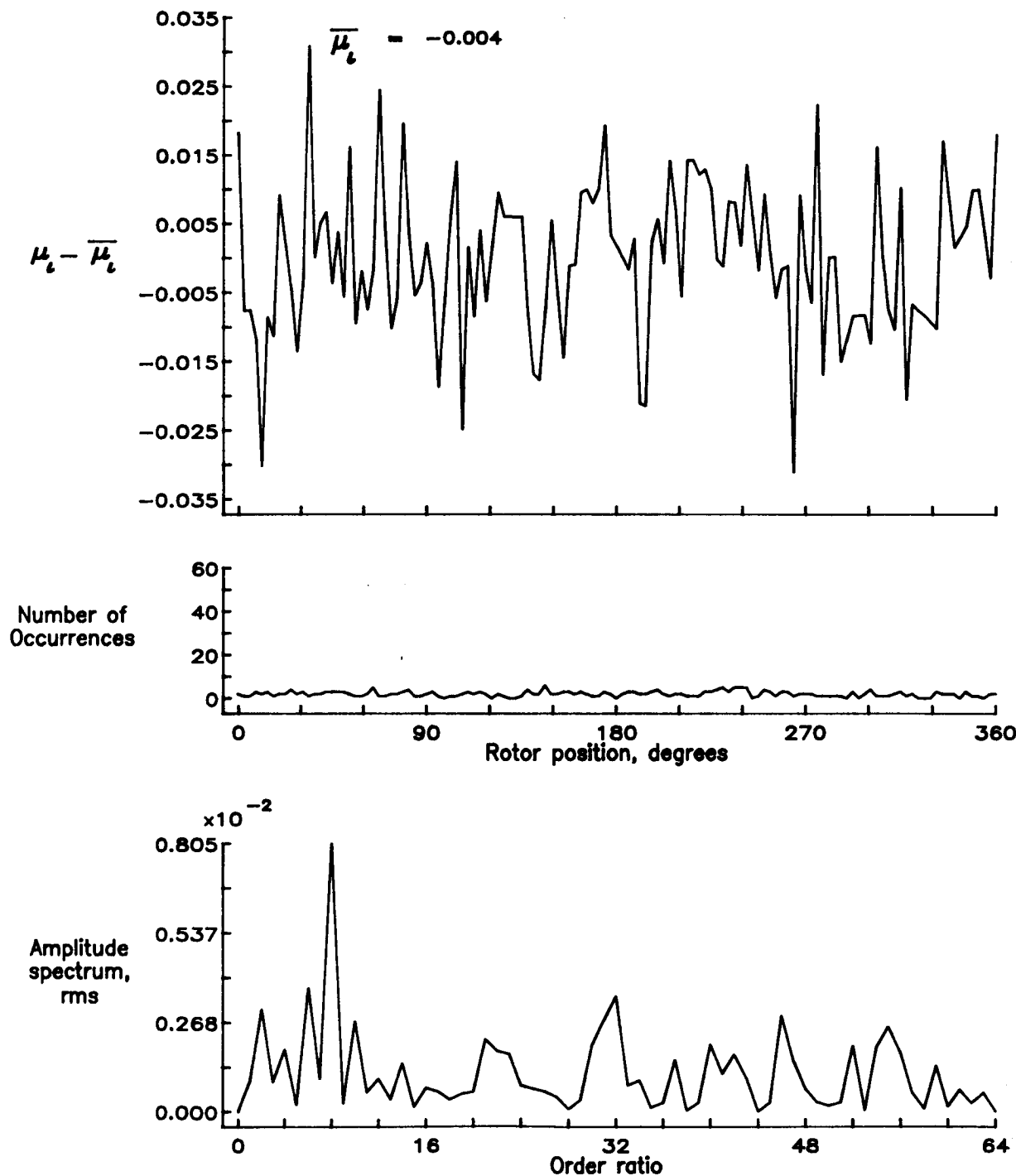


Figure 69.— Induced inflow velocity measured at 90 degrees and  $r/R$  of 1.04.

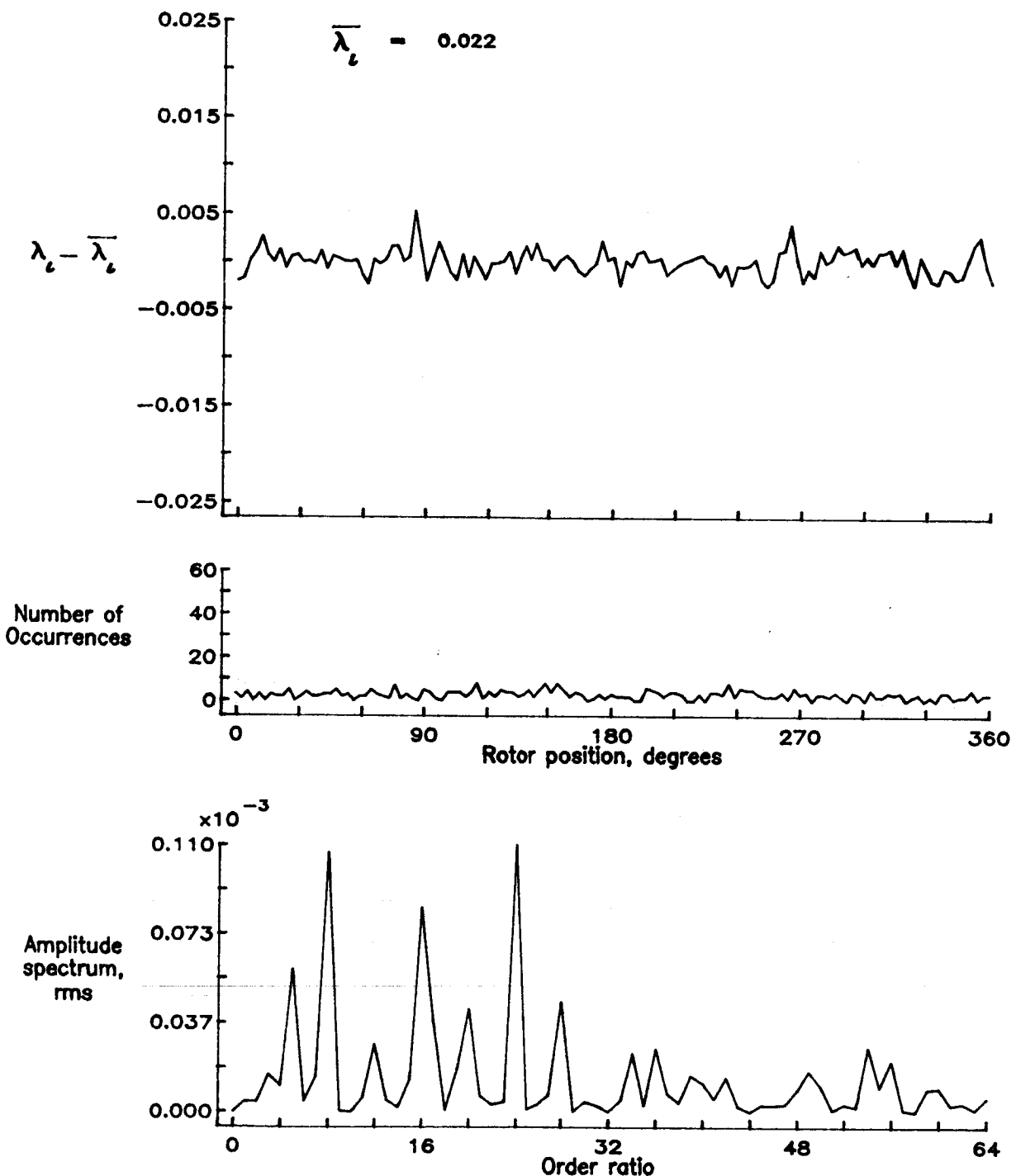


Figure 69.— Concluded.

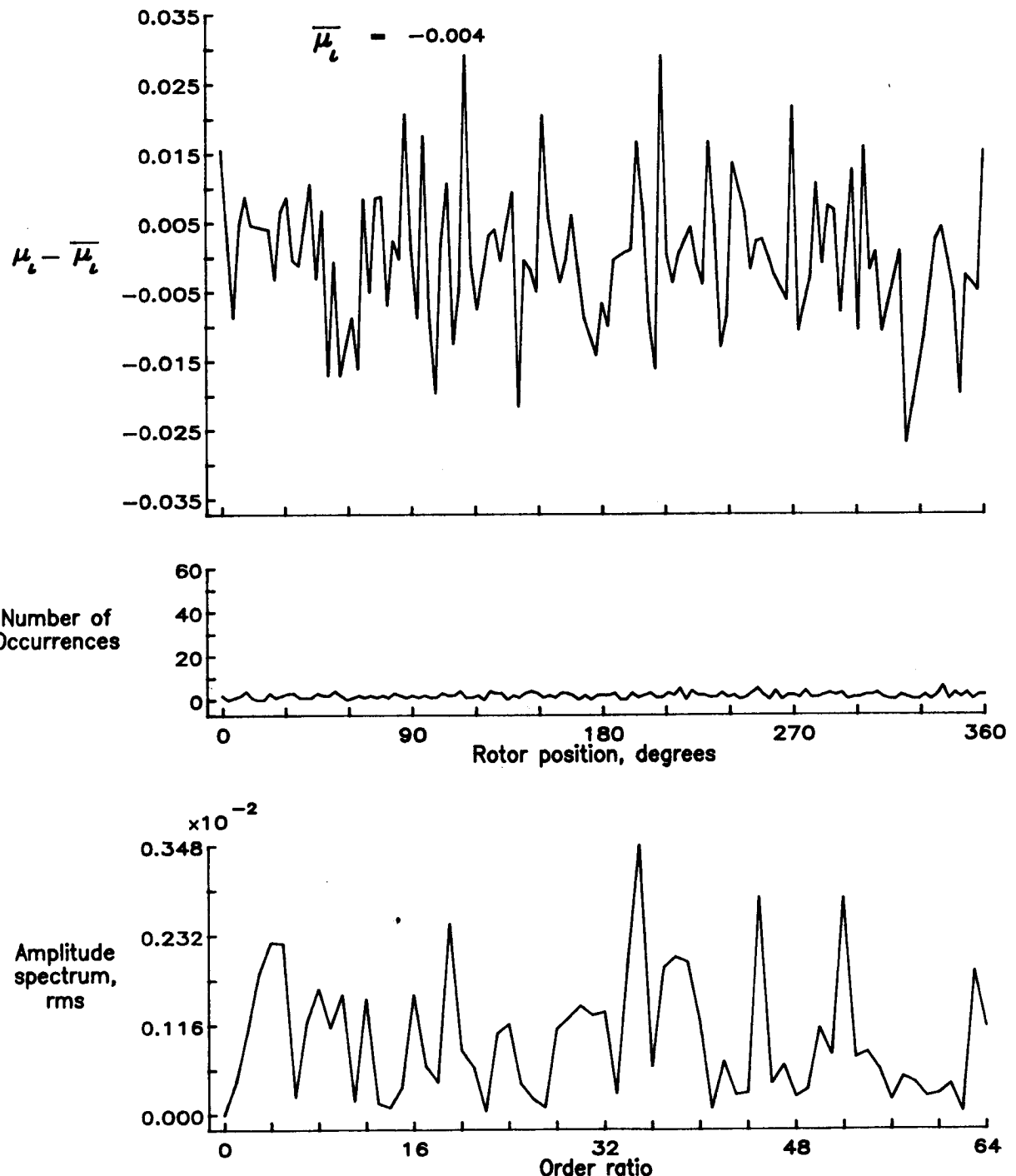


Figure 70.— Induced inflow velocity measured at 90 degrees and r/R of 1.10.

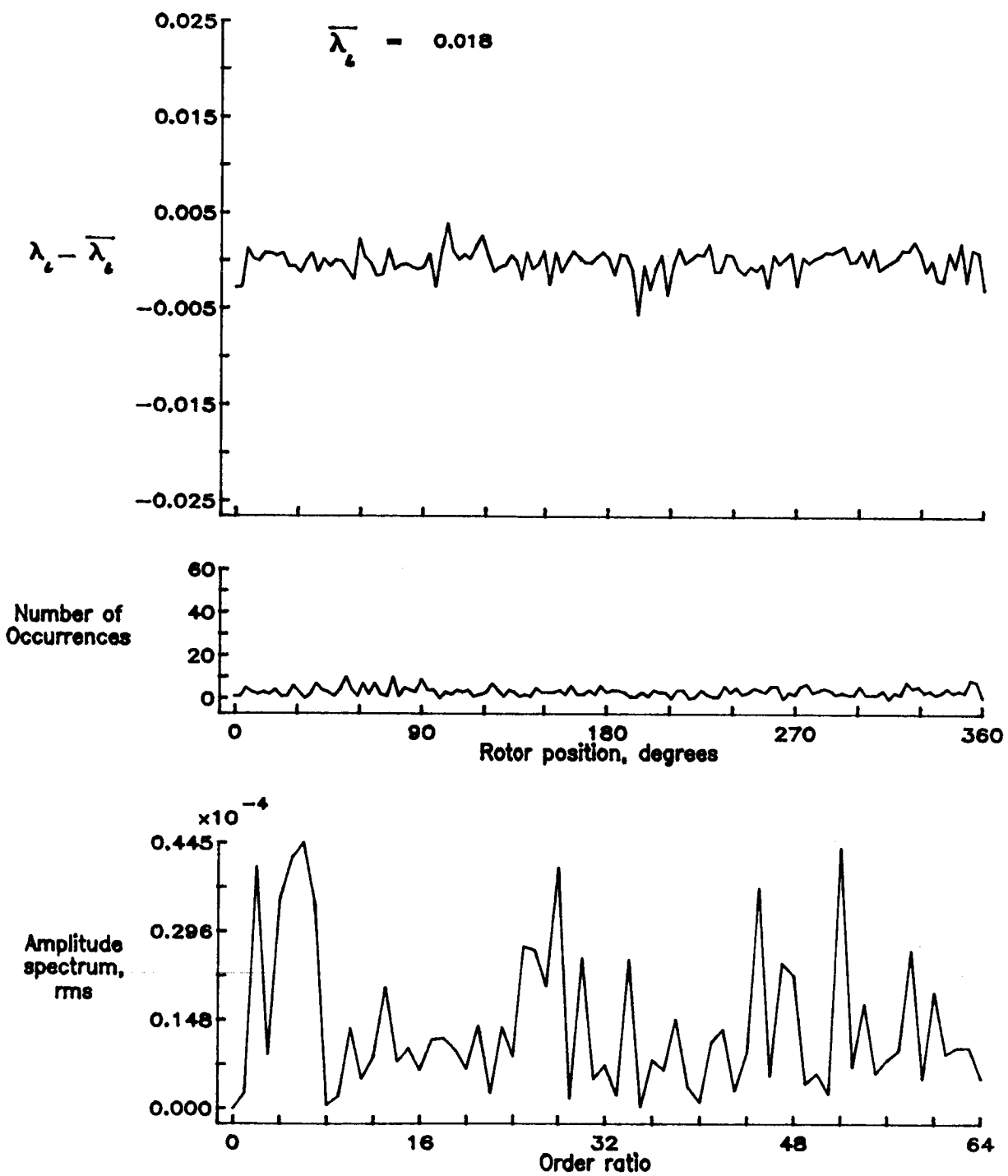


Figure 70.— Concluded.

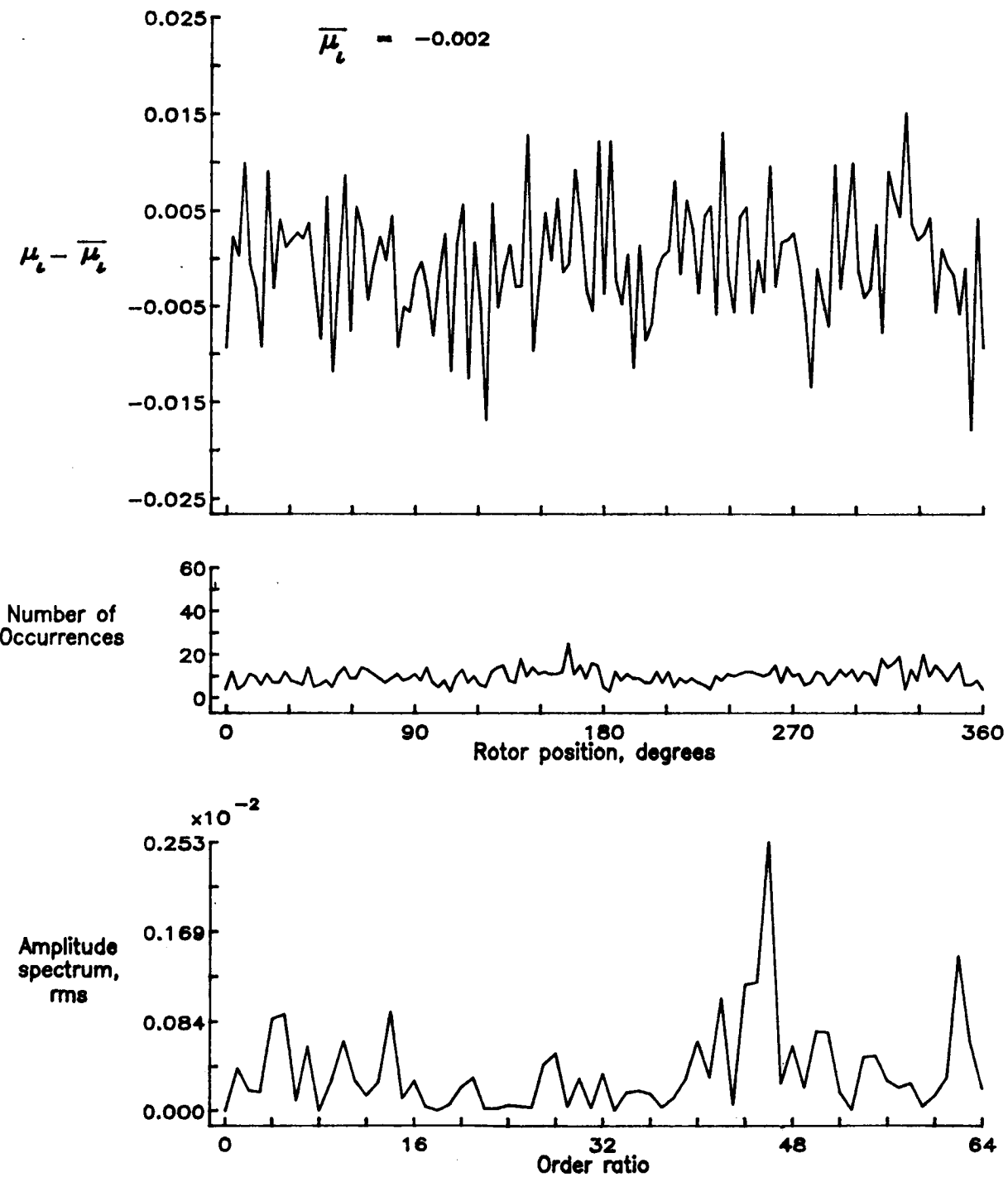


Figure 71.— Induced inflow velocity measured at 150 degrees and  $r/R$  of 0.20.

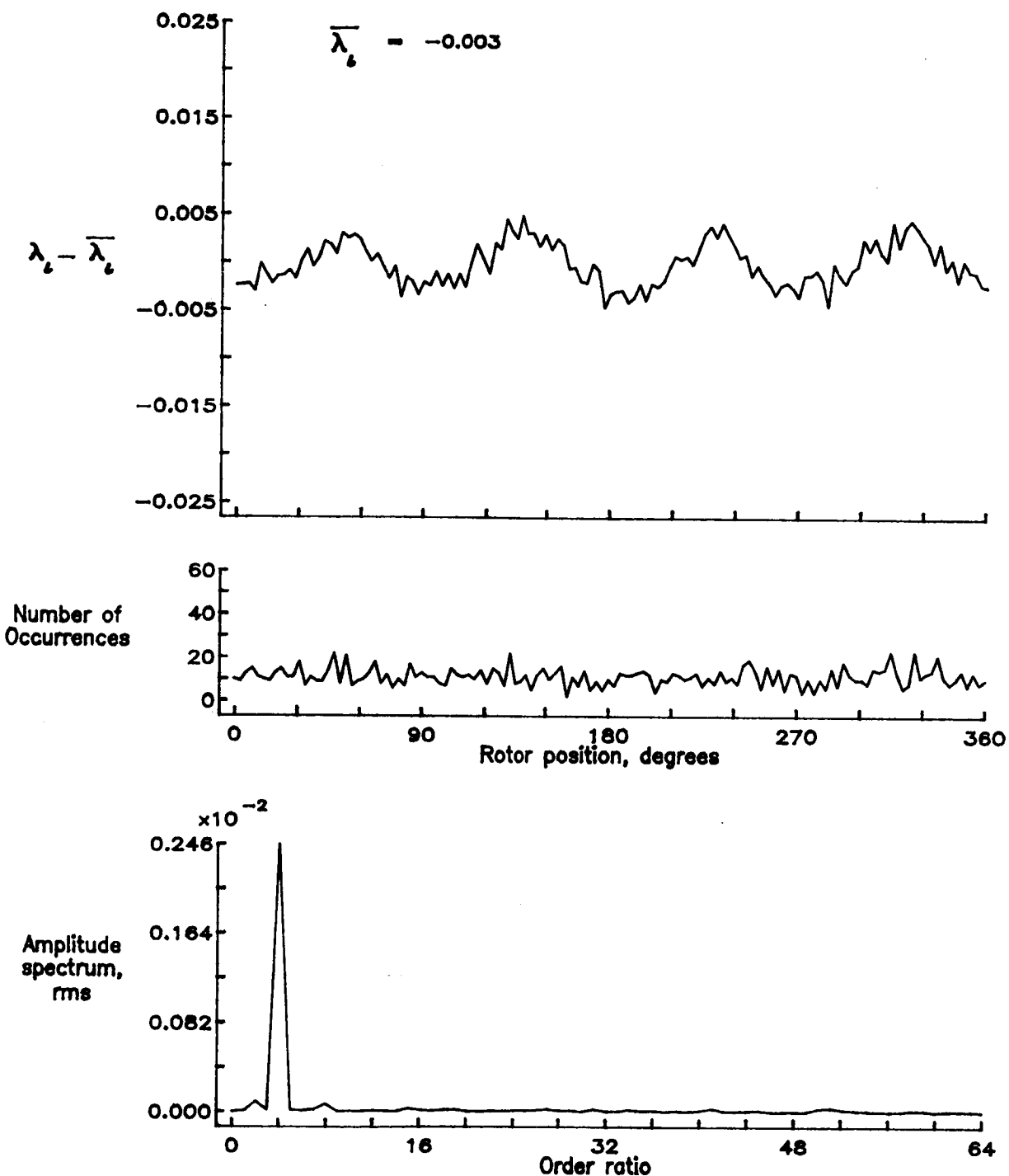


Figure 71.— Concluded.

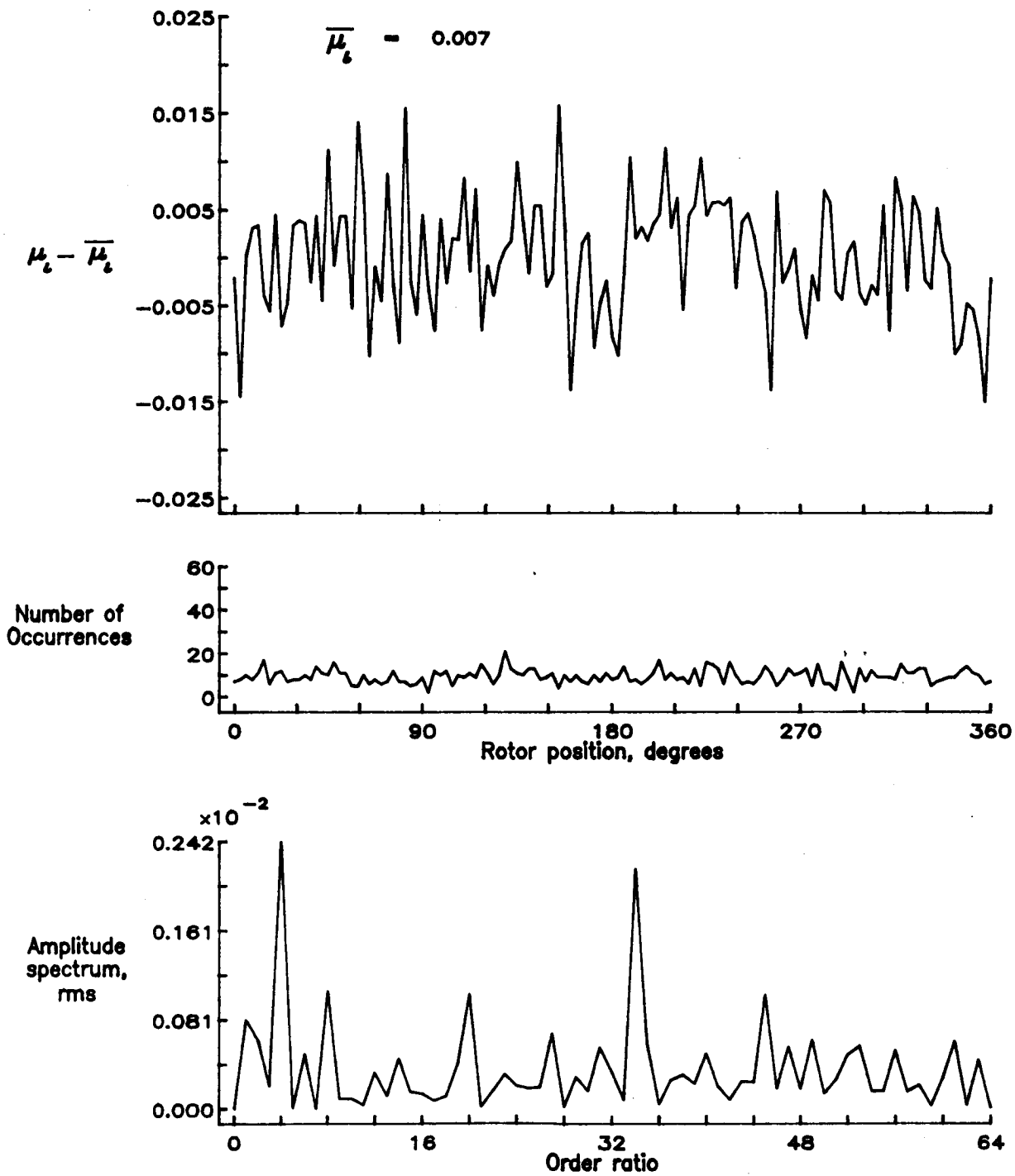


Figure 72.— Induced inflow velocity measured at 150 degrees and r/R of 0.40.

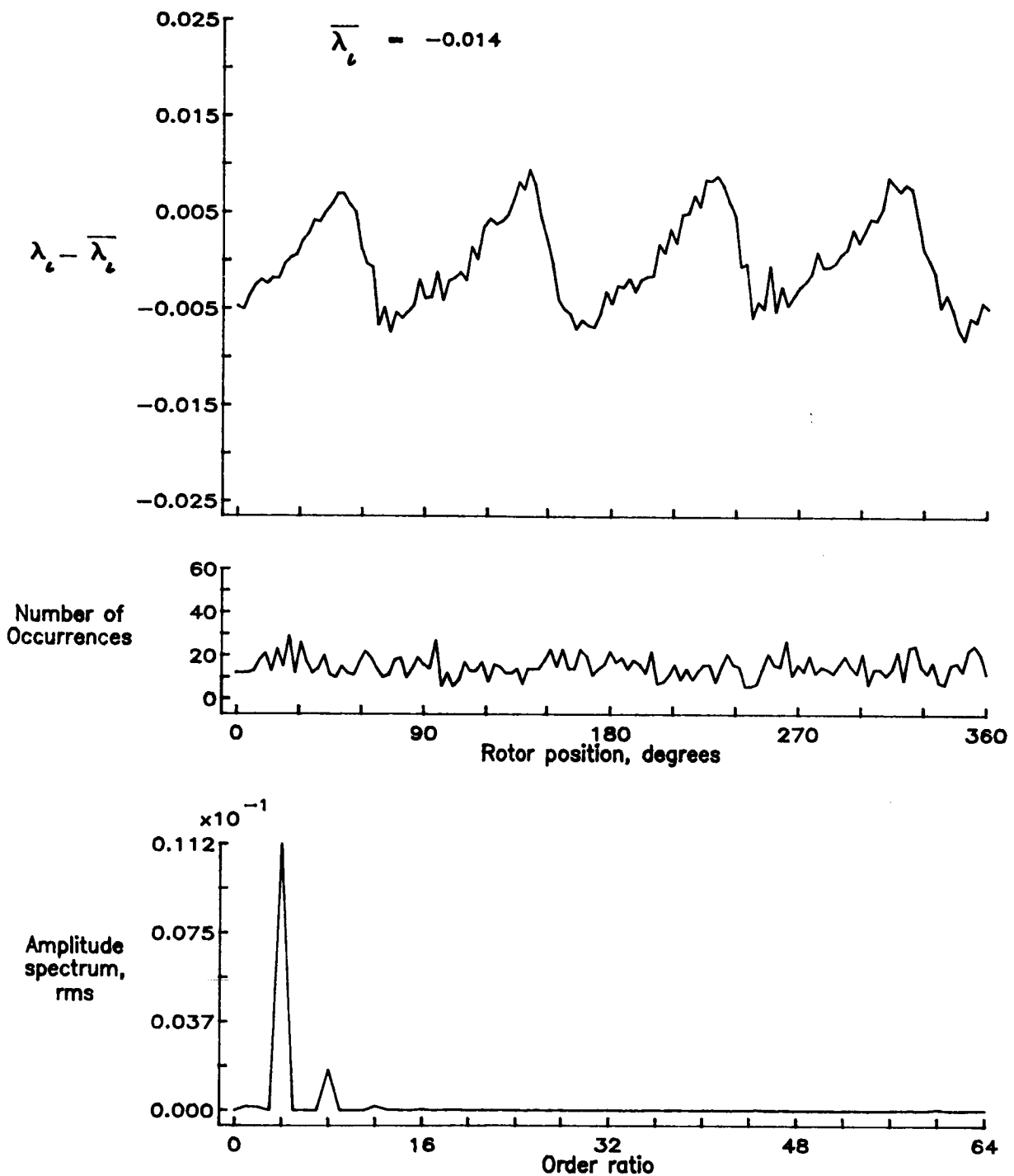


Figure 72.— Concluded.

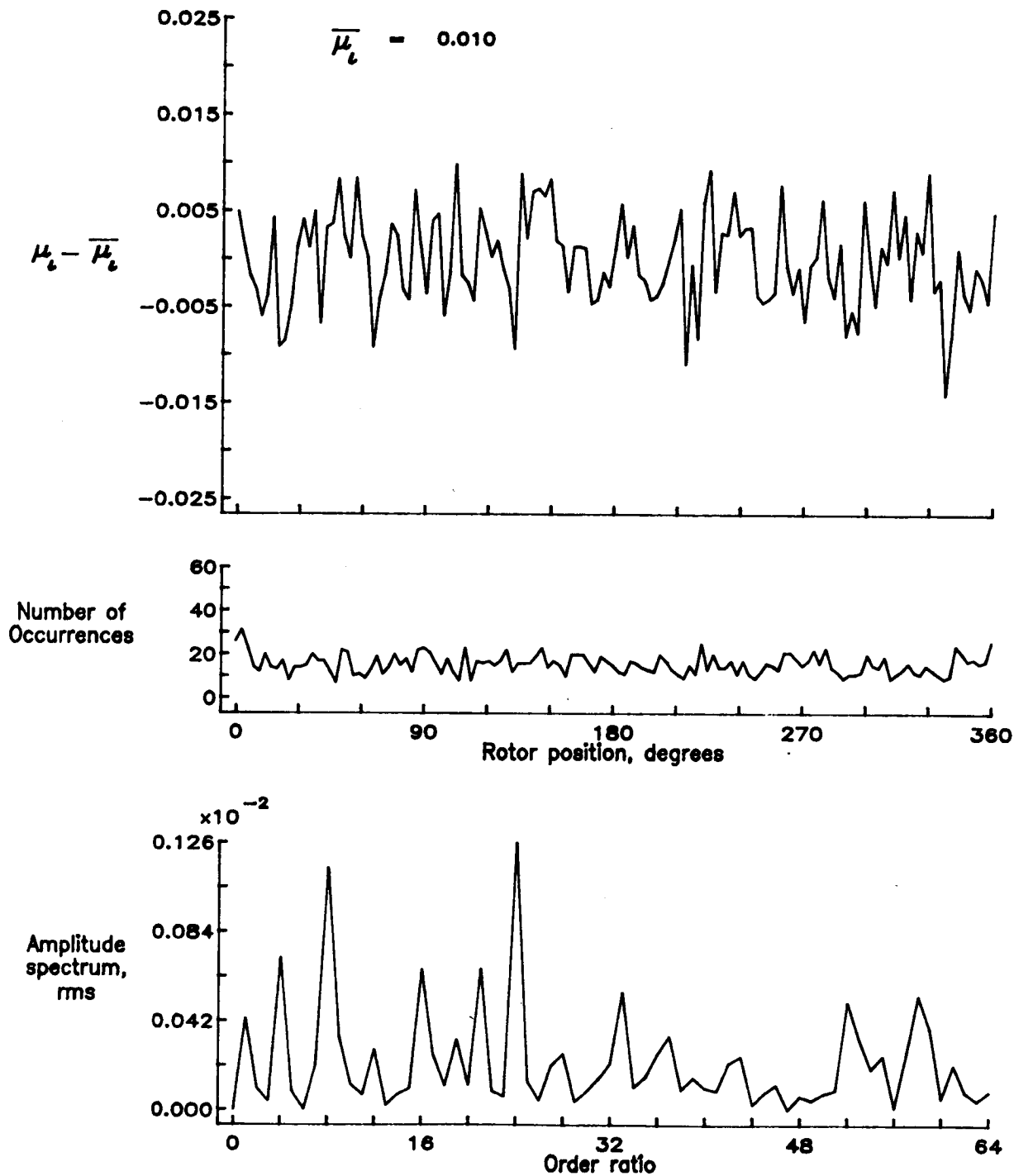


Figure 73.— Induced inflow velocity measured at 150 degrees and r/R of 0.50.

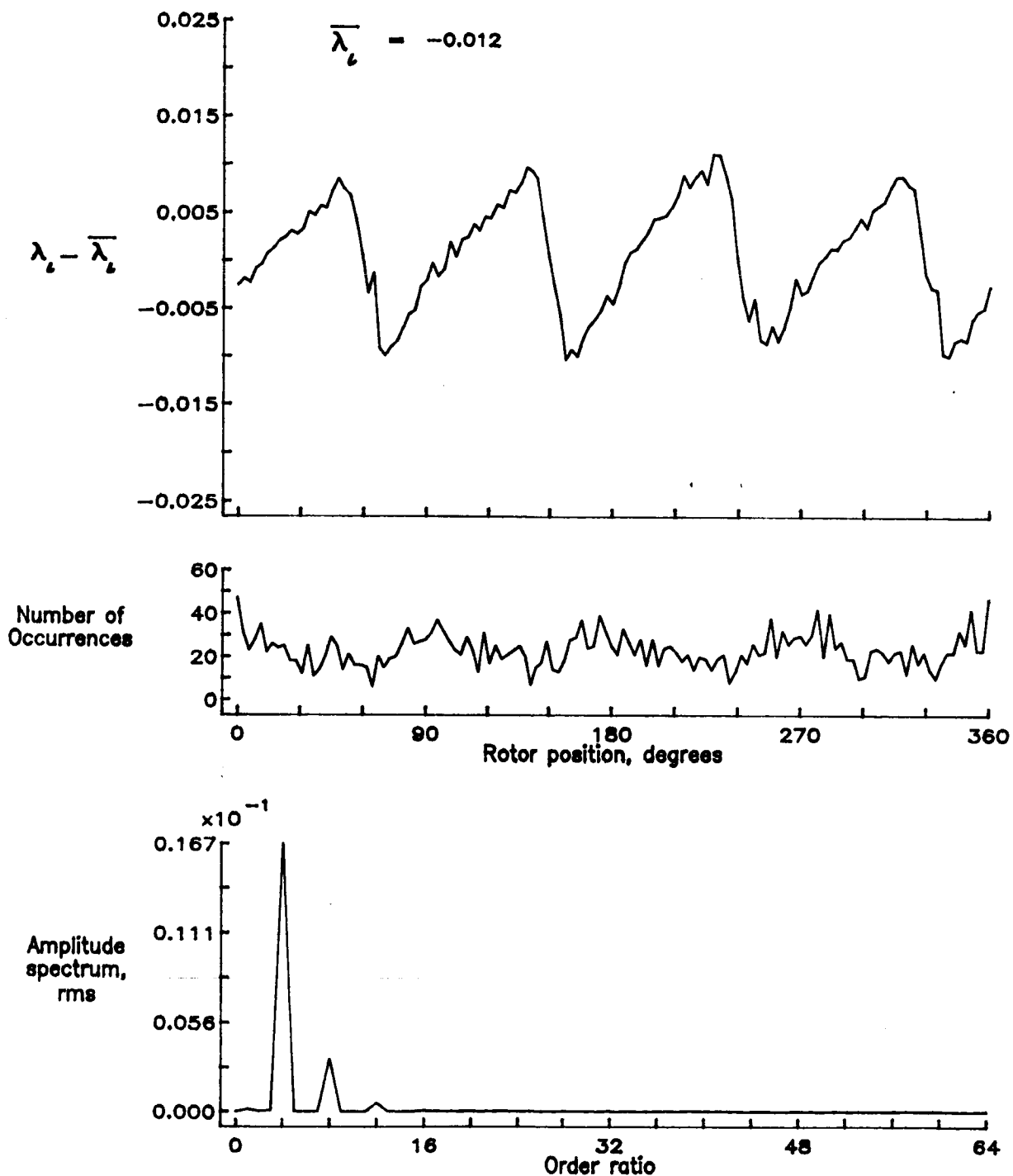


Figure 73.— Concluded.

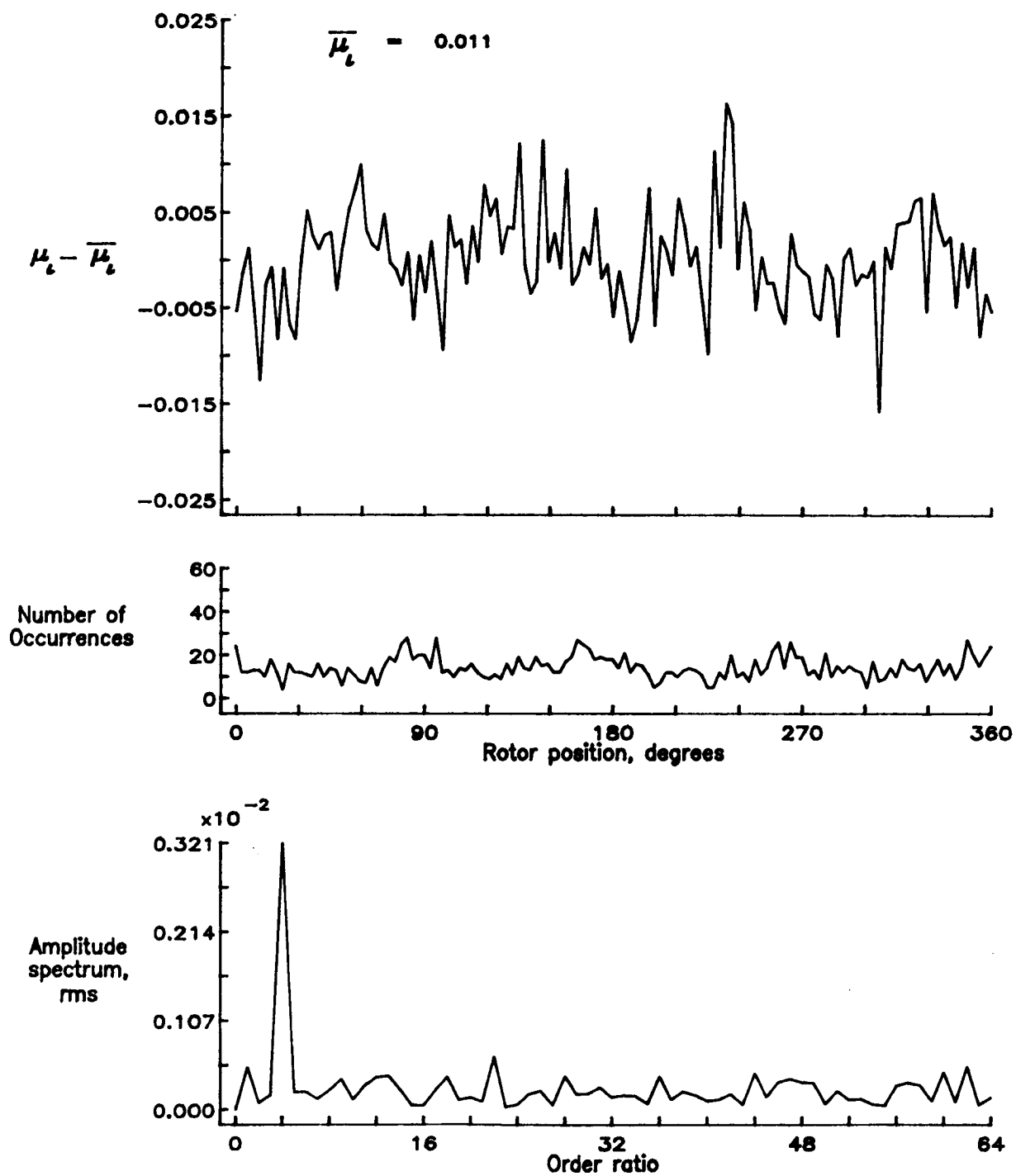


Figure 74.— Induced inflow velocity measured at 150 degrees and r/R of 0.60.

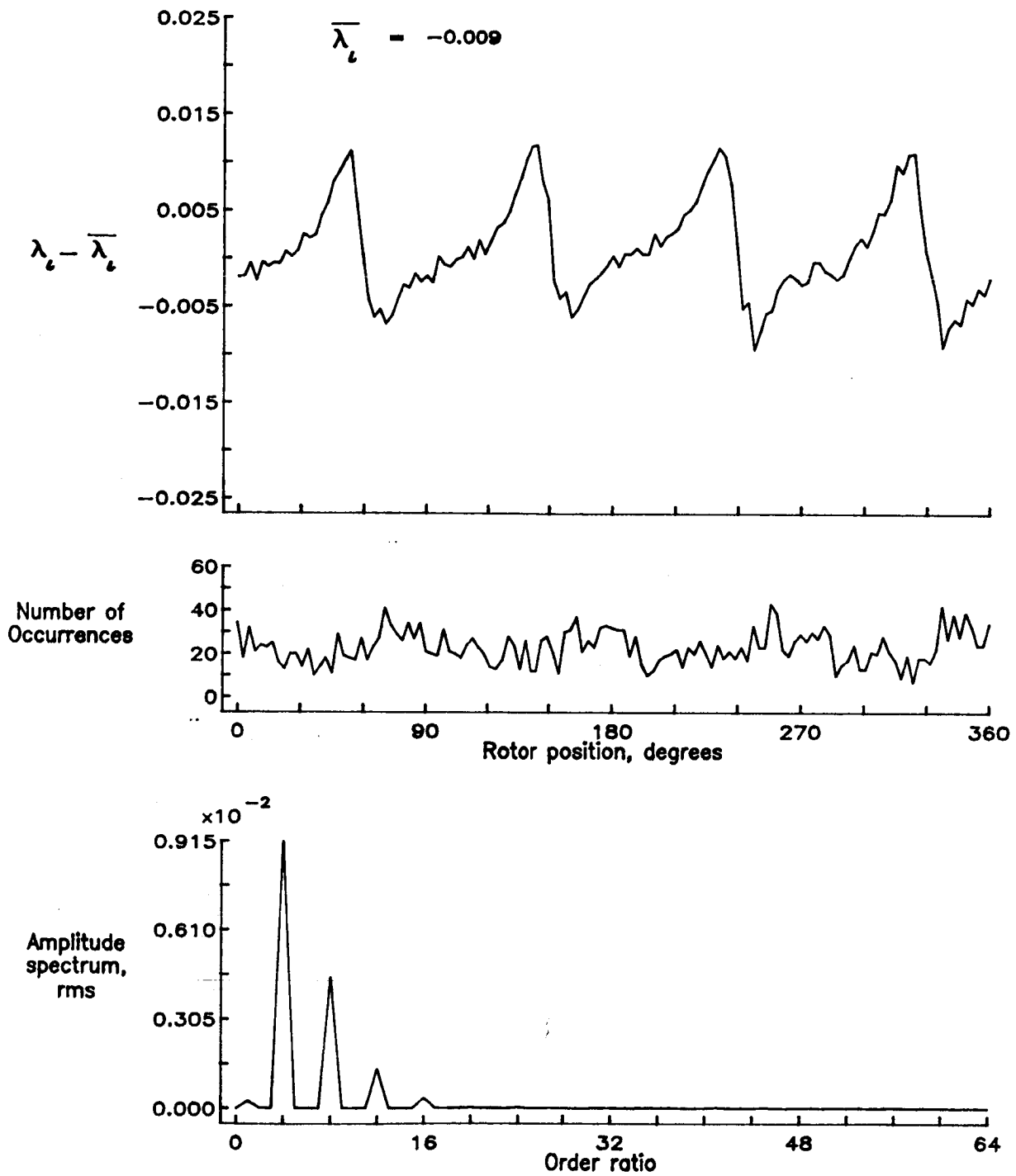


Figure 74.— Concluded.

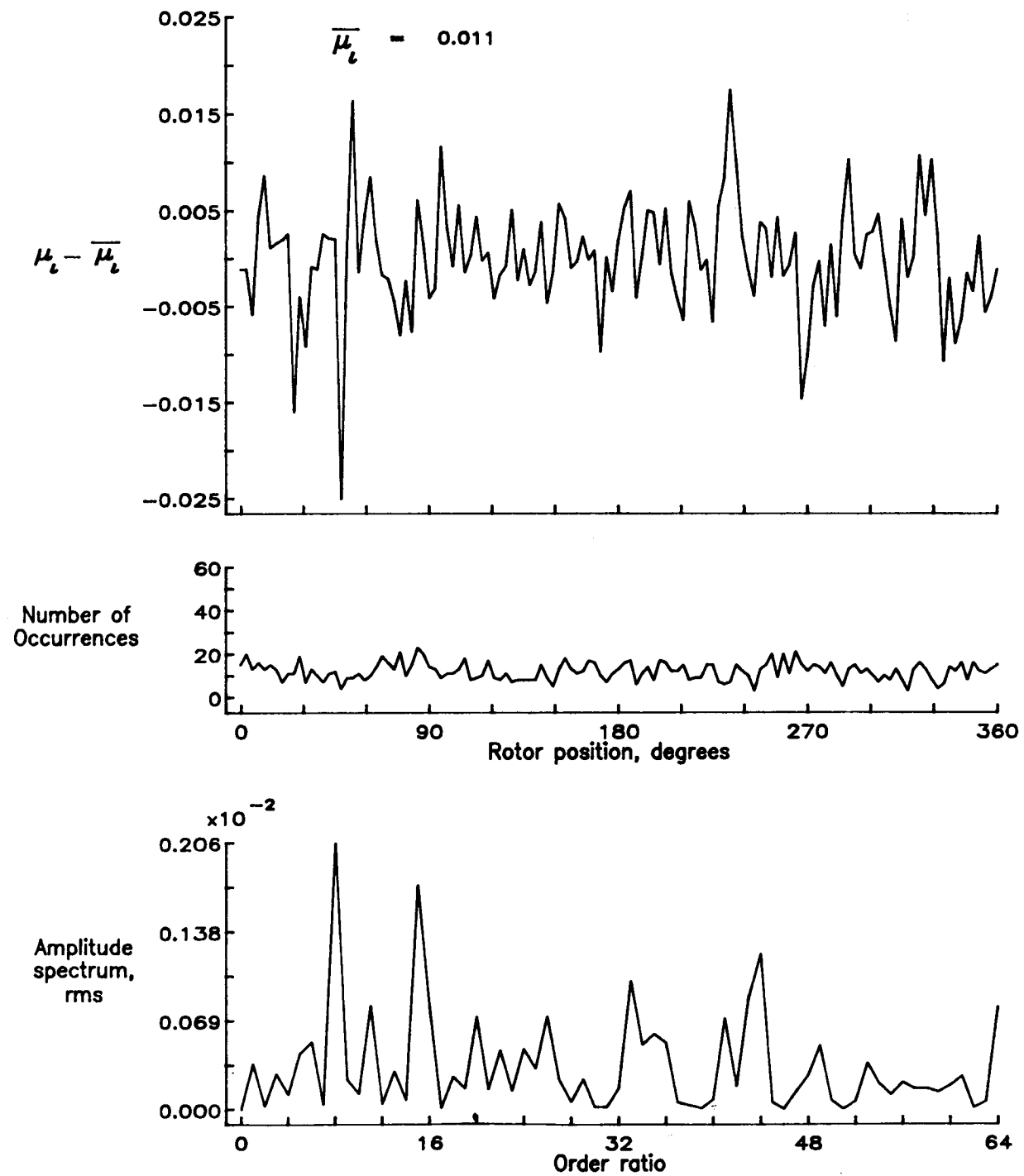


Figure 75.— Induced inflow velocity measured at 150 degrees and  $r/R$  of 0.70.

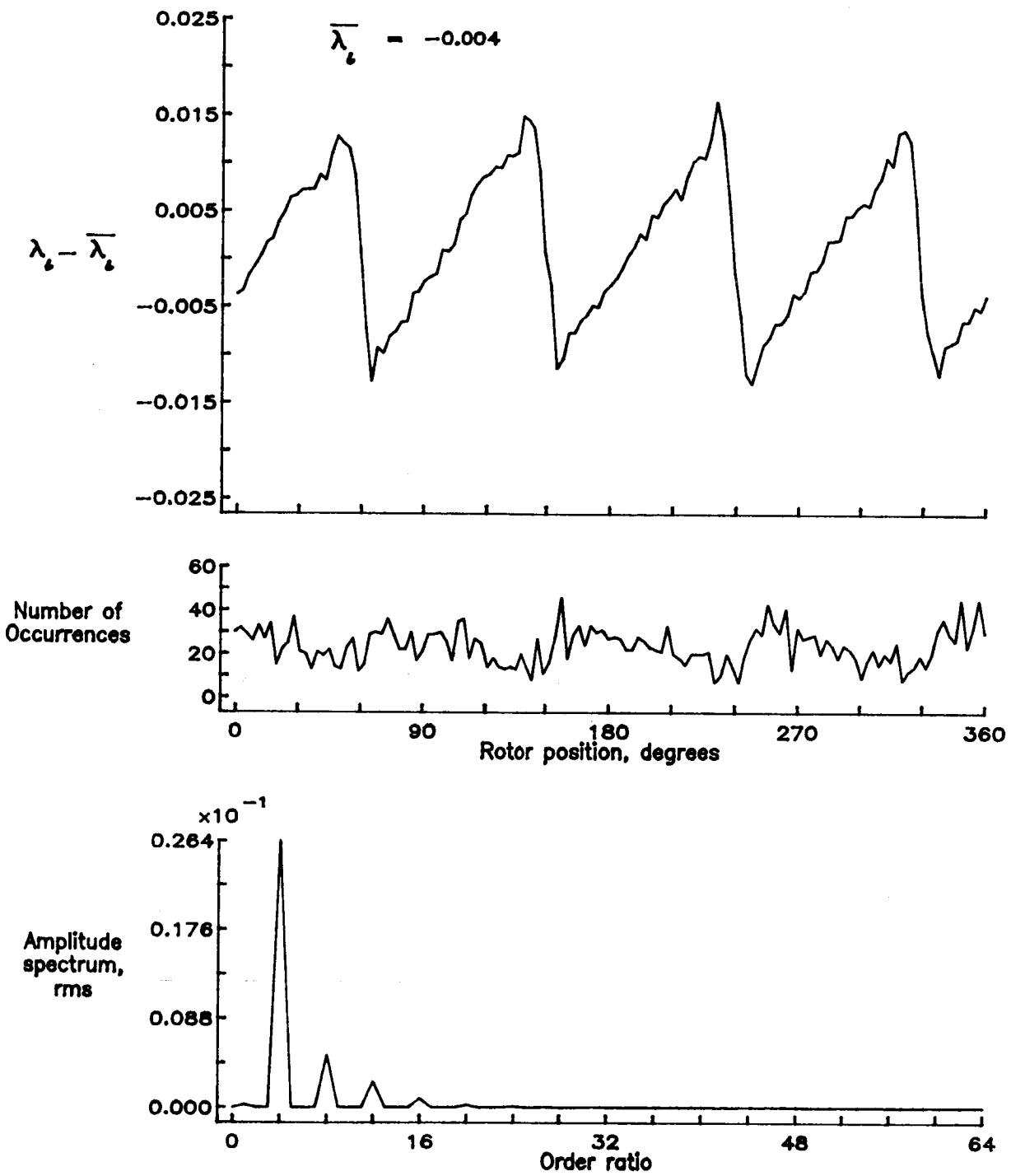


Figure 75.— Concluded.

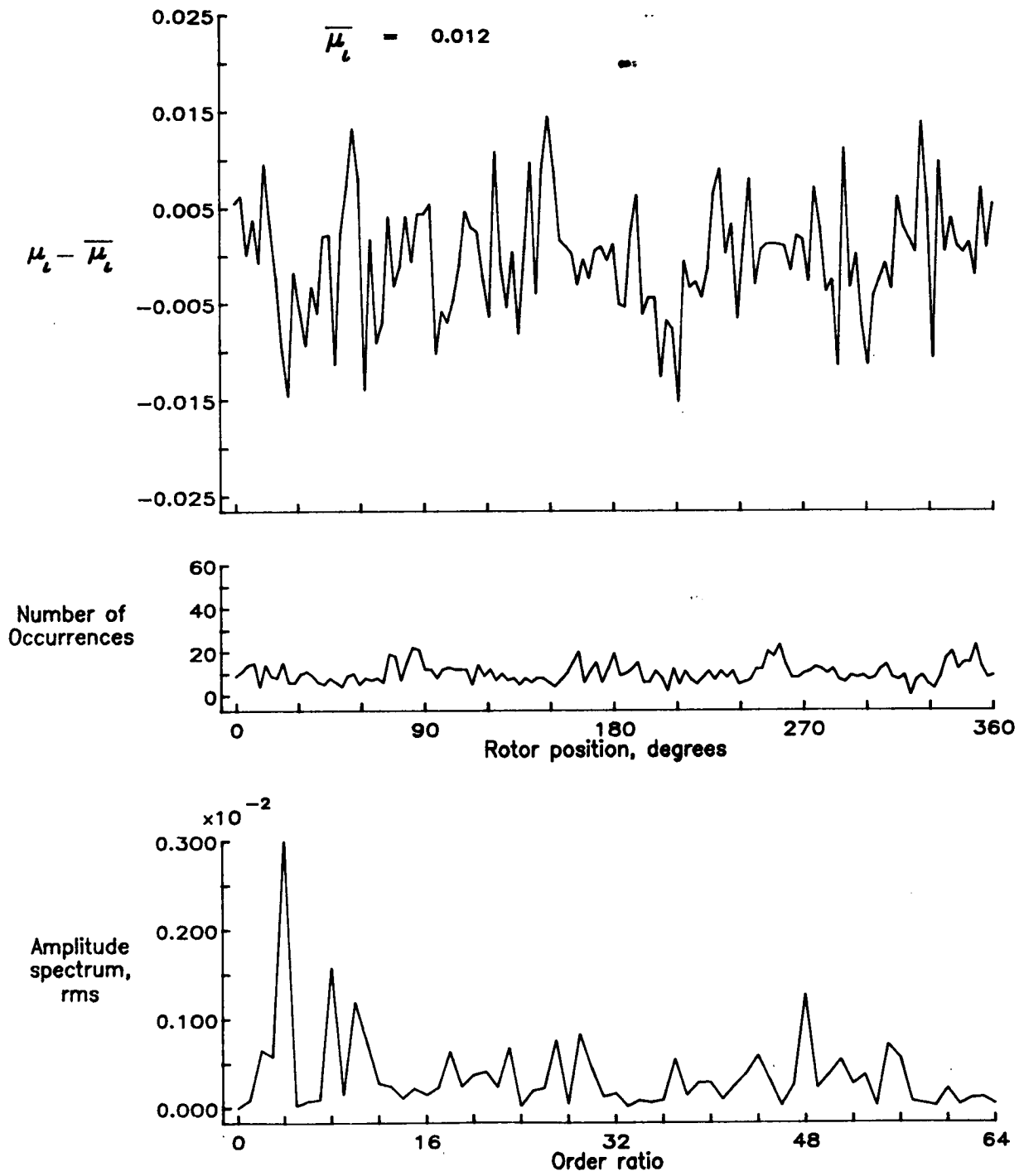


Figure 76.— Induced inflow velocity measured at 150 degrees and r/R of 0.74.

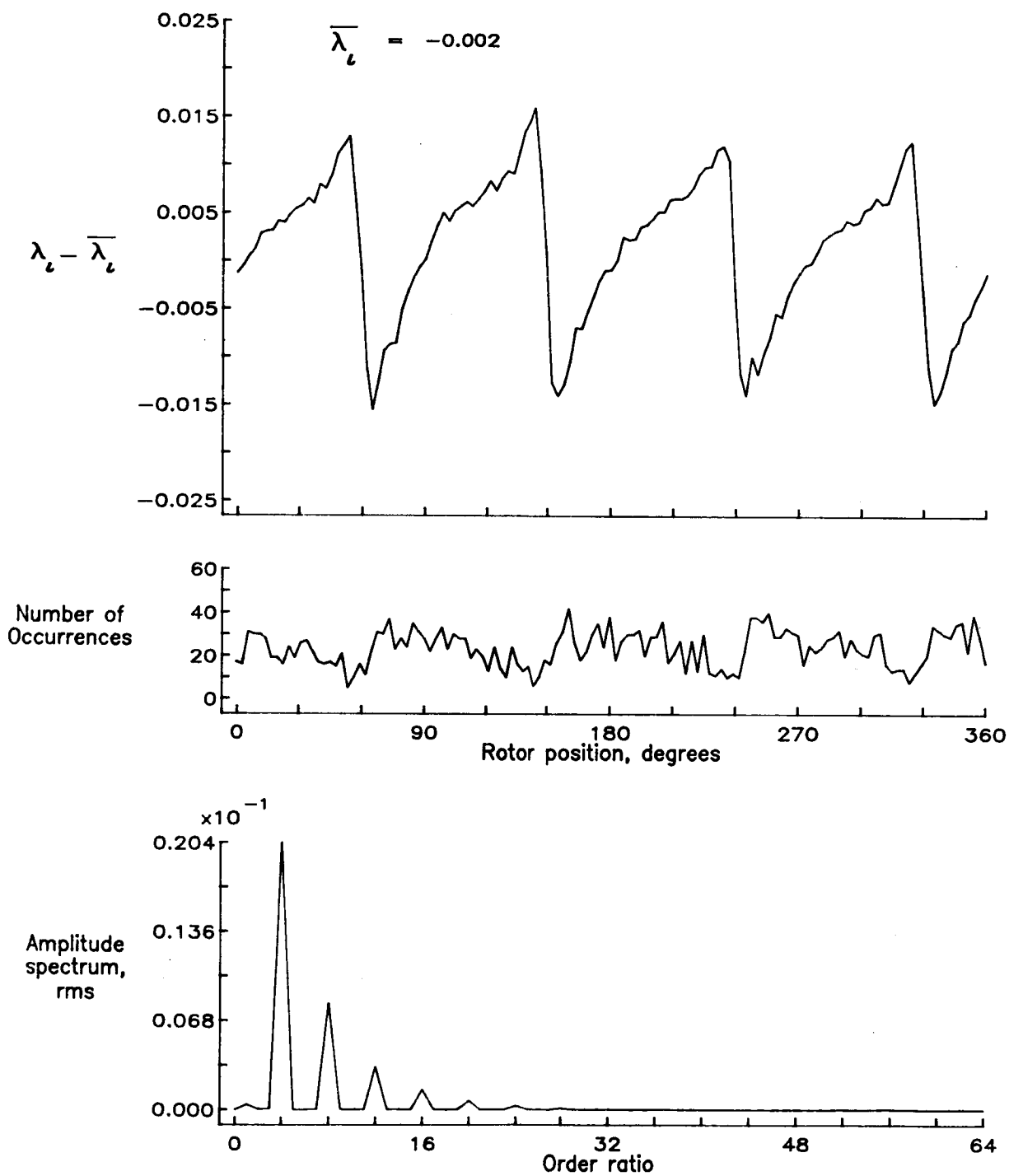


Figure 76.— Concluded.

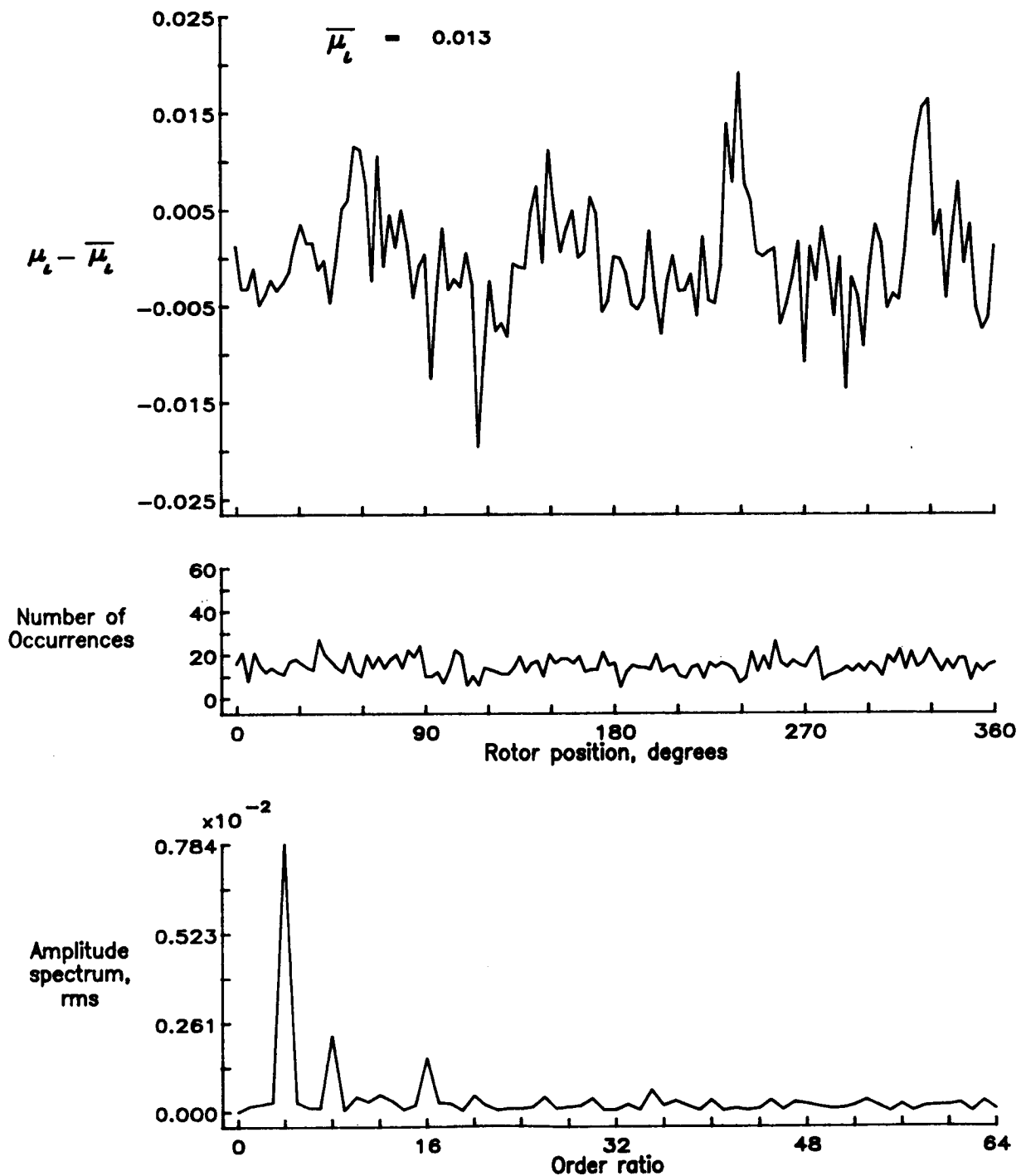


Figure 77.— Induced inflow velocity measured at 150 degrees and r/R of 0.78.

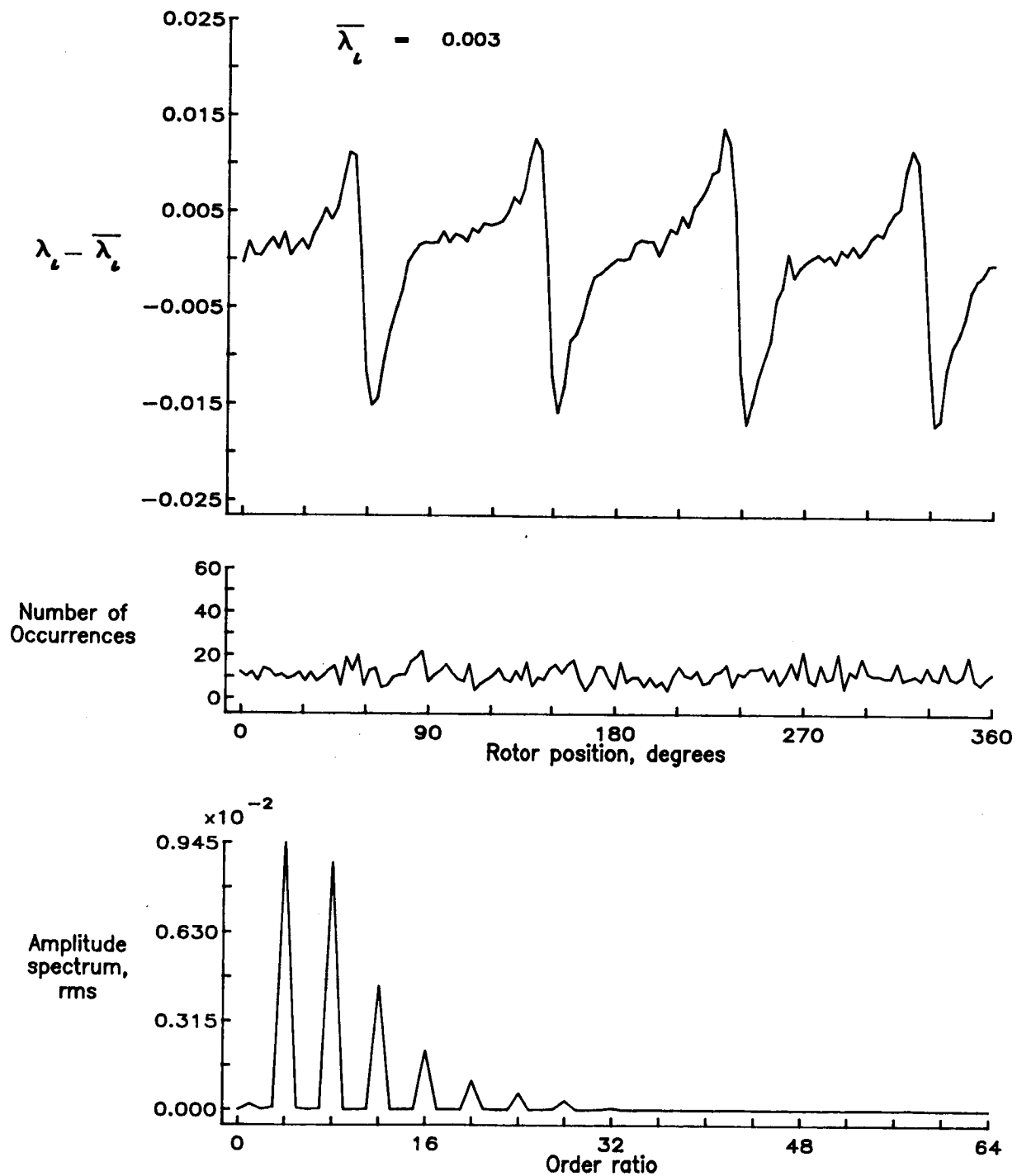


Figure 77.— Concluded.

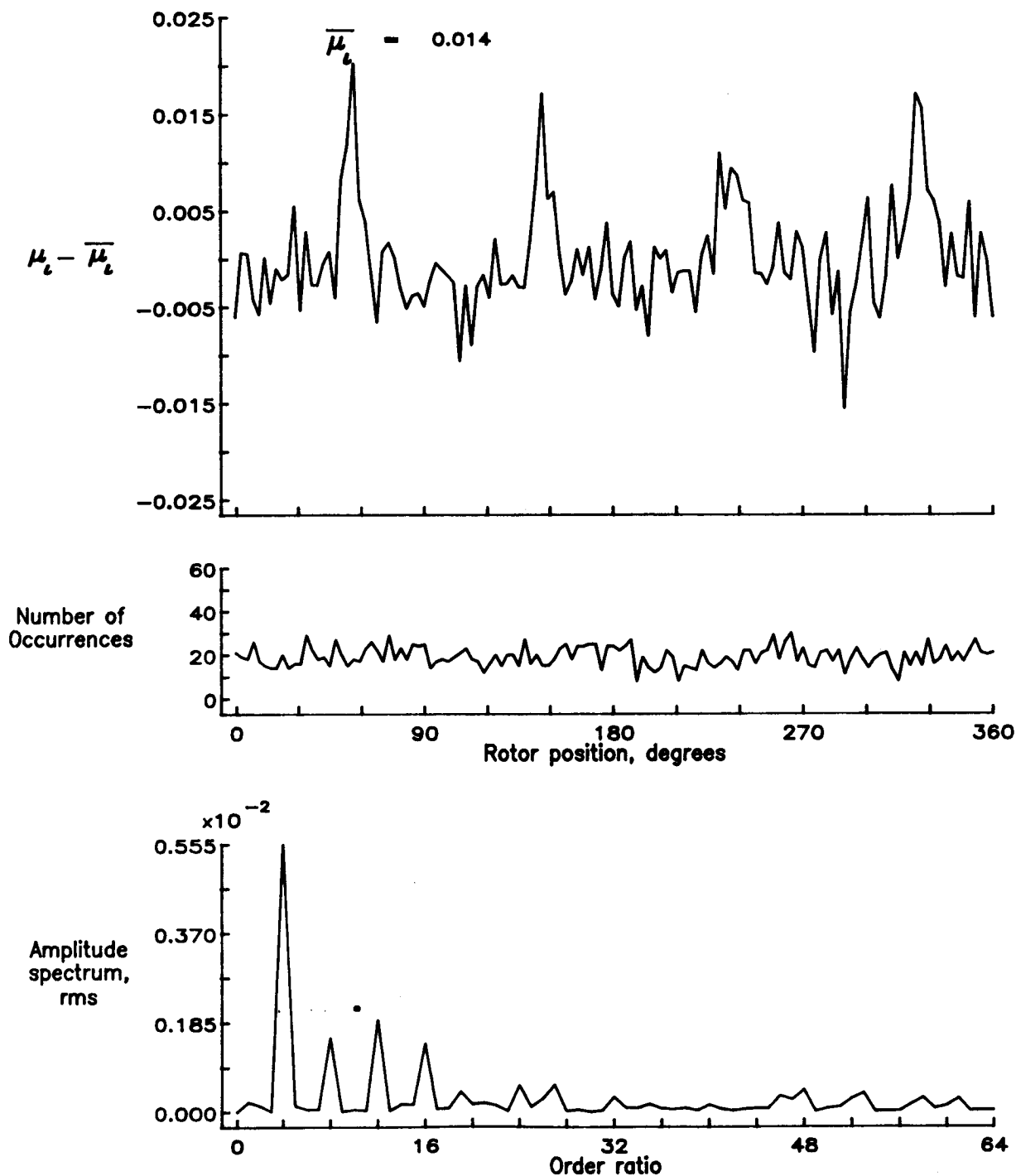


Figure 78.— Induced inflow velocity measured at 150 degrees and r/R of 0.82.

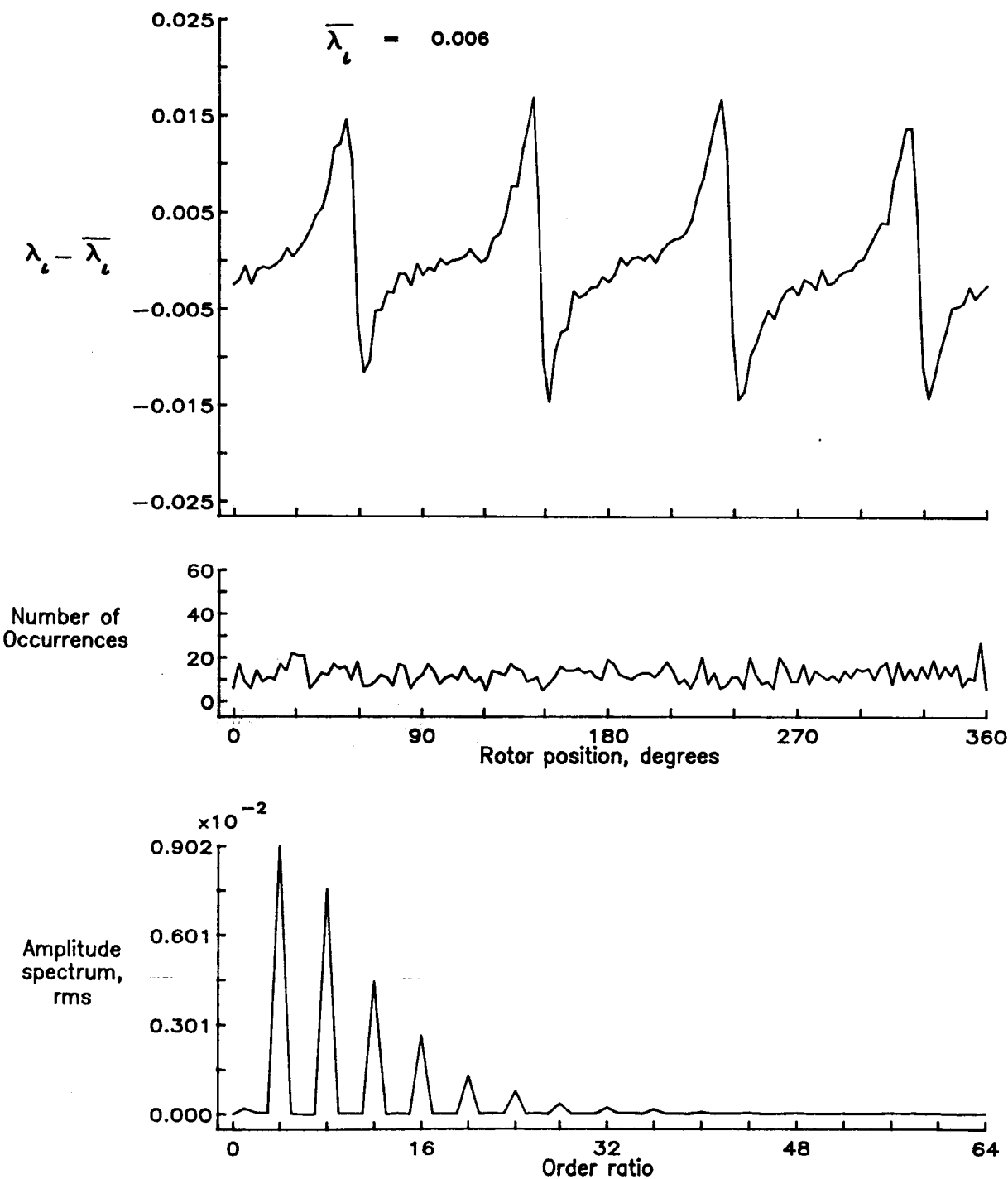


Figure 78.— Concluded.

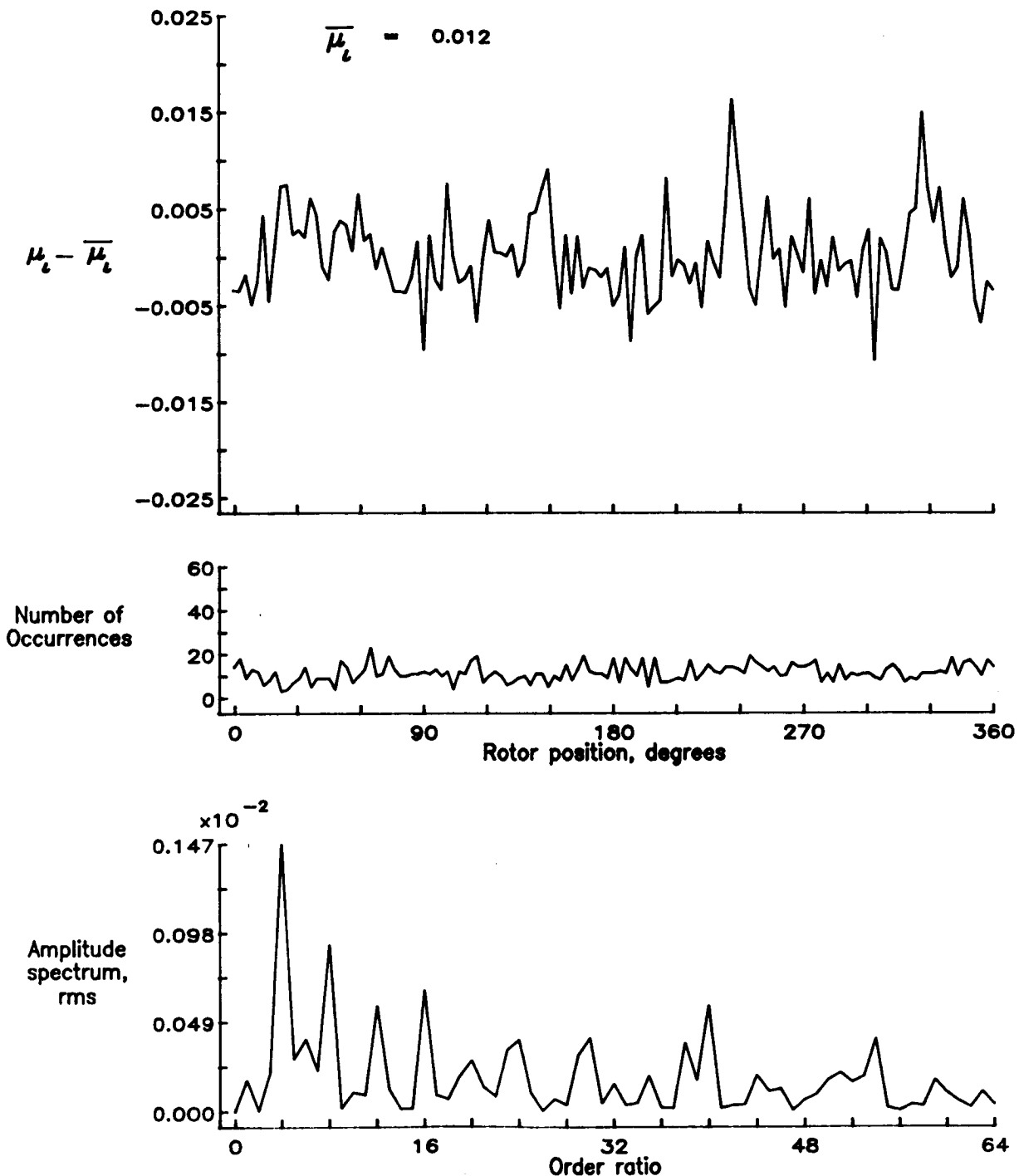


Figure 79.— Induced inflow velocity measured at 150 degrees and  $r/R$  of 0.86.

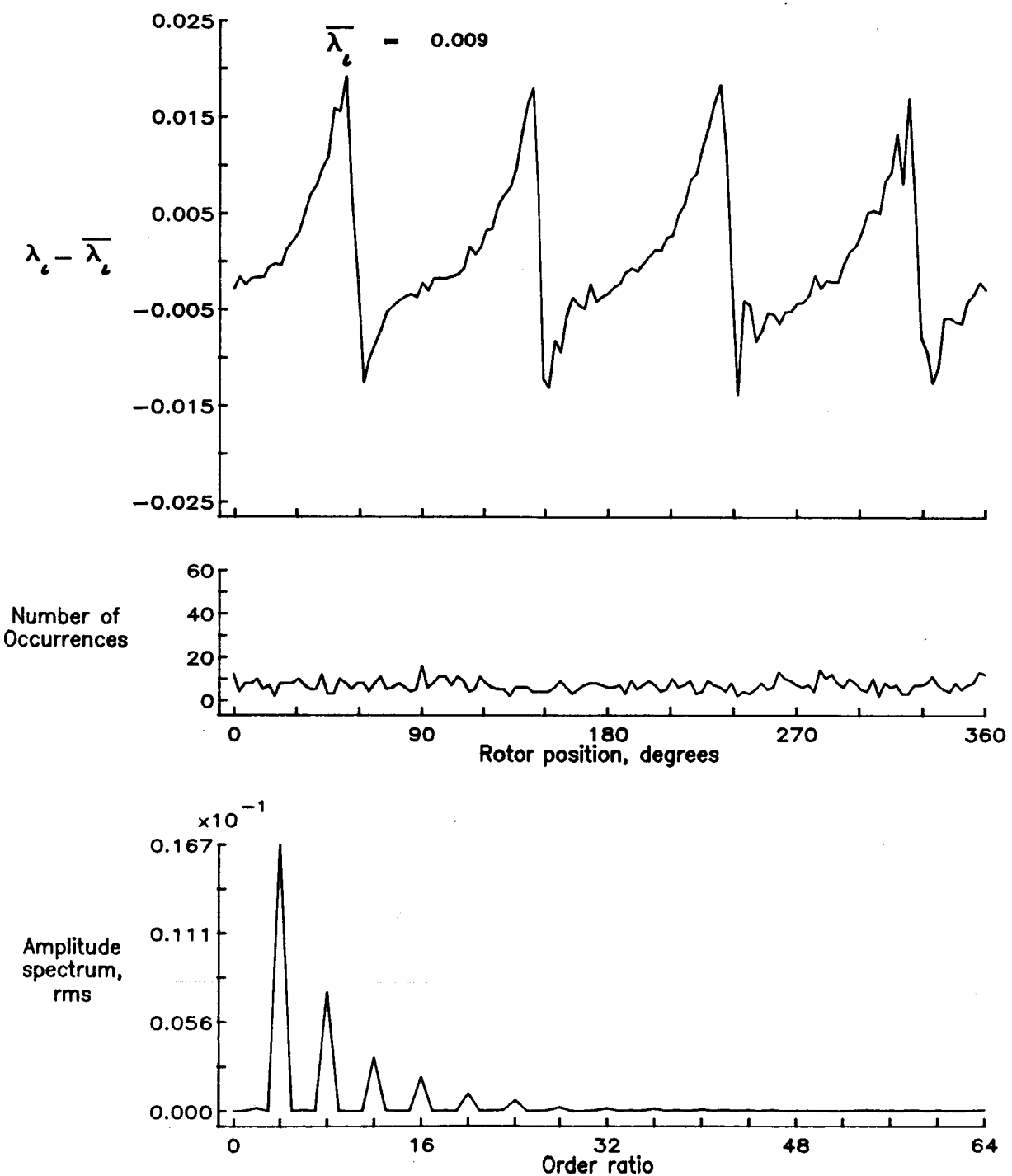


Figure 79.— Concluded.

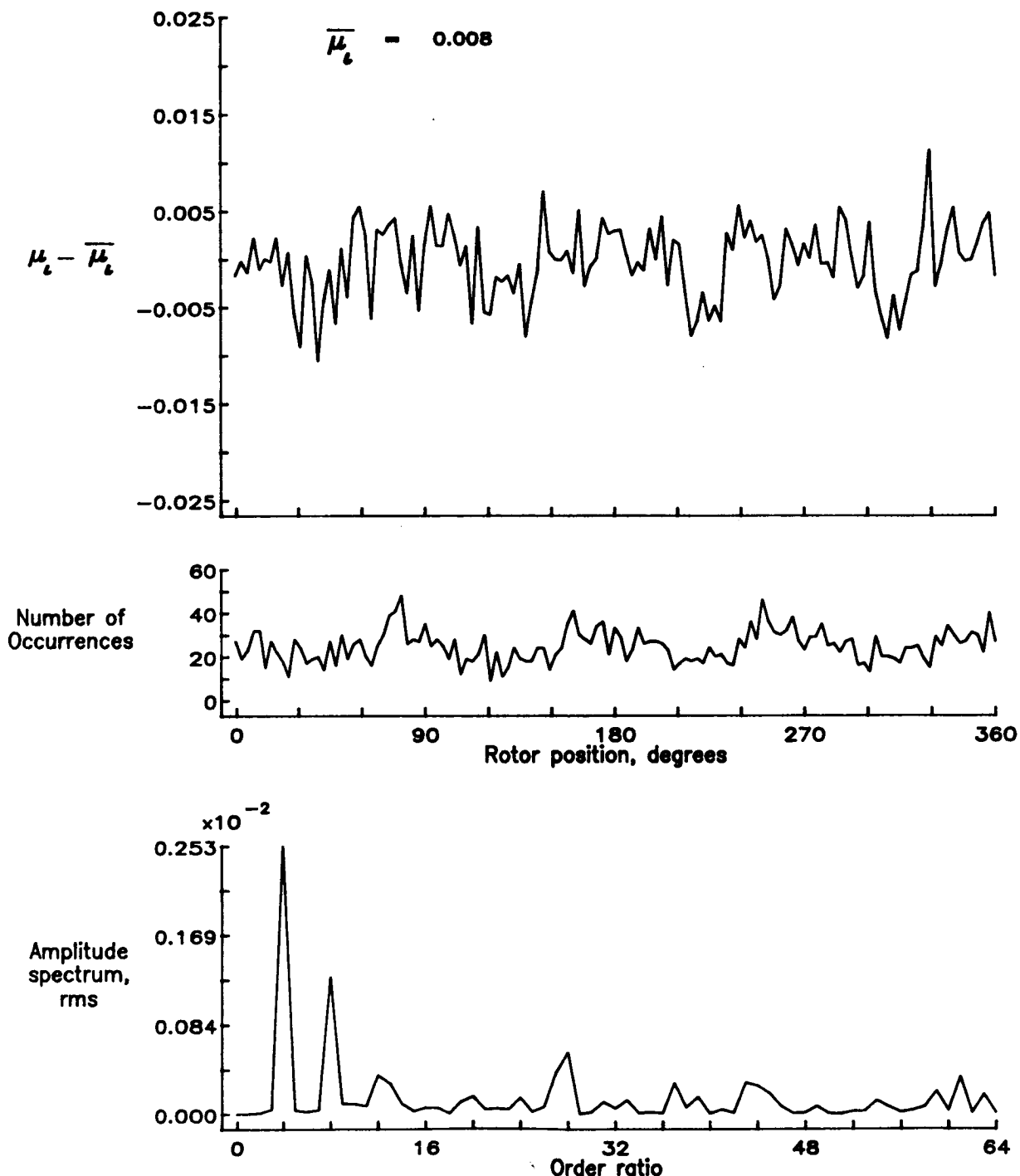


Figure 80.— Induced inflow velocity measured at 150 degrees and  $r/R$  of 0.90.

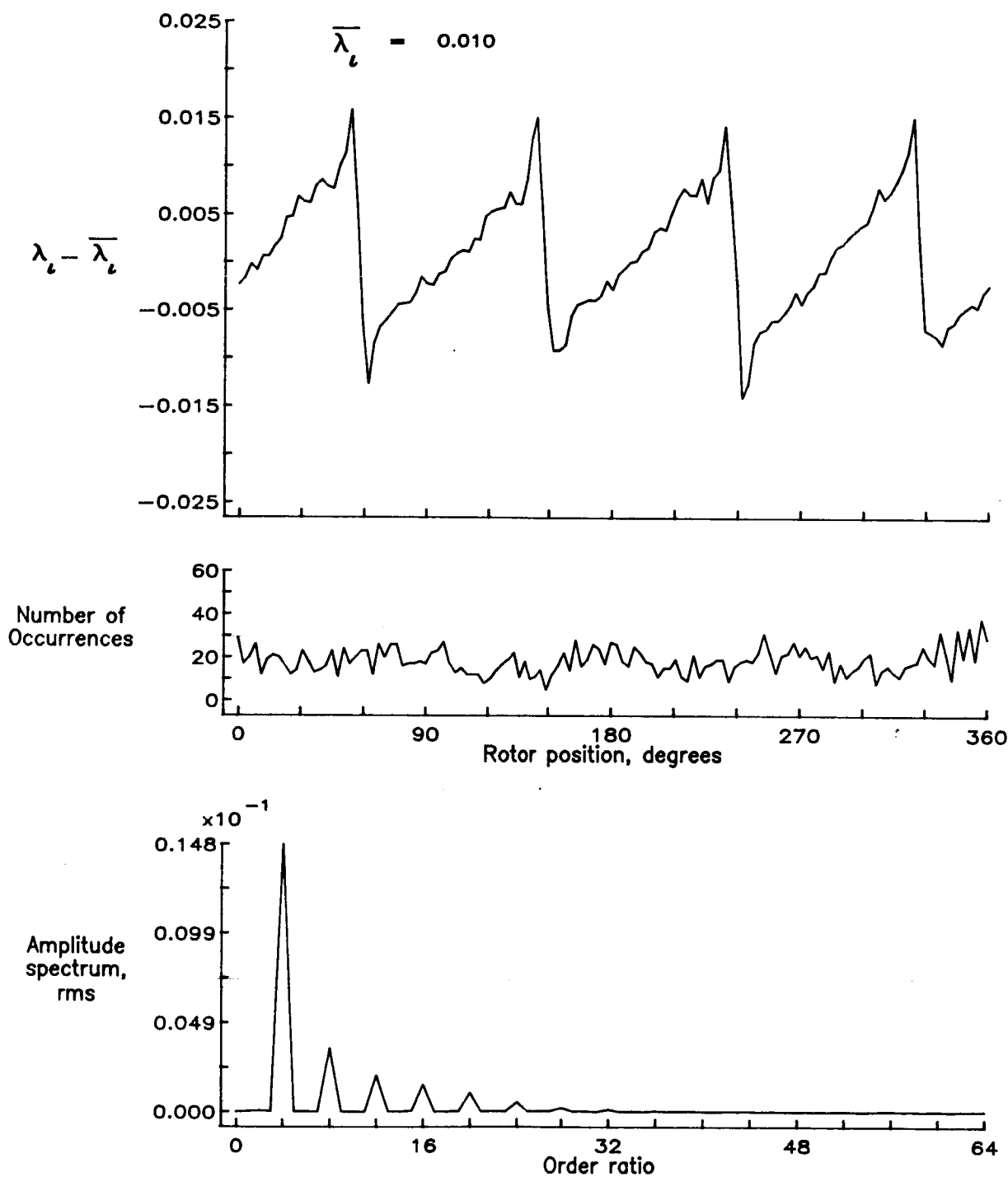


Figure 80.— Concluded.

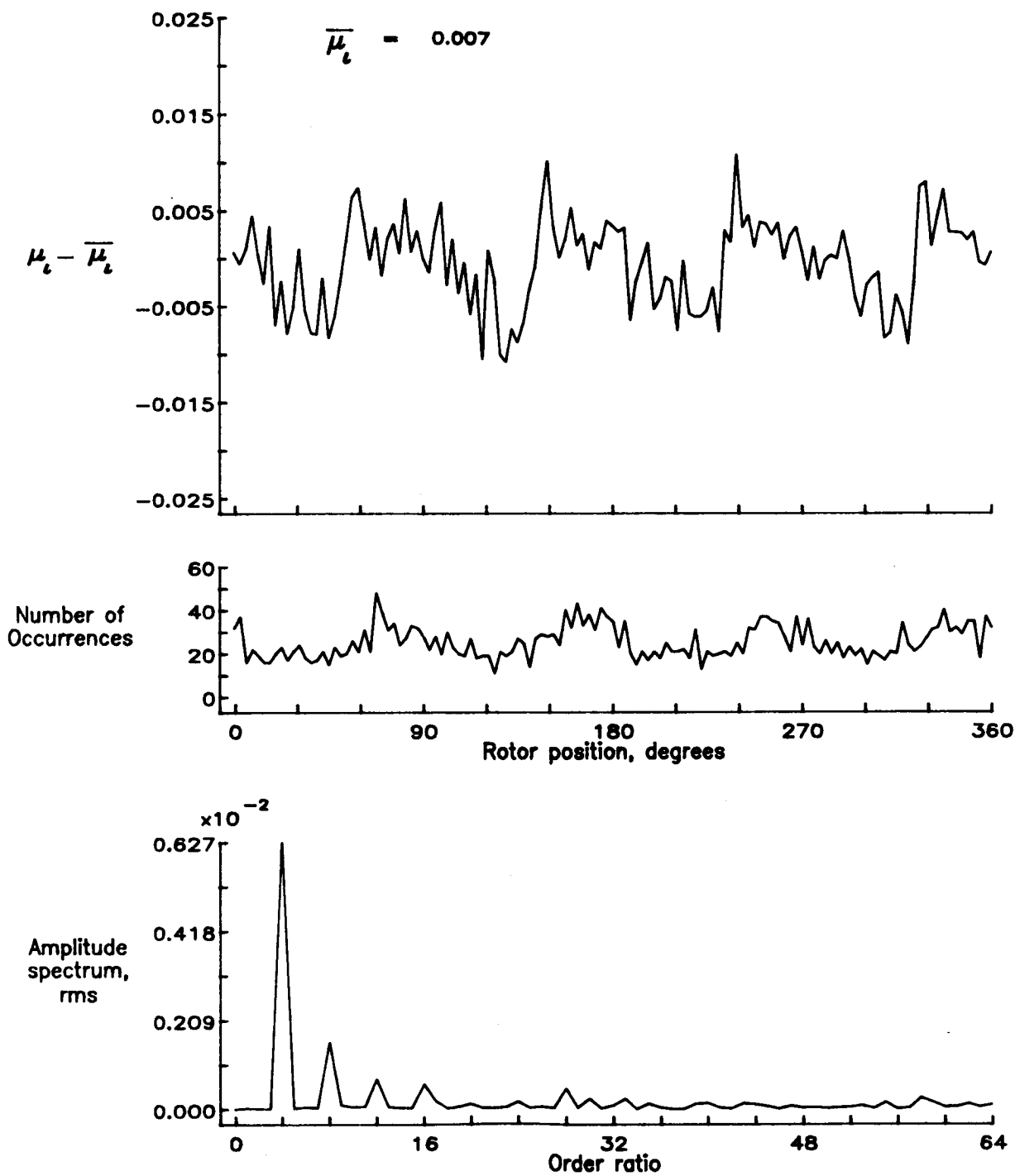


Figure 81.— Induced inflow velocity measured at 150 degrees and r/R of 0.94.

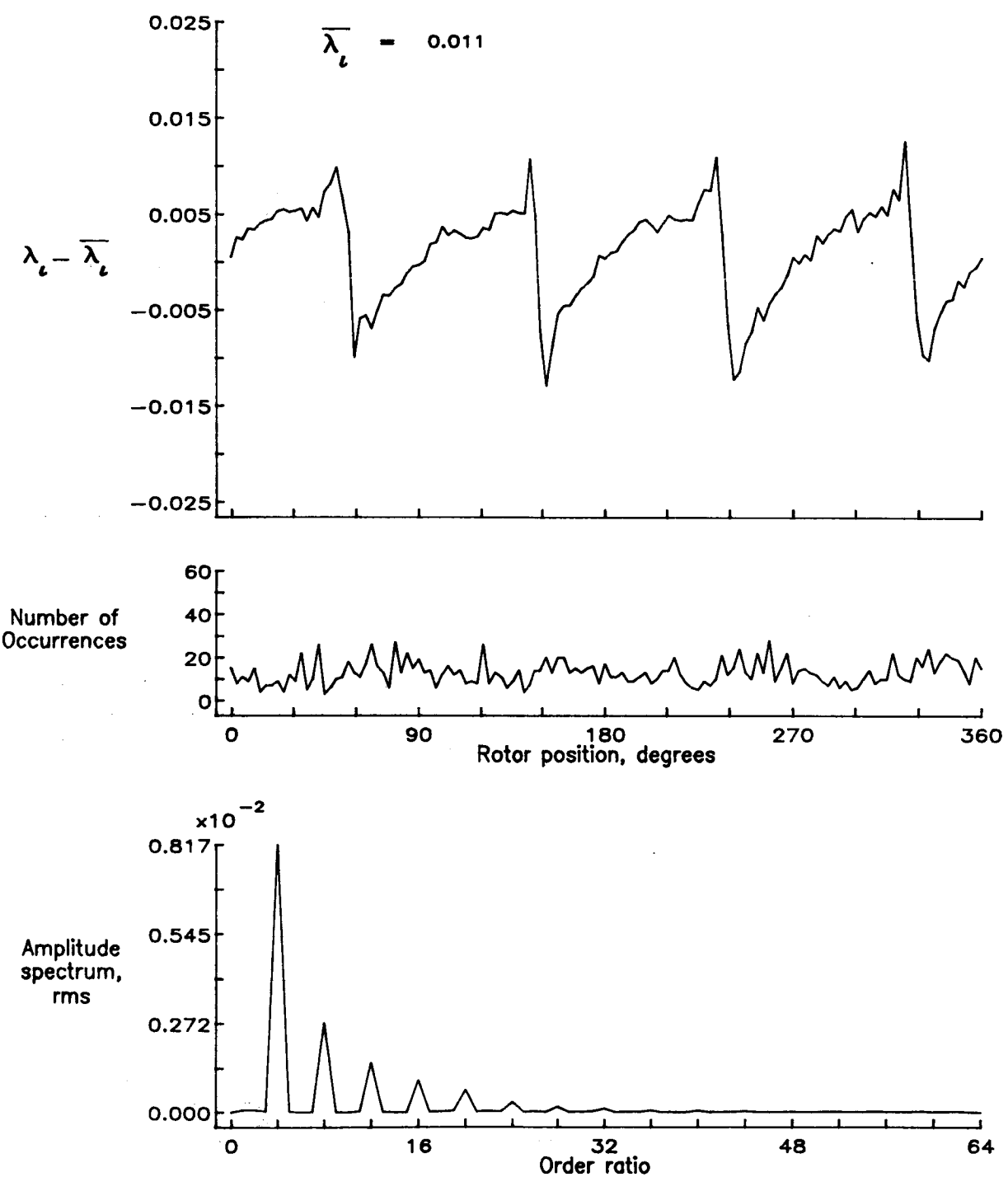


Figure 81.— Concluded.

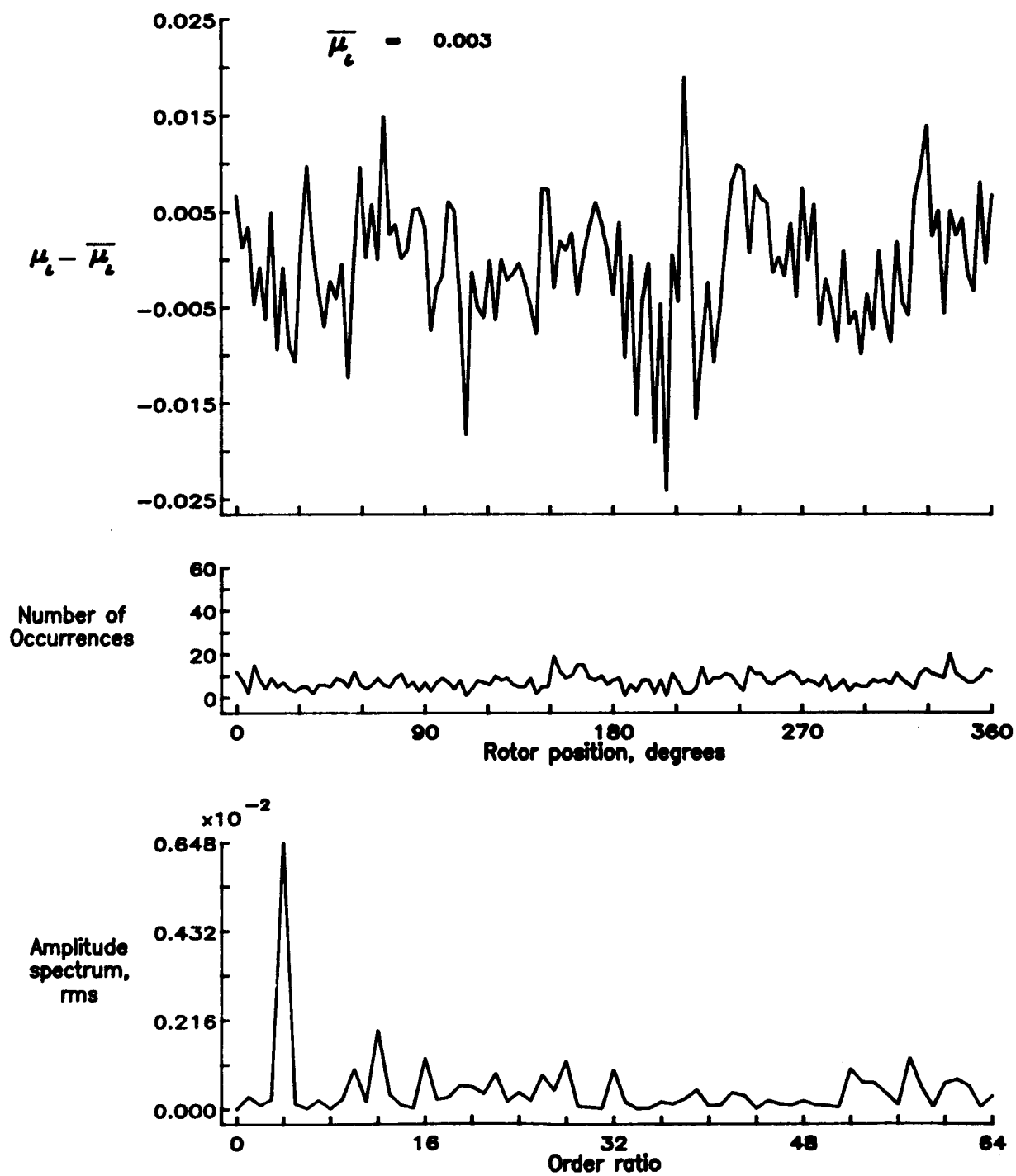


Figure 82.— Induced inflow velocity measured at 150 degrees and r/R of 0.98.

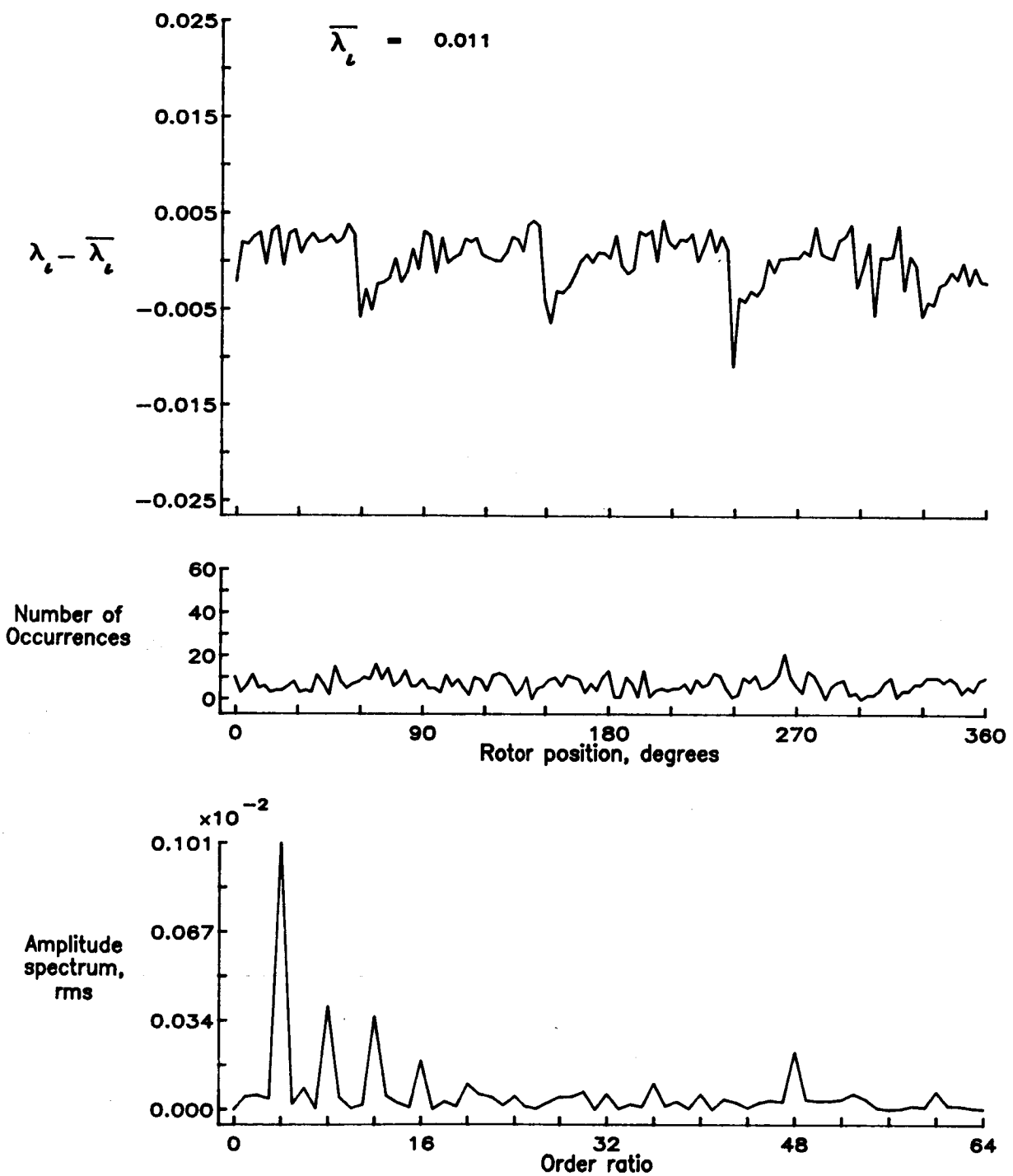
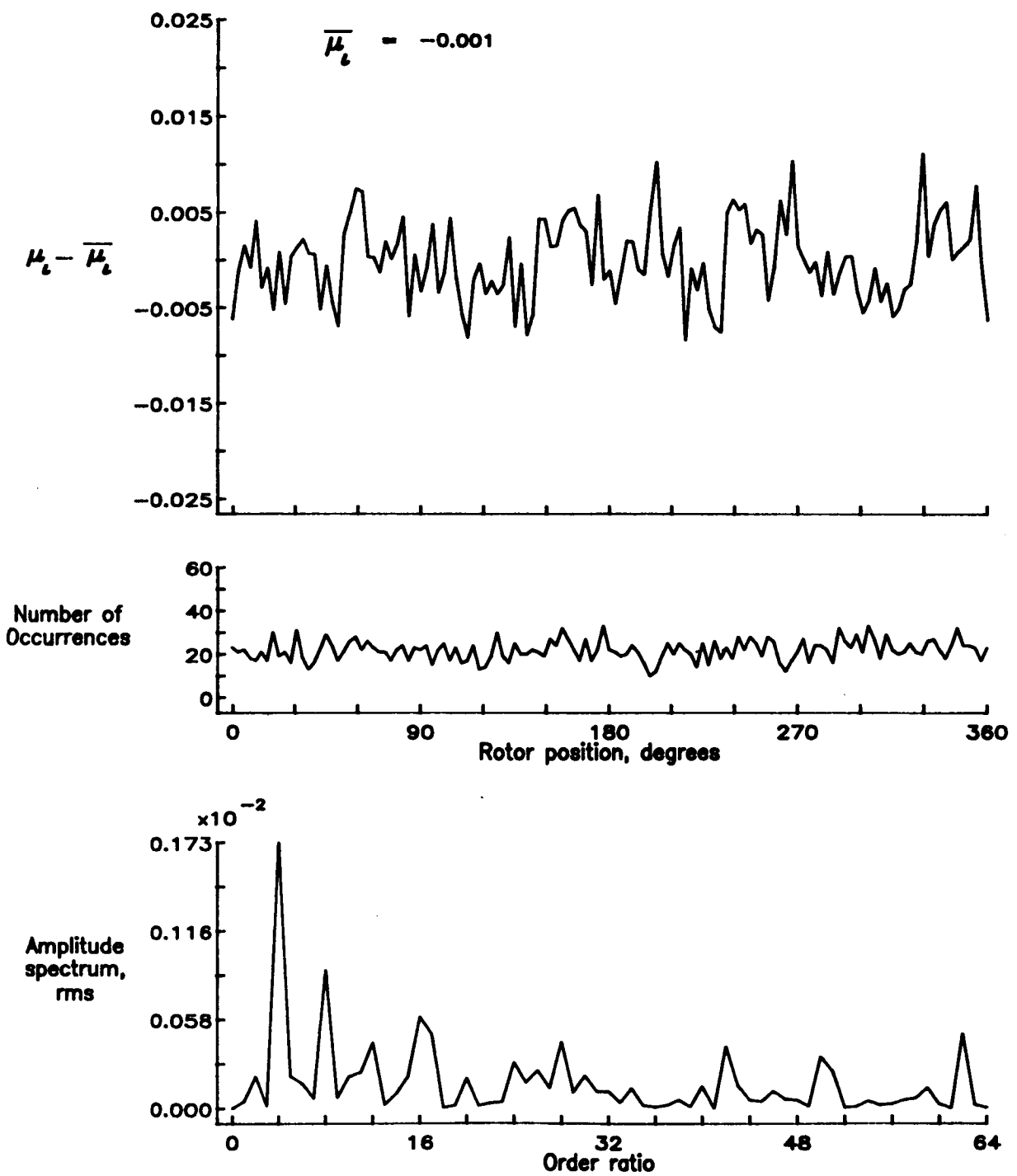


Figure 82.— Concluded.



**Figure 83.— Induced inflow velocity measured at 150 degrees and r/R of 1.02.**

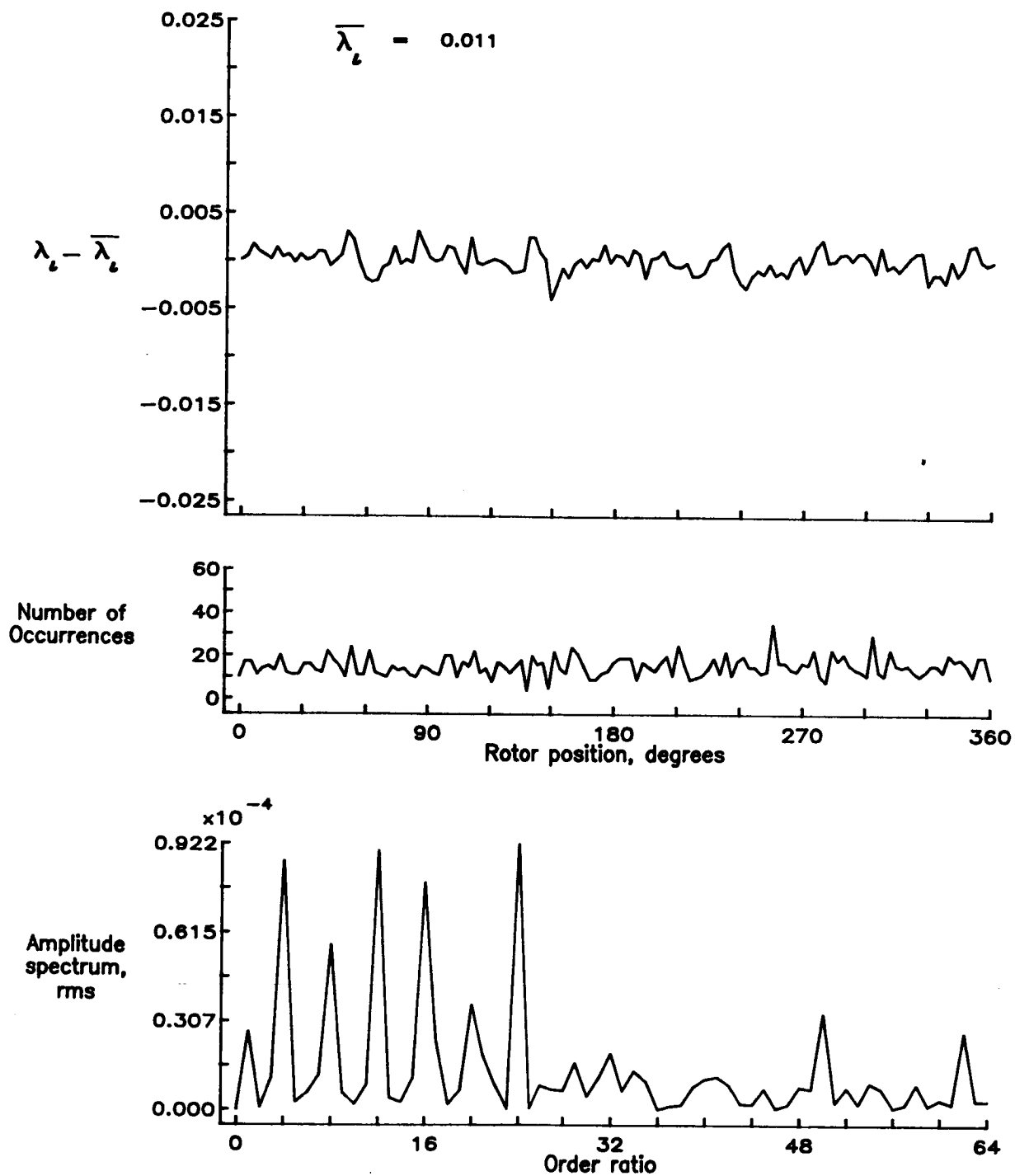


Figure 83.— Concluded.

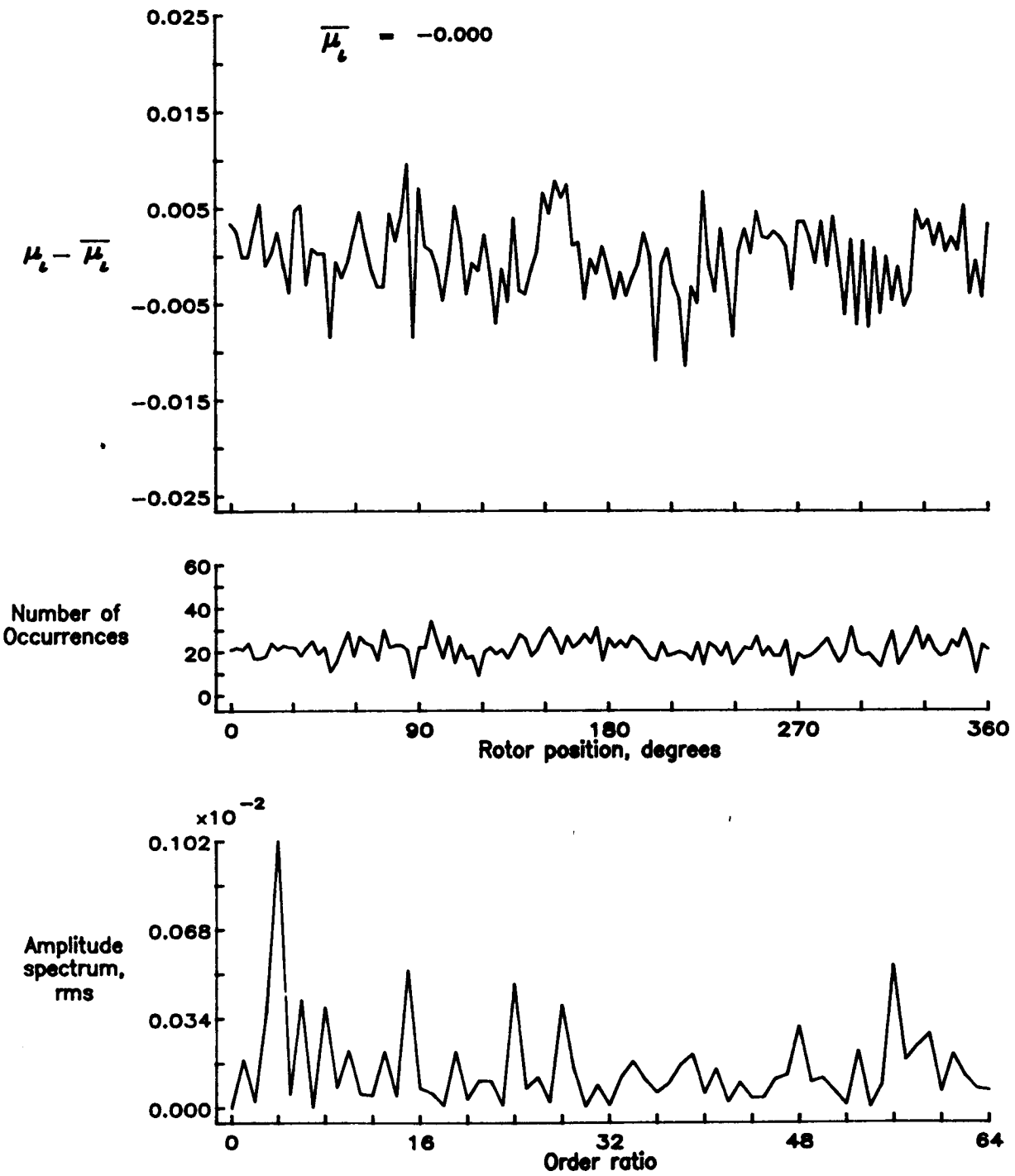


Figure 84.— Induced inflow velocity measured at 150 degrees and r/R of 1.04.

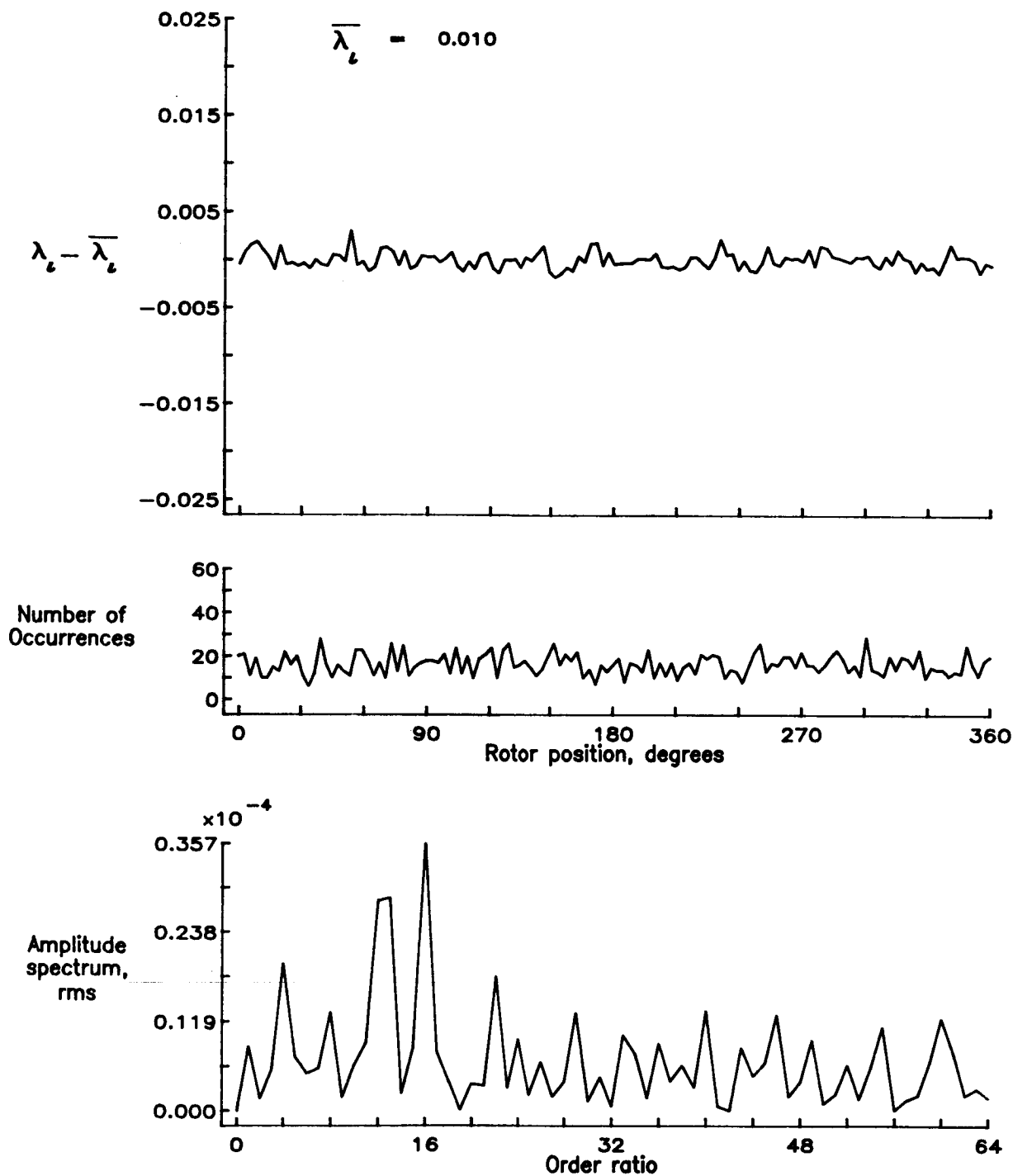


Figure 84.— Concluded.

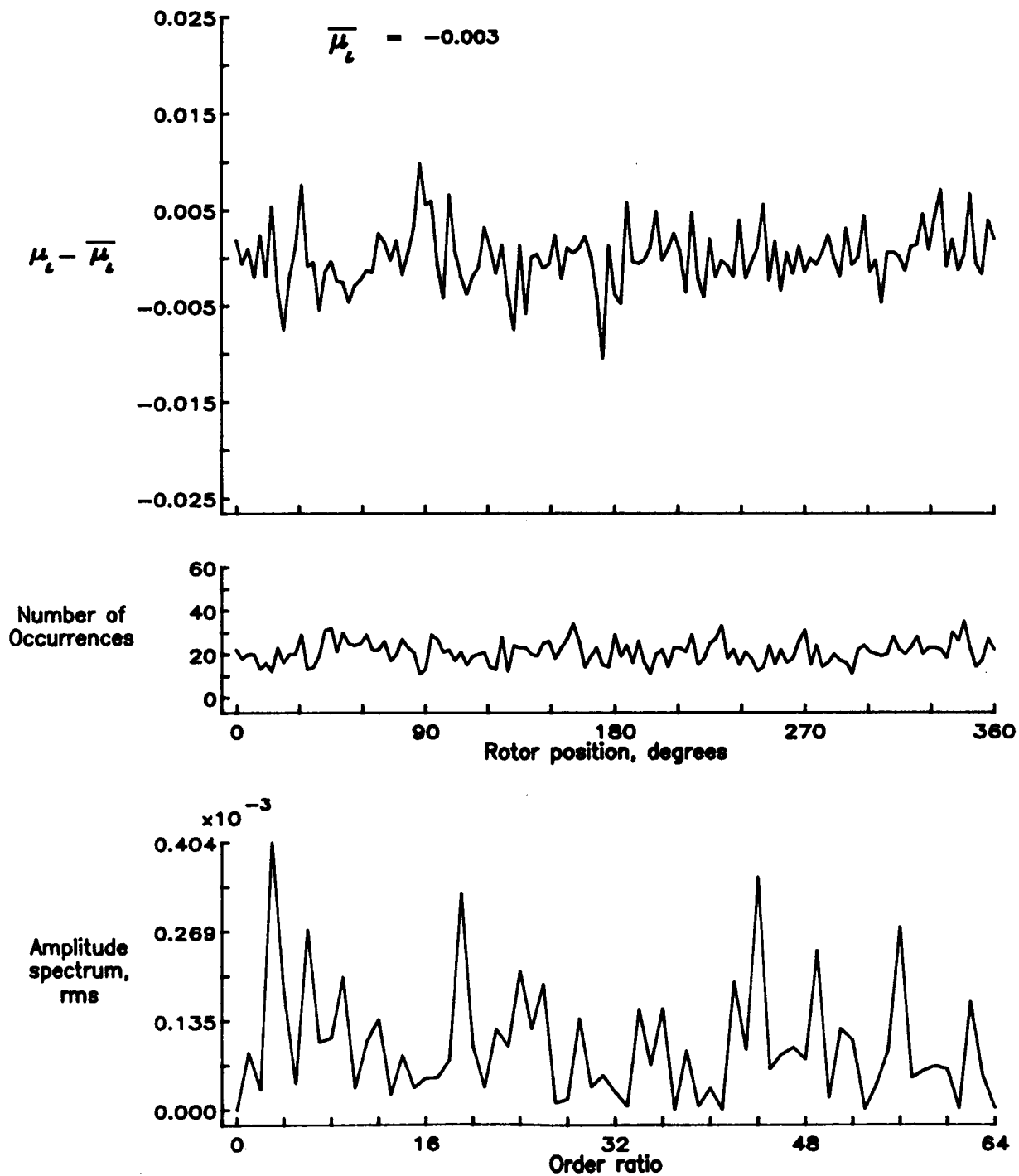


Figure 85.— Induced inflow velocity measured at 150 degrees and r/R of 1.10.

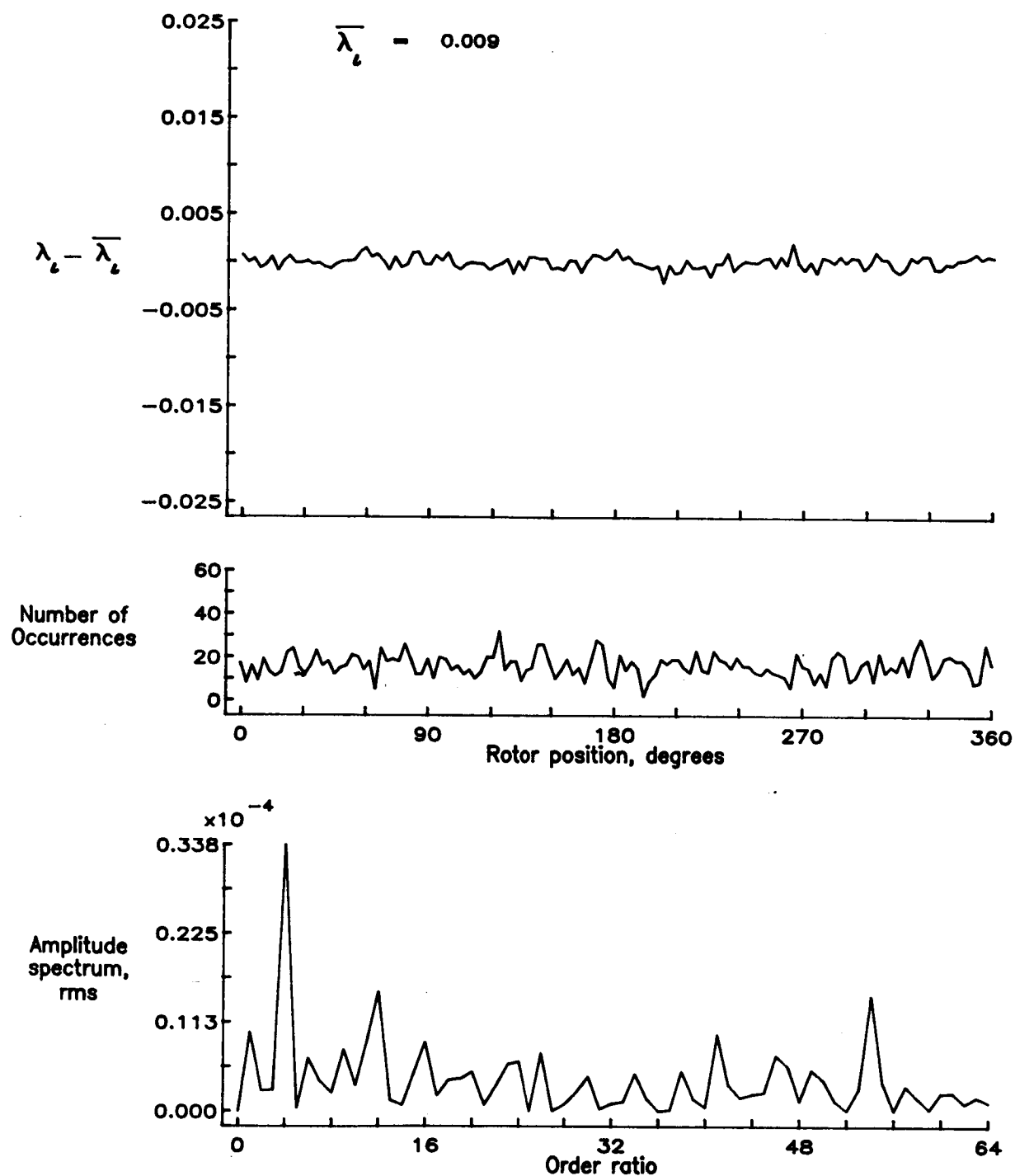


Figure 85.— Concluded.

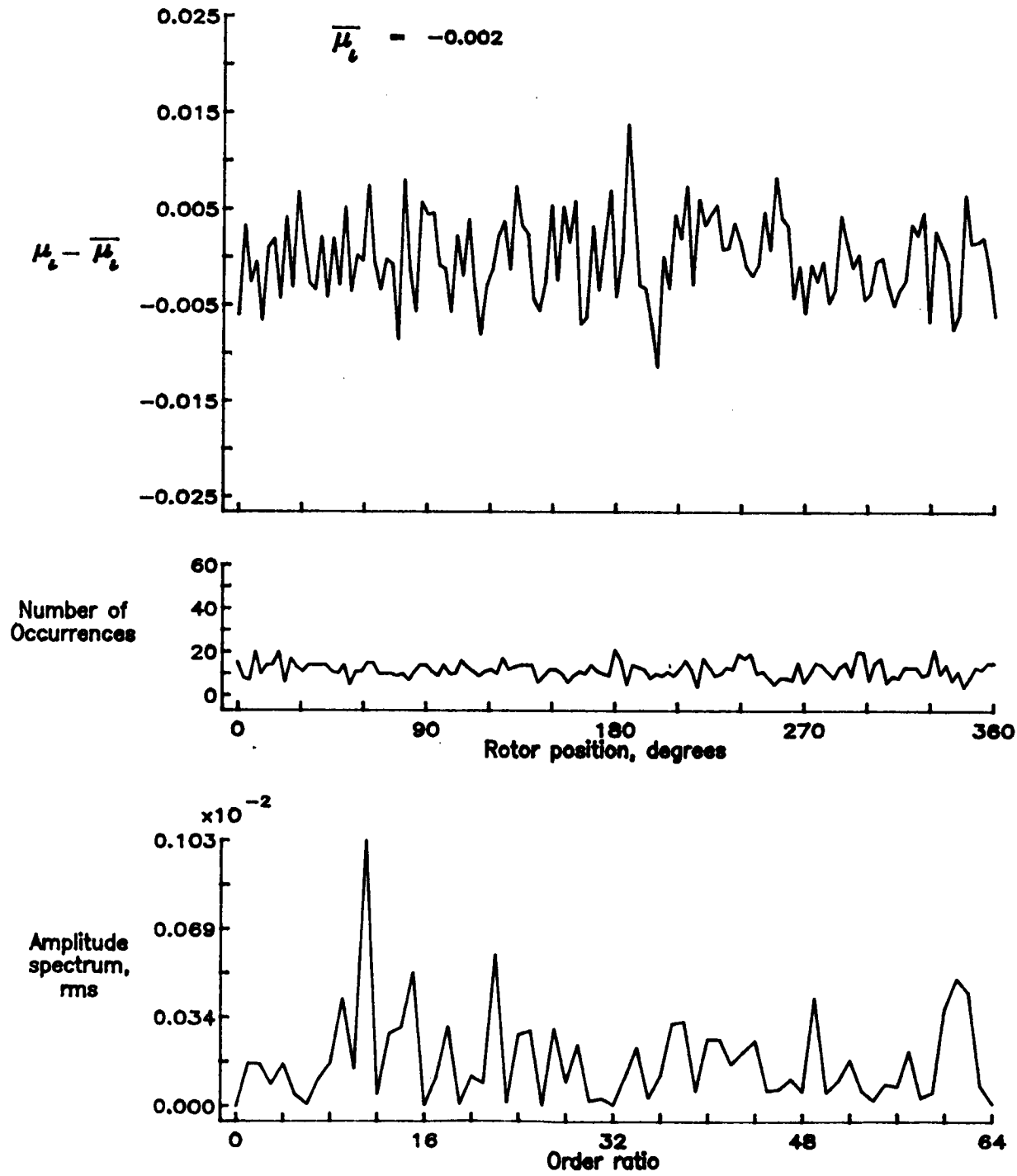


Figure 86.— Induced inflow velocity measured at 180 degrees and  $r/R$  of 0.20.

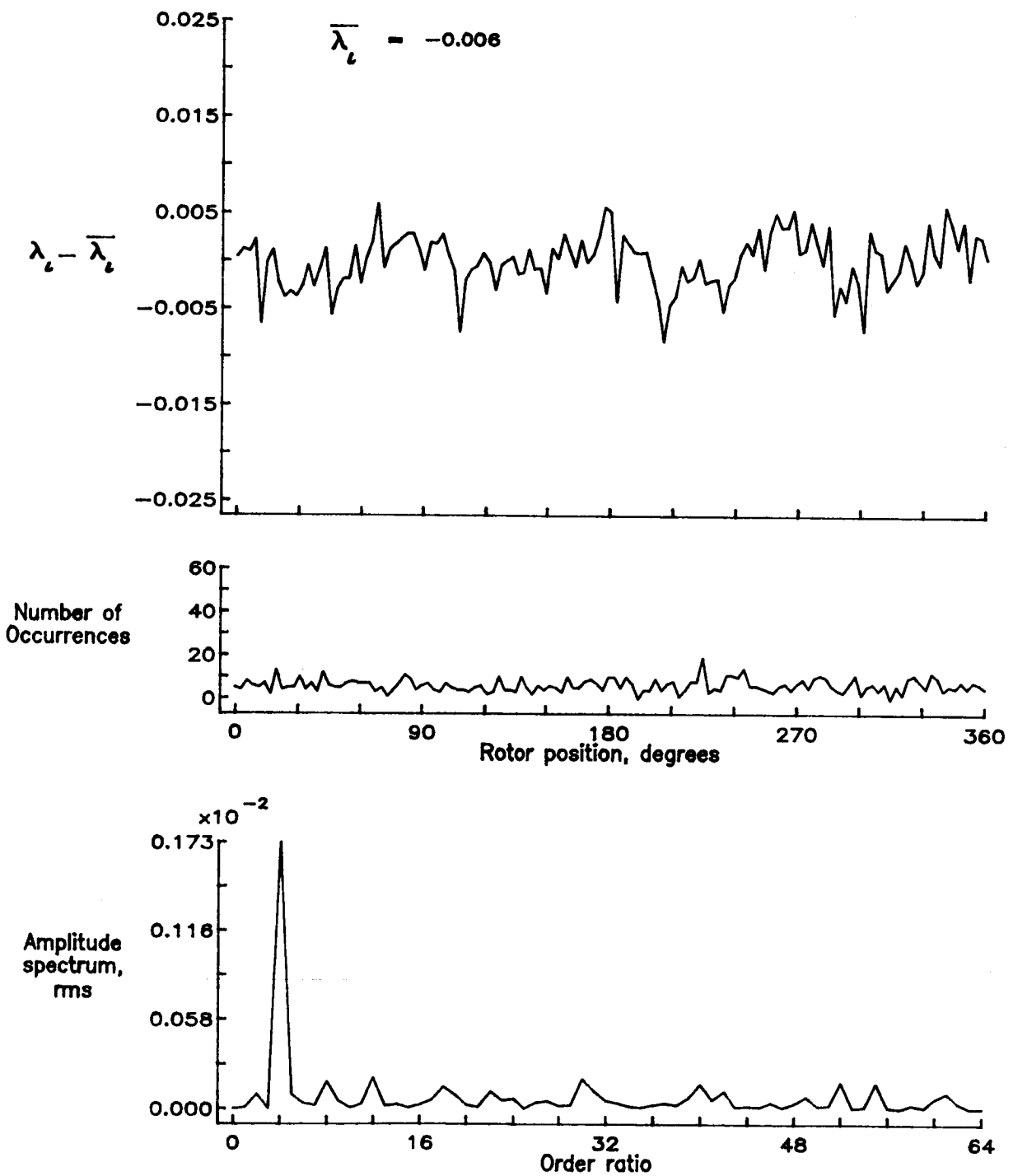


Figure 86.— Concluded.

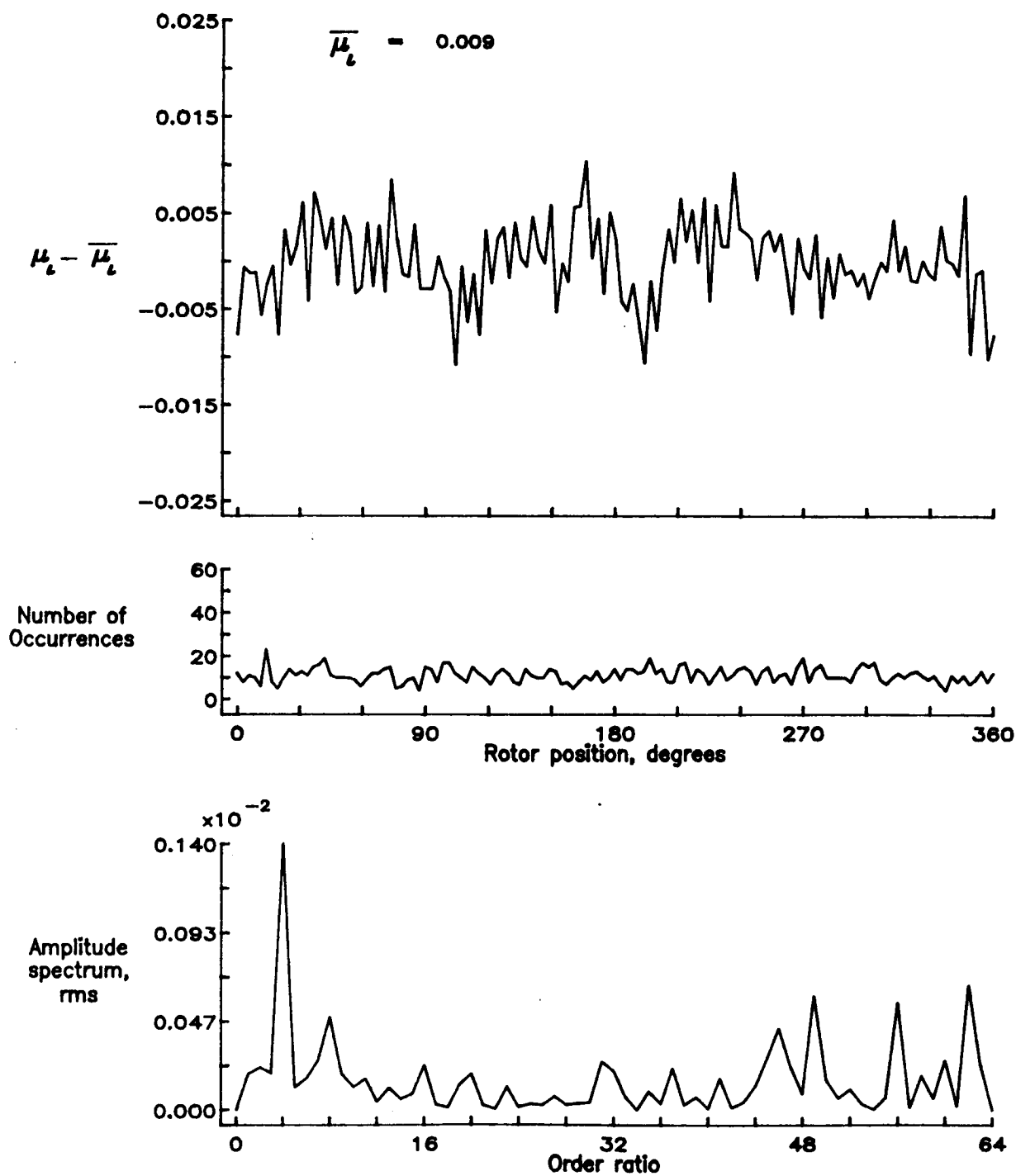


Figure 87.— Induced inflow velocity measured at 180 degrees and  $r/R$  of 0.40.

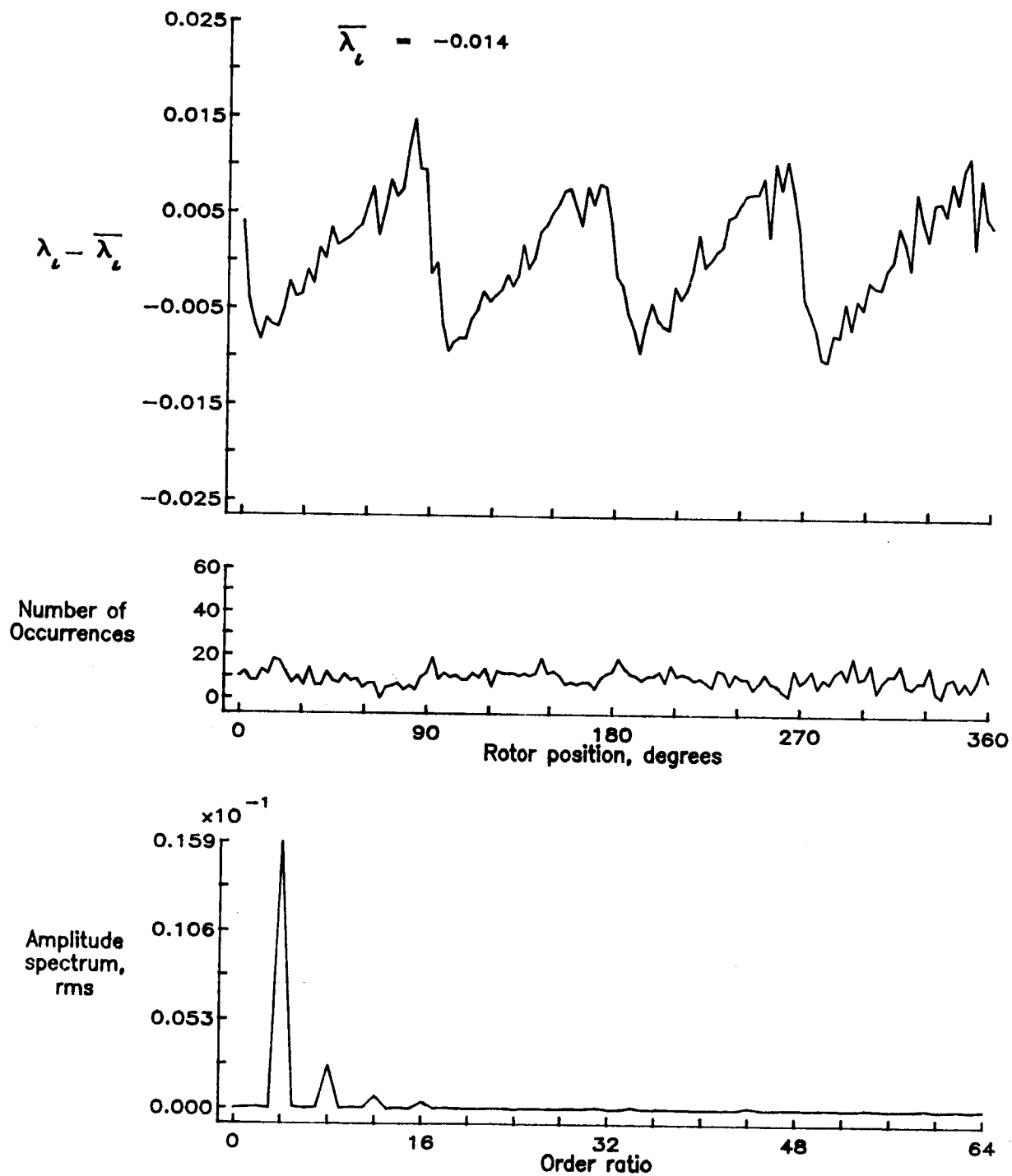


Figure 87.— Concluded.

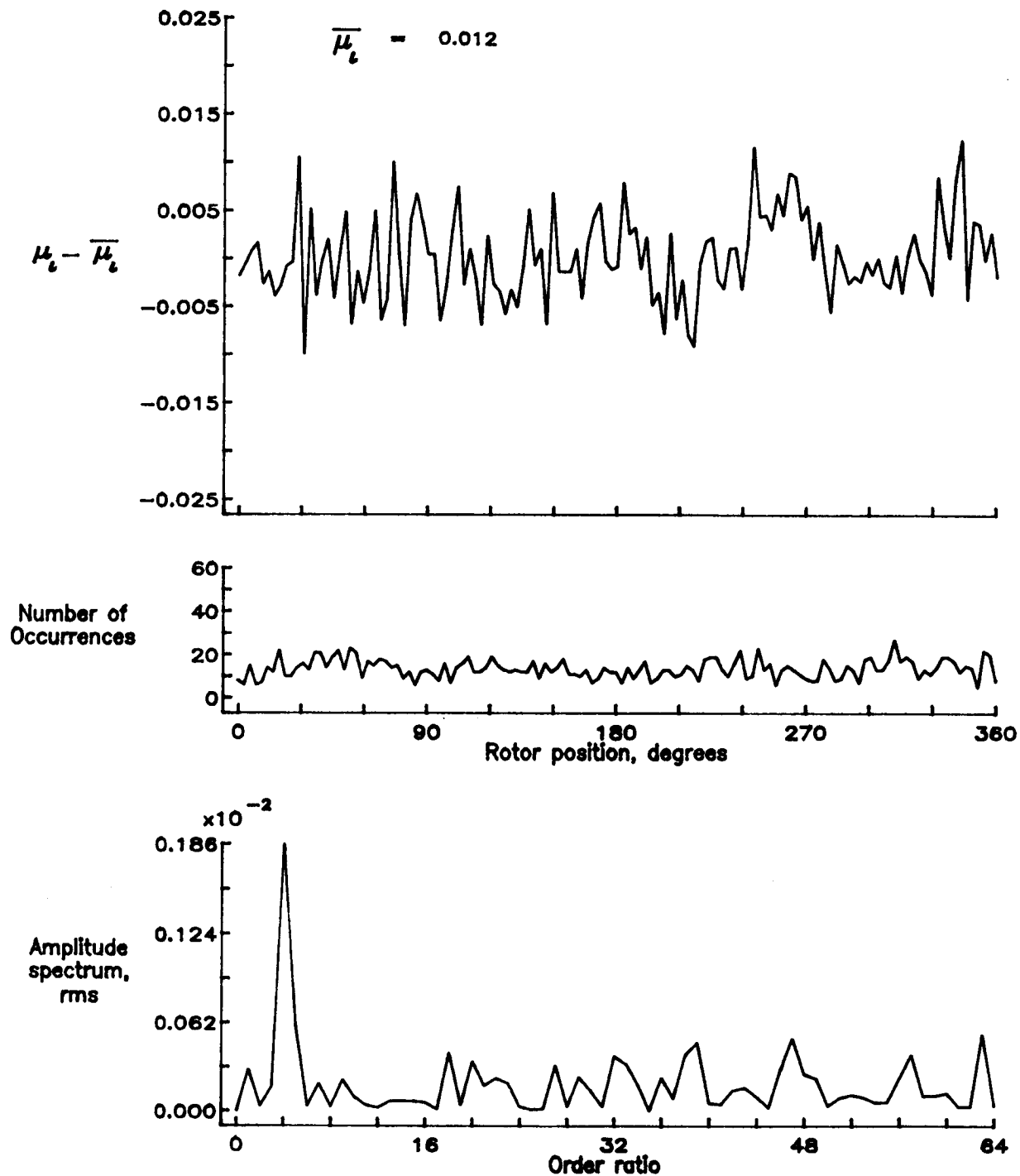


Figure 88.— Induced inflow velocity measured at 180 degrees and r/R of 0.50.

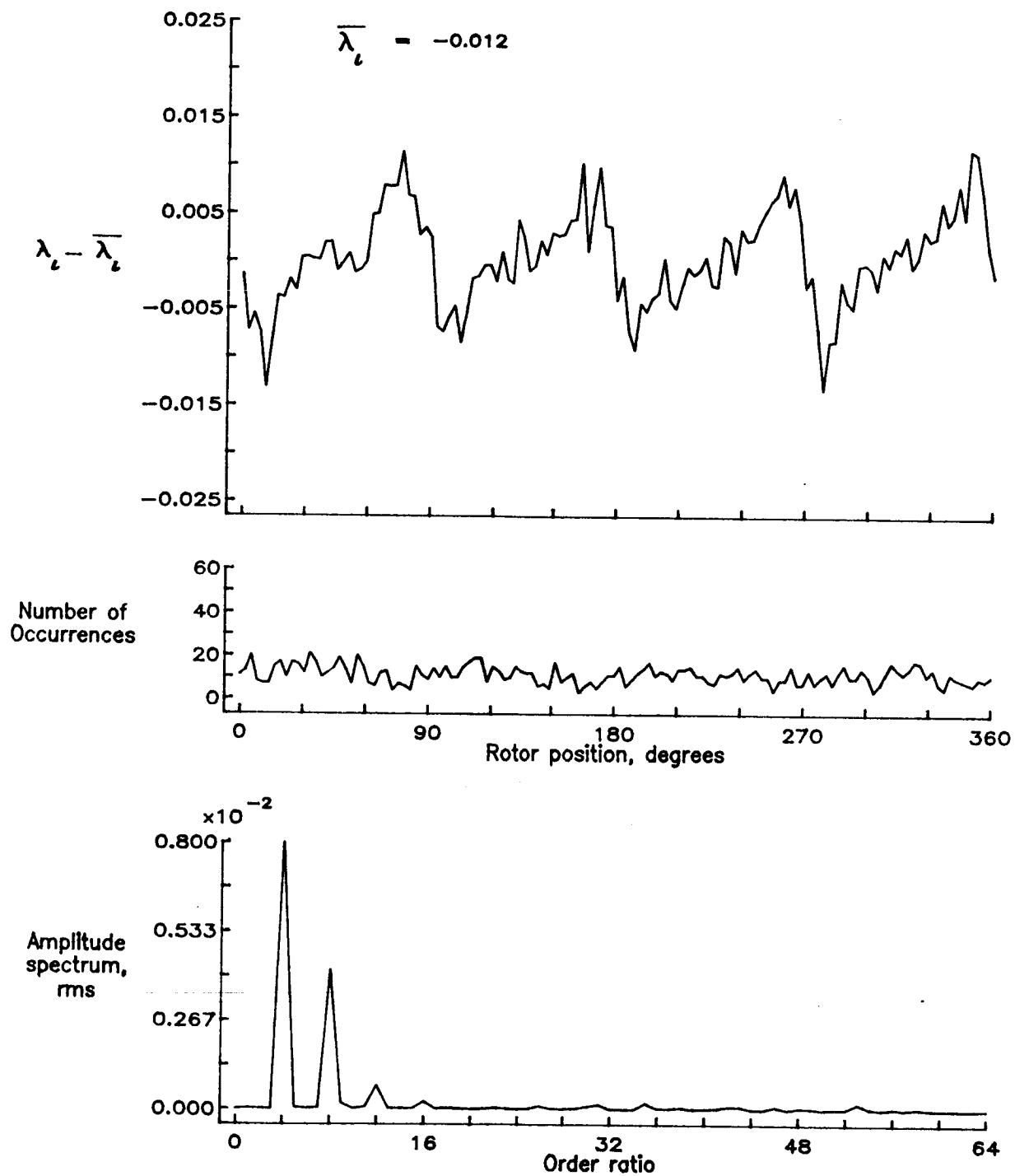


Figure 88.— Concluded.

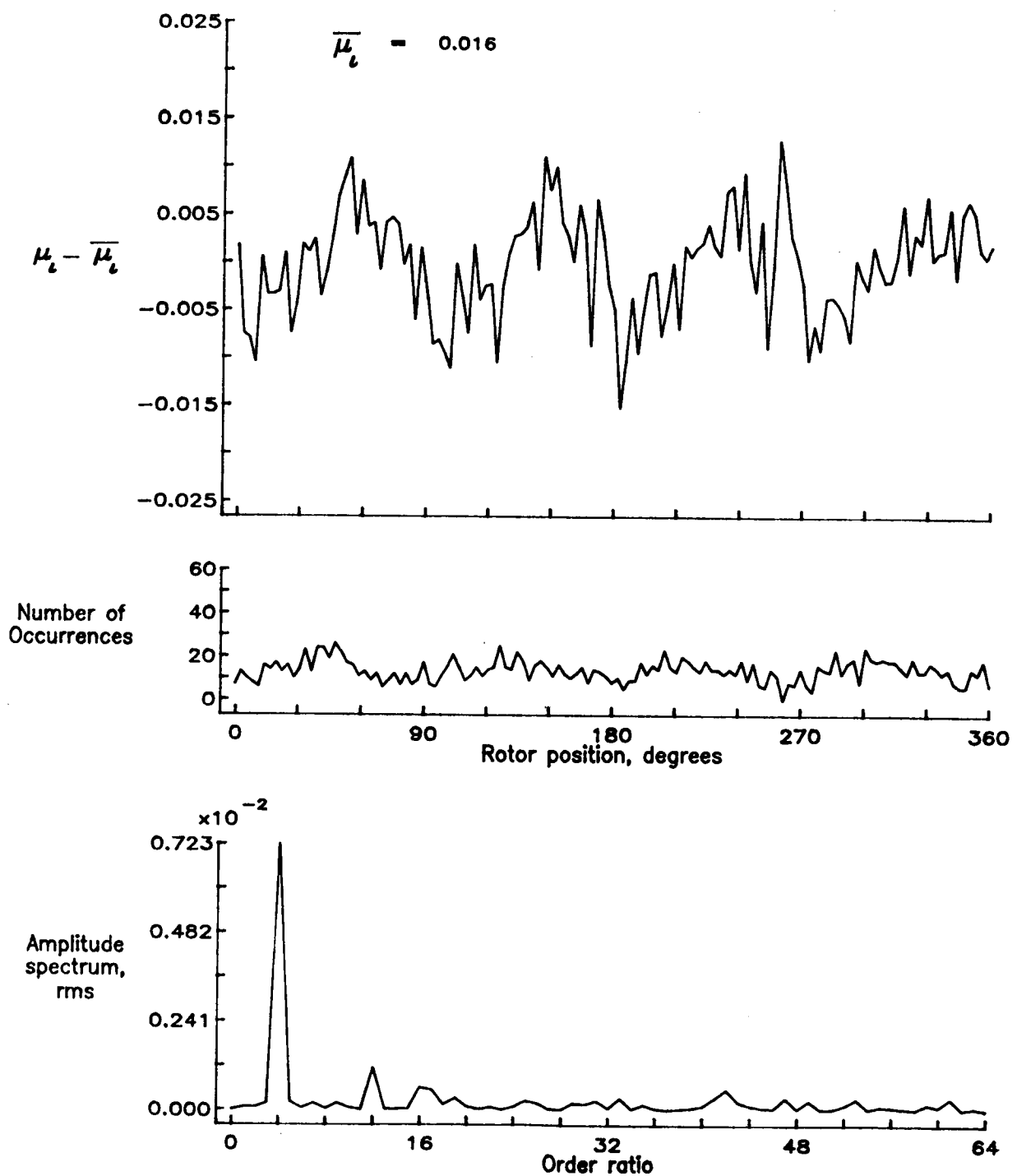


Figure 89.— Induced inflow velocity measured at 180 degrees and r/R of 0.60.

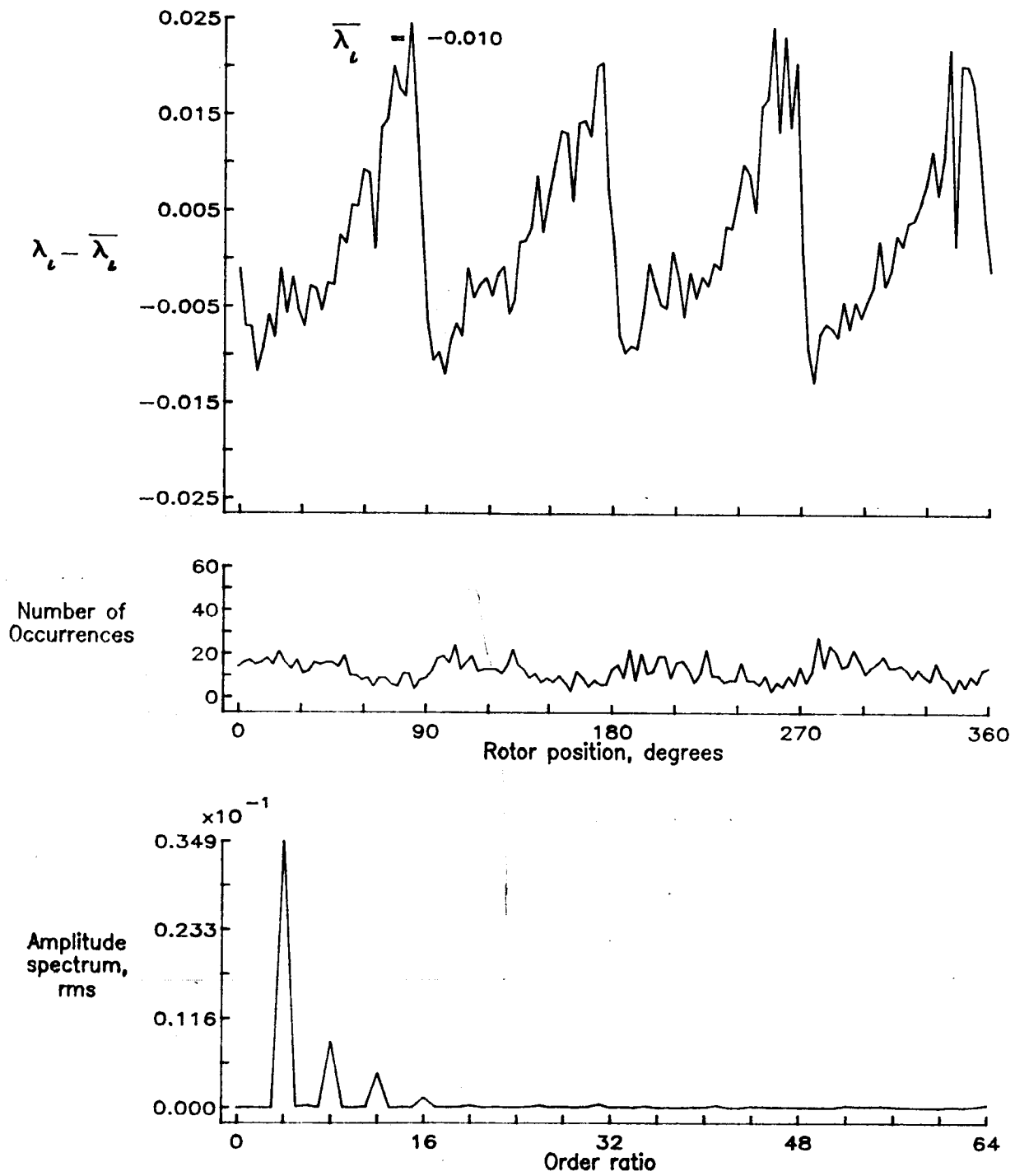


Figure 89.— Concluded.

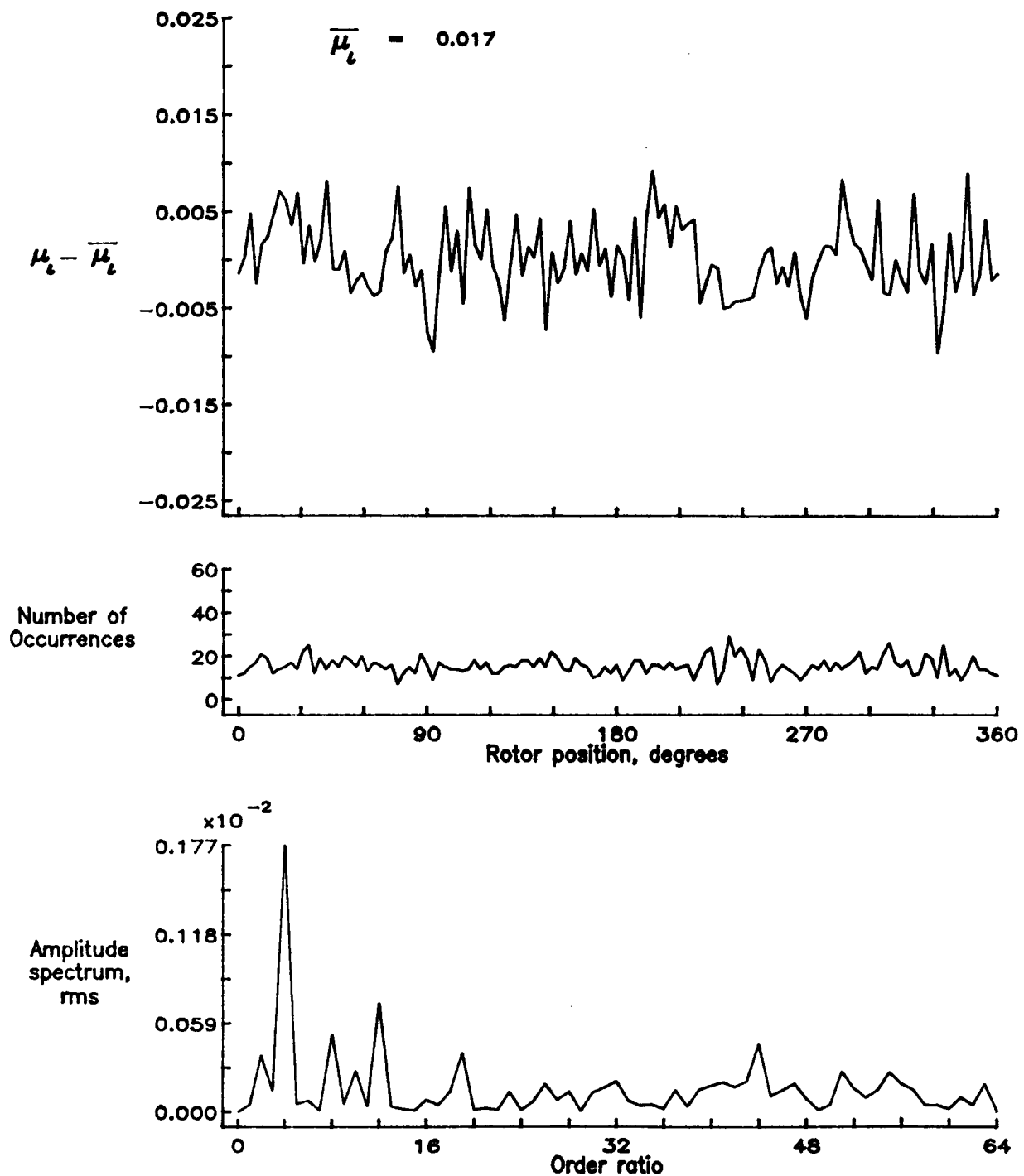


Figure 90.— Induced inflow velocity measured at 180 degrees and r/R of 0.70.

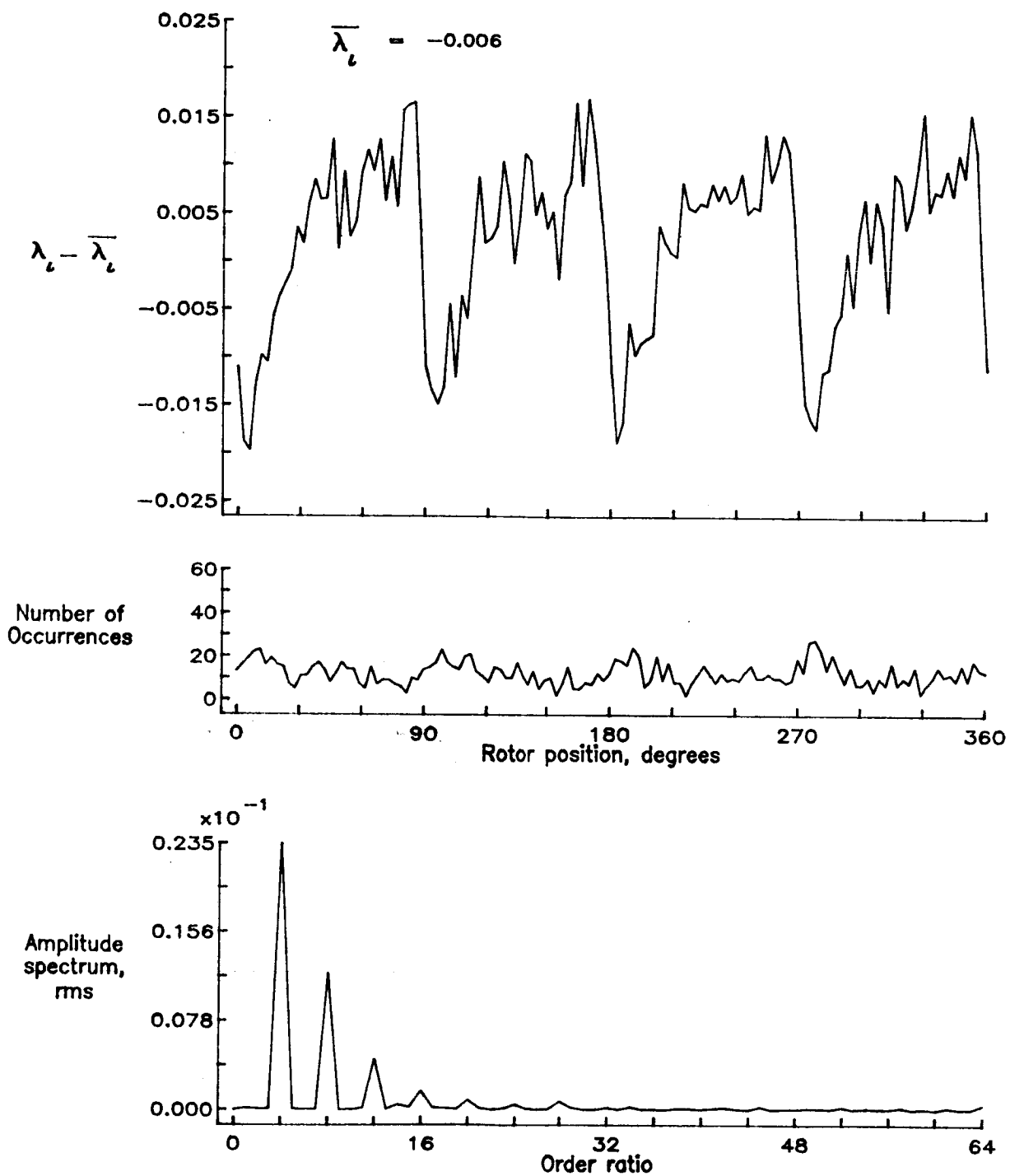


Figure 90.— Concluded.

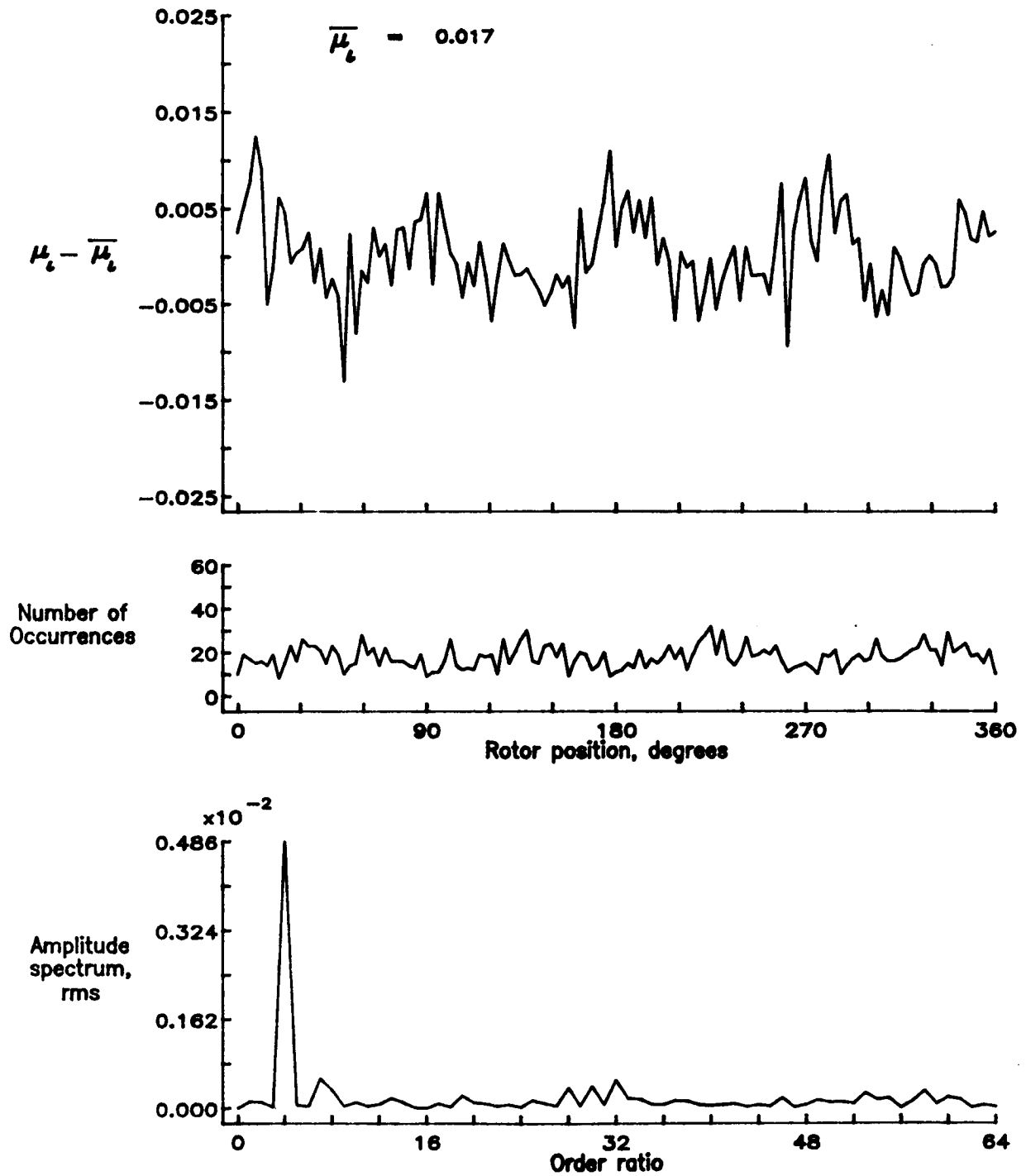


Figure 91.— Induced inflow velocity measured at 180 degrees and r/R of 0.74.

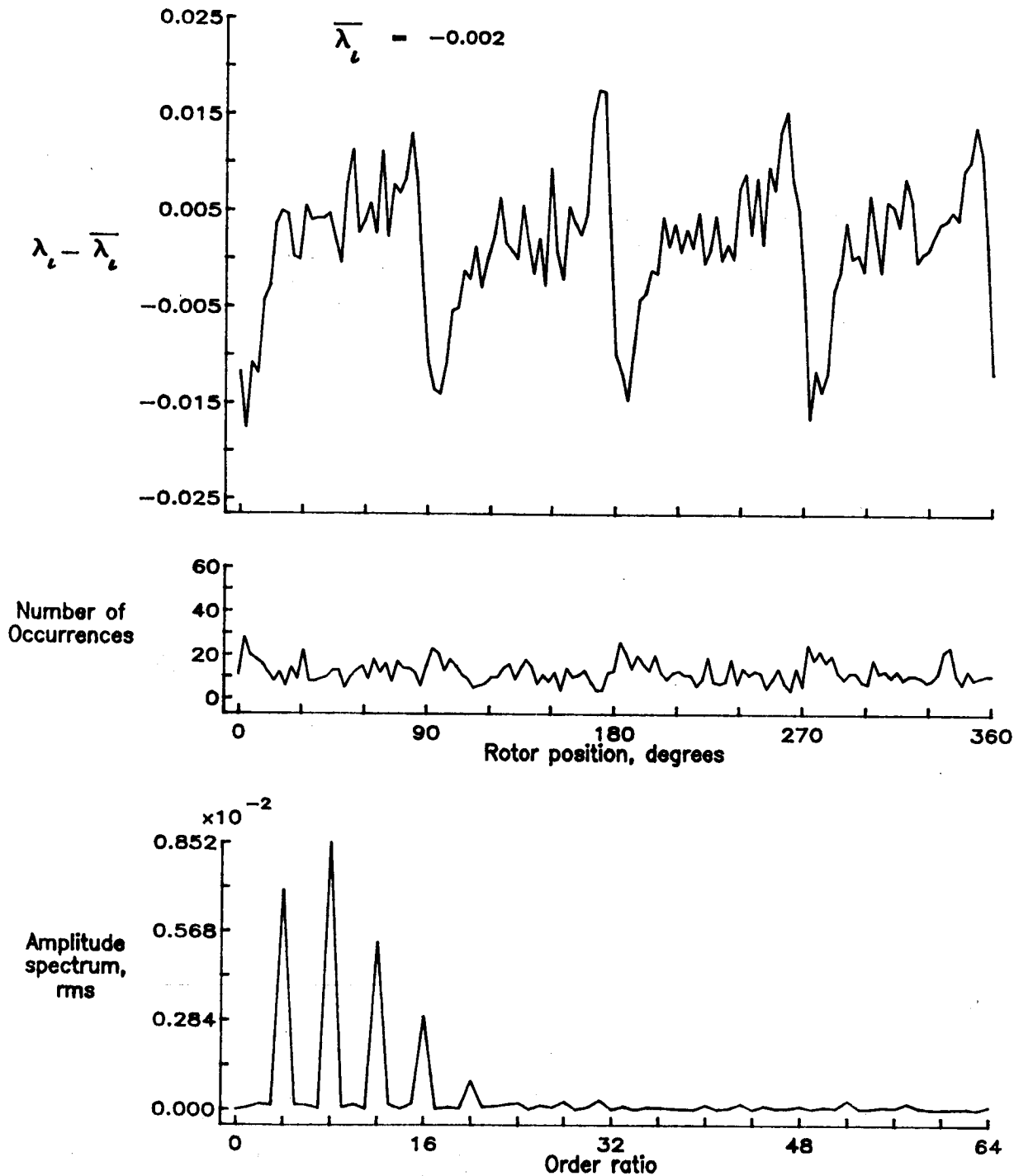


Figure 91.— Concluded.

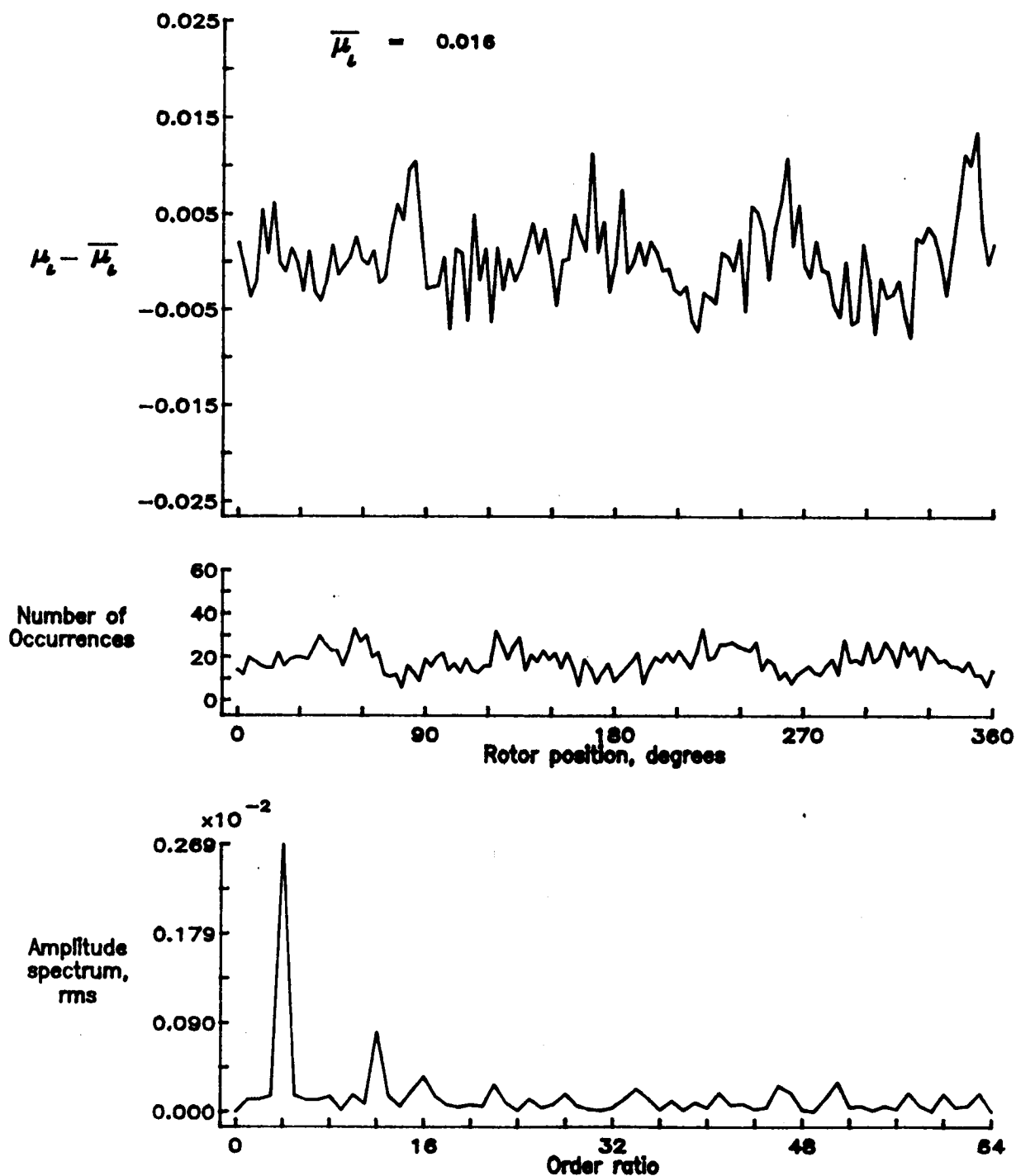


Figure 92.— Induced inflow velocity measured at 180 degrees and r/R of 0.78.

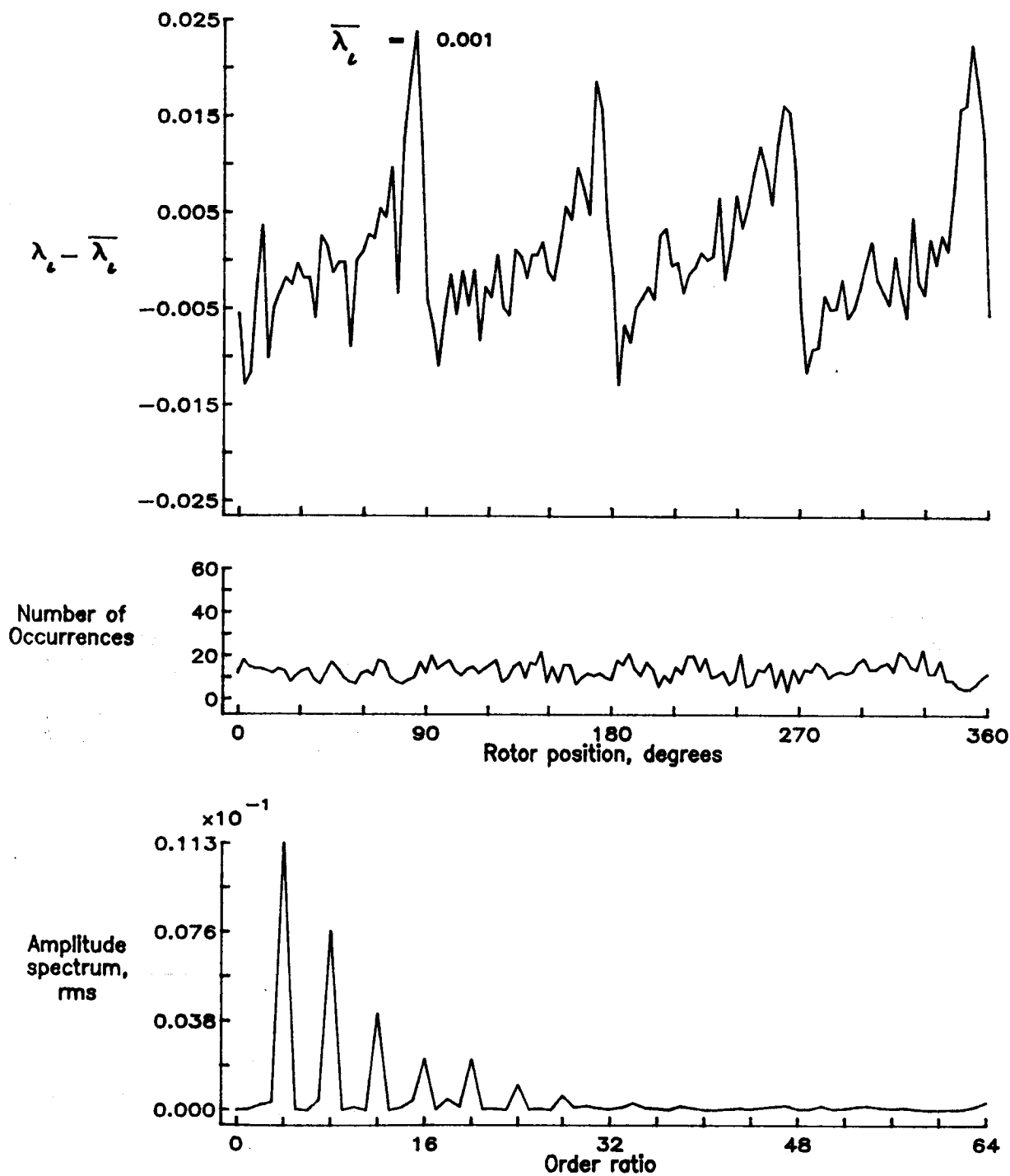


Figure 92.— Concluded.

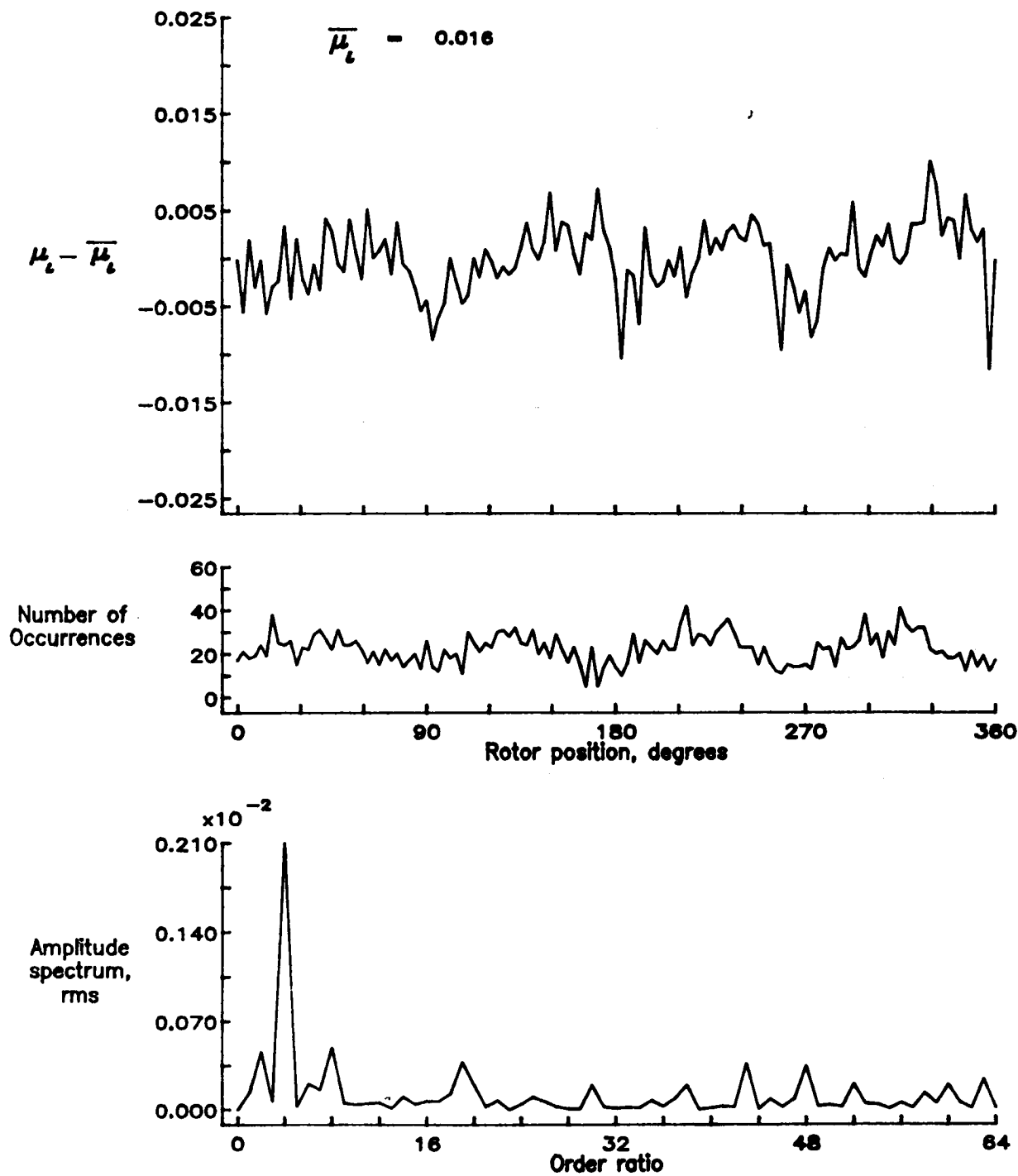


Figure 93.— Induced inflow velocity measured at 180 degrees and r/R of 0.82.

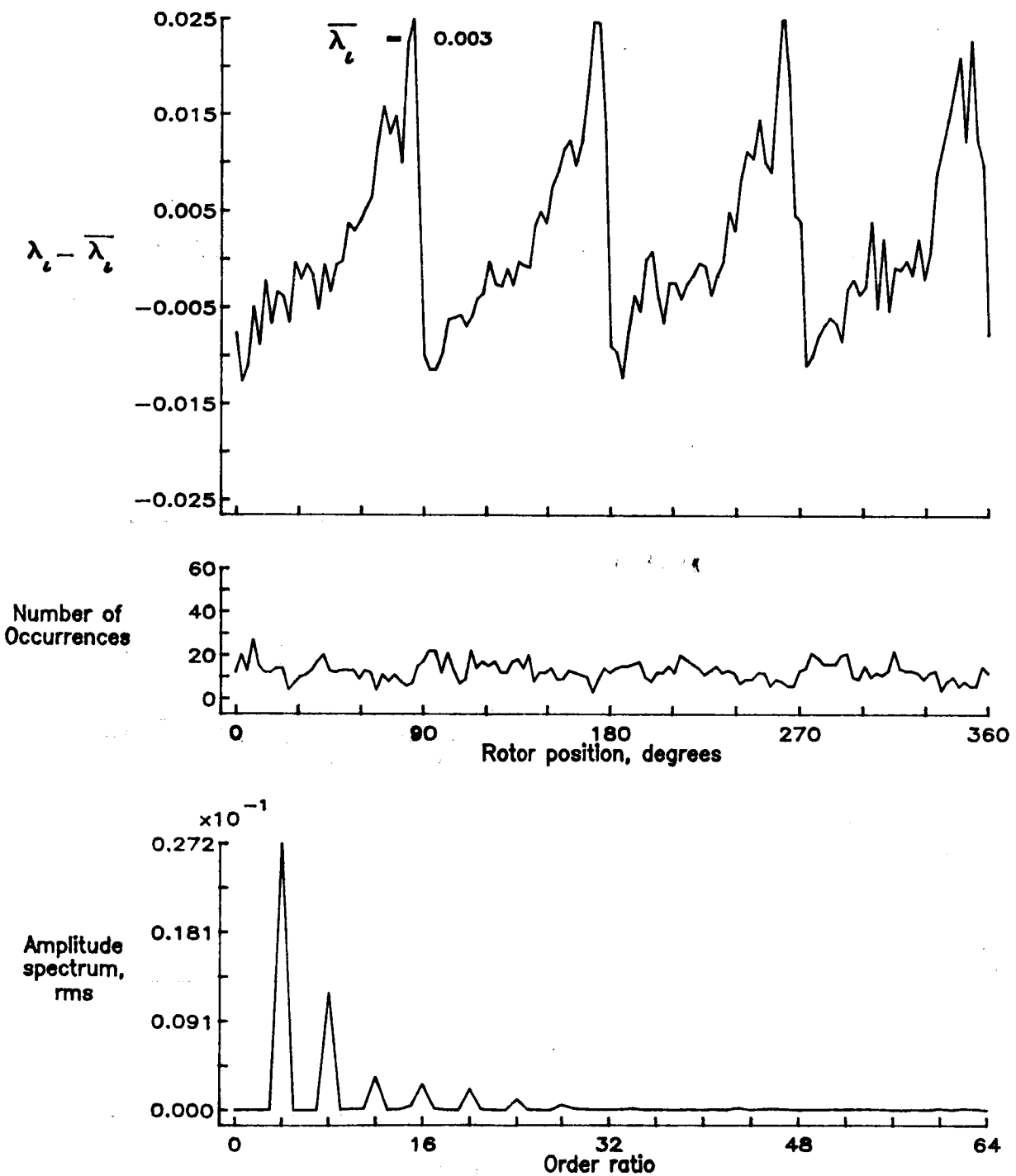


Figure 93.— Concluded.

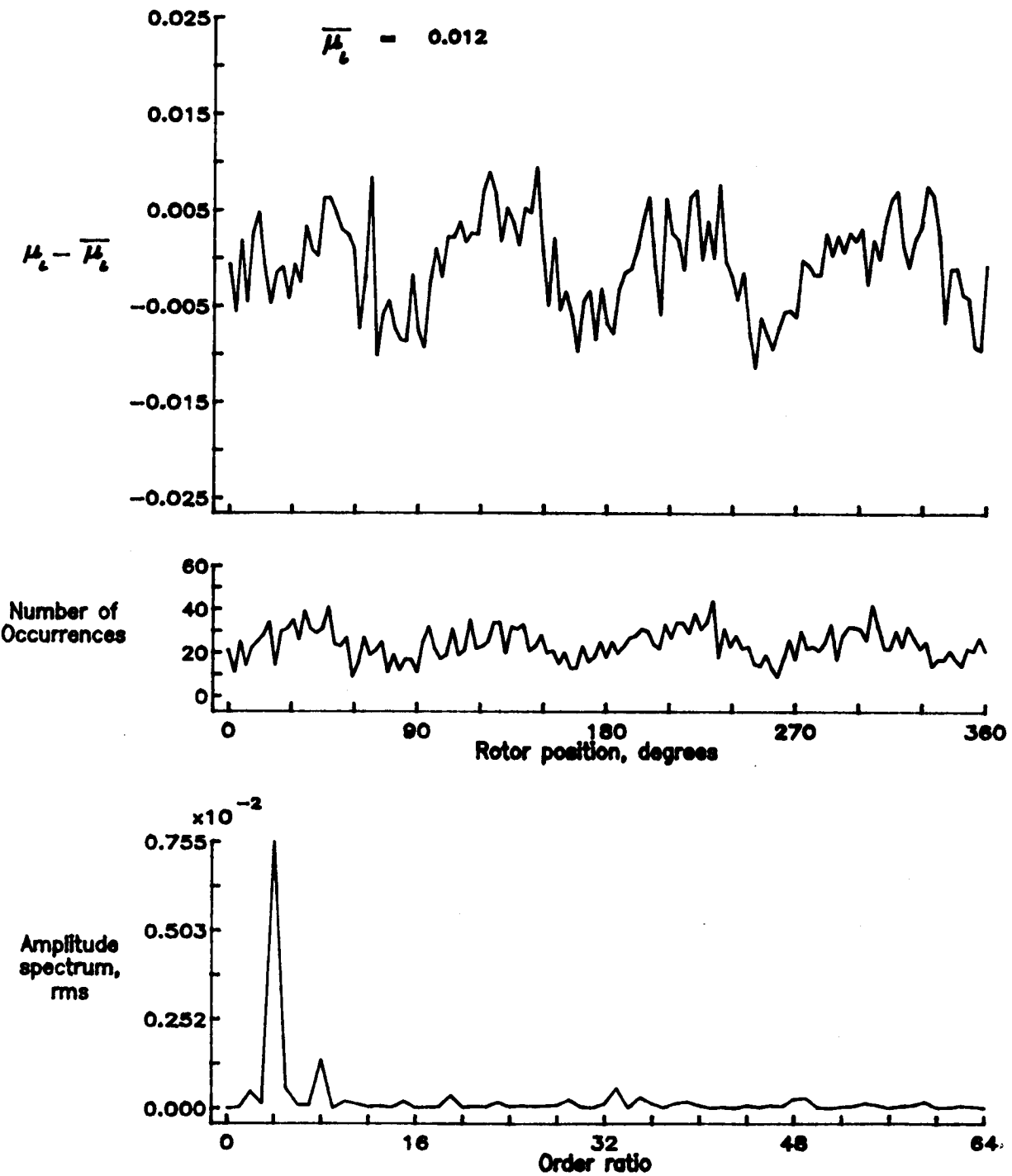


Figure 94.— Induced inflow velocity measured at 180 degrees and r/R of 0.86.

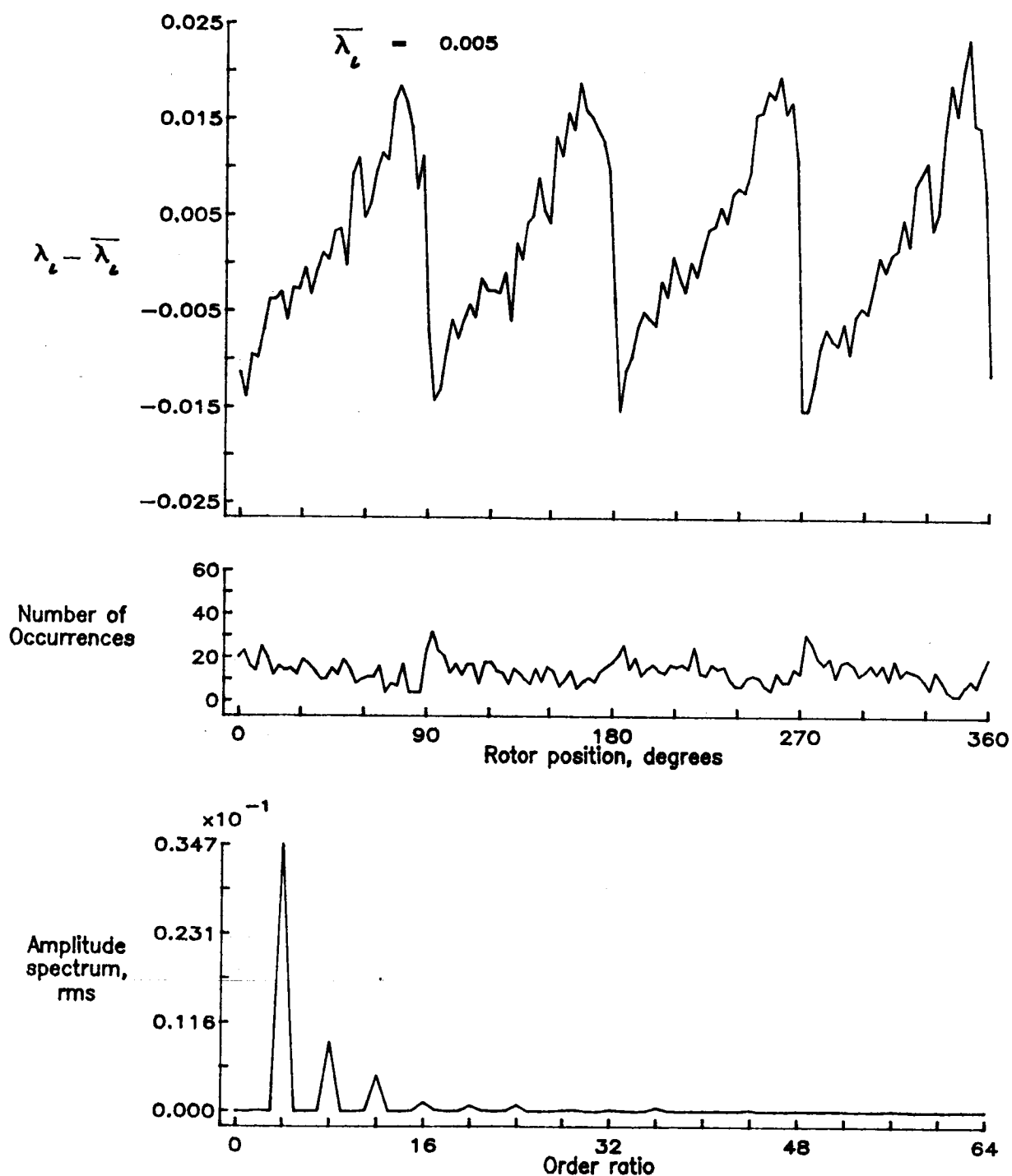


Figure 94.— Concluded.

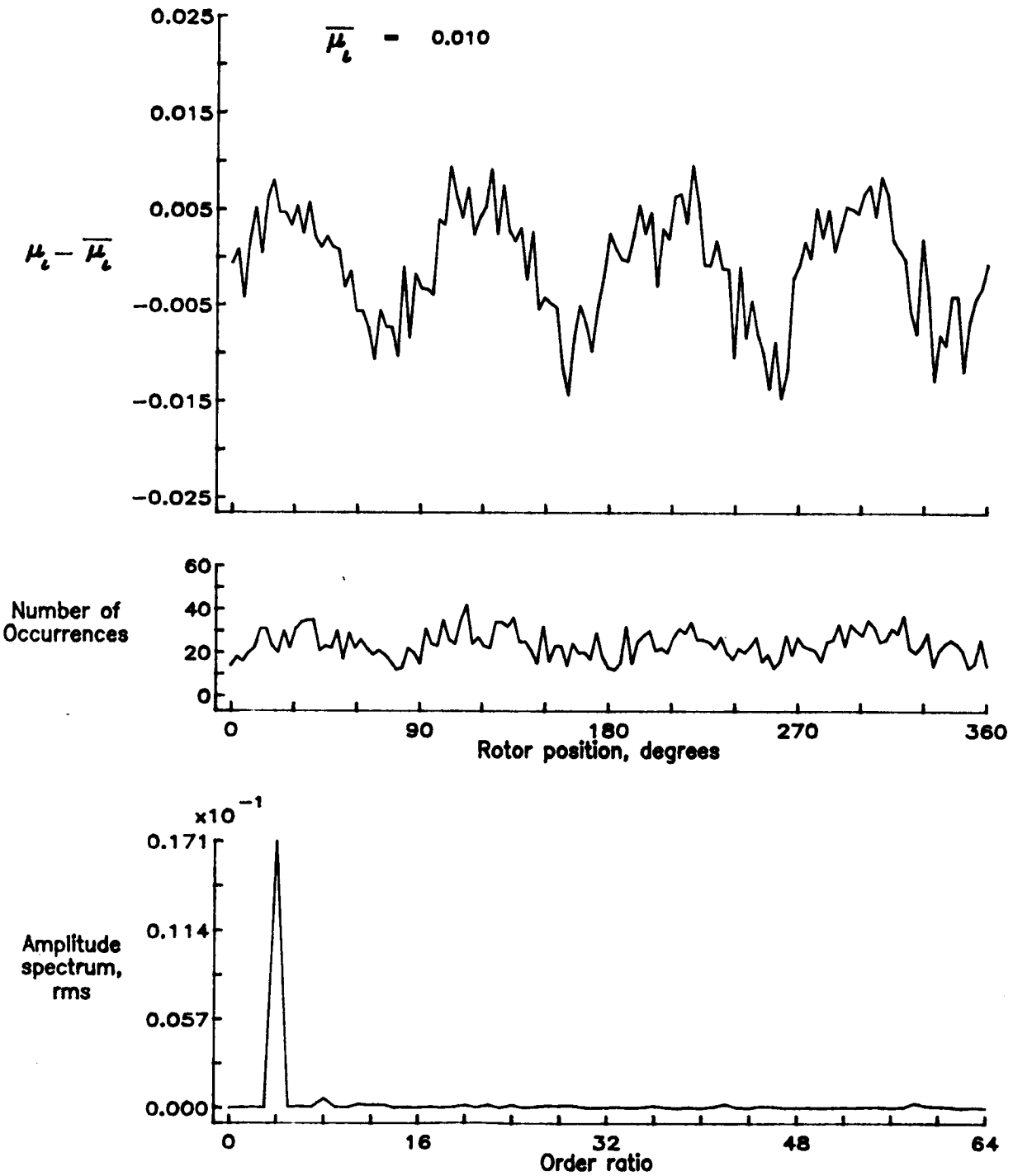


Figure 95.— Induced inflow velocity measured at 180 degrees and r/R of 0.90.

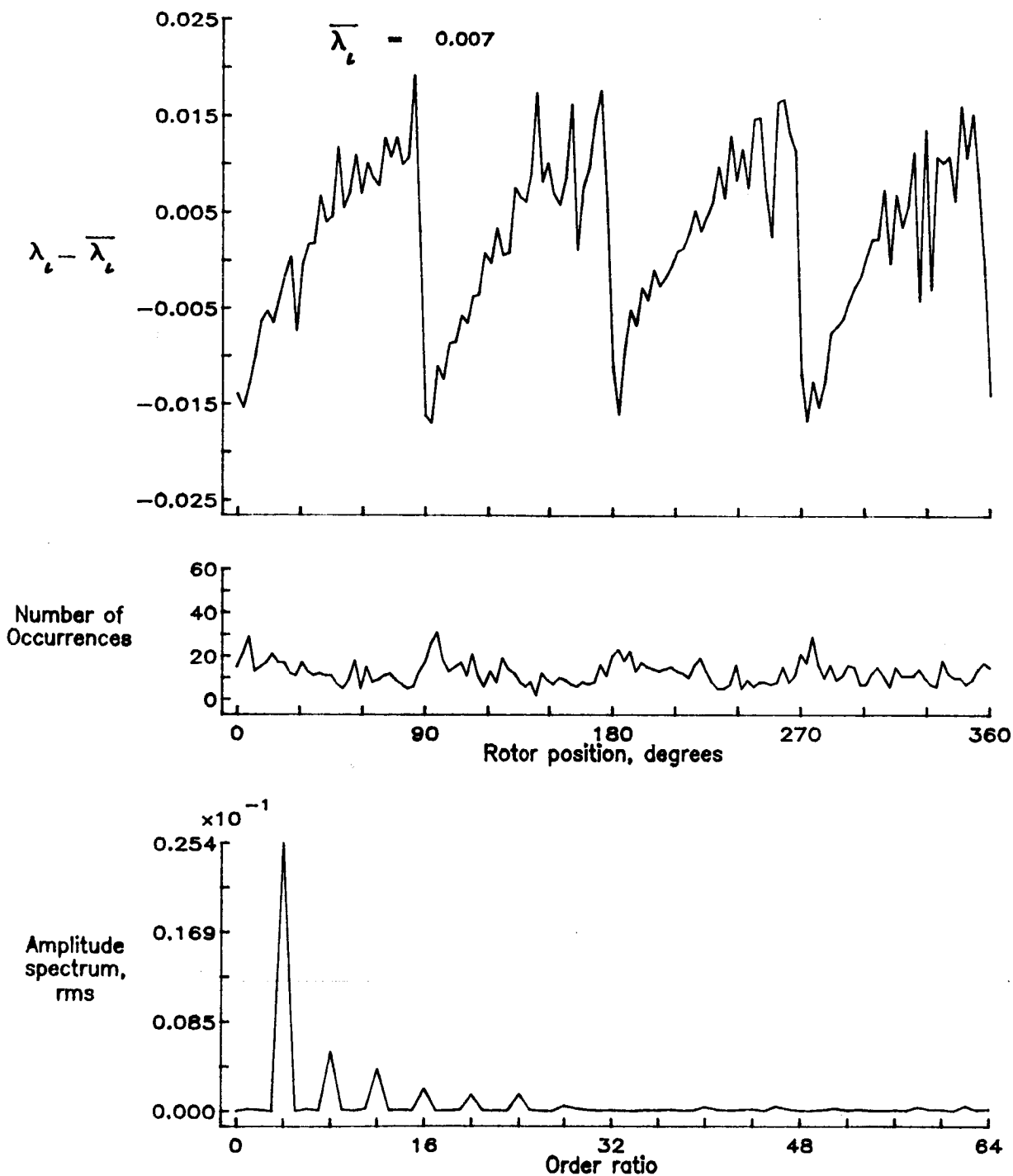


Figure 95.— Concluded.

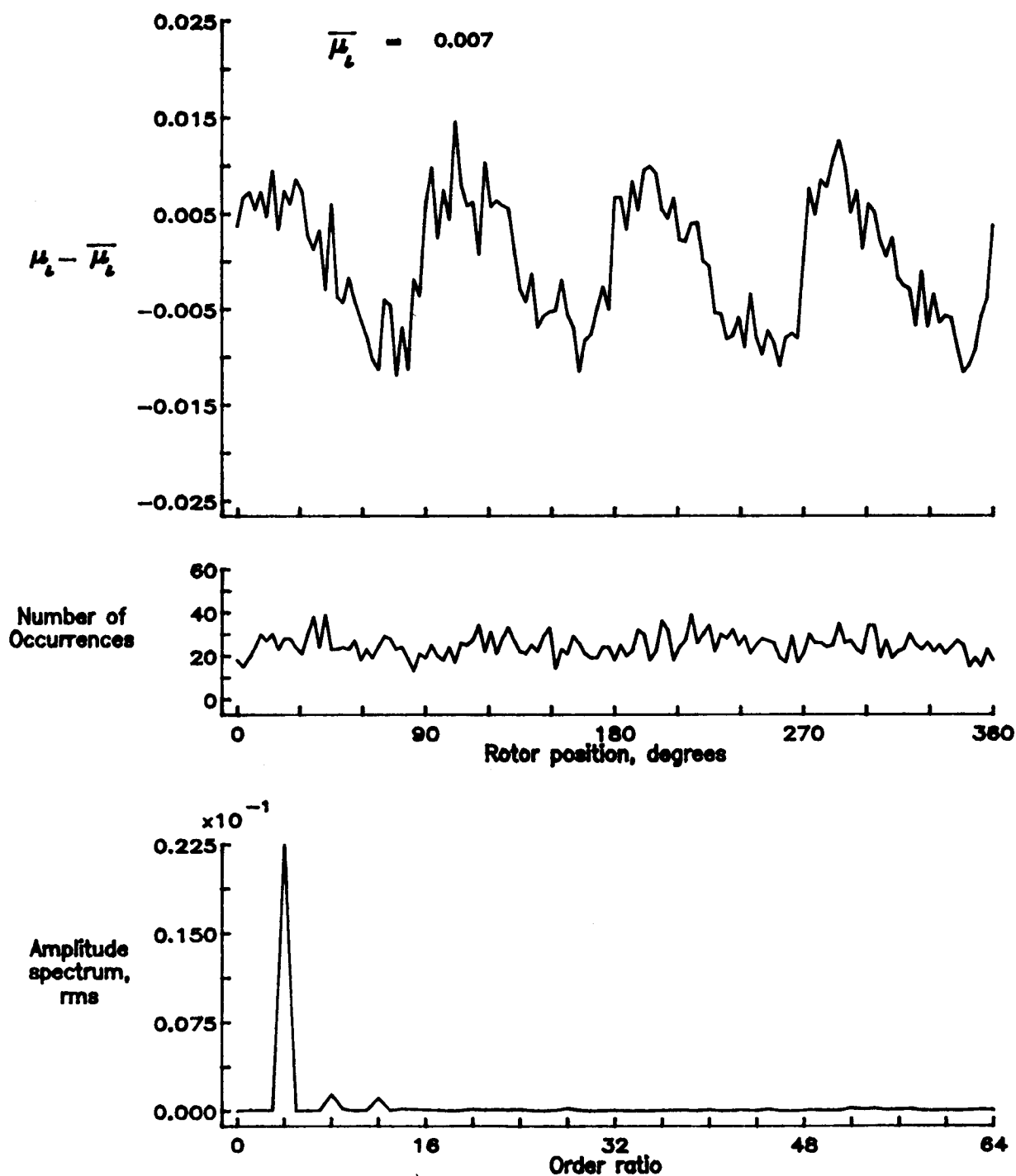


Figure 96.— Induced inflow velocity measured at 180 degrees and r/R of 0.94.

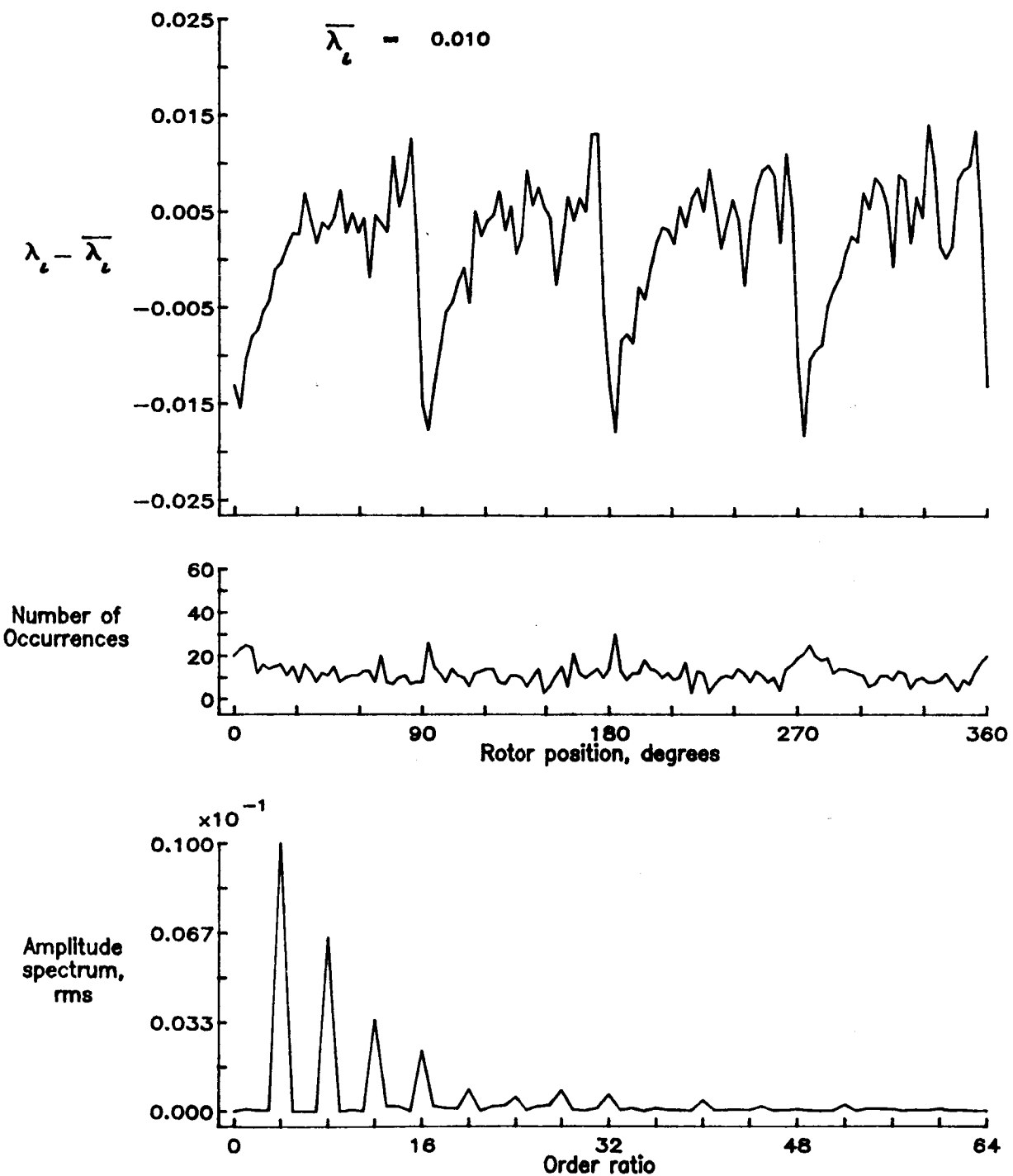


Figure 96.— Concluded.

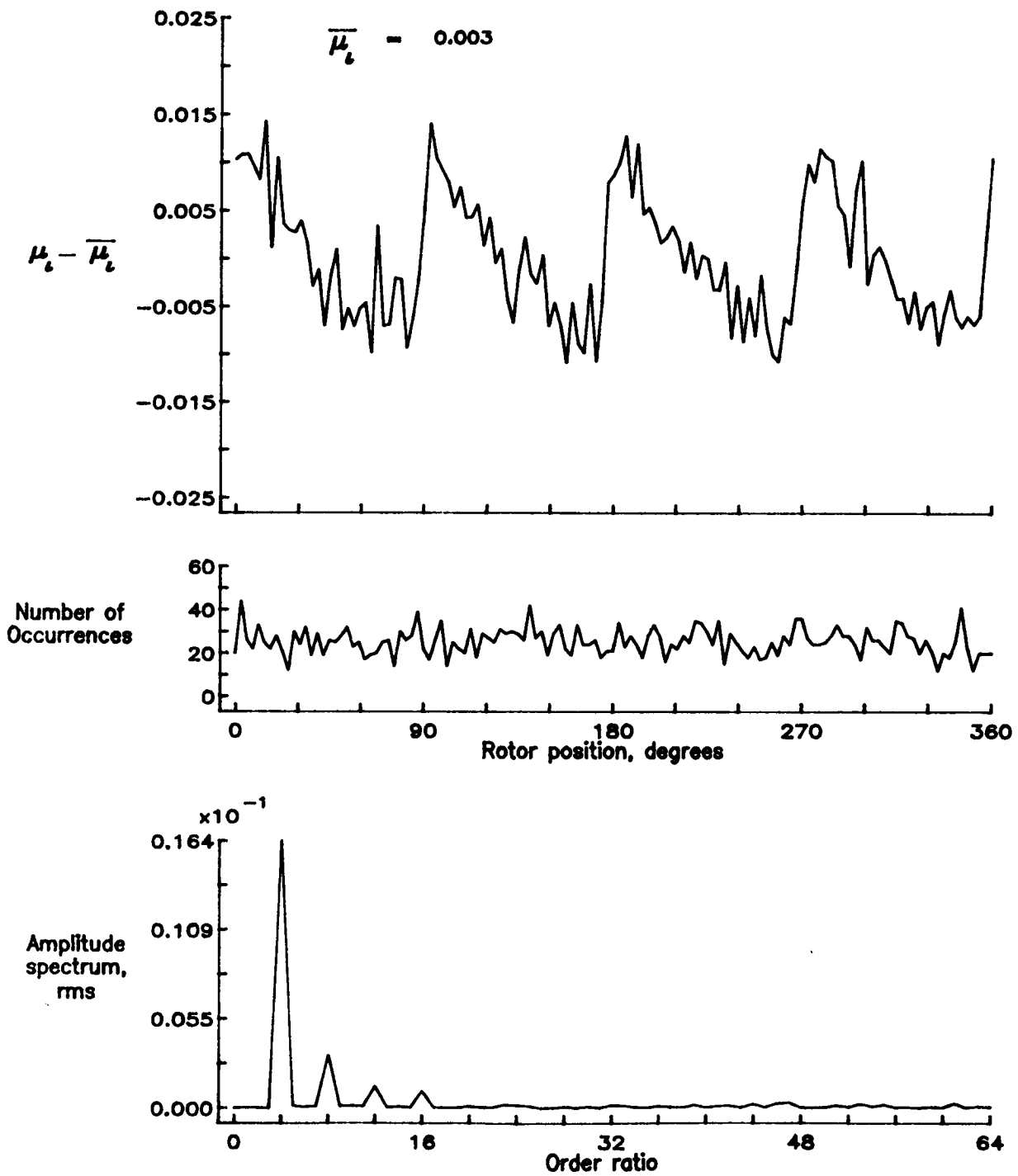


Figure 97.— Induced inflow velocity measured at 180 degrees and r/R of 0.98.

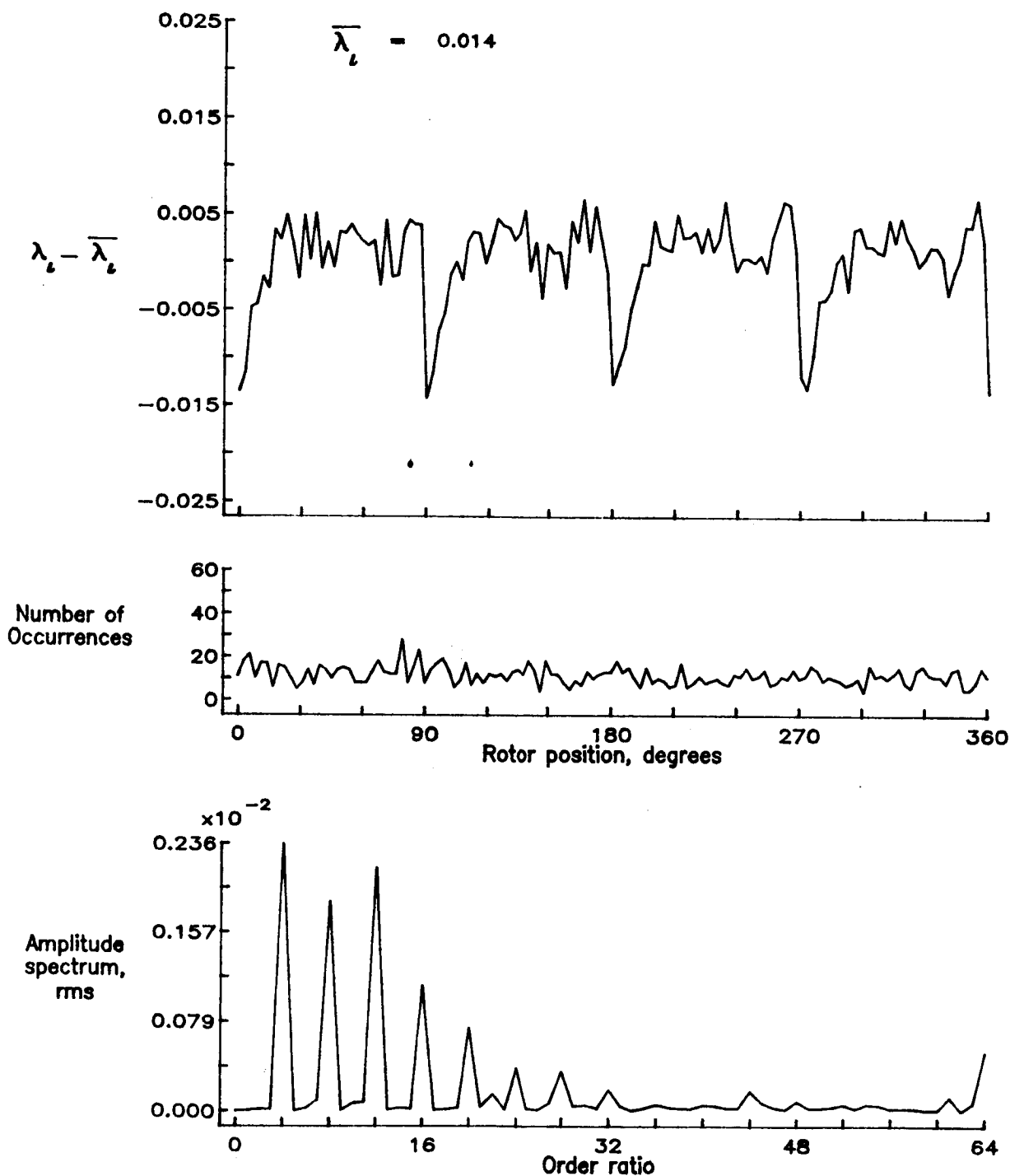


Figure 97.— Concluded.

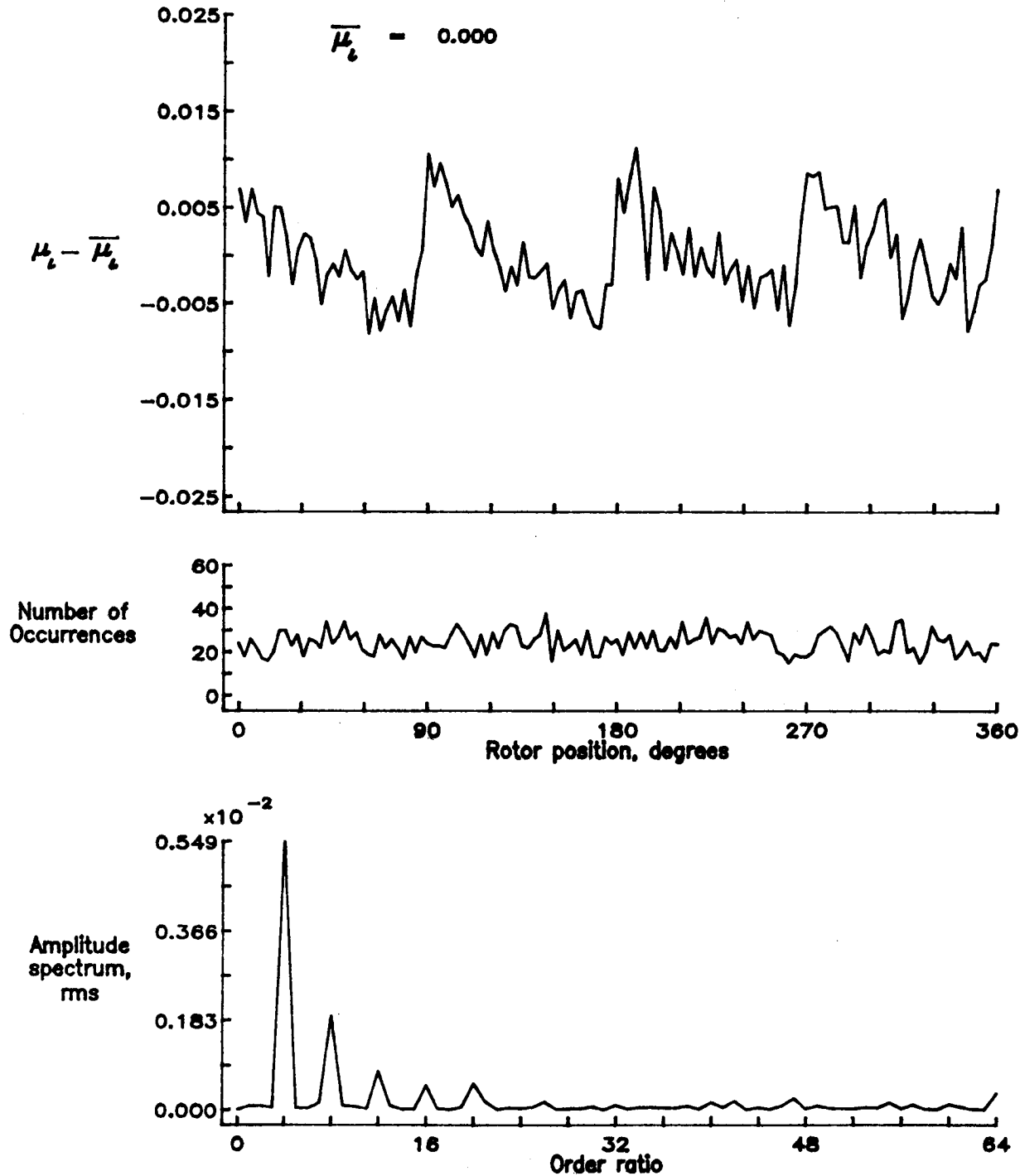


Figure 98.— Induced inflow velocity measured at 180 degrees and r/R of 1.02.

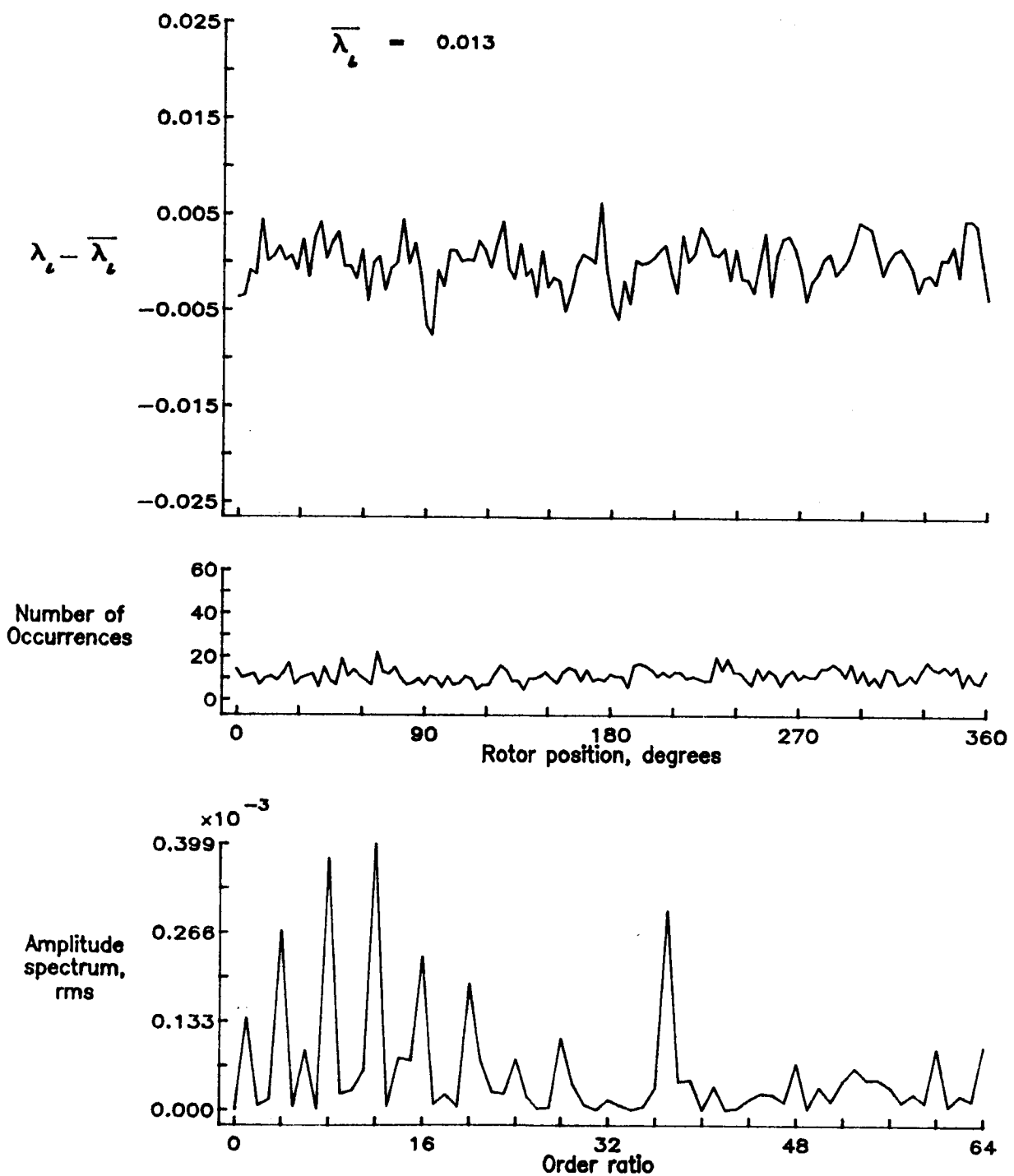


Figure 98.— Concluded.

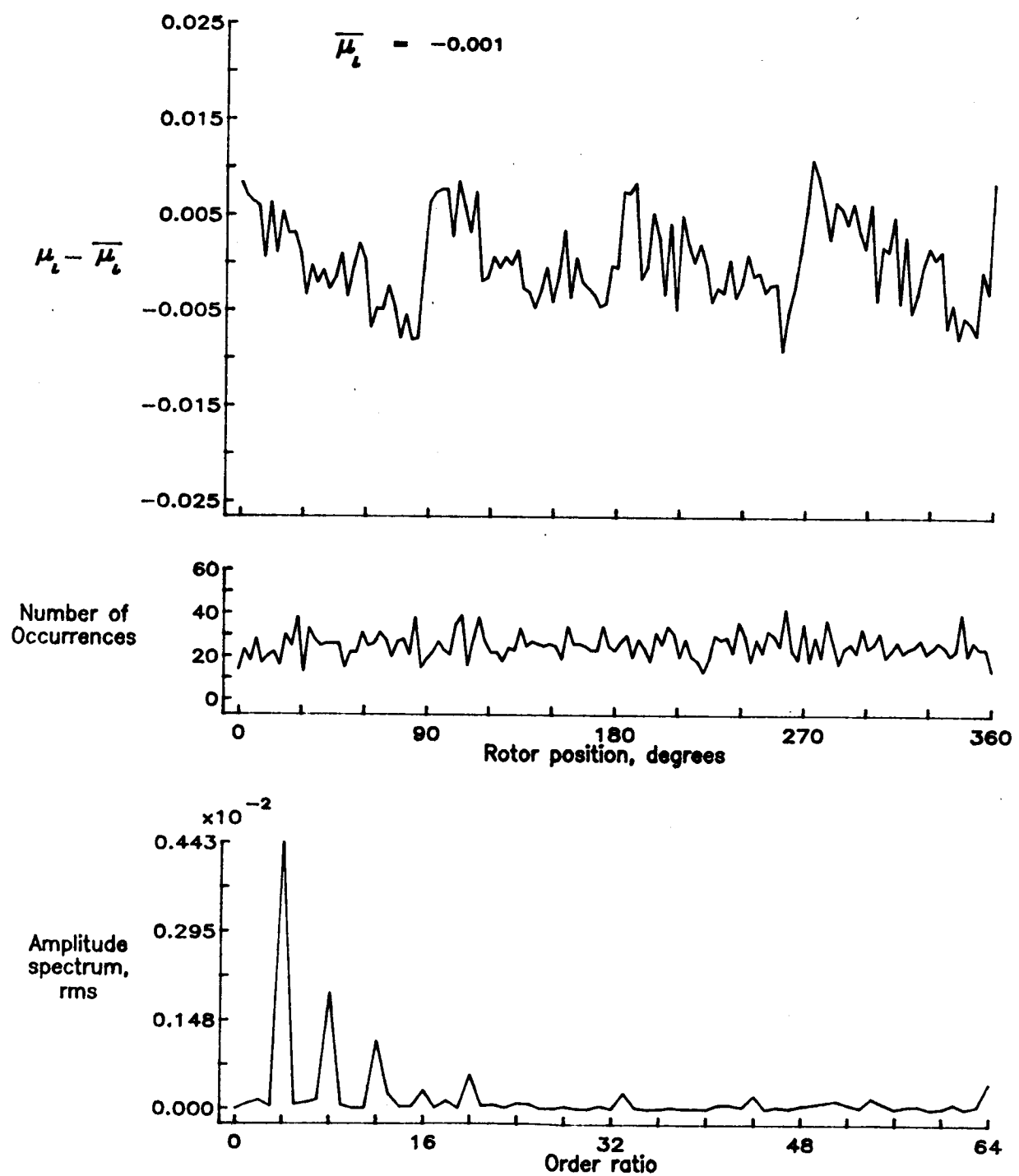


Figure 99.— Induced inflow velocity measured at 180 degrees and r/R of 1.04.

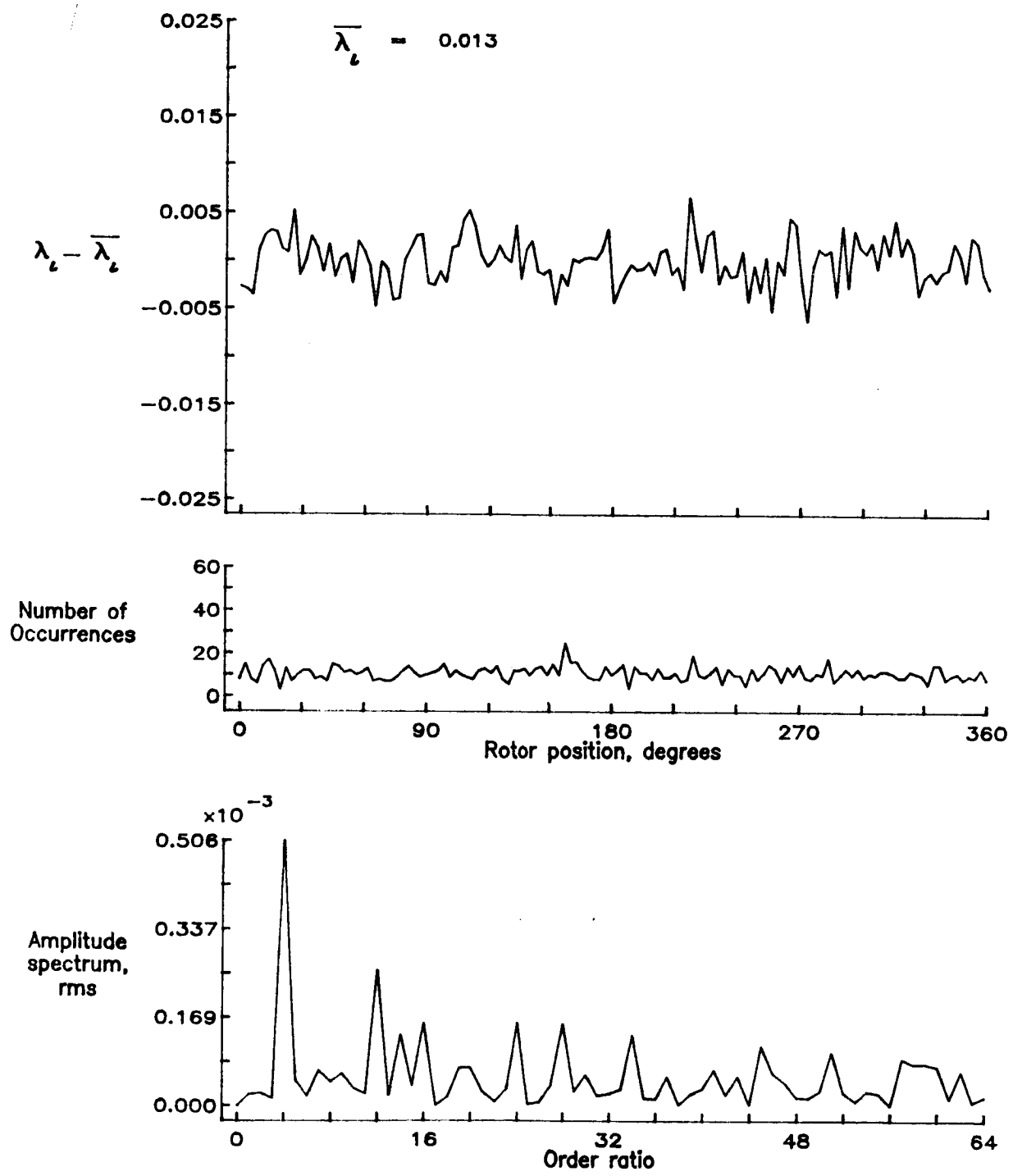


Figure 99.— Concluded.

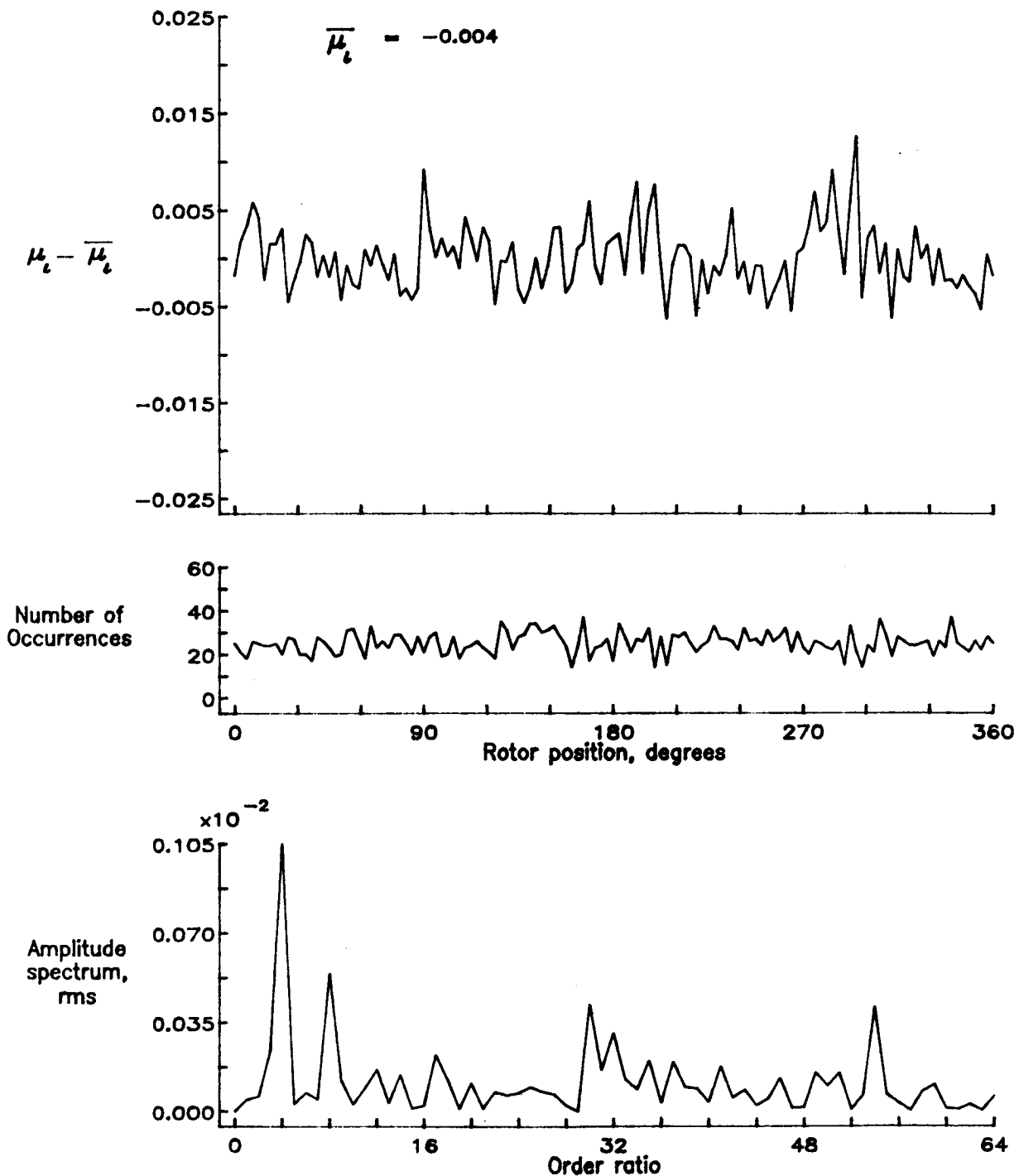


Figure 100.— Induced inflow velocity measured at 180 degrees and  $r/R$  of 1.10.

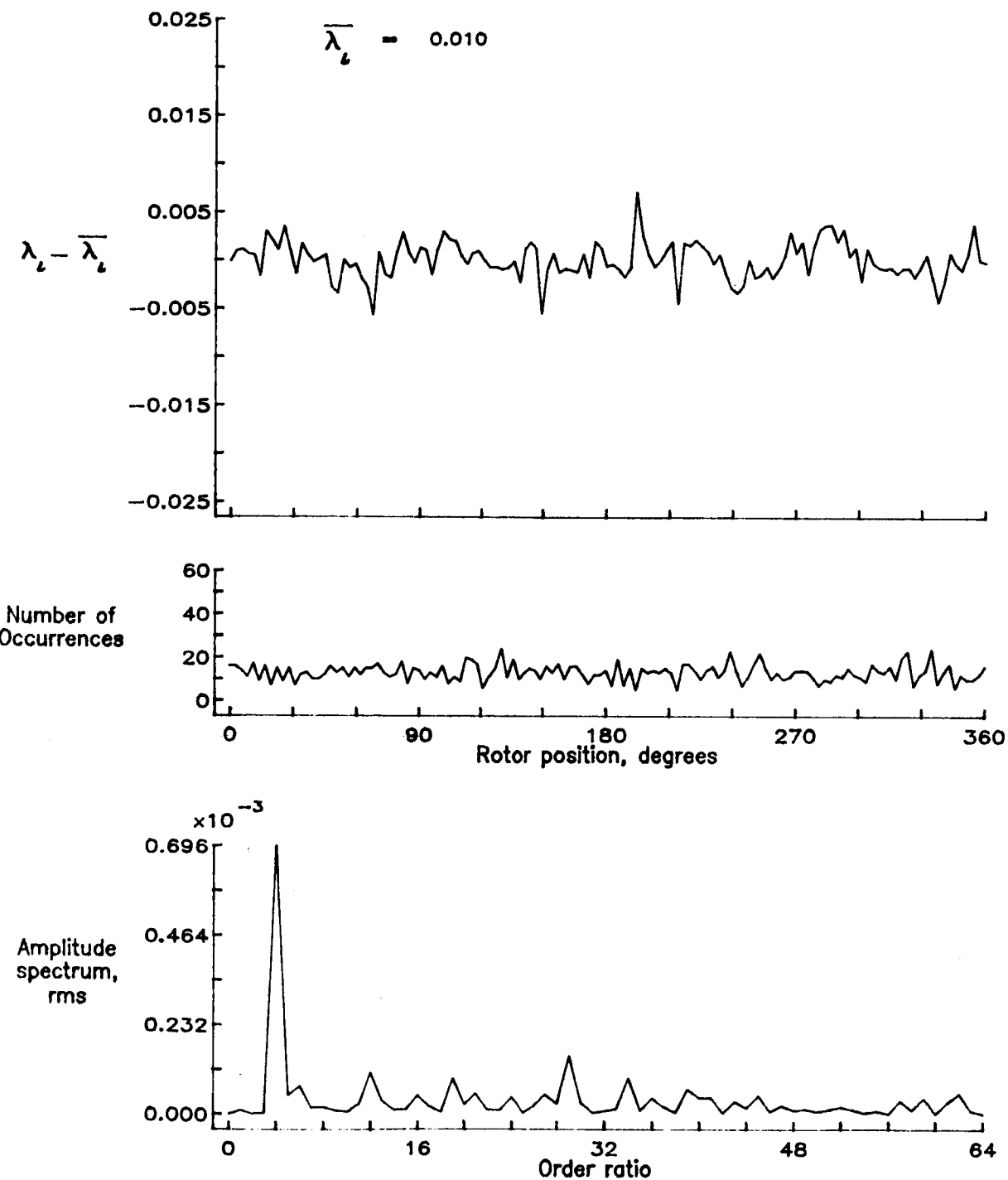


Figure 100.— Concluded.

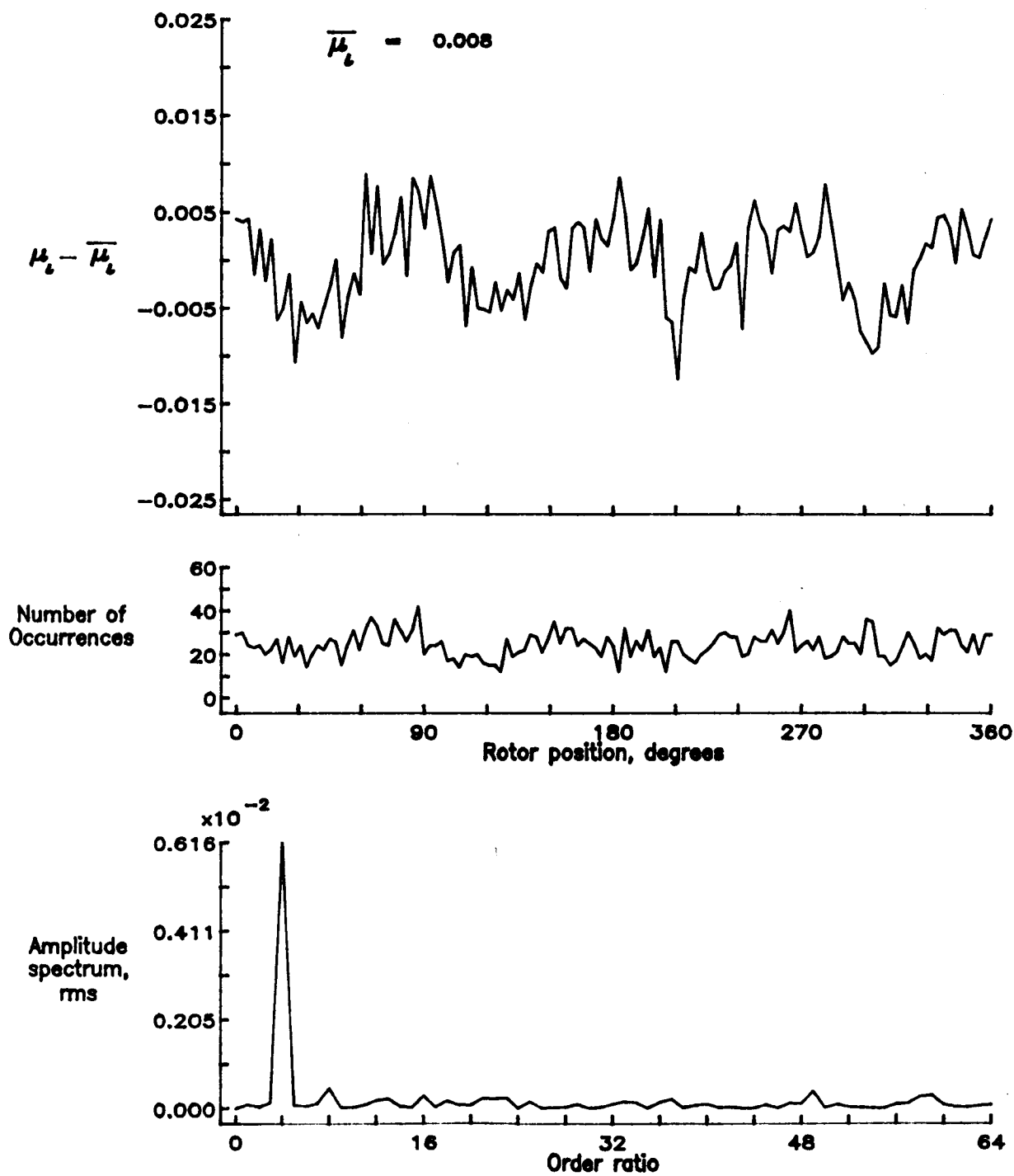


Figure 101.— Induced inflow velocity measured at 210 degrees and r/R of 0.40.

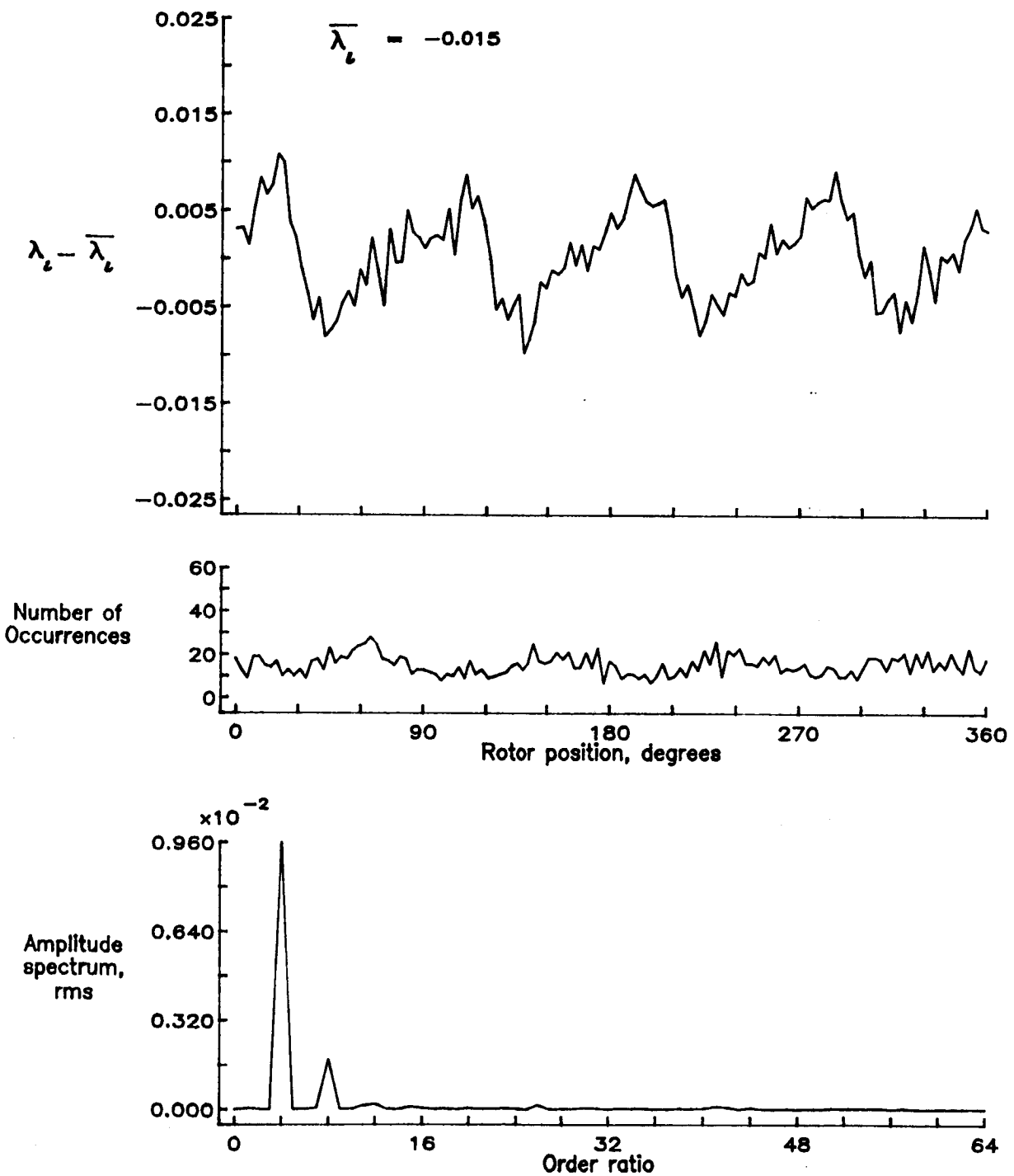


Figure 101.— Concluded.

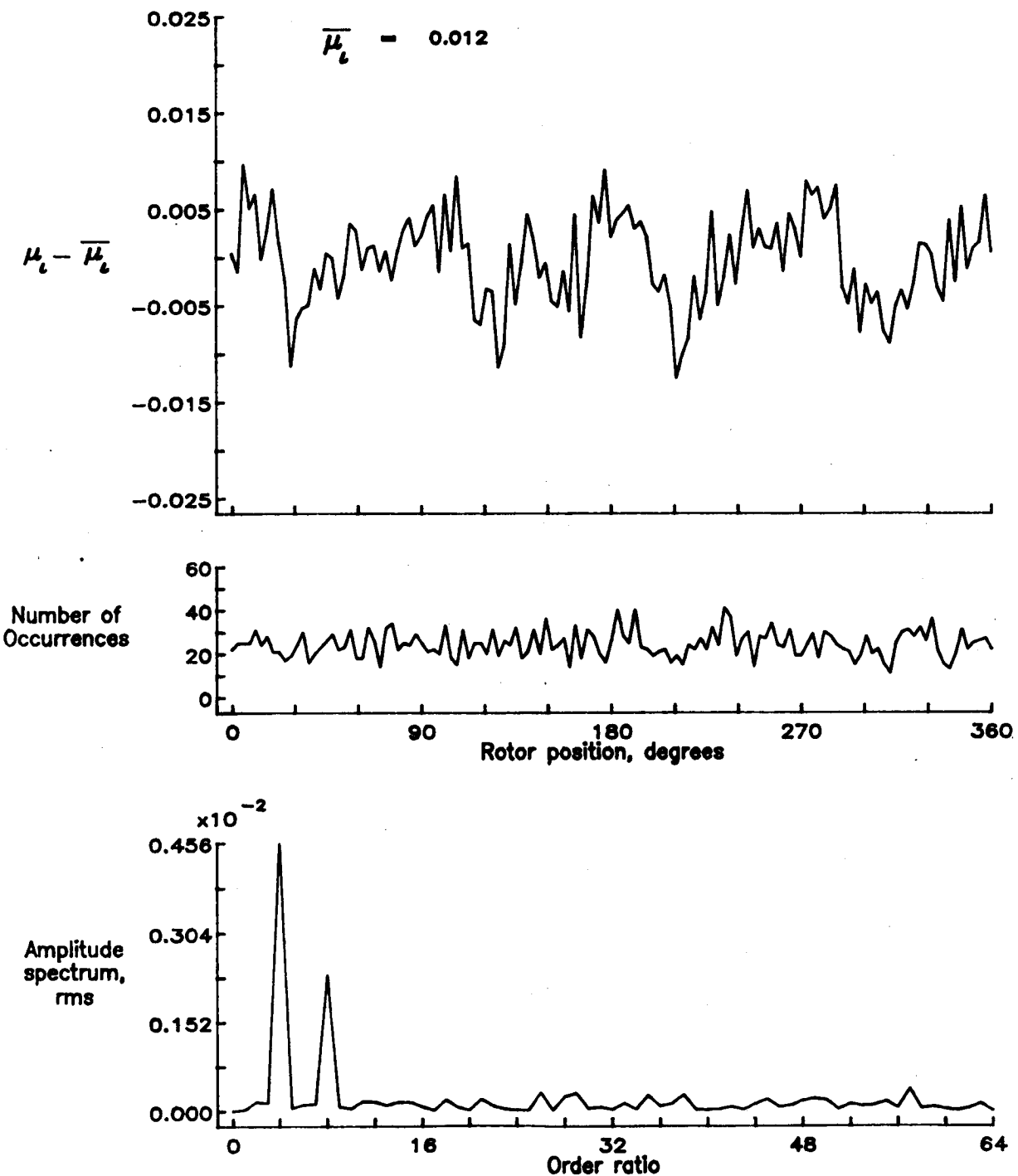


Figure 102.— Induced inflow velocity measured at 210 degrees and r/R of 0.50.

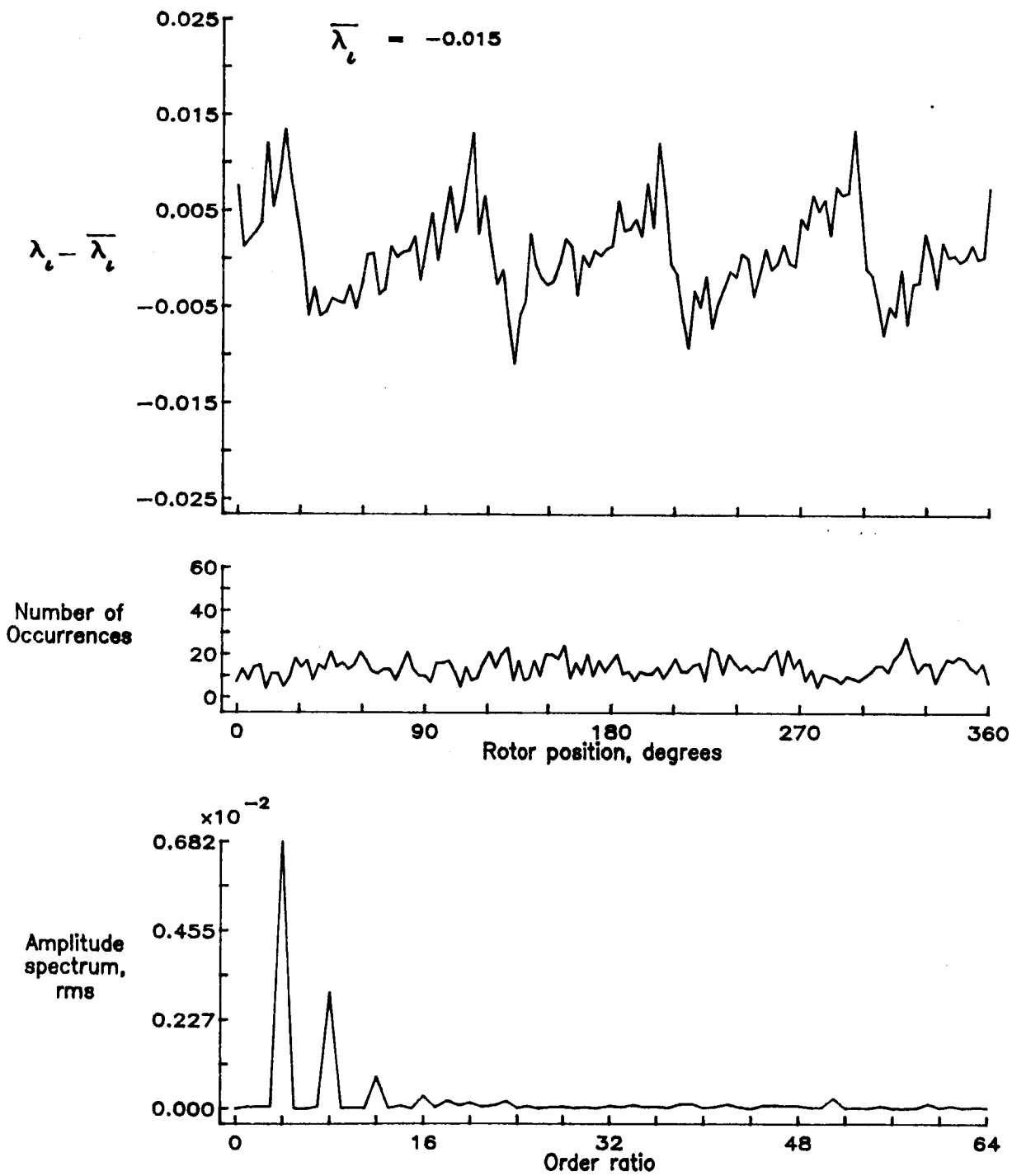


Figure 102.— Concluded.

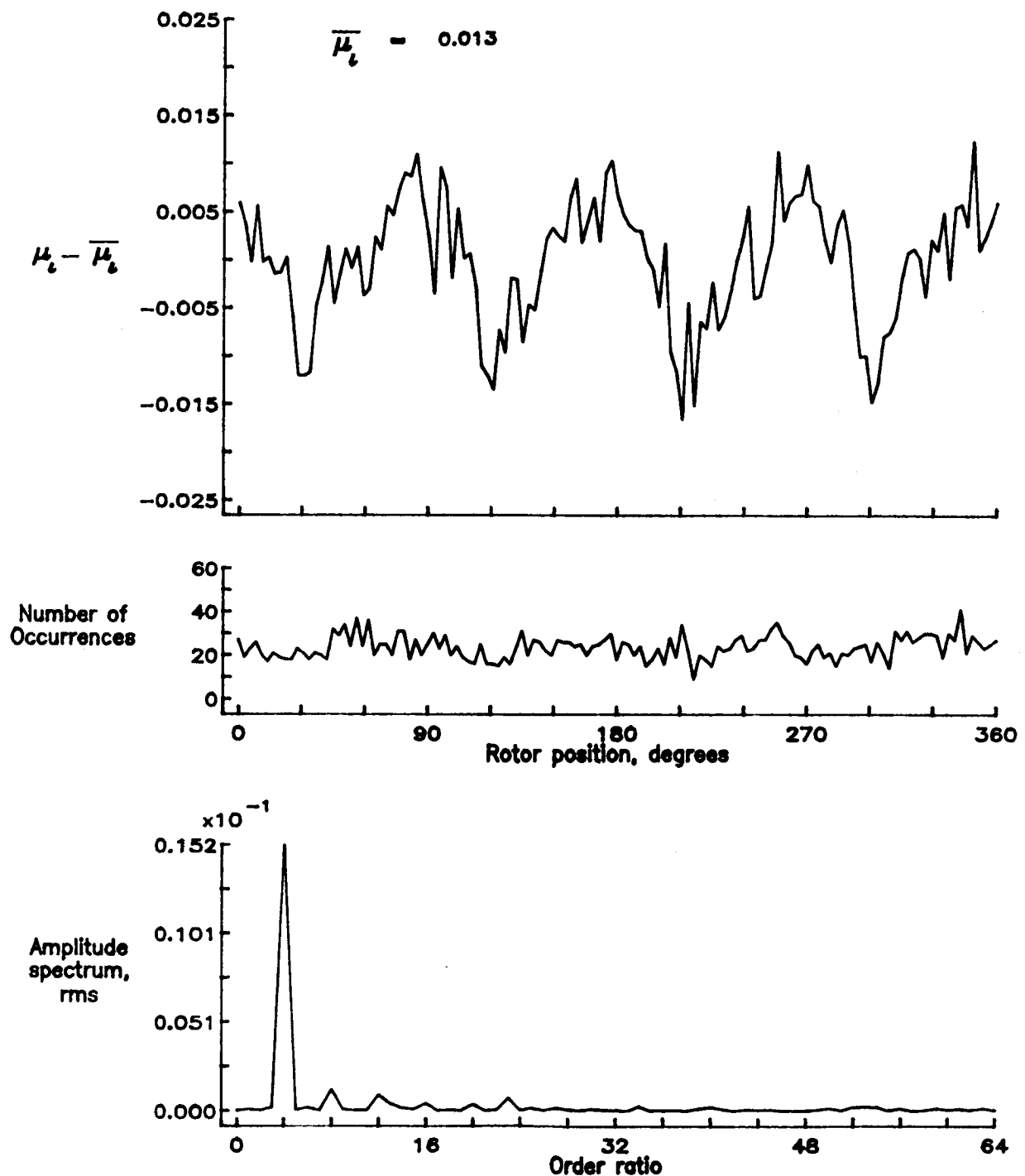


Figure 103.— Induced inflow velocity measured at 210 degrees and r/R of 0.60.

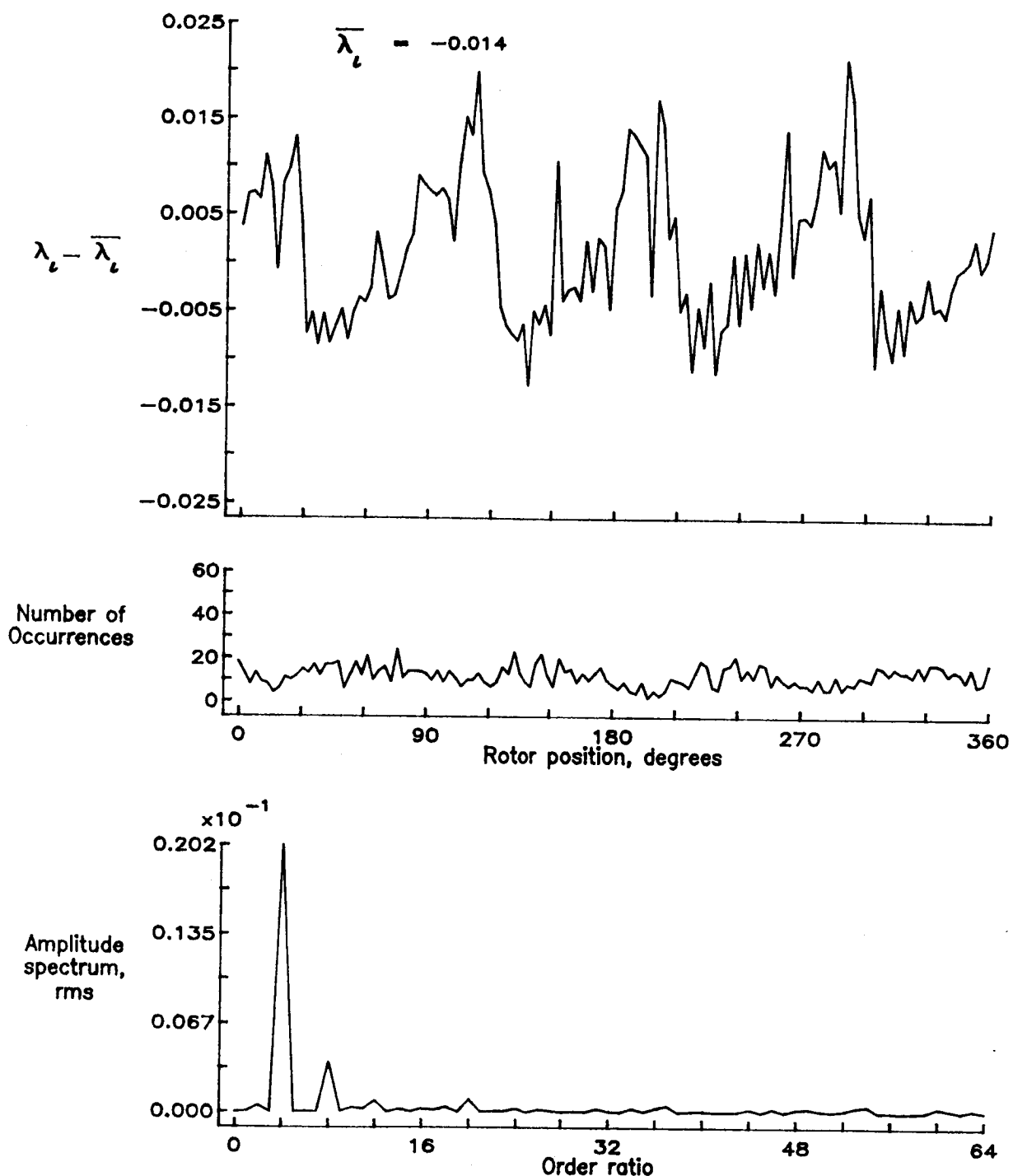


Figure 103.— Concluded.

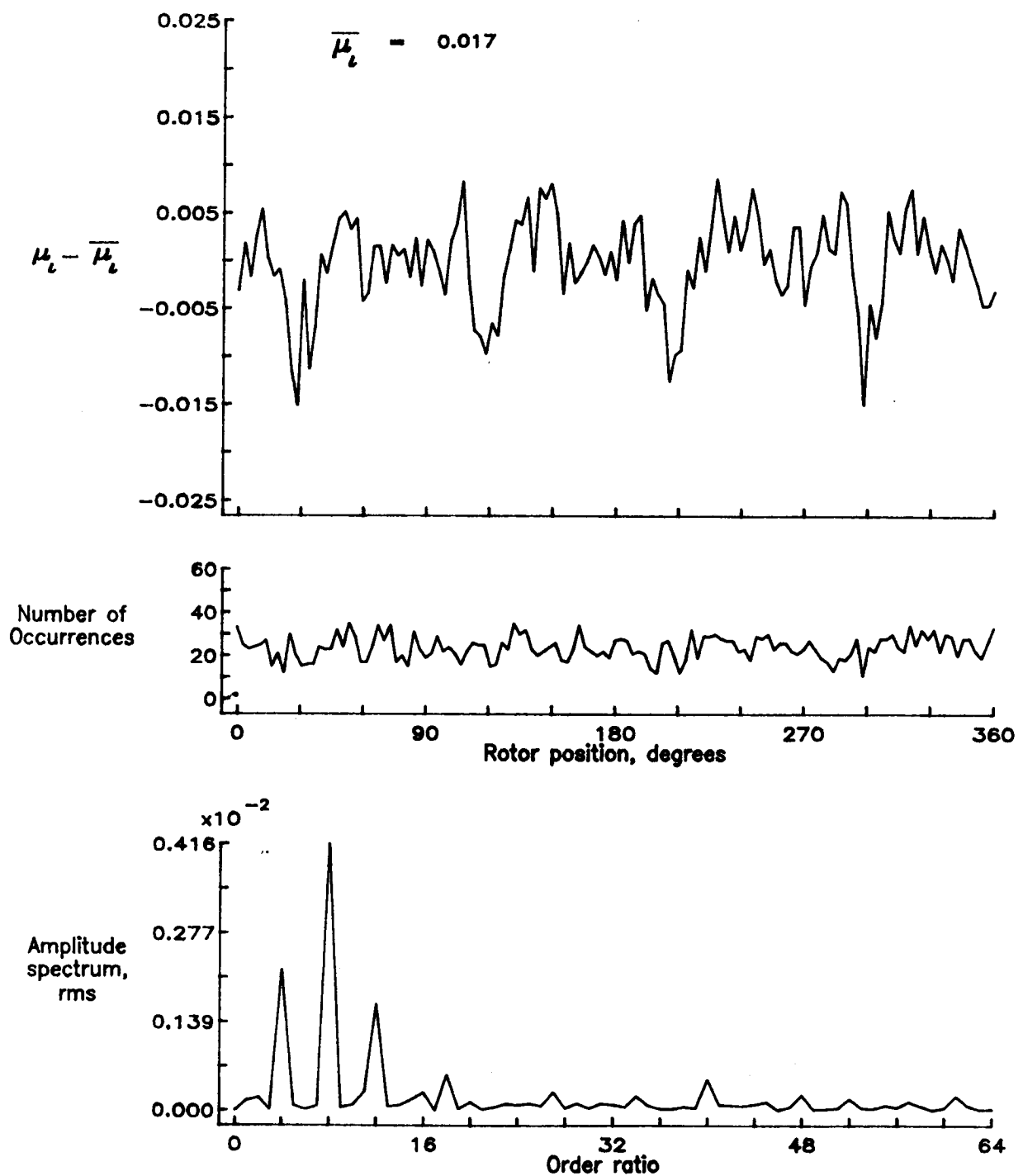


Figure 104.— Induced inflow velocity measured at 210 degrees and r/R of 0.70.

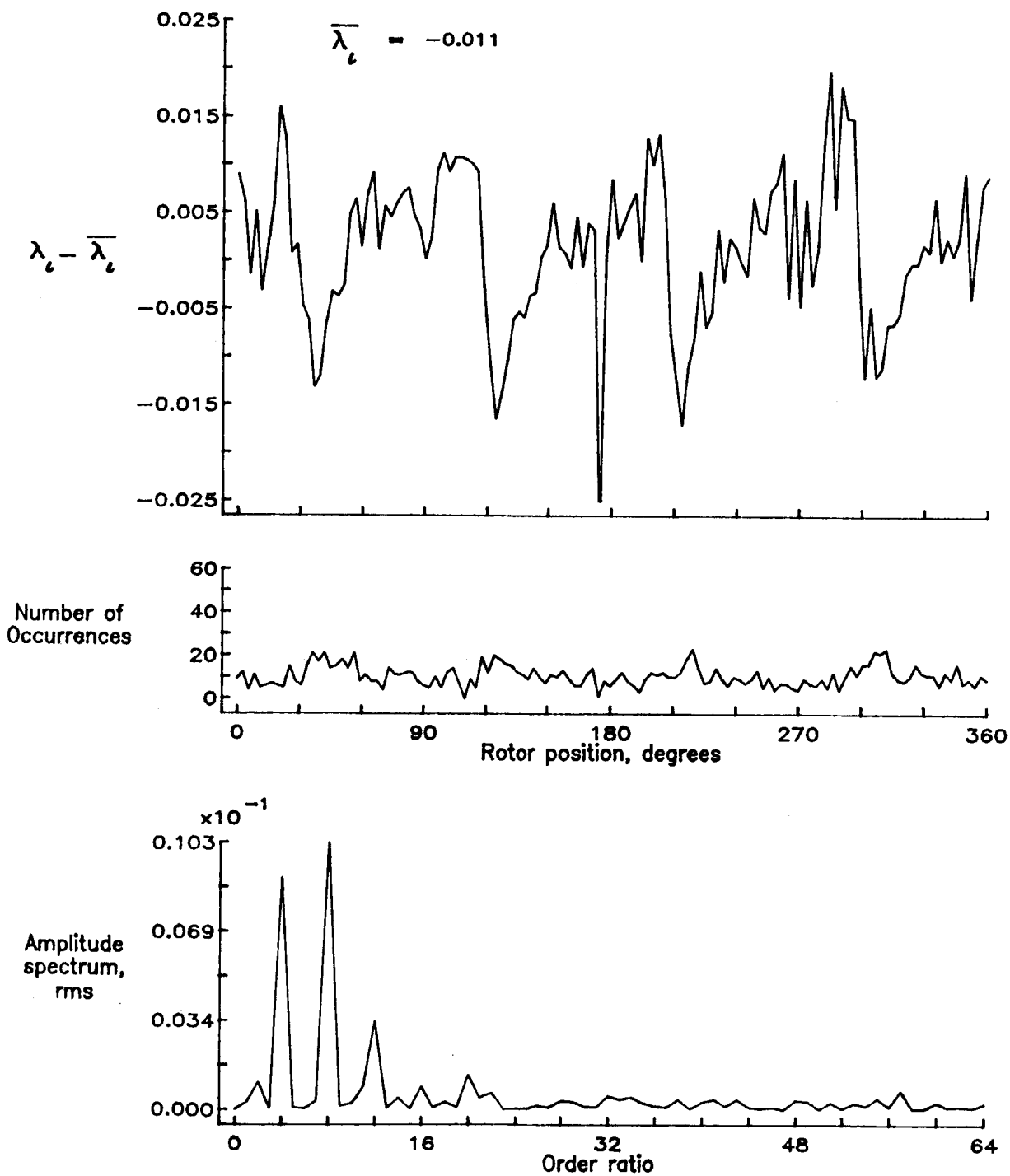


Figure 104.— Concluded.

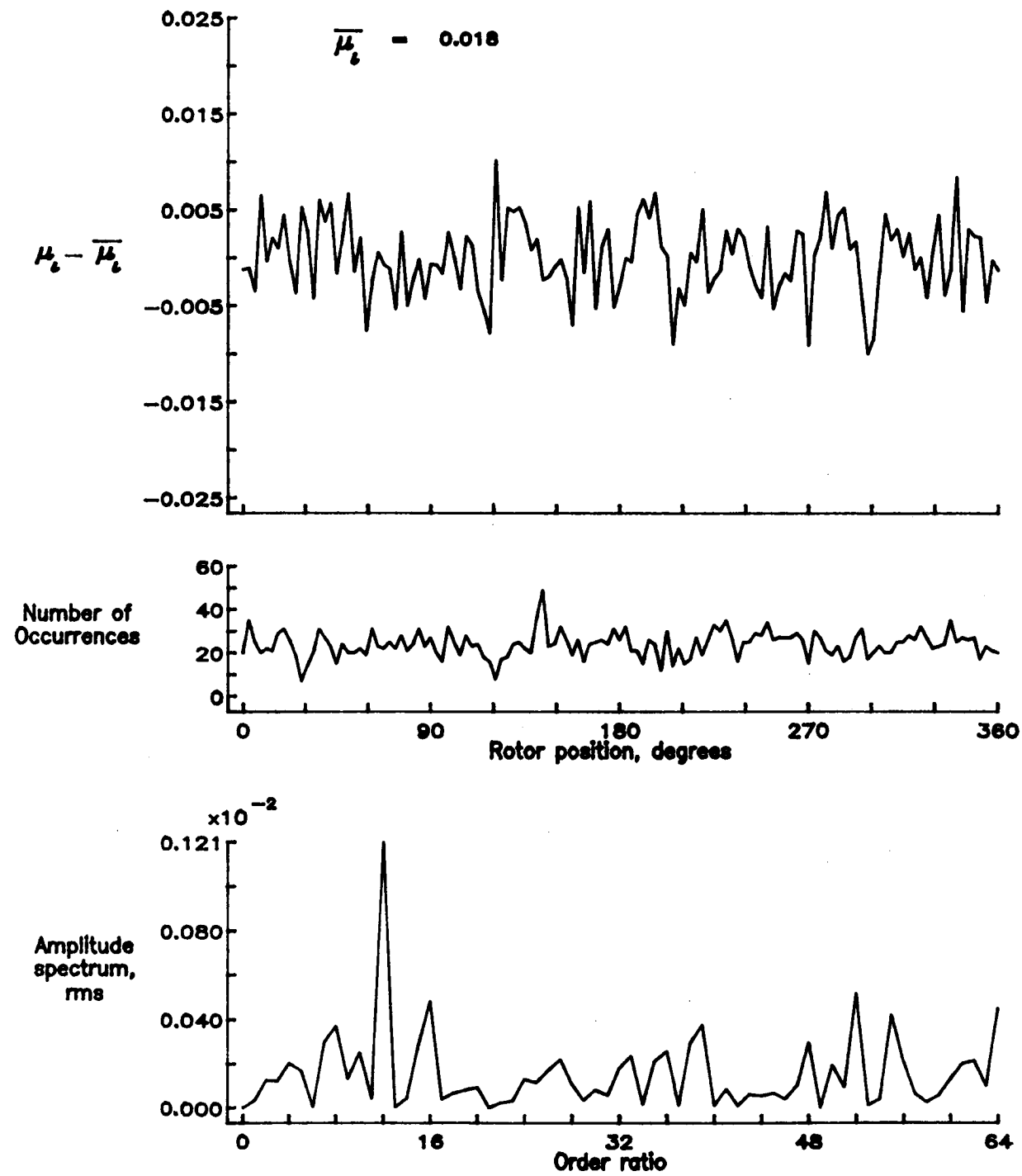


Figure 105.— Induced inflow velocity measured at 210 degrees and  $r/R$  of 0.74.

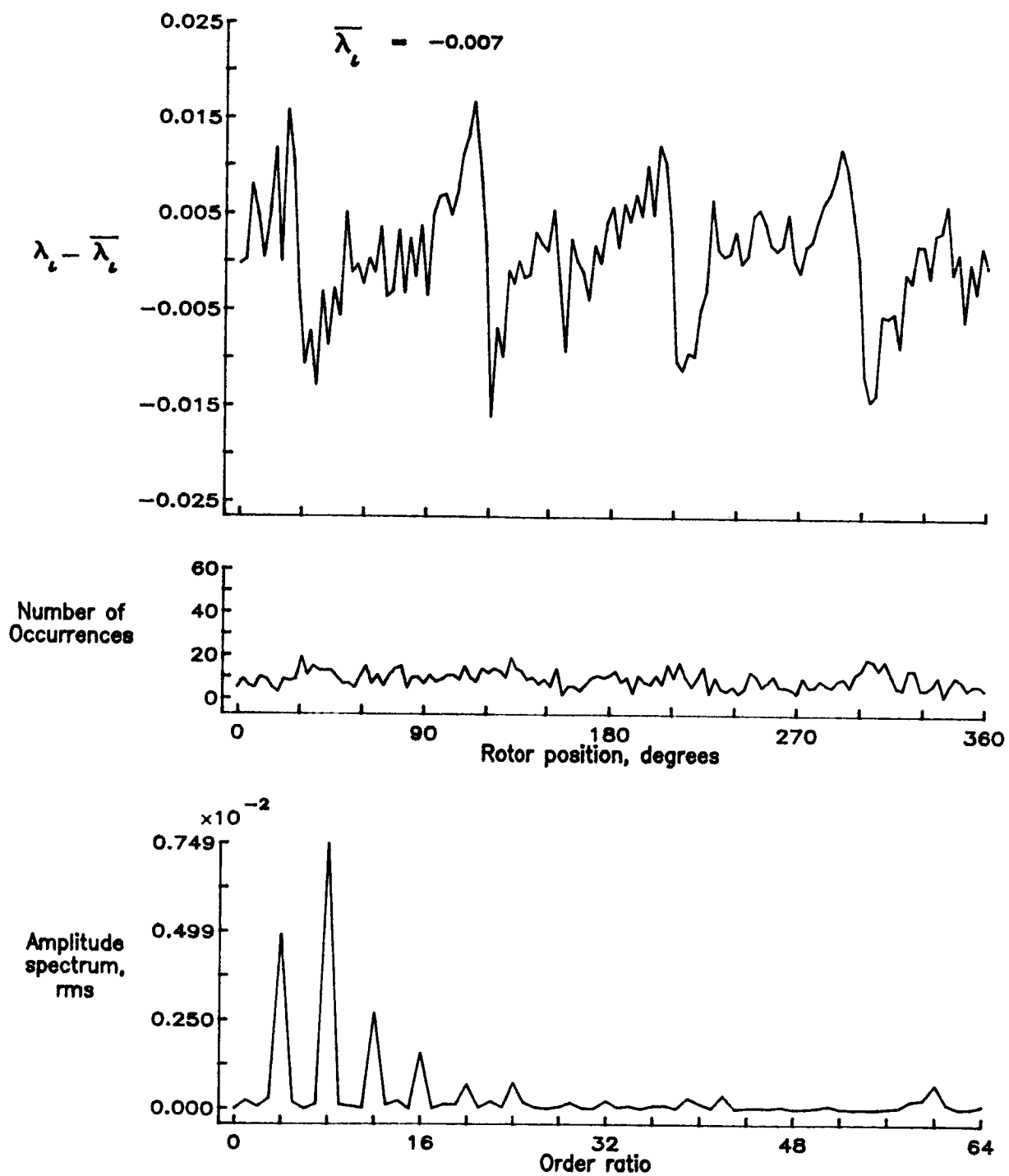


Figure 105.— Concluded.

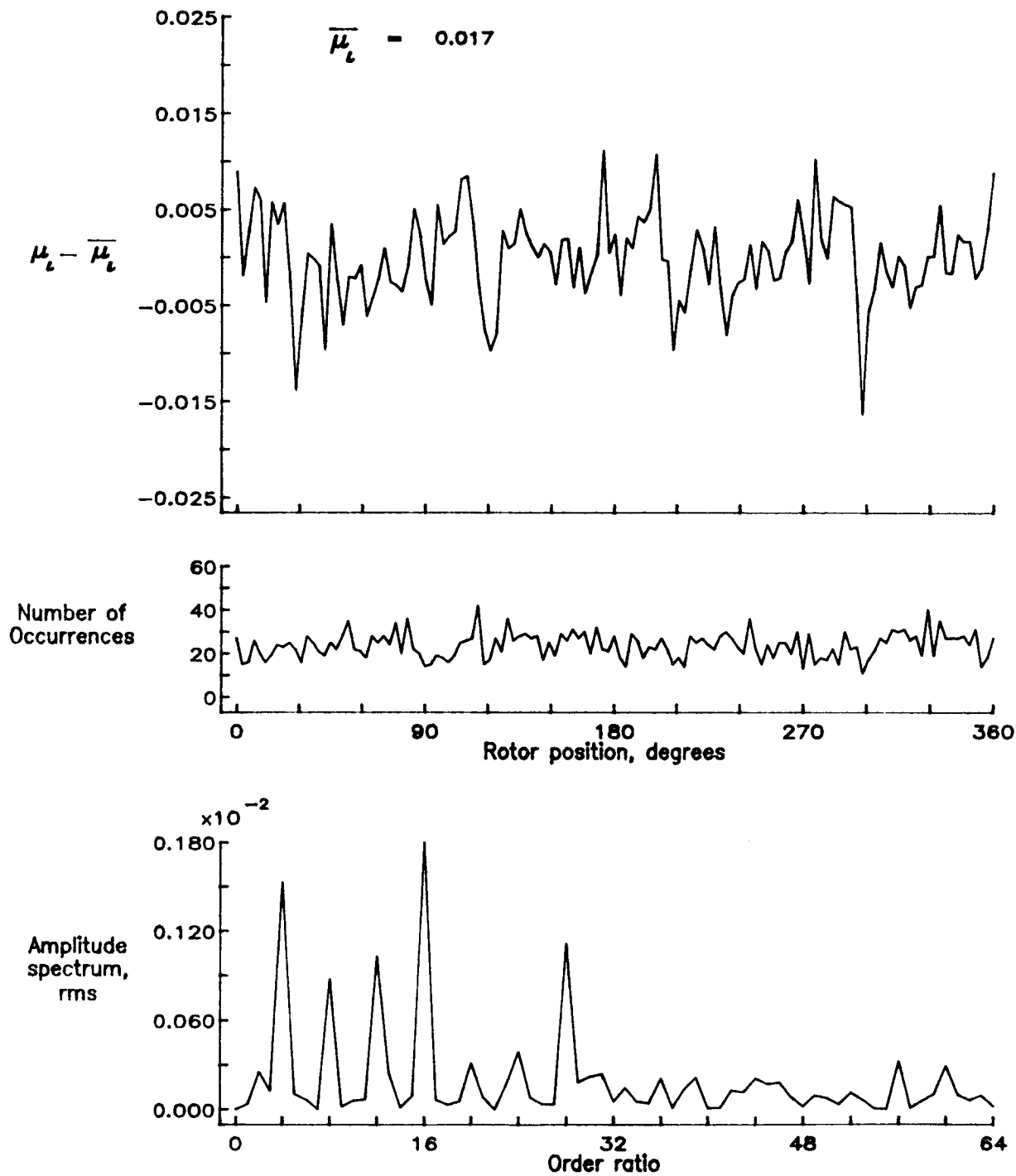


Figure 106.— Induced inflow velocity measured at 210 degrees and  $r/R$  of 0.78.

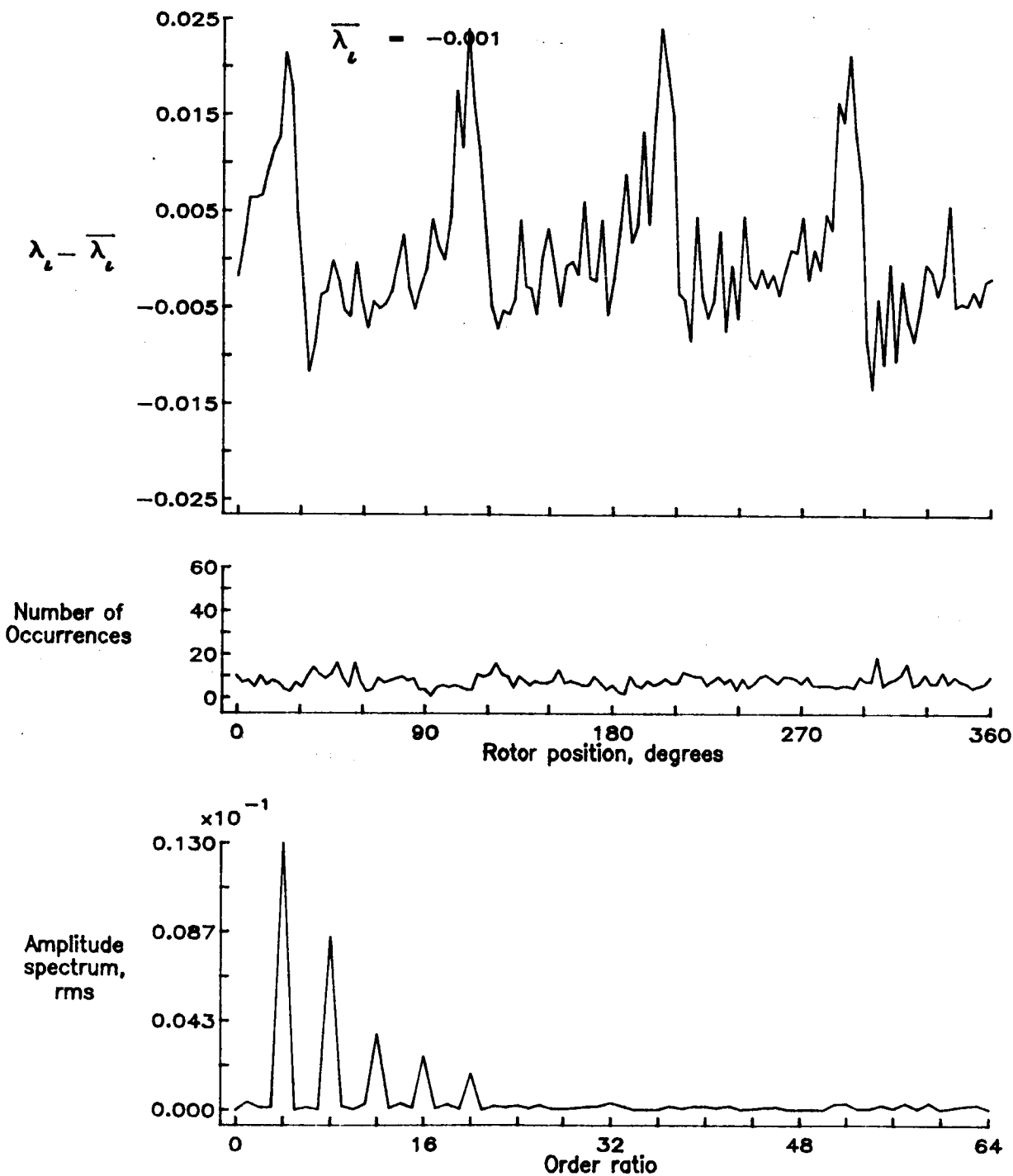


Figure 106.— Concluded.

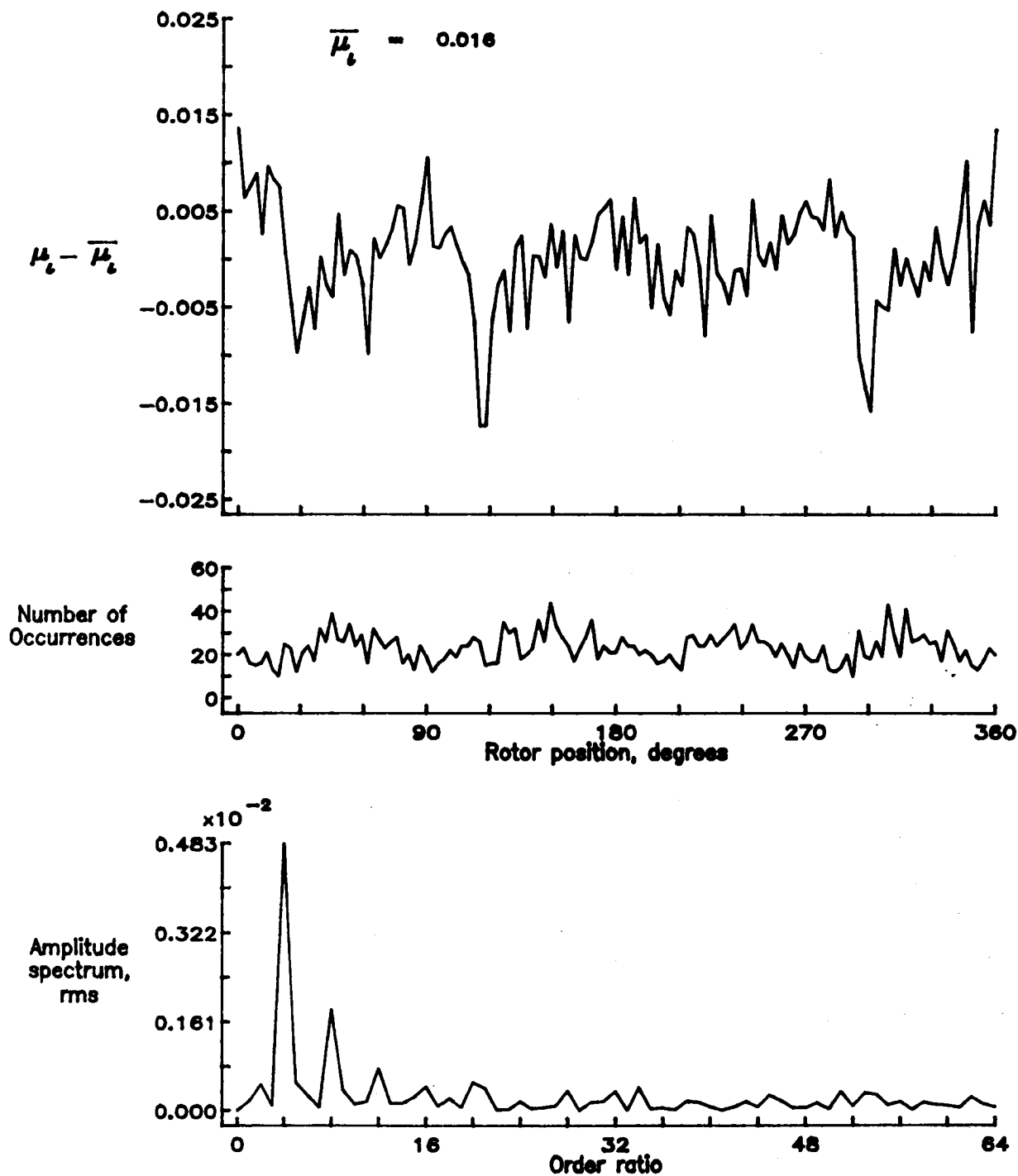


Figure 107.— Induced inflow velocity measured at 210 degrees and r/R of 0.82.

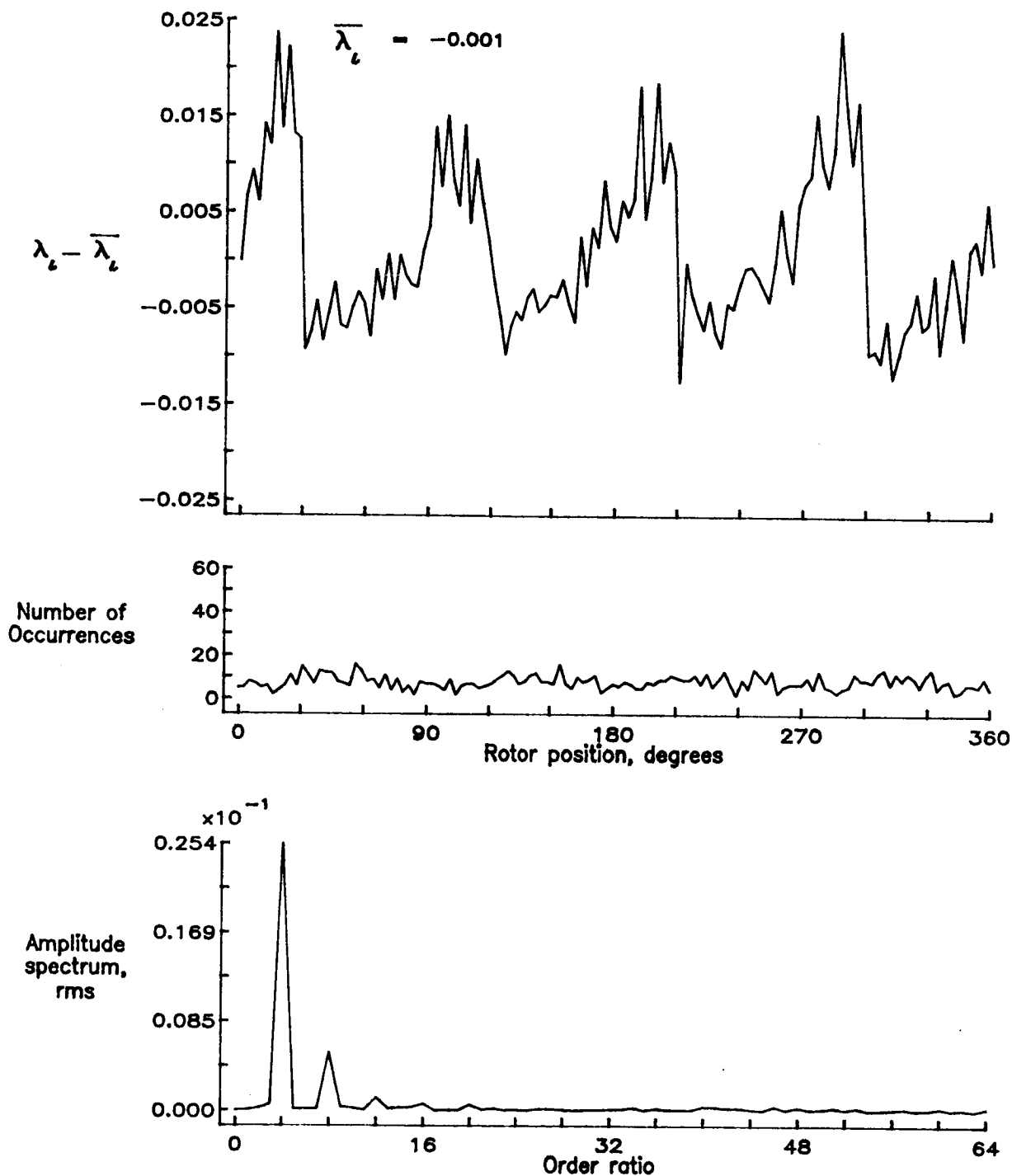


Figure 107.— Concluded.

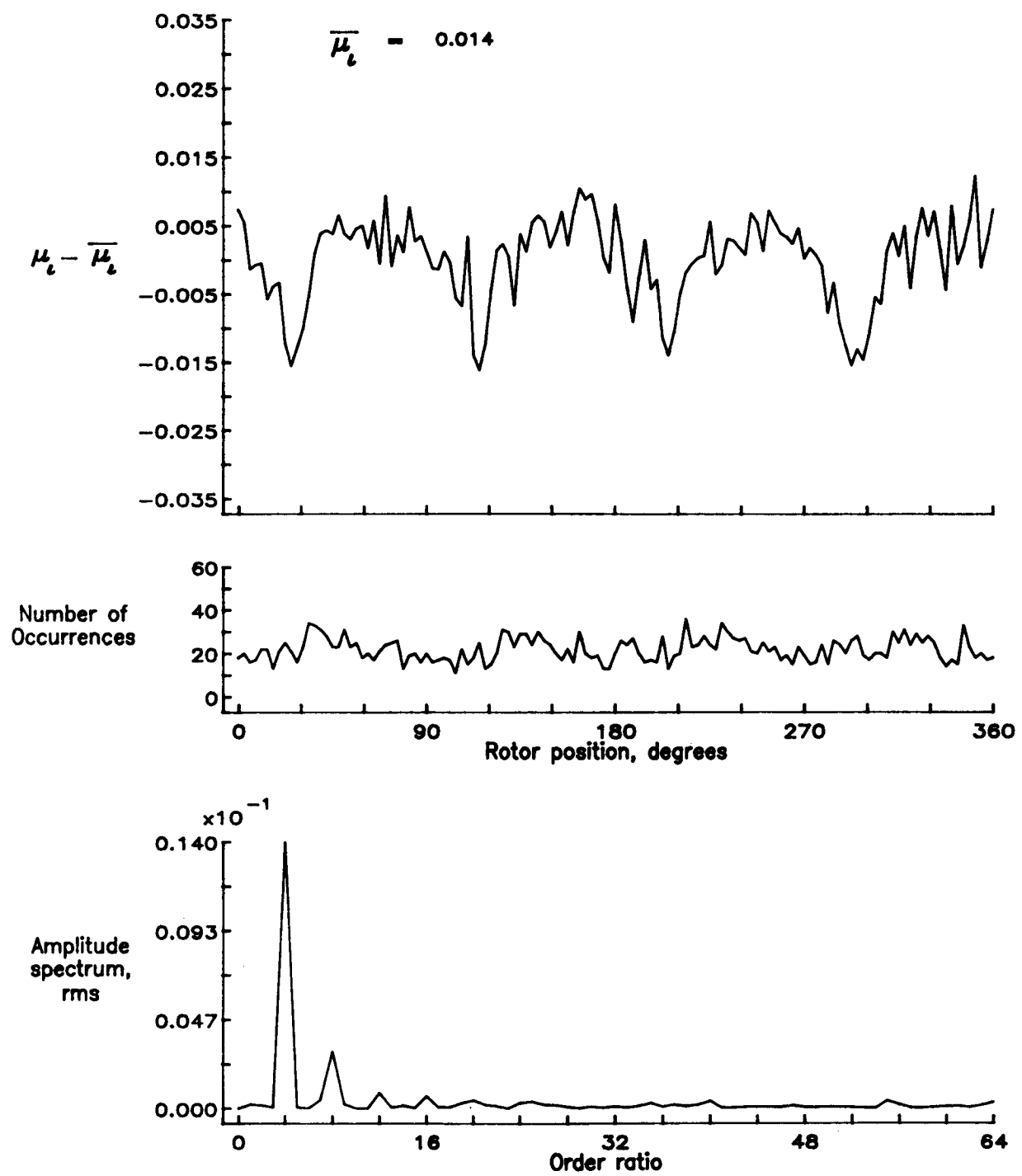


Figure 108.— Induced inflow velocity measured at 210 degrees and r/R of 0.86.

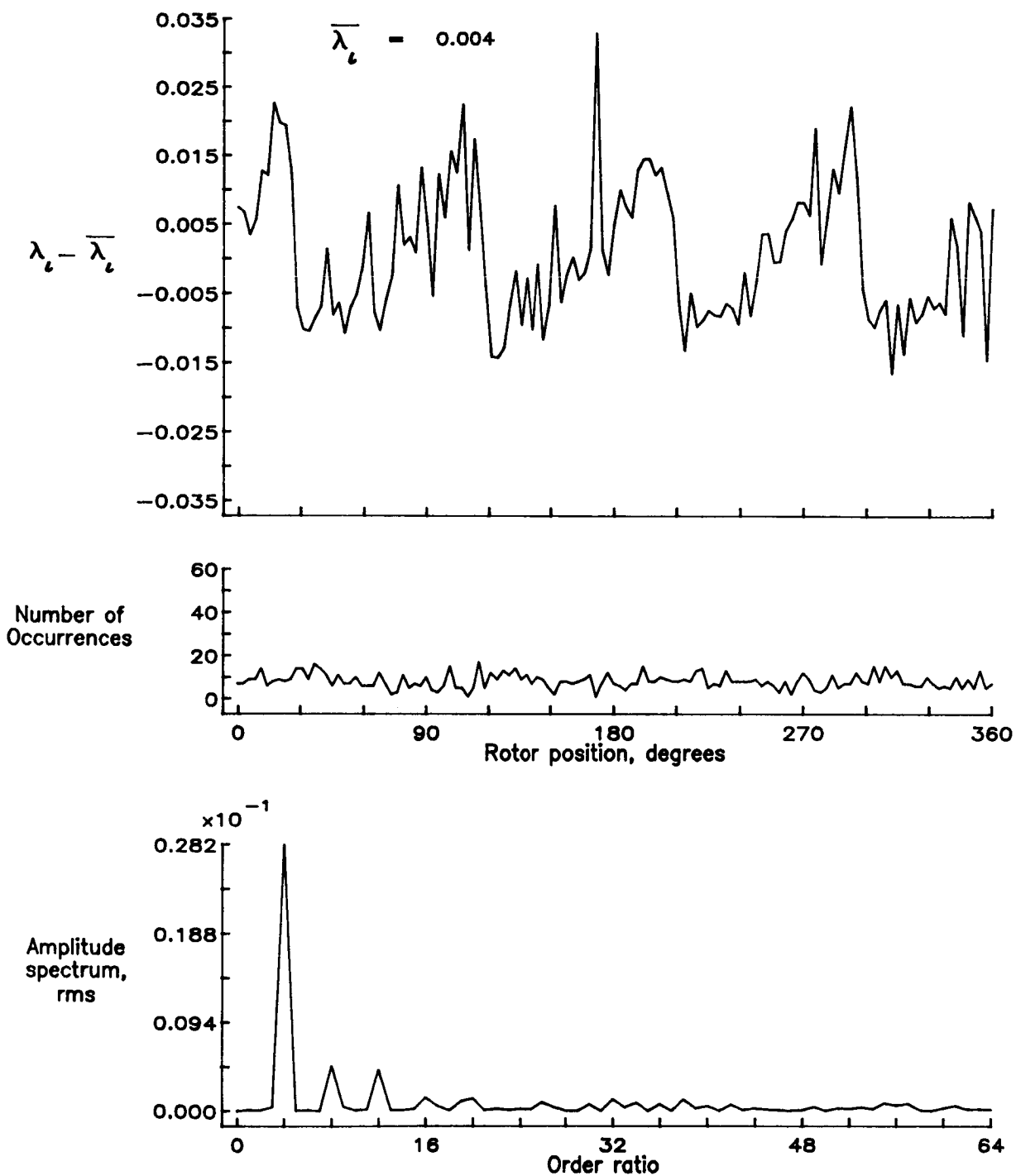


Figure 108.— Concluded.

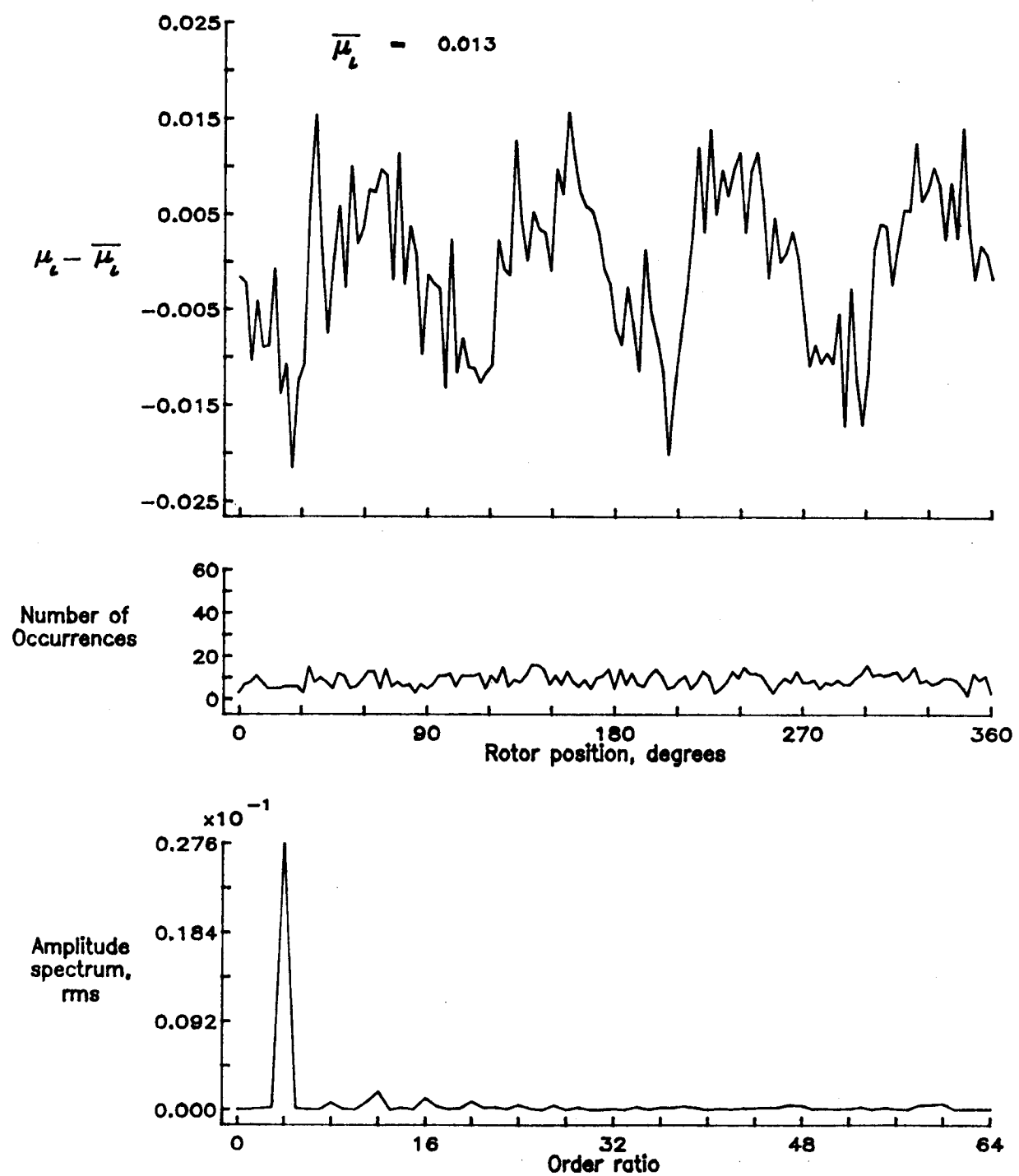


Figure 109.— Induced inflow velocity measured at 210 degrees and r/R of 0.90.

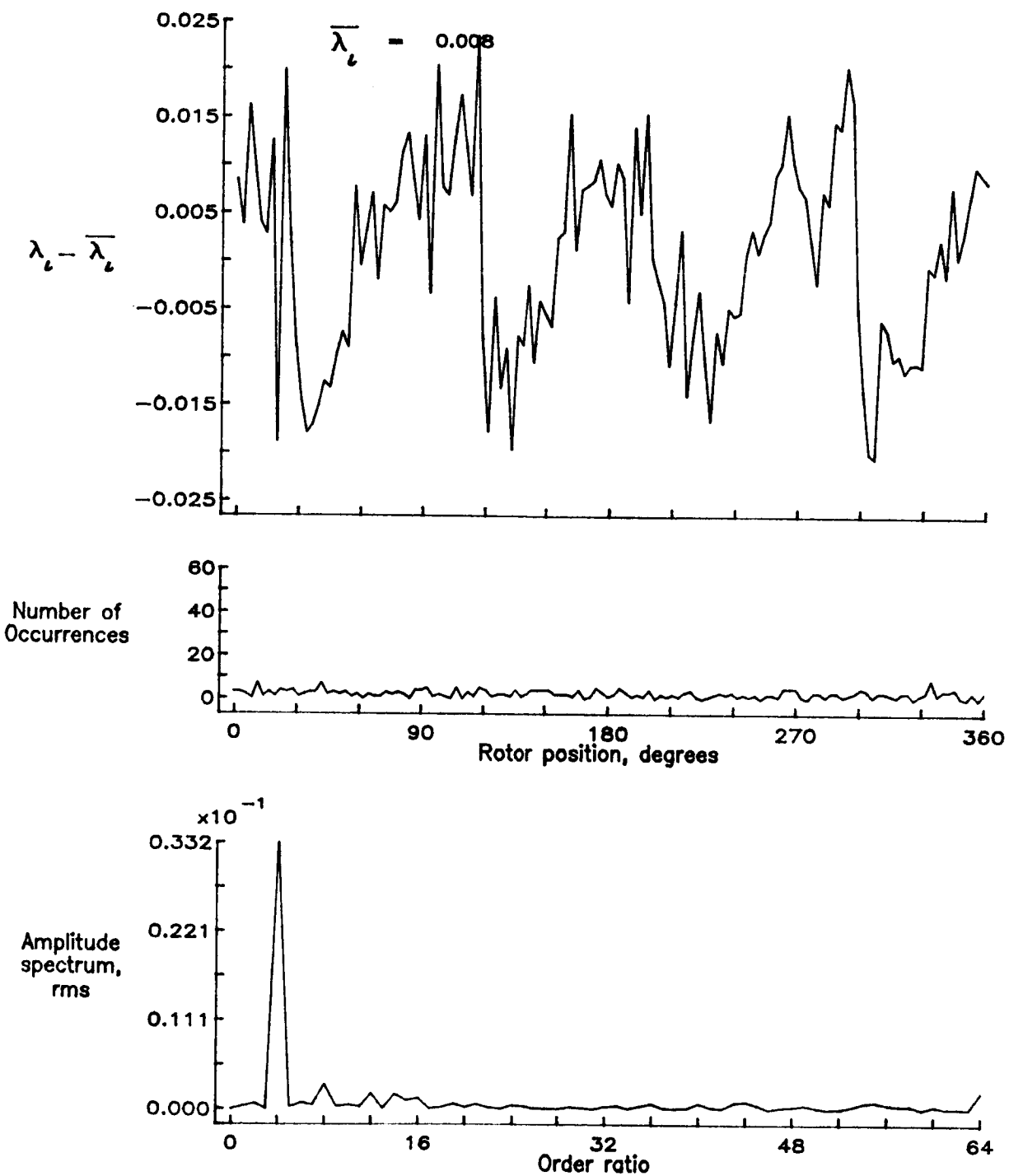


Figure 109.— Concluded.

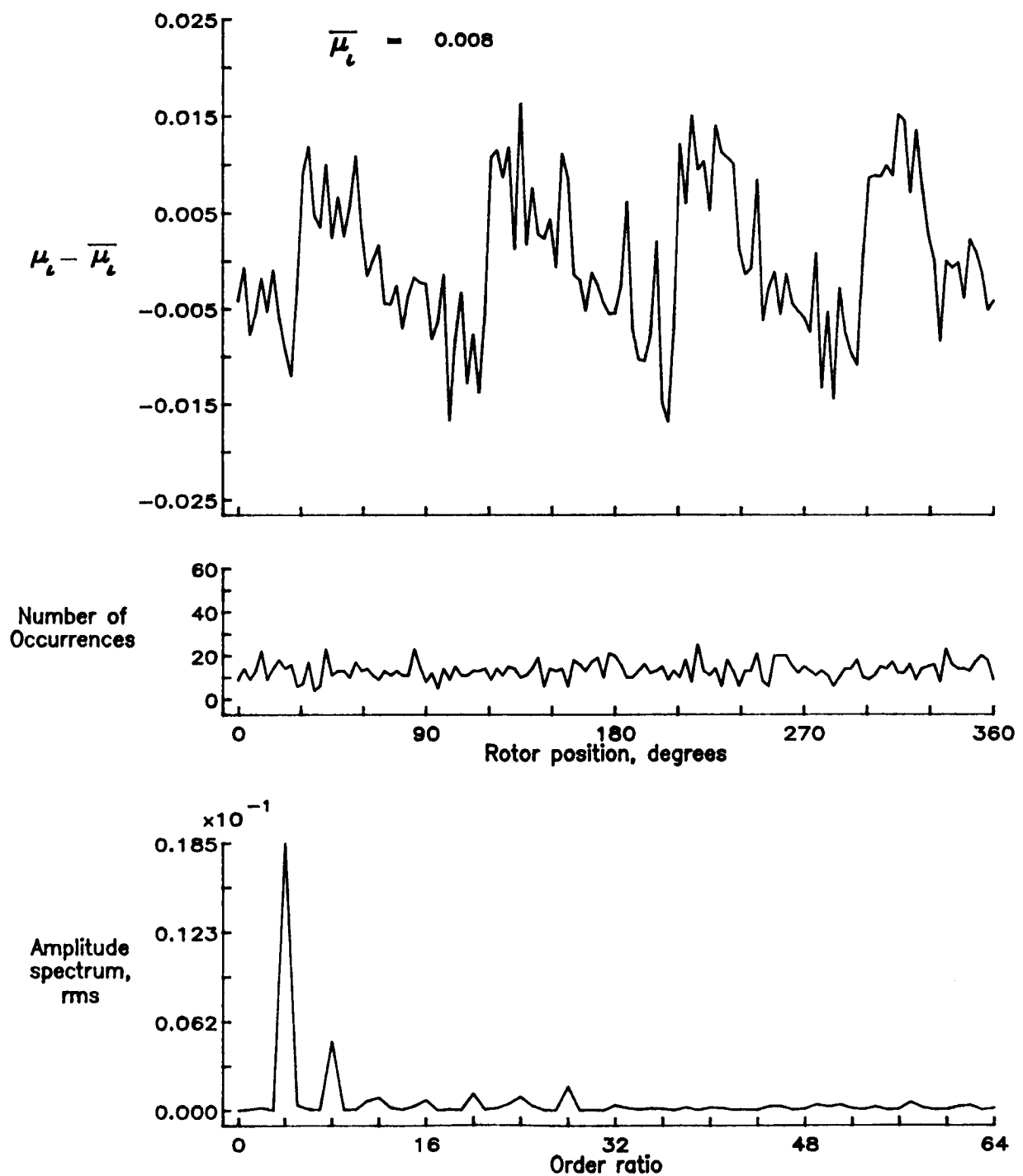


Figure 110.— Induced inflow velocity measured at 210 degrees and r/R of 0.94.

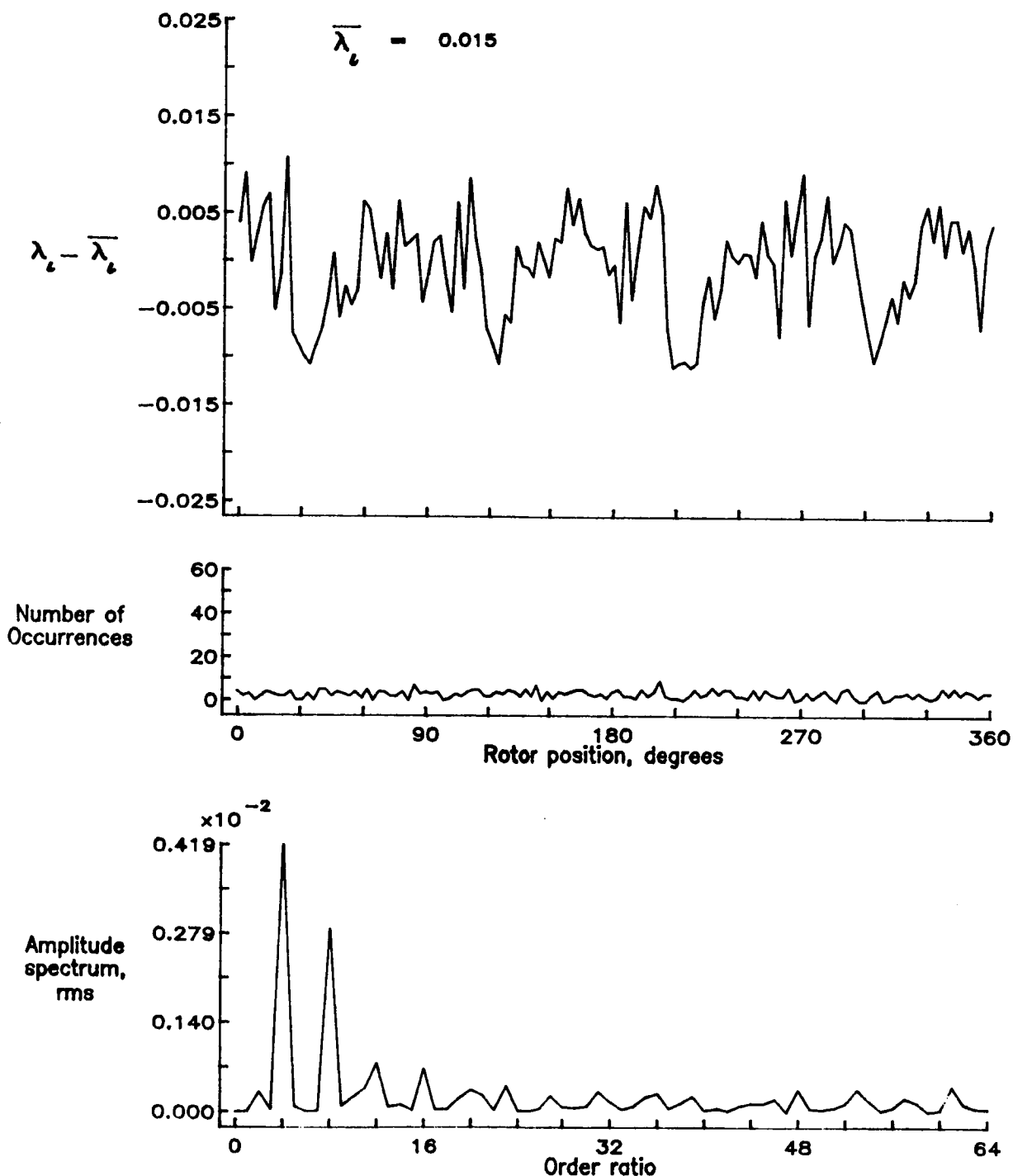


Figure 110.— Concluded.

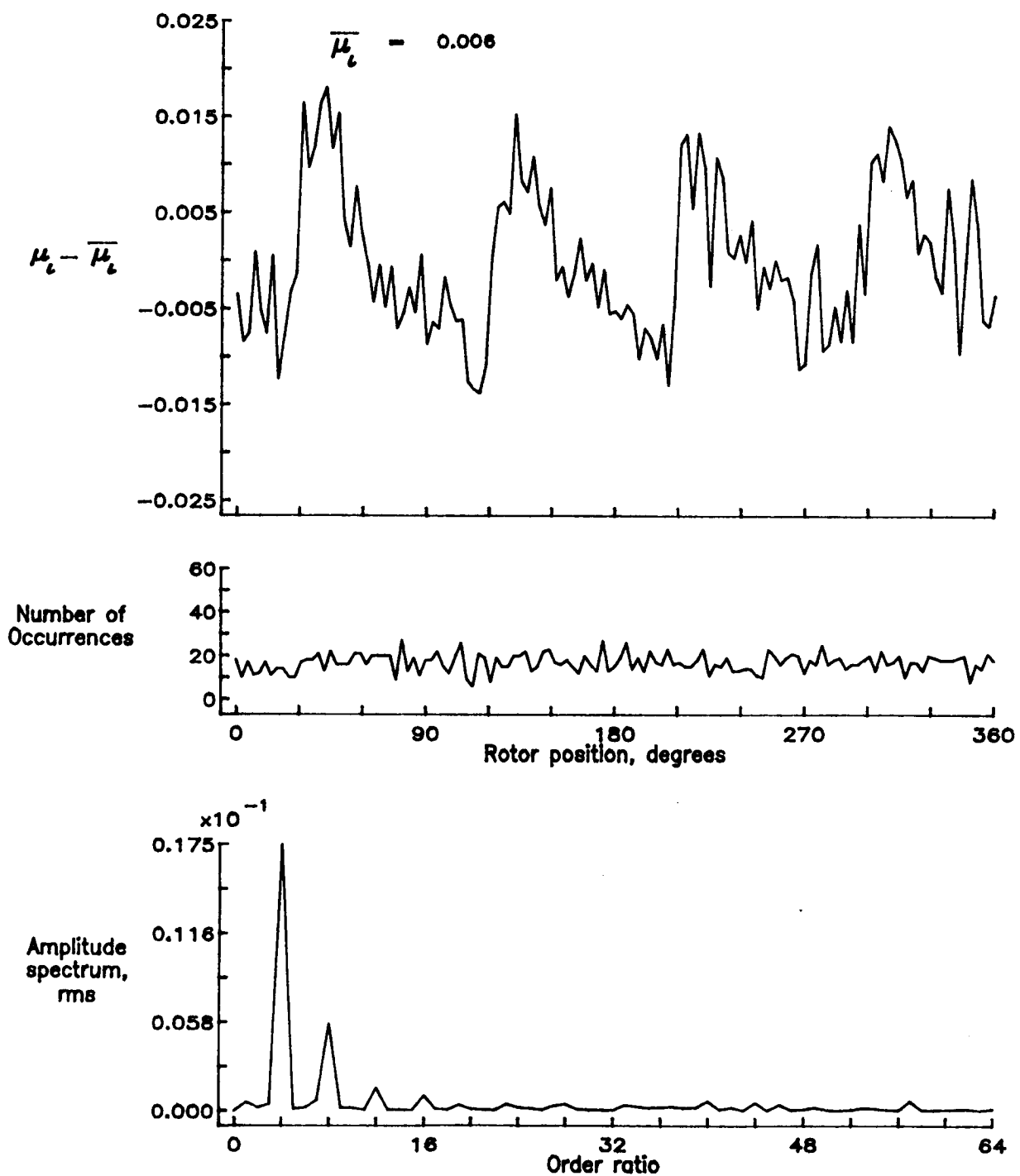


Figure 111.— Induced inflow velocity measured at 210 degrees and r/R of 0.98.

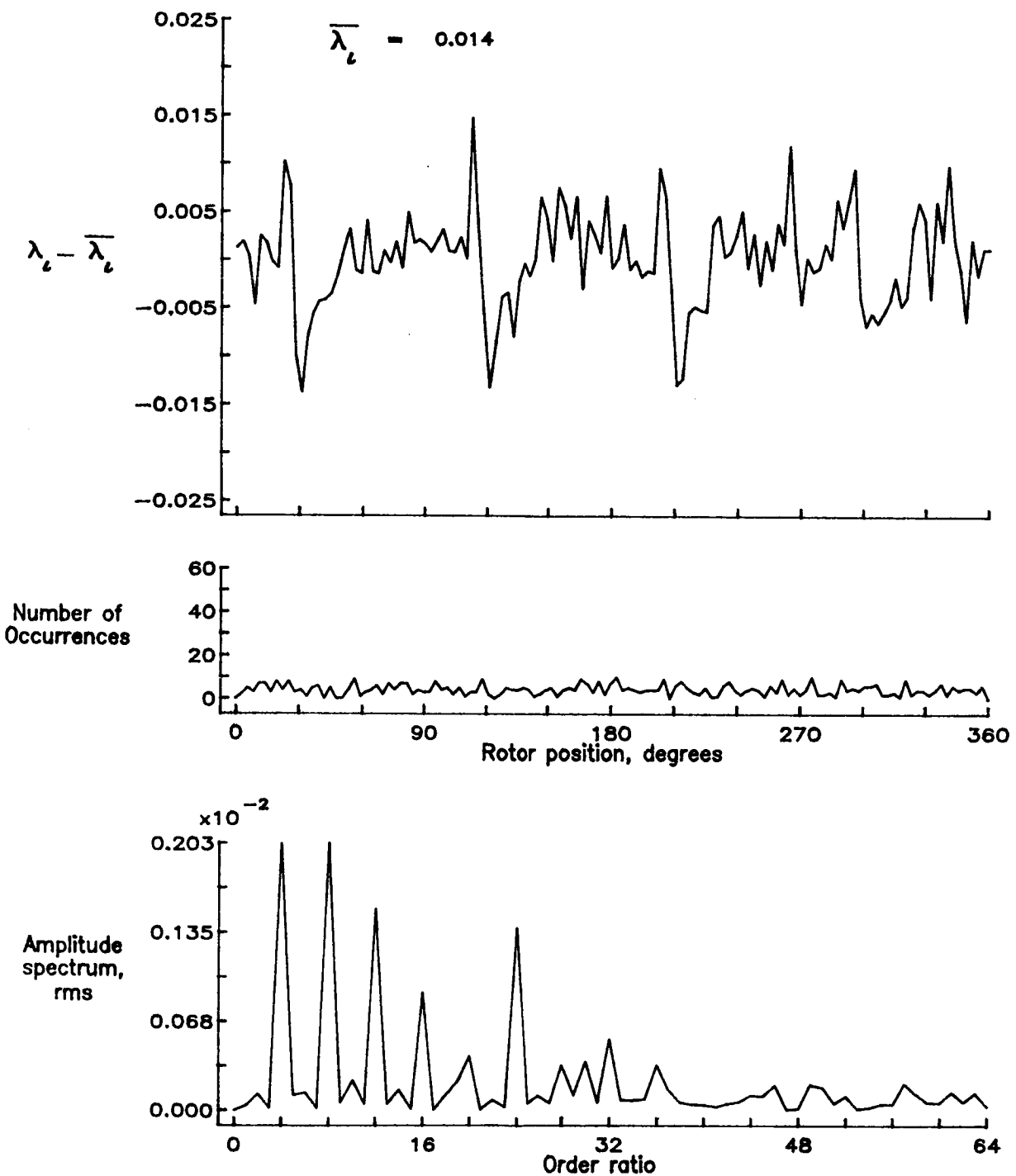


Figure 111.— Concluded.

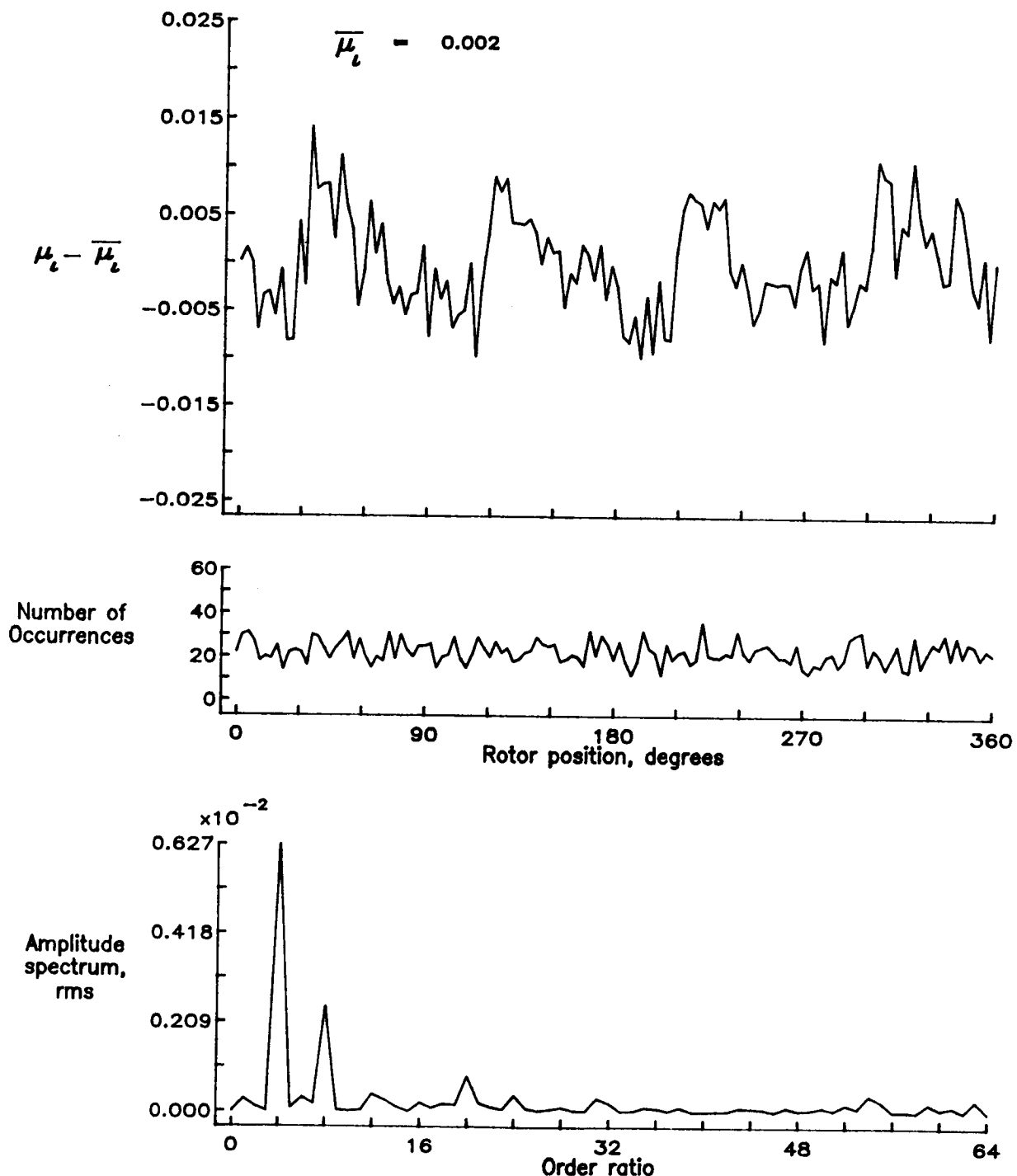


Figure 112.— Induced inflow velocity measured at 210 degrees and  $r/R$  of 1.02.

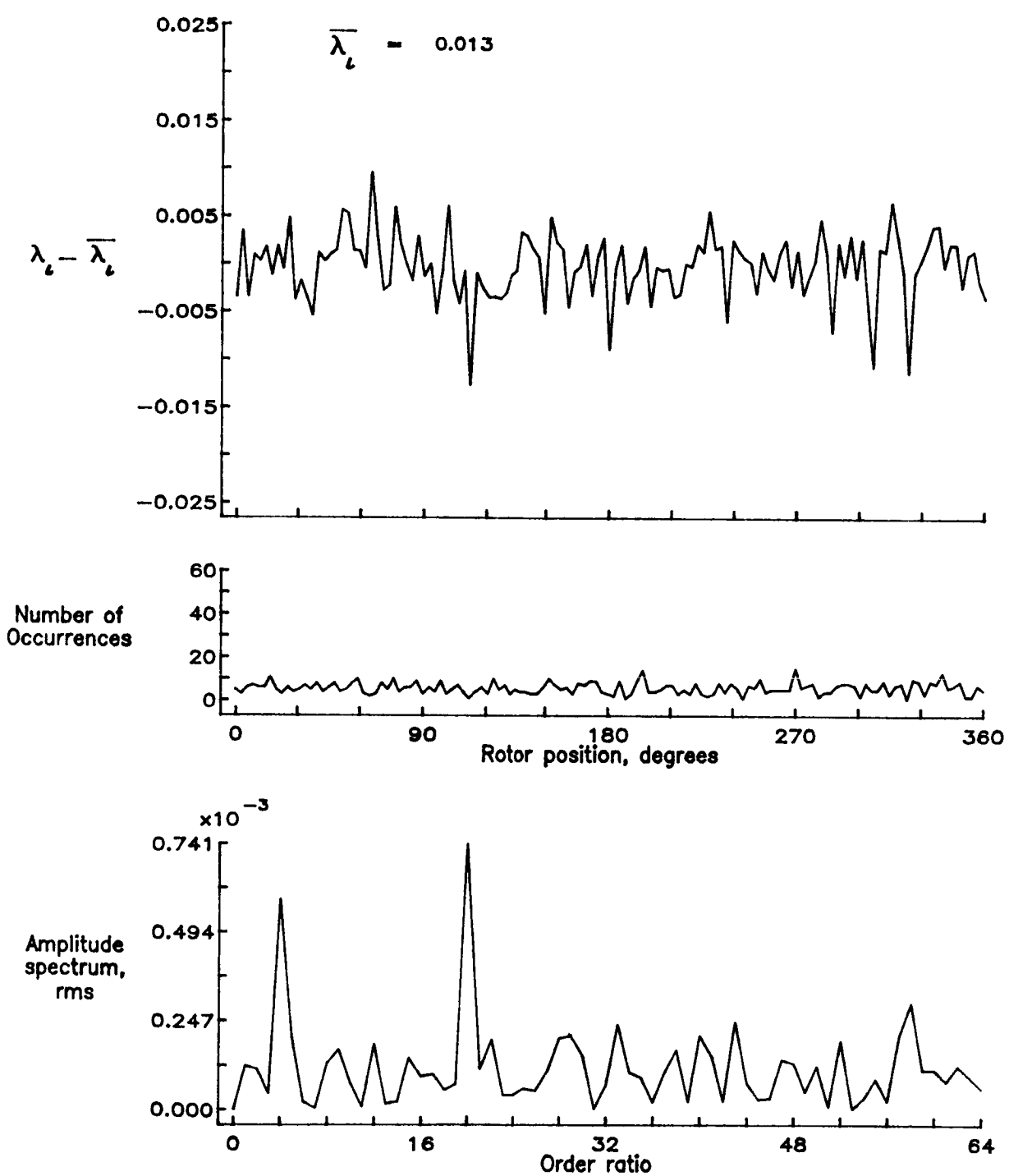


Figure 112.— Concluded.

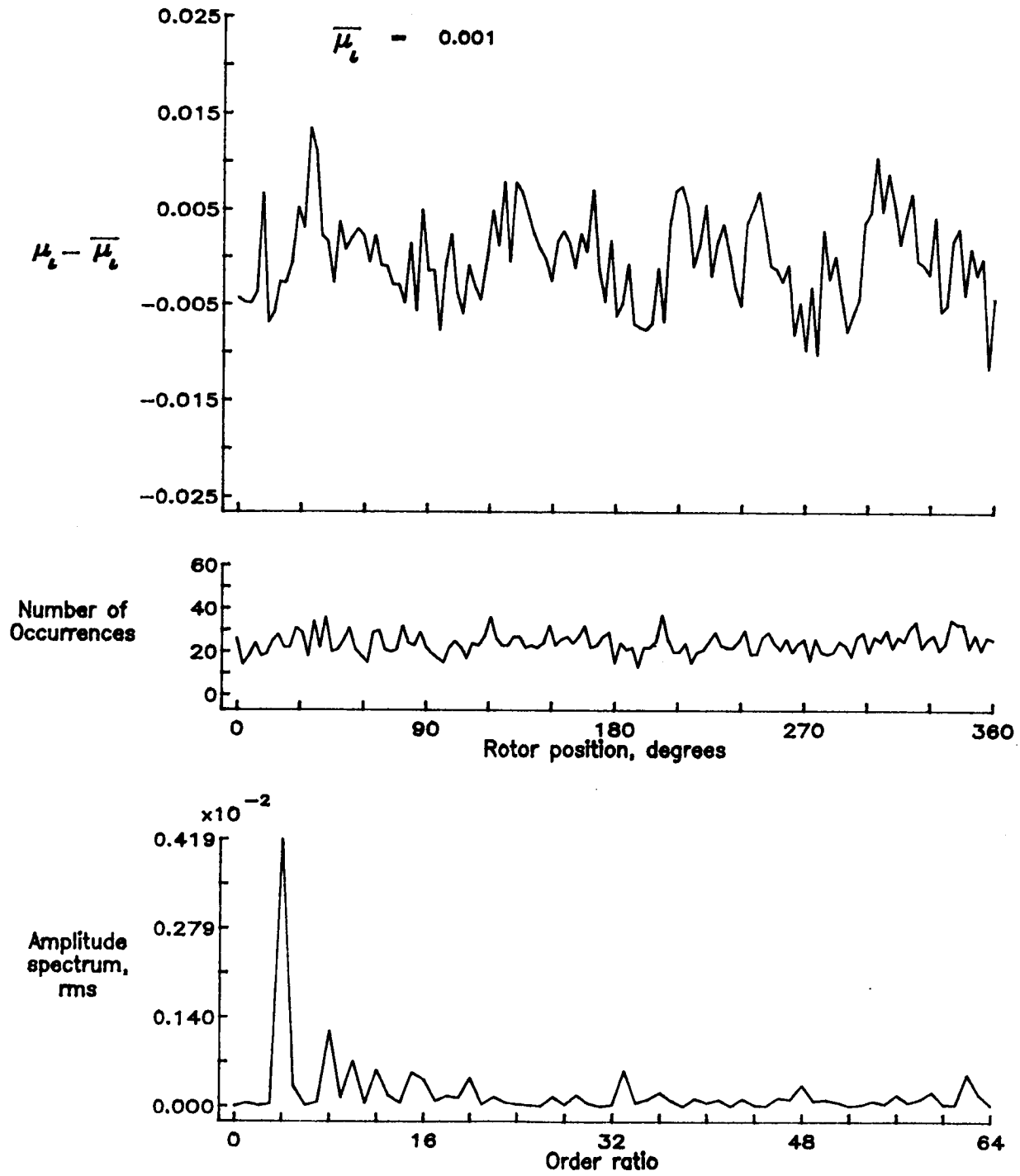


Figure 113.— Induced inflow velocity measured at 210 degrees and r/R of 1.04.

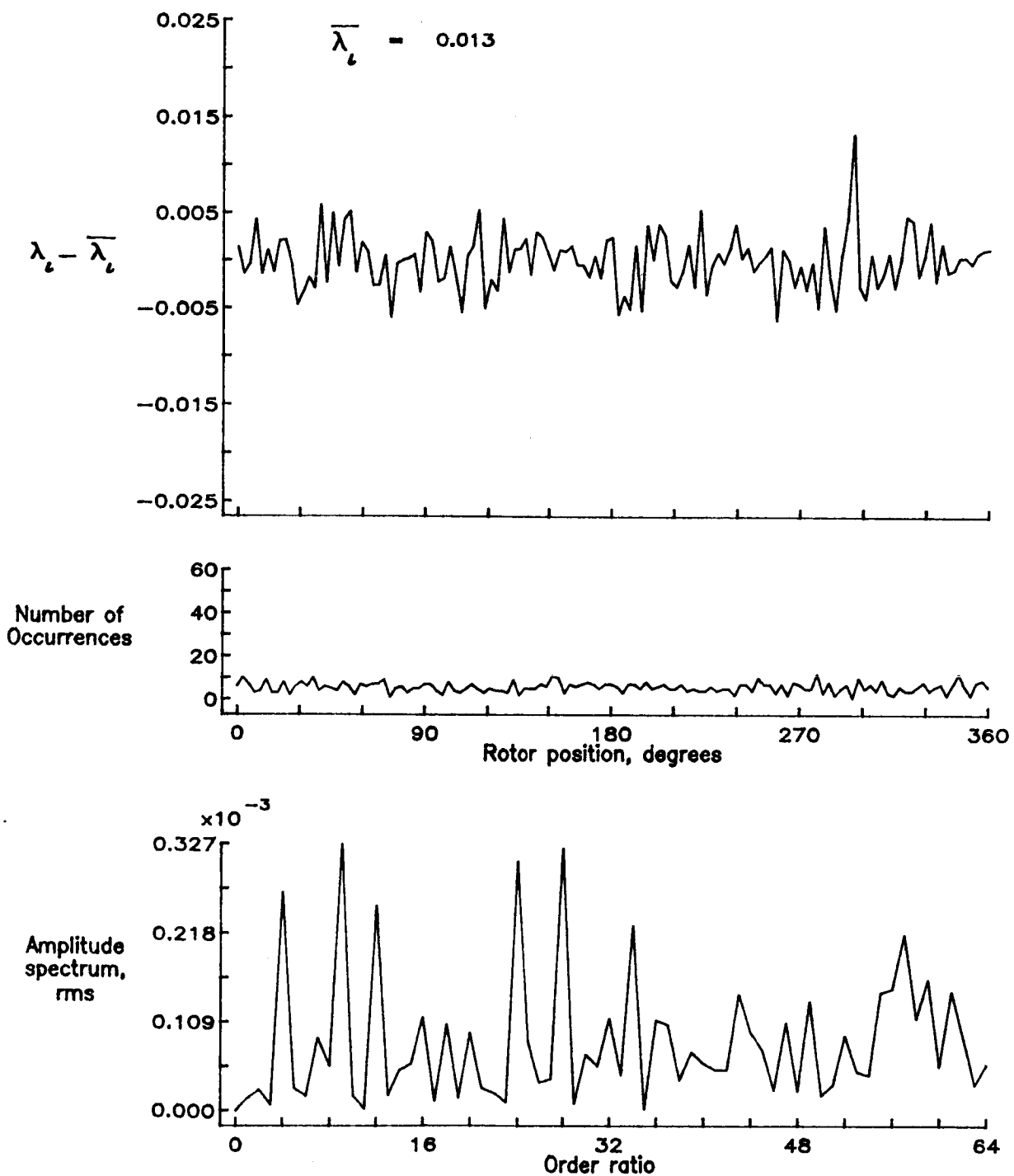


Figure 113.— Concluded.

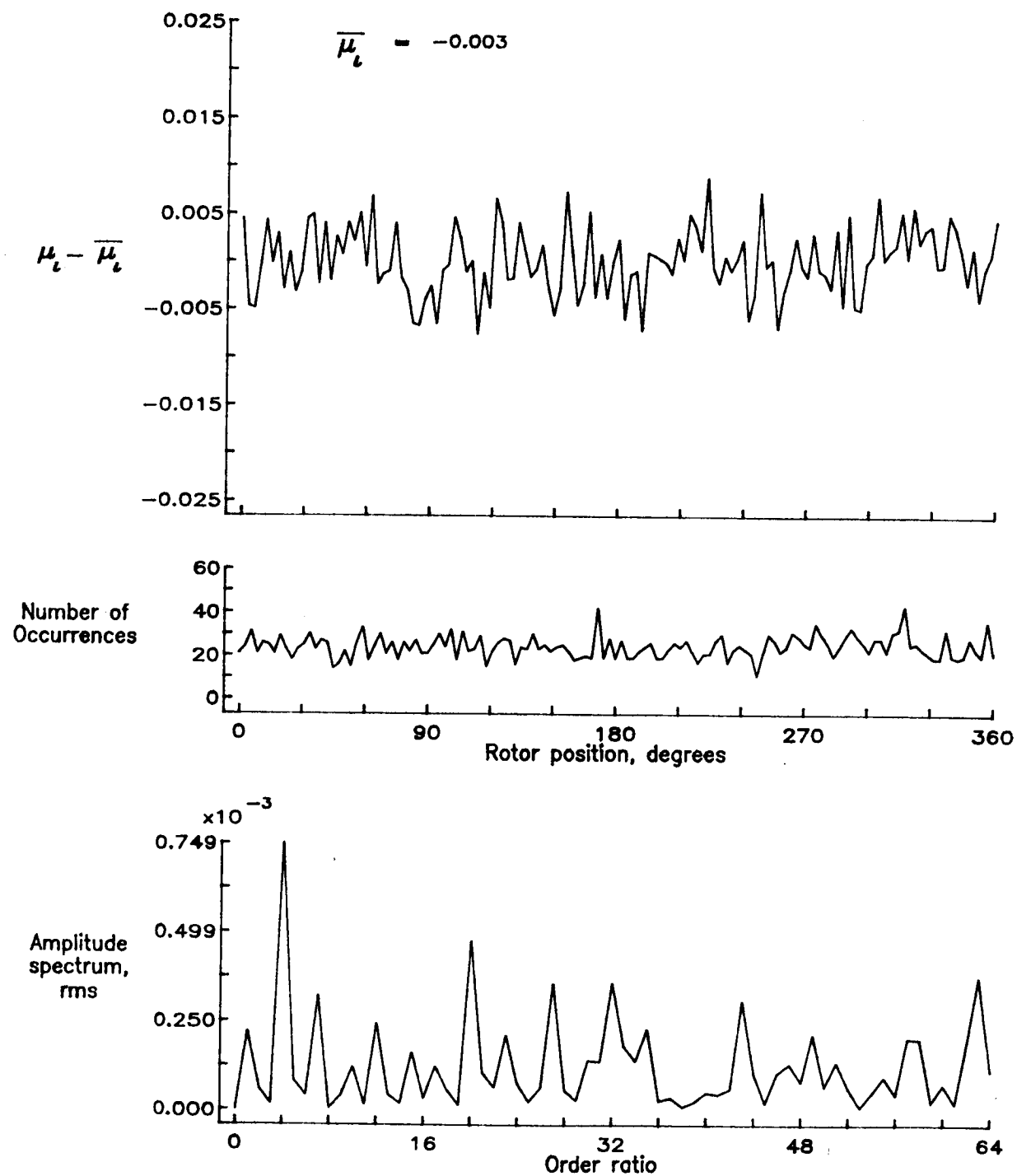


Figure 114.— Induced inflow velocity measured at 210 degrees and  $r/R$  of 1.10.

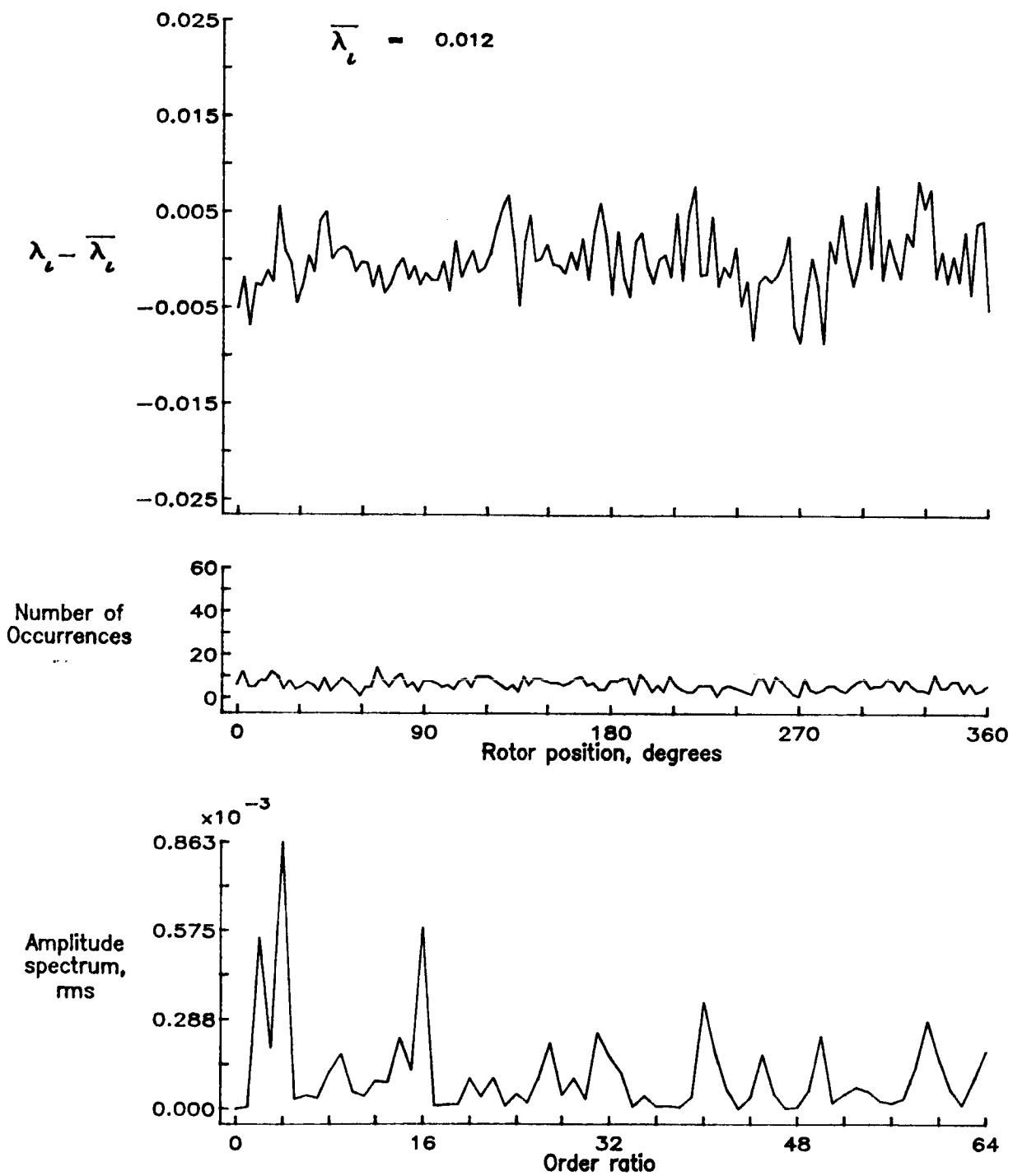


Figure 114.— Concluded.

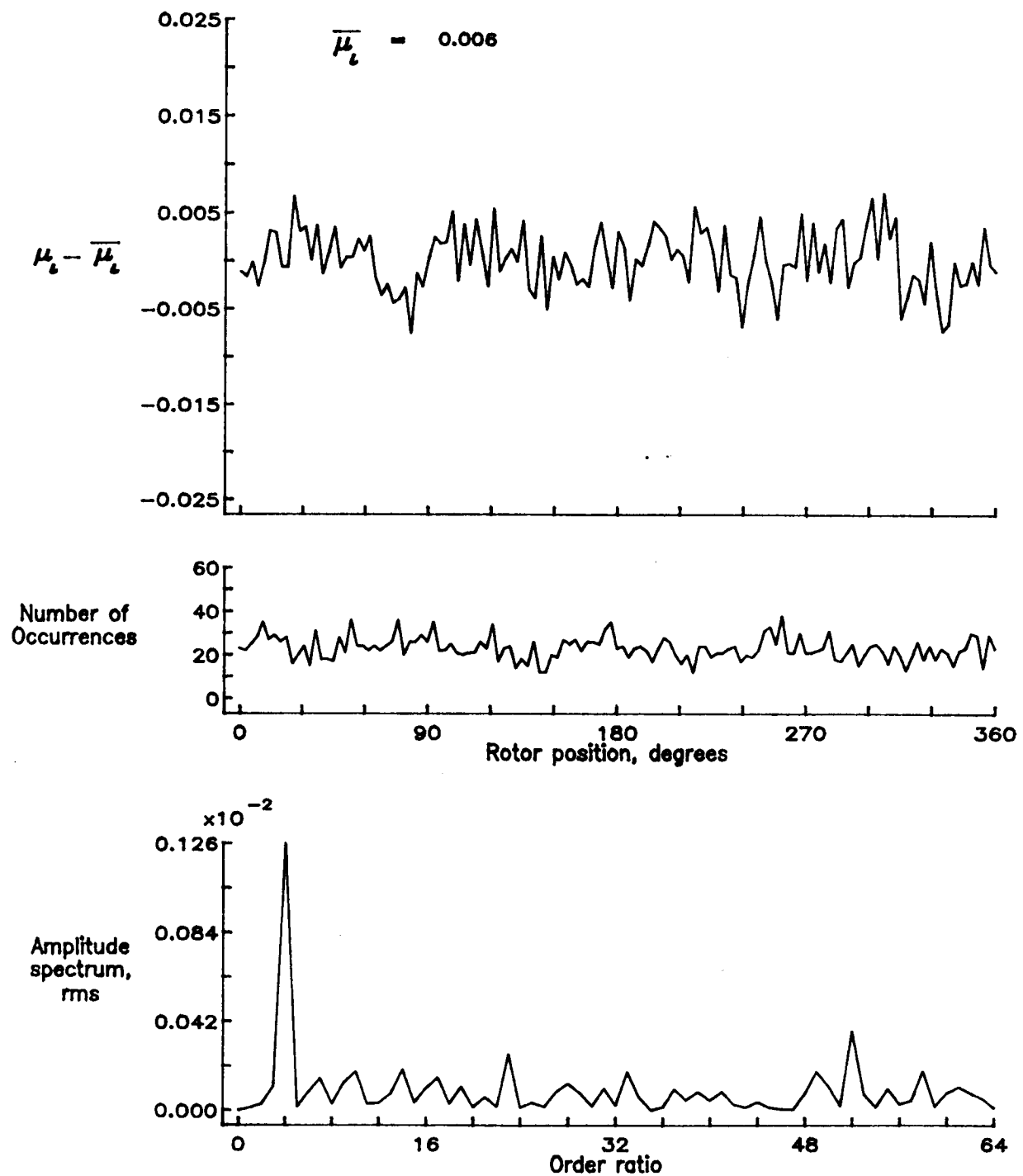


Figure 115.— Induced inflow velocity measured at 240 degrees and  $r/R$  of 0.20.

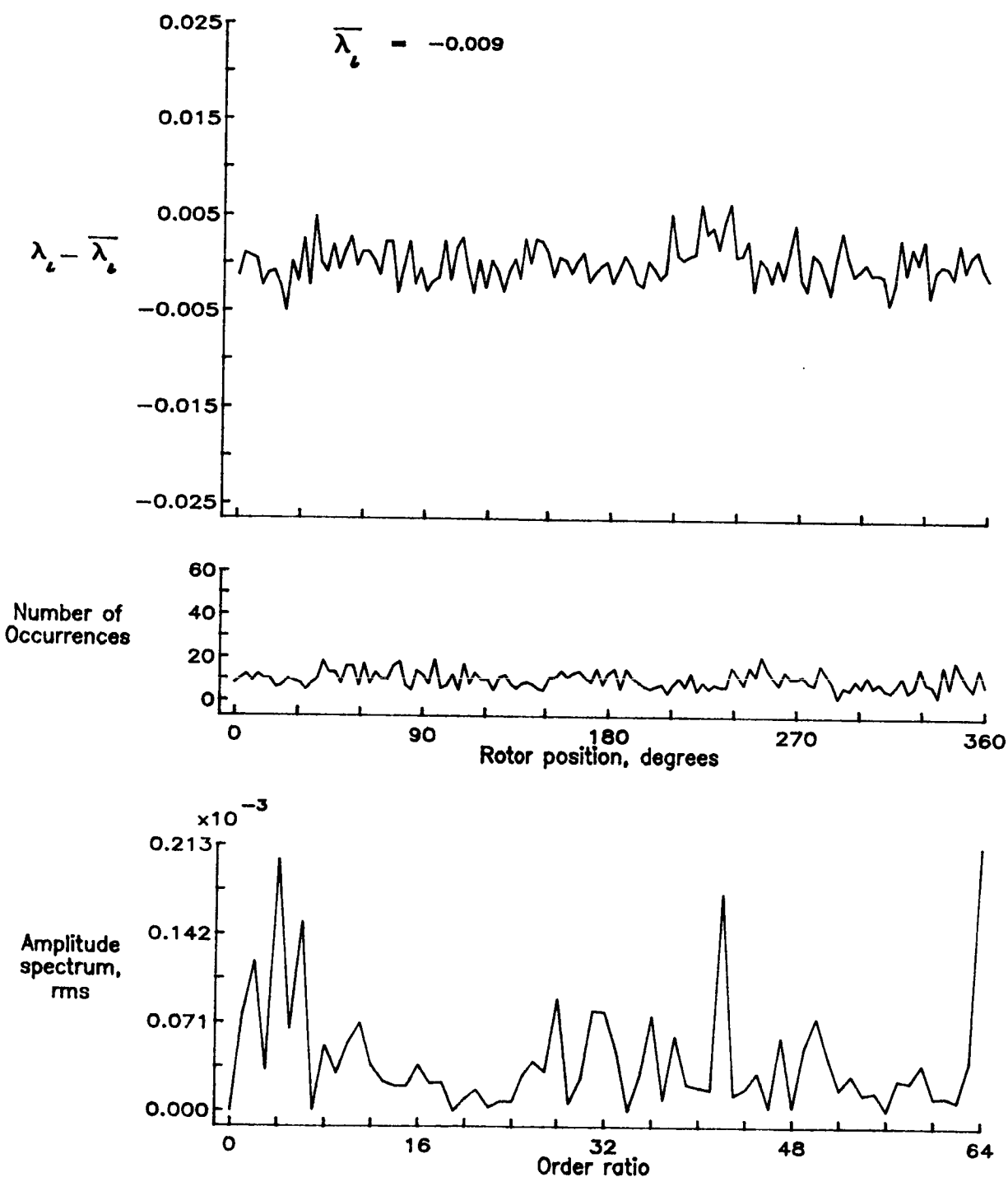


Figure 115.— Concluded.

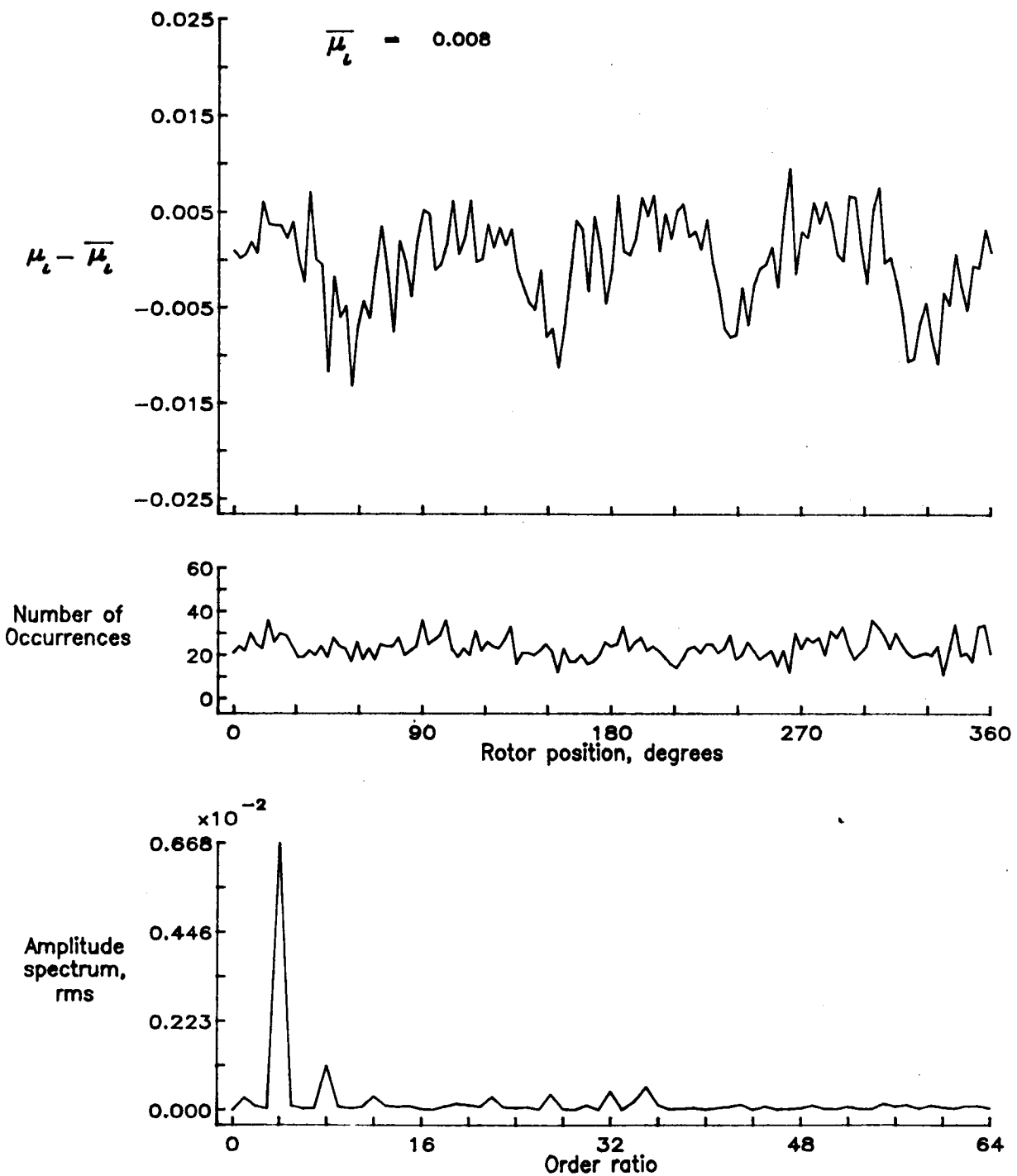


Figure 116.— Induced inflow velocity measured at 240 degrees and r/R of 0.40.

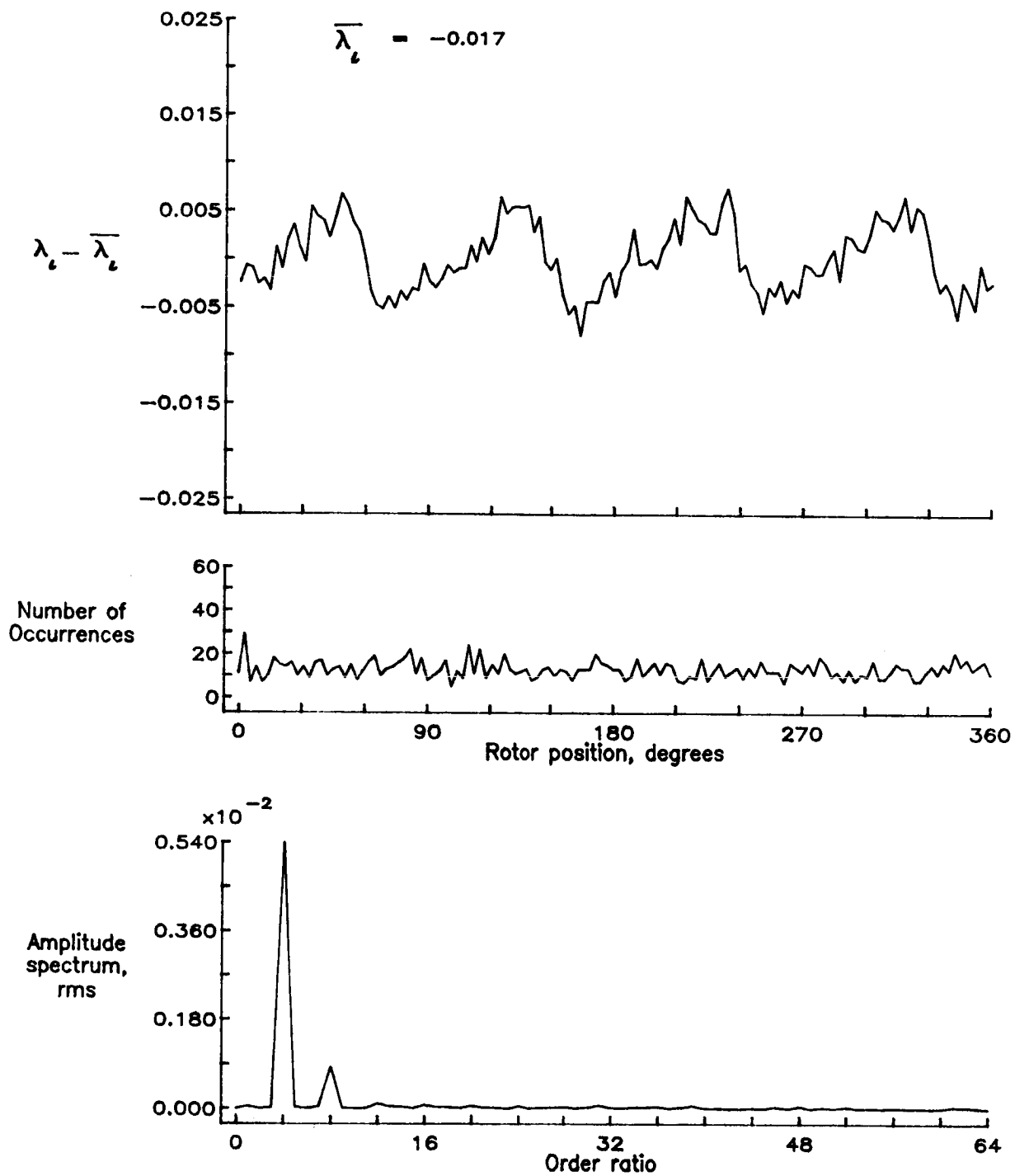


Figure 116.— Concluded.

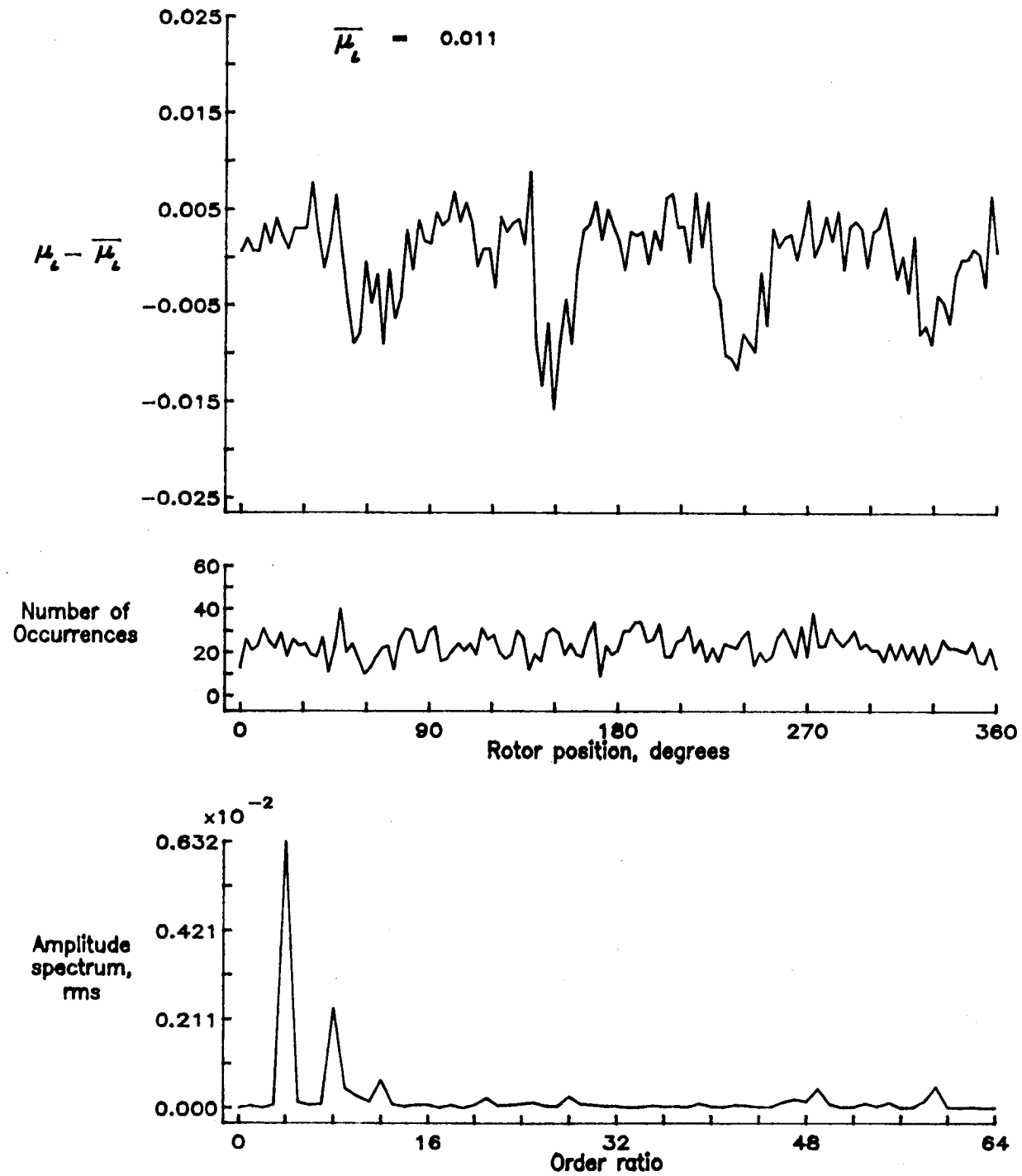


Figure 117.— Induced inflow velocity measured at 240 degrees and  $r/R$  of 0.50.

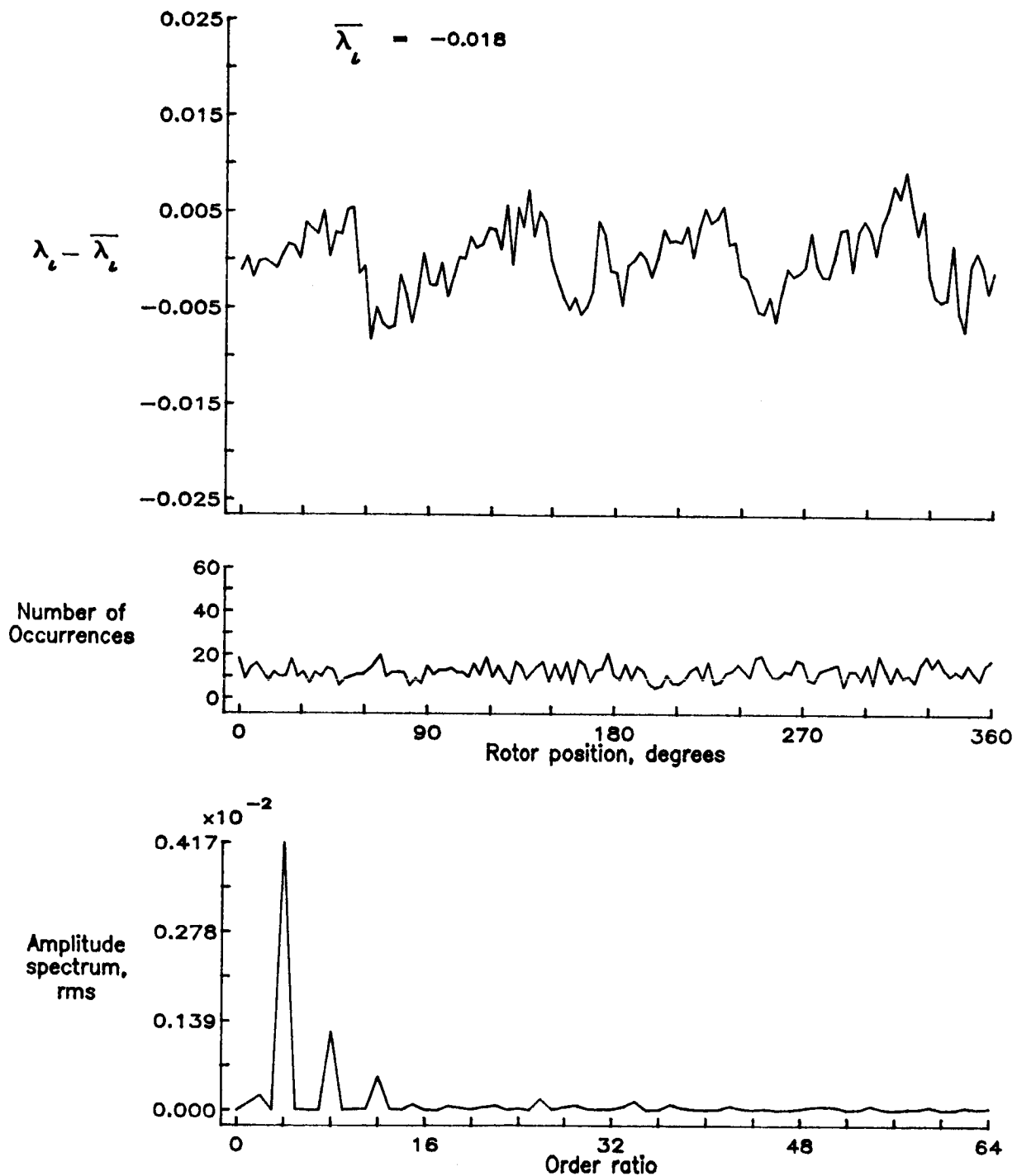


Figure 117.— Concluded.

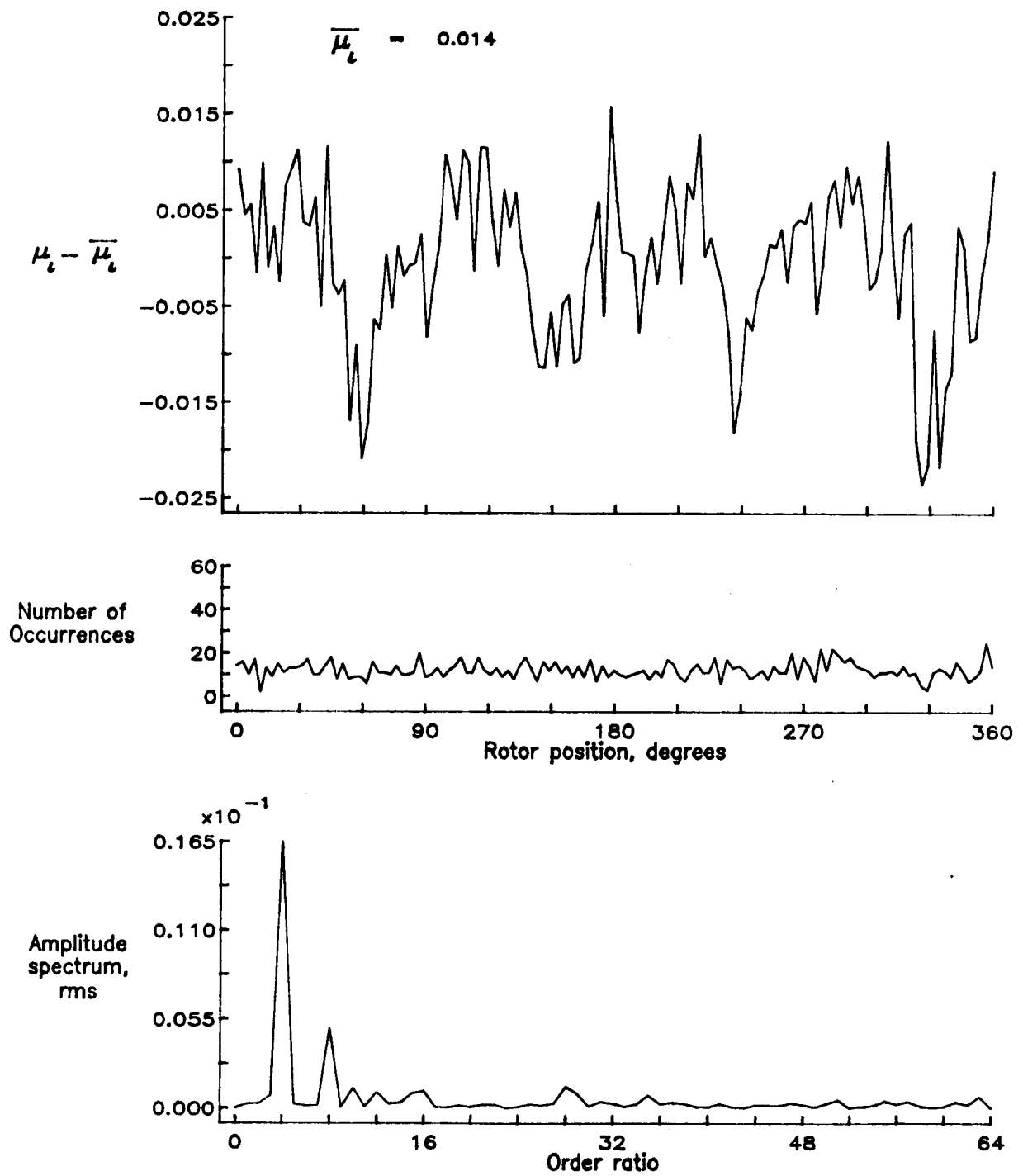


Figure 118.— Induced inflow velocity measured at 240 degrees and r/R of 0.60.

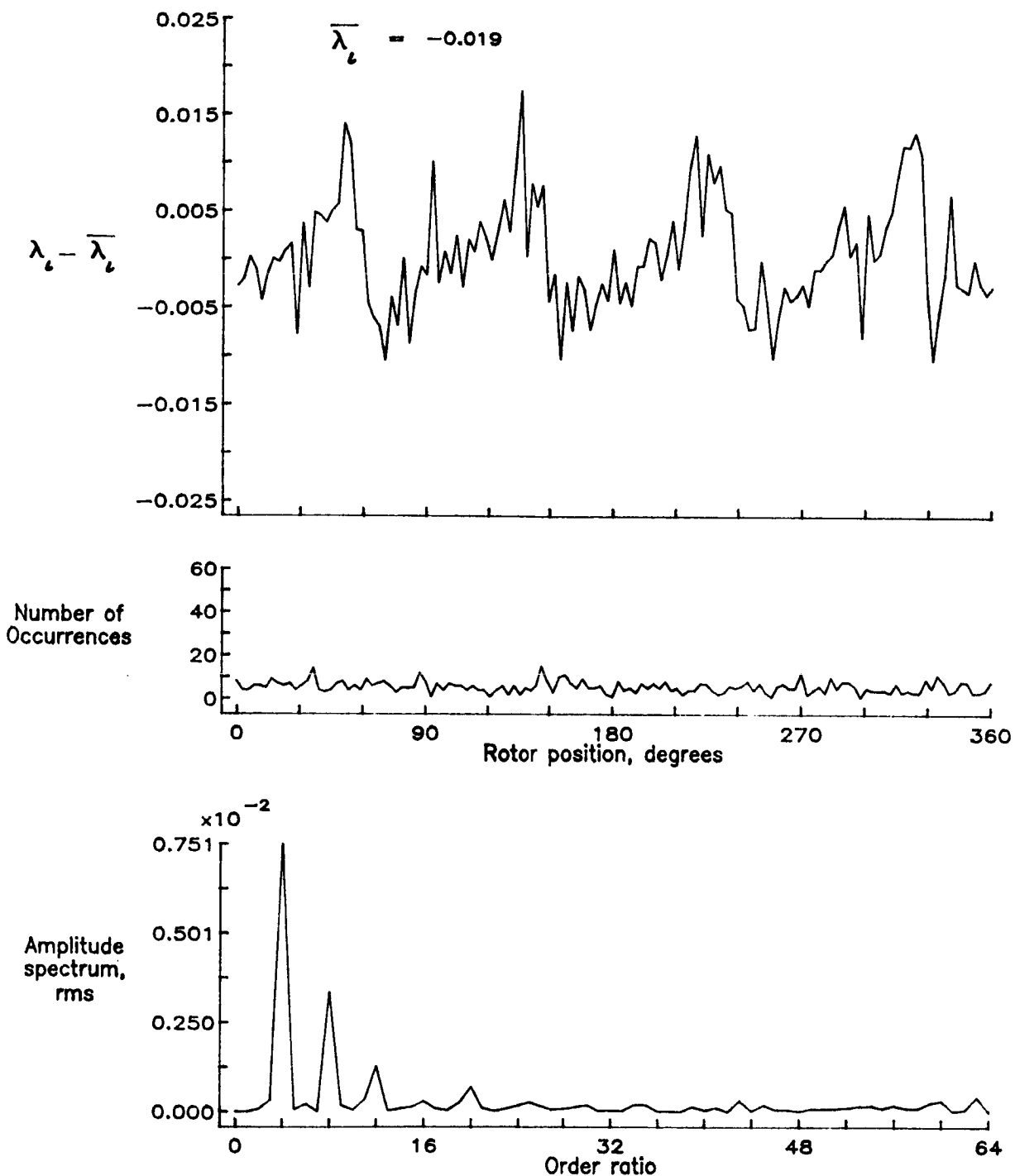


Figure 118.— Concluded.

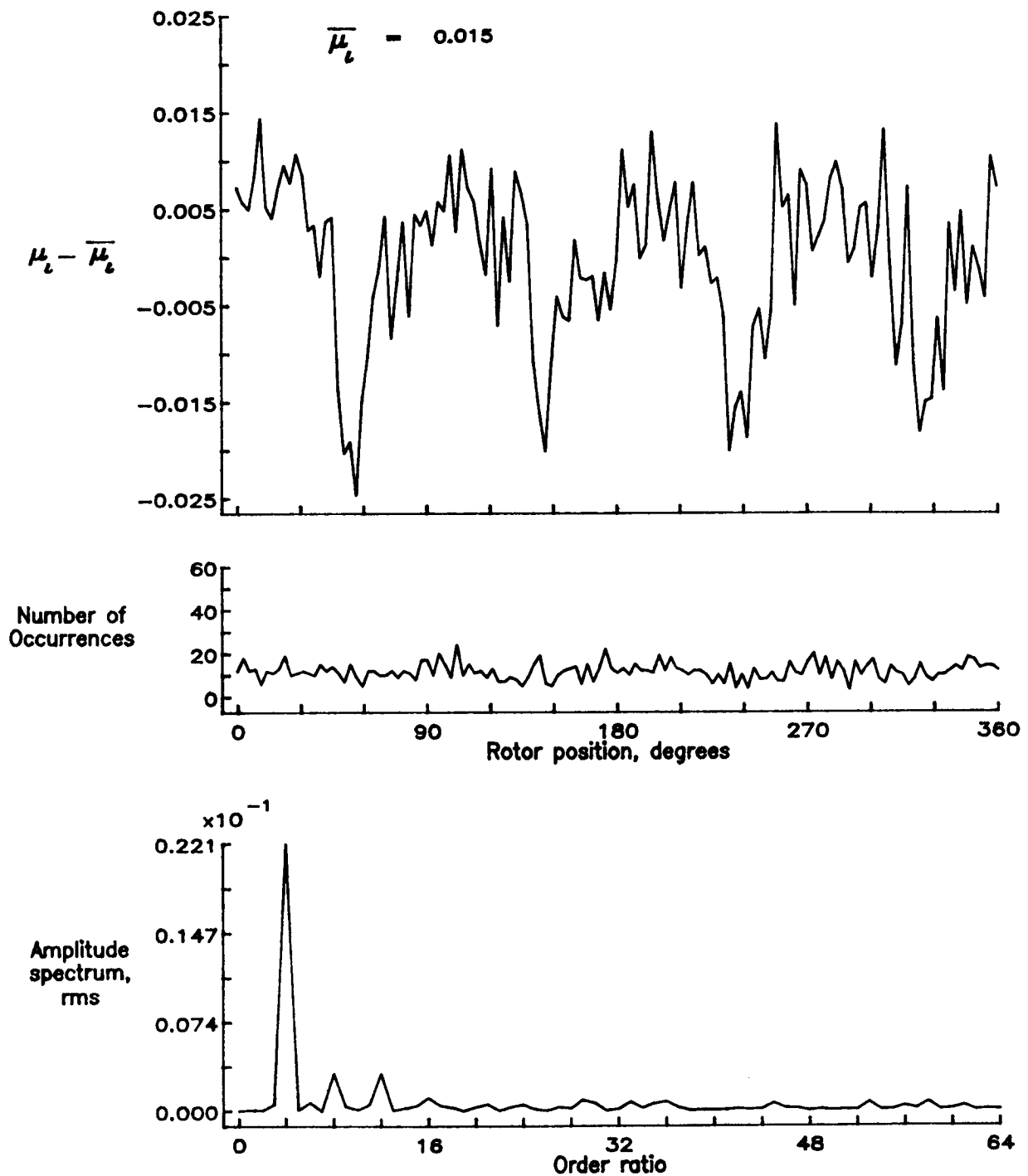


Figure 119.— Induced inflow velocity measured at 240 degrees and r/R of 0.70.

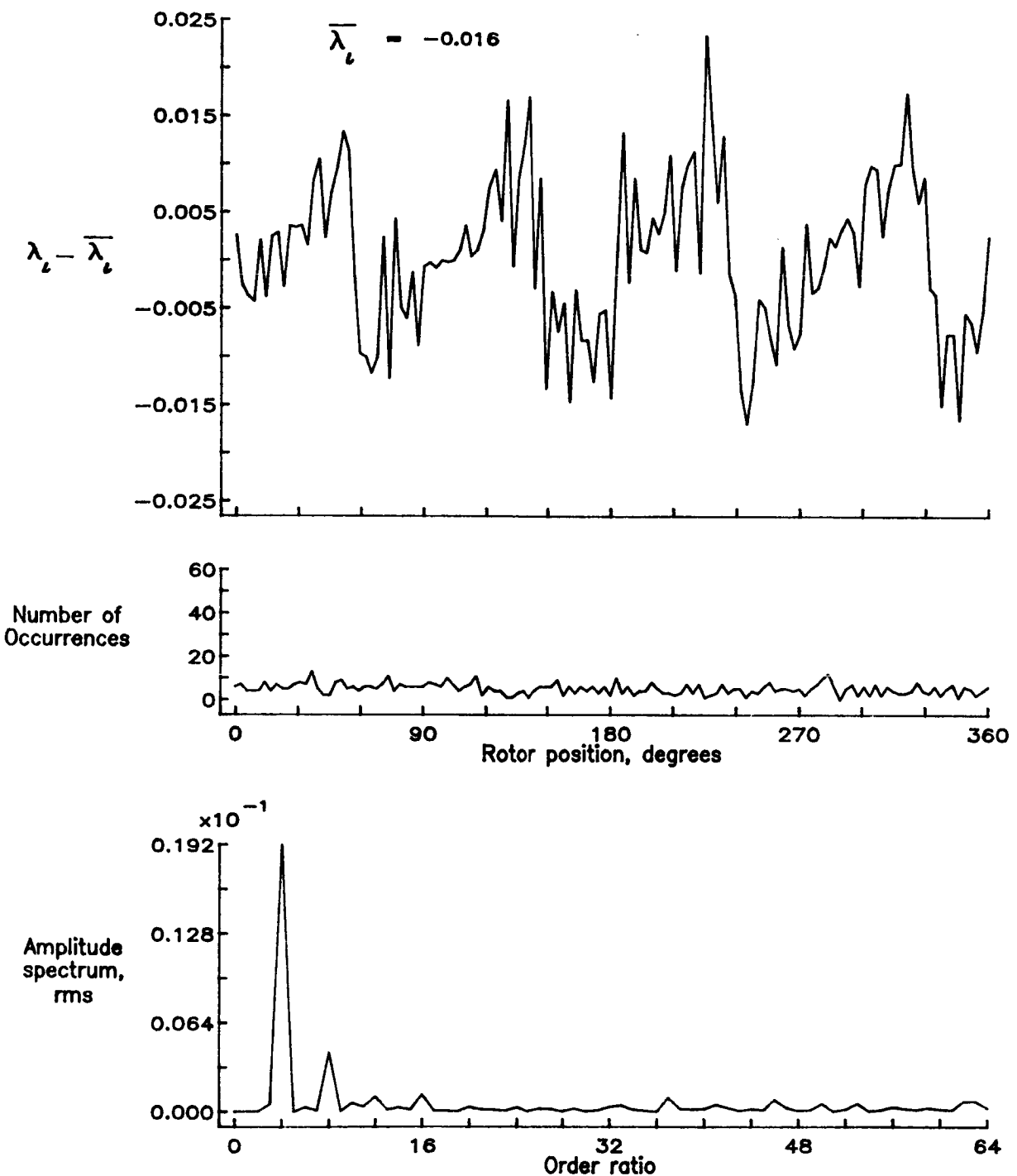


Figure 119.— Concluded.

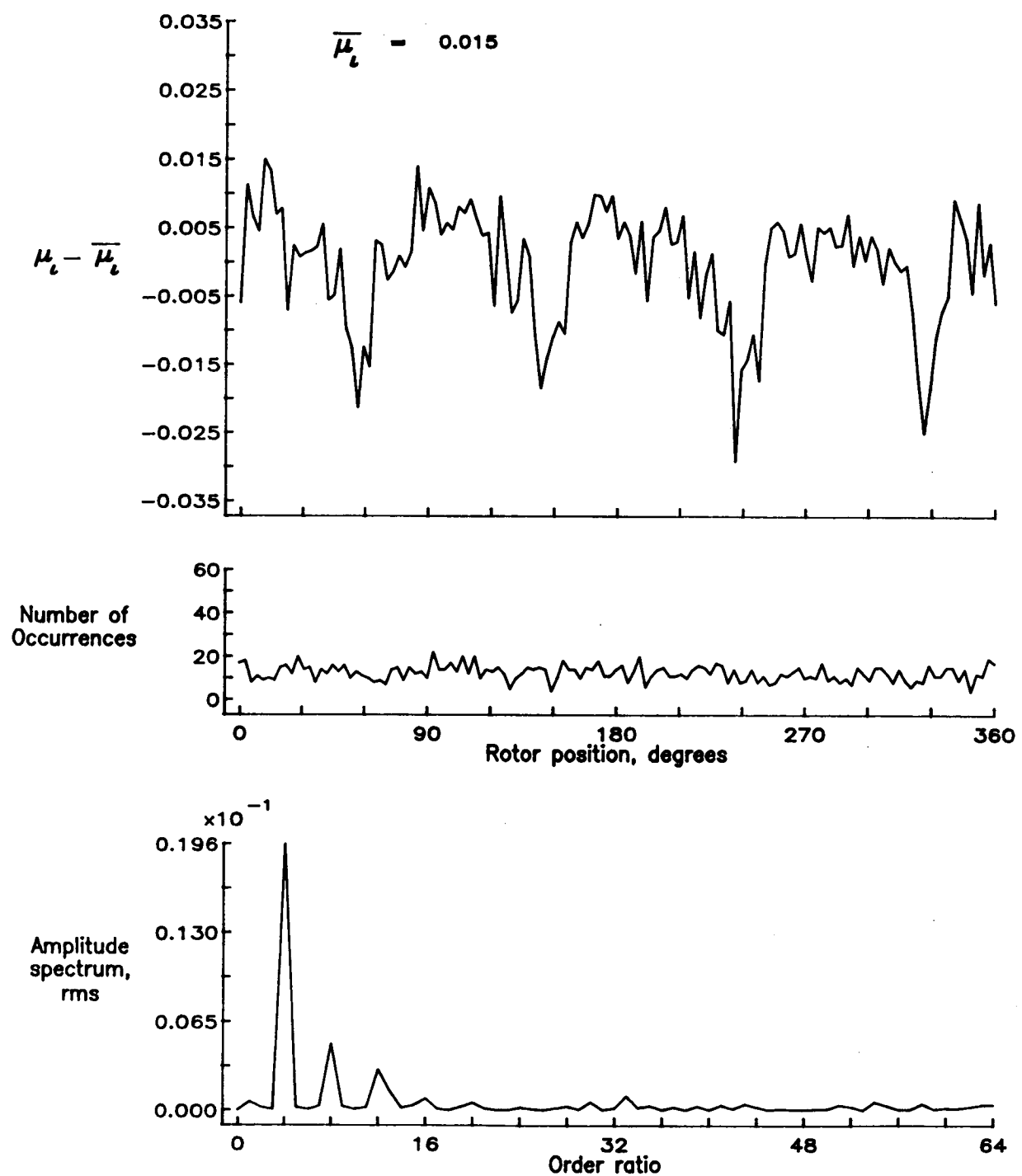


Figure 120.— Induced inflow velocity measured at 240 degrees and r/R of 0.74.

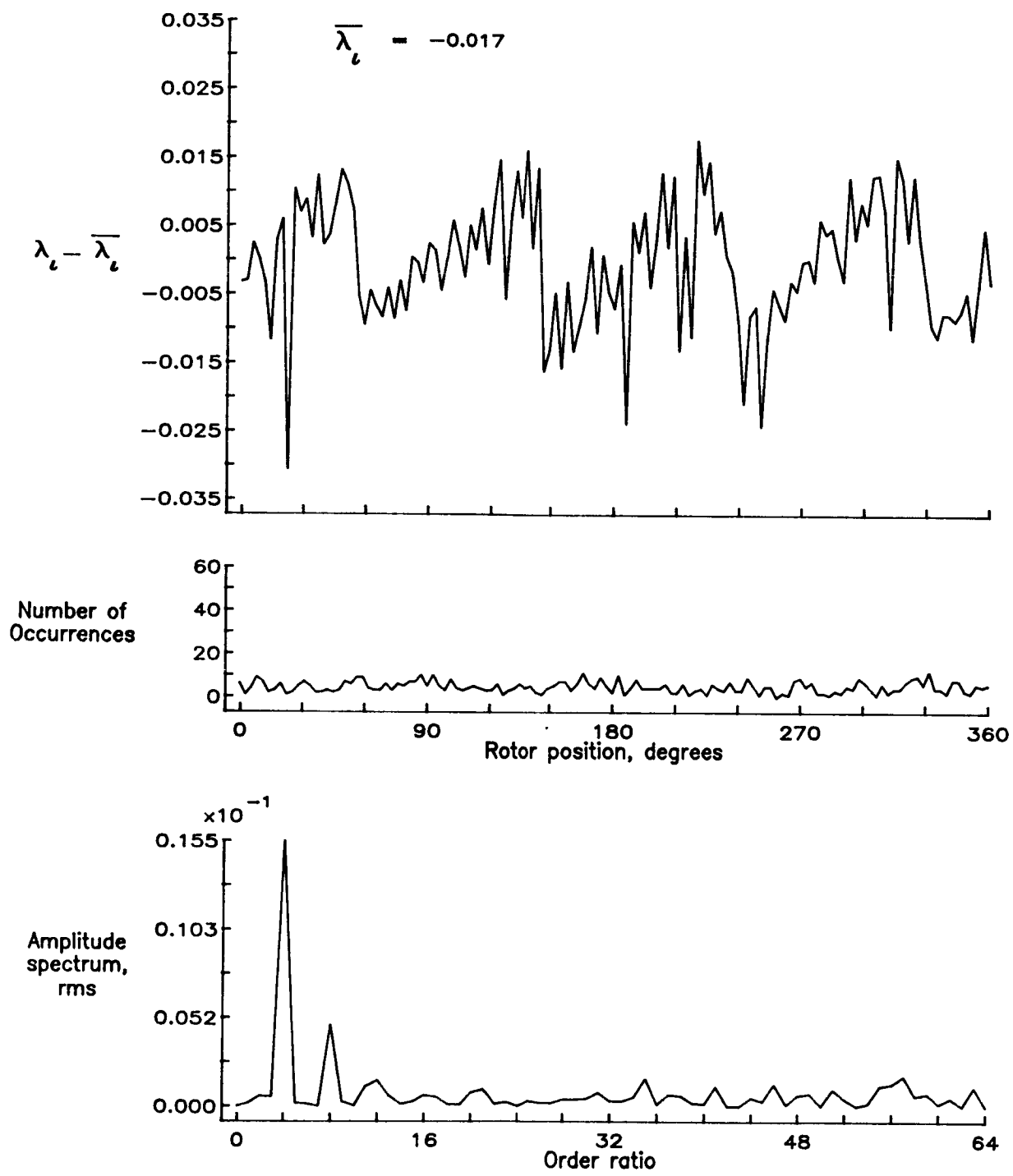


Figure 120.— Concluded.

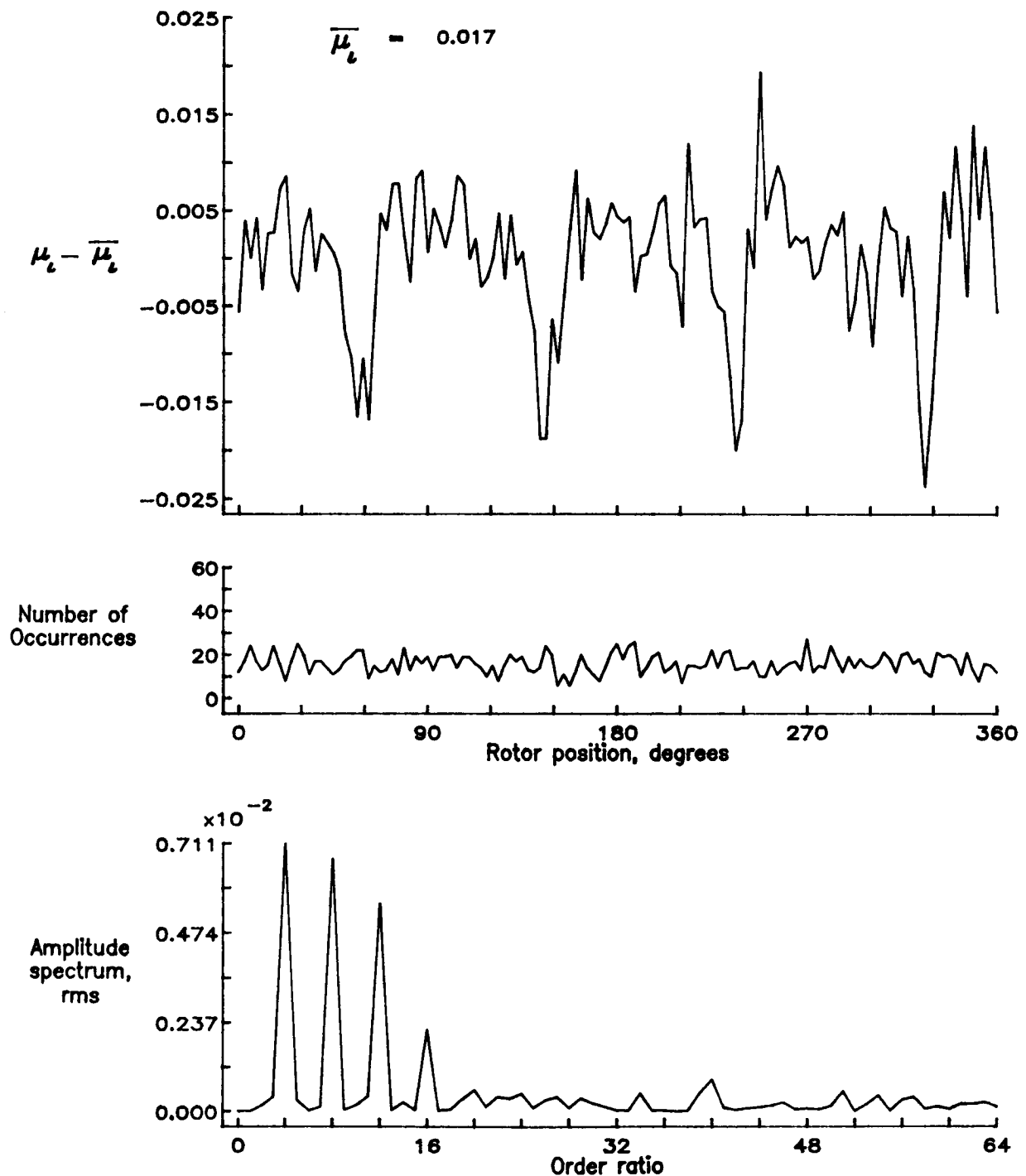


Figure 121.— Induced inflow velocity measured at 240 degrees and r/R of 0.78.

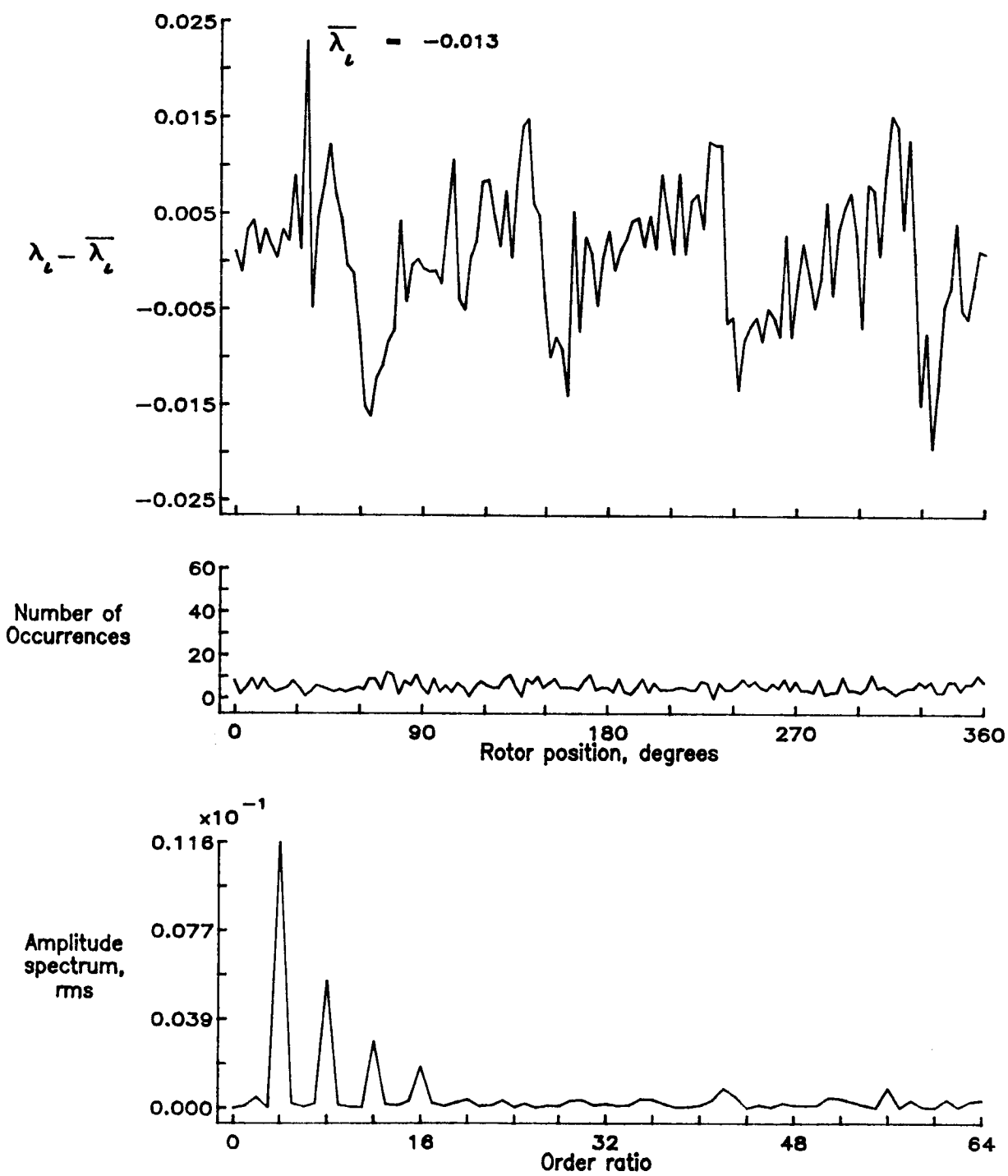


Figure 121.— Concluded.

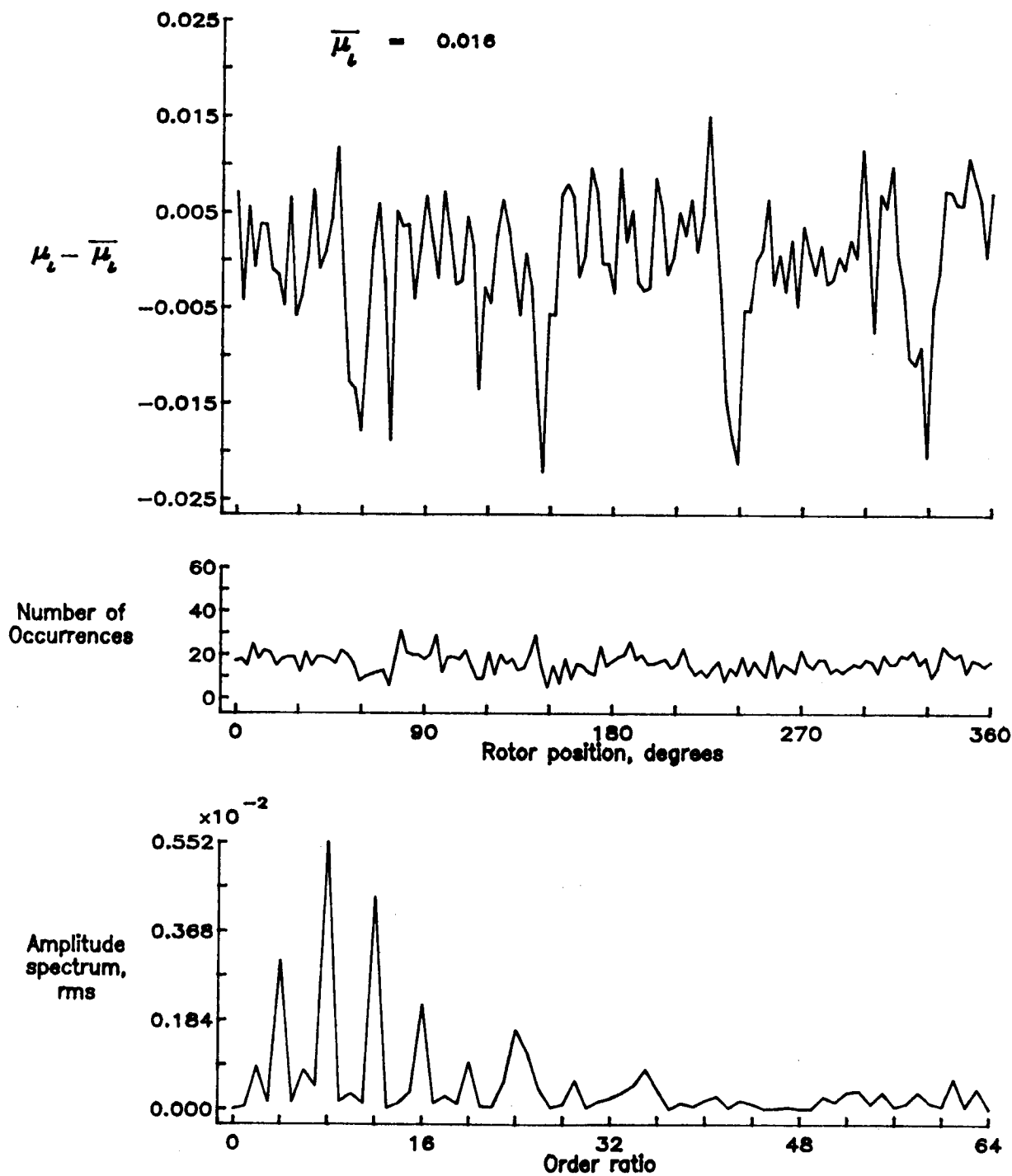


Figure 122.— Induced inflow velocity measured at 240 degrees and r/R of 0.82.

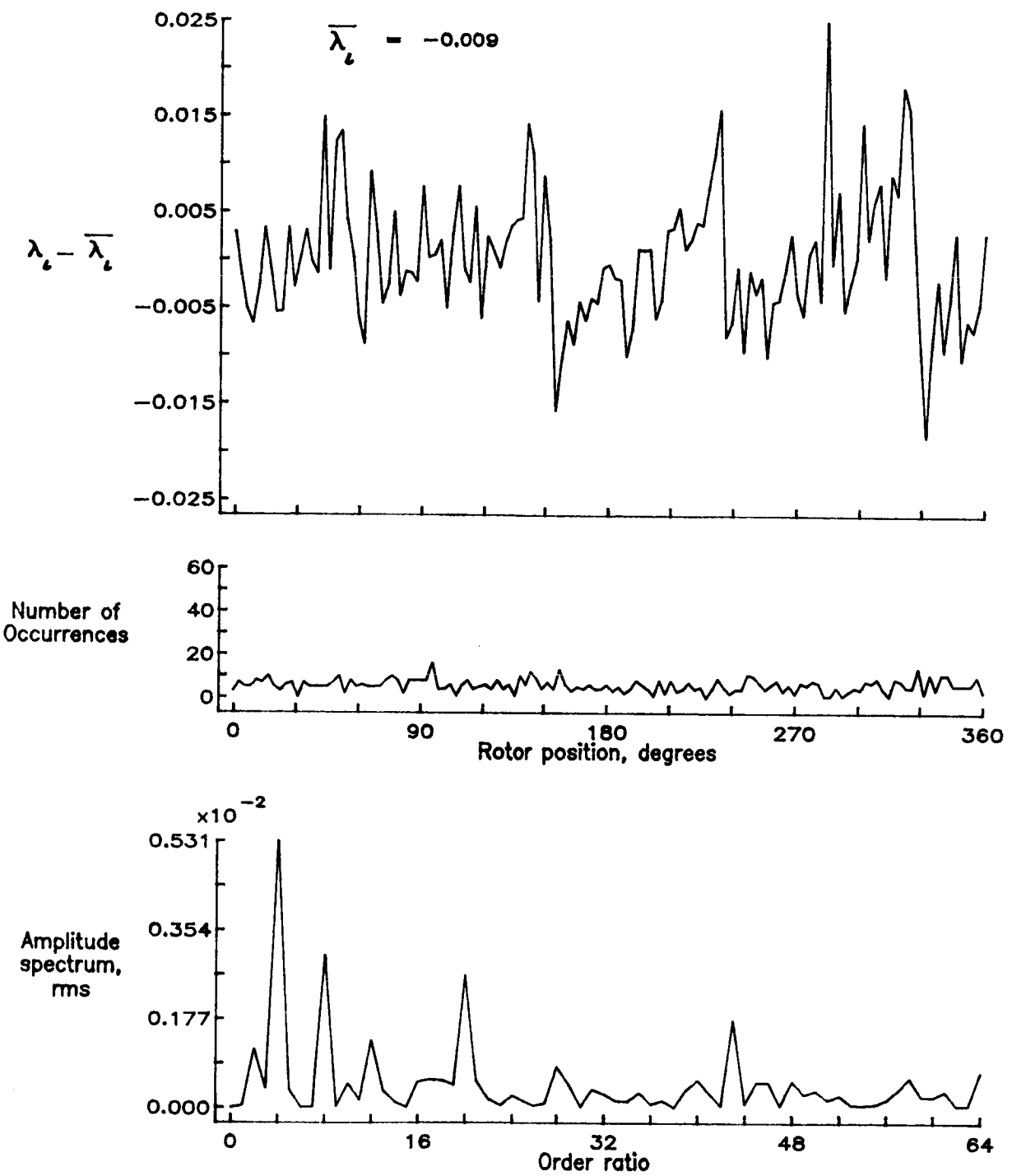


Figure 122.-- Concluded.

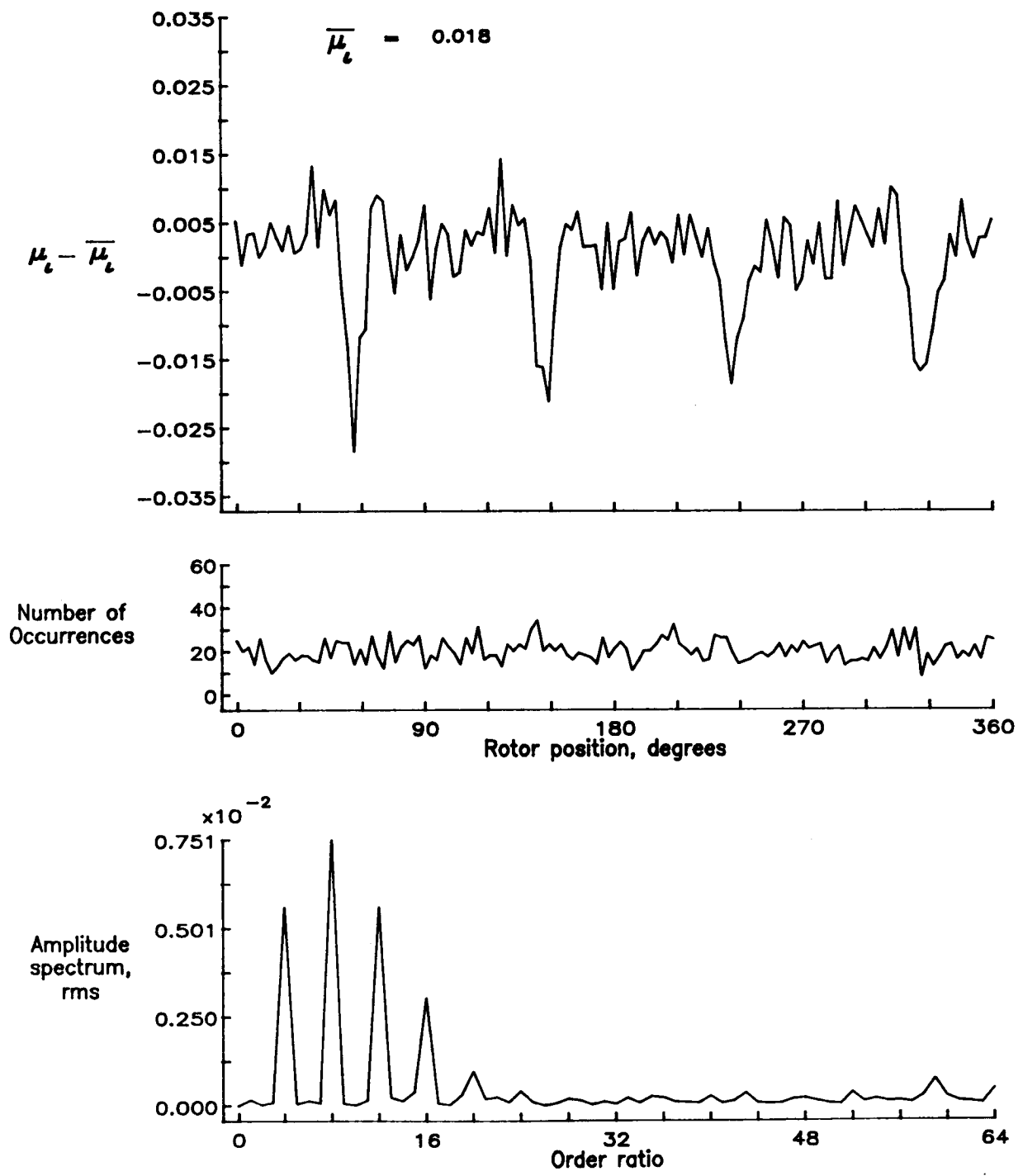


Figure 123.— Induced inflow velocity measured at 240 degrees and r/R of 0.86.

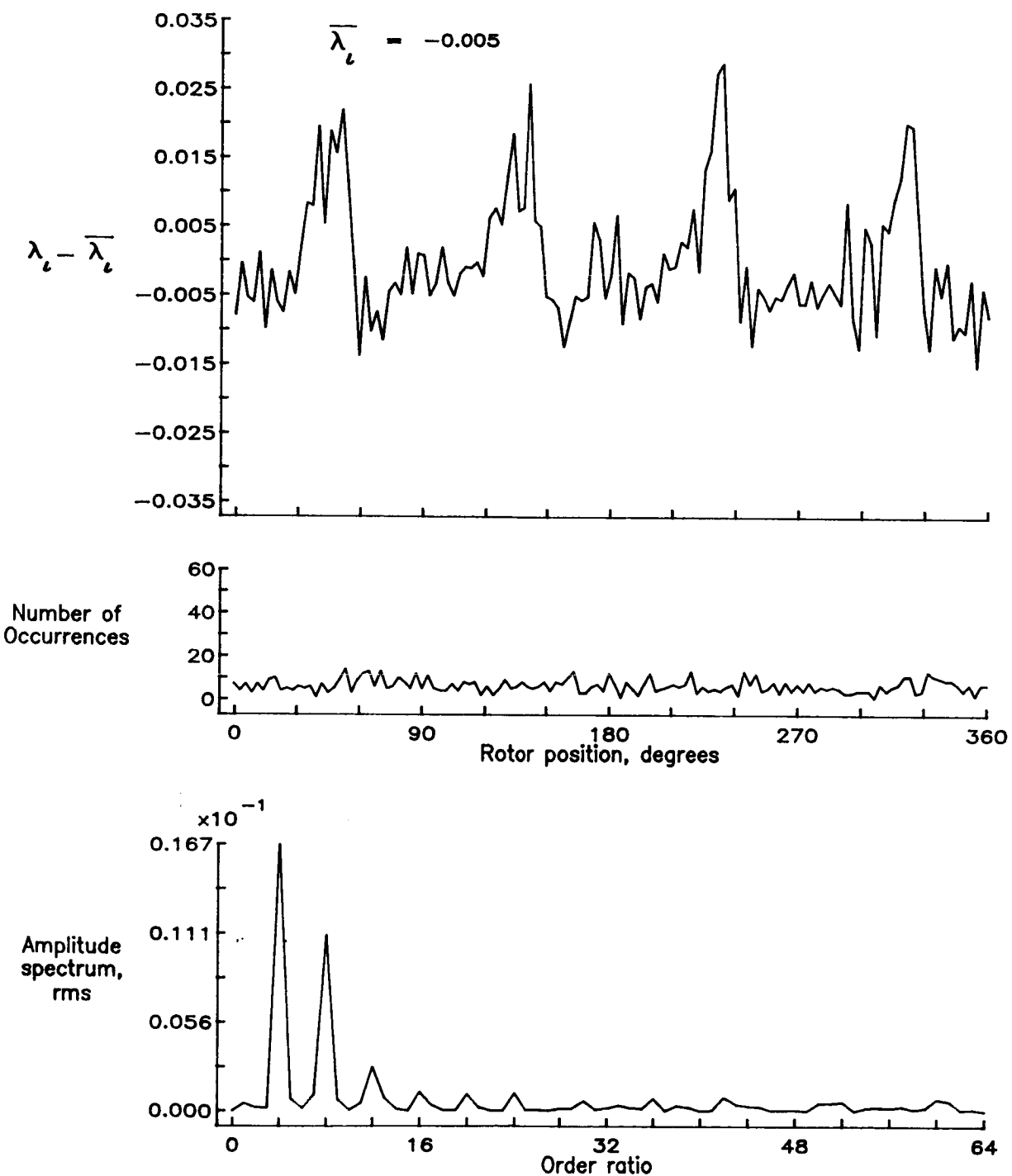


Figure 123.— Concluded.

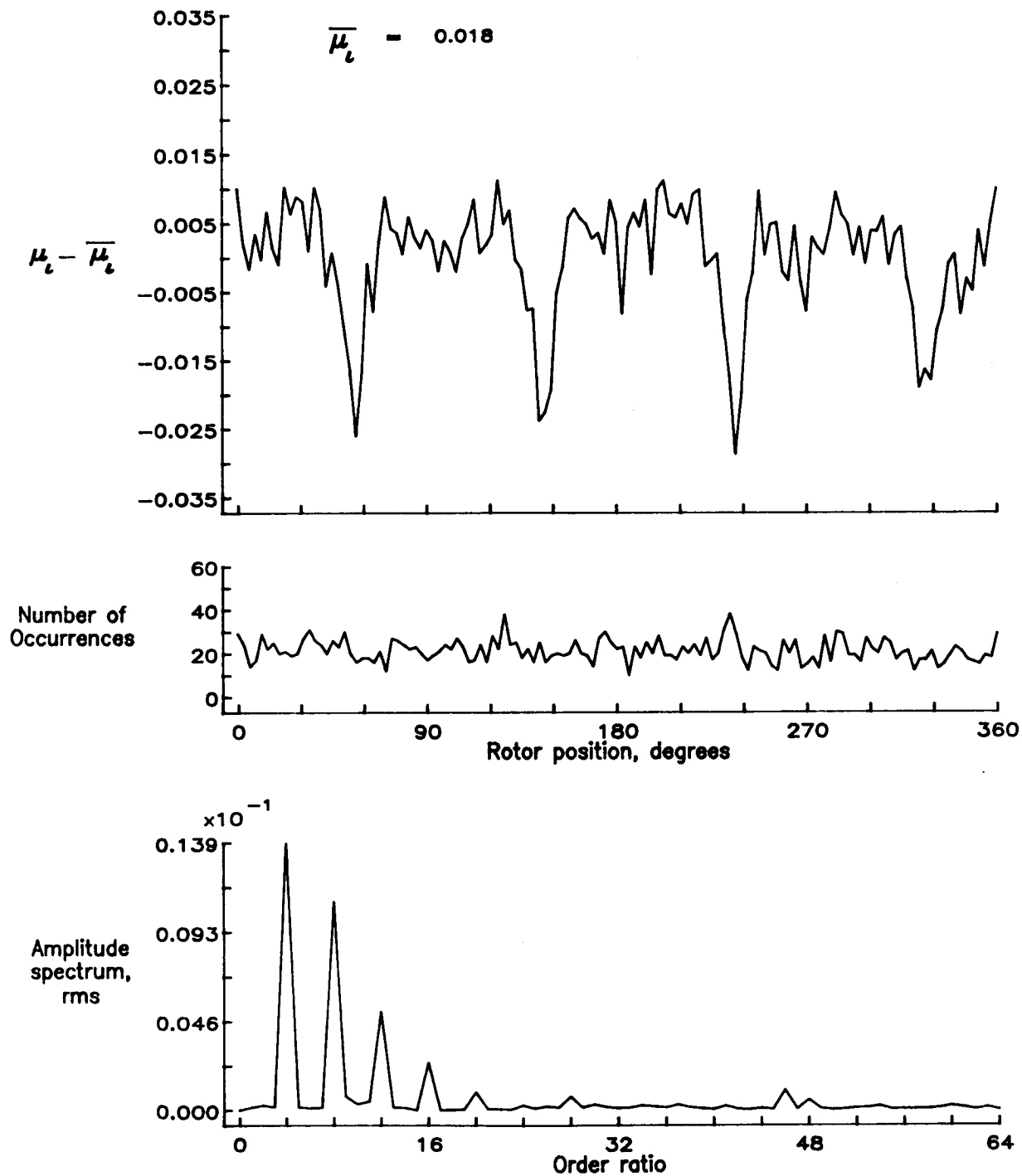


Figure 124.— Induced inflow velocity measured at 240 degrees and r/R of 0.90.

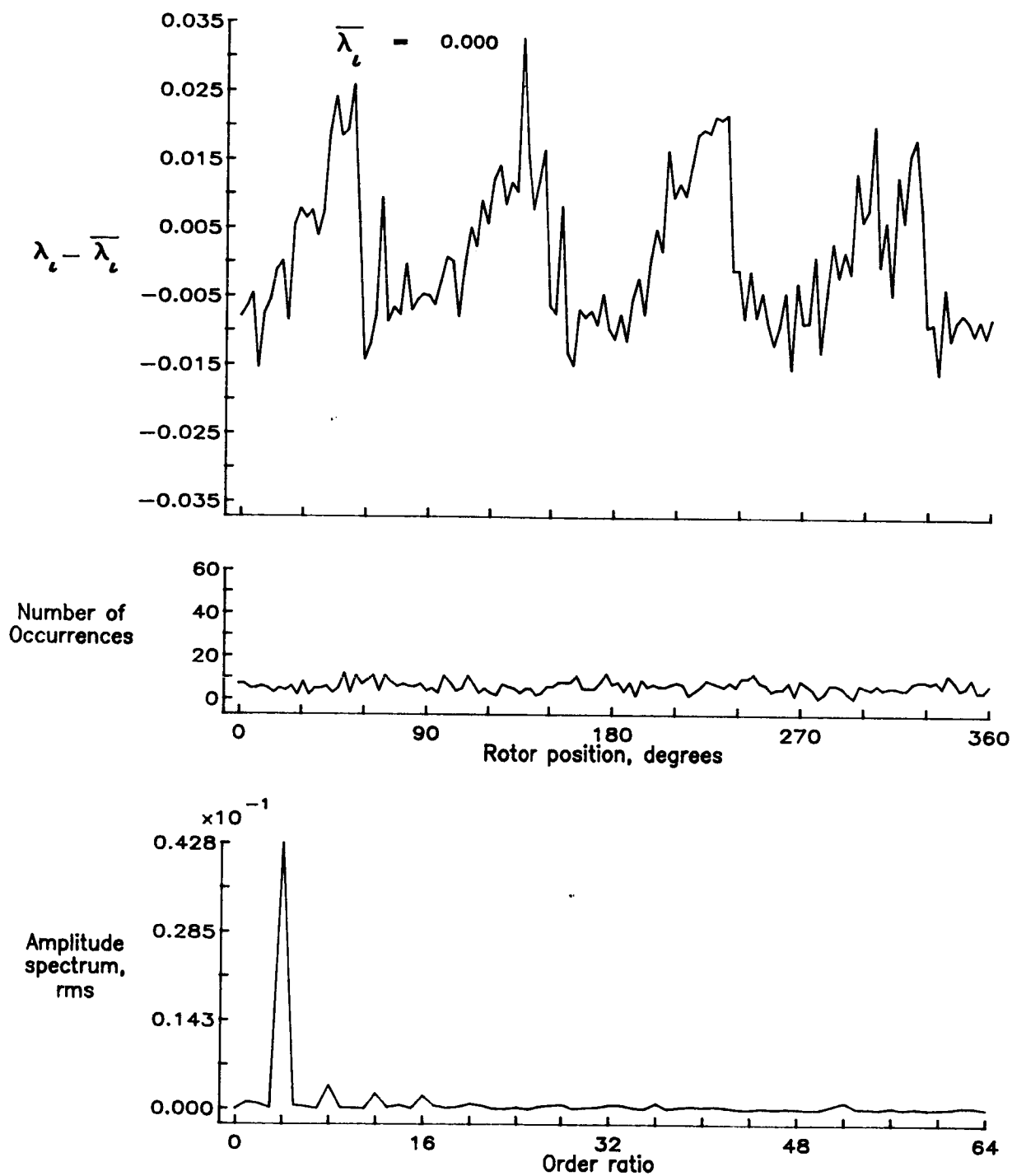


Figure 124.— Concluded.

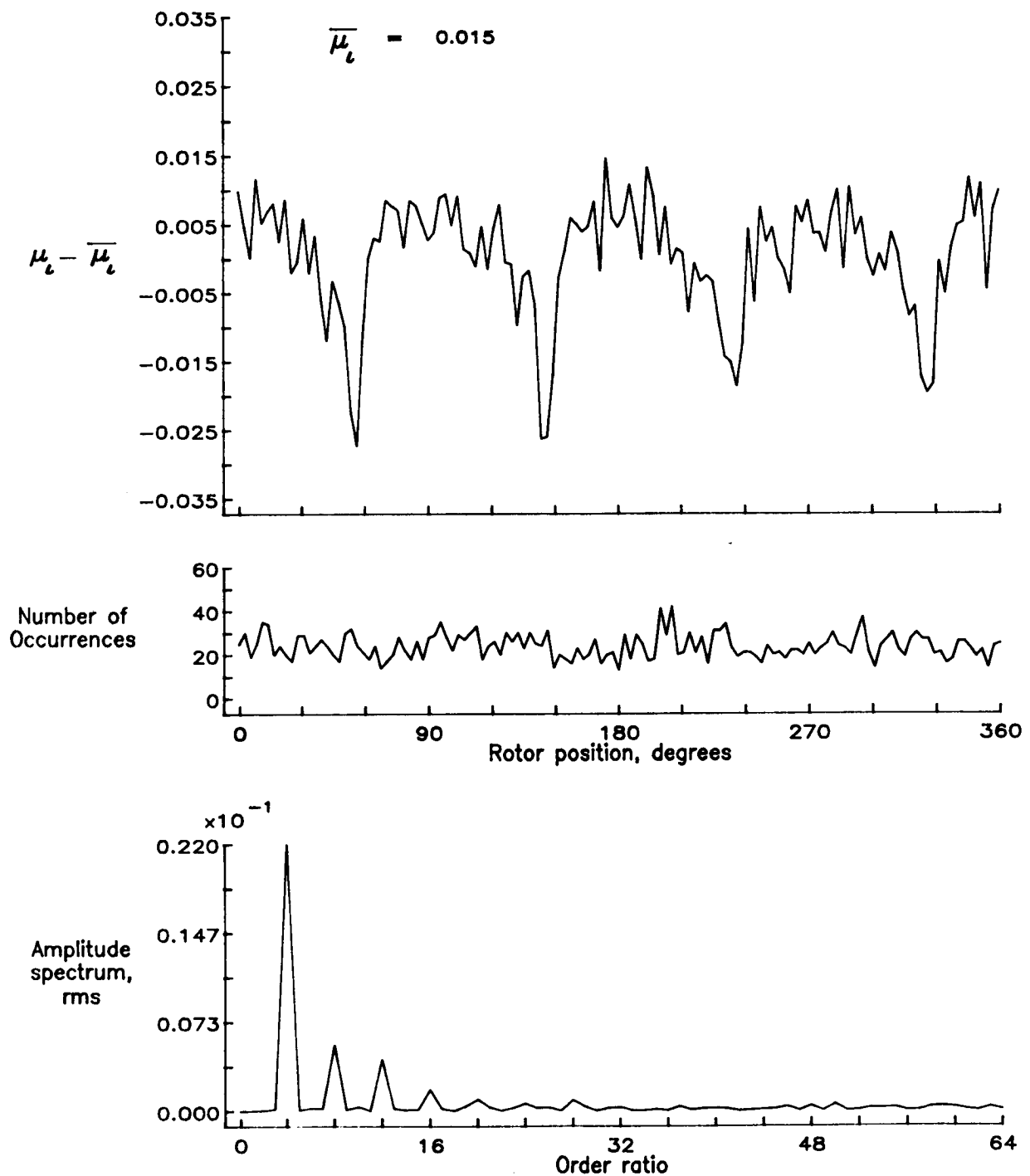


Figure 125.— Induced inflow velocity measured at 240 degrees and r/R of 0.94.

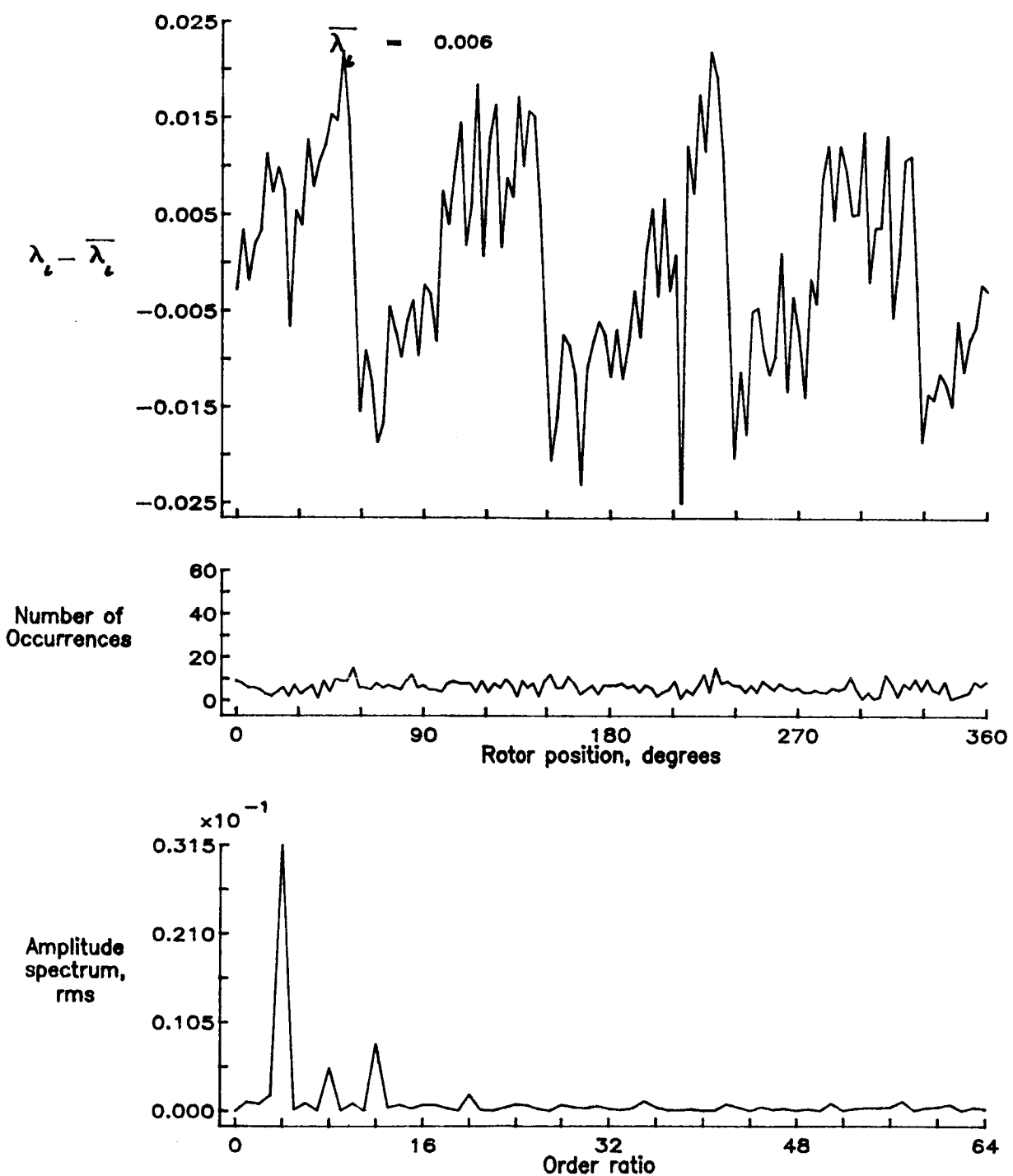


Figure 125.— Concluded.

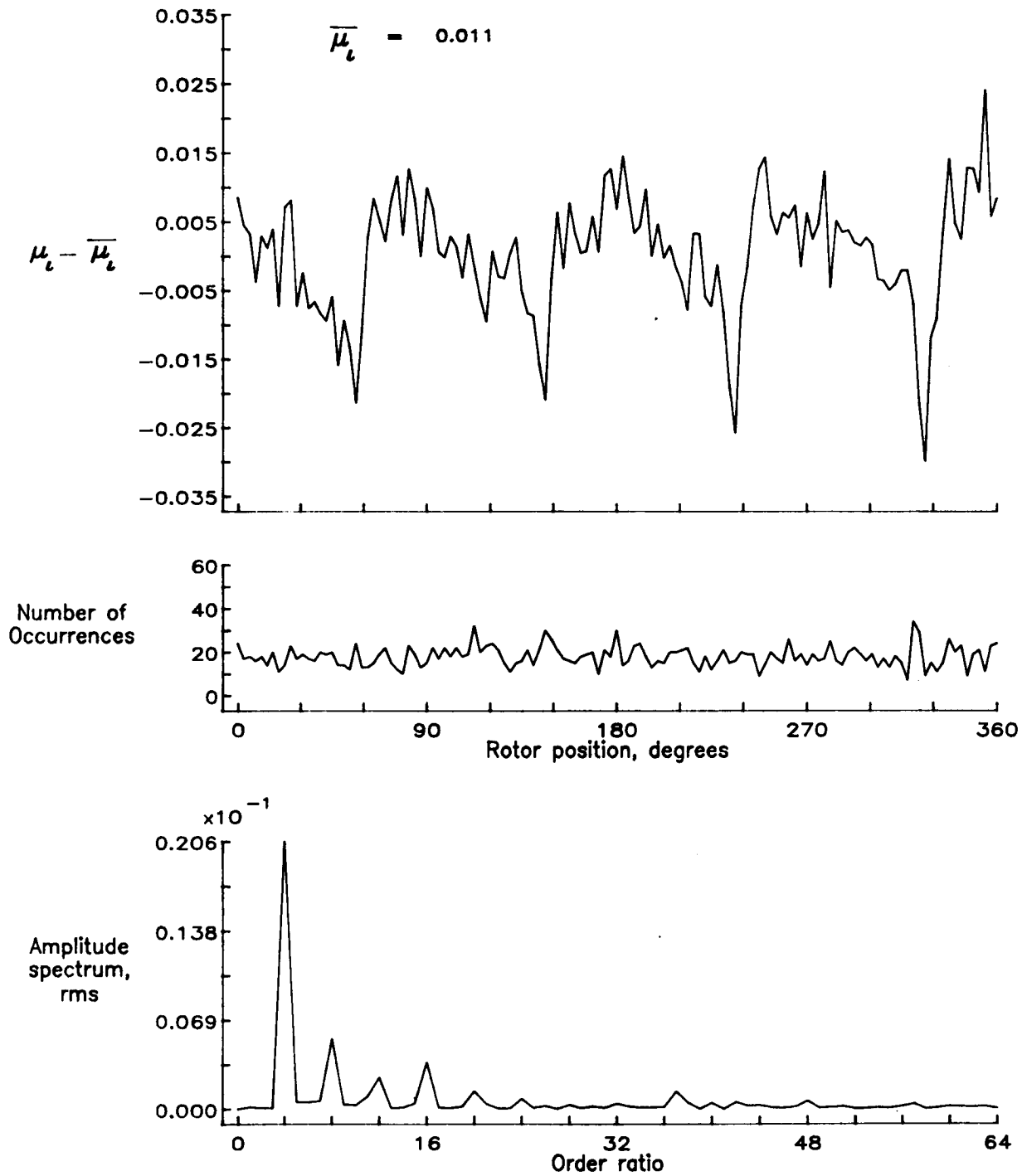


Figure 126.— Induced inflow velocity measured at 240 degrees and r/R of 0.98.

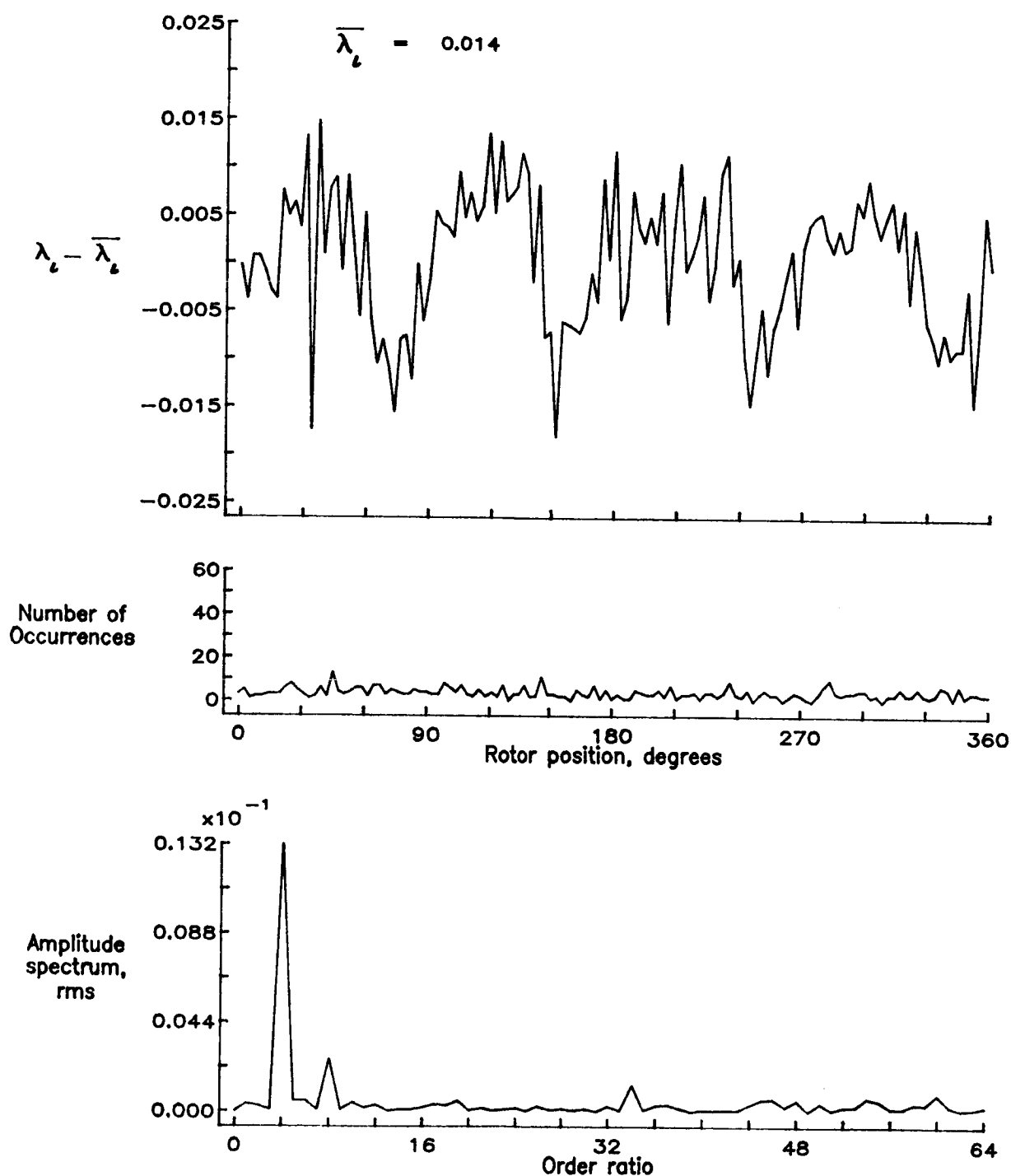


Figure 126.— Concluded.

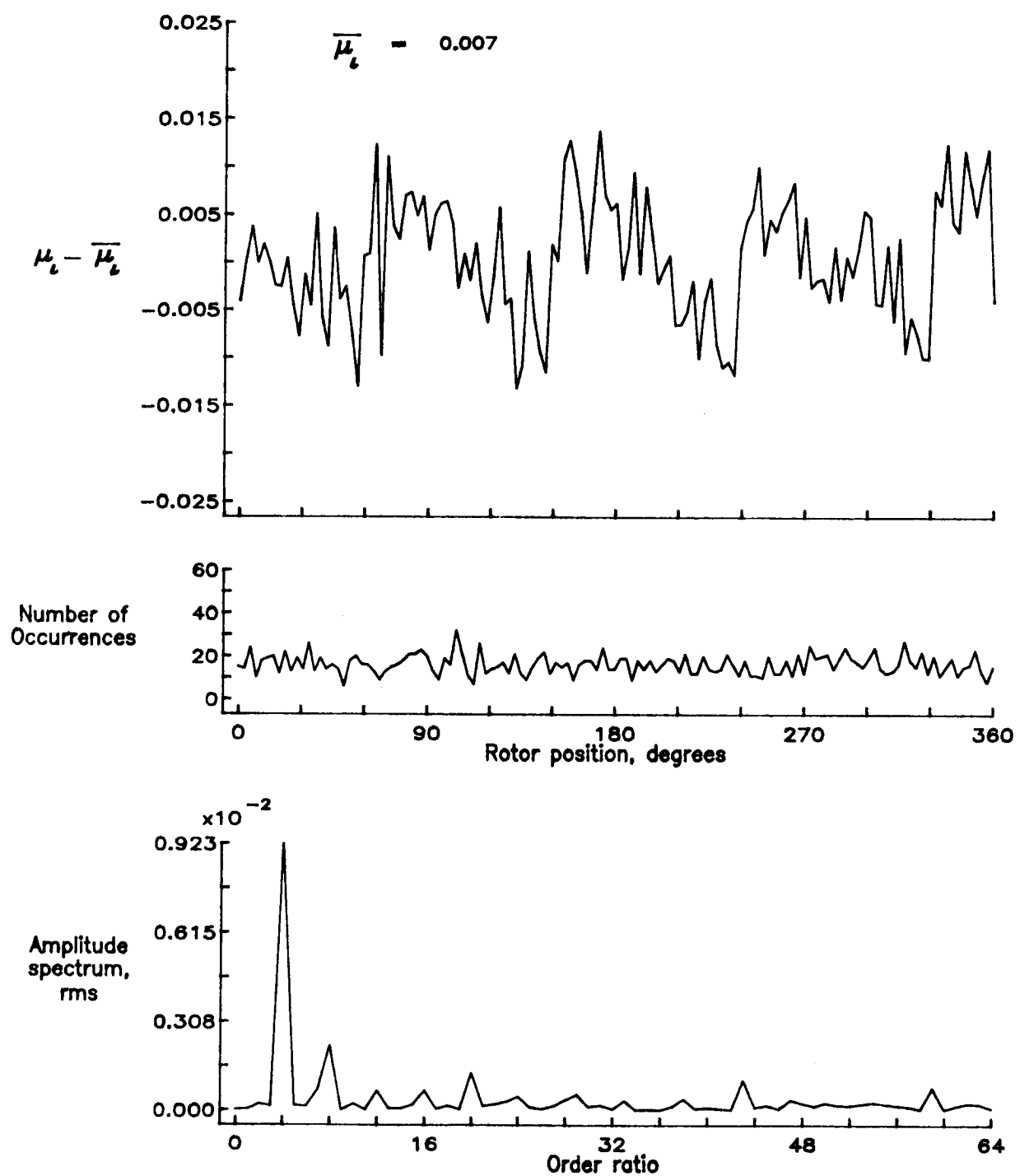


Figure 127.— Induced inflow velocity measured at 240 degrees and r/R of 1.02.

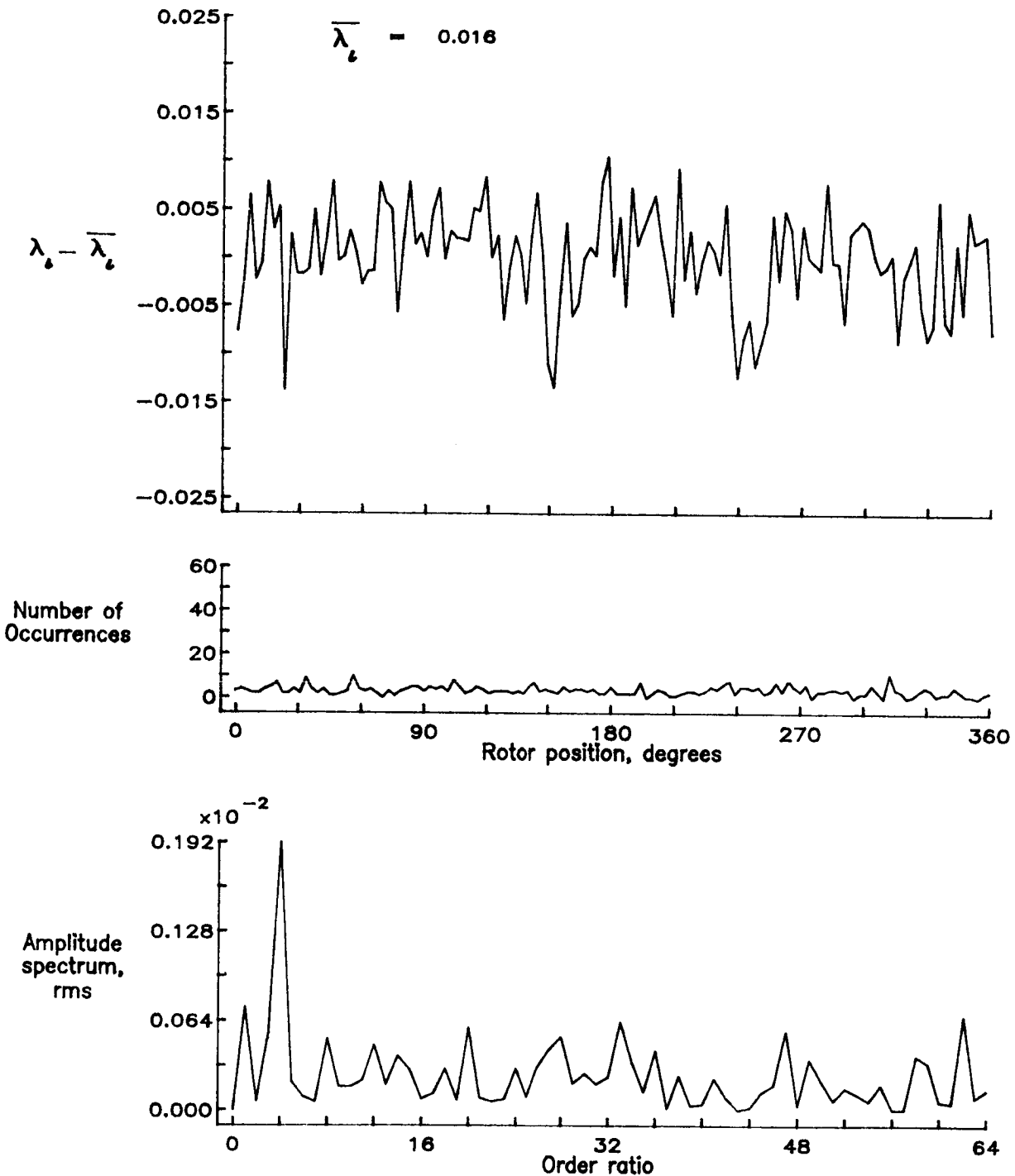


Figure 127.— Concluded.

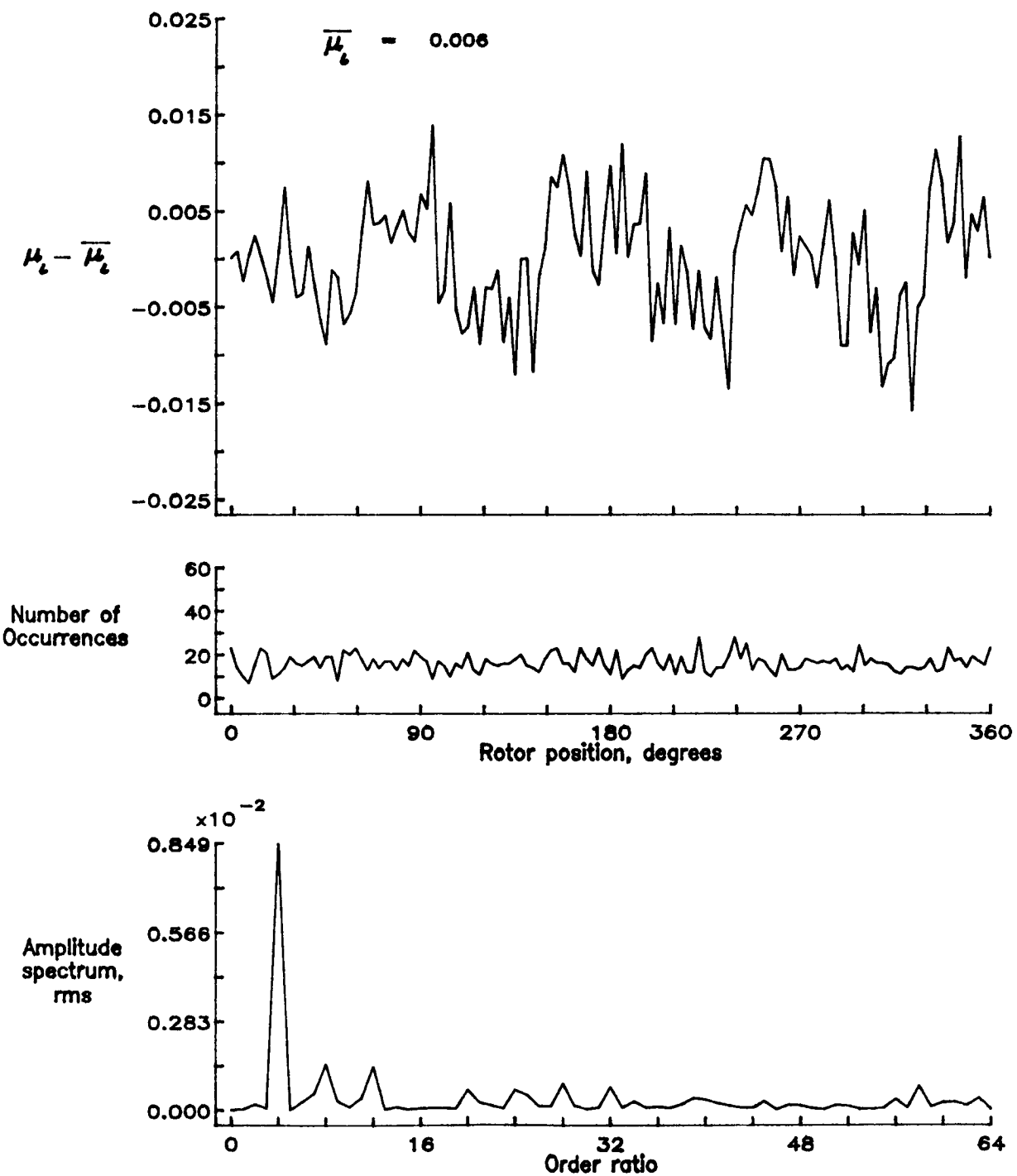


Figure 128.— Induced inflow velocity measured at 240 degrees and r/R of 1.04.

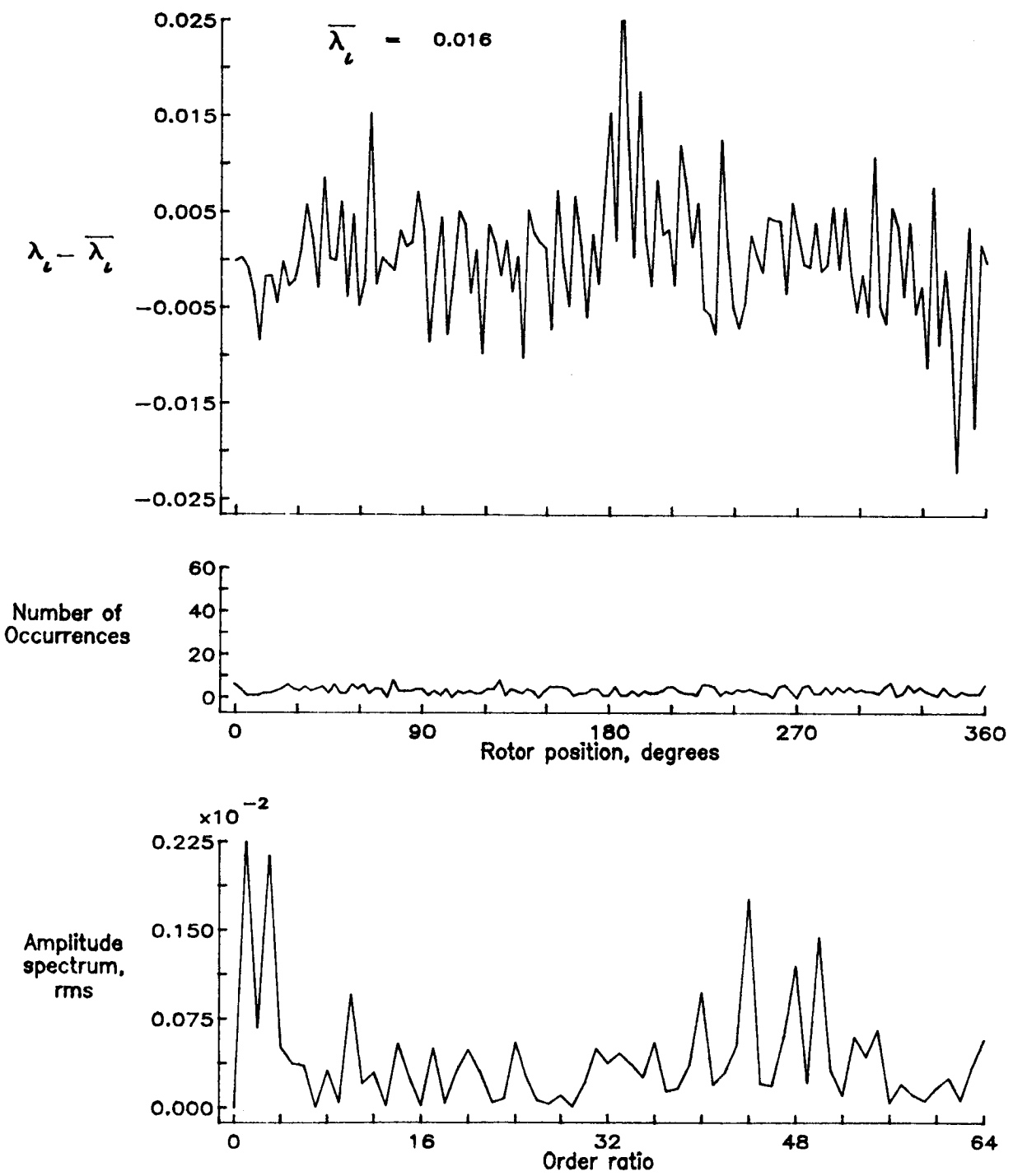


Figure 128.— Concluded.

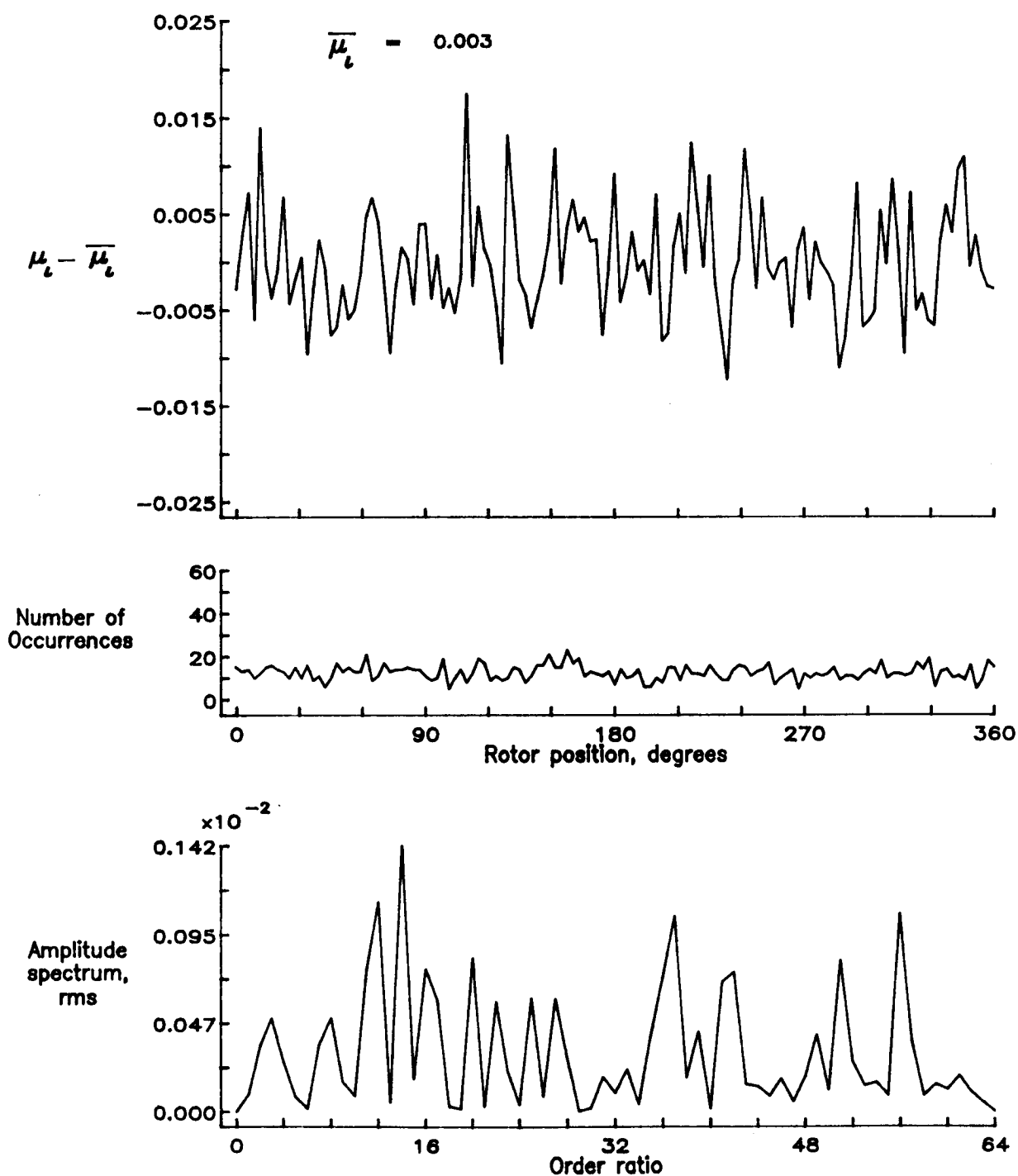


Figure 129.— Induced inflow velocity measured at 240 degrees and r/R of 1.10.

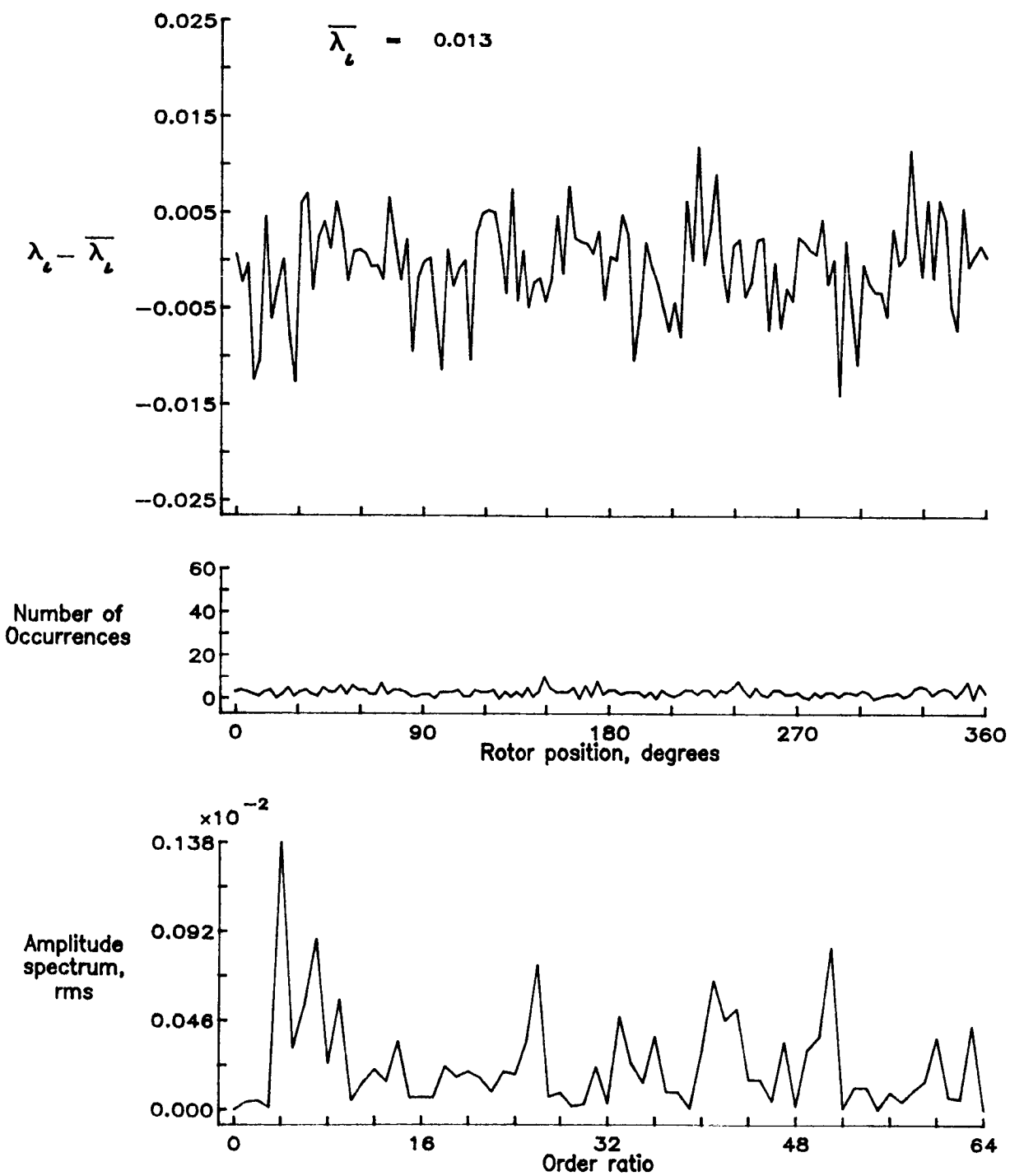


Figure 129.— Concluded.

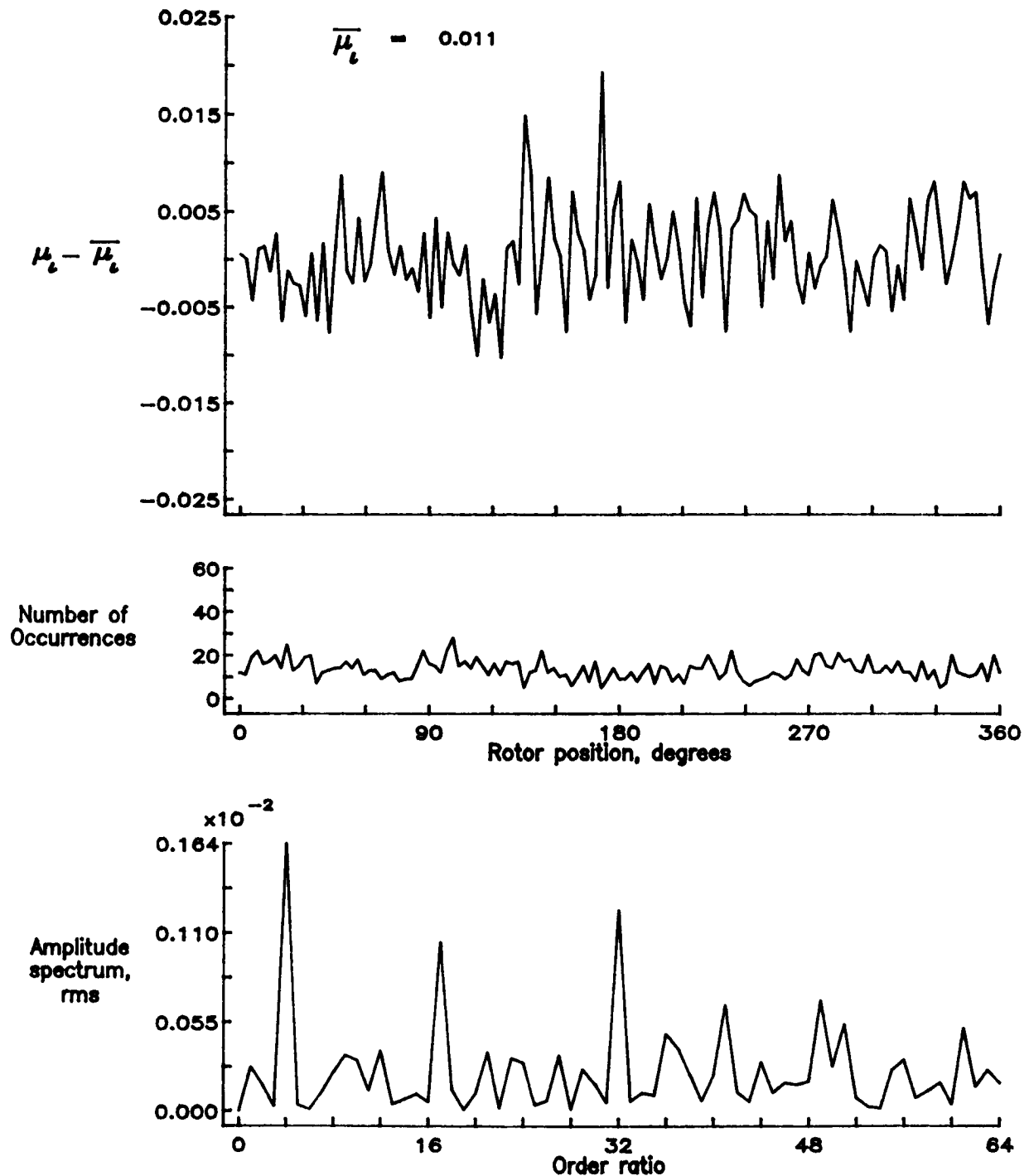


Figure 130.— Induced inflow velocity measured at 300 degrees and  $r/R$  of 0.20.

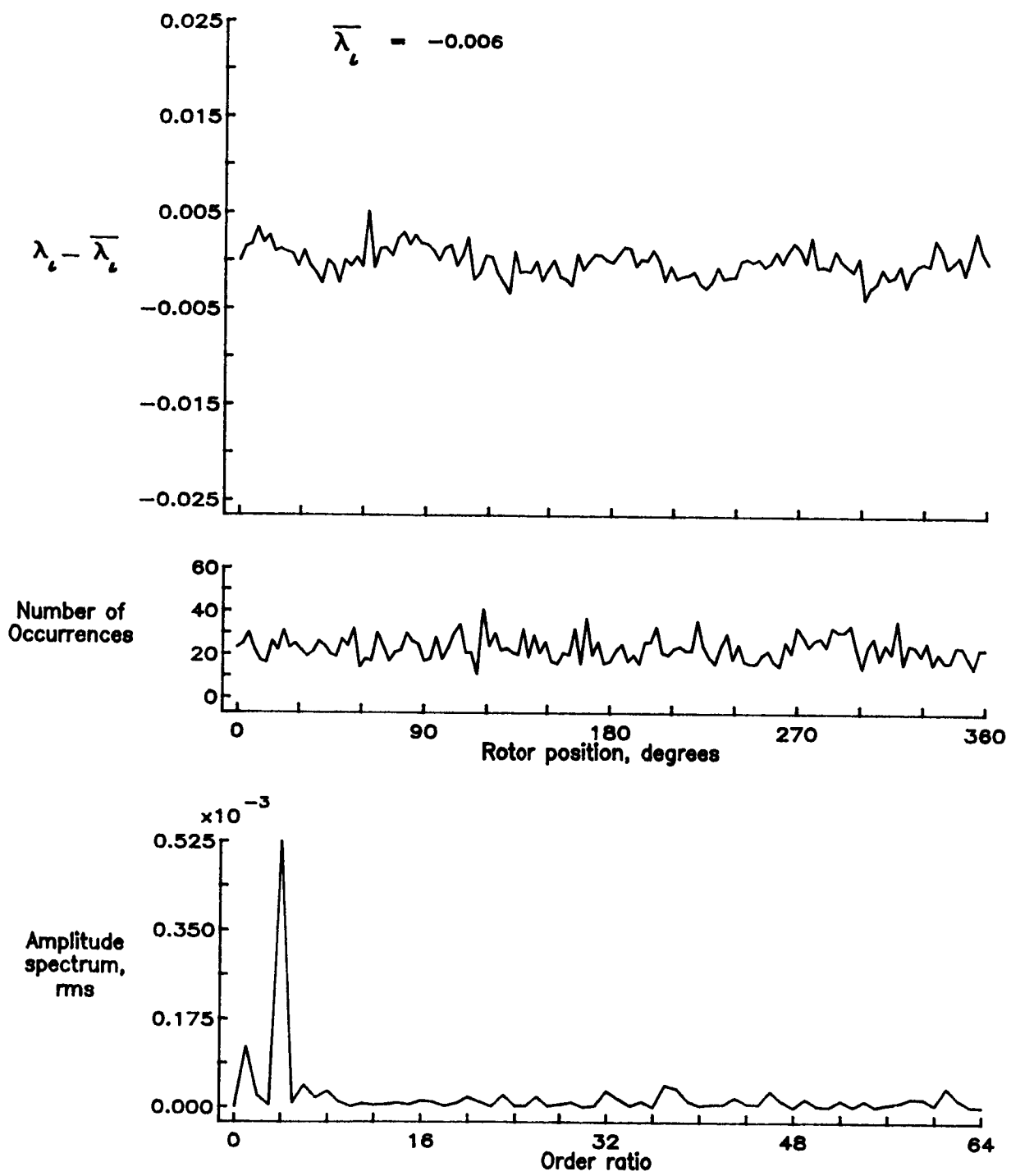


Figure 130.— Concluded.

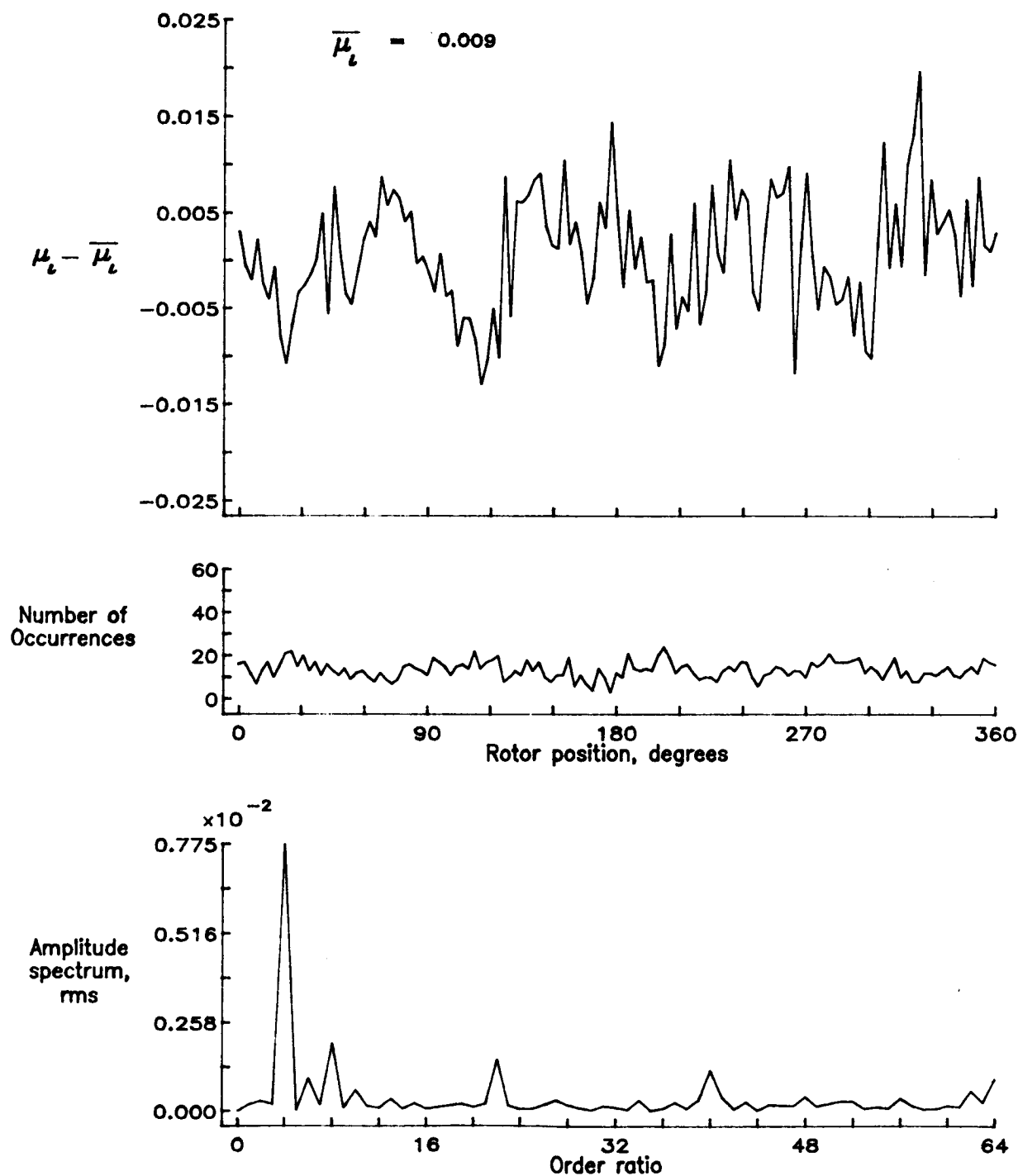


Figure 131.— Induced inflow velocity measured at 300 degrees and r/R of 0.40.

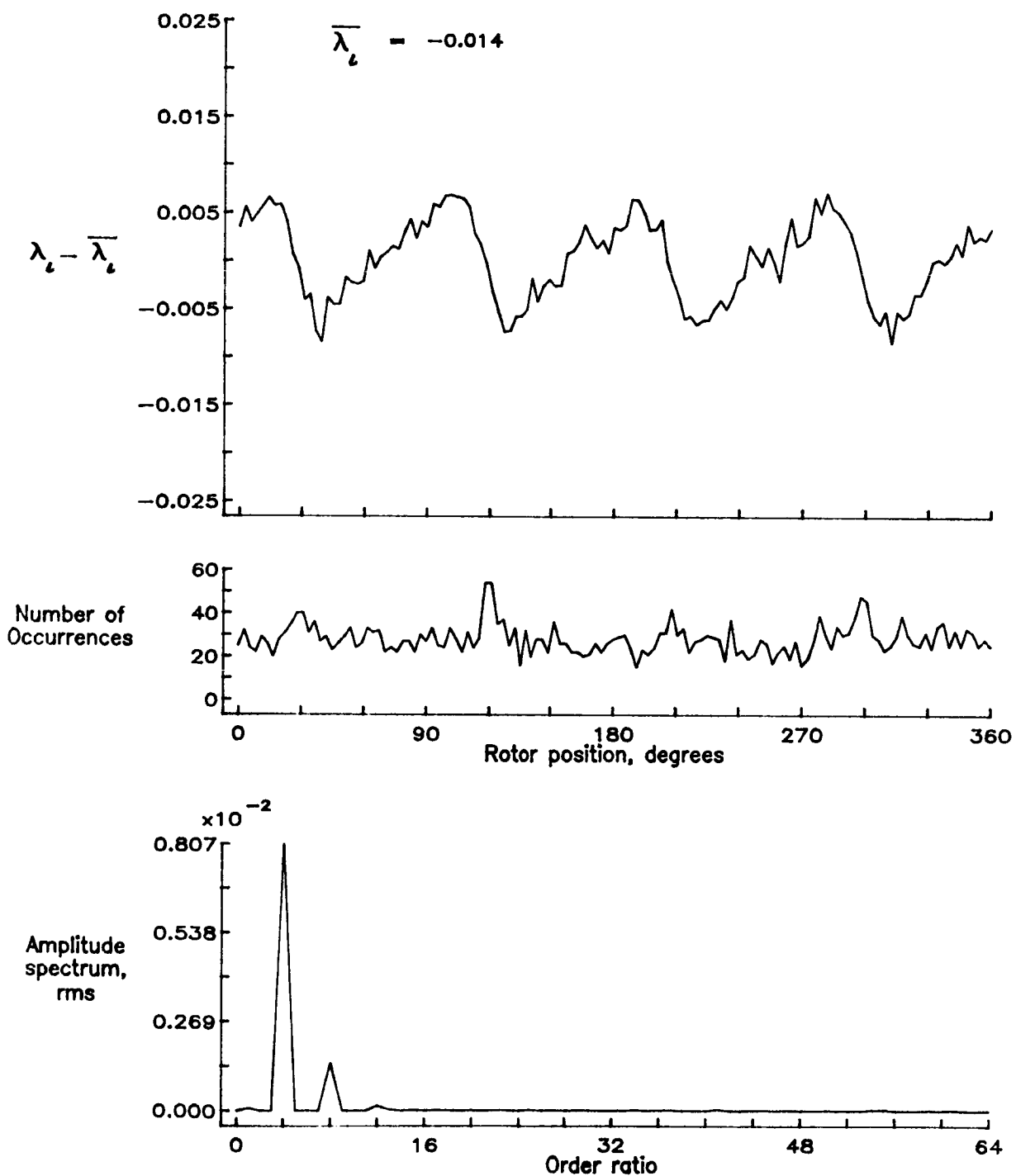


Figure 131.— Concluded.

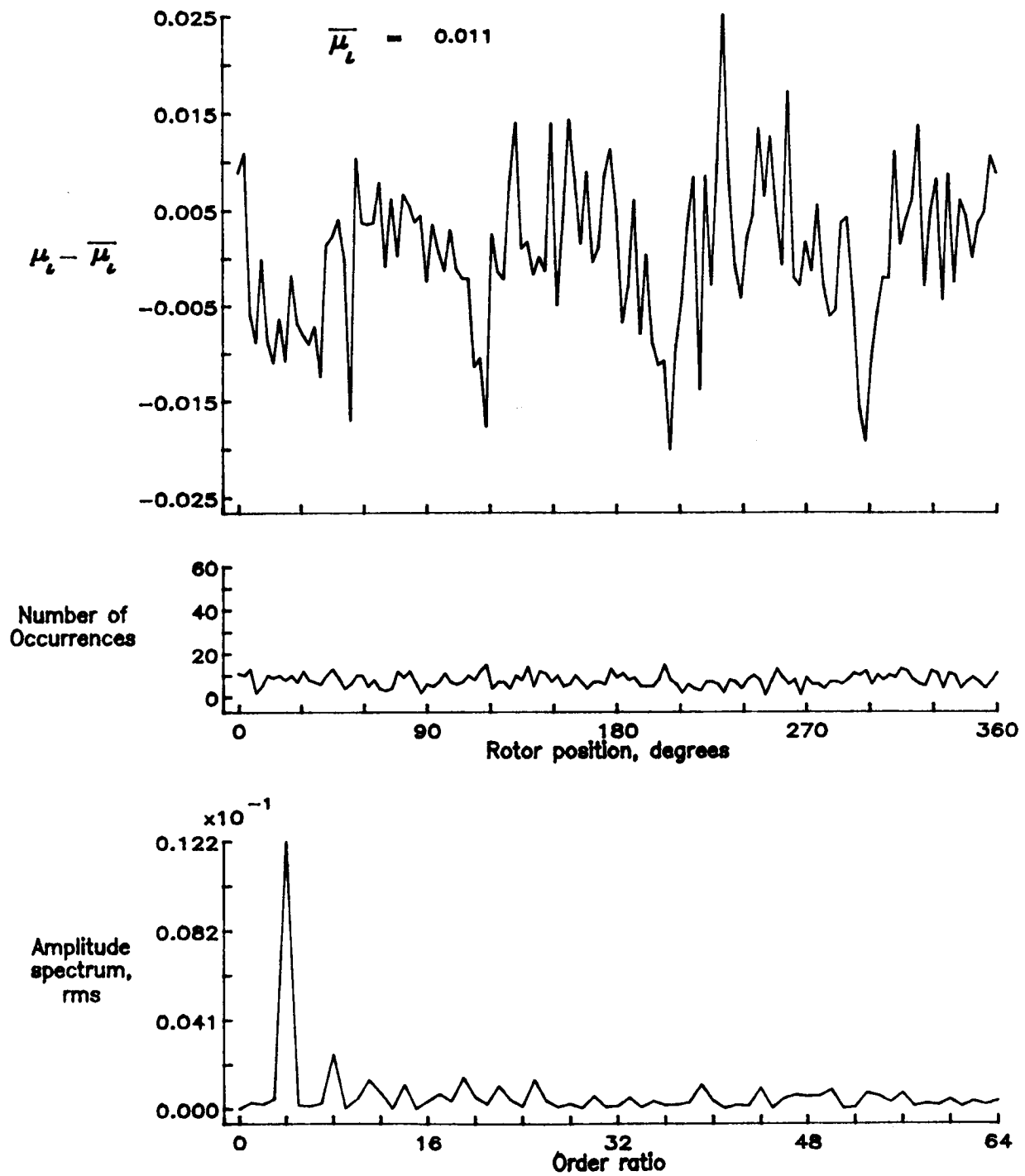


Figure 132.— Induced inflow velocity measured at 300 degrees and  $r/R$  of 0.50.

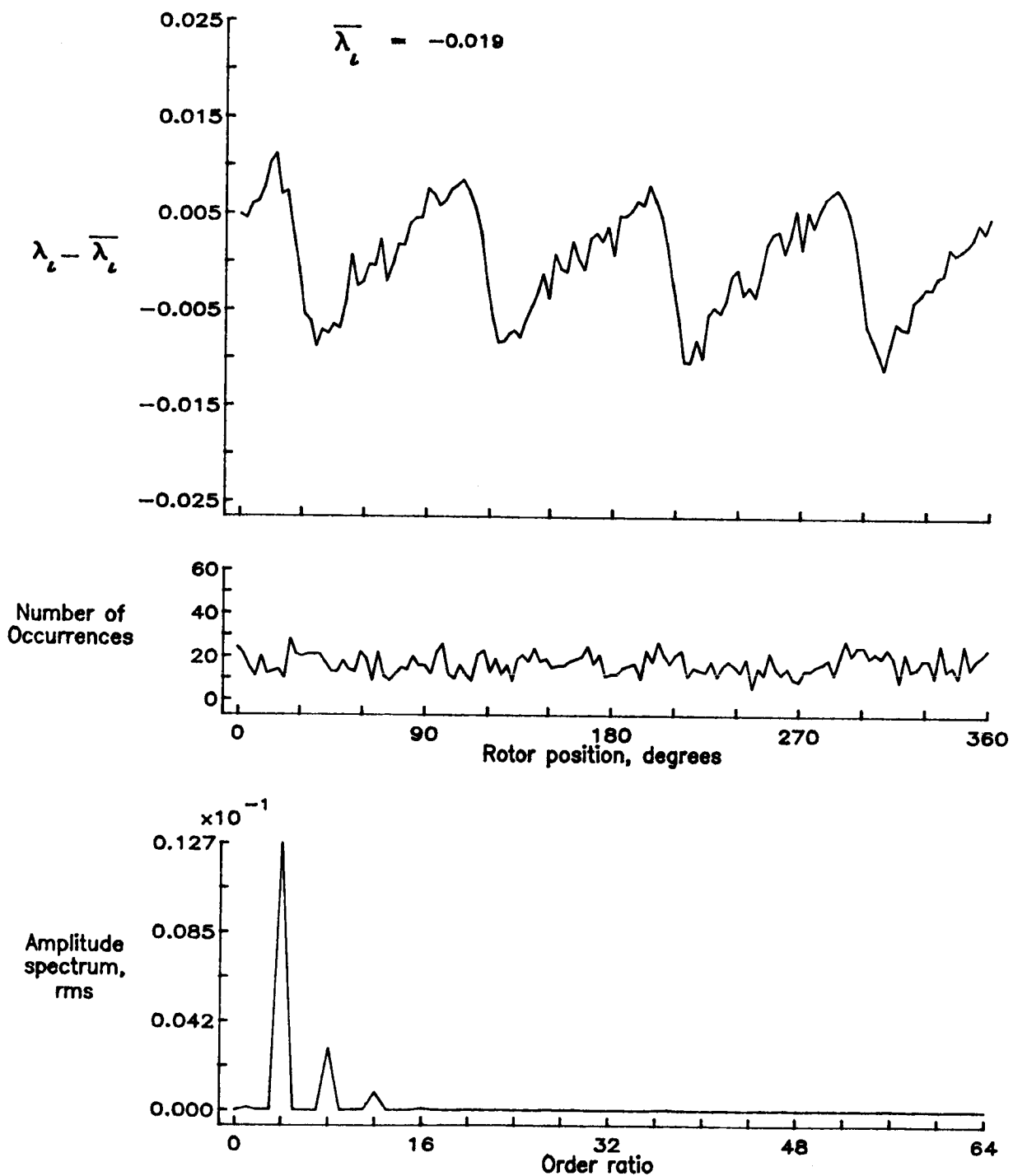


Figure 132.— Concluded.

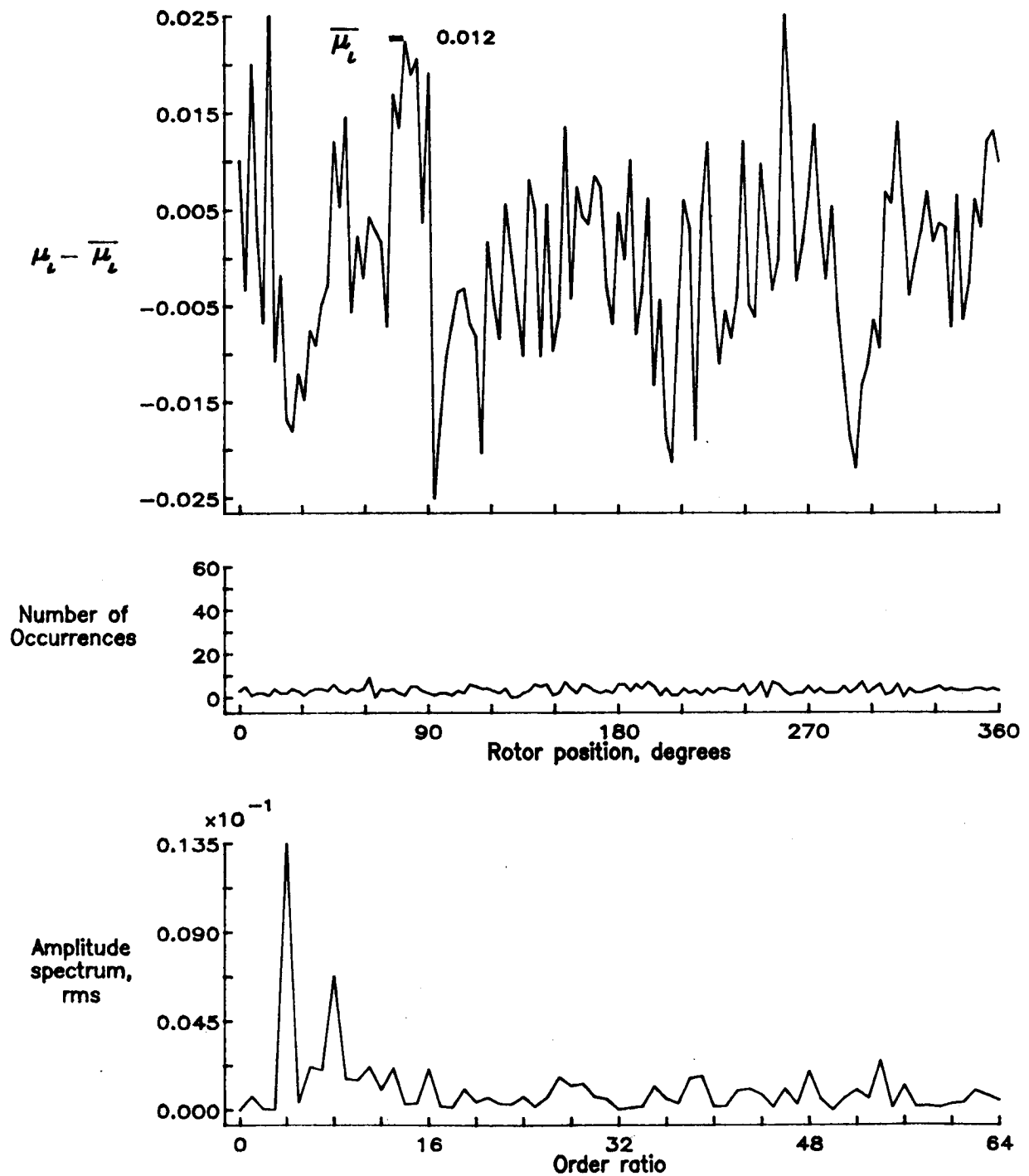


Figure 133.— Induced inflow velocity measured at 300 degrees and r/R of 0.60.

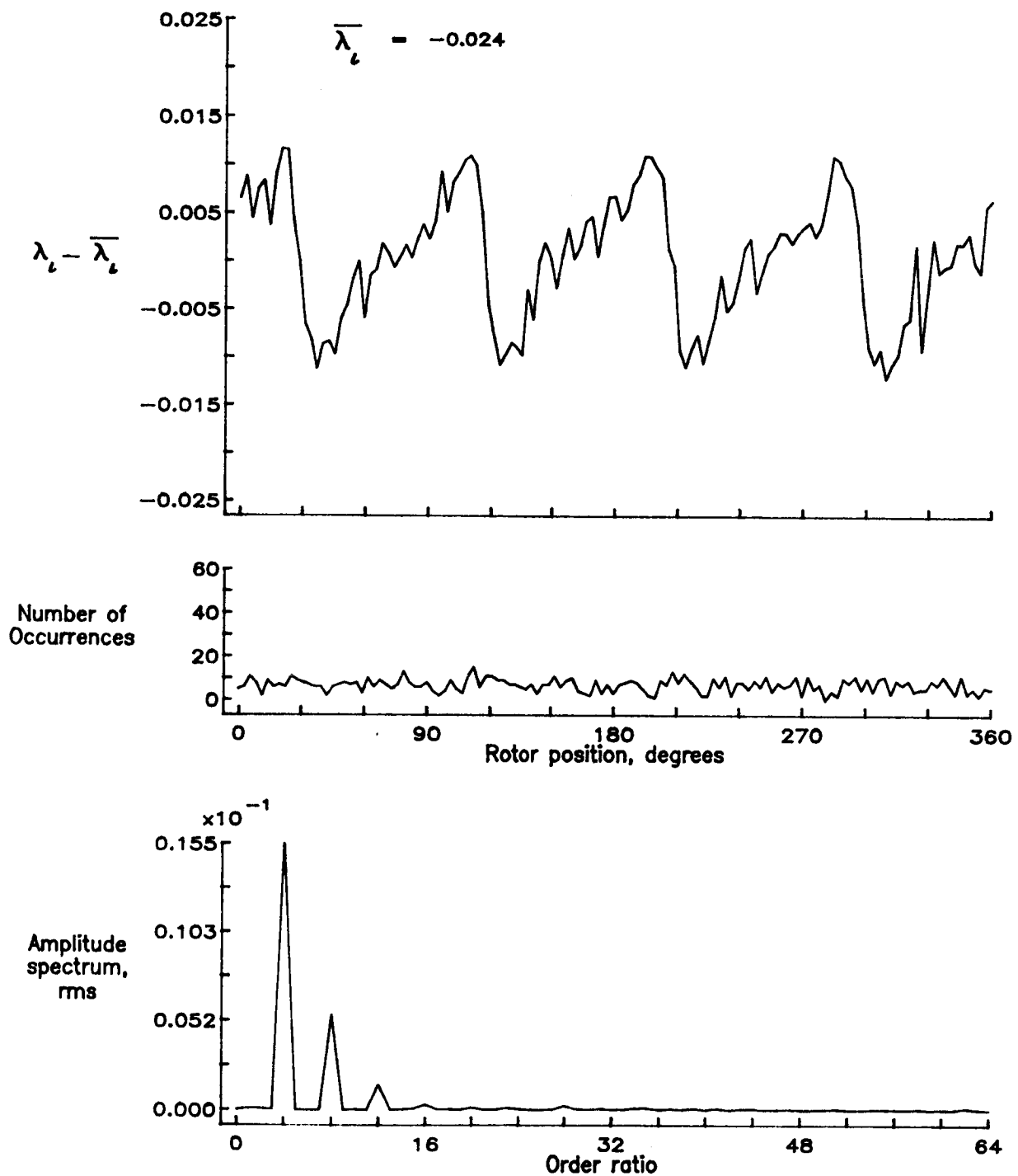


Figure 133.— Concluded.

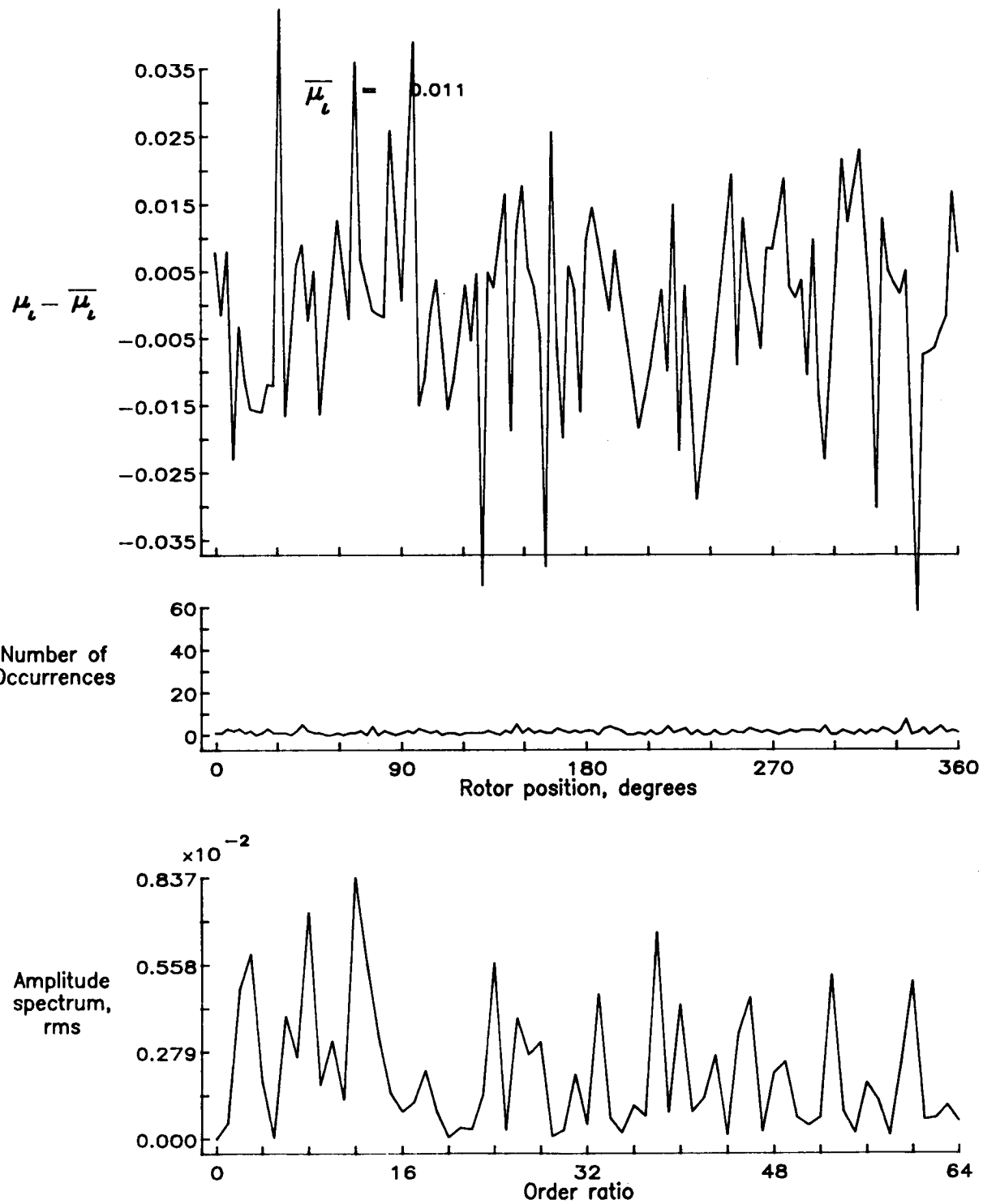


Figure 134.— Induced inflow velocity measured at 300 degrees and  $r/R$  of 0.70.

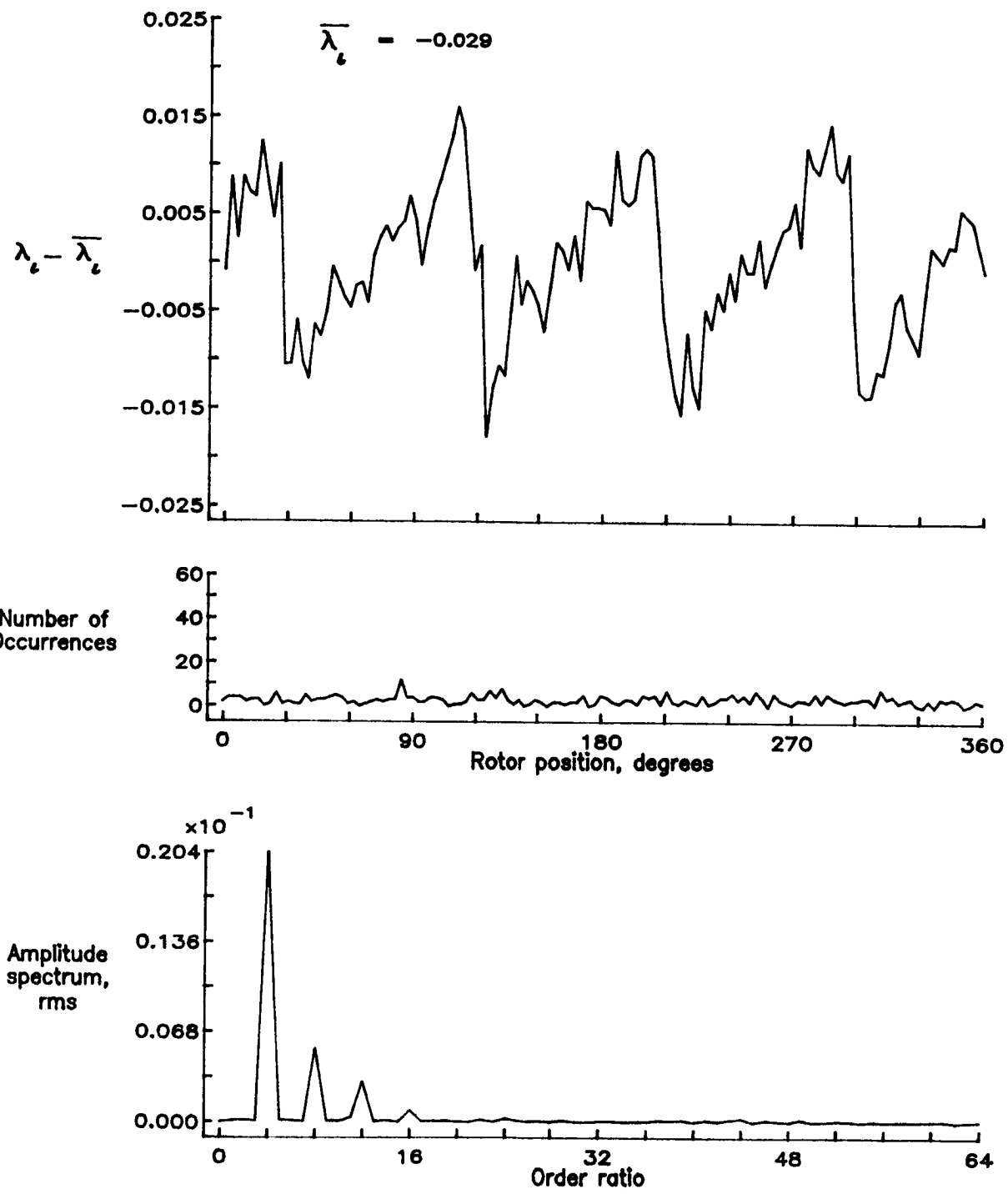


Figure 134.— Concluded.

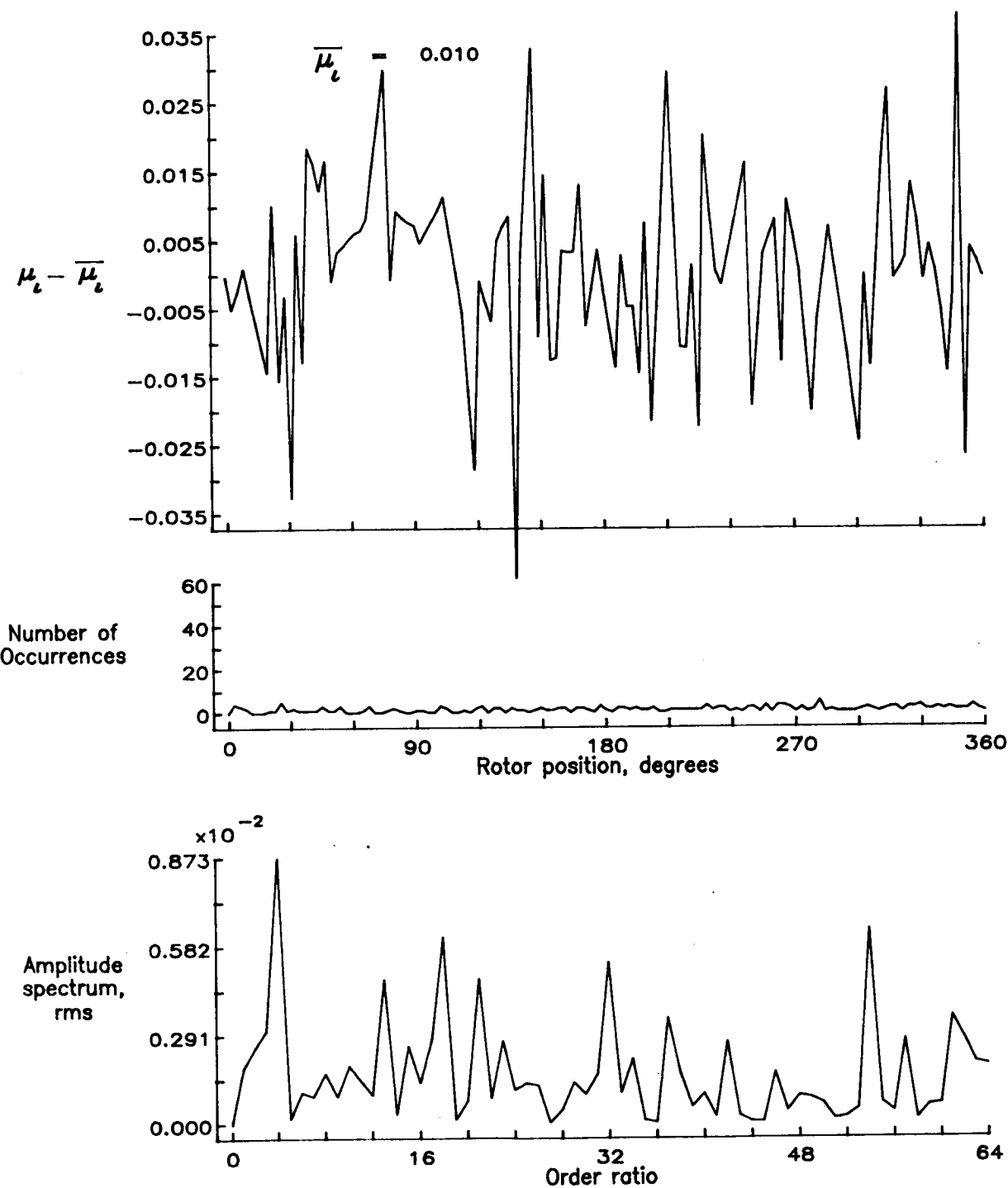


Figure 135.— Induced inflow velocity measured at 300 degrees and r/R of 0.74.

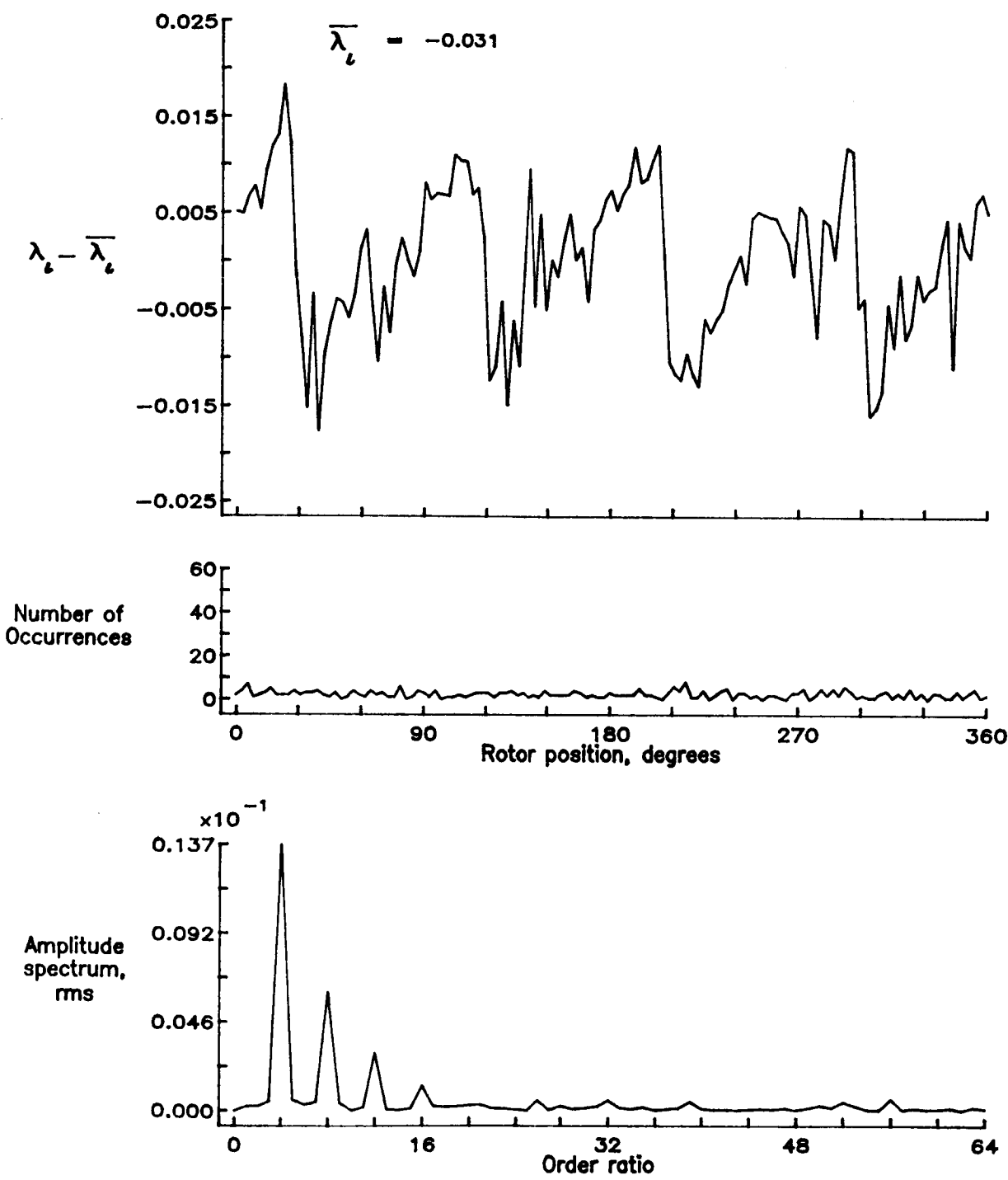


Figure 135.— Concluded.

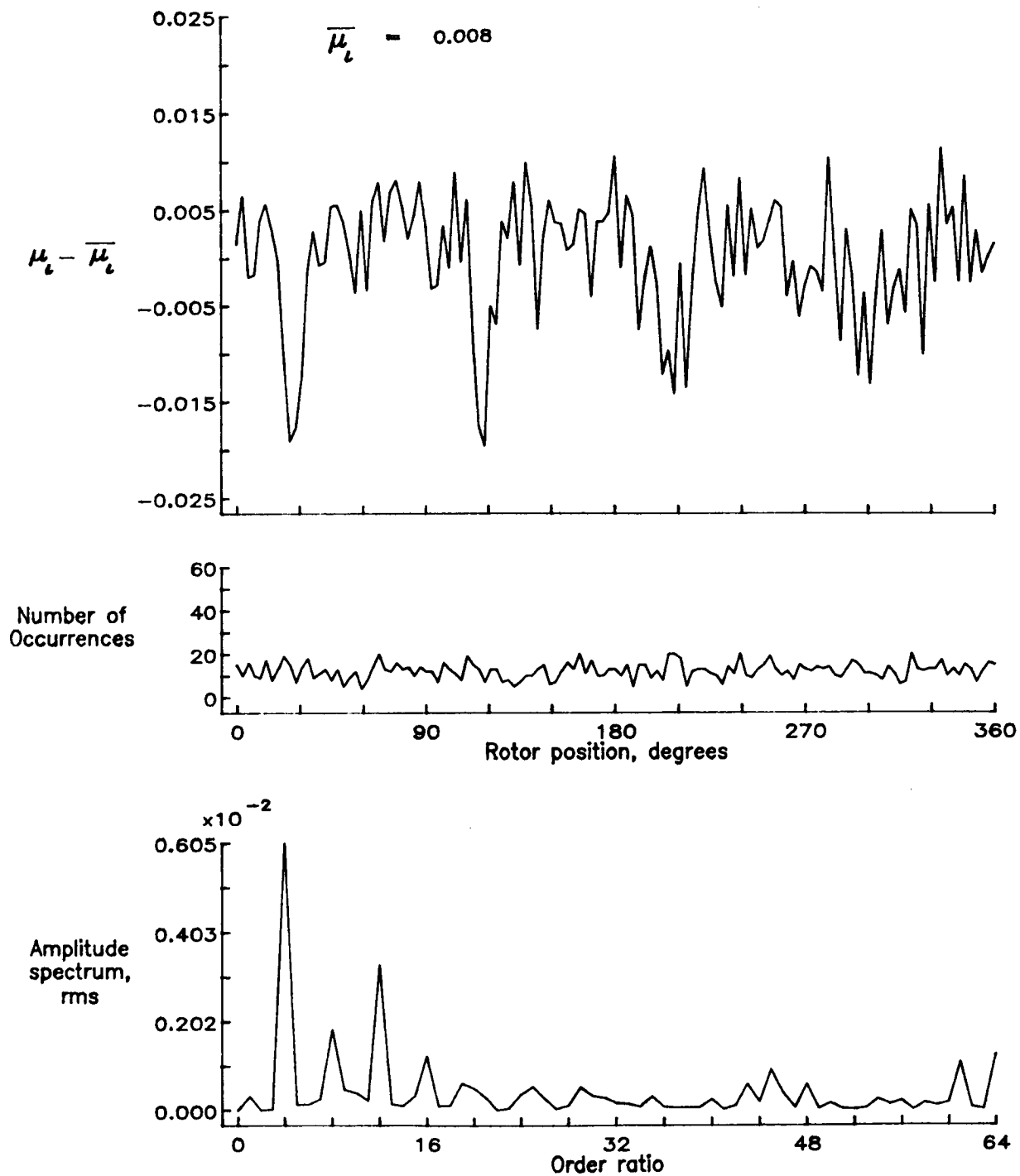


Figure 136.— Induced inflow velocity measured at 300 degrees and r/R of 0.78.

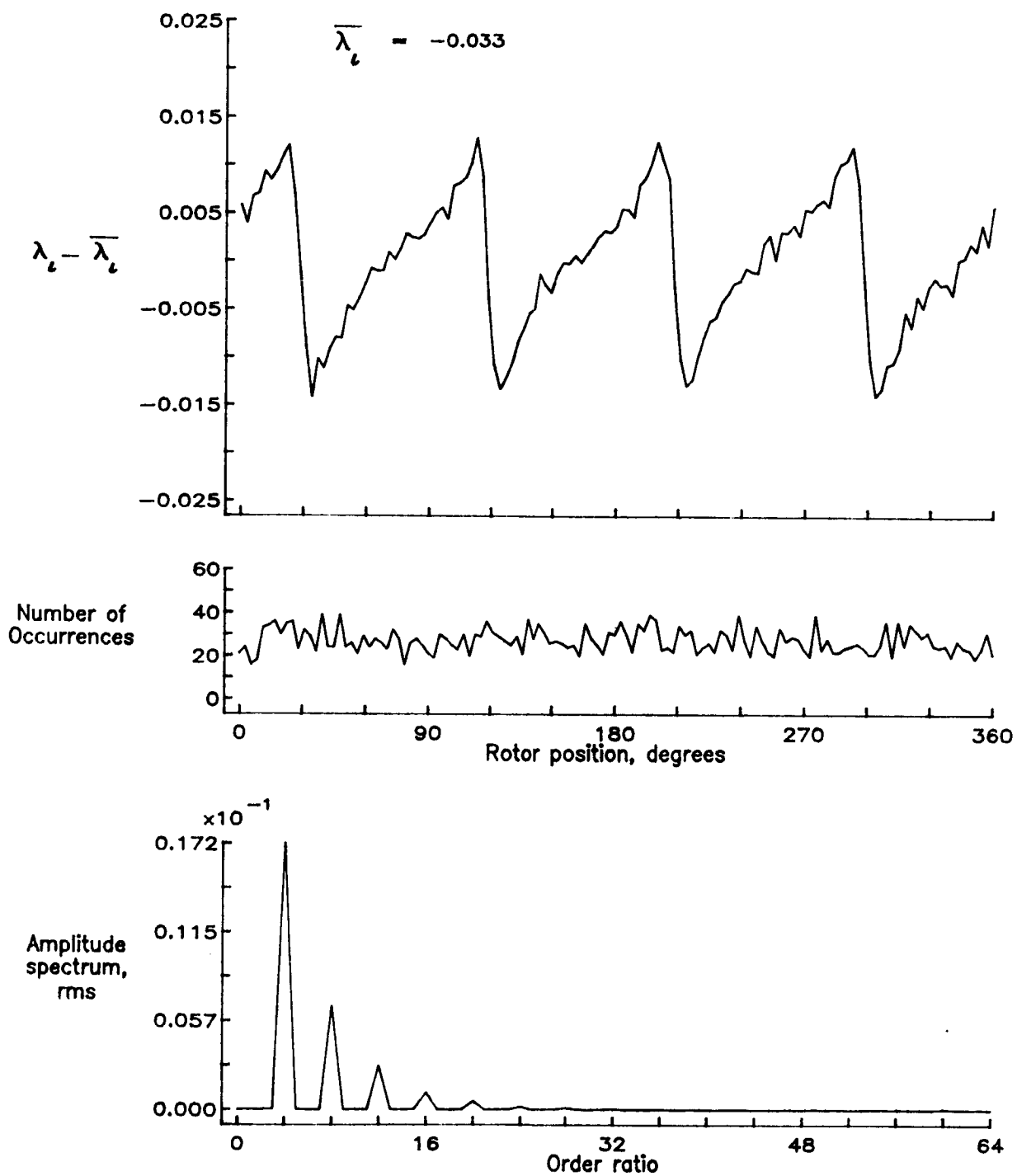


Figure 136.— Concluded.

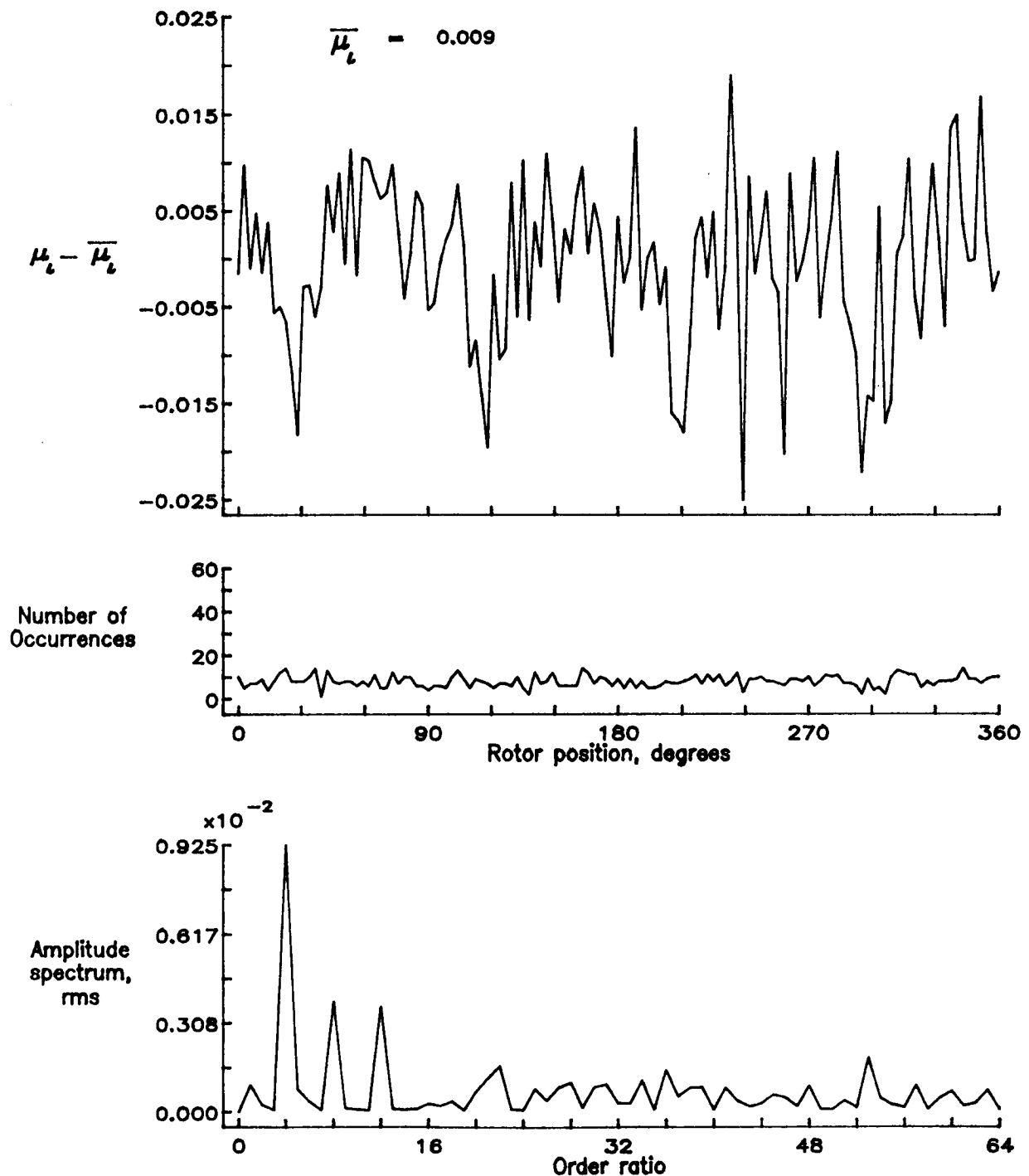


Figure 137.— Induced inflow velocity measured at 300 degrees and  $r/R$  of 0.82.

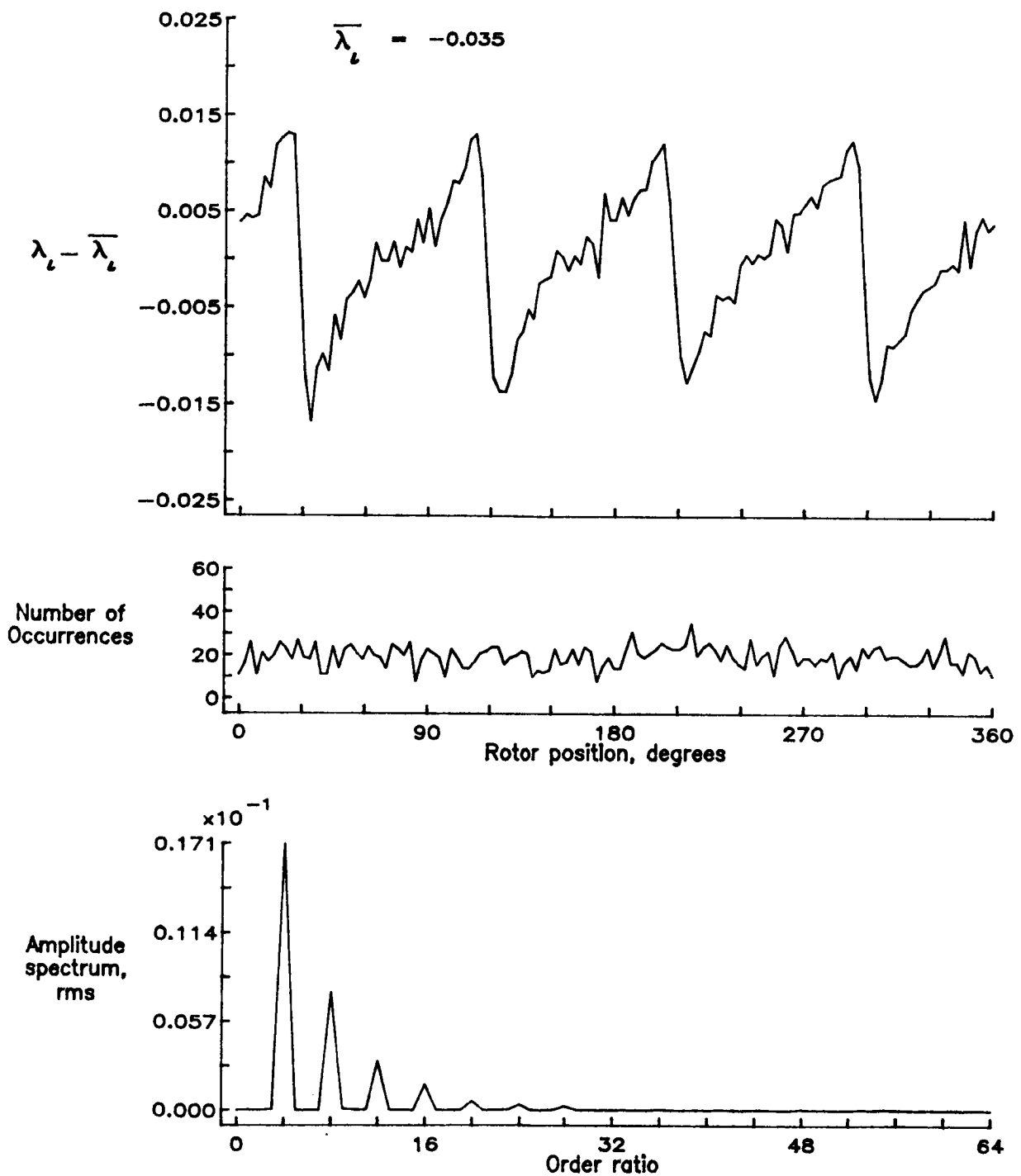


Figure 137.— Concluded.

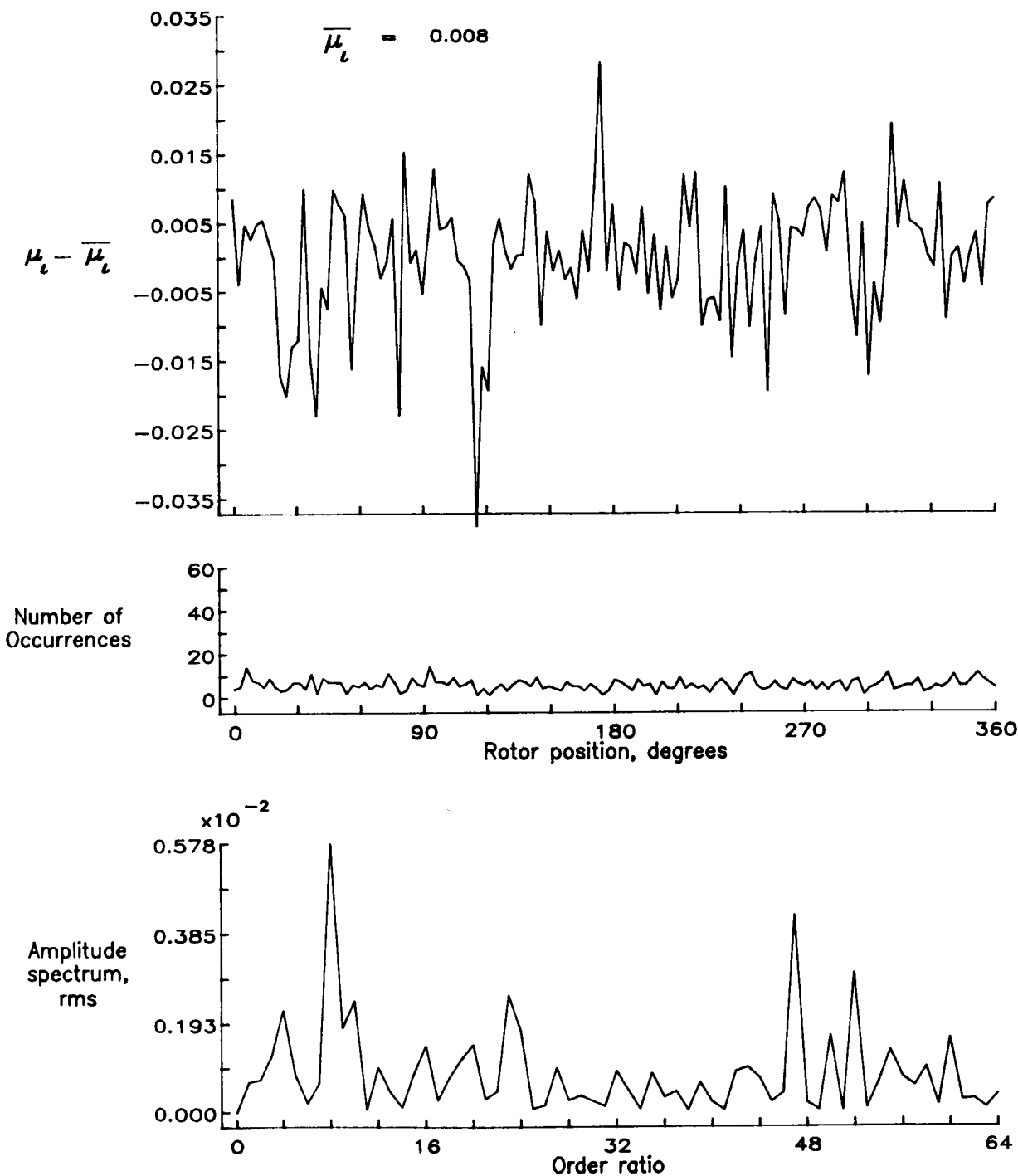


Figure 138.— Induced inflow velocity measured at 300 degrees and  $r/R$  of 0.86.

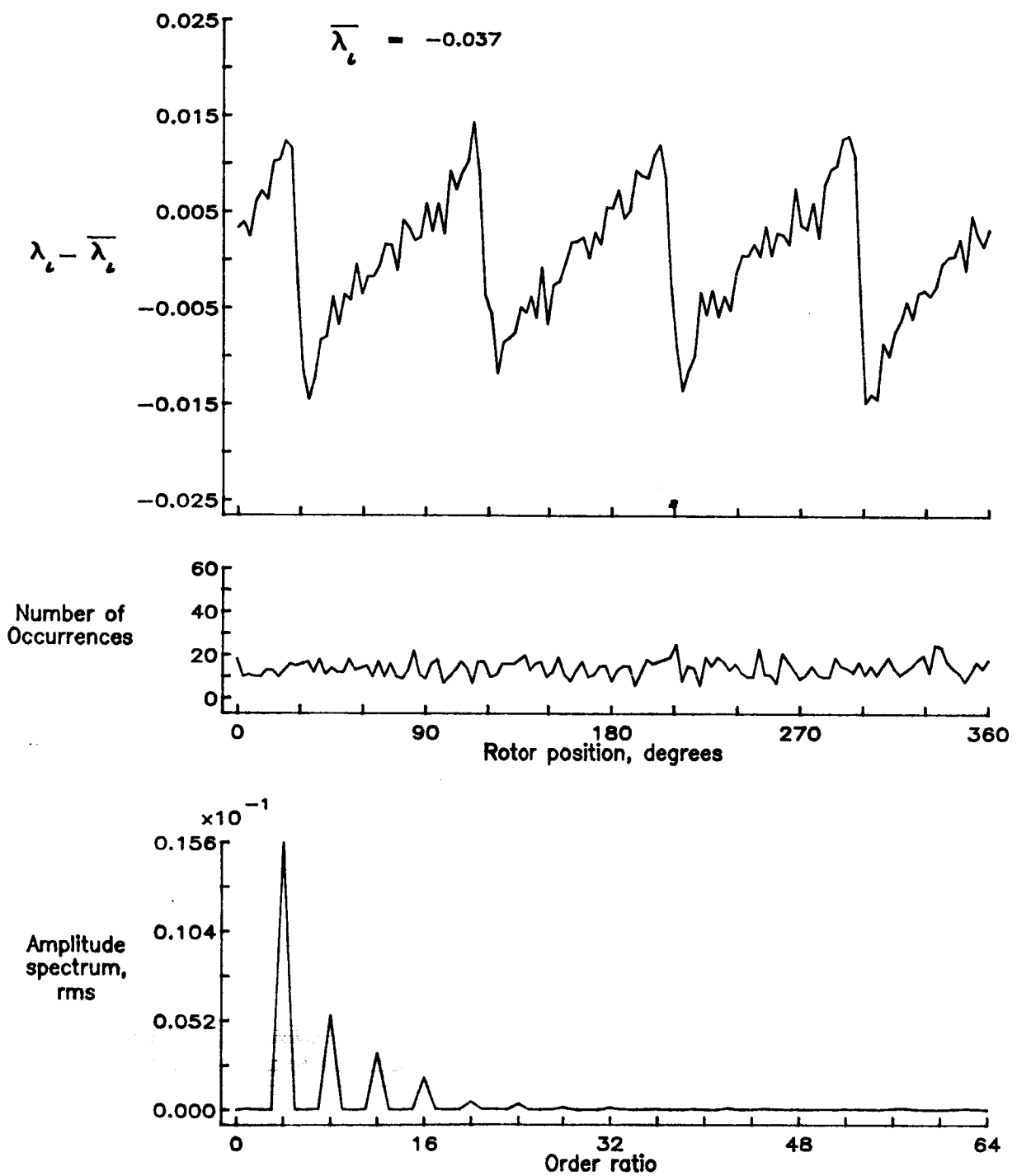


Figure 138.— Concluded.

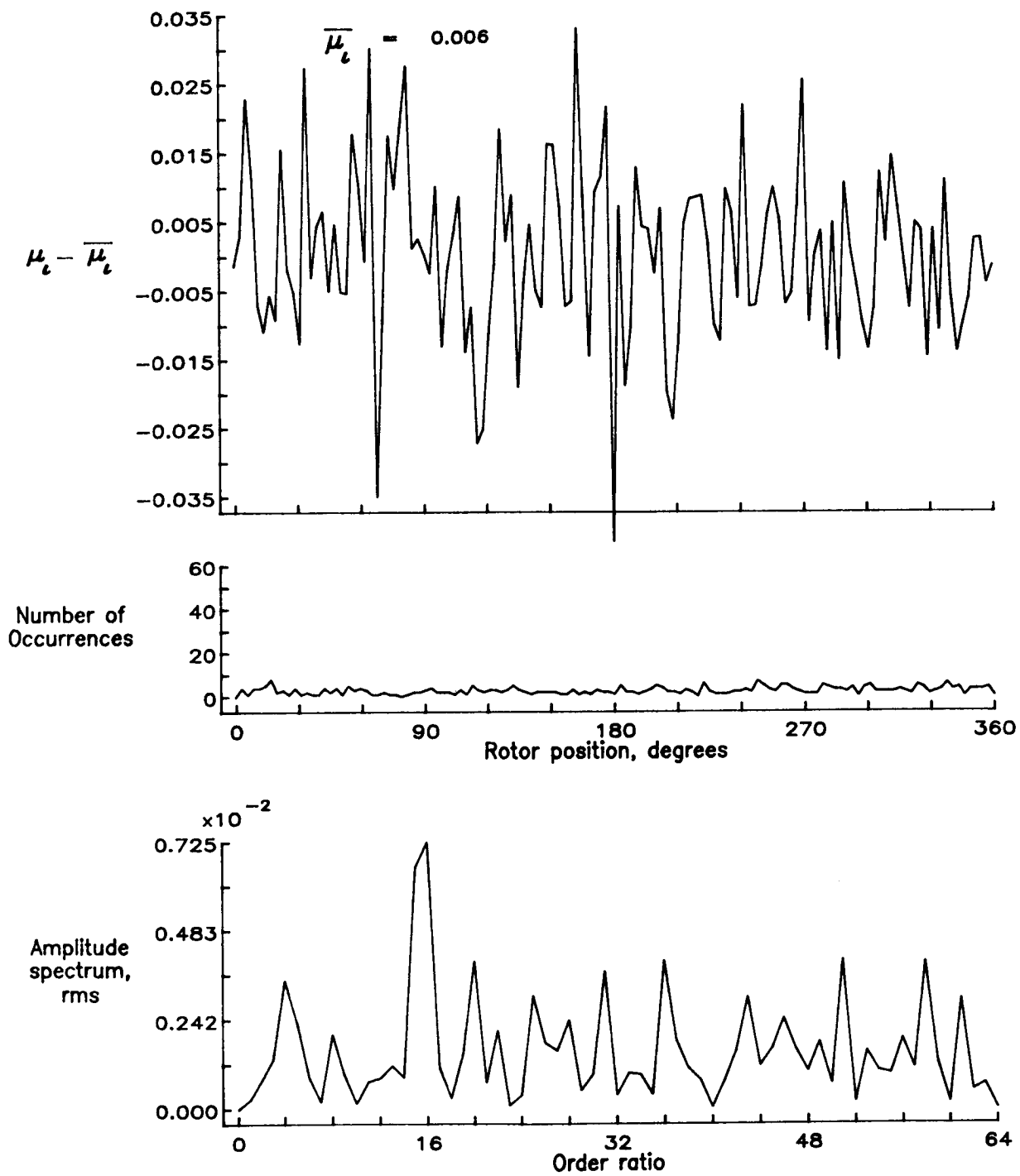


Figure 139.— Induced inflow velocity measured at 300 degrees and  $r/R$  of 0.90.

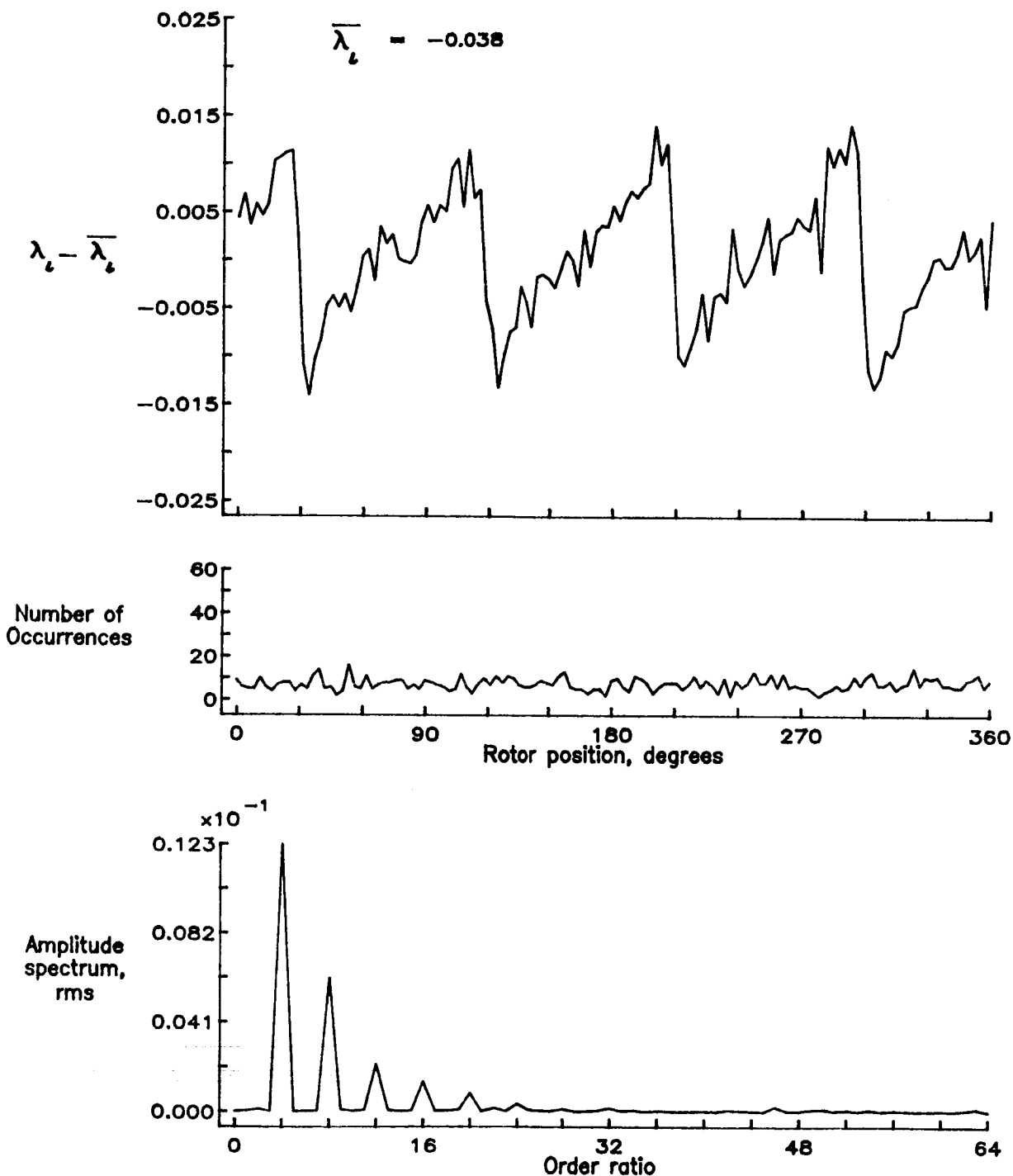


Figure 139.— Concluded.

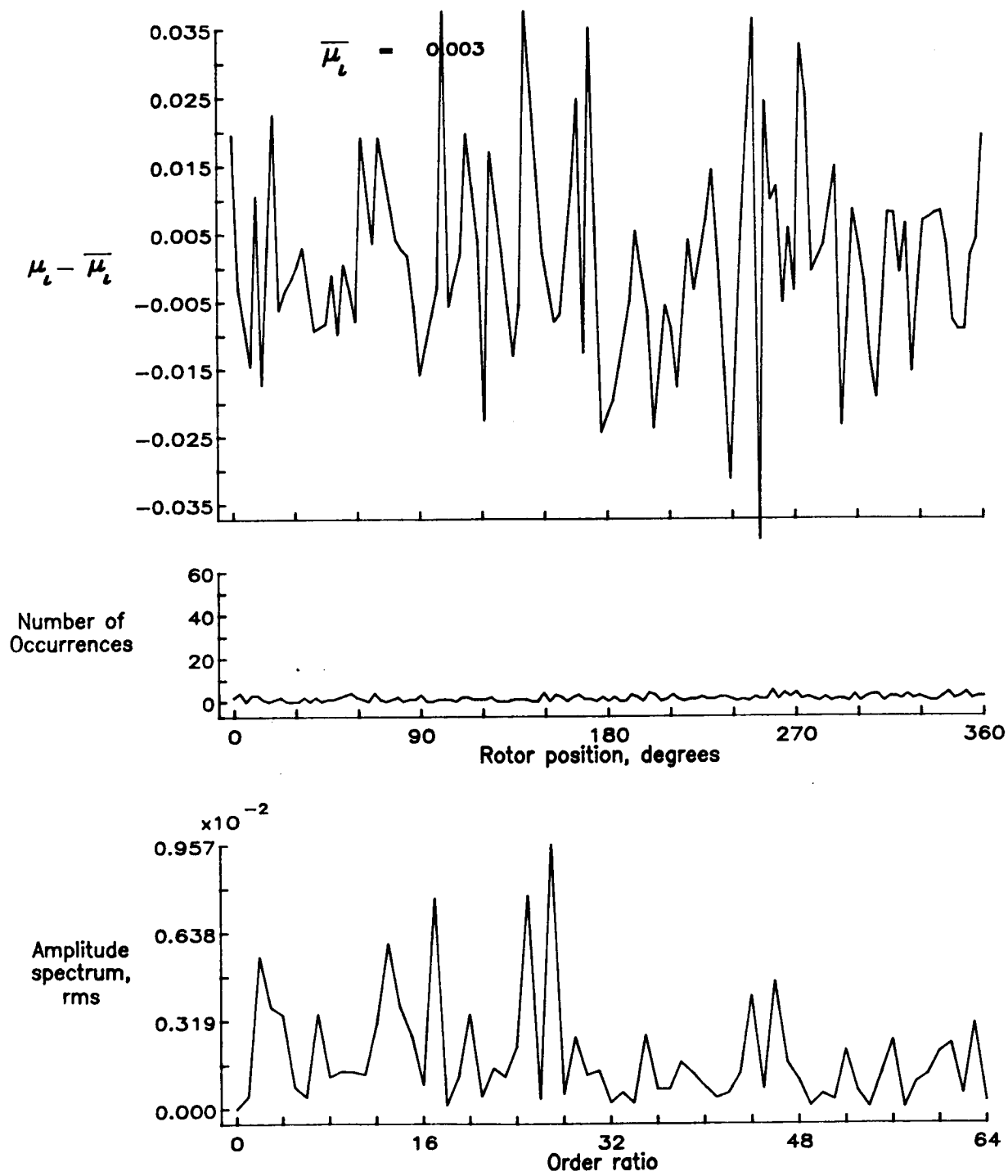


Figure 140.— Induced inflow velocity measured at 300 degrees and r/R of 0.94.

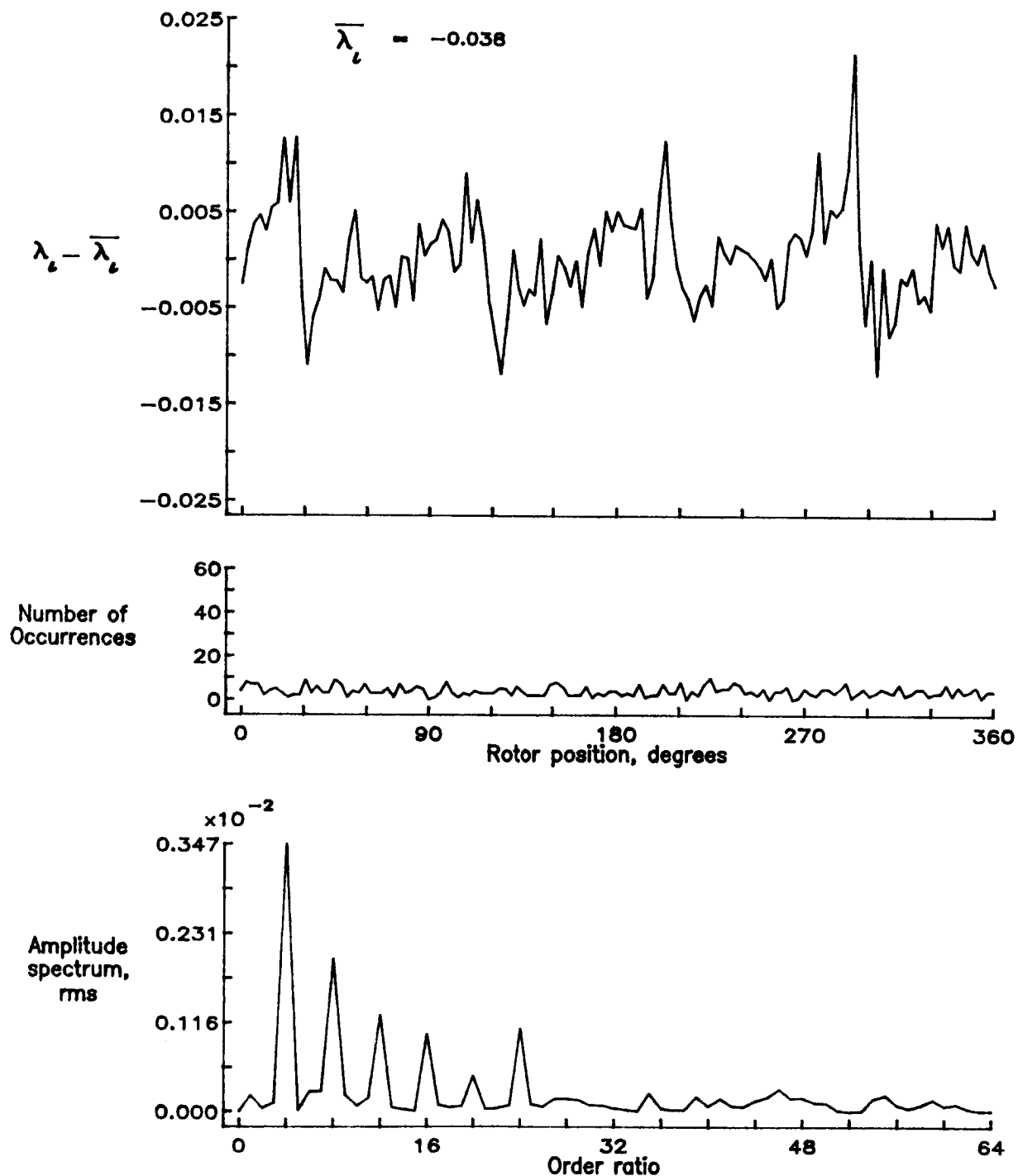


Figure 140.— Concluded.

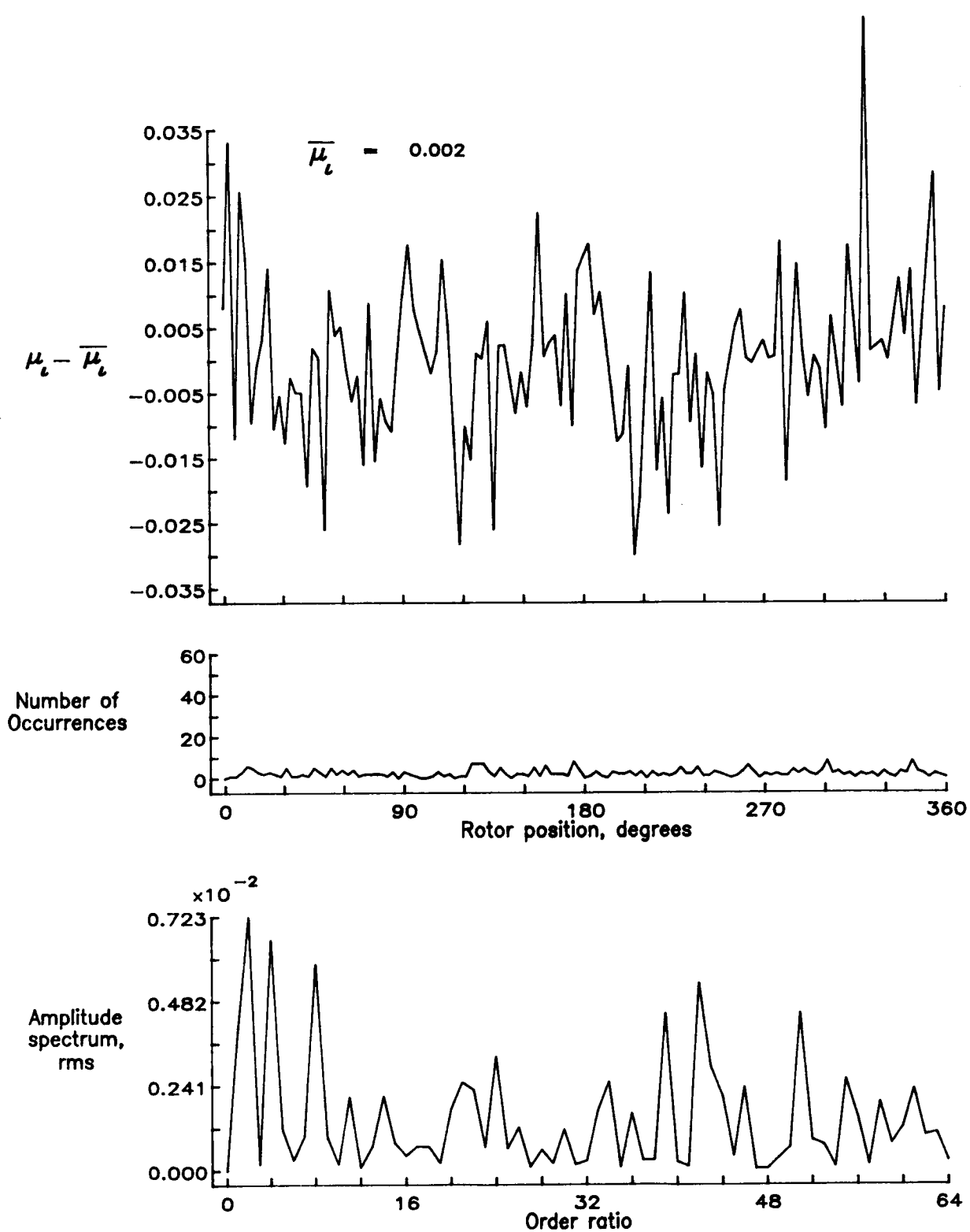


Figure 141.— Induced inflow velocity measured at 300 degrees and r/R of 0.98.

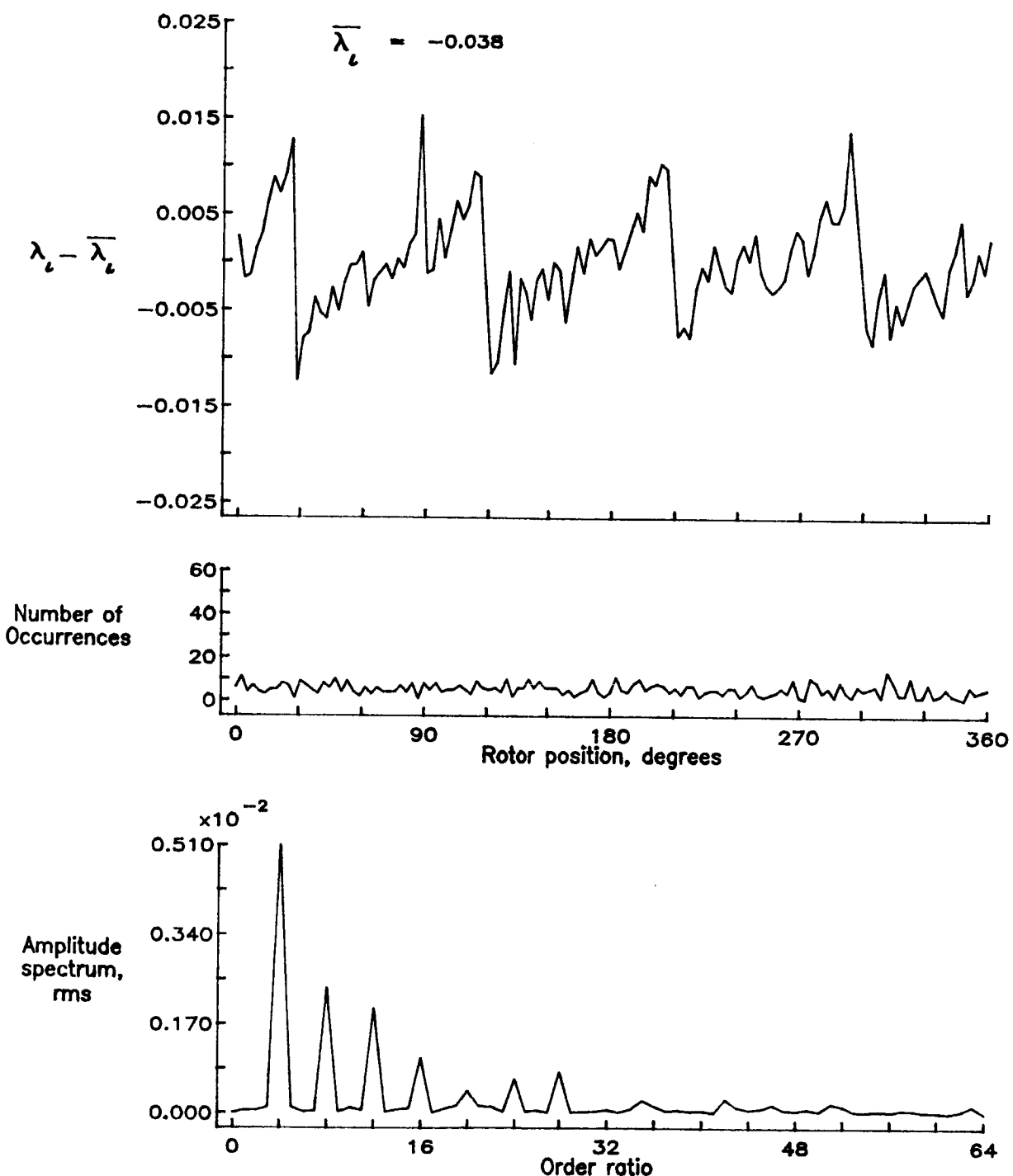


Figure 141.— Concluded.

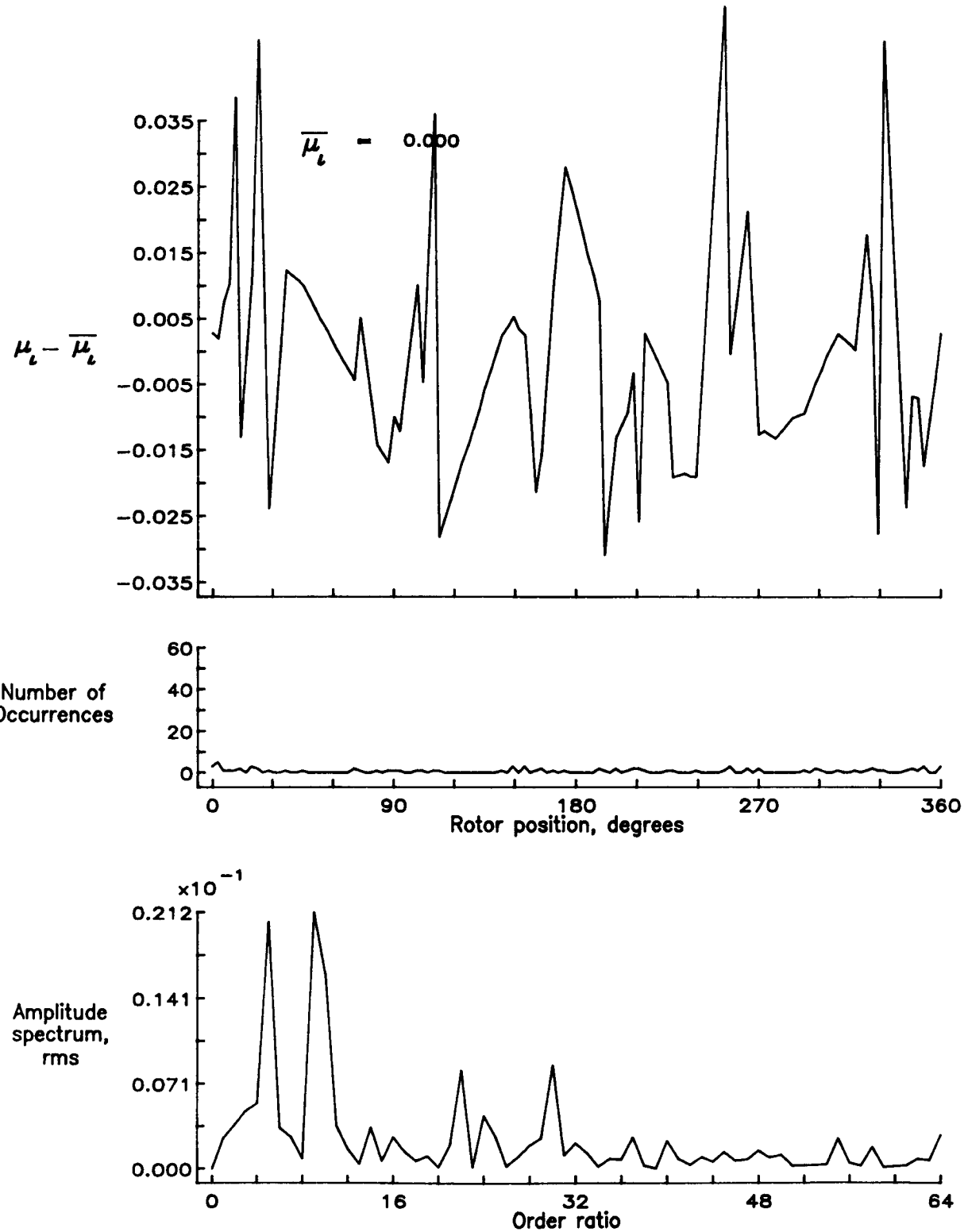


Figure 142.— Induced inflow velocity measured at 300 degrees and  $r/R$  of 1.02.

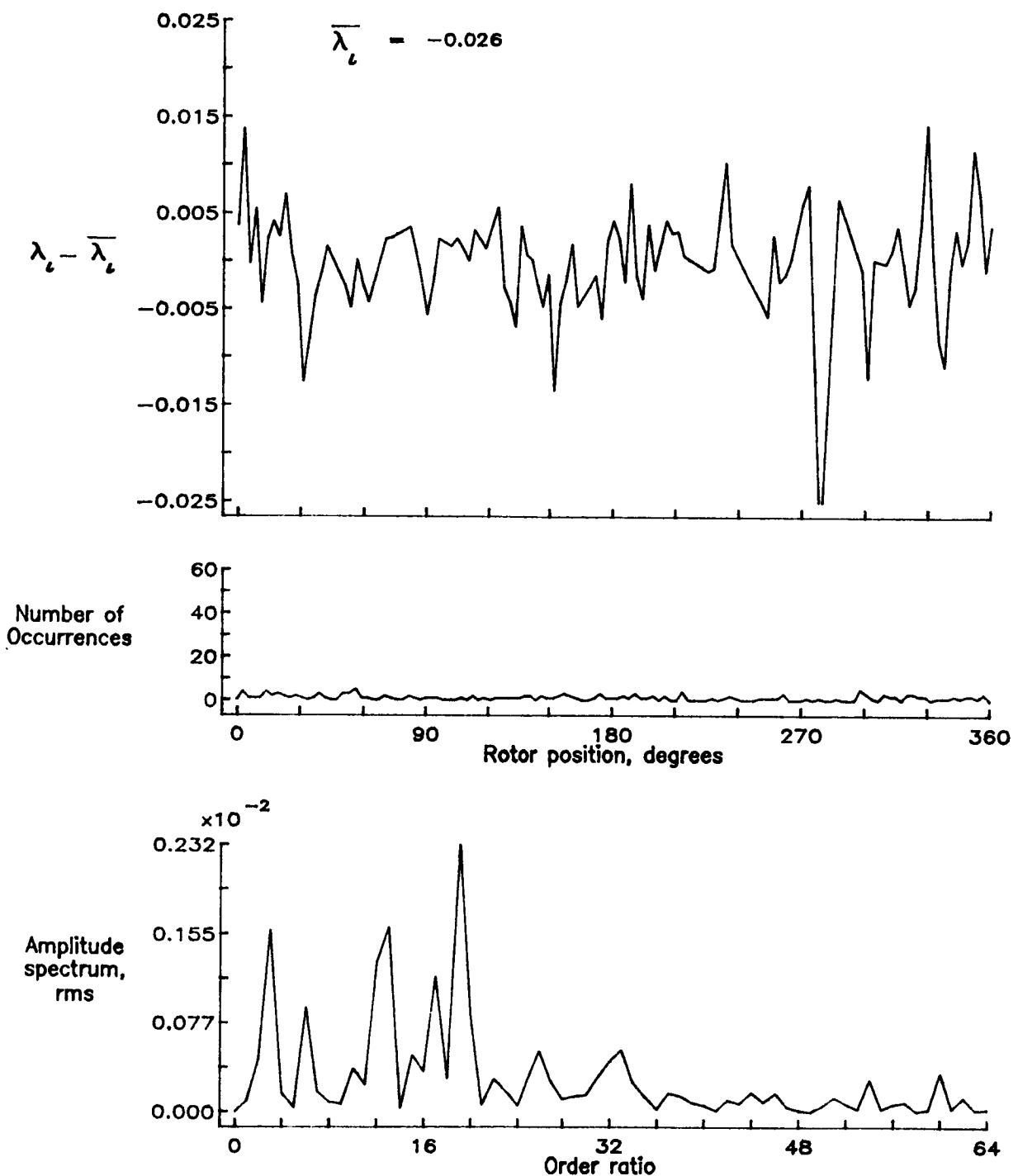


Figure 142.— Concluded.

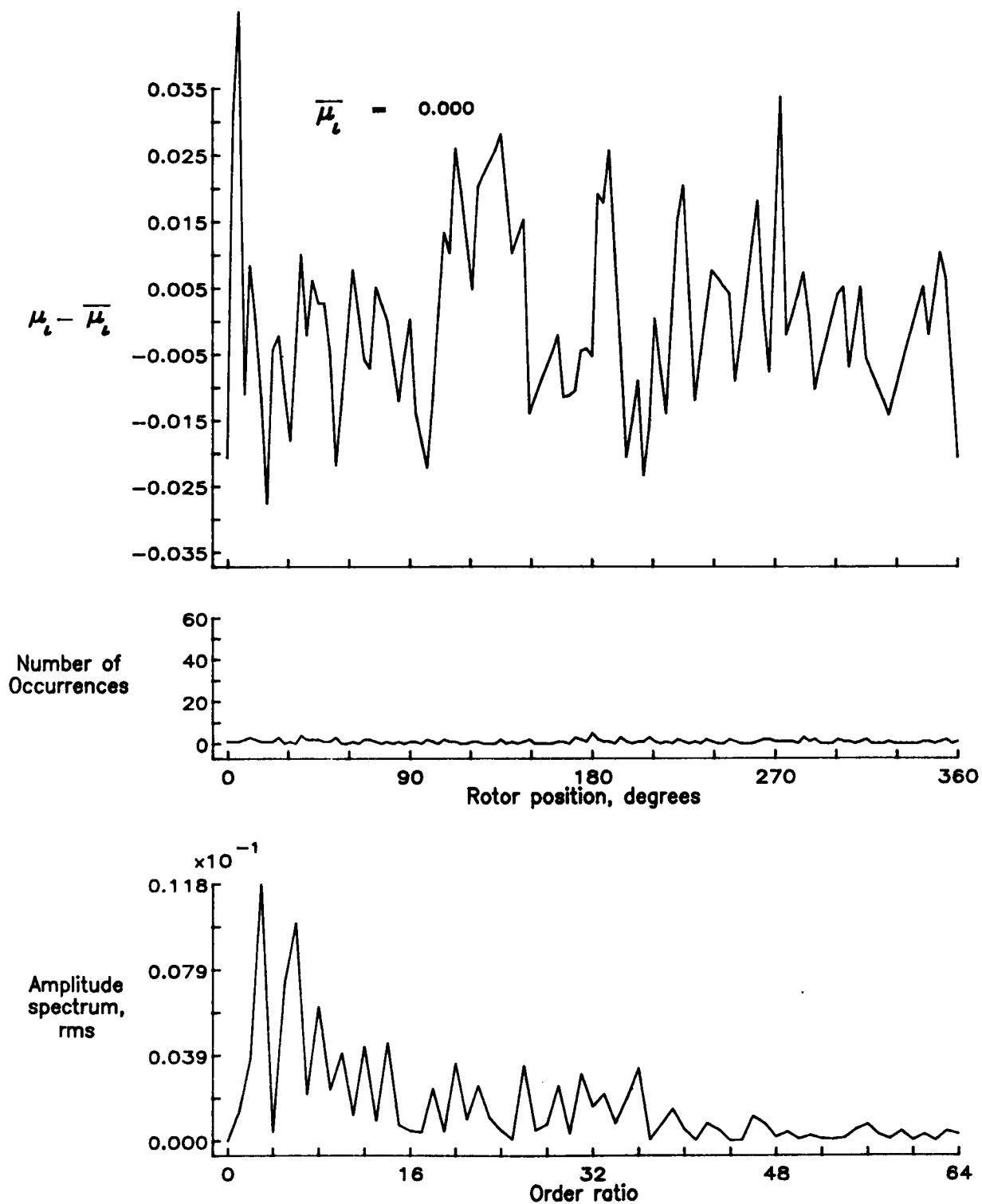


Figure 143.— Induced inflow velocity measured at 300 degrees and r/R of 1.04.

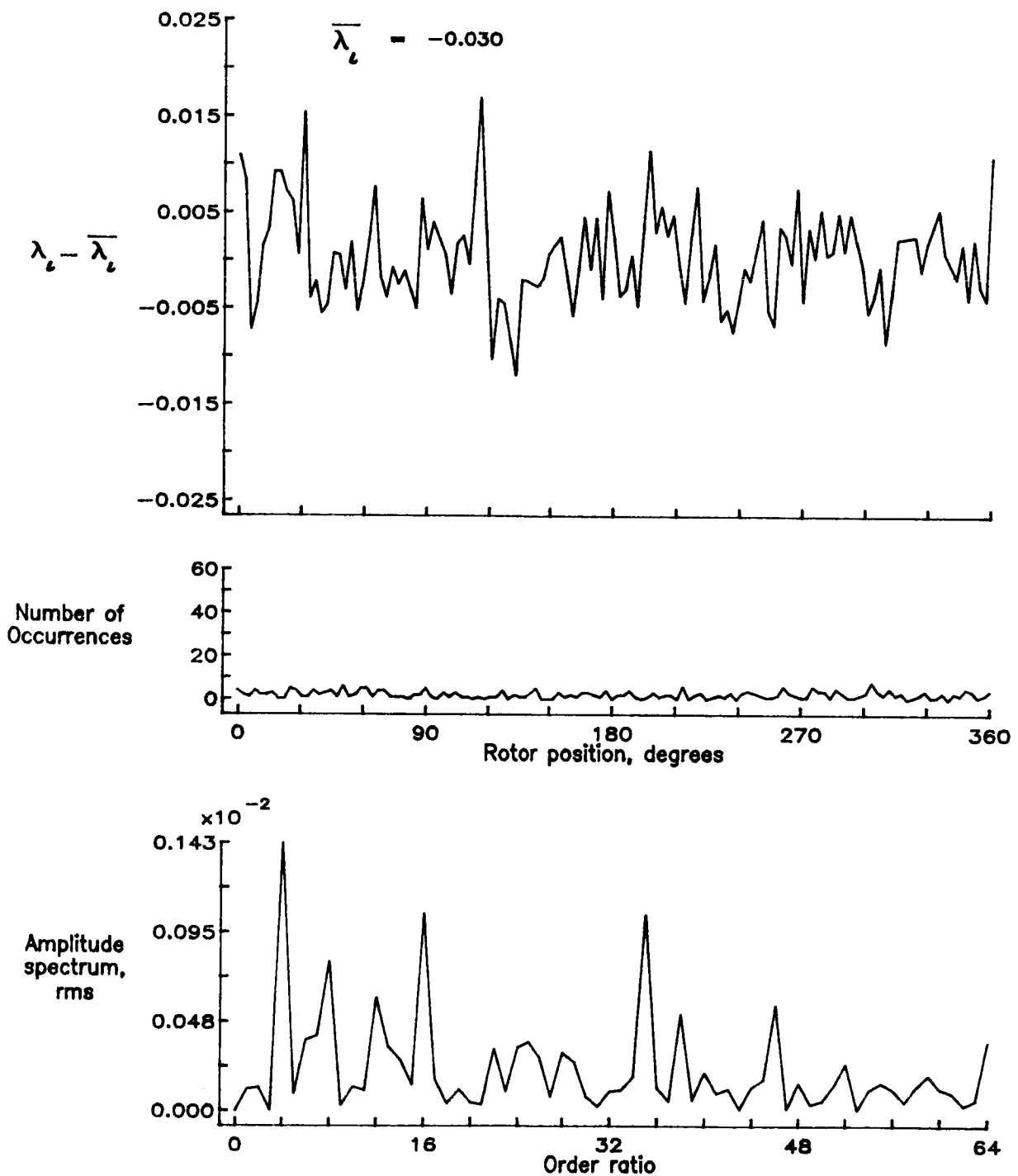


Figure 143.— Concluded.

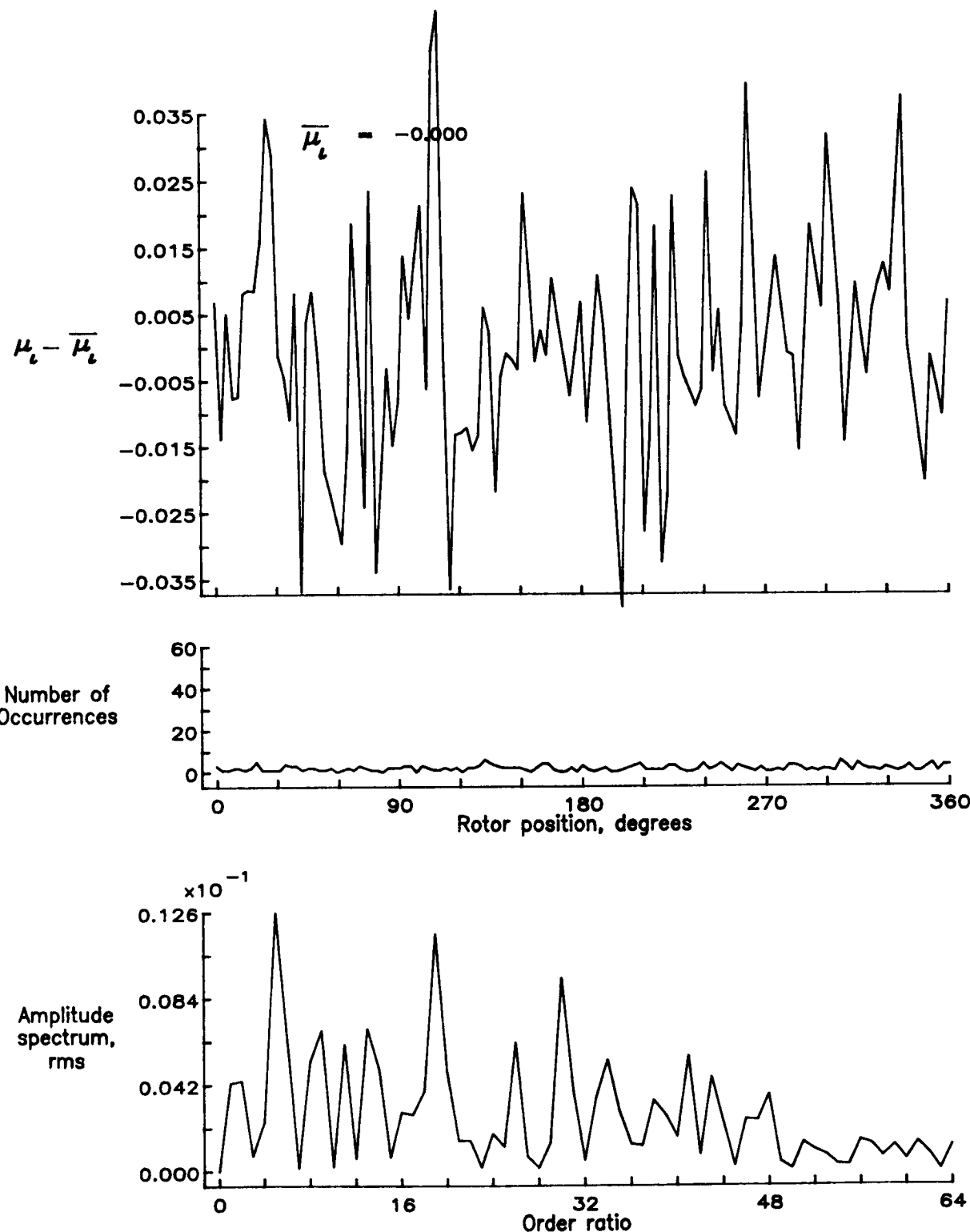


Figure 144.— Induced inflow velocity measured at 300 degrees and r/R of 1.10.

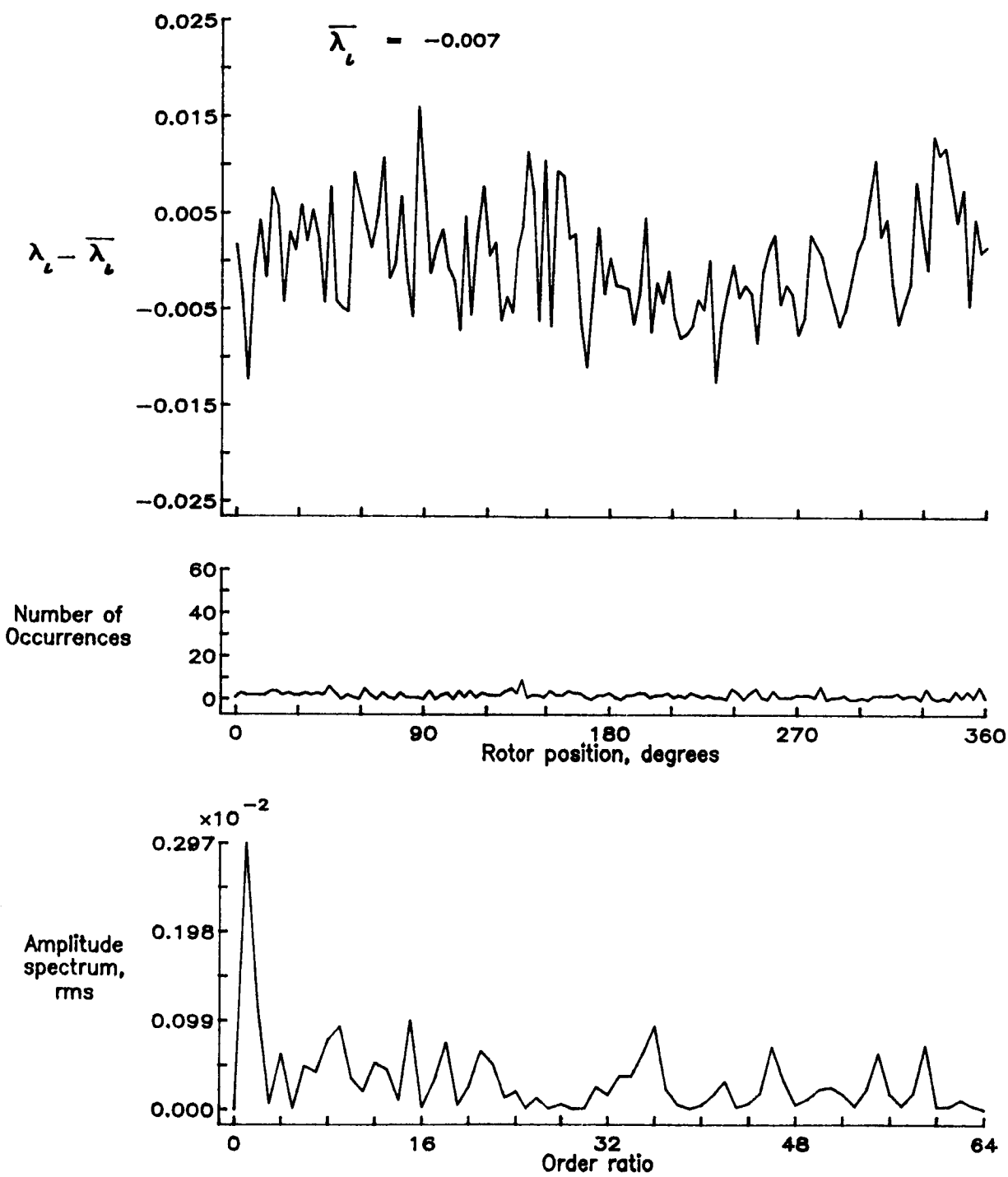


Figure 144.— Concluded.

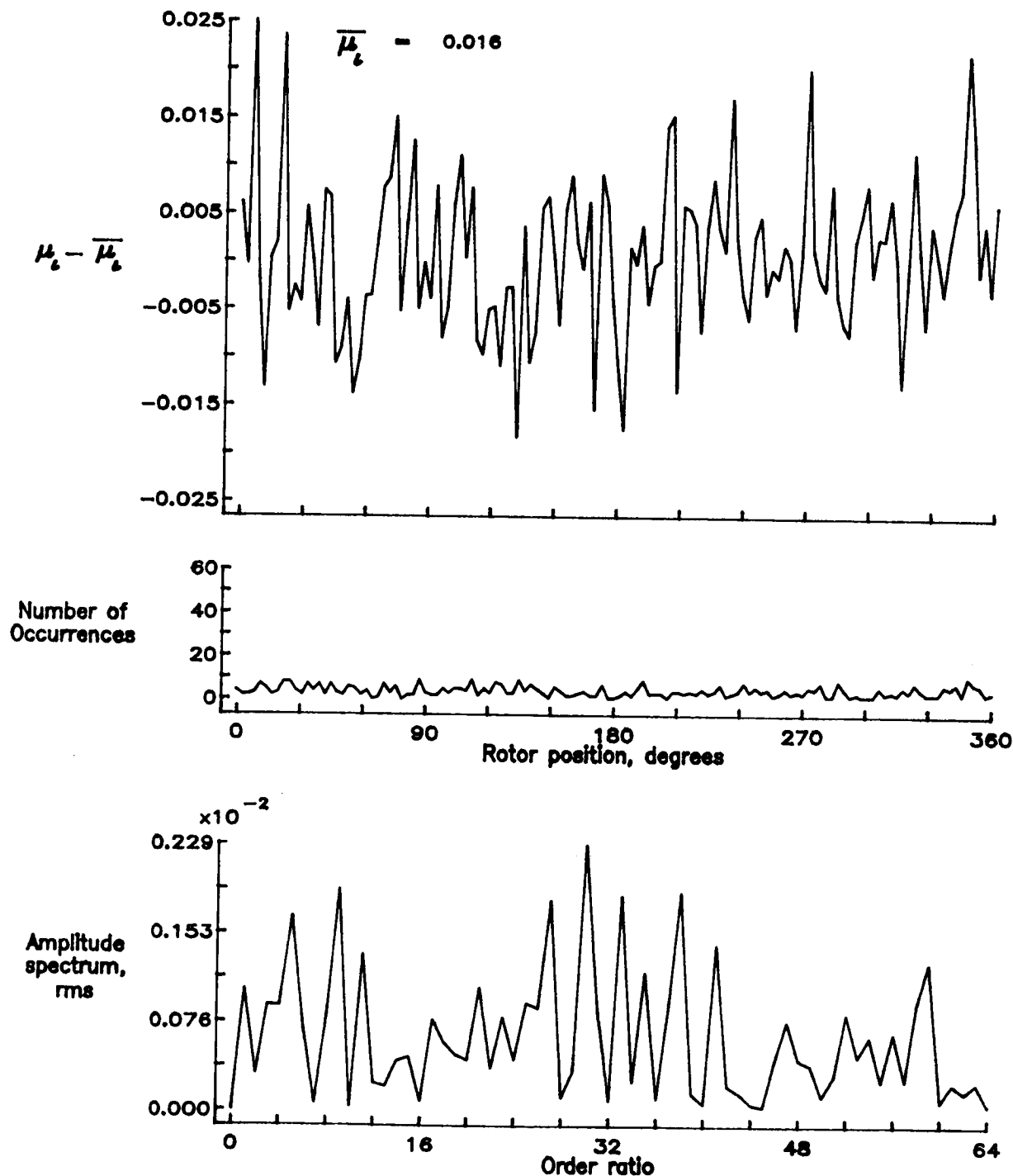


Figure 145.— Induced inflow velocity measured at 330 degrees and  $r/R$  of 0.20.

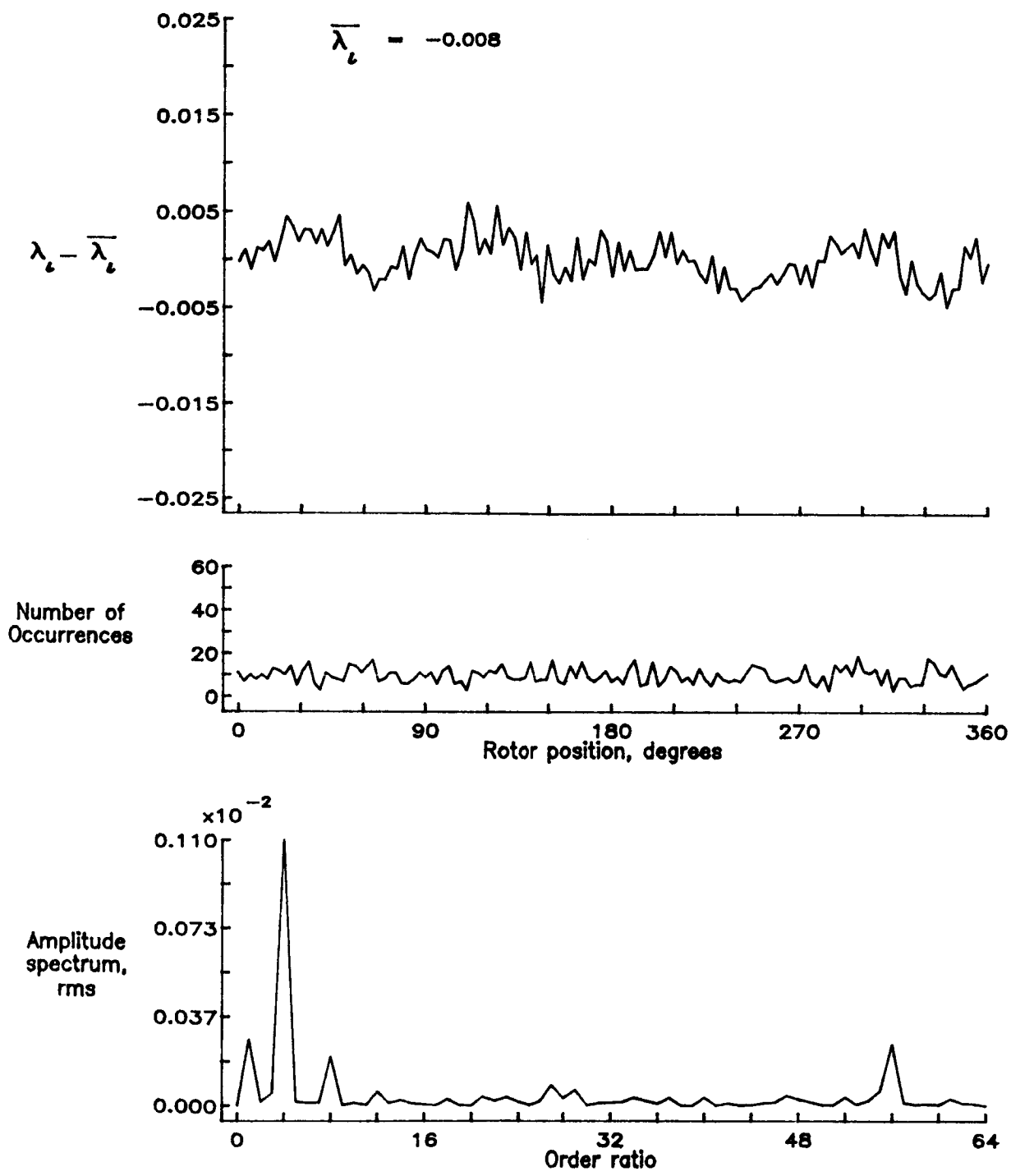


Figure 145.— Concluded.

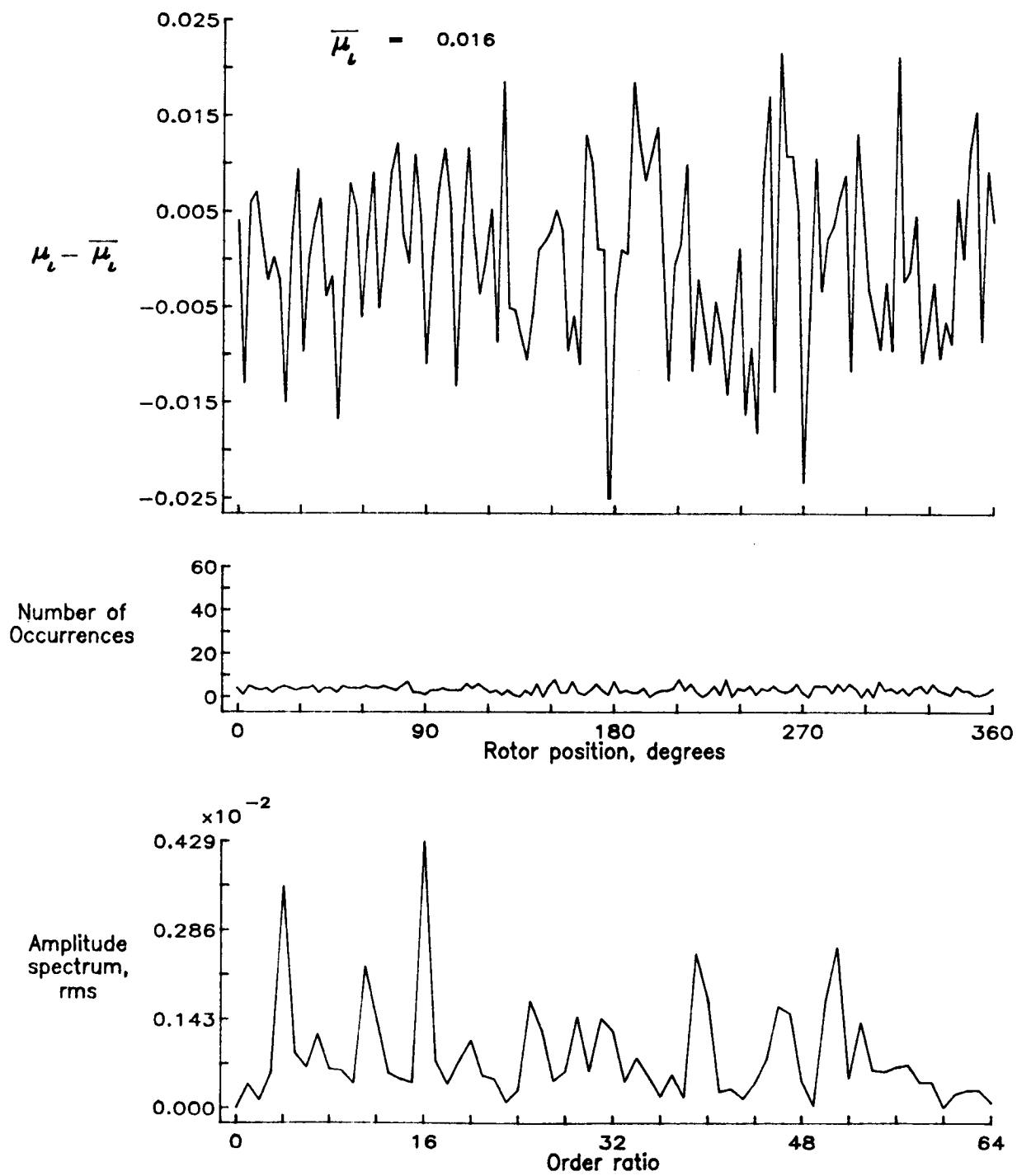


Figure 146.— Induced inflow velocity measured at 330 degrees and r/R of 0.40.

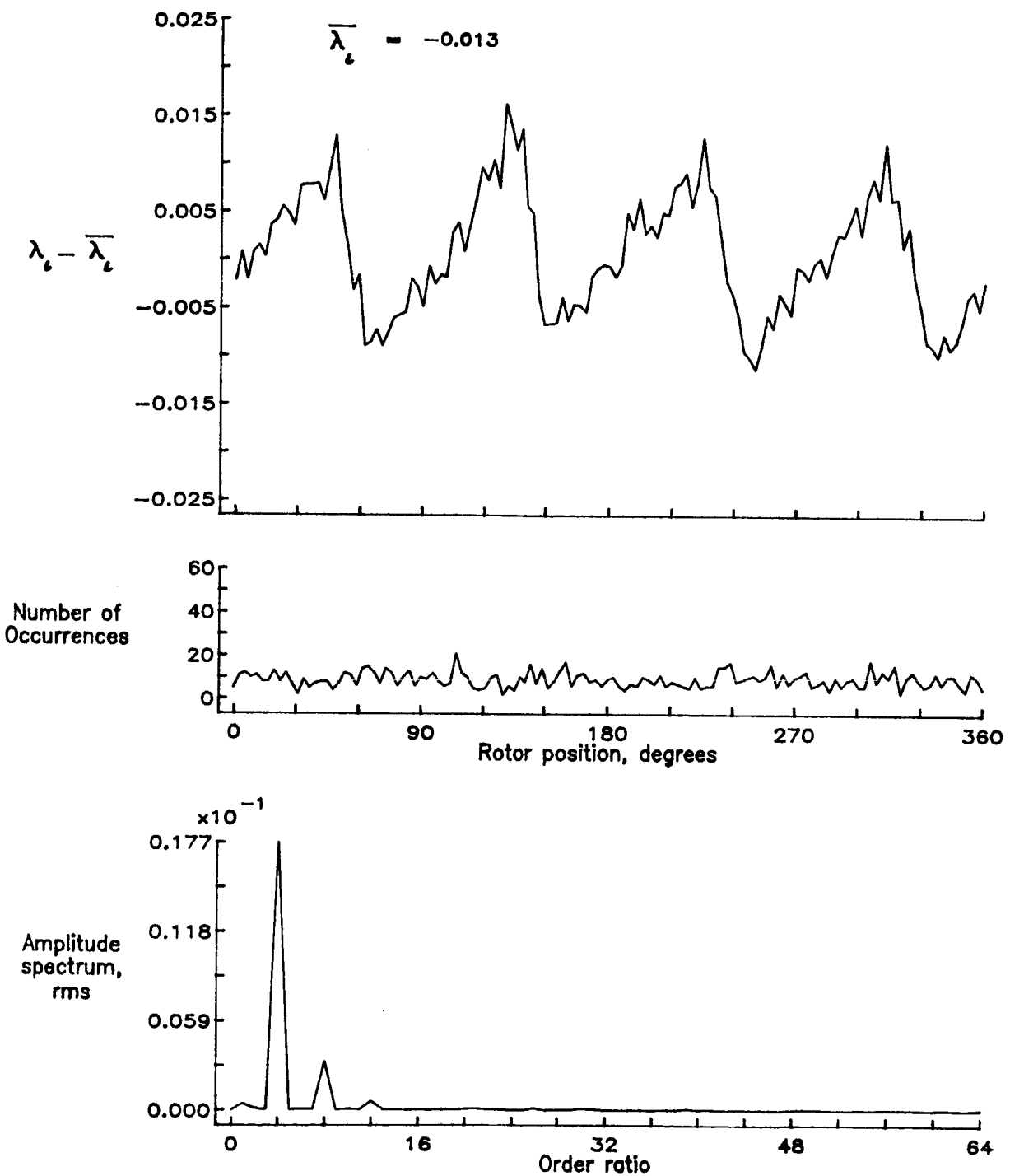


Figure 146.— Concluded.

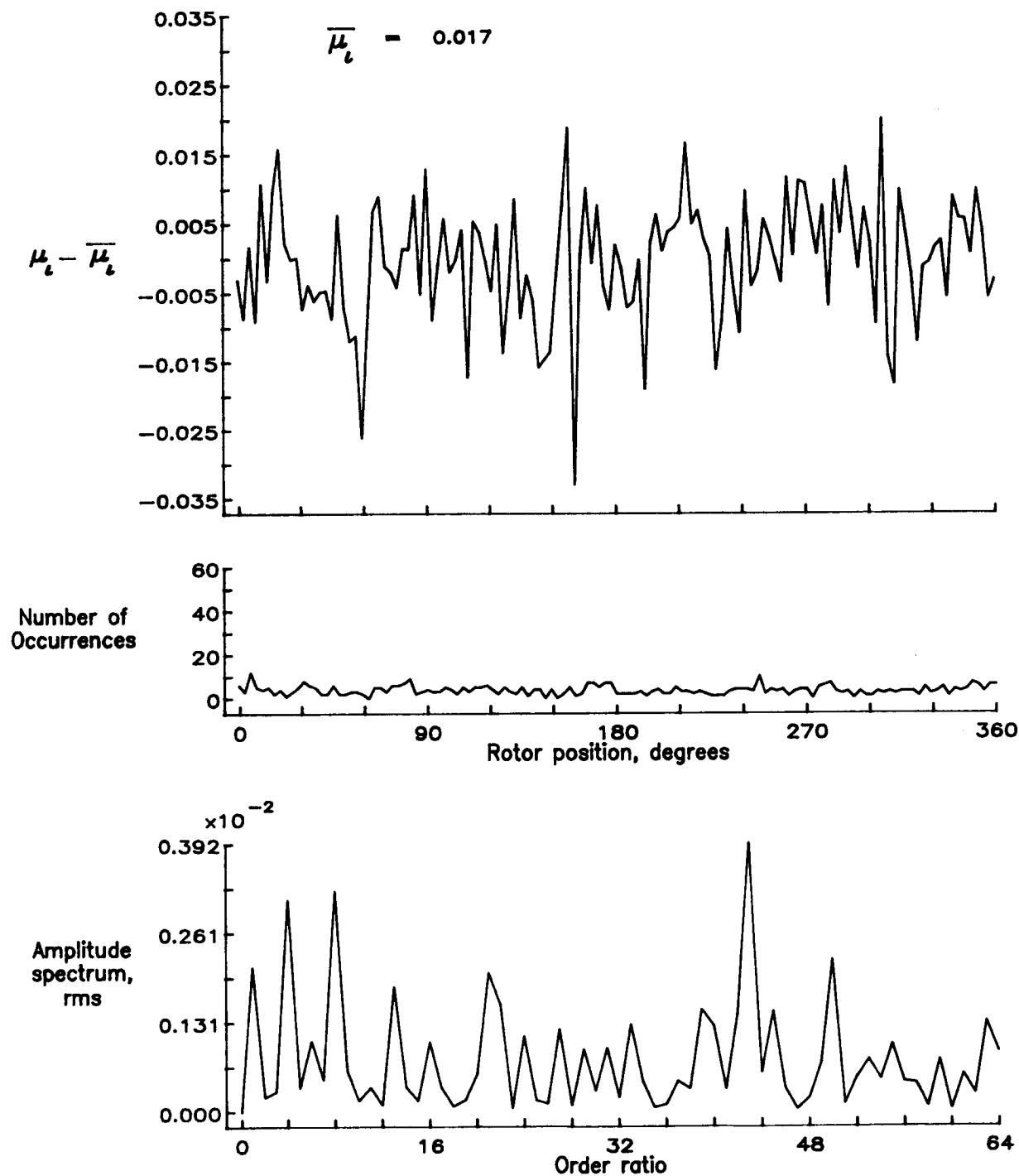


Figure 147.— Induced inflow velocity measured at 330 degrees and r/R of 0.50.

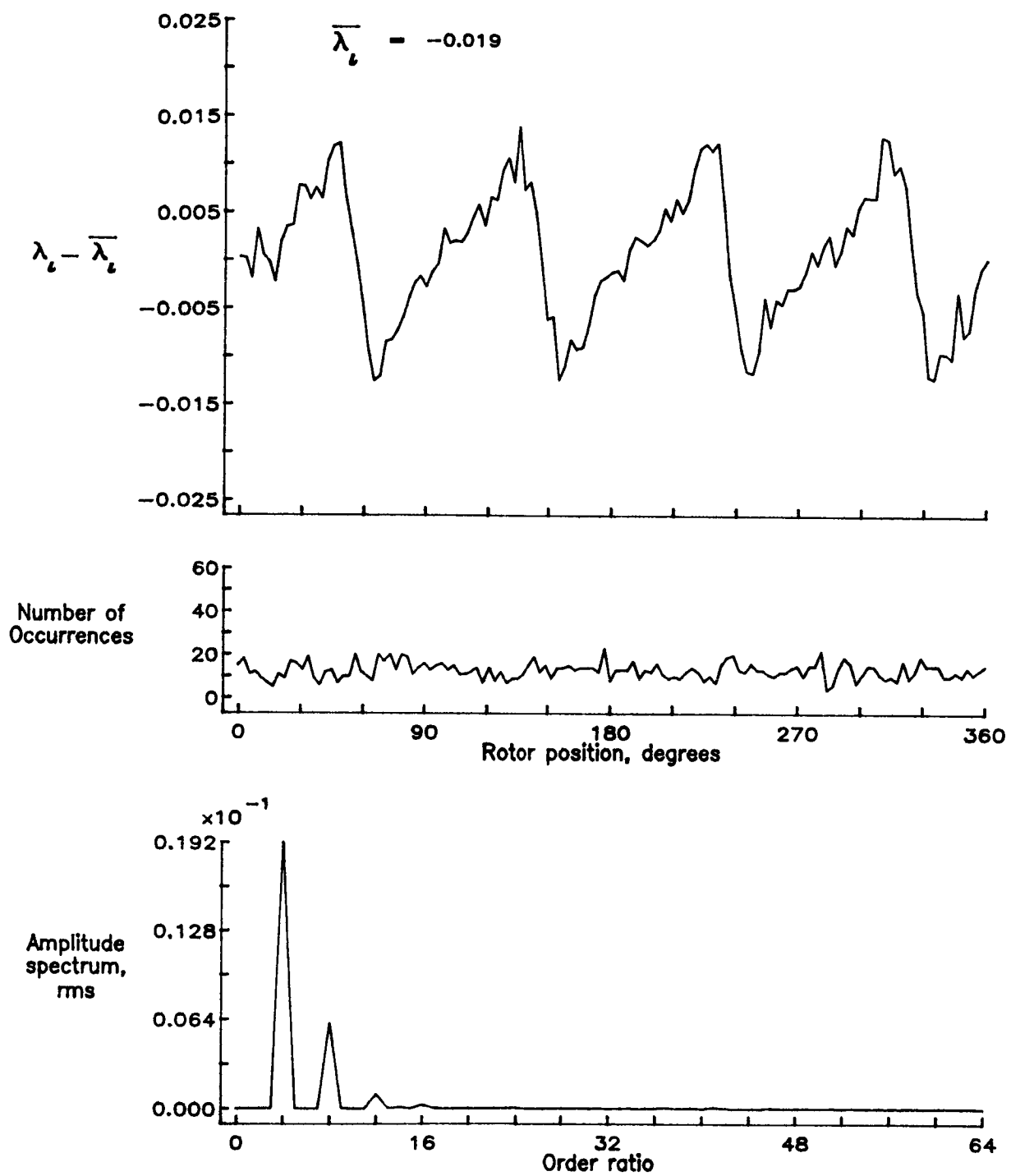


Figure 147.— Concluded.

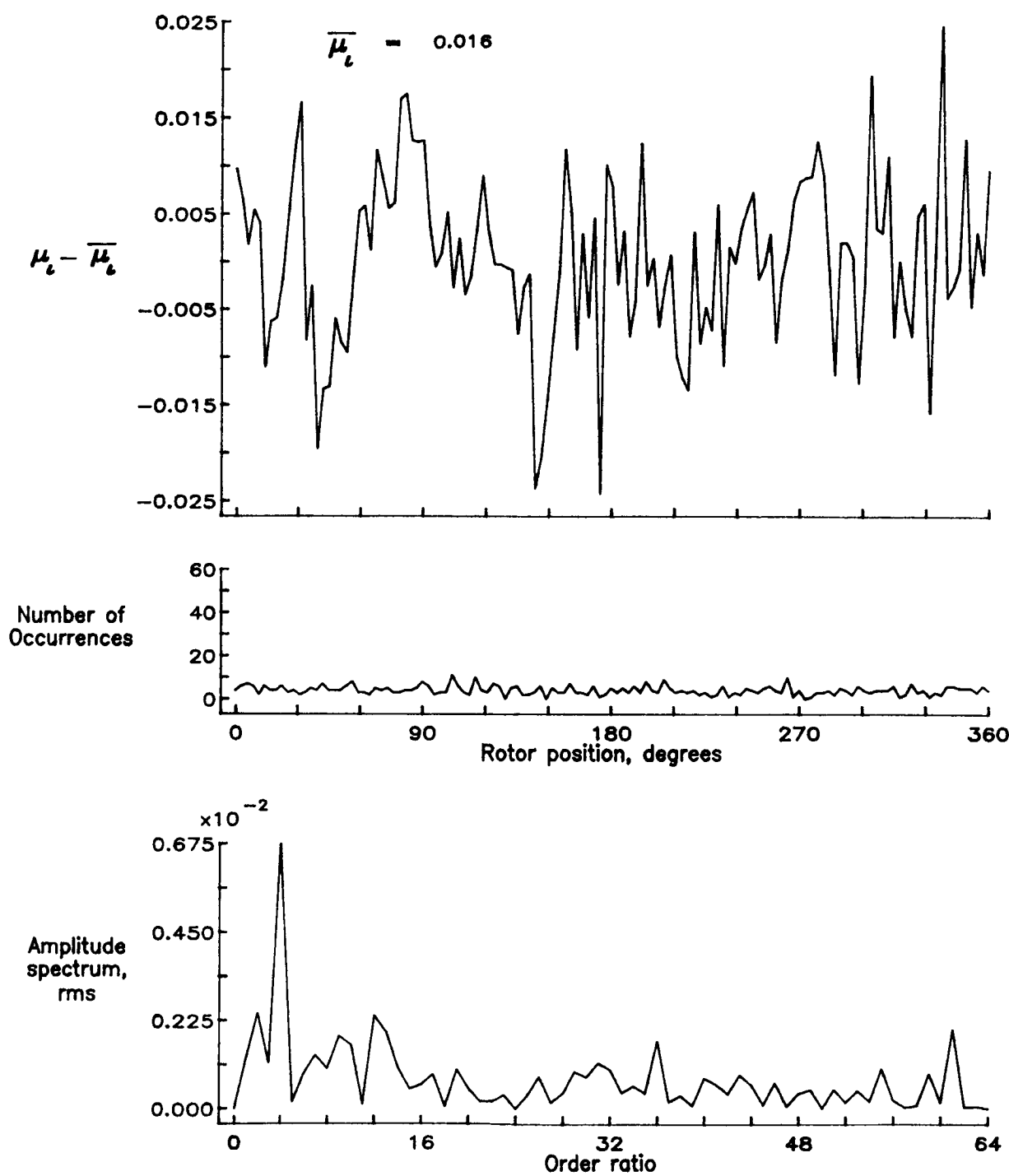


Figure 148.— Induced inflow velocity measured at 330 degrees and r/R of 0.60.

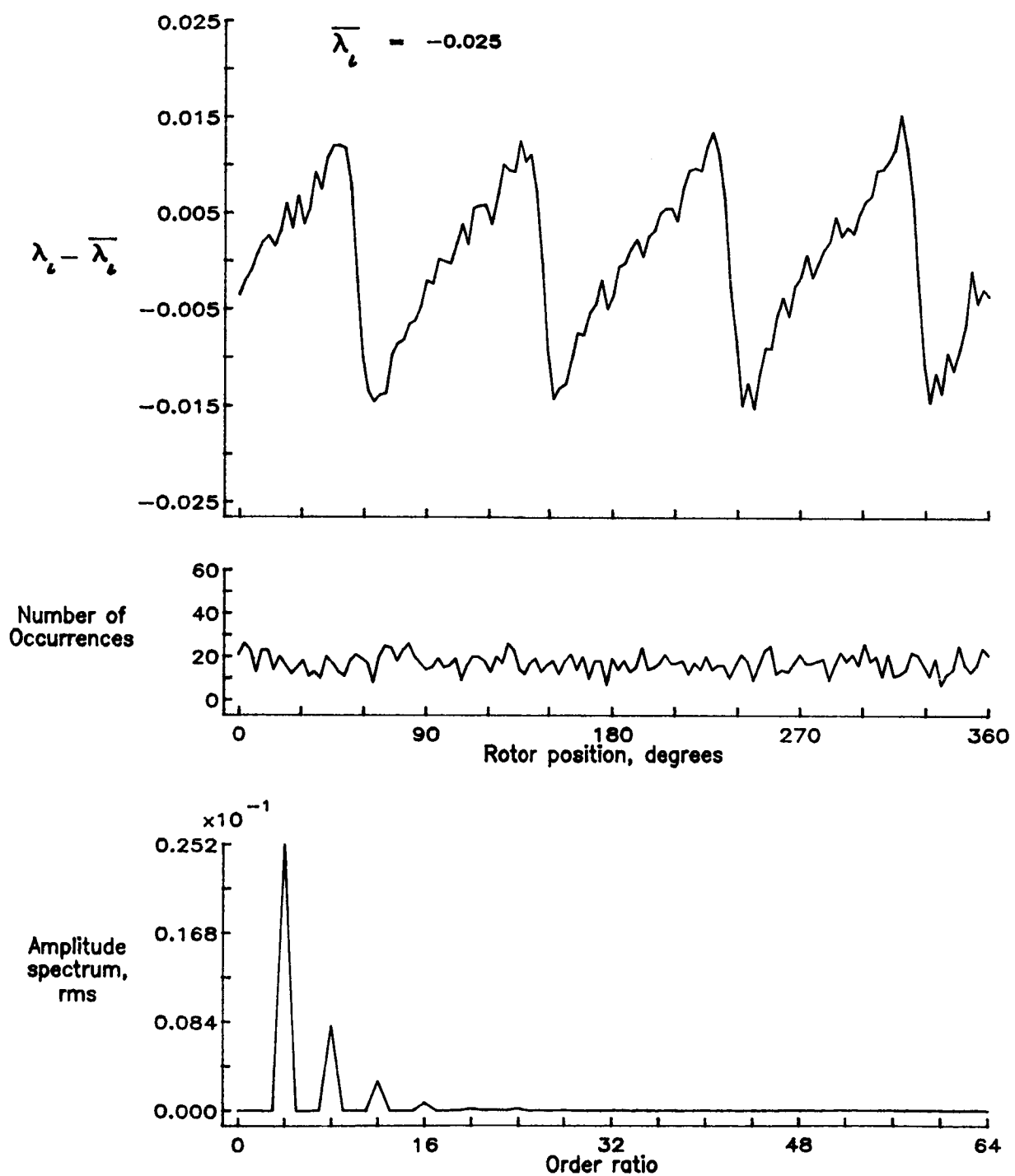


Figure 148.— Concluded.

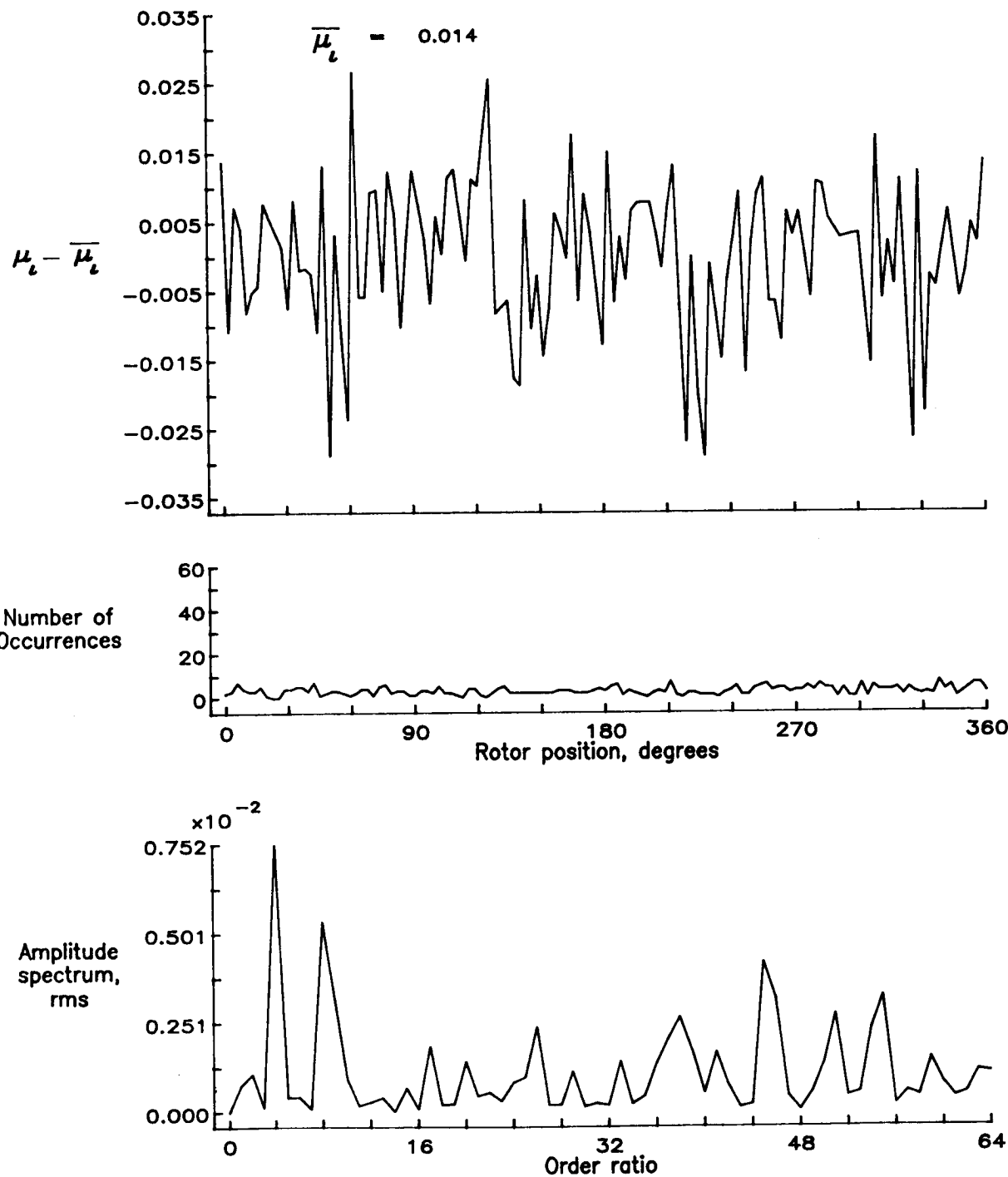


Figure 149.— Induced inflow velocity measured at 330 degrees and r/R of 0.74.

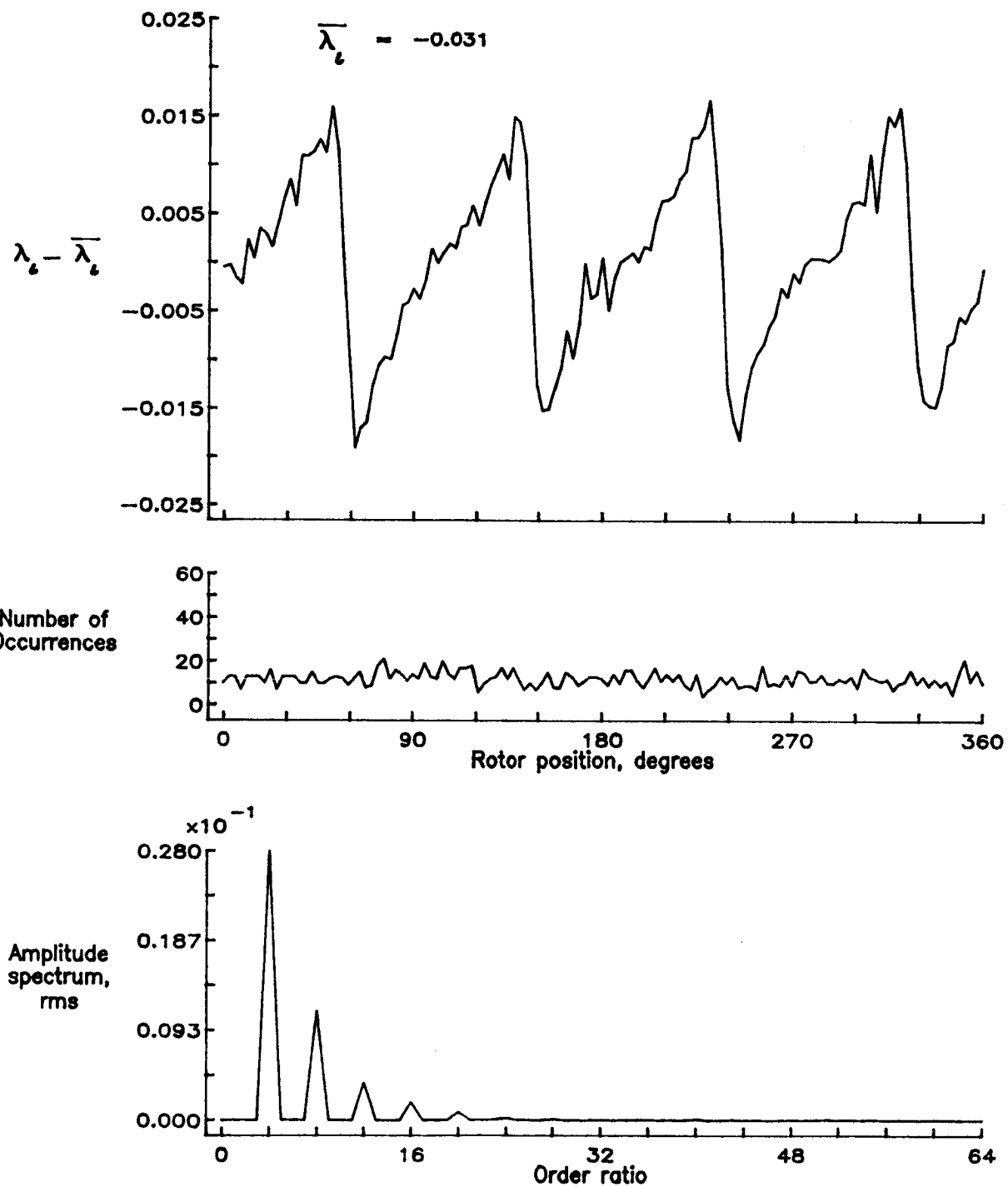


Figure 149.— Concluded.

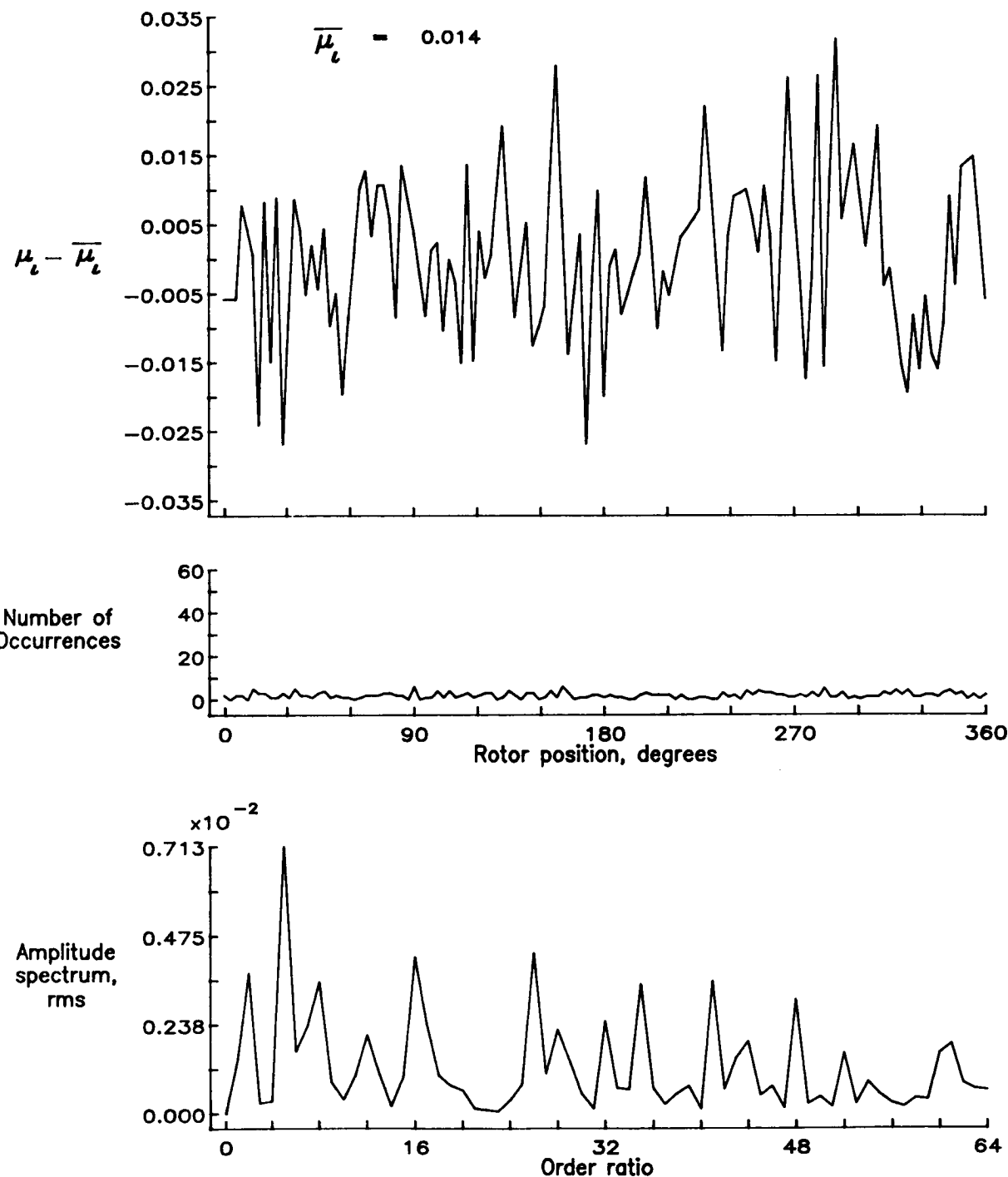


Figure 150.— Induced inflow velocity measured at 330 degrees and r/R of 0.78.

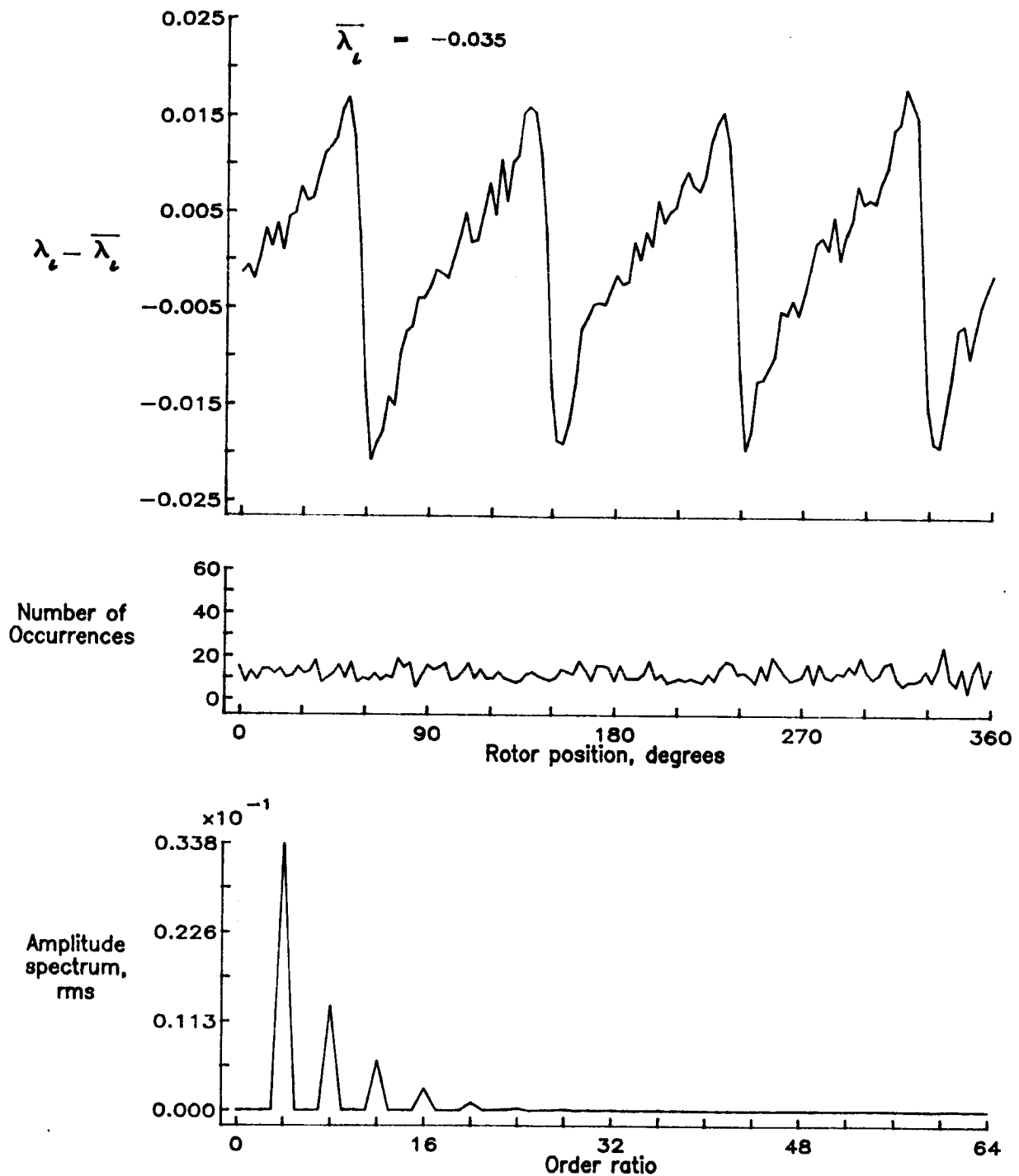


Figure 150.— Concluded.

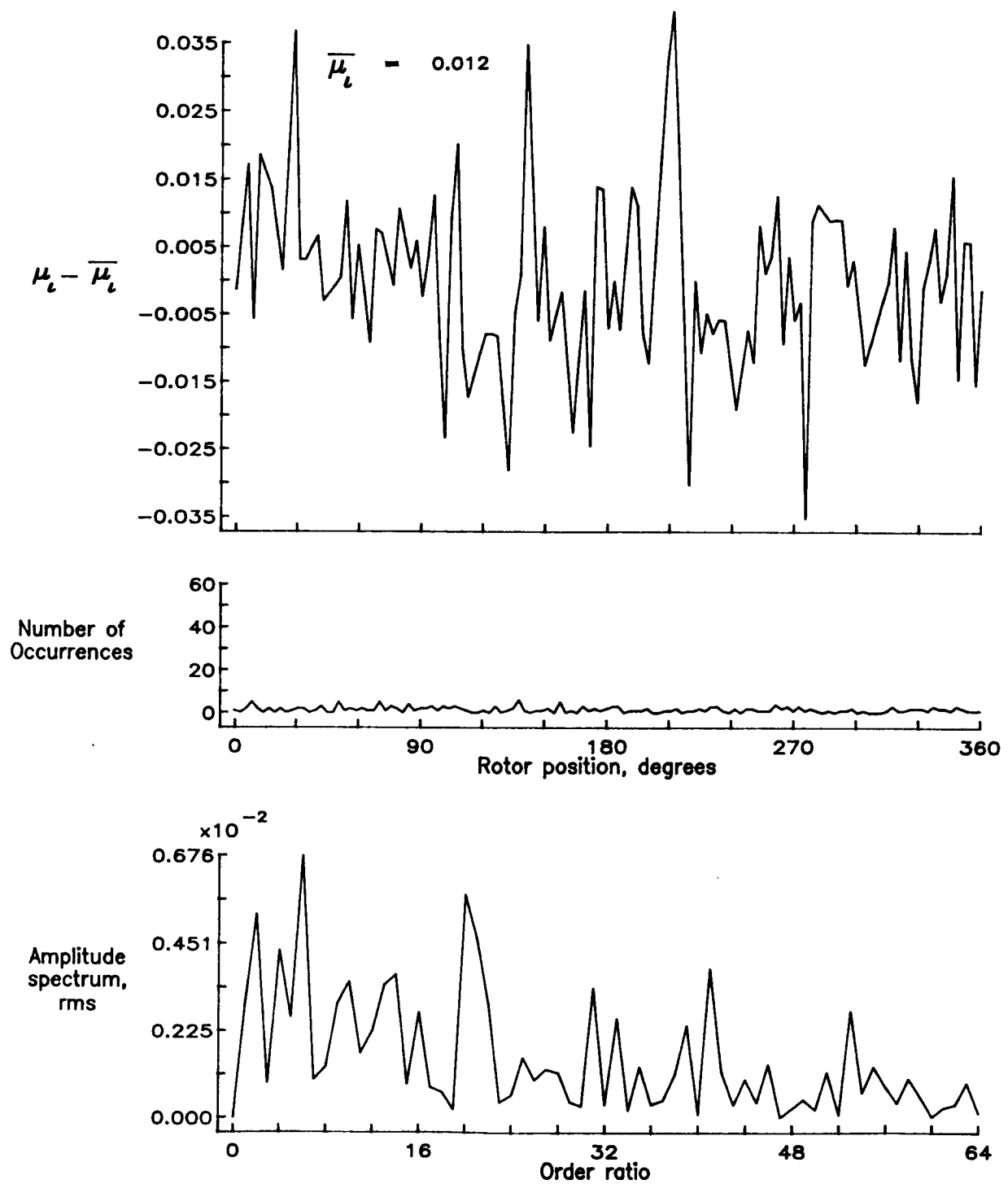


Figure 151.— Induced inflow velocity measured at 330 degrees and r/R of 0.82.

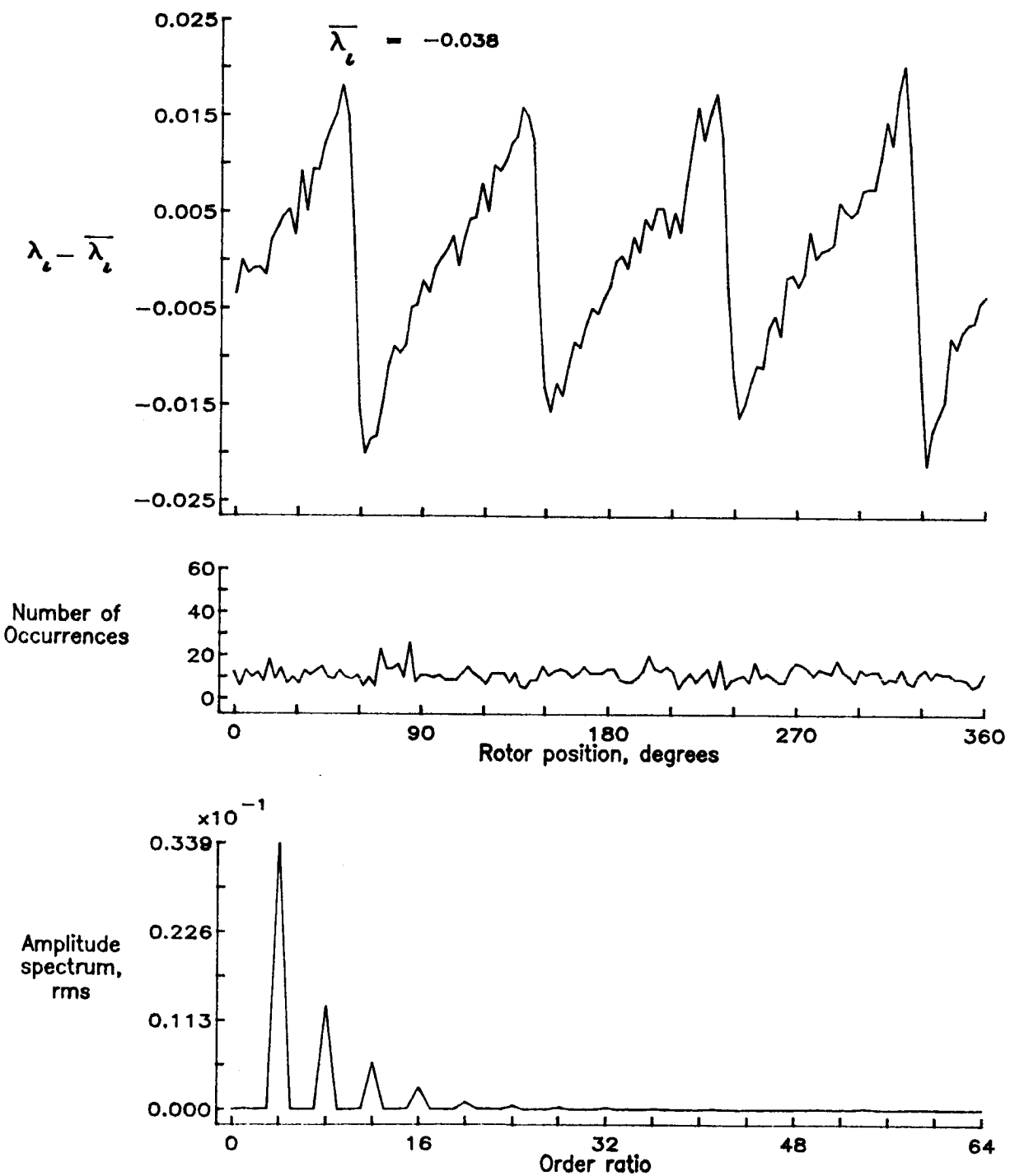


Figure 151.— Concluded.

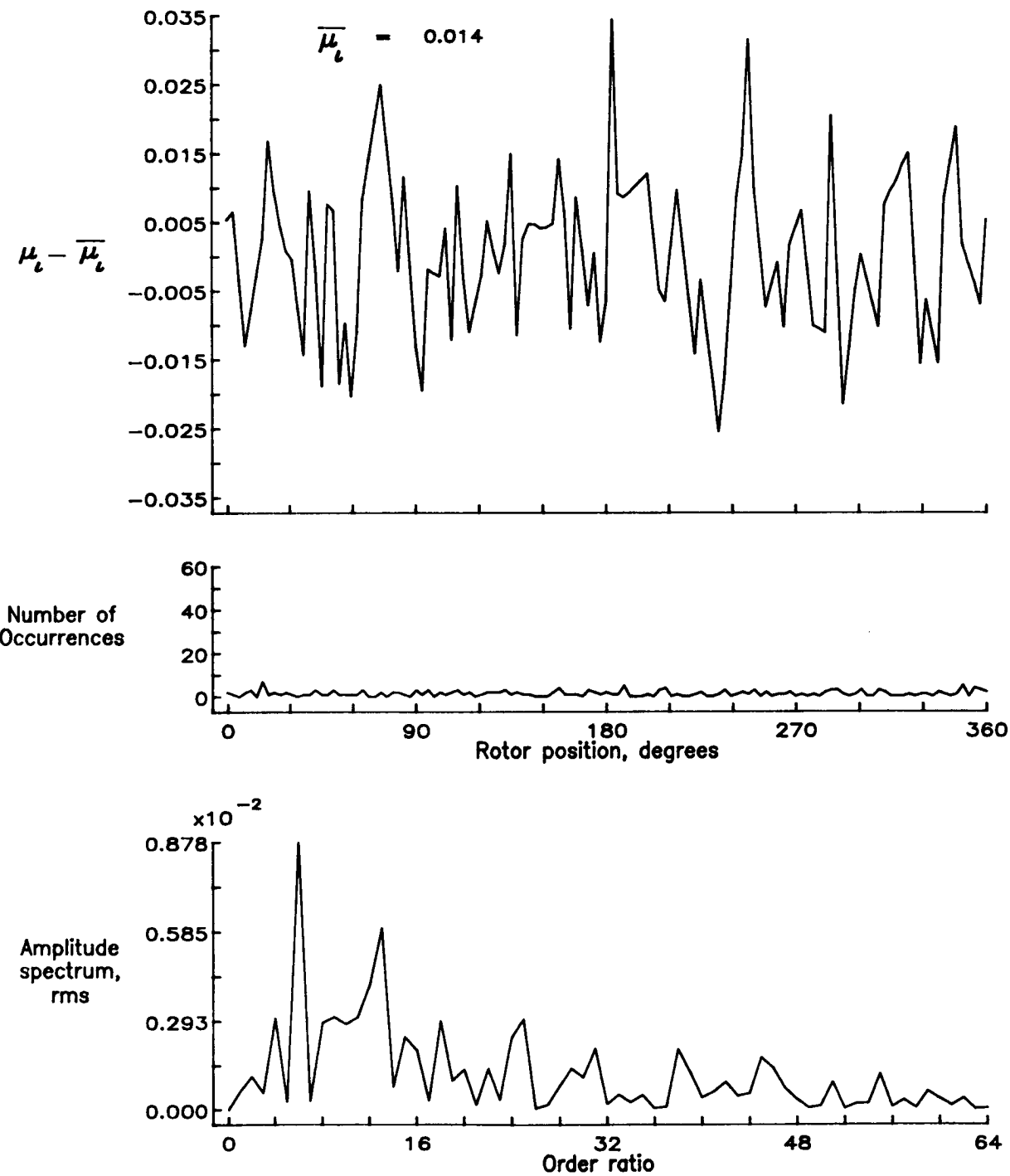


Figure 152.— Induced inflow velocity measured at 330 degrees and r/R of 0.86.

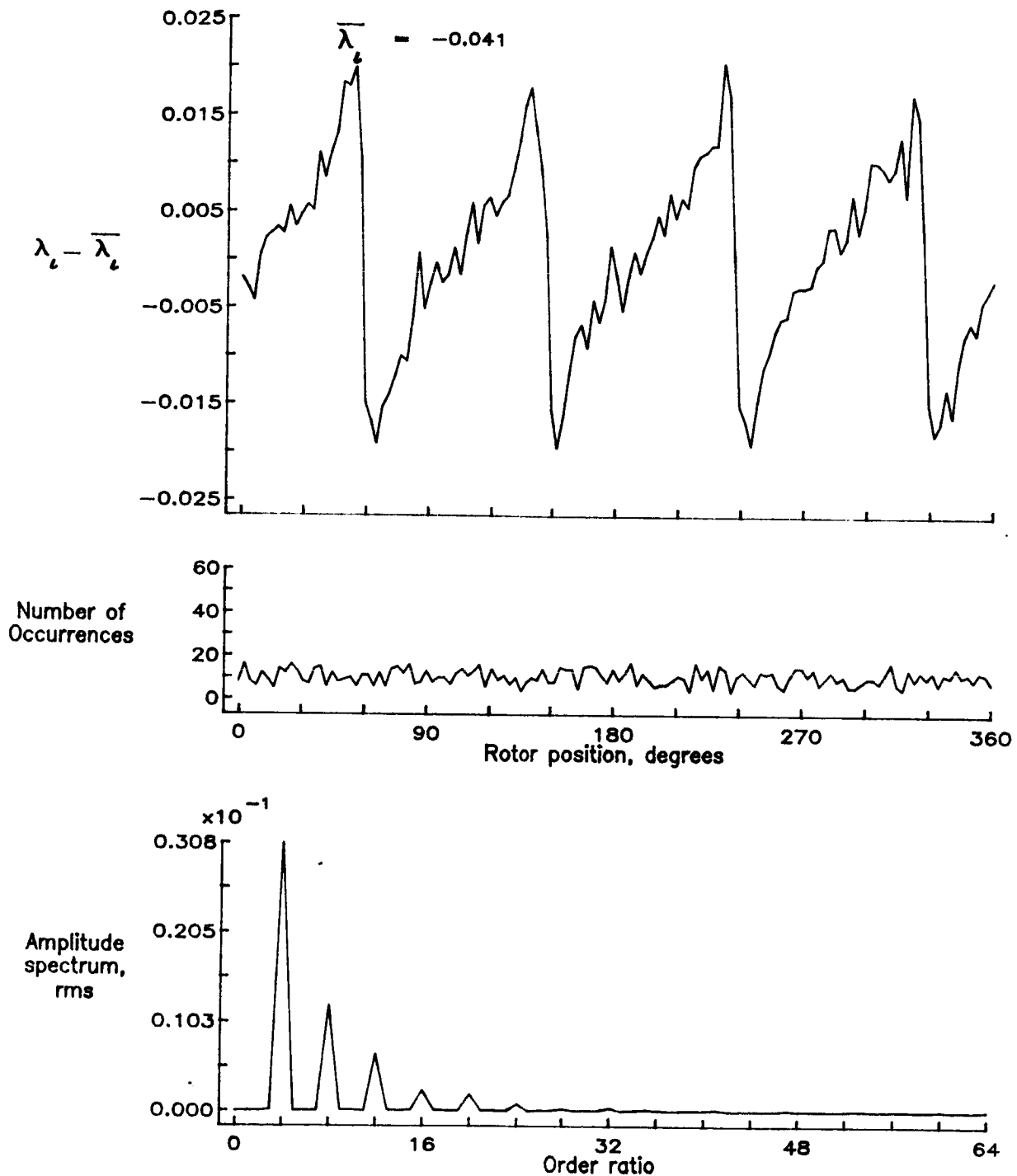


Figure 152.— Concluded.

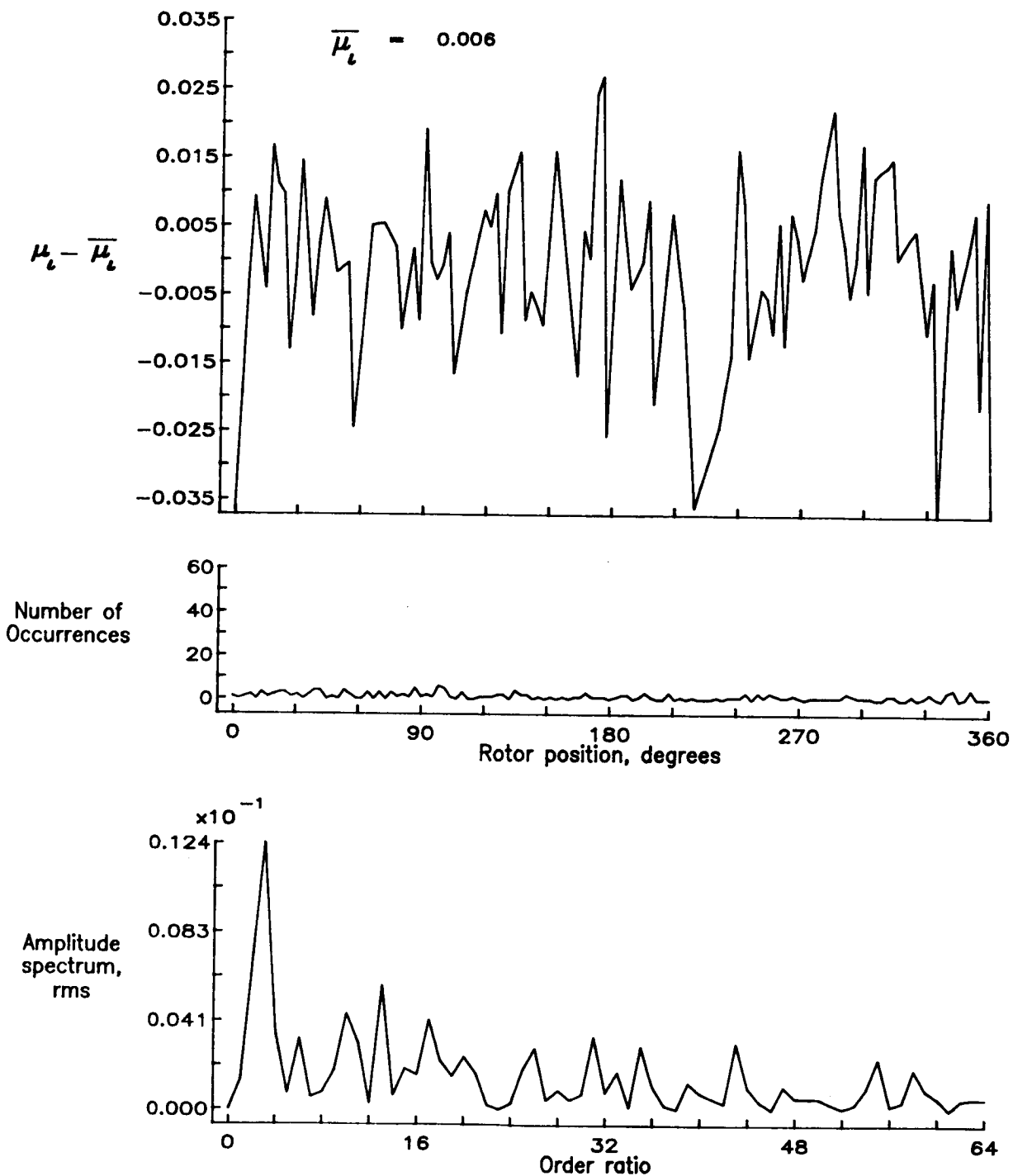


Figure 153.— Induced inflow velocity measured at 330 degrees and  $r/R$  of 0.90.

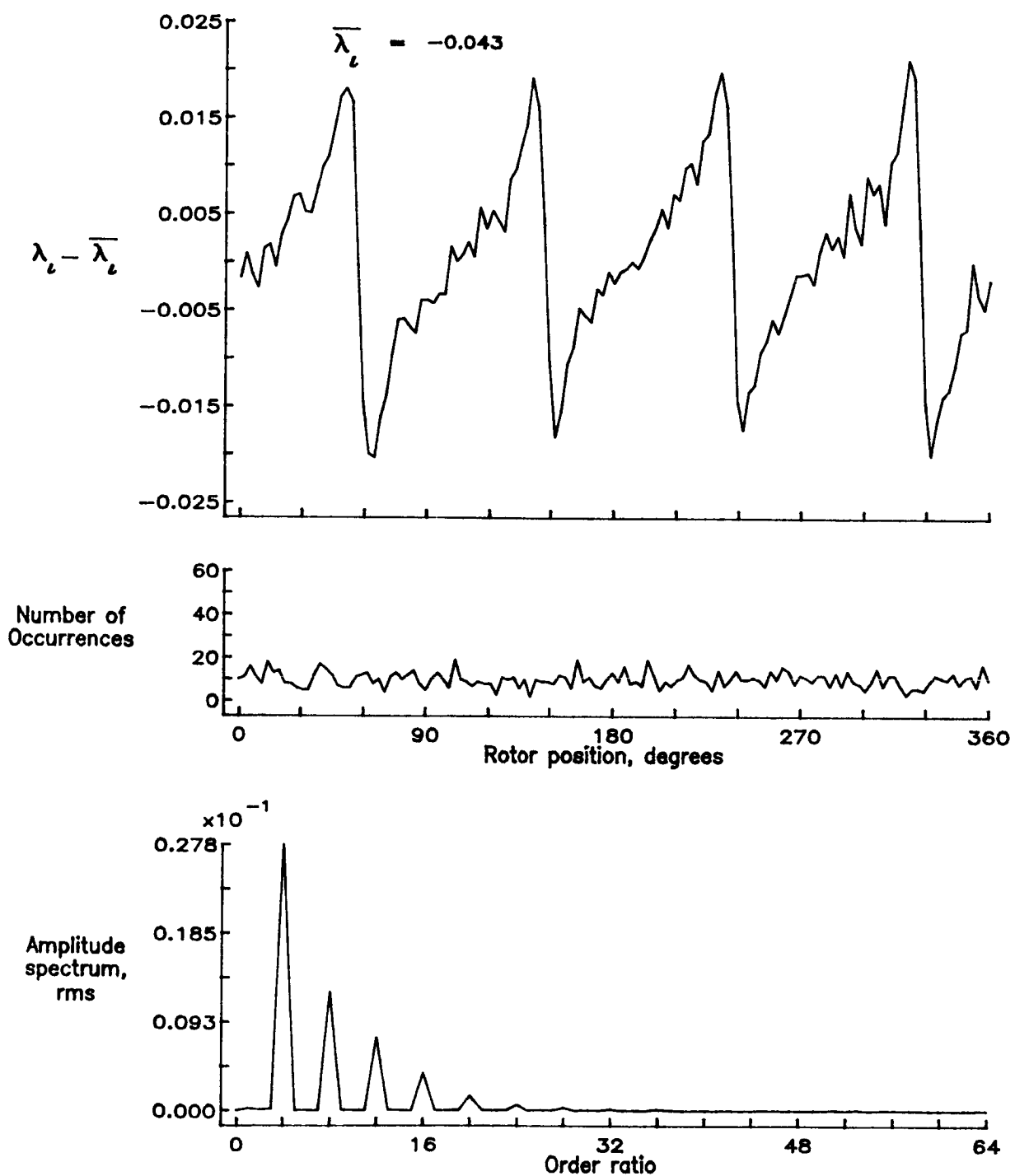


Figure 153.— Concluded.

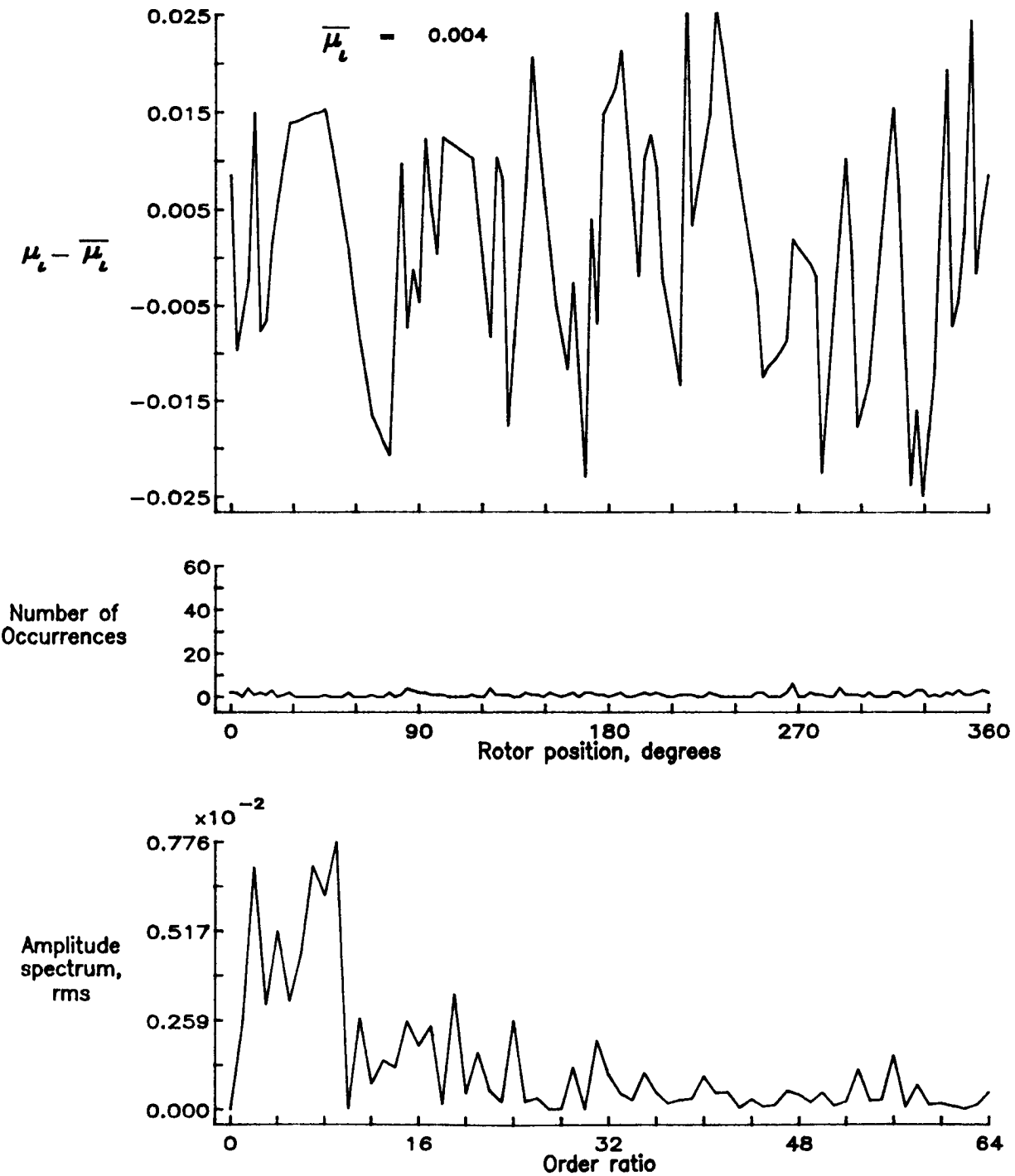


Figure 154.— Induced inflow velocity measured at 330 degrees and  $r/R$  of 0.94.

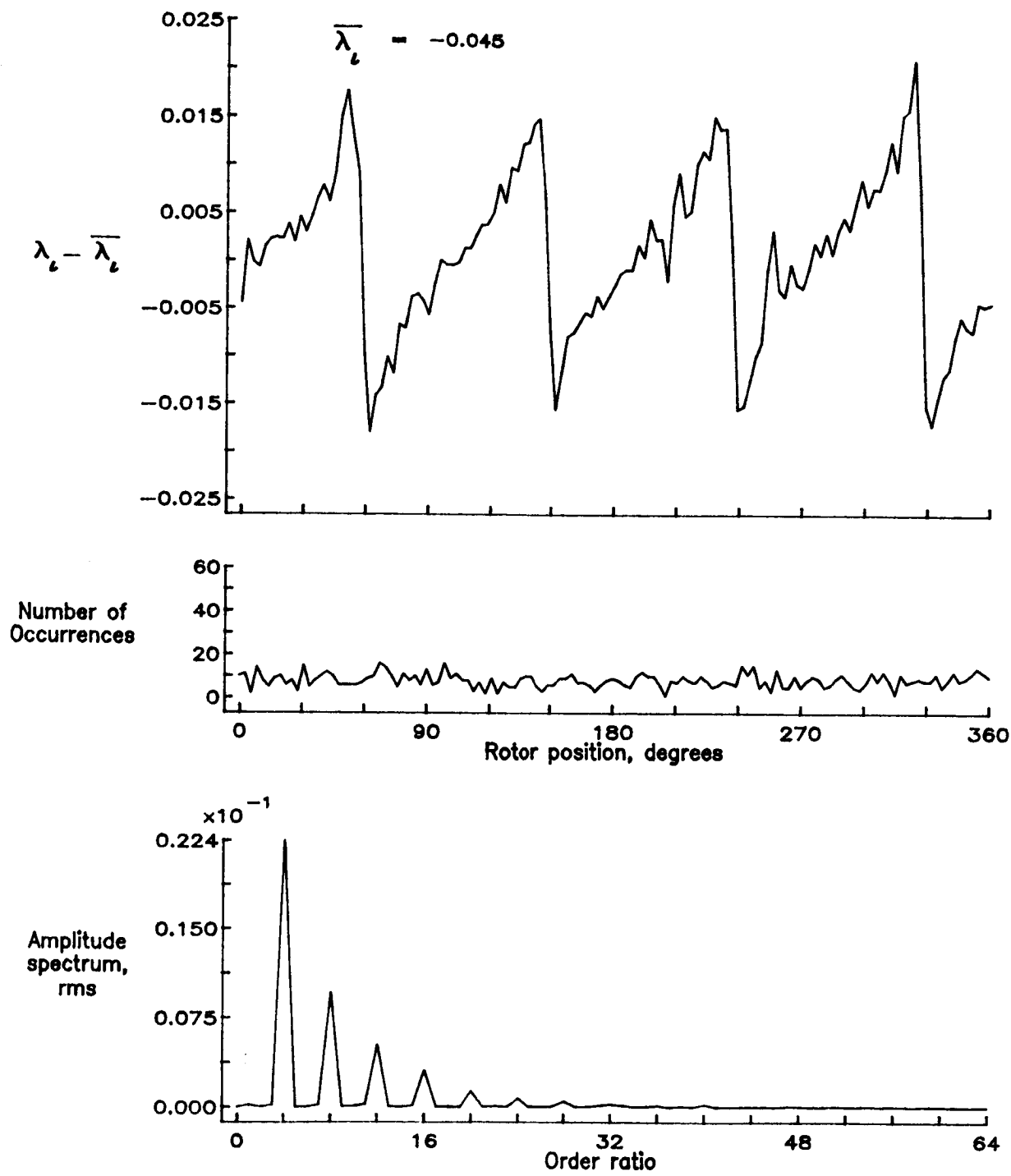


Figure 154.— Concluded.

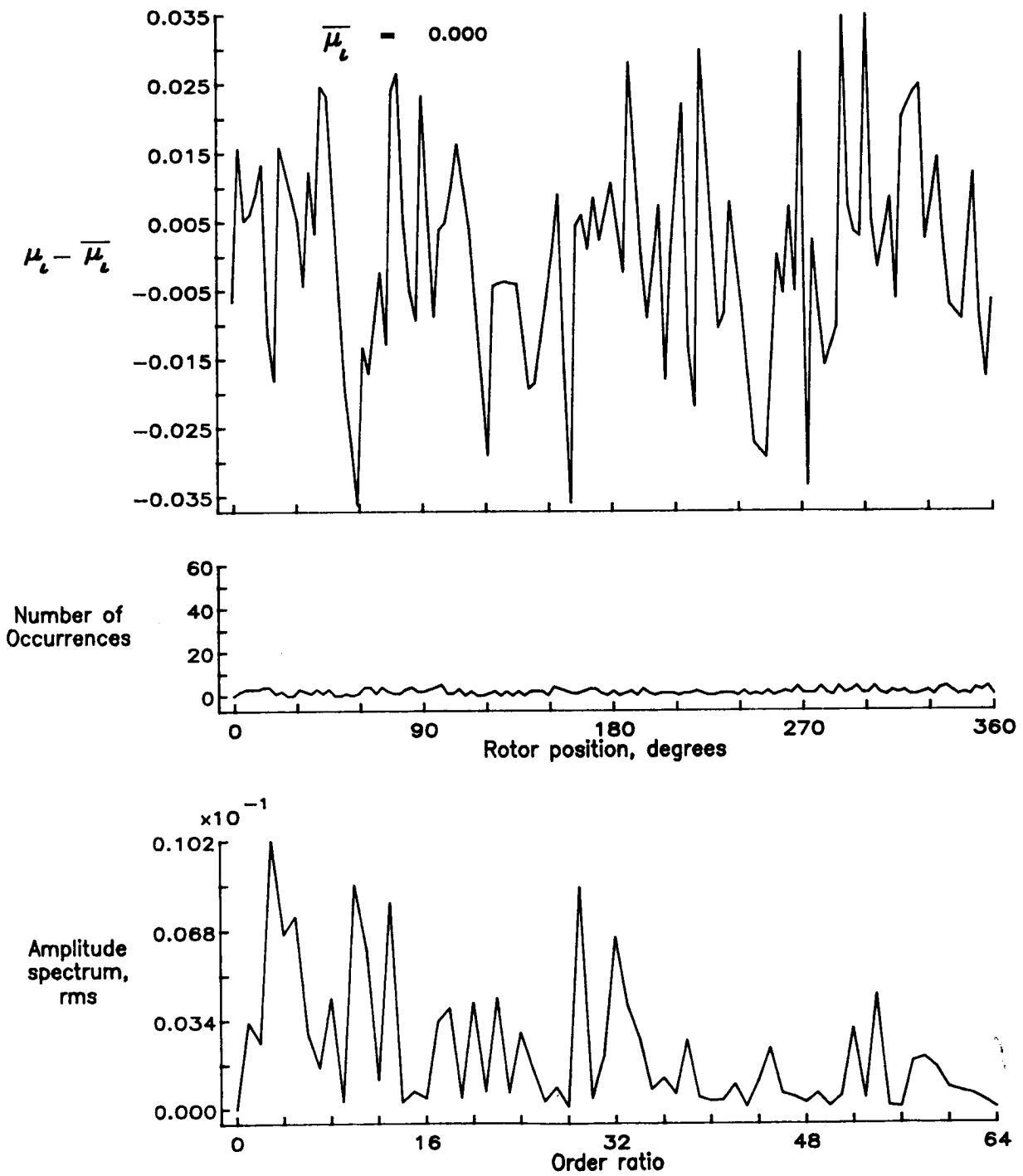


Figure 155.— Induced inflow velocity measured at 330 degrees and  $r/R$  of 0.98.

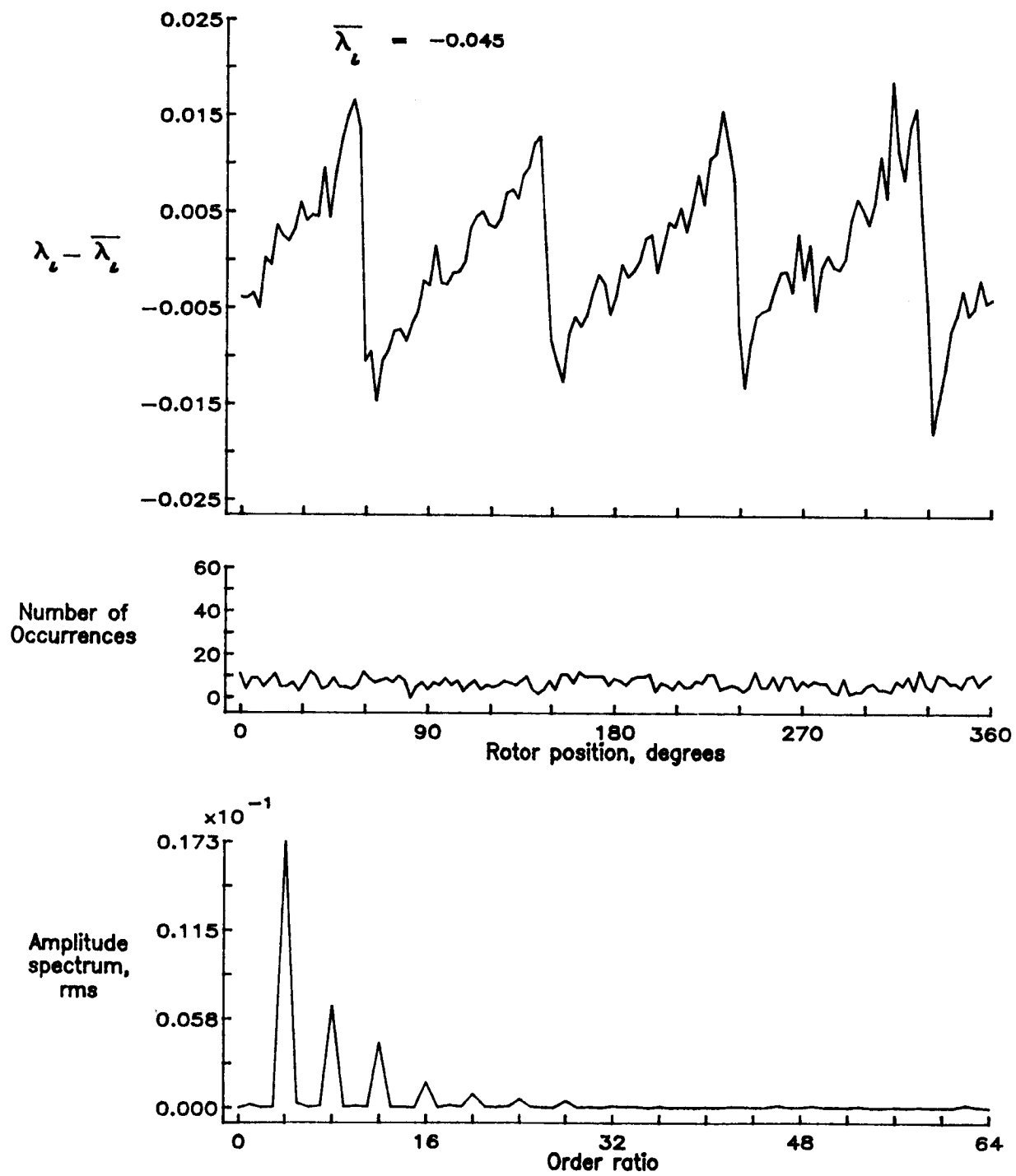


Figure 155.— Concluded.

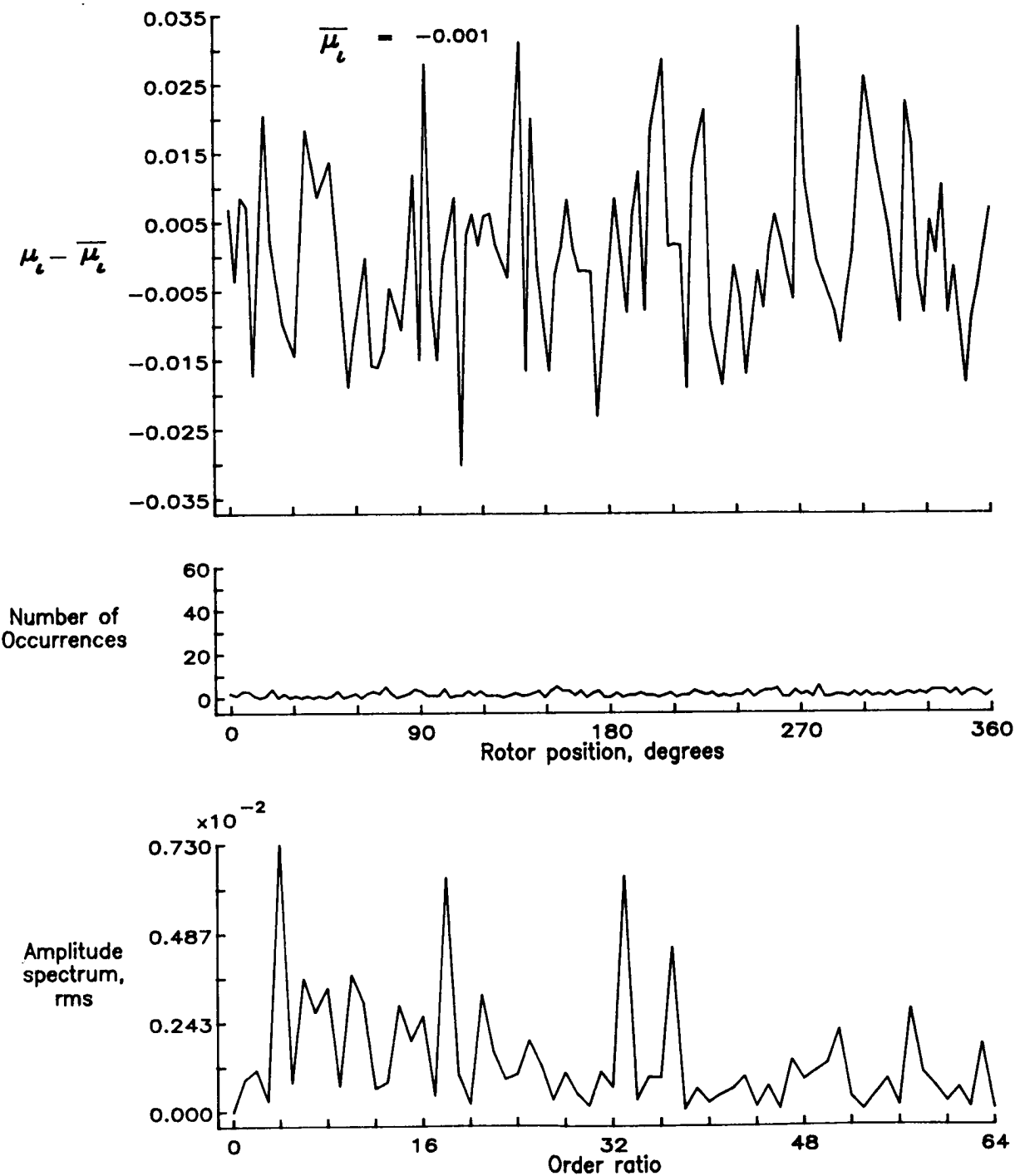


Figure 156.— Induced inflow velocity measured at 330 degrees and r/R of 1.02.

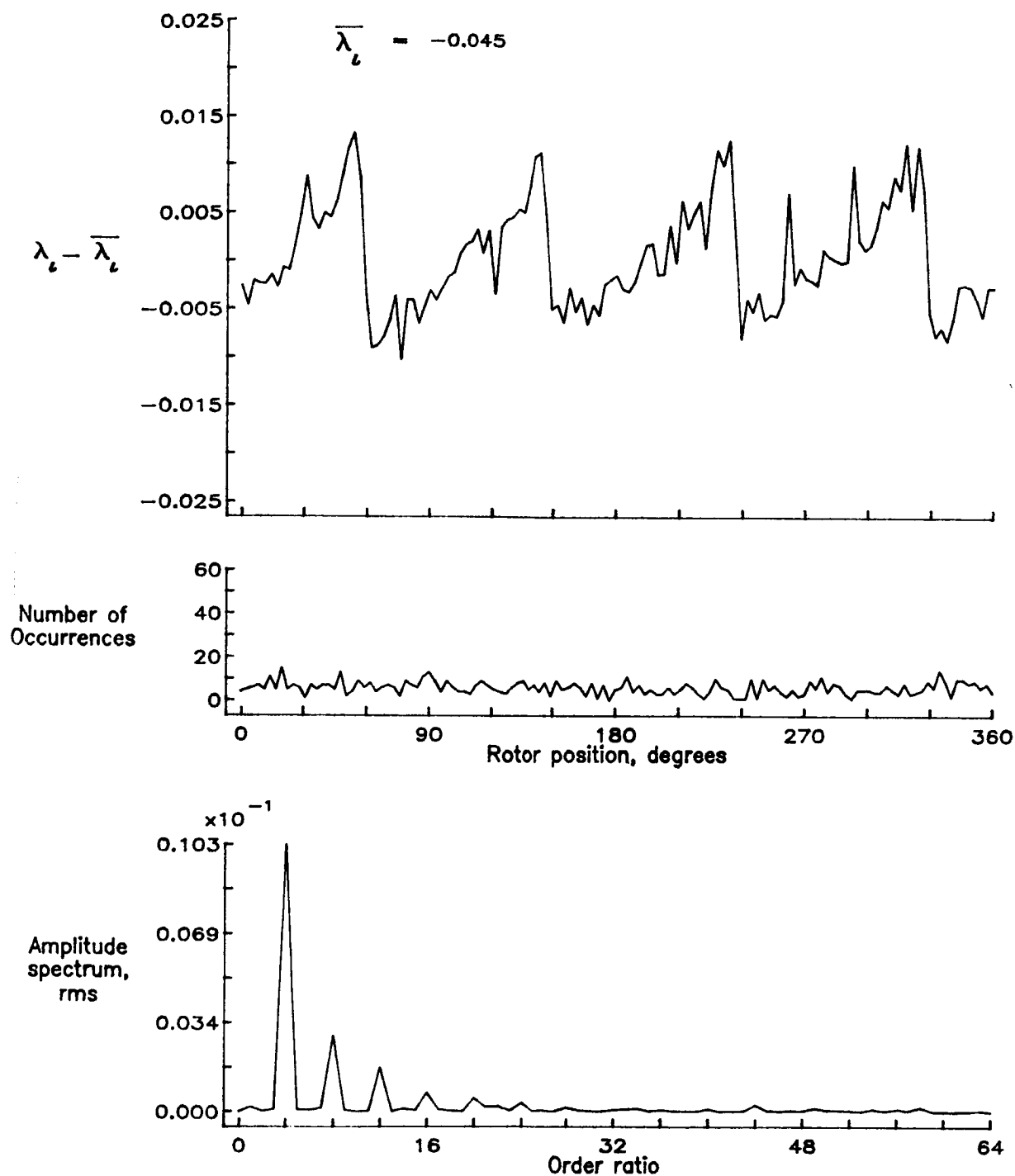


Figure 156.— Concluded.

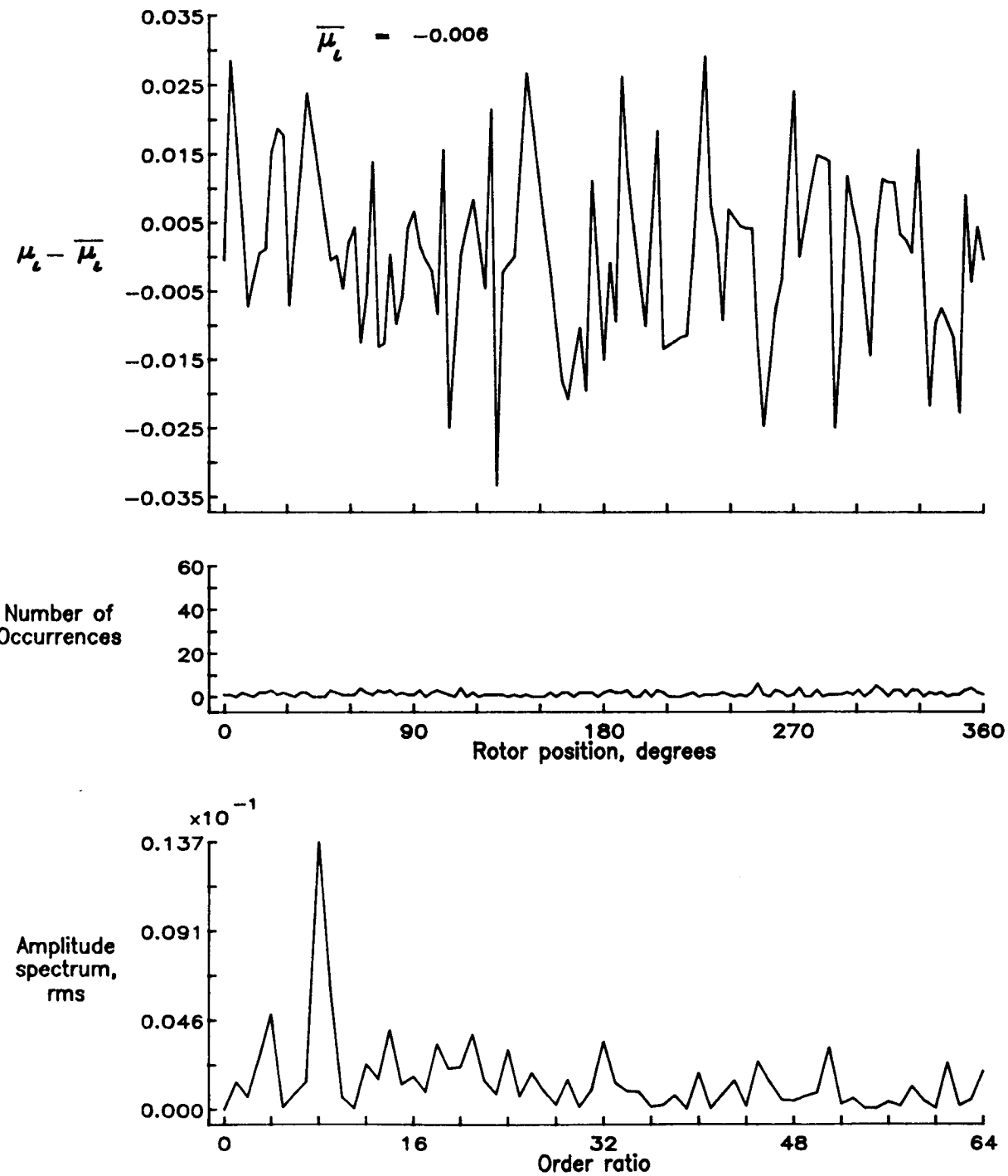


Figure 157.— Induced inflow velocity measured at 330 degrees and r/R of 1.04.

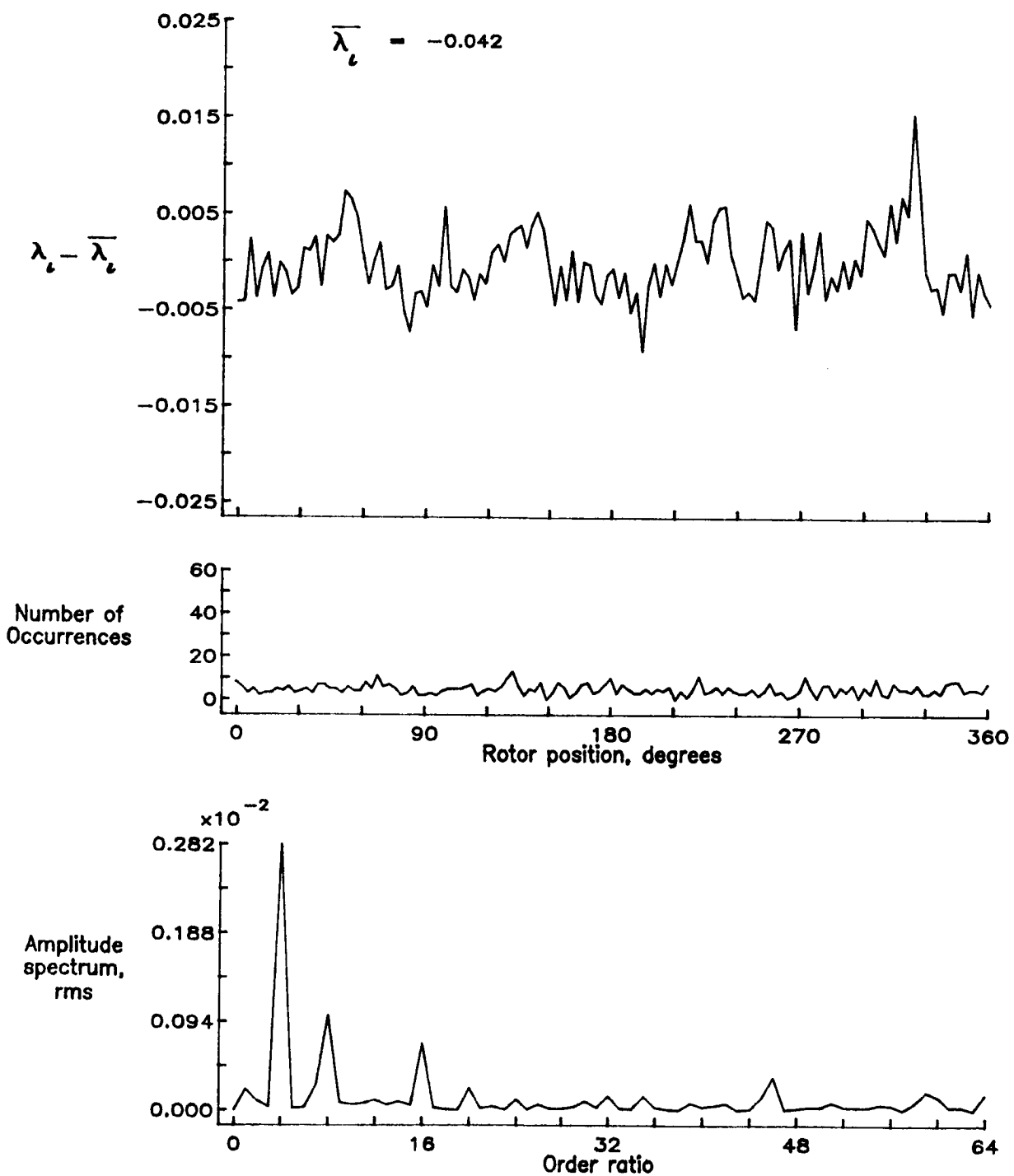


Figure 157.— Concluded.

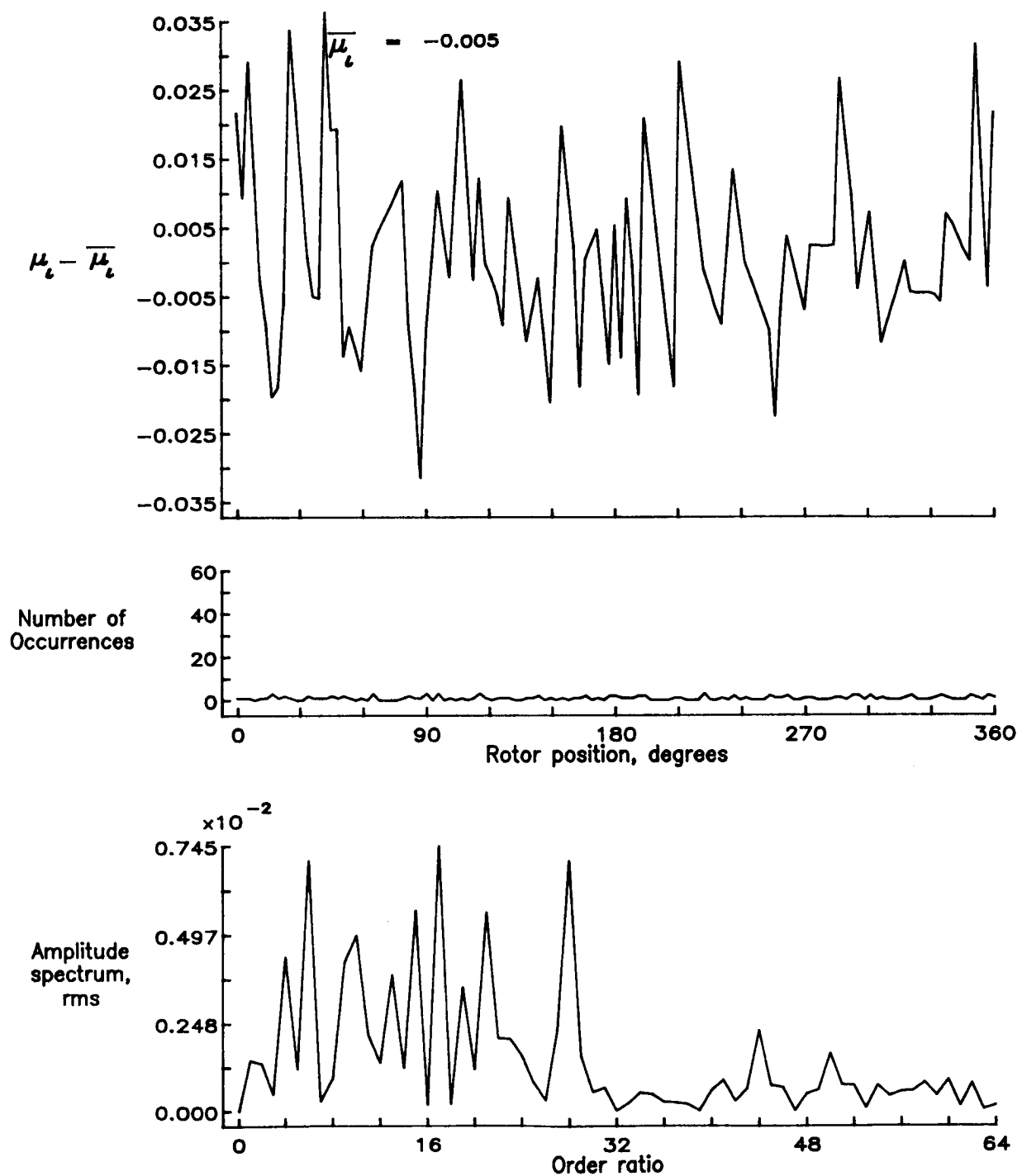


Figure 158.— Induced inflow velocity measured at 330 degrees and r/R of 1.10.

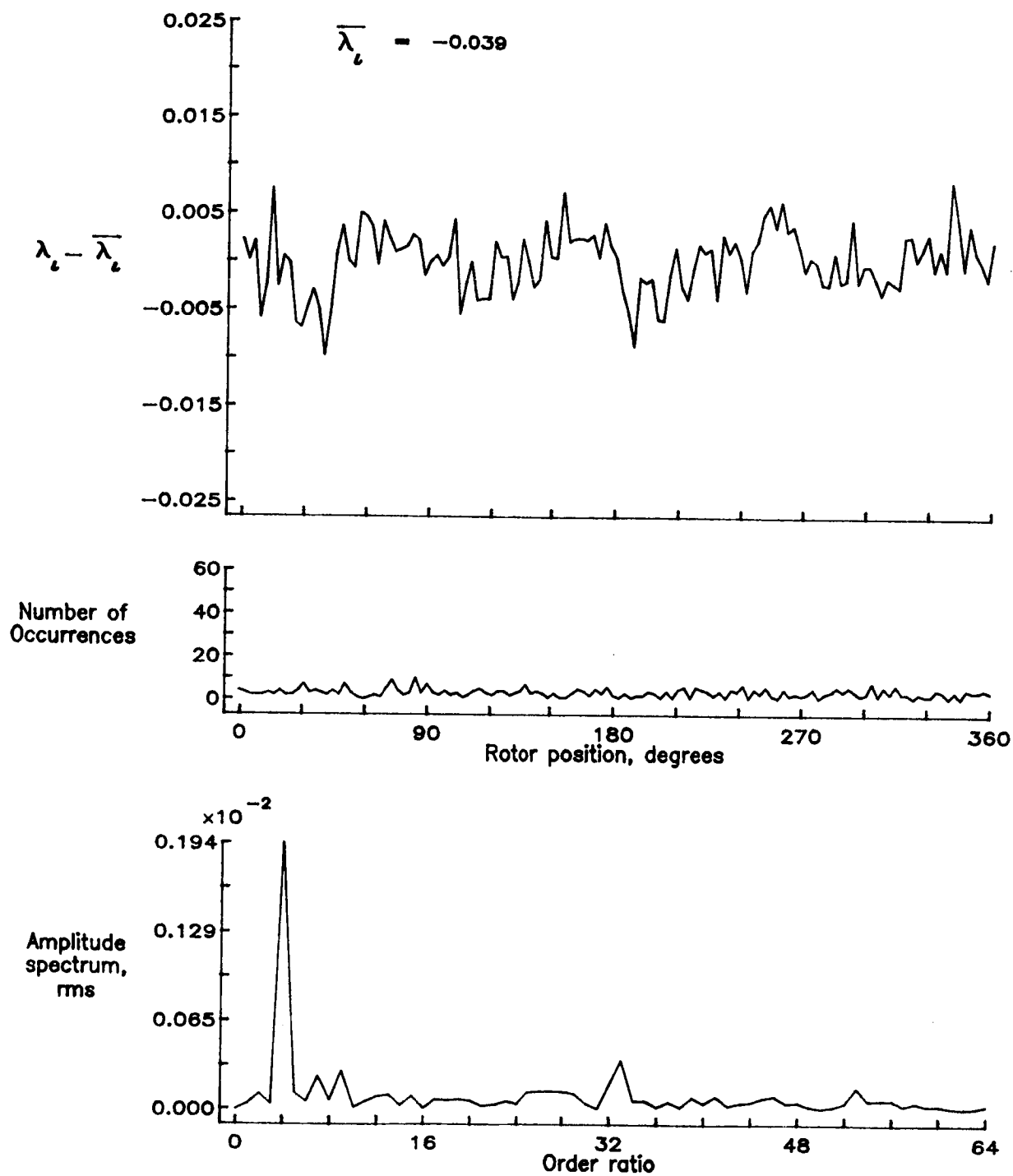


Figure 158.— Concluded.



National Aeronautics and Space Administration

## Report Documentation Page

1. Report No.  NASA TM-100541 AVSCOM TM 88-B-004	2. Government Accession No.	3. Recipient's Catalog No.	
4. Title and Subtitle  Inflow Measurements Made With A Laser Velocimeter On A Helicopter Model In Forward Flight, Volume I Rectangular Planform Blades at an Advance Ratio of 0.15		5. Report Date  April 1988	6. Performing Organization Code
7. Author(s)  Joe W. Elliott, Susan L. Althoff, and Richard H. Sailey		8. Performing Organization Report No.	
9. Performing Organization Name and Address  Aerostructures Directorate USAARTA-AVSCOM Langley Research Center Hampton, VA 23665-5225		10. Work Unit No.  505-61-51-10	11. Contract or Grant No.
12. Sponsoring Agency Name and Address  National Aeronautics and Space Administration Washington, DC 20546-0001 and US Army Aviation Systems Command St. Louis, MO 63120-1798		13. Type of Report and Period Covered  Technical Memorandum	14. Sponsoring Agency Code
15. Supplementary Notes  Joe W. Elliott and Susan L. Althoff: Aerostructures Directorate, USAARTA-AVSCOM, Langley Research Center, Hampton, VA Richard H. Sailey: PRC Kentron, Inc., Hampton, VA			
16. Abstract  An experimental investigation was conducted in the 14- by 22-Foot Subsonic Tunnel at NASA Langley Research Center to measure the inflow into a scale model helicopter rotor in forward flight ( $\mu_\infty = 0.15$ ). The measurements were made with a two component Laser Velocimeter (LV) one chord above the plane formed by the path of the rotor tips (tip path plane). A conditional sampling technique was employed to determine the azimuthal position of the rotor at the time that each velocity measurement was made so that the azimuthal fluctuations in velocity could be determined. Measurements were made at a total of 147 separate locations in order to clearly define the inflow character. This data is presented herein without analysis. In order to increase the availability of the resulting data, both the mean and azimuthally dependent values are included as part of this report on two 5.25 inch floppy disks in Microsoft Corporation MS-DOS format.			
17. Key Words (Suggested by Author(s))  Rotor model Inflow Laser Velocimetry		18. Distribution Statement  Unclassified - Unlimited  Subject Category 02	
19. Security Classif. (of this report)  Unclassified	20. Security Classif. (of this page)  Unclassified	21. No. of pages  322	22. Price  A14